AD/A-005 818

ANALYTICAL INVESTIGATION OF MEDIUM STOL TRANSPORT STRUCTURAL CONCEPTS. VOLUME I. STUDY RESULTS

R. E. Adkisson, et al

Douglas Aircraft Company

Prepared for:

Air Force Flight Dynamics Laboratory

August 1974

DISTRIBUTED BY:

NTIS

National Technical Information Service
U. S. DEPARTMENT OF COMMERCE
5285 Port Royal Road, Springfield Va. 22151

AFFDL-TR-74-109
Volume I

ANALYTICAL INVESTIGATION OF MEDIUM STOL TRANSPORT STRUCTURAL CONCEPTS

Volume I – Study Results

R. E. Adkisson
G. V. Deneff
Et Al

Douglas Aircraft Company
McDonnell Douglas Corporation

TECHNICAL REPORT AFFDL-TR-74-109, VOLUME I
August 1974

Approved for public release; distribution unlimited.

Air Force Flight Dynamics Laboratory
Air Force Systems Command
Wright-Patterson Air Force Base, Ohio

NOTICE

When Government drawings, specifications, or other data are used for any purpose other than in connection with a definitely related Government procurement operation, the United States Government thereby incurs no responsibility nor any obligation whatsoever; and the fact that the government may have formulated, furnished, or in any way supplied the said drawings, specifications, or other data, is not to be regarded by implication or otherwise as in any manner licensing the holder or any other person or corporation, or conveying any rights or permission to manufacture, use, or sell any patented invention that may in any way be related thereto.

Copies of this report should not be returned unless return is required by security considerations, contractual obligations, or notice on a specific document.

AIR FORCE/56780/5 February 1975 — 300

Unclassified

SECURITY CLASSIFICATION OF THIS PAGE (When Data Entered)

REPORT DOCUMENTATION PAGE

READ INSTRUCTIONS BEFORE COMPLETING FORM

1. REPORT NUMBER: AFFDL-TR-74-109, Volume I
2. GOVT ACCESSION NO.:
3. RECIPIENT'S CATALOG NUMBER: AD/A-005818
4. TITLE (and Subtitle): ANALYTICAL INVESTIGATION OF MEDIUM STOL TRANSPORT STRUCTURAL CONCEPTS, Study Results
5. TYPE OF REPORT & PERIOD COVERED: Final Technical Report of work performed between 15 March 1973 and 24 June 1974
6. PERFORMING ORG. REPORT NUMBER: MDC J-6625, Volume I
7. AUTHOR(s): Adkisson, R.E.; Deneff, G.V.; et al
8. CONTRACT OR GRANT NUMBER(s): F33615-73-C-3049
9. PERFORMING ORGANIZATION NAME AND ADDRESS: McDonnell Douglas Corporation, Douglas Aircraft Company, Long Beach, California 90846
10. PROGRAM ELEMENT, PROJECT, TASK AREA & WORK UNIT NUMBERS: Project 1368, Task 0212
11. CONTROLLING OFFICE NAME AND ADDRESS: Air Force Flight Dynamics Laboratory, Air Force Systems Command, Wright-Patterson Air Force Base, Ohio 45433
12. REPORT DATE: August 1974
13. NUMBER OF PAGES: 452
14. MONITORING AGENCY NAME & ADDRESS (if different from Controlling Office):
15. SECURITY CLASS. (of this report): Unclassified
15a. DECLASSIFICATION/DOWNGRADING SCHEDULE:
16. DISTRIBUTION STATEMENT (of this Report): Approved for public release; distribution unlimited
17. DISTRIBUTION STATEMENT (of the abstract entered in Block 20, if different from Report):
18. SUPPLEMENTARY NOTES:

19. KEY WORDS (Continue on reverse side if necessary and identify by block number)

STOL Structural Concepts, C-15 (AMST) Aircraft, STOL Design Criteria, STOL Loads, Structural Materials, Structural Evaluation, Manufacturing Methods, Nondestructive Inspection, Acquisition Costs, Life Cycle Costs, Performance Payoffs, STOL Wing Concepts, STOL Fuselage Concepts, STOL Empennage Concepts.

20. ABSTRACT (Continue on reverse side if necessary and identify by block number)

Results of a study program to devise and evaluate new structural concepts of lower weight and cost for a medium STOL transport aircraft are presented. The wing box, fuselage shell and empennage stabilizer structure of the projected C-15 production airplane were designated as the study (and baseline) components. Selected concepts are evaluated for structural integrity, weight, manufacturing methods, applicability of NDI methods, production and life cycle costs and aircraft performance payoffs. Structural integrity analyses of both

DD FORM 1473, 1 JAN 73 EDITION OF 1 NOV 65 IS OBSOLETE

Unclassified

SECURITY CLASSIFICATION OF THIS PAGE (When Data Entered)

the baseline and new concepts are based on a common set of requirements for ultimate strength, fatigue life, damage tolerance and flutter rigidity.

The primary materials considered are aluminum, titanium, steel and beryllium. Of these, aluminum 7050 and 7475 are a best choice for minimum production cost and low weight. The primary geometry concepts considered include integral stiffened, honeycomb and isogrid (a special form of integral stiffened). Integral stiffened and honeycomb geometry, in conjunction with the selected aluminum materials, produce weight and cost savings in the participating individual components of up to 10% which are further reflected as overall life cycle cost savings and performance payoffs at the aircraft system level. Innovative concepts for wing cover panel spanwise skin splices are also shown.

Requirements for simple "design-for-weight" and "design-for-cost" methods are identified. A simple "design-for-weight" method integrating materials, geometries and requirements was conceived and is implemented. A simple concept selection parameter based on unit weight and cost is also identified. Methods for developing consistent material property data and correlating of notched specimen fatigue data are also presented.

*U.S.Government Printing Office: 1974 — 657-017/370

ANALYTICAL INVESTIGATION OF MEDIUM STOL TRANSPORT STRUCTURAL CONCEPTS

Volume I – Study Results

R. E. Adkisson
G. V. Deneff
Et Al

Approved for public release; distribution unlimited.

FOREWORD

The analytical study described in this report was performed by Douglas Aircraft Company, McDonnell Douglas Corporation, Long Beach, California and sponsored by the Air Force Flight Dynamics Laboratory (AFFDL), Wright-Patterson Air Force Base, Ohio. The work was conducted under contract F33615-73-C-3049 Project 1368 and Task 0212. Lt. J. E. Malinak (AFFDL/FBR) was the project engineer for the work conducted.

This report covers work conducted between March 15, 1973, and June 24, 1974. This report was submitted by the authors on 26 July 1974, for AFFDL review. This report is also released as McDonnell Douglas report MDC-J6625A for internal control at the Douglas Aircraft Company.

This report is published in two volumes. Volume I, Study Results, presents the capabilities and costs of the baseline medium STOL transport wing, fuselage, and empennage structural concepts. This volume also includes the concept improvements resulting from the integration of new structural geometries, new materials, and manufacturing advances along with the resulting aircraft cost and performance payoffs. Volume II, Isogrid Fuselage Study, presents: (1) the design and analysis of a new isogrid fuselage concept, (2) the associated manufacturing methods and nondestructive inspection techniques, and (3) an aircraft cost and performance analysis for the isogrid fuselage and the new wing and empennage concepts, described in Volume I.

Mr. R. E. Adkisson was the Program Technical Director for Douglas Aircraft Company. Principle investigators in the associated disciplines include R. E. Adkisson - Structural Design, G. V. Deneff - Structural Analyses, B. J. Alperin - Material and Processes, R. L. Zwart - Manufacturing, M. L. Platte - System Analysis, and D. P. Marsh - Weight Engineering.

This technical report has been reviewed and is approved.

Francis J. Janik, Jr.
Chief, Structural Development Branch
Structures Division
Air Force Flight Dynamics Laboratory

ABSTRACT

Results of a study program to devise and evaluate new structural concepts of lower weight and cost for a medium STOL transport aircraft are presented. The wing box, fuselage shell and empennage stabilizer structure of the projected C-15 production airplane were designated as the study (and baseline) components. Selected concepts are evaluated for structural integrity, weight, manufacturing methods, applicability of NDI methods, production and life cycle costs and aircraft performance payoffs. Structural integrity analyses of both the baseline and new concepts are based on a common set of requirements for ultimate strength, fatigue life, damage tolerance and flutter rigidity.

The primary materials considered are aluminum, titanium, steel and beryllium. Of these, aluminum 7050 and 7475 are a best choice for minimum production cost and low weight. The primary geometry concepts considered include integral stiffened, honeycomb and isogrid (a special form of integral stiffened). Integral stiffened and honeycomb geometry, in conjunction with the selected aluminum materials, produce weight and cost savings in the participating individual components of up to 10% which are further reflected as overall life cycle cost savings and performance payoffs at the aircraft system level. Innovative concepts for wing cover panel spanwise skin splices are also shown.

Requirements for simple "design-for-weight" and "design-for-cost" methods are identified. A simple "design-for-weight" method integrating materials, geometries and requirements was conceived and is implemented. A simple concept selection parameter based on unit weight and cost is also identified. Methods for developing consistent material property data and correlating of notched specimen fatigue data are also presented.

VOLUME I

TABLE OF CONTENTS

TABLE OF CONTENTS (Continued)

TABLE OF CONTENTS (Continued)

TABLE OF CONTENTS (Continued)

TABLE OF CONTENTS (Concluded)

LIST OF ILLUSTRATIONS

LIST OF ILLUSTRATIONS (Continued)

LIST OF ILLUSTRATIONS (Continued)

LIST OF ILLUSTRATIONS (Continued)

LIST OF ILLUSTRATIONS (Continued)

LIST OF ILLUSTRATIONS (Concluded)

LIST OF TABLES

LIST OF TABLES (Continued)

LIST OF TABLES (Continued)

LIST OF TABLES (Concluded)

LIST OF ABBREVIATIONS AND SYMBOLS

SYMBOL		UNITS
a	Panel length (parallel to an edge), crack length (usually one-half total length), crack depth (part through crack), or hole diameter	inches
A	Area, constant or pertaining to materials with properties with 90% probability and 95% confidence	inches^2
A_1, A_{sk}	Skin area	inches^2
A_2, A_s, A_{st}	Stiffener area	inches^2
A_b	Back surface correction factor for a corner flaw from a hole	
A_c	Channel flange or composite area	inches^2
ACFT	Aircraft	
AGE	Aerospace Ground Equipment	
a_i	Load path (i = 1, 2, 3, etc.)	
A.J.	Assembly jig	
A1	Best aluminum materials for baseline geometry	
A1'	Best aluminum materials for integral Z geometry	
AMPR	Aircraft Manufacturer's Planning Report	
Ann	Annealed	
A_R	Total intercostal area	inches^2
A_{tot}	Total area	inches^2
ATP	Auxiliary tool - production	
b	Panel width, wing span, or isogrid rib width	inches
B	Panel width or pertaining to material with properties based on 99% probability and 95% confidence	inches
b_e	Skin effective width	inches
B.J.	Bonding jig	
b/1	Baseline geometry and any material	

LIST OF ABBREVIATIONS AND SYMBOLS (Continued)

SYMBOL		UNITS
$\overline{b/l}$	Initial baseline geometry and materials	
B/L	Baseline geometry and materials	
b_s	Stiffener spacing	inches
c	Compression, end fixity coefficient, or distance from neutral axis	
C	Coefficient in crack growth rate equation or chordwise	
2c	Crack length (part-through crack)	inches
C_{adv}	Cost of advanced component	$/#
C_{BL}	Cost of baseline component	$/#
C_c	Cost coefficient	
CCW	Counterclockwise	
C_F	Complexity factor	
Cf	Frame stiffness coefficient	
CKF	Check fixture	
C_{lc}	Life cycle costs	$\$/ft^2$
C_H	Cost of new concept component	
C_n	Horizontal tail chord	
C_s	Manufacturing cost	$\$/ft^2$
C_t	Tip chord	inches
CTOL	Conventional take-off and landing	
C_w	Wing chord	inches
c/z	Composite reinforced Z wing structure	
$C_{\#}$	Manufacturing cost per unit weight	$/#
d	Isogrid rib depth	inches
D	Diameter	inches

LIST OF ABBREVIATIONS AND SYMBOLS (Continued)

SYMBOL		UNITS
da/dN	Crack growth rate	inches/cycle
db	Decibels	
D.F.	Dynamic factor	
DJ	Drill jig	
DLC	Drawing control list	
D/T	Damage tolerance	
$D_R = \sum \frac{n_i}{N_i}$	Total damage in fatigue analysis	
E	Elastic modulus or extrusion	psi
E'	Modified modulus $(EE_T)^{1/2}$	psi
E_R	Intercostal elastic modulus	psi
E_T	Tangent modulus	psi
E.O.P.	Edge of part	
f	Applied stress, number of cycles, or frequency of occurrence	psi
F	Allowable stress, fatigue, or forging material	psi
$f(\frac{a}{r})$	Stress intensity factor coefficient for cracks at holes	
FA	Of each	
F_c	Allowable compressive stress	psi
F_{cs}	Allowable compression stress for design shear stress for honeycomb panels = $R_{ca} \times F_{cy}$	ksi
$f(\frac{L}{r})$	Stress intensity factor coefficient for corner cracks at holes	
F_{LT}	One lifetime	hours
FRP	Fuselage reference plane	
F/S	Full-size or front spar	

LIST OF ABBREVIATIONS AND SYMBOLS (Continued)

SYMBOL		UNITS
F_{ts}	Allowable tensile stress for design shear stress for honeycomb panels = $R_{TA} \times F_T$	ksi
F_{xx}	Minimum period of unrepaired service usage	hours
g	Load factor	
G	Shear modulus	psi
G&A	General and Administrative	
GAG	Ground-air-ground	
G+M	Gust + maneuver	
GW	Gross weight	pounds
h	Channel depth, distance between facing centroids, depth, height of isogrid triangle, honeycomb core depth, or thickness	inches
H/C	Honeycomb geometry and selected materials	
H-Core	Honeycomb core	
HF	Handling Fixture	
HFLD	Handling Fixture - Line Dolly	
HFPR	Handling Fixture - Production	
HL	Hole	
HS	Horizontal Stabilizer	
HT	Heat treat	
H_z	Hertz	cycle/sec
I	Moment of inertia	$inches^4$
I_R	Intercostal moment of inertia	$inches^4$
i/z	Integral Z geometry and any material	
I/Z	Integral Z geometry and selected materials	
J	Torsional moment of inertia	$inches^4$

LIST OF ABBREVIATIONS AND SYMBOLS (Continued)

SYMBOL		UNITS
K	Stress intensity factor, applied scatter factor to account for variability in Pd, or constant	ksi $\sqrt{in}$
K_A, K_B	One sided tolerance limits	
K_c	Critical stress intensity factor (plane stress fracture toughness)	ksi $\sqrt{ins.}$
K_f	Stress concentration factor in fatigue	
K_{I_c}	Critical stress intensity factor (plane strain fracture toughness	ksi $\sqrt{ins.}$
K_n	Modified stress concentration factor	
K_o	Factor for hole out, notch, etc.	
K_q	Tentative value of plane strain fracture toughness	ksi $\sqrt{ins.}$
K_t	Stress concentration factor	
L	Panel total length, longitudinal, shell length, longitudinal grain direction, or rib and spar web stiffening	inches
L'	Panel effective length	inches
$L = \frac{a}{\sqrt{2}}$	In $f(\frac{L}{r})$ coefficient	inches
LB	pounds	pounds
L.E.	Leading edge	
LF	Load factor	
LLM+G	Low level maneuver plus gust	
L_N	Distance between wing and horizontal tail 0.25MAC's	inches
LS,RS	Left side, right side	
LT	Long transverse grain direction or layout template	
L_V	Distance between wing and vertical tail 0.25 MAC's	inches
m	Material or mode	
M	Mach number, bending moment, or mode	inch-lbs

SYMBOL		UNITS
MAC	Mean aerodynamic chord	inches
MC	Mill cutter	
MCM	Machine control medium	
MF	Mill fixture	
M+G	Maneuver + gust loads	
M_H	Mach number at V_H	
M_k	Elastic stress magnification factor for deep surface discontinuities in tension in Δk equation	
M_L	Mach number at V_L	
MLG	Main landing gear	
MLP	Multiple load path structure	
M_{tu}	Ultimate mode design moment	inch-lbs
MP	Midpoint Manufacturer's Planning Report	
n	Number of occurrences, load factor, exponent in crack growth rate equation, or shape factor in stress strain equation $\mathcal{E} = \frac{T}{E} + K\,(T)^n$	
N	Allowable number of occurrences or load intensity	lbs/inch
N.A.	Neutral axis	
NC	Numerically controlled	
NDT	Non-destructive testing	
NDI	Non-destructive inspection	
NLG	Nose landing gear	
N.MI.	Nautical miles	
NT	No tool	
N_{xc}	Longitudinal compression loading	#/in.
N_{xt}	Longitudinal tension loading	#/in.

LIST OF ABBREVIATIONS AND SYMBOLS (Continued)

SYMBOL		UNITS
OEW	Operator's empty weight	pounds
P	Load or plate material	pounds
P_b	Bypassing load	pounds
P_{DM}	Load occurring once in 100 depot or base level inspection intervals	
P_{LT}	Minimum required residual strength for non-inspectable structure	
PME	Prime mission equipment	
POL	Petroleum, oil, and lubricant	
P_t	Transfer load	pounds
P_{xx}	Minimum required residual strength	
P_{yy}	Minimum load for fail-safe structure	
q	Notch sensitivity factor = $(K_f-1)/(K_t-1)$	
Q	Flaw shape parameter	
r	Hole radius	inches
R	Radius or ratio of minimum to maximum stress	inches
R_{CA}	Allowable compression stress ratio for design shear stress for honeycomb panels	
R_{CT}	Ratio of stress intensity factors in unstiffened to stiffened sheet	
RDT&E	Research, Development, Test, & Engineering	
RT	Room temperature	
R_{TA}	Allowable tensile stress ratio for design shear stress for honeycomb panels	
R.S.	Rear spar	
s	Intercostal length	inches
S	Sheet material, spanwise stringer number or specification	
SBR	System Benefit Rate	$/#

LIST OF ABBREVIATIONS AND SYMBOLS (Continued)

SYMBOL		UNITS
SCF	Stress concentration factor	
SCG	Slow crack growth	
SD	Standard Deviation	
S_F	Scale factor	
SL	Sea level	
SLS	Sea level static	
$S_{n(K_t=x)}$	Net area stress in fatigue	psi
$S_{n(K_t=x)}$	$= S_{n(K_t=1)}K_f$	psi
ST	Short transverse grain direction	
STA	Solution treated and aged	
STOGW	STOL gross weight	
t	Intercostal web thickness, thickness, temperature, or time	inches °F, seconds
T	Transverse, tension, or torque	
$\overline{t}$	Equivalent weight thickness	inches
t_c	Honeycomb core depth	inches
t_f	Honeycomb face sheet thickness	inches
TH	Tooling hole	
TOGW	Take-off gross weight	pounds
t_s	Skin thickness	inches
U_{de}	Gust velocity	ft/sec
UE	Unit equipment	
V	Airspeed, shear	KEAS,pounds
V_d	Dive speed (FAR)	KEAS
VG	Vertical gust	ft/sec

LIST OF ABBREVIATIONS AND SYMBOLS (Continued)

SYMBOL		UNITS
V_H	Level flight maximum speed	KEAS
V_L	Limit operational speed	KEAS
V_{LF}	Limit speed for landing approach and take-off	KEAS
V_{PTA}	Limit load factor stall speed	KEAS
VS	Vertical stabilizer	
w	Weight, weight per unit area, plate width or notch flank angle	$\#/ft^2$
W	Weight or wrought material	
W_R	Intercostal weight	$\#/ft^2$
WRP	Wing Reference Plane	
W_s	Structural weight	pounds
X_H	Horizontal stabilizer station	inches
XYZ	Principle axis of aircraft and external load coordinates	
X_w	Wing station	inches
y	Vertical distance above top of fuselage	inches
Z,J	Stringer configuration	
Z_{RS}	Vertical stabilizer station	inches
α	Thermal expansion coefficient and angle of attack	in/in °F, degrees
α_b	Backside correction factor	
β	Angle of attack in yaw or modification factor in stress intensity equation to account for load transfer	degrees
γ	Stress correlation factor (classical vs FORMAT) or transfer load/total load = $\dfrac{P_t}{P_t + P_b}$	
δ	Control surface deflection or deflection	degrees
ε	Strain or geometric efficiency factor	inches/inch

SYMBOL		UNITS
ϵ_g	Efficiency = $\frac{\text{actual panel capability}}{\text{ideal panel capability}}$	
λ	$\lambda = 1 - \mu_{ab}\ \mu_{ab}$ or panel width correction factor	
μ	Poisson's ratio	
η	Material constant	
$\bar{\eta}$	$= (E_t/E)^{0.75}$	
ρ	Material density	$lb/in.^3$
ρ'	Grain size factor	inches
ρ'_f	Grain size factor in fatigue	inches
σ_g	Gross area stress	psi
σ	Applied stress	psi
τ_e	Effective area stress	ksi
ω	Notch flank angle	radians

SUBSCRIPTS

bt	Bending tension
c	Compression
cu	Compression ultimate
cy	Compression yield
Crit	Critical
DM	Depot Maintenance (relative to inspection periods)
eq	Equivalent
f	Frame
F	Flap or flutter
FE	Flight evident
GE	Ground evident
H	Horizontal tail

LIST OF ABBREVIATIONS AND SYMBOLS (Concluded)

SUBSCRIPTS

H/C	Honeycomb
i	Point in time
I/G	Isogrid
LLM+G	Low level maneuver plus gust
m	Mode
min	Minimum
N	Normal load on vertical tail
o	Base value
req'd	Required
RES	Residual
S	Shear
ssc	Stress corrosion cracking
s_v	Special Visual (relative to inspection periods)
sy	Shear yield
t	Tensile
TH	Threshold
tu	Ultimate tensile
ty	Tensile yield
ULT	Ultimate
WY	Walk around visual
WV	Walk around (relative to inspection periods)
X,Y,Z, or x,y,z	Axes
n	Power

SUPERSCRIPTS

n	Constant in Format equation for da/dn

SECTION I

INTRODUCTION AND SUMMARY

1.1 INTRODUCTION

The structural weight fraction of an aircraft system determines, to a great extent, the success of that aircraft. The STOL transport structural weight fraction is even more critical due to the requirements of short field landing and takeoffs. A reduction in the structural weight fraction will enhance the productivity of the aircraft in that more payload and/or range is possible for the same size aircraft. Similarly, a structural weight reduction can be the basis for resizing the aircraft to reduce production and life cycle costs.

The structural weight fractions of various aircraft, including that of the AMST are listed in Table I. The basic fraction for a CTOL version of the AMST is in the range of existing aircraft; however, for the STOL mode, the structural weight becomes an even more significant portion of the TOGW.

Efforts to reduce the structural weight were concentrated on the structural boxes of the wing and empennage and on the fuselage shell, including the cargo floor. The primary structure weight reduction goal was 15%. The weight reduction was to be made at the same or reduced cost from the existing baseline structure.

The AMST, a medium STOL transport (frontispiece), is a four engine high wing vehicle incorporating an externally blown high lift flap system. The cargo box is approximately 12 x 12 x 47 feet in size with an aft entrance provided by a single door in conjunction with a loading ramp. The STOL midpoint TOGW is 150,000 pounds. The design takeoff and landing distances are 2000 feet.

1.2 STUDY APPROACH

The study approach was first to determine the capabilities and costs of the baseline structural concepts and then to improve these concepts by integrating new structural geometries, new materials and manufacturing advances. The program followed the flow chart as presented in Figure 1. A more comprehensive discussion of this integration is in Section VI.

Four structural stations were selected as analysis points for the wing box, fuselage shell and the horizontal and vertical stabilizer structural boxes. These are shown in Figure 2. The weights of the various concepts were calculated for the primary structure at these stations and used to determine the total airframe weight.

Cost estimates for the metal baseline and the advanced metallic structure concept aircraft in this study are based on historical data and detailed discrete component estimates for the airframe and the airframe systems, engine company prices for the propulsion system, and subcontractor cost data for avionics. This provides a consistent and solid approach for developing and comparing the differential weights and costs between these aircraft.

TABLE I STRUCTURAL WEIGHT FRACTION COMPARISON									
NO	ITEM	DC9-32	DC8-55F	DC10-10	C-133B	C-130E	C-141	C-5	C-15*
1	WING WEIGHT	11541	35454	49533	27064	14075	34392	81985	18765
2	FUSELAGE WEIGHT	11157	25214	44899	32123	14561	29212	114954	24367
3	EMPENNAGE WEIGHT	2790	4952	13404	6147	3409	5745	12344	6694
4	STRUCTURE WEIGHT	25488	65620	107836	65334	32045	69349	209283	49826
5	WING AREA	1001	2883	3550	2673	1808	3002	6200	1740
6	T.O.G.W. (CTOL)	108000	325000	430000	286000	155000	316100	728000	198500
7	WING LOADING (CTOL)	108	113	121	107	86	105	118	114
8	STRUCTURAL WEIGHT FRACTION (CTOL)	.236	.202	.250	.229	.207	.219	.288	.251
9	MIDPOINT T.O.G.W.	-	-	-	-	-	-	-	150000
10	WING LOADING (STOL)	-	-	-	-	-	-	-	86
11	STRUCTURAL WEIGHT FRACTION (STOL)	-	-	-	-	-	-	-	.332

* AMST

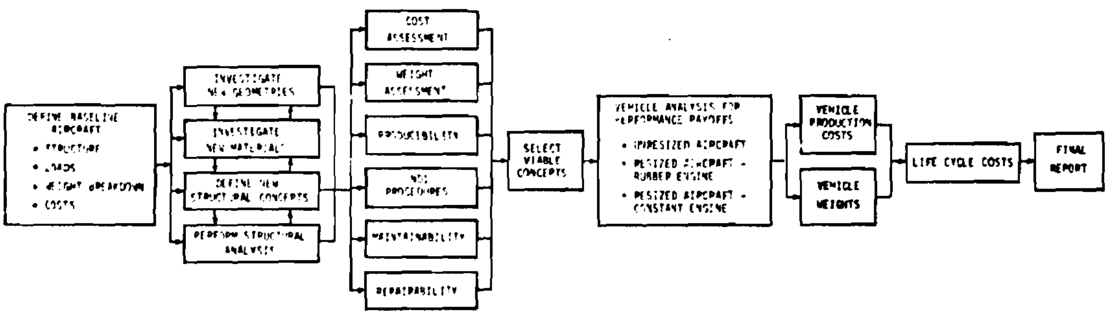

Figure 1 TASK FLOW DIAGRAM

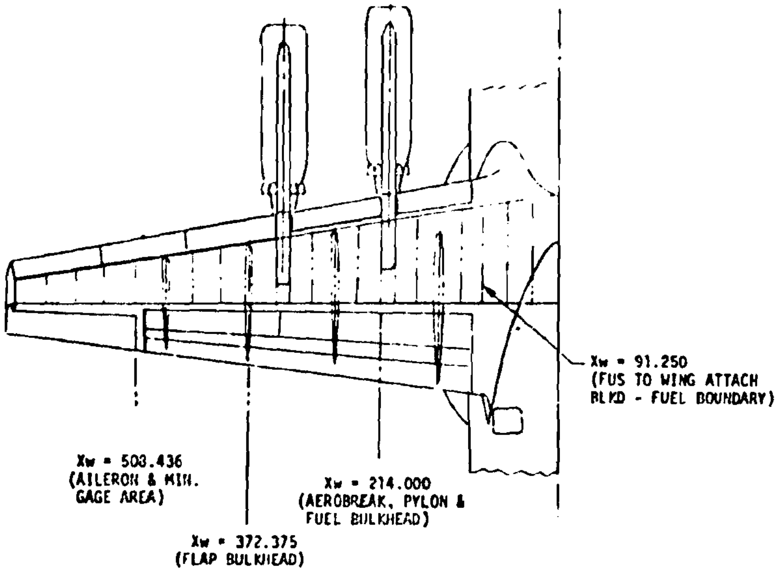

(a) LOCATION OF WING SPANWISE STRUCTURAL STUDY STATIONS

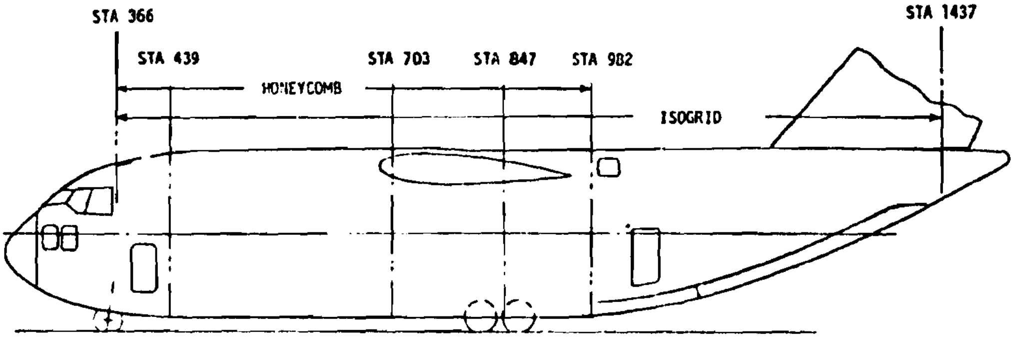

(b) LOCATION OF FUSELAGE STRUCTURAL STUDY STATIONS

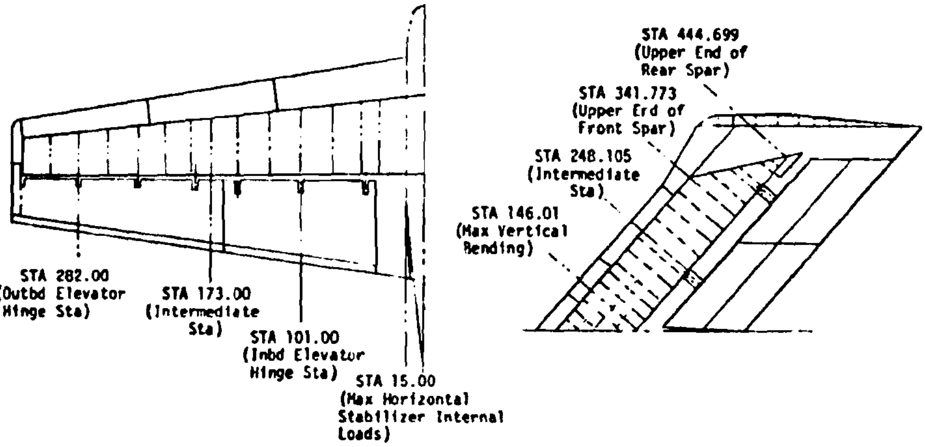

(c) LOCATION OF EMPENNAGE STRUCTURAL STUDY STATIONS

Figure 2 STRUCTURAL STATIONS FOR ANALYSIS

The metal baseline aircraft is similar in physical characteristics and performance to the projected C-15 production aircraft; however, the C-15 aircraft has been tailored to a production "design-to-cost" program, and emphasizes primary cost reductions compared to traditional design and program concepts. Therefore, $10.1M in FY 1973 dollars for the study baseline aircraft using commercial transport historical data compares to a $6.6M price in FY 1972 dollars for the AMST Proposal "design-to-cost" production aircraft. These cost figures are based on the cumulative average for 300 aircraft.

For purposes of this study, the specific intent was to establish and maintain throughout a consistent basis for comparing the baseline and new concept aircraft so that the comparative weight and cost results obtained are indicative of the potential for advanced structural designs. However, in the future, it also is essential to examine the potential of applying these new concepts to a projected design-to-cost aircraft where the challenge is to achieve a significant reduction in airframe cost. A final proof of achievement would entail design, fabrication, test, evaluation and cost tracking of full-scale primary structural components.

1.3 SUMMARY

The study program to develop new and innovative concepts for structural components for the AMST aircraft has been completed and the results are presented in this two volume report.

The baseline vehicle, a production version of the McDonnell Douglas YC-15 prototype, was established and is described in detail for the wing and empennage boxes and for the fuselage shell, including the cargo floor. The final external loads were determined and the associated internal loads summarized. These external loads are representative of the STOL loads. The corresponding internal loads are representative of the baseline aircraft. Parametric studies were conducted to determine panel geometry weight comparisons by assuming various load intensities. The actual weight comparisons were then made by using the correct loads at each design station of the wing, fuselage and empennage.

A comprehensive material data search was completed for advanced alloys of aluminum, titanium, steel, beryllium and composites. The properties considered were static and fatigue strengths, corrosion and stress corrosion, toughness and crack growth rates. Promising aluminum alloys identified for applications to the primary structure of the wing and empennage boxes and to the fuselage shell are 7050 and 7475. The airframe loads and expected environment did not justify the use of titanium or steel. Beryllium was not cost effective and projected sheet sizes were less than optimum for airframe utilization. Composites were used as selective reinforcement for the cargo floor planks, the vertical stabilizer spar caps, and were considered for use on the wing cover skin stringers.

Structural concepts were considered and evaluated for the wing and empennage structural boxes, the fuselage shell and for the cargo floor. The selected designs were combined into a new concept airframe for weight and cost studies. Two basic airframe configurations were established. The wing and empennage structure is identical for both. One arrangement has a honeycomb sandwich fuselage shell and the other an isogrid shell. The descriptions and analyses for all except the isogrid shell are in Volume I. The isogrid study is documented in Volume II. Each of the two configurations have been resized keeping the same performance characteristics.

The wing cover skins are integrally stiffened panels with integral rib caps. These are combined with integrally machined spars and bulkheads to present a wing structure with few details.

The horizontal and vertical stabilizer cover panels are an aluminum honeycomb sandwich. The spar caps and bulkhead caps are bonded to the panels reducing the number of attachments through highly stressed areas. The spar webs and bulkhead webs are integrally stiffened.

The aluminum honeycomb sandwich fuselage shell extends from Station 366 to Station 982. The panels have "picture frame" edge members with provisions for tension bolt attachments both circumferentially and longitudinally. The panels are nine feet wide and vary in length from 11 feet to 28 feet. The major wing and landing gear frames are integrally machined. The cargo floor loads are distributed into the sandwich shell through partial frames extending from below the floor to 45 degrees above the fuselage reference line.

The isogrid fuselage shell concept application ran from Station 366 to Station 1347. The discussion of the study effort is presented in Volume II.

A new approach has been formulated to provide better visibility in the selection and integration of structural geometries and materials. A series of charts have been constructed to show the relative weights of various combinations based on ultimate strength, fatigue life, damage tolerance and flutter considerations.

Weight estimates were made for the new geometries established for the wing, empennage and fuselage primary structure. The wing box weight is 11 percent below the baseline counterpart. The horizontal stabilizer box weight is 11.6 percent less than the baseline. The vertical stabilizer box weight is 11.7 percent less than the baseline. The honeycomb fuselage shell is 3.3 percent lighter than the conventional baseline skin and longeron concept. These primary structure weight reductions are for the full sized aircraft. The total primary structural weight is 8.6 percent less than the baseline. The weight of the resized components are 10.2 percent less. The isogrid shell weight is 6.1 percent heavier than the baseline, as indicated in Volume II.

Manufacturing methods and non-destructive inspection procedures are discussed as they relate to the selected structural concepts.

Cost estimates were made for the baseline aircraft and for the new concepts. The acquisition and life cycle costs of the new concepts were established for both the full sized and completely resized aircraft.

The resized airframe component production cost comparisons are; 1) wing box, 35 percent less; 2) horizontal tail box, 42 percent less; 3) vertical tail box, 29 percent less; 4) honeycomb fuselage shell, 20.2 percent more; and 5) isogrid fuselage shell, 66.7 percent more.

The production costs for the resized airframe containing the new concepts of the wing and empennage boxes and the honeycomb fuselage shell are 7 percent less than those for the baseline.

Production costs for the resized airframe utilizing the isogrid fuselage shell and the wing and empennage new structural concepts are 0.7 percent more than the baseline.

Life cycle costs for the honeycomb fuselage shell airframe are 1.8 percent less than the baseline for the full size and 2.8 percent less for the resized. Similarly, the life cycle costs for the isogrid fuselage shell airframe are 1.1 percent more for the full size and 0.4 percent less for the resized.

Aircraft performance payoff studies were conducted for three sizes of aircraft utilizing the new design concepts. The results for the honeycomb fuselage shell concept are in this volume. The isogrid fuselage shell arrangement results are presented in Volume II. The sizes include: 1) unresized, or fixed, geometry; 2) completely resized airframe, including "rubberized" engines and 3) partially resized airframe with the baseline engines. Three performance options were considered. They are: 1) a reduction in field length, 2) an increase in payload and 3) an increase in mission radius.

SECTION II

STRUCTURAL INTEGRITY REQUIREMENTS

The baseline and new structural concepts are required to: 1) possess adequate ultimate and yield strength to withstand the loads and pressures in the expected operating environments, 2) meet the fatigue and damage tolerance service life requirements and 3) possess sufficient stiffness to prevent flutter and excessive deformation in accordance with the classical relationship

$$\text{Margin of Safety} = \frac{\text{Structural Capability}}{\text{Structural Requirements}} - 1 \geq 0 \qquad (1)$$

Provisions of capability to equal or exceed the requirements defines the concept characteristics; therefore, the structural integrity requirements are an integral part of the new concept development procedure.

2.1 BASELINE DESCRIPTION

The baseline airplane used for this study was the production version of the YC-15 medium STOL transport prototype whose general arrangement is shown in Figure 3. The C-15 has the same arrangement as the prototype YC-15; however, the material selection changed due to the different fatigue life requirements.

The structural concepts of the baseline airplane were used for comparison in this analytical study. This structure represents the current state-of-the-art for design and manufacturing for the major components of the wing, fuselage shell and empennage.

The basic structural arrangement is shown in Figure 4. The material for all primary structure is aluminum alloy. The utilization of a particular alloy for a specific component has been determined by loading conditions or expected environmental use.

The baseline structural weight breakdown in percent of the midpoint STOL TOGW is shown in Figure 5. The wing and fuselage primary structure constitutes a major portion of the total weight. The empennage structure weight is a small fraction; hence, the wing and fuselage structure received the major study consideration for weight and cost reduction. The primary structural weight breakdown, in percent of the total structural weight, is shown in Figure 6.

Baseline design criteria, external load conditions and internal member sizing were obtained from the YC-15 prototype design effort. Damage tolerance requirements were furnished by the Air Force (Revision C of the proposed criteria) and are found in Appendix A.

The requirements are progressively developed from the general air vehicle level (design criteria) to the more detailed airframe component and panel levels (design loads and rigidities) in the following subsections.

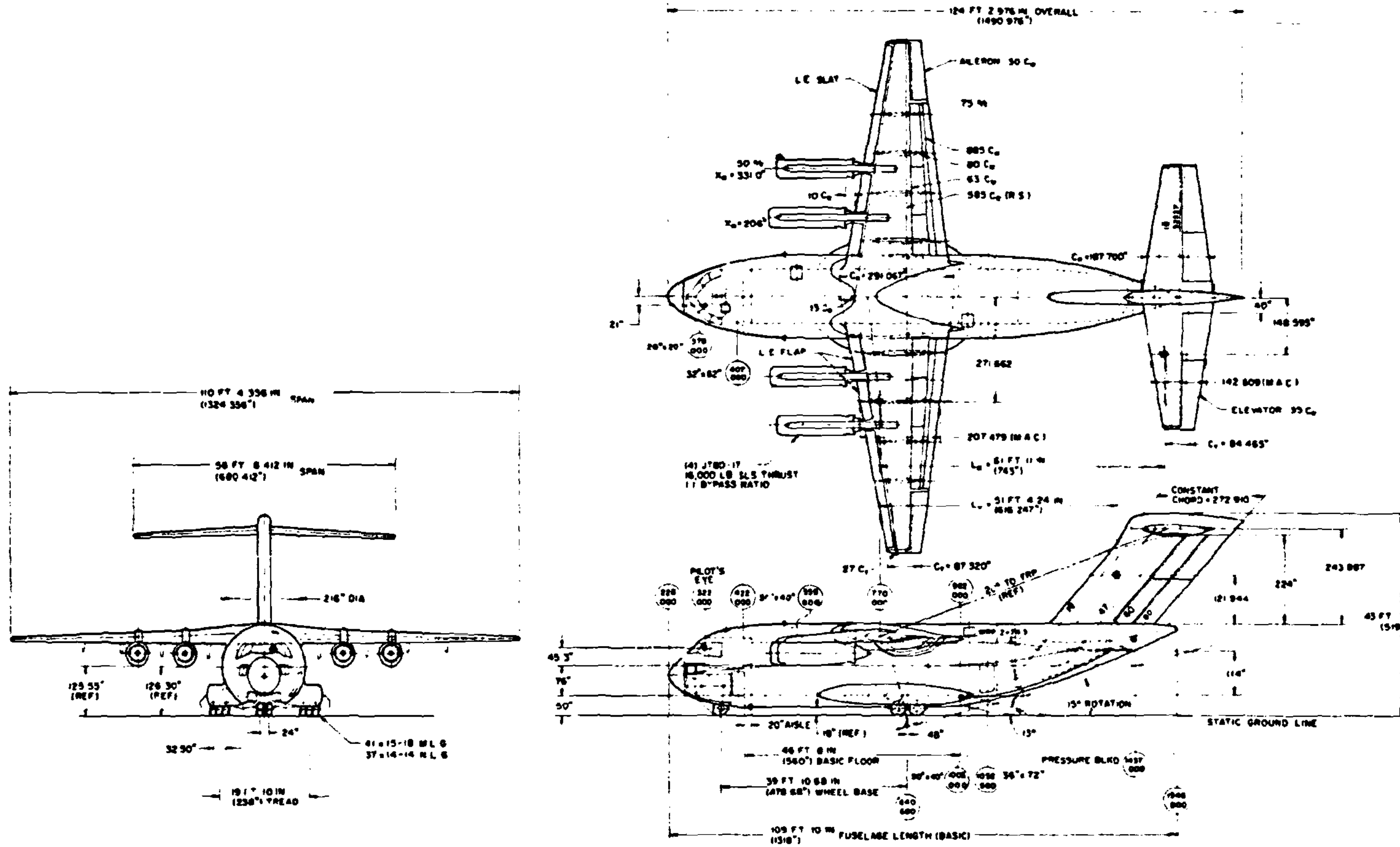

Figure 3   BASELINE AIRPLANE GENERAL ARRANGEMENT

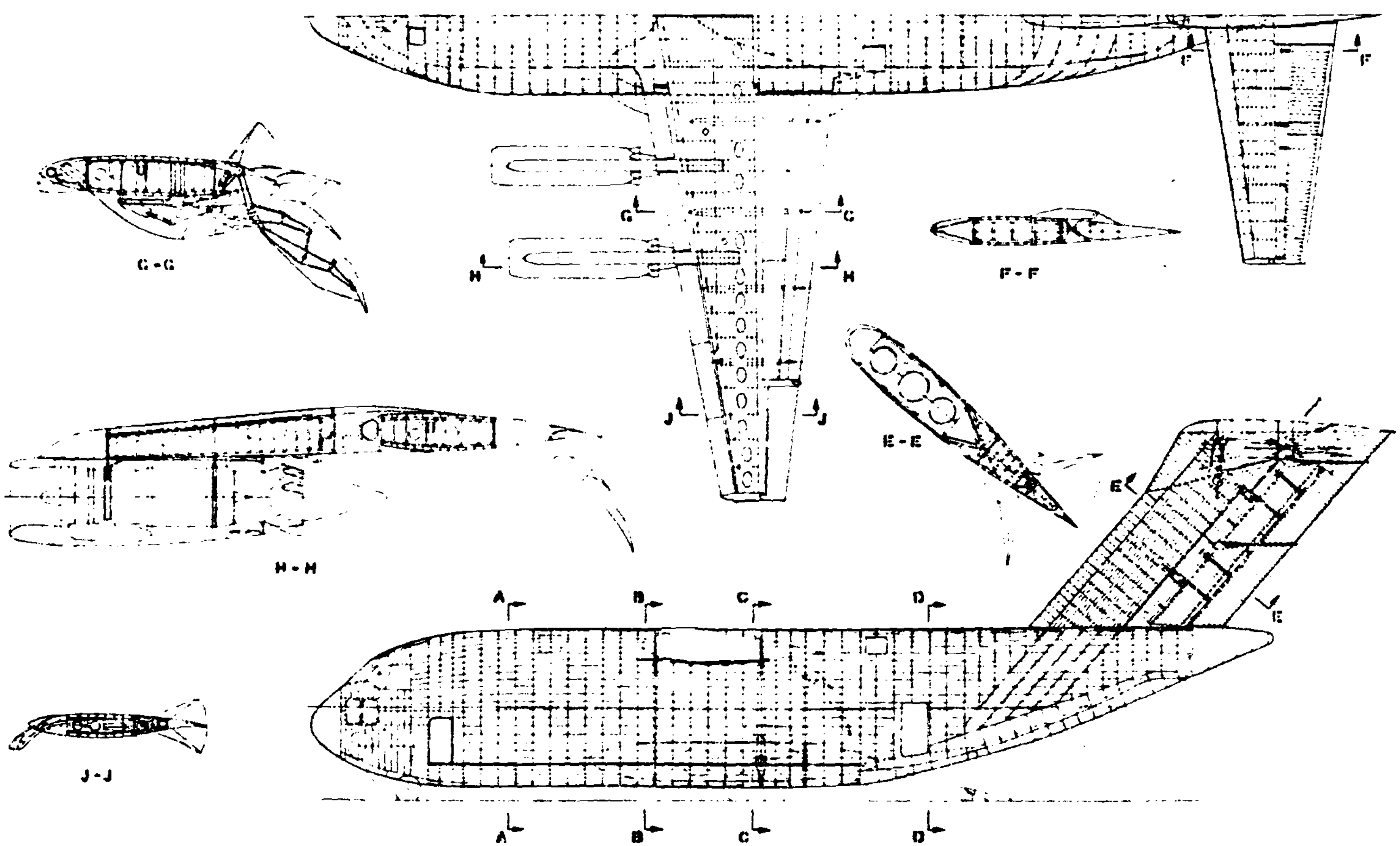

Figure 4 BASELINE AIRPLANE STRUCTURAL ARRANGEMENT (Sheet 1)

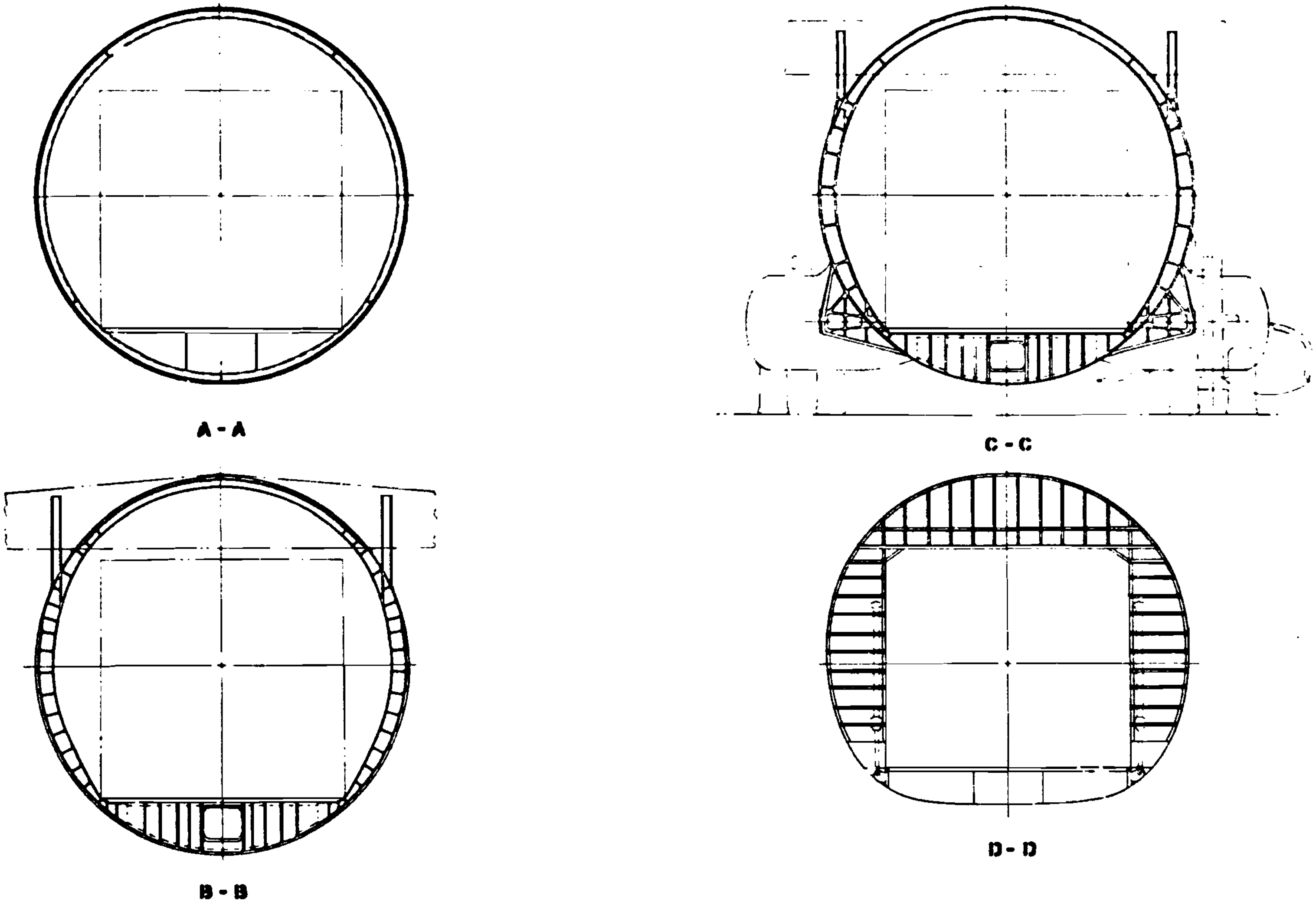

Figure 4 BASELINE AIRPLANE STRUCTURAL ARRANGEMENT (Concluded) (Sheet 2)

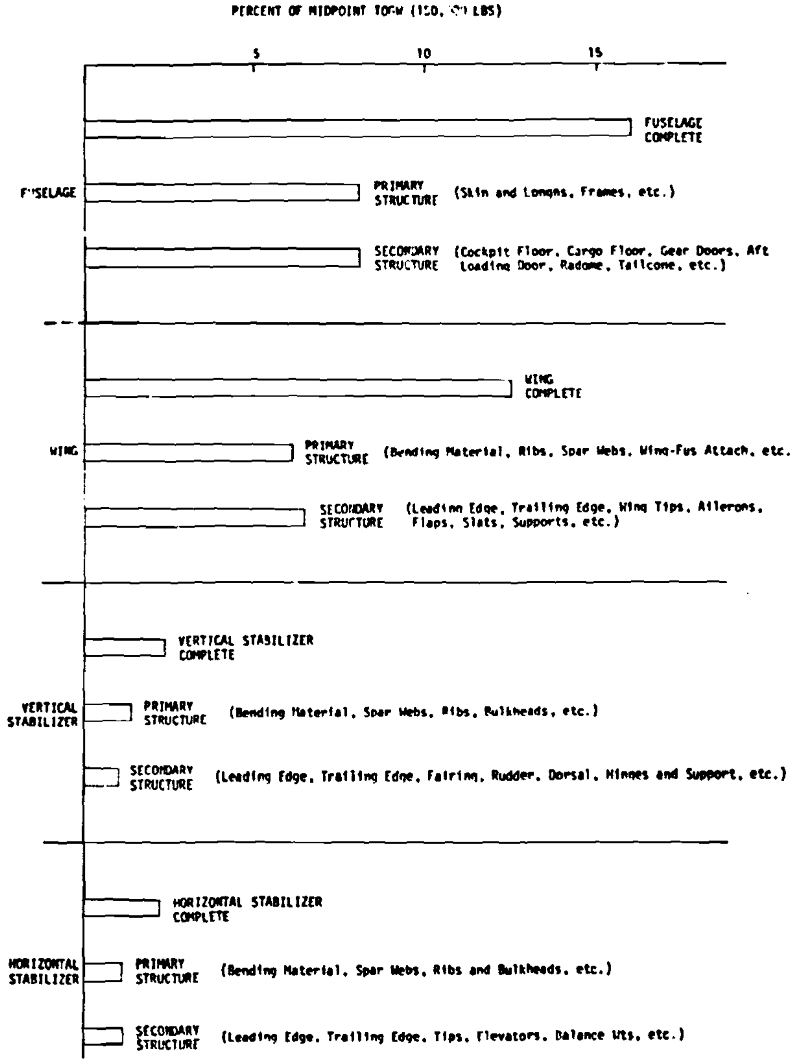

Figure 5 STRUCTURAL WEIGHT vs MIDPOINT STOL TOGW

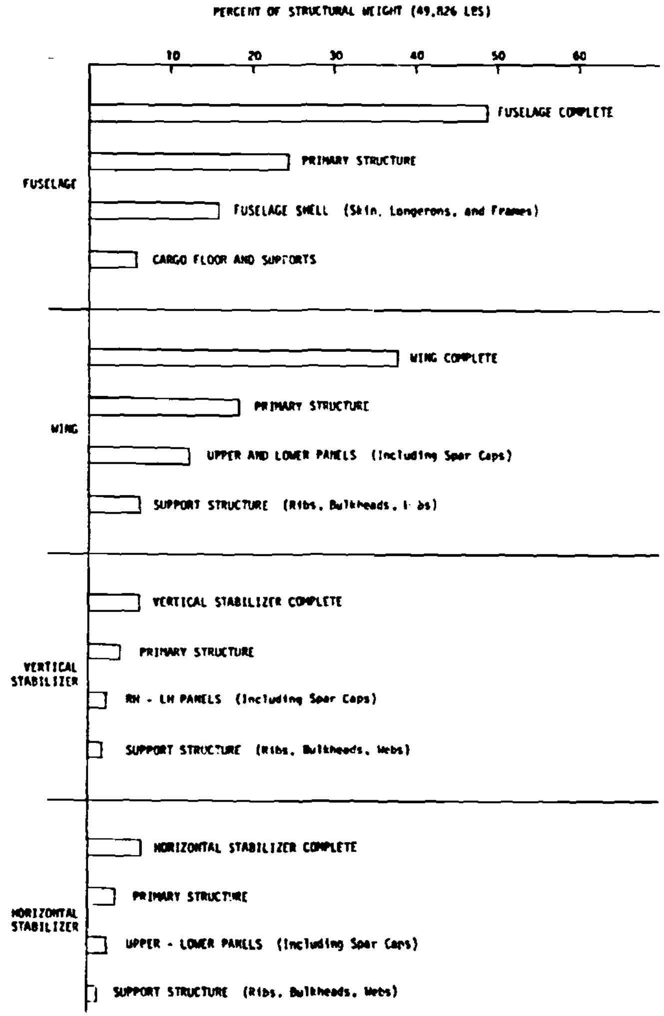

Figure 6 STRUCTURAL WEIGHT DISTRIBUTION

2.2 DESIGN CRITERIA

The design criteria define the requirements which the structural concepts must meet. The basis for the criteria used in this study is the MIL-A-008860A series (and related) Air Force specifications. The applicable general requirements of these specifications are interpreted and used to define the specific criteria for this STOL study baseline configuration. These criteria are identical to those defined for the production STOL aircraft. Pertinent criteria elements for ultimate strength, fatigue endurance, damage tolerance and rigidity are defined in the following subsections. These requirements are applicable to both the baseline and the advanced concept structure.

2.2.1 Ultimate Strength

General requirements and definitions for design gross weights and speeds are based on MIL-A-008860A. Flight, ground and miscellaneous loads are derived in accordance with MIL-A-008861A, MIL-A-008862A and MIL-A-008865A, respectively. In a limited number of instances, justifiable deviations are taken as summarized in Table II.

2.2.1.1 Design Weights - The baseline design weights in pounds, are as follows:

	CTOL	STOL
Maximum Design Gross Weight	198,420	-
Maximum Landing Design Weight	198,420	-
Basic Flight Design Gross Weight	150,000	150,000
Landplane Landing Design Gross Weight	177,285	150,000
Maximum Zero Fuel Gross Weight	160,150	134,150
Minimum Flying Weight	103,140	103,140
Jacking Weight: Gear	198,420	-
Fuselage	150,000	150,000
Maximum Design Payload	53,000	27,000
Maximum Design Fuel Weight @ 6.5 lbs/gal	77,715	46,850

The maximum and the basic flight design gross weights are used at altitude (i.e., no fuel burnoff) in establishing critical conditions and flight loads. The fuel schedule is established by the requirement that each engine be supplied from its associated individual tank. The center wing tank fuel is pumped to the other tanks as soon as volume is available.

The payload may be composed of vehicles and pallets. Design payload vehicle combinations are summarized in Table III.

2.2.1.2 Design Speeds - Design speeds for power on and leading and trailing edge devices retracted are summarized on Figure 7. The maximum level flight speed V_H = 350 KEAS (and M_H =0.76) is associated with cargo loads $\leq$ 27,000 lbs.

TABLE II LIST OF DEVIATIONS FOR AMST			
MILITARY SPECIFICATION	SUBJECT	DEVIATION	JUSTIFICATION
MIL-A-008860A Para. 6.2.2.8	V_{LF} Limit Flap Speed	(1) Landing, Approach, and Take-Off Limit Speed(V_{LF}) (a) Leading edge devices (wing and tail) extended: V_{LF} = 235 KEAS (b) Trailing edge devices extension: For Actuation - All systems working (3000 psi or less) 1g flight loads 65° power at all speeds No DLC 0° - 23° @ 200 KEAS 23° - 44° @ 150 KEAS 44° - 55° @ 100 KEAS For Holding - All systems working, @ 100% power and 2g for all flap angles, loads shall be limit. For Holding - One system out (engine and/or hydraulic) or single structural failure, loads shall be ultimate. 0 - 2.0g flight loads With DLC 100% power at all speeds and angles noted above. Hydraulic pressure not to exceed 7500 psi ultimate.	Limit flap speeds for powered lift aircraft should not be established in strict accordance with the criteria stated in MIL-A-008860A, paragraph 6.2.2.8 since these criteria would establish unrealistic design conditions (1) with respect to airplane operational attitudes and speeds. The design criteria selected for limit flap speeds in specific flight configurations are established to provide more than adequate speed and angle of attack margins for maneuver and stall protection within a realistic extreme flight envelope.
MIL-A-008860A Para. 6.2.2.8 (Continued)		For Holding - 55° flaps @ 100 KEAS @ 100% power, one system out - the resulting loads are ultimate. Add 10% to all flap extended loads for buffet considerations.	
MIL-A-008861A Para. 3.12	Positions of Adjustable Fixed Surfaces	The positions of the adjustable horizontal stabilizer fixed surface shall be limited to the extreme positions obtainable from a maximum of 3.0 seconds of trim motor operation.	This criteria has been successfully used for all DC-8 and DC-10 airplanes and is established using the recommended criteria set by FAA. (Reference FAA Special Conditions No. 25-18-WE-7).
MIL-A-008865A Para. 3.3	Crash Loads	The basic crash load factors shall be: All seats — 9g FWD* Cargo with no troops (Crew located above cargo) — 3g FWD for cargo Cargo with troops — 3g FWD for cargo; 9g FWD for net forward of cargo	As recommended in USAF report ASD-TR-73-17 (An appendix to USAF technical report AFFDL-TR-71-139) *Per FAA criteria for DC-10 seats.

(1) "Unrealistic design conditions" refers to the singular conservative flap speed that results from direct use of MIL-A-008860A criteria which must be considered with all flap and power settings and gross weights. For the AMST landing conditions, for example, this would result in flap speeds over twice those that are actually being used for design per the deviated criteria.

TABLE III VEHICLE PAYLOAD		
PAYLOAD COMBINATION	VEHICLES	WEIGHT (LB)
1	5 Ton Cargo Truck (M54A2) Without Winch Ammunition Trailer 2 Jeeps (M38 Truck)	44,000
2	5 Ton Cargo Truck (M54A2) With Winch Towed 155MM Howitzer	44,300
3	155 SP Howitzer (M109A1)	53,060
4	5 Ton Medium Wrecker (M543A2) Command Recon. Carrier (M114A1)	51,000
5	2.5 Ton Maintenance Van 1.5 Ton Trailer	27,000

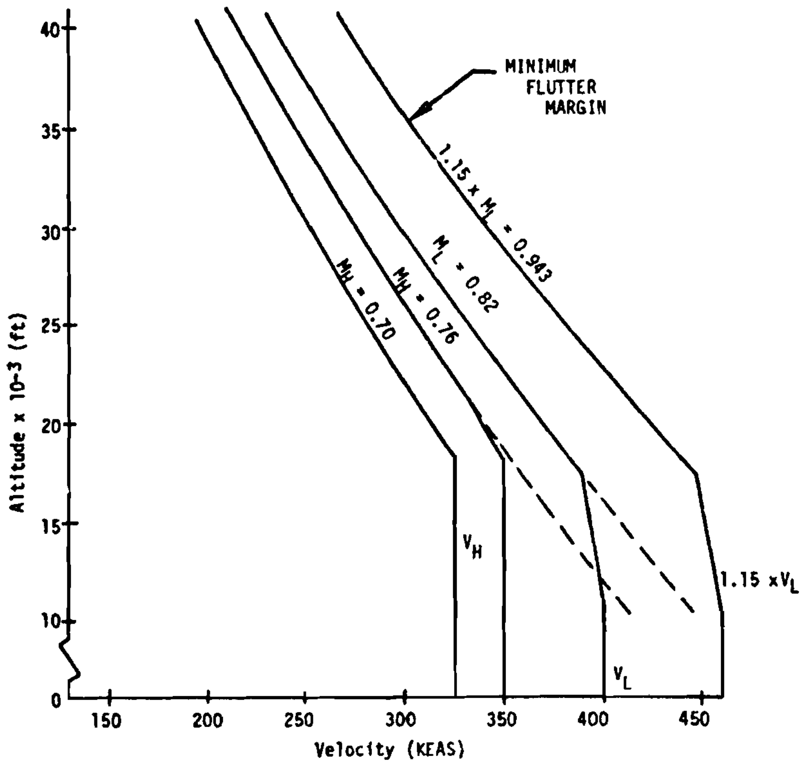

Figure 7 AMST DESIGN SPEEDS

and V_H = 325 KEAS (and M_H =0.70) with cargo loads $\geq$ 27,000 lbs. Design speeds for power on and off and flaps down are summarized as follows: V_{LF} = 100 KEAS is associated with landing flap settings ($44° \leq \delta_F \leq 55°$), 150 KEAS with approach settings ($23° \leq \delta_F \leq 44°$), 200 KEAS with takeoff settings ($\delta_F = 23°$) and 235 KEAS for leading edge devices only extended.

2.2.1.3 Load Factors - The STOL airplane is designed for maneuver and gust conditions. This is illustrated by V-n diagrams for representative cruise configuration flight conditions and gross weights (Figure 8). Maximum maneuver load factor limits (for high life devices retracted) are +3.0/-1.00 and +2.25/0 for basic flight and maximum design gross weights, respectively. The maximum limits are +2.0 and 0 (Figure 9) for high lift devices extended. A load factor of +2.00 is applicable at all gross weights for ground taxi conditions. Load factors associated with the following design limit sink speeds (fps) are applicable for landing conditions.

	CTOL	STOL
Maximum Landing Design Weight (198,420 lbs.)	6.0	0
Landplane Landing Design Weights (177,285 lbs.)	10.0	16

2.2.1.4 Factors-of-Safety - The structure is required to sustain without yielding the applied limit loads and without failing the applied ultimate loads. Ultimate loads are limit loads times the factor-of-safety, 1.5.

2.2.1.5 Center of Gravity Limits - The center of gravity envelope for design is that shown in Figure 10.

2.2.2 Fatigue

"Safe-life" design is employed as the primary means of satisfying the service life requirements for primary structure. The general fatigue requirements of MIL-A-008866A are used as a basis. These general requirements are further supplemented by specific service life, usage and spectra requirements for the STOL aircraft. Service requirements for the STOL aircraft are based on projected utilization and are as follows:

Flight Service Life (hours)	15,000
Number of Missions	7,392
Total Number of Landings	23,755
Number of "Full Stop" Landings	15,586
Number of "Touch and Go" Landings	8,169
Number of Fuselage Pressurizations	12,431

A scatter factor of 4 is applicable to the service life requirements to establish the design life requirements. USAF projected utilization in the form of representative mission profiles is shown in Figure 11. Five missions are identified to represent basic employment, an alternate employment, deployment, low altitude resupply and training usages. Individual mission

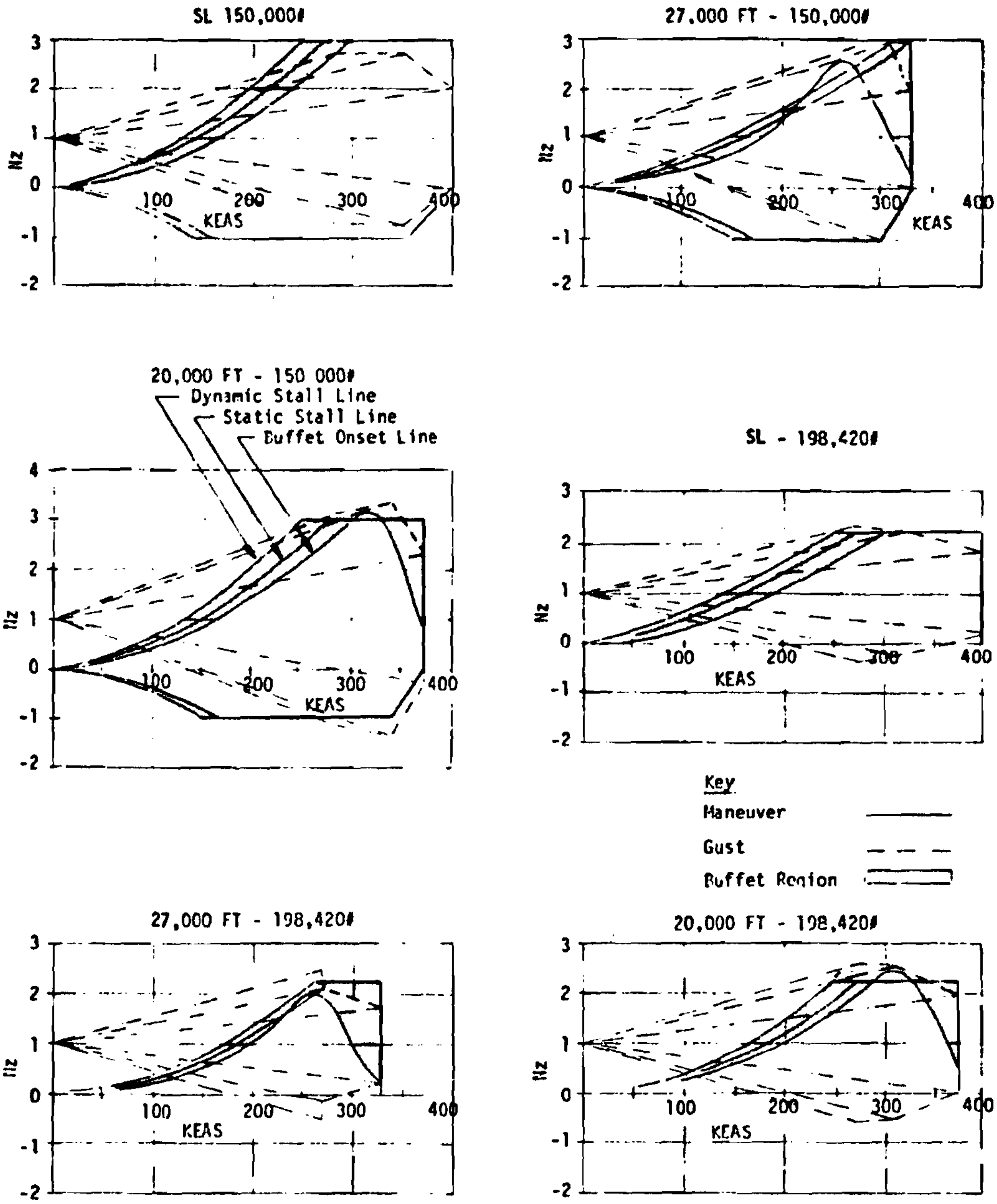

Figure 8 V-n DIAGRAMS (CRUISE CONFIGURATION)

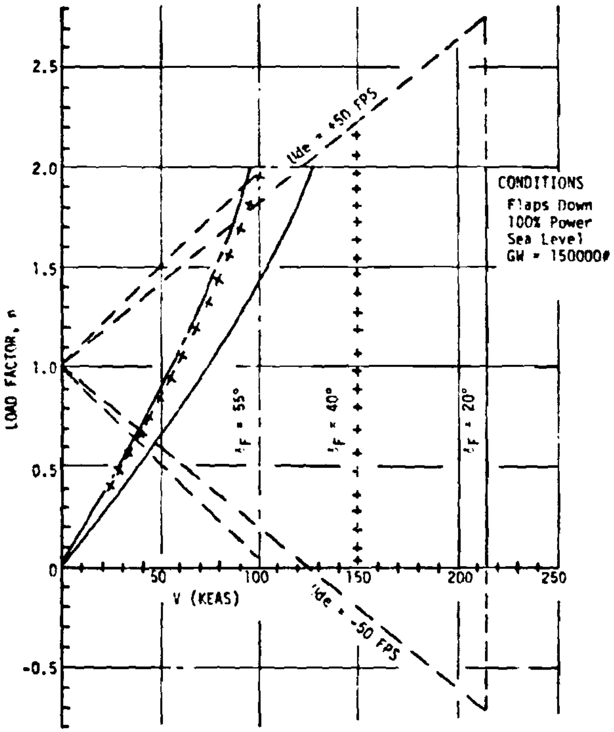

Figure 9 V-n DIAGRAM (HIGH LIFT)

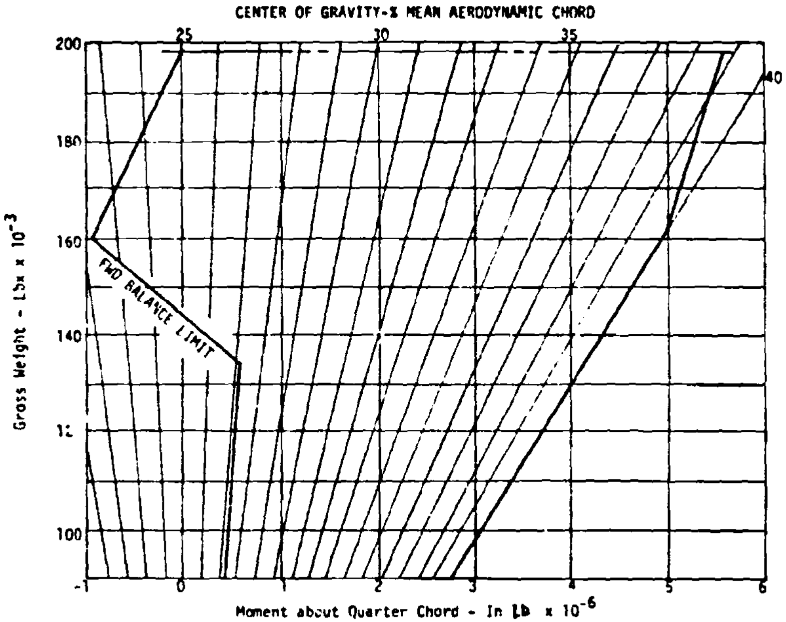

Figure 10 CENTER OF GRAVITY LIMITS

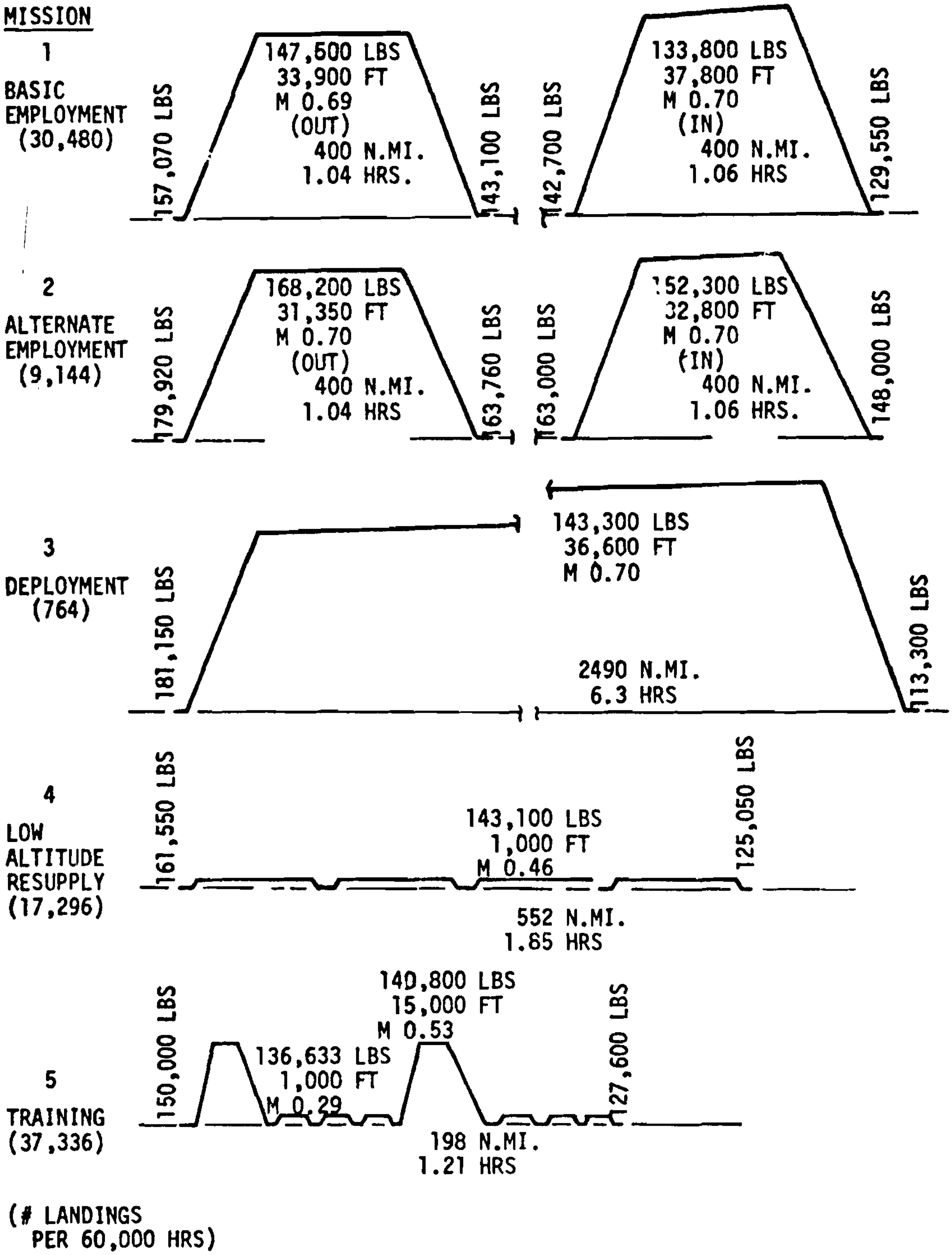

Figure 11 MEDIUM STOL TRANSPORT MISSION PROFILES

general characteristics and utilization are further defined and summarized in Table IV. No fuselage pressurizations are associated with flight segments of 1000 foot altitude or less.

Basic C.G. load factor spectra data from MIL-A-008866A are used for flight and ground conditions. Maneuver and gust spectra data are considered for flight conditions; taxi and landing impact data for ground conditions. The basic MIL-A-008866A spectra data are modified for STOL usage where required. For example, ground taxi operations on paved fields (CTOL) and on semi-prepared fields (STOL) are considered. For CTOL operations, the data of MIL-A-008866A are used directly. For STOL operations, the given data are increased in severity to reflect the rougher field conditions. Further definition of the STOL airplane C.G. load factor spectra data is presented in Section 2.3.2.

Ground-Air-Ground (GAG) cycles are considered as part of the fatigue loads spectrum. A GAG cycle is defined by the maximum flight and maximum ground loads which occur during one flight, as illustrated below. One flight is associated with each landing.

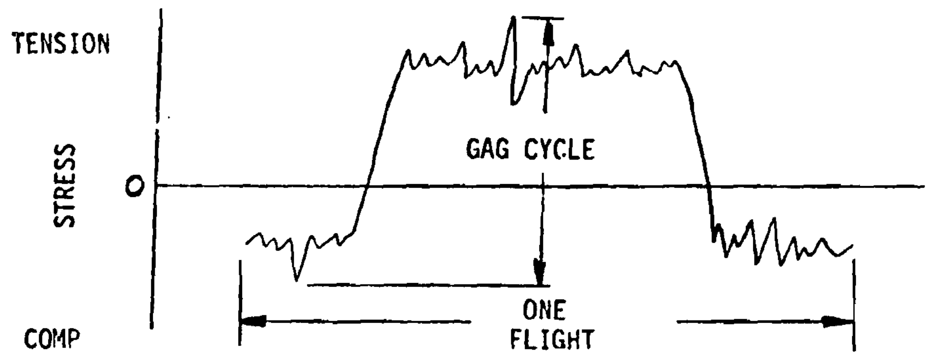

2.2.3 Damage Tolerance

Primary structure vital to the integrity of the aircraft or the safety of personnel is required to be damage tolerant as a backup to the safe life requirements. Damage tolerance requirements with respect to degree of inspectability, frequency of inspection, minimum period of unrepaired service usage, minimum required residual strength, minimum initial and in-service damage sizes and damage growth limits shall be as defined in Appendix A. The minimum residual strength requirement is based on the fatigue load spectra. The frequency of inspection associated with the inspection plan elements is as follows:

Inspection Plan Element	Inspection Interval (Hours)
Walk Around Visual	25
Special Visual	1,000
Depot or Base Level	3,750

2.2.4 Rigidity

The structure is required to meet the MIL-A-008870 specified minimum flutter speed of 1.15 V_L (see Figure 7).

2.3 DESIGN LOADS AND RIGIDITIES

The design loads and rigidities are determined in accordance with the design criteria, Section 2.2, and are summarized in the following subsections. Ultimate, fatigue, damage tolerance and flutter mode data used to design and screen the structural concepts are presented. Information is provided as to the critical conditions, external and internal loads and load spectra. More detailed loads data are given in Reference 1.

2.3.1 Ultimate Mode

The critical conditions and loads for the baseline wing, fuselage and empennage are those of the YC-15 prototype STOL aircraft. The loads presented include the external and internal loads from flight and ground conditions.

The internal loads for the baseline structure were derived from the external loads using FORMAT (References 2 through 4), a generalized energy analysis method. The structure was represented by bar and panel elements and the resulting matrix equations were solved by computer to obtain bar loads (axial, shear and moment) and panel shear flow loads. The structural idealization of the center fuselage shown in Figure 12 is typical of the sophistication used in defining the structure for loads analysis. The FORMAT analysis technique has been verified by full-scale proof load tests of the DC-10 and other aircraft and its use provides an accurate detailed distribution of loads for the study, including regions of redistribution such as at doors or the wing-fuselage intersection. These loads, sufficient to design flight structure, serve as a more accurate basis for developing structural concepts than the preliminary design loads normally available for parametric studies.

2.3.1.1 Wing Loads - The critical conditions for the wing control stations (91.25, 214.0, 372.275, and 508.436) are given in Table V. These conditions were identified from critical internal loads and margins of safety at the four stations based on 24 external flight load conditions (symmetric and unsymmetric) and on 7 external ground load conditions (including landing, taxiing and braking). The resulting critical external load envelopes for wing shear, moment and torque are shown in Figure 13.

Envelopes of internal loads for the wing cover panels, spars, ribs and bulkheads have been generated for the control stations and are presented in Reference 1. (NOTE: In addition to the loads from flight and ground conditions,

NO.	MISSION DESCRIPTION	MISSION LENGTH		LANDINGS PER MISSION		HOURS PER LANDING	SERVICE LIFE: FLIGHT HOURS	% OF TOTAL FLT. HRS.	LANDINGS: STOL	CTOL	TOTAL	% TOTAL	NO. OF MISSIONS	L.F.
1	BASIC EMPLOYMENT 400 N.Mi. Radius (157,070/36,420/17,500)(2)	2.1	800	1	1	1.05	8,000	53.5	3,810	3,810	7,620	32.1	3,810	3.0 @ Mid-Point
2	ALT. EMPLOYMENT 400 N.Mi. Radius (179,920/42,270/34,500)(2)	2.1	800	1	1	1.05	2,400	16	1,143	1,143	2,286	9.6	1,143	2.25
3	DEPLOYMENT (181,150/78,000/0)(2)	6.3	2,490	0	1	6.3	1,200	8	0	191	191	.8	191	2.5
4	LOW ALT. RESUPPLY (3) 270 N.Mi. Radius (161,550/41,000/17,400)(2)	1.85	552	3	1	.463	2,000	13.2	3,243	1,081	4,324	18.2	1,081	3.0
5	TRAINING High & Low Alt. (150,000/46,850/0)(2)	1.2	198	4	4	.15	1,400	9.3	4,667	4,667	9,334	39.3	1,167	3.0
1-5							15,000		12,863	10,892	23,755		7,392	

Caption: TABLE IV ADVANCED STOL TRANSPORT (MEDIUM) PROJECTED UTILIZATION (1)

(1) Required Service Life = 15,000 flight hours
= 15,586 "Full Stop" + 8,169 "Touch and Go" Landings

(2) Ramp Weights (Gross/Fuel/Payload)

(3) V_{L_L} = 300 KEAS @ 1000 feet

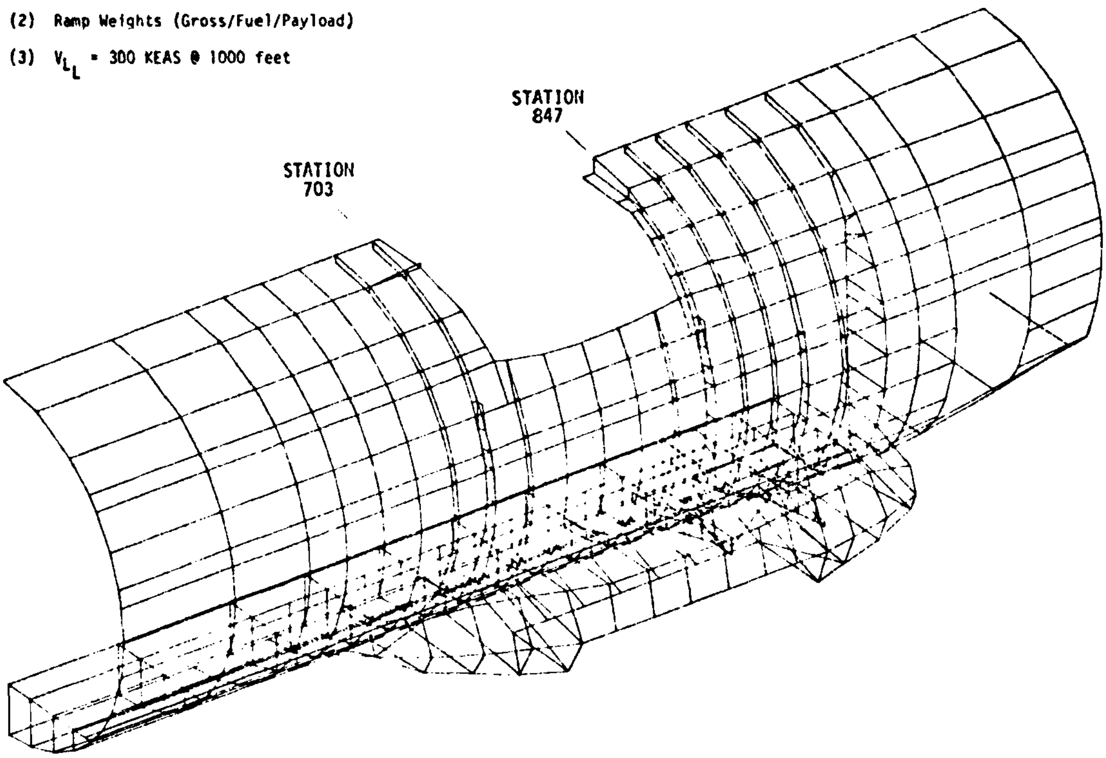

Figure 12 YC-15 CENTER FUSELAGE STRUCTURAL IDEALIZATION USED IN FORMAT ANALYSIS

TABLE V WING CRITICAL CONDITION SUMMARY											
TYPE	DESCRIPTION	CONDITION NUMBER	GROSS WT. (#)	ALT. (ft)	SPEED		LOAD FACTOR			ANGLE OF ATTACK	
					XEAS	MACH NO.	NX	NY	NZ	α°	β°
MANEUVER	Steady Pitch Maneuver - Cruise Configuration	1	150000	12400	396.7	0.758	.043	0	3.0	1.2	0
	Steady Pitch Maneuver - Speed Brake Configuration	2	150000	12400	396.7	0.758	.065	0	3.0	5.2	0
	Steady Pitch Maneuver - Cruise Configuration	3	150000	39000	155.3	0.533	-.105	0	-1.0	-1477	0
	Steady Pitch Maneuver - 40° Flaps Down Configuration	4	160150	SL	150	0.226	.033	0	2.0	3.6	0
LDG.	Dynamic Landing, 16 fps (.29 sec)	5	15000	SL	87	0.131	--	--	2.615	0.7	--

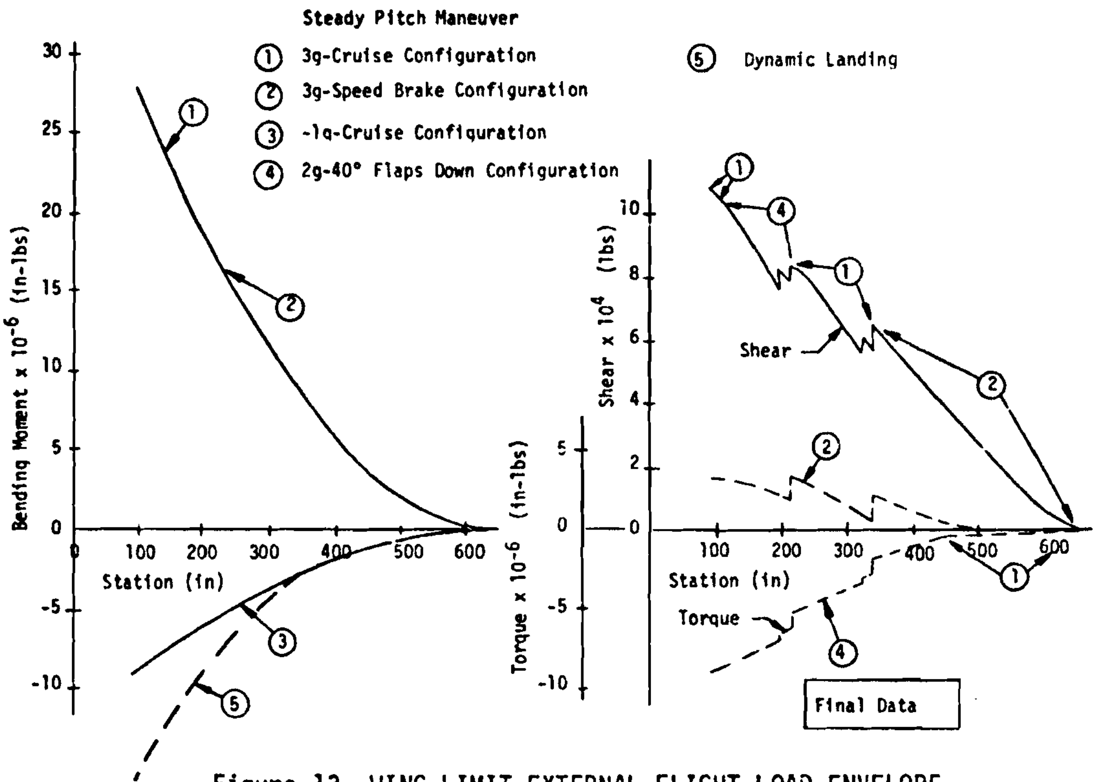

Figure 13 WING LIMIT EXTERNAL FLIGHT LOAD ENVELOPE

fuel pressure, aerodynamic pressure and crushing loads are also presented in Reference 1.) A summary of maximum load levels for the cover panels at the control stations are summarized in Figure 14. Wing upper and lower cover loadings are equal to or less than 14,000 #/in. compression and 12,400 #/in. tension. The wing cover panel shear flows are equal to or less than 4,600 #/in. Individual critical load curves which fall within the load envelopes were generated for use in design. These are also summarized in Reference 1.

2.3.1.2 Fuselage Loads - The critical conditions for the four fuselage control stations (439, 703, 847 and 982) are summarized in Table VI. These conditions were identified from YC-15 critical internal loads and margins of safety. The corresponding external load envelopes are shown in Figures 15 through 18 for vertical and lateral shear, moment and torque loads. Loads are derived from both symmetric and unsymmetric flight and ground conditions. Only flexible body landing conditions were run, i.e., no rigid body solutions.

Internal loads for the fuselage cover structure, frames and floor, at the control stations, are given in Reference 1. Maximum values of the cover structure loads are summarized in Figure 14. The maximum load levels occur at Station 847, varying from a maximum tension load of 3770 #/in. in the wing-fuselage intersection area to a maximum compression load of 3850 #/in. in the gear-fuselage intersection area and with 2470 #/in. compression load at the floor line. The panel shear flow maximum value is 2820 #/in. Individual critical load curves which fall within the load envelopes were generated for use in design.

2.3.1.3 Empennage Loads - The critical conditions for the empennage are summarized in Table VII. The associated normal and in-plane external load envelopes for the vertical stabilizer are summarized in Figures 19 and 20, respectively.

The external load envelopes for the horizontal stabilizer are presented in Figure 21.

Internal load envelopes for the cover panels, spars, ribs and bulkheads at the vertical and horizontal stabilizer control stations are presented in Reference 1. The representative envelope values for empennage cover structure are summarized in Figure 22. The left and right vertical stabilizer cover loadings are equal to or less than 4,200 #/in. compression and 4,500 #/in. tension. The cover panel maximum shear flow is 2,950 #/in. The upper and lower horizontal cover loadings are equal to or less than 9,000 #/in. compression and 10,280 #/in. tension except at the pivot (where 25,000 #/in. compression and 23,000 #/in. tension are the maximum values). The maximum cover panel shear flow is 5,170 #/in. Individual critical load curves which fall within the load envelopes were generated for use in design.

2.3.2 Fatigue and Damage Tolerance Load Factor Spectra

Load spectra are based on the five basic mission profiles defined in the design criteria (Figure 11). Included are taxi, gust, landing impact, and low level gust plus maneuver. The derivation is described in Reference 1.

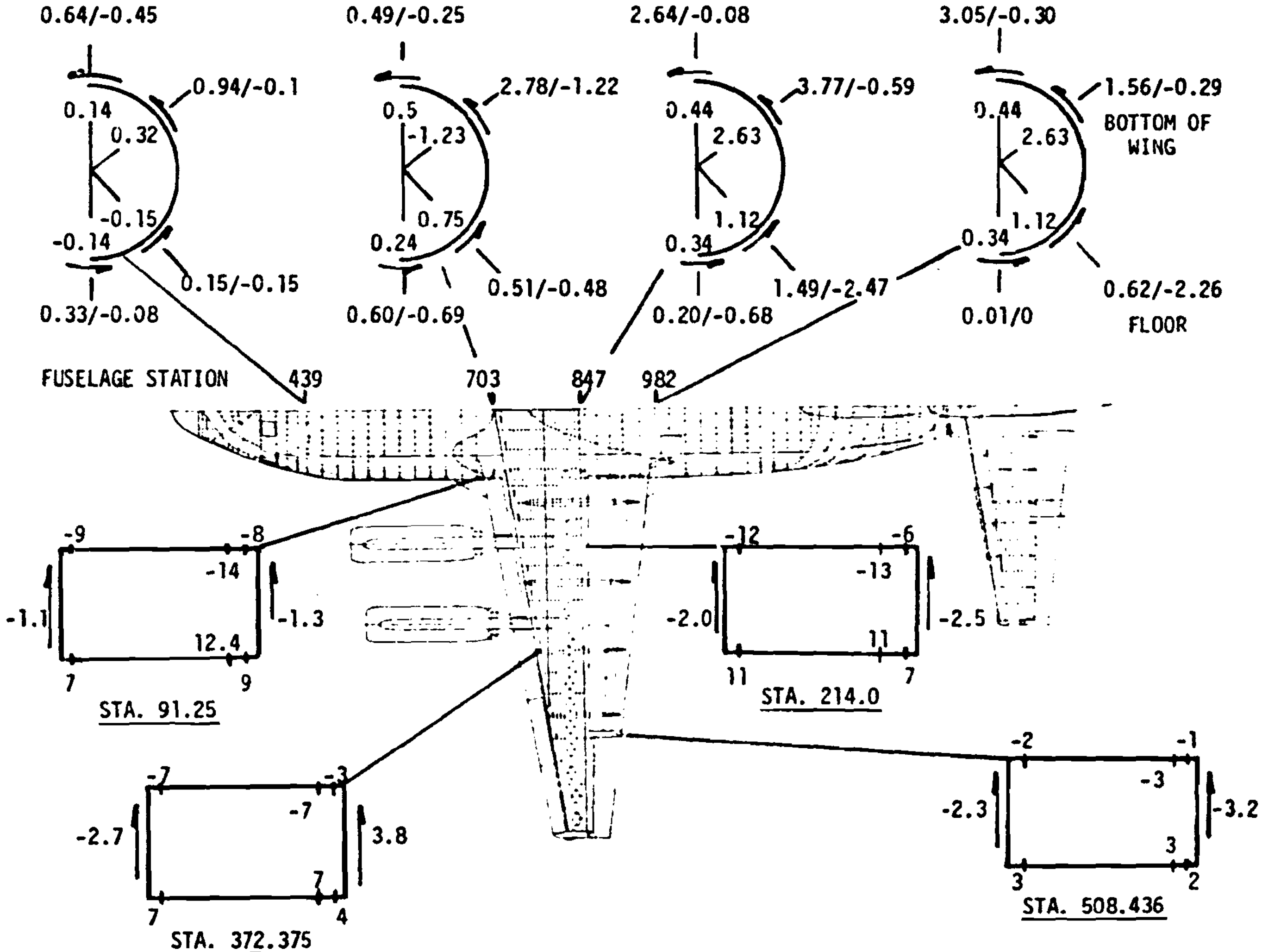

Figure 14 WING AND FUSELAGE ULTIMATE ENVELOPE LOADING AT CONTROL STATIONS

TABLE VI FUSELAGE CRITICAL CONDITION SUMMARY

DESCRIPTION	CONDITION NUMBER	GROSS WT. (#)	ALT (FT)	SPEED		LOAD FACTOR (1)			ANGLE OF ATTACK (DEGREE)	
				KEAS	MACH NO.	NX	NY	NZ	α	β
Nose Gear Tow	1	198,504	SL	--	--	-.15	0	1.0	--	--
Nose Gear Taxi	2	198,506	SL	--	--	.44	0	1.117	--	--
1g Balanced Maneuver	3	134,150	27,000	302	.783	0	0	±1.0	.77	0
VG Gust	4	198,506	20,000	270	.602	0	0	2.387	7.32	0
1g Balanced Maneuver with Mistrim	5	150,000	30,000	250	.694	0	0	-1.0	-2.64	0
3g Balanced Maneuver with Mistrim	6	150,000	17,200	389.7	.82	0	0	3.0	2.24	0
First Peak Pull Up	7	150,000	SL	214	.32	0	0	1.026	-2.74	0
2 Point 3.8° Tail Down Landing (2)	8	150,000	SL	--	--	1.543	0	3.33	--	--
2 Point 3.8° Tail Down Landing (2)	9	134,200	SL	--	--	-1.13	0	varies	--	--
3 Point Level Landing (2)	10	150,086	SL	--	--	varies	varies	varies	--	--
3g Balanced Maneuver	11	134,150	14,700	400	.80	0	0	3.0	.55	0
Taxi/Takeoff Run	12	198,500	SL	--	--	0	0	2.0	--	--
Second Peak Pull Up	13	150,000	20,000	240	.53	0	0	3.0	7.91	0
Second Peak Push Over	14	198,506	SL	214	.32	0	0	0	-7.94	0
2 Point Level Landing (2)	15	150,000	SL	--	--	1.71	0	3.33	--	--
2 Point 3.8° Tail Down Landing (2)	16	134,000	SL	--	--	varies	varies	varies	--	--
V_{LF} Gust	17	160,150	SL	214	.32	0	0	2.393	4.12	0
Lateral Gust	18	134,150	18,000	350	.75	.213	-.57	1.0	- .44	4.84
Left Turn with Symmetrical Braking	19	198,506	SL	--	--	.461	.052	1.389	--	--
STOL Drift Landing	20	150,000	SL	--	--	0	.665	1.95	--	--
Right Turn (0.5g)	21	198,504	SL			0	.5	1.0		
Uncoordinated Roll	22	103,000	17,200	390	.82	0	±.985	1.0	-1.21	4.64
Lateral Gust	23	103,140	20,000	270	.60	0	-.744	1.0	- .02	8.24
Engine Failure	24	198,506	SL	200	.302	-.022	.366	1.0	6.38	-11.31

(1) Limit
(2) Varies with Time

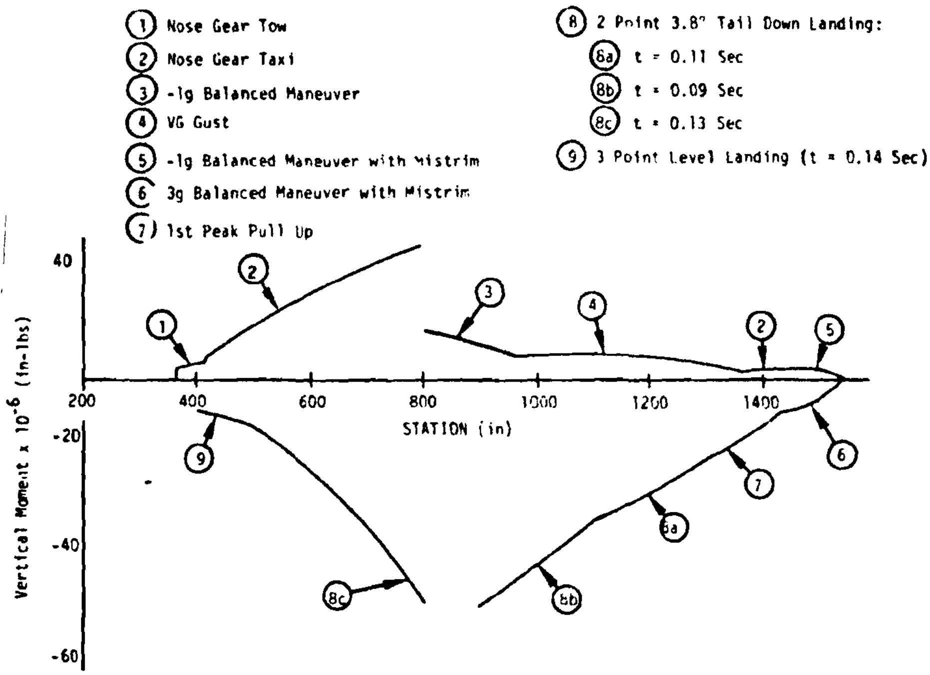

Figure 15 FUSELAGE LIMIT VERTICAL MOMENT ENVELOPE

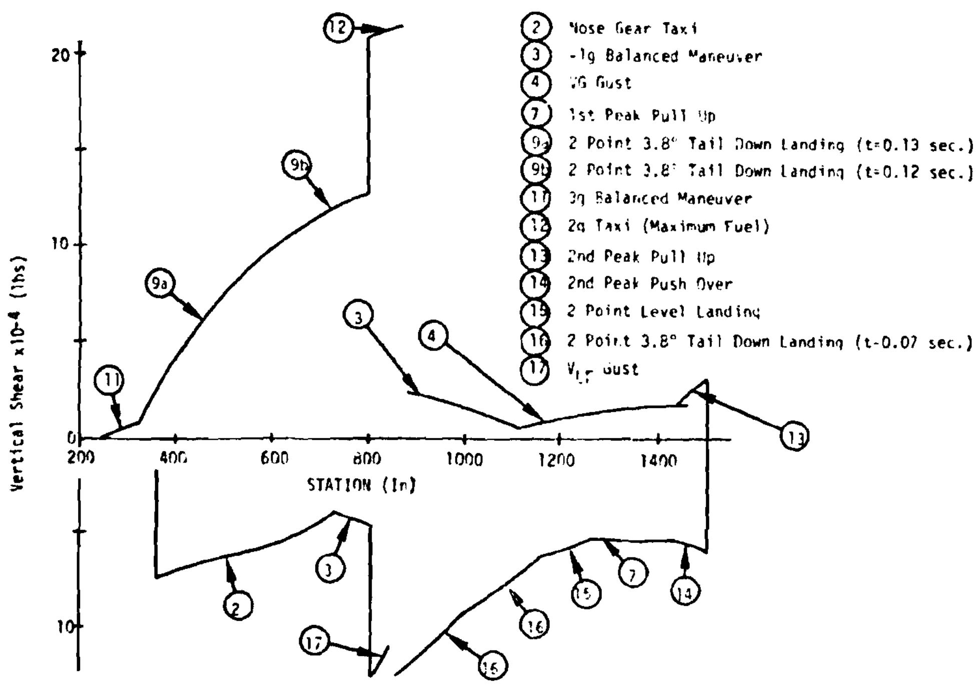

Figure 16 FUSELAGE LIMIT VERTICAL SHEAR ENVELOPE

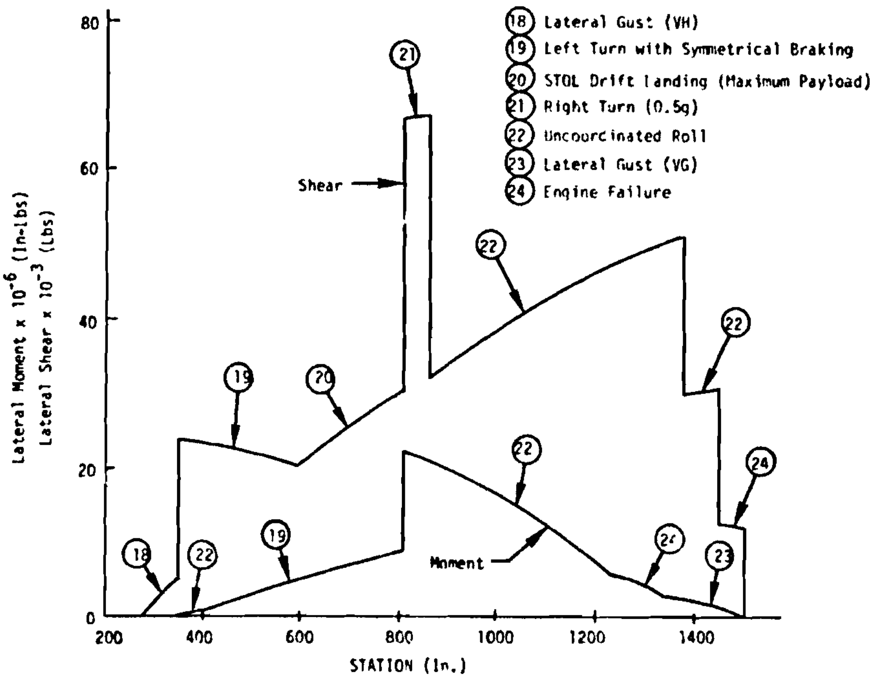

Figure 17 FUSELAGE LIMIT LATERAL MOMENT AND SHEAR ENVELOPE

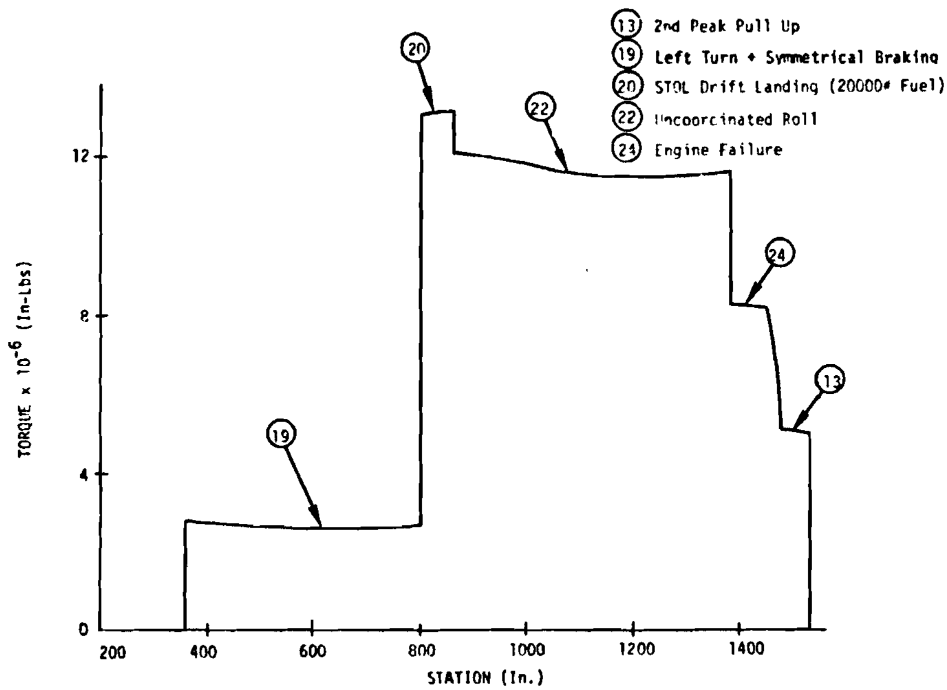

Figure 18 FUSELAGE LIMIT TORQUE ENVELOPE

TABLE VII EMPENNAGE CRITICAL CONDITION SUMMARY

TYPE	DESCRIPTION	CONDITION NUMBERS	GROSS WT. (#)	ALT. (ft)	SPEED KEAS	SPEED MACH NO.	LOAD FACTOR NX	LOAD FACTOR NY	LOAD FACTOR NZ	ANGLE OF ATTACK α	ANGLE OF ATTACK β
Roll	Uncoordinated Roll With Yaw Dampers	1	103000	17200	390	0.82	--	0.985	1.0	-1.21	-4.64
Side-Slip	Steady Sideslip With Rudders Neutralized	2	142582	S.L.	150	0.22	--	-0.745	1.0	8.5	30.0
Push Over	2nd Peak Abrupt Push Over	3	198506	S.L.	200	0.3	--	0	0	-7.24	0
Pull Up	2nd Peak Abrupt Pull Up	4	150000	20000	240	0.53	--	0	3.0	7.91	0
	1st Peak Abrupt Pull Up	5	150000	17200	390	0.82	--	0	1.46	0.01	0
Mis-trim	Nose Up Mistrim	6	150000	18000	350	0.75	--	0	3.0	2.81	0
	Nose Down Mistrim	7	150000	18000	350	0.75	--	0	-1.0	-3.39	0
Gust	Discrete Lateral Gust	8	198506	20000	270	0.6	--	-0.385	1.0	1.95	8.24

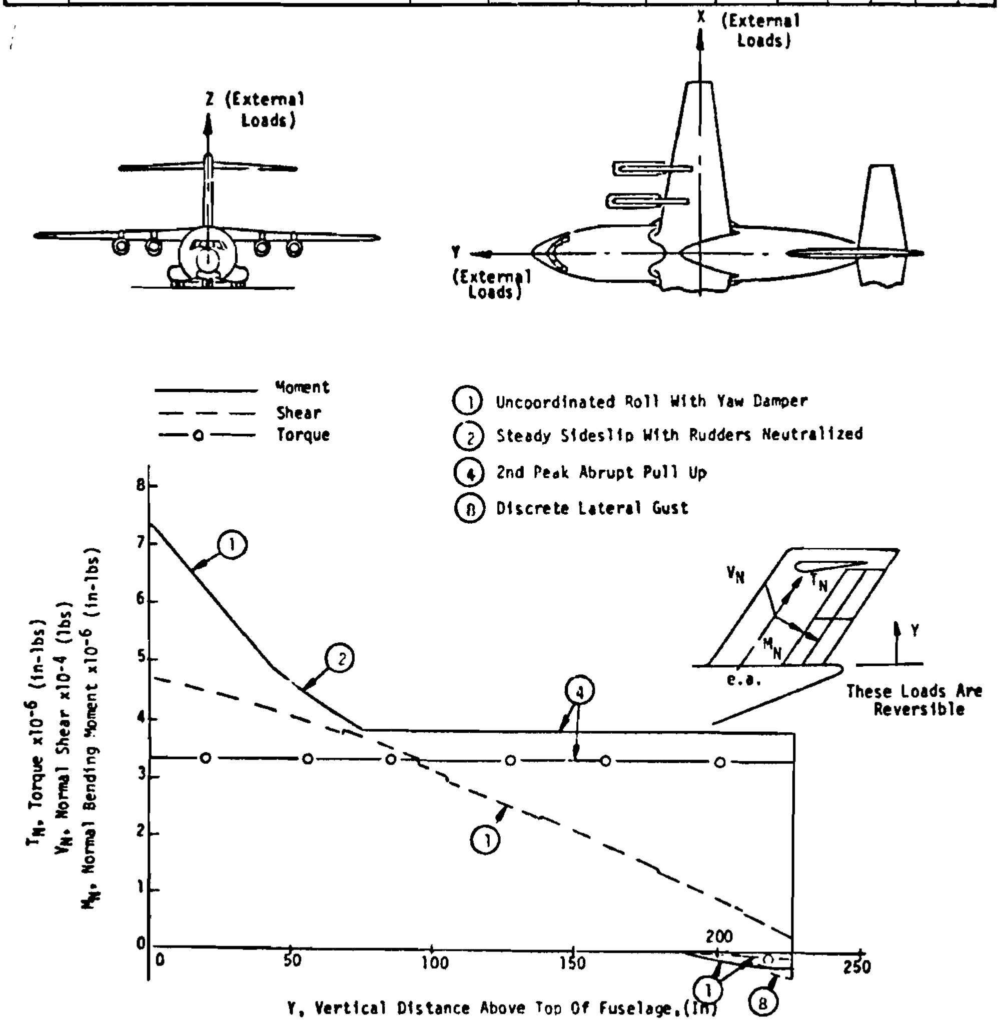

Figure 19 VERTICAL STABILIZER LIMIT NORMAL LOAD ENVELOPE

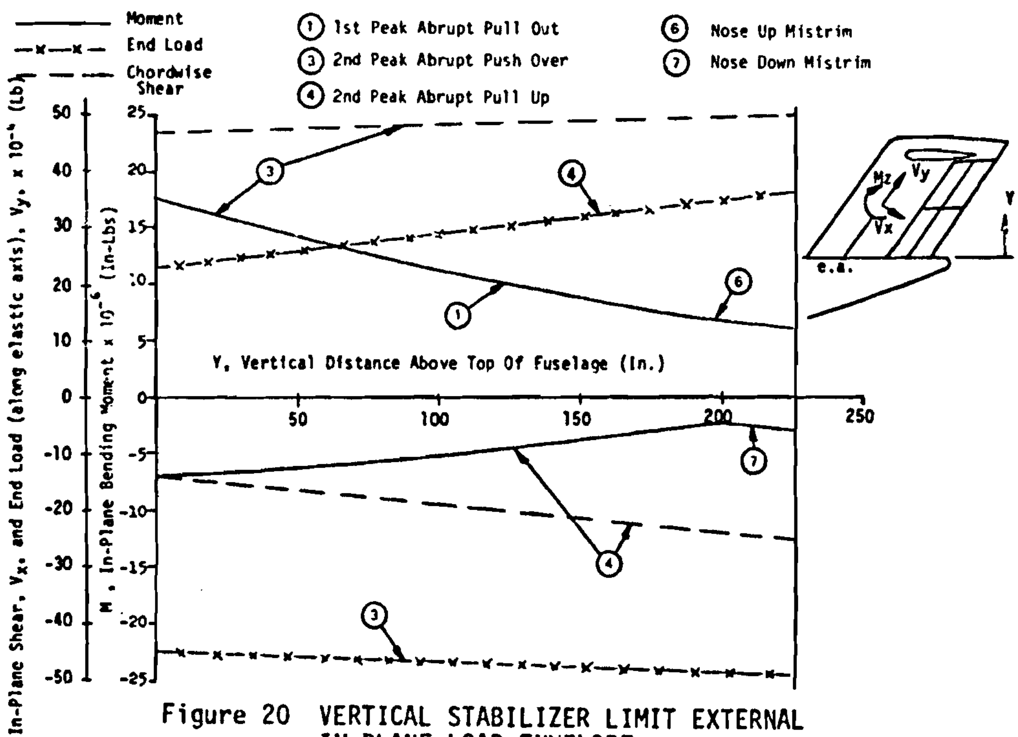

Figure 20 VERTICAL STABILIZER LIMIT EXTERNAL IN-PLANE LOAD ENVELOPE

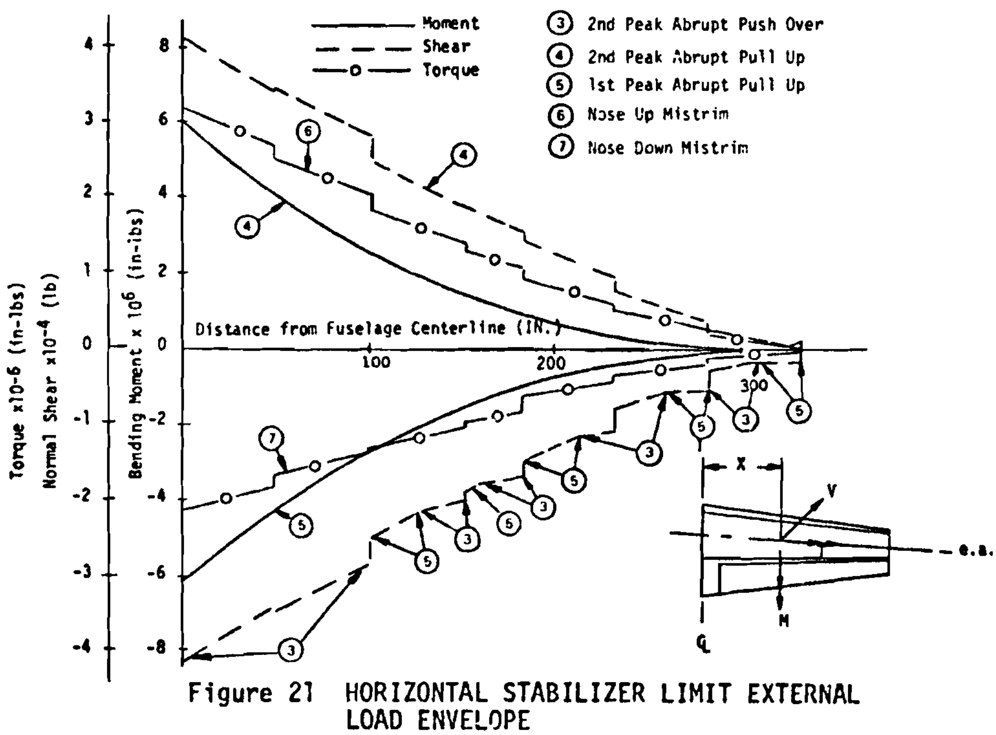

Figure 21 HORIZONTAL STABILIZER LIMIT EXTERNAL LOAD ENVELOPE

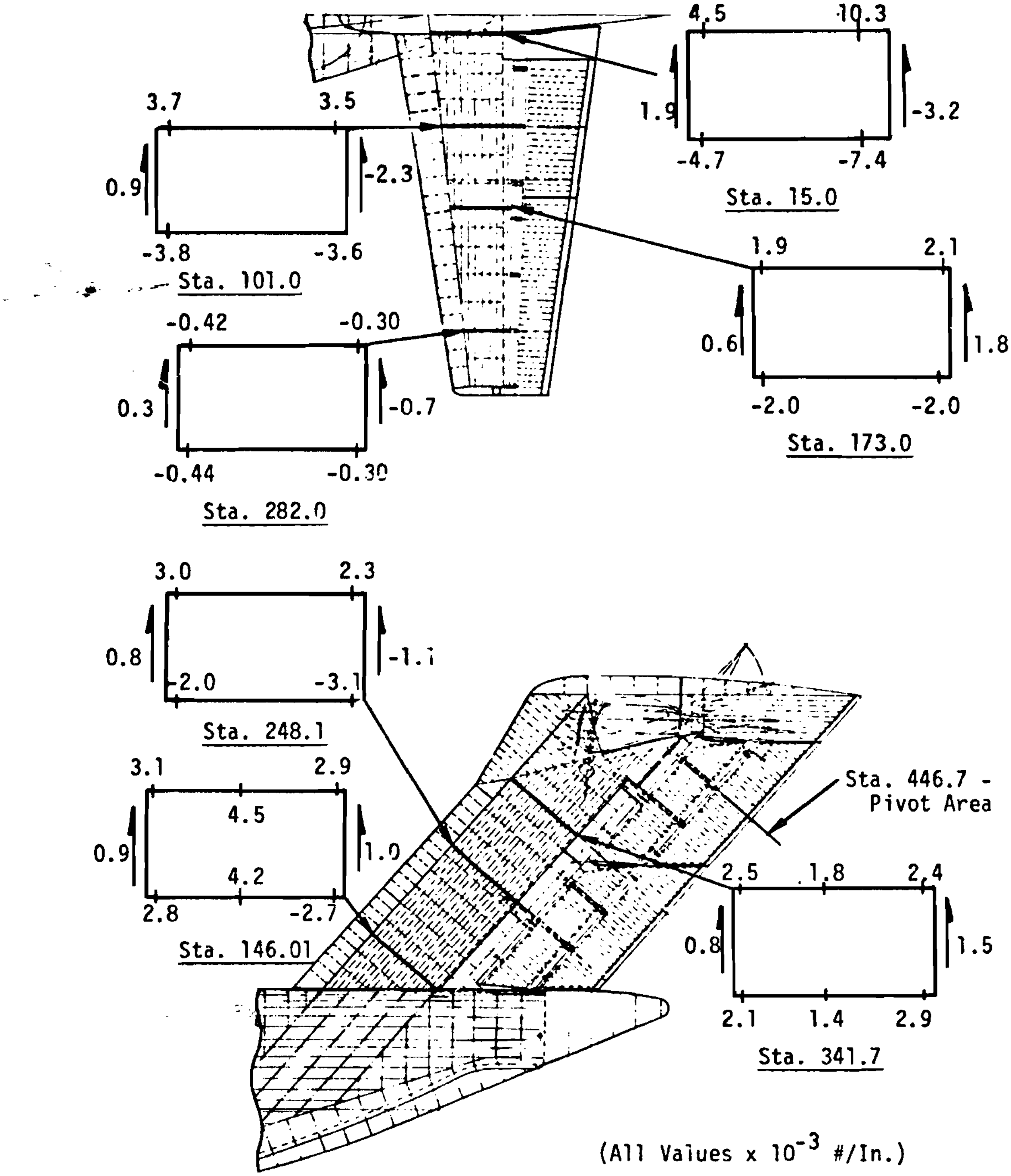

(All Values x 10^{-3} #/In.)

Figure 22 EMPENNAGE ULTIMATE ENVELOPE LOADINGS AT CONTROL STATIONS

The resulting load spectra for all missions for a design life of 60,000 hours are summarized by environmental mode for frequency content and distribution in Table VIII.

Over 93% of the frequency content is supplied by taxi and low level gust-plus-maneuver. Maximum load factor excursions result from landing impact and from maneuver spectra. Landing load factors, however, apply to inertia loadings only, thus diminishing their importance.

Experience has shown that the ground-air-ground (GAG) cycle is a major influence in structural fatigue damage. The data in Table VIII have been used to develop the GAG cycle for the baseline. A cumulative frequency of flight condition cycles and of ground condition cycles is made to define the peak flight and peak ground load factor excursions. Only every other peak excursion is used to define a GAG cycle, thus reflecting that: 1) the maximum load factor excursion is not always associated with maximum stress (for example, incremental gust load factors are inversely proportional to gross weight) and 2) more than one large load factor excursion may occur per flight cycle. Thus, the 95,020th GAG cycle, corresponding to 95,020 landings per 60,000 hours, is defined at Σf = 190,040 cycles. The C.G. load factor exceedance spectra resulting from the analysis is shown in Figure 23. The typical, or average, GAG cycle excursion is approximately defined at Σf = 95,020 where flight Δn = 0.56 and ground Δg = 0.47.

2.3.2.1 Acoustic Loads - The STOL is also subjected to acoustic loads from the engines. Estimates of acoustic loads have been obtained for various flap settings at takeoff thrust with the airplane stationary. These estimated pressure spectrum levels are summarized in Reference 1 for the critical locations on the wing, fuselage, and empennage, along with db reduction values for forward velocity, ground clearance and reduced thrust. The maximum unreduced levels for the wing, fuselage and empennage are 139 db, 134 db and 124 db, respectively, all occurring at a frequency of approximately 50 hz.

2.3.3 Flutter Rigidity Requirements

Wing rigidity constraints are established by the flutter speed requirements (1.15 V_L), Section 2.2.4. A preliminary flutter analysis was made of the YC-15 wing using the bending (I_{yy}) and torsional (J) rigidities shown in Figure 24. (Note: The YC-15 and the initial baseline wing rigidities are approximately the same.) This unique rigidity solution, however, is not the only one which can meet the flutter requirement. Alternate flutter solutions also can be defined by trading off EI_{yy} and GJ magnitudes and distributions.

Flutter sensitivity analyses, based on a finer grid idealization, were performed to determine the effect of incremental changes in stiffness on structural damping, g, (Figures 25 and 26) which is related to flutter speed. Using this tool, the EI_{yy} and GJ magnitudes and distributions of the new wing concepts (reflecting weight and concept variations) are controlled to produce designs for which the flutter "margin of safety" is equal to or greater than zero.

TABLE VIII FATIGUE LOAD FACTOR SPECTRA SUMMARY BY ENVIRONMENTAL MODE[1]

MODE / ΔN_{ave}	TAXI	GUST	LANDING IMPACT (CTOL)	LANDING IMPACT GW 153K (STOL)	LANDING IMPACT GW 153K (STOL)	LOW LEVEL M + G	MANEUVER $\pm \Delta N$	MANEUVER $\pm \frac{\Delta N}{2}$
.15	24,796,000	788,797	20,917	---	4,537	9,105,753	590,336	1,168,283
.25	6,964,000	99,085	1,726	12,768	1,156	2,690,332	103,757	322,217
.35	1,928,000	14,164	205	6,384	587	1,117,523	19,334	96,926
.45	309,466	2,457	93	5,532	302	362,161	3,817	30,973
.55	46,615	585	39	2,979	186	134,517	887	10,447
.65	6,070	195	29	1,703	125	12,417	268	3,744
.75	827	81	28	2,000	97	19,143	103	1,445
.85	122	36		1,276	27	9,830	47	610
.95	17	17	ΔN_{ave}	979	57		23	283
1.05	3	8	1.1	1,703	41		12	144
1.15		4	1.3	851			7	79
1.25		2	1.5	553			4	44
1.35		1	1.7	468			2	26
1.45			1.9	256			1	16
1.55			2.1	192				10
1.65			2.3	78				5
1.75			2.5	167				4
1.85			2.7	110				2
			2.9	69				2
			3.1	44				
			3.3	93				

(1) ALL MISSIONS FOR 60,000 HOURS

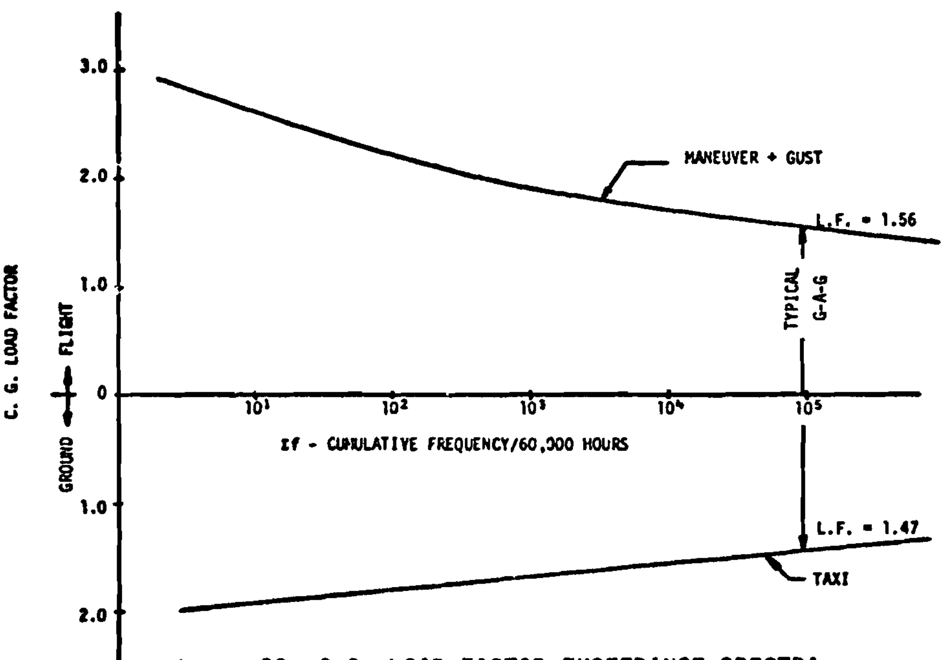

Figure 23 C.G. LOAD FACTOR EXCEEDANCE SPECTRA

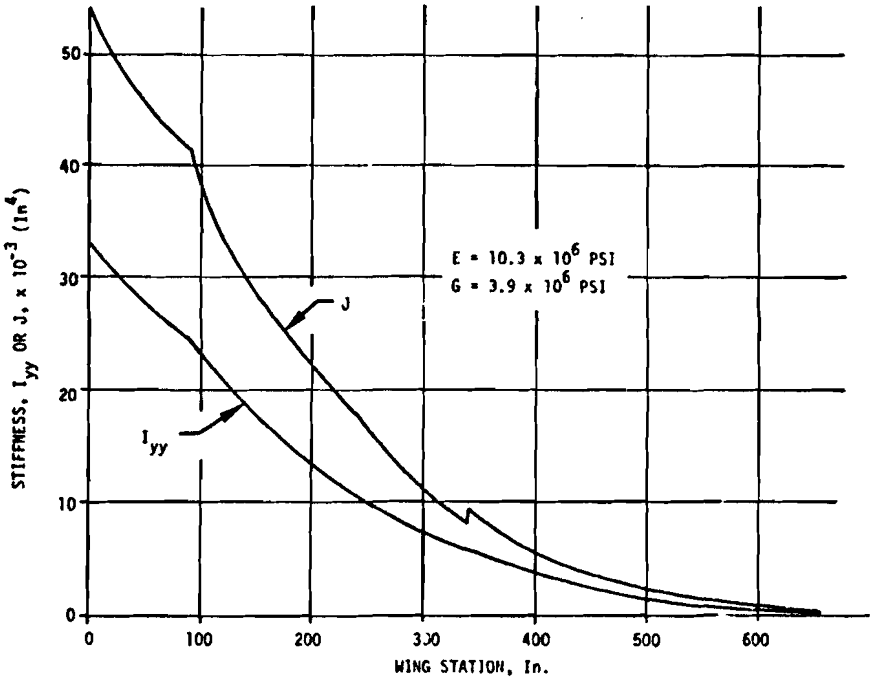

Figure 24 INITIAL BASELINE WING BENDING AND TORSIONAL RIGIDITIES

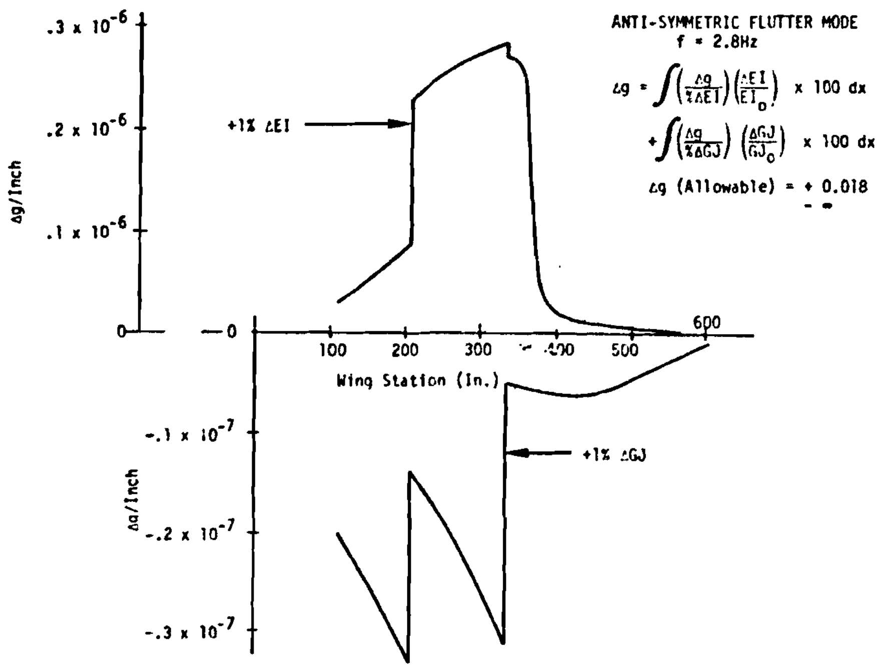

Figure 25 EFFECT OF WING LOCAL RIGIDITY CHANGES ON DAMPING FOR FLUTTER ASSESSMENT (f = 2.8 Hz)

In the same manner, a flutter analysis was made of the baseline empennage using the bending I_{yy} and torsional (J) rigidities shown in Figures 27 and 28. As in the case of the wing, this unique rigidity solution is only one of many that can meet the flutter requirement. Flutter sensitivity analyses, based on a finer grid idealization, were performed to determine the effect of incremental changes in stiffness on flutter speed, Figure 29. It should be noted that the vertical and horizontal stabilizers influence the flutter speed simultaneously. Using Figure 29 it was, therefore, possible to adjust the EI_{yy} and GJ distribution of both stabilizers for the new study concepts to obtain the lightest total empennage primary structure with a positive "margin of safety" for the flutter mode.

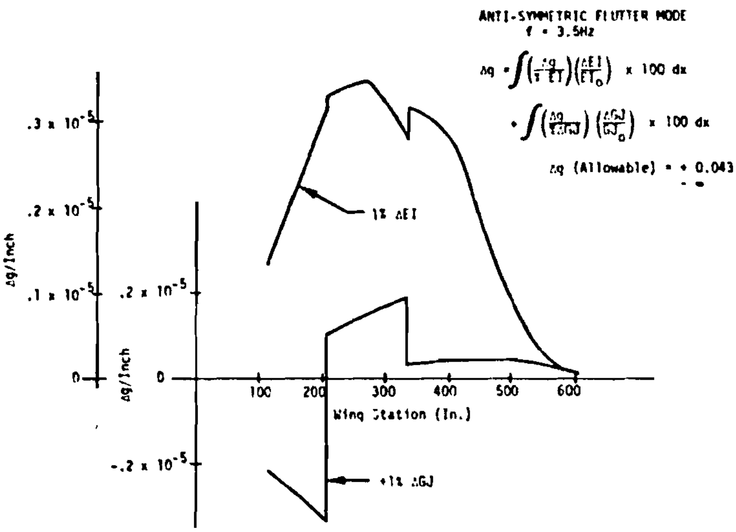

Figure 26 EFFECT OF WING LOCAL RIGIDITY CHANGES ON DAMPING FOR FLUTTER ASSESSMENT (f = 3.5 Hz)

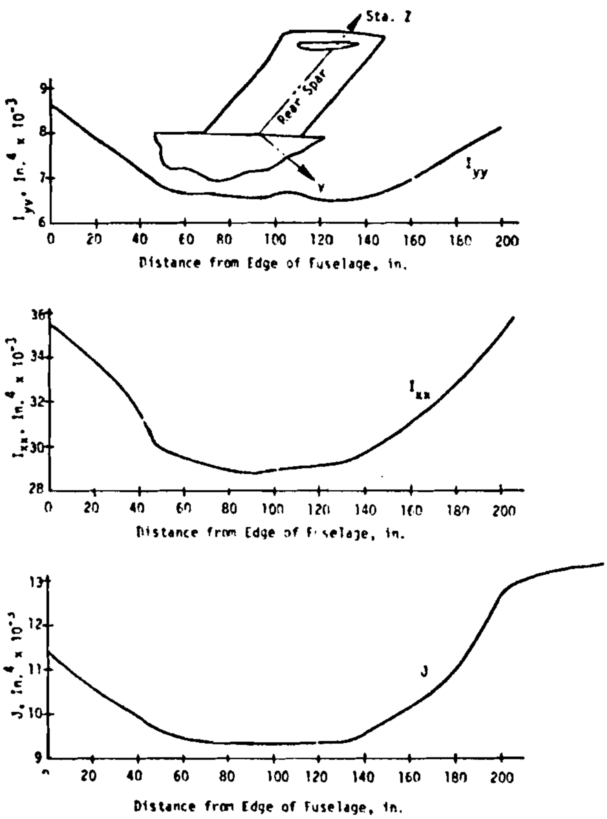

Figure 27 BASELINE VERTICAL STABILIZER BENDING AND TORSIONAL RIGIDITIES

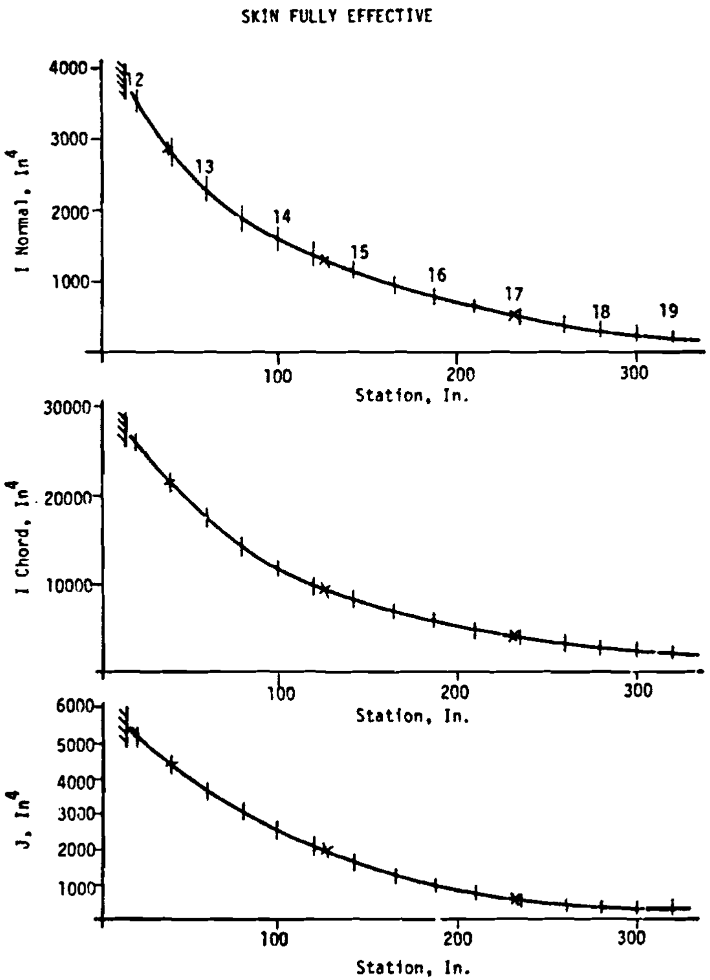

Figure 28 BASELINE HORIZONTAL STABILIZER BENDING & TORSIONAL RIGIDITIES

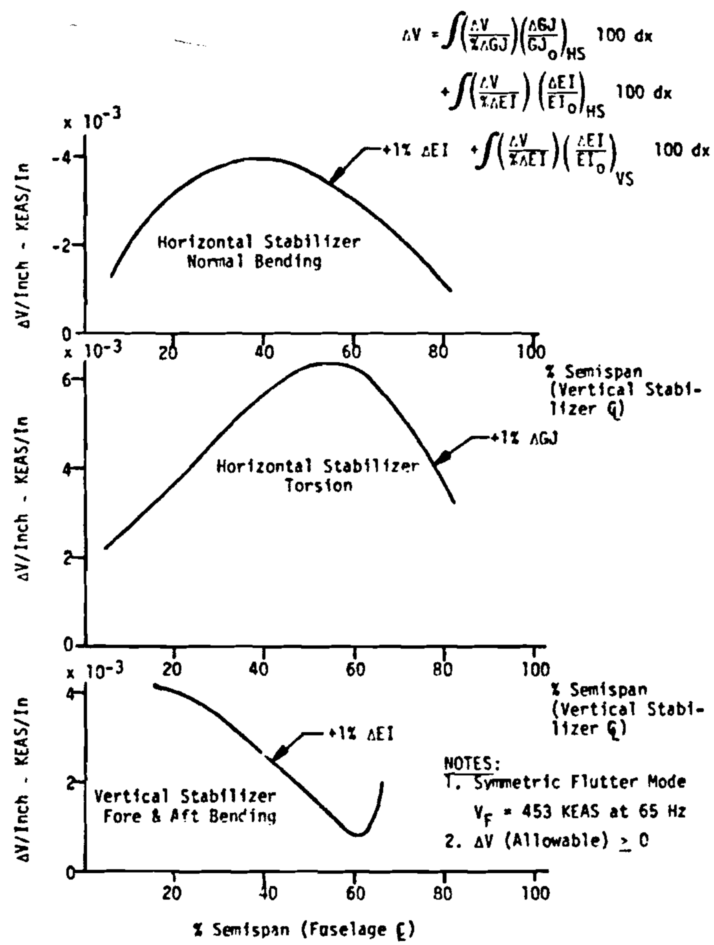

Figure 29 CHANGE IN EMPENNAGE FLUTTER SPEED WITH SPANWISE VERTICAL AND HORIZONTAL STABILIZEP STIFFNESS VARIATIONS

SECTION III

STRUCTURAL MATERIALS

One of the basic variables affecting structural weight (and cost) is material. A material selection criterion is developed in Section 3.1 which is based on a consideration of each integrity mode (such as ultimate tension, fatigue, etc).

Material property data for implementing the material selection criteria (including ultimate and yield strength, modulus, stress corrosion resistance, fatigue and plane stress/strain crack growth factors) for the study materials are given in Section 3.2. Materials are limited by the study scope to beryllium, aluminum, titanium and steel alloys, and selective composite reinforcement. It is common in parametric studies to find that required fatigue data are unavailable for particular notch conditions. Therefore, a procedure is described in Appendix B to normalize and thereby extend existing notched specimen data. Evaluation of materials, especially for the ultimate compression mode, requires basic stress strain data. The procedure used and resulting data are also summarized in Appendix B.

These material data are subsequently used in support of the design and analysis of new structural concepts.

3.1 MATERIAL SELECTION CRITERIA

Development of more efficient (i.e., lighter) structural concepts relies on improved geometry and/or material characteristics which, for "fixed requirements," are defined by the critical integrity mode capabilities. Hence, for the "geometry constant" case, material selection criteria are established directly from the analytical models defining structural capability for each mode.

The integrity modes considered are: 1) ultimate (tension, compression and shear), 2) fatigue, 3) damage tolerance, 4) flutter and 5) stress corrosion. The selection criteria, along with appropriate remarks on the development of the criterion parameters, are summarized in Table IX. As previously stated, the basis for the criteria is "minimum weight" except for stress corrosion, which is "maximum reliability."

The results, in general, are classical in nature and are a function of the mode, the associated analysis model and the geometry. In order to enhance the accuracy of the material comparisons, representative criteria conditions are also defined for fatigue ($N_{GAG} = 10^5$, $R = 0$, $K_t = 1$ and 3) and for damage tolerance ($da/dn = 10^{-5}$, $R = 0$).

The required important material properties are identified directly from the material selection criteria parameters. When implemented over a range of new material candidates, these parameters provide a means of determining the best material for each mode, ranking the materials selected in order and showing how much better one material is with respect to another.

TABLE 9 - MATERIAL SELECTION CRITERIA		
INTEGRITY MODE	CRITERION	REMARKS & RATIONALE
ULTIMATE TENSION	$(F_{tu}/\rho)_{max}$ (1)	(1) $w = \rho \bar{t} = \rho \frac{Nx}{F} = \frac{Nx}{(F/\rho)}$ Loading Nx = constant Failure stress $F \doteq F_{tu}$ ρ = material density $w_{min} = \frac{1}{(F_{tu}/\rho)_{max}}$
COMPRESSION	$(E_{c}/\rho)_{max}$ (1)	(2) General or local instability stress $F = F_{c_{crit}}$ $F_{c_{crit}} = E_c$ f (panel concept, geometry ratios) $= E_c$ f (panel concept, geometry ratios) = constant
	$(F_{cy}/\rho)_{max}$ (1)	(3) Same rationale as (1), limiting instability stress $F = F_{cy}$
SHEAR	$(E_{c}/\rho)_{max}$ (1)	(4) Same rationale as (2), $F_{s_{crit}}$ in lieu of $F_{c_{crit}}$
	$(F_{sy}/\rho)_{max}$ (1)	(5) Same rationale as (3), F_{sy} in lieu of F_{cy}
	$(F_{tu}/\rho)_{max}$ (1)	(6) Same rationale as (1), (tension field)
FATIGUE	$(\sigma_{max}/\rho)_{max}$ (1) @ N, R, K_t	(7) Spectrum loadings $Nx = N_{x_{max_i}}$ = constant Spectrum stresses $F = \sigma_{max_i}$ Determine σ_{max_i} from S-N data on basis of: Ground-air-ground cycle (GAG) most damaging $N = N_{GAG} = 10^5$ cycles $R = R_{GAG} = 0$ (representative and convenient value) $1 \leq K_t \leq 3$ (use upper & lower limit values)
DAMAGE TOLERANCE	$(\Delta K/\rho)_{max}$ (1) @ da/dn, R	(8) The A/F criteria "period" requirement is primarily achieved at early conditions of crack growth, i.e., $a_i < a \leq \frac{a_{crit}}{10}$ $N_x = N_{x_{max_i}}$ = constant F_i = spectrum stress $= \sigma_{max_i}$ $\sigma_{max_i} = K_{max_i}$ f (panel concept & crack geometry) $\sigma_{max_i} \propto K_{max_i} = \frac{\Delta K_i}{1 - R_i} \propto \Delta K_i$ since R_i & f (panel concept & crack geometry) = constant Determine ΔK from "da/dn vs. ΔK" data on basis of: $da/dn = \frac{C \Delta K^n}{(1-R)K_c} = 10^{-5}$ inches/cycle = representative value which also corresponds to lower limit of data availability. R = 0 (representative and convenient value)
	$(K_c/\rho)_{max}$ (1)	(9) "Detectability" is primarily achieved at later conditions of crack growth, i.e., $\frac{a_{crit}}{10} \leq a \leq a_{crit}$ $N_x = N_{x_{max_i}}$ = constant Maximum spectrum stress $F_i = \sigma_{max_i}$ $\sigma_{max_i} \propto K_{max_i} = K_c$ (See 8)

TABLE 9 MATERIAL SELECTION CRITERIA -- Concluded		
INTEGRITY MODE	CRITERION	REMARKS & RATIONALE
DAMAGE TOLERANCE (CON'T)	$\left[\frac{K_c}{F_{ty}}\right]^2_{max}$ (1)	(10) Achievement of "period" requirement enhanced by retardation. Maximum retardation corresponds to maximum "plasticity," i.e., plastic zone radius $r_{y_{max}} \propto \left[\frac{K_c}{F_{ty}}\right]^2_{max}$
FLUTTER RIGIDITY		
BENDING	$(E/\rho)_{max}$ (1)	(11) Sizing basis: $E\ I$ = constant $w = \rho\ \bar{t} = \rho\ \left(\frac{I}{2h^2}\right) = \frac{\rho\ \text{constant}}{E(2h^2)}$ Configuration geometry (h) = constant $w_{min} = \frac{1}{(E/\rho)_{max}}$
TORSION	$(E/\rho)_{max}$ (1)	(12) Same rationale as (11) to define $w_{min} = \frac{1}{(G/\rho)_{max}} = \frac{1}{(E/\rho)_{max}}$ since $G = E/_{2(1+\mu)} \propto E$
STRESS CORROSION		
"SMOOTH" CONDITIONS	$\left[\frac{\sigma_{TH}}{E}\right]_{max}$ (2)	(13) Assume bending moment due to "misfit" clamping on assembly $M_{max} \propto \frac{E\ I\ \delta}{L^2}$ Bending stress $f_{bt} \propto \frac{E\ \delta\ c}{L^2}$ For constant panel concept & panel geometry ratios $c \propto \frac{1}{E},\ L = \frac{1}{E},\ \delta = f(L) \propto \frac{1}{E}$ $\sigma_{res.} = f_{bt} \propto E$ On the basis of reliability, $R = 1 + M.S = \frac{\sigma_{TH}}{\sigma_{res}}$ $R_{max} \propto \left[\frac{\sigma_{TH}}{E}\right]_{max}$
"FLAWED" CONDITIONS	$\left[\frac{K_{I_{scc}}}{E}\right]_{max}$ (2)	(14) For surface flaw(3)/stress couple, $K = M_k \sigma A \sigma \sqrt{\pi a} \propto \sigma$ Q, A, M_k, a = constant for fixed NDI capability $\sigma = \sigma_{res} \propto E$ for bending (See 13) Then $K \propto E$; $K_{max} = K_{I_{scc}}$ $R_{max} = 1 + M.S_{max} = \left[\frac{K_{I_{scc}}}{K}\right]_{max} \propto \left[\frac{K_{I_{scc}}}{E}\right]_{max}$

(1) For minimum weight (w)
(2) For maximum reliability (R)
(3) Result applies to hole flaw subject to attachment interference fit stress, also.

3.2 MATERIAL PROPERTIES

The properties of various candidate aluminum, titanium, steel and beryllium alloys have been obtained from the general literature and from preliminary reports from the AMS/ADP Program, McDonnell Douglas Corporation, and other published and unpublished data sources. Approximations have been used where data were unavailable.

The initial baseline airplane alloys include the following:

Clad sheet	2024-T3, 7075-T6
Plate	7075-T76
Extrusions	7075-T6511
Forgings	7075-T6, 7075-T73

These alloys are considered current (January 1973) "state-of-the-art" materials and are applicable to the study structures.

The material properties used for the initial baseline design are "B" values as listed in MIL-HDBK-5. The data for the new materials are available as "S" values or typical values. A common basis is required to make valid weight comparisons between the various concepts utilizing new materials. Therefore, a method for converting new material data to a "B" value basis was evolved and is presented in Appendix B.

The properties of the baseline and selected materials appear in Tables X and XI. The data sources are noted by reference numbers (5 through 30) in the tables.

The following comments are made in regard to interpretation of the tables and notations:

1. Column headings are in accordance with material properties and selection criteria found in Section 3.1.

2. Typical or average values have been supplied for K_c, K_{I_c}, $K_{I_{scc}}$, fatigue and ΔK properties.

3. Threshold values are listed for smooth bar stress corrosion (σ_{th}) conditions.

4. Correction factors for fatigue data obtained under conditions other than R = 0 and K_T = 3 were determined by the method described in Appendix B. When the data base to implement this method was not available, typical properties were estimated.

5. The fatigue data for all candidate aluminum alloys except sheet have been evaluated to fall within the general scatterband for 7075 alloy. Although the data may appear to show some slight differences between the newer alloys, it is deemed premature to invoke these values since data are only available from a very few heats or producers. The fatigue values for 7075 in the

TABLE X PROPERTIES OF INITIAL BASELINE STRUCTURE MATERIALS

ALLOY		Ftu KSI	Ftu/ρ	Fty KSI	Fty/ρ	Fcy KSI	Fcy/ρ	Fsu KSI	Fsu/ρ	Ec	Ec/ρ	ρ	0.7 SECANT STRESS KSI	SHAPE FACTOR n	KIC	Kc	Kc/ρ	(a/Q)	STRESS CORROSION			FATIGUE				CRACK GROWTH		REFERENCES
2024-T3 CLAD SHEET		B		B		B		B		10.[illegible]	107	.100										43	23	430	230	14	140	
.063 to .249	L	64	[illegible]	[illegible]	[illegible]	[illegible]	[illegible]	[illegible]	[illegible]				[illegible]	10.7					≥35									5,6,7,[illegible]
	LT	[illegible]	[illegible]	[illegible]	[illegible]	[illegible]	[illegible]								.175		.750	12.8	≥35	8	.769							6,9,10
	TL														.148		.480											
	ST																											
	SL																											
7075-T76 BARE SHEET		(B)		(B)		(B)		(B)		10.5	104	.101										45	19	446	186	12	118	5
.125 to .249	L	7[illegible]	.733	66	[illegible]	[illegible]	[illegible]	46	.455				61.8	(20)					45									5,6,11,12
	LT	75	[illegible]	66	[illegible]	.67	.662								.25		.763	1.37	42									13
	TL														.62		.614	.938		(47)	4.48							
	ST																											
	SL																											
7075-T6 CLAD SHEET		B		B		B		B		10.5	104	.101										40	21	396	208			5
.063 to .187	L	75	[illegible]	67	.663	.66	[illegible]	.45	.444				67.9	11.6					49									5,6
	LT	73	.723	65	.644	.65	.693								60		596	.726	46									
	TL														57		564		(45)	4.29						10	99	8
	ST																											
	SL																											
7075-T6 DIE FORGING		B		B		B		B		10.4	103	.101										55	21	545	228			6
≤ 1.0	L	78	.772	67	.663	[illegible]	.693	.45	.450				71.4	(20)					35									5,14,15,16
	LT																		25									
	TL																											
	ST	75	.743	67	.664	.66	.673												7							10	99	
	SL																											
7075-T6 DIE FORGING		B		B		B		B		10.4	101	.101										55	23	545	228			
1.0 to 2.0	L	77	.762	66	.653	.69	.683	.44	.436				70.3	(20)														12
	LT															26	257	.142										
	TL															23	228	.118										
	ST	74	.733	66	.654	.57	.564																					
	SL															17	168	.064										

[illegible]

(*) Estimated, F values based on actual F values

(**) Estimated E values based on estimated F values

(20) Assumed values for n (0.7 secant stress calculated)

TABLE X PROPERTIES OF INITIAL BASELINE STRUCTURE MATERIALS (CONCLUDED)

ALLOY		Ftu KSI	Ftu/ρ	Fty KSI	Fty/ρ	Fcy KSI	Fcy/ρ	Fsu KSI	Fsu/ρ	Ec	Ec/ρ	ρ	0.7 SECANT STRESS KSI	SHAPE FACTOR n	KIC	Kc	Kc/ρ	(a/Q)	STRESS CORROSION			FATIGUE				CRACK GROWTH		REFERENCES
7075-T6 DIE FORGING		B		B		B		B		10.4	103	.101										55	23	545	228			
2.0 to 3.0	L	76	.752	65	.644	.66	.673	[illegible]	.426				69.2	(20)														
	LT																											
	TL																											
	ST	73	[illegible]	63	.624	[illegible]	.653																					
	SL																											
7075-T73 DIE FORGING		(B)		B		(B)		(B)		10.4	103	.101										55	23	545	228	12.5	123	5
≥ 3.0	L	6[illegible]	[illegible]	5[illegible]	.544	61	[illegible]	42	.416				61.7	(20)					50									5,14,17,18
	TL															31	307	.286	48									
	ST	65	.644	56	.554	[illegible]	[illegible]									25	248	.200										
	SL																		41									
7075-T6511 EXTRUSION		B		B		B		B		10.7	109	.101																5
≤ .249	L	82	[illegible]	76	[illegible]	7[illegible]	[illegible]	.44	[illegible]				75.6	(20)														14,15,19
	LT	80	[illegible]	70	[illegible]	76	[illegible]																					
	TL																											
	ST																											
	SL																											
7075-T6511 EXTRUSION		B		B		B		B		10.7	106	.101																
.250 to .499	L	85	.842	77	.762	77	.762	.45	.446				78.8	(20)														
	LT	83	.822	72	.713	78	.772																					
	TL																											
	ST																											
	SL																											

[illegible]

(*) Estimated, F values based on actual F values

(**) Estimated E values based on estimated F values

(20) Assumed values for n (0.7 secant stress calculated)

TABLE XI PROPERTIES OF SELECTED STRUCTURE MATERIALS (IMPROVED BASELINE & NEW CONCEPTS)

Alloy		F_{tu} KSI	F_{tu}/ρ 10^3 inch	F_{ty} KSI	F_{ty}/ρ 10^3 inch	F_{cy} KSI	F_{cy}/ρ 10^3 inch	F_{su} KSI	F_{su}/ρ 10^3 inch	E_c 10^6 psi	E_c/ρ 10^6 inch	ρ lb/in^3	.7 Secant Stress KSI	Shape Factor (n)	K_c * KSI$\sqrt{\text{inch}}$	K_{Ic} * KSI$\sqrt{\text{inch}}$	K^*/ρ 10^3 in$^{1/2}$	$(K^*/F_{ty})^2$ inch	Stress Corrosion Smooth σ_{th} KSI	Stress Corrosion Notched K_{Iscc} ($\frac{da}{dt}$ 10^{-4}) KSI	Stress Corrosion Notched K_{Iscc}/F_c 10^{-1} KSI	Fatigue 10^7 Cycles σ max $K_t=1$ KSI	Fatigue 10^7 Cycles σ max $K_t=3$ KSI	Fatigue σ_0/ρ max $K_t=1$ 10^3 inch	Fatigue σ_0/ρ max $K_t=3$ 10^3 inch	Crack Growth Δa ($\frac{da}{dN}$ 10^{-4}) KSI$\sqrt{\text{inch}}$	Crack Growth $\Delta a/\rho$ 10^3 in$^{1/2}$	References
7050-T76 CLAD SHEET		((B))		((B))		((B))		((B))		10.6	104	.102										(40)	(21)	382	206	(14)	137	20
.020 to .063	L	79	774	72	706	73	716	47	461				74.5	(20)														
	LT	79	774	70	686	76	745								(60)		588	.695										
	TL																											
	ST																											
	SL																											
7050-T73651 PLATE		(B)		(B)		(B)		(B)		10.6	104	.102										55	23	539	22[illegible]			17,21
≥ 2.0	L	73	716	65	637	64	627	43	422				64.9	(20)														
	LT	74	725	65	637	67	657									36	353	.307								16	157	17,22,23
	TL															30	294	.213		30	2.83							13
	ST																		30									
	SL															26	255	.155		26	2.45							17,24
7050-T7651 PLATE		(B)		(B)		(B)		(B)		10.6	104	.102										55	23	539	225			17
≥ 2.0	L	79	775	71	696	70	686	46	451				72.1	13												14	137	25
	LT	80	784	69	676	72	706									34	333	.229										19
	TL															28	275	.165		20	1.89							
	ST																		25									
	SL															24	235	.121										
7475-T7351 PLATE		(B)		(B)		(B)		(B)		10.6	105	.101										55	23	545	228			26
1.5 to 2.0	L	69	683	58	574	57	564	43	426				57.4	(20)					47									
	LT	70	693	58	574	60	594									50	495	.743	42	30	4.72					14	139	17,24,27
	TL															45	446			45	4.25							27
	ST	67	663	55	545	59	584												42									
	SL															33	327	.360		33	3.11							
7475-T7651 PLATE		(B		(B)		(B)		(B)		10.6	105	.101										55	23	545	228	12	119	
1.0 to 1.5	L	71	703	61	604	60	594	41	406				60.6	(20)					50									17,25,27
	LT	72	713	61	604	63	624									43	426	.497	45	43	4.06					14	139	
	TL															38	376	.388		35	3.30							
	ST																		25		2.64							
	SL															29	287			28								

* Kc or KIc as applicable

( ) Estimated "B" values based on Actual "S" Values

((B)) Estimated "B" values based on estimated "S" values

(20) Assumed values for "n" (0.7 secant stress calculated)

TABLE XI PROPERTIES OF SELECTED STRUCTURE MATERIALS (CONT'D)

ALLOY		1	2	3	4	5	6	7	8	9	10	ρ	12	13	14	15	16	17	18	19	20	21	22	23	24	25	REFERENCES
7049-T73 DIE FORGING		(B)		(B)		(B)		(B)		10.6	136	.102									55	23	539	225	12.5	123	5,28,29
1.0 to 2.0	L	75	715	65	617	[illegible]	[illegible]	44	431				69.1 (20)														5,11,28
	LT														30	296	.213										
	TL														25	265	.184										
	ST	73	712	63	618	65	637											62									
	SL														24	235	145		20	1.89							
7049-T73 DIE FORGING		(B)		(B)		(B)		(B)		[illegible]	[illegible]	.102									55	23	539	225	12.5	123	
2.0 to 4.0	L	[illegible]	725	66	[illegible]	[illegible]	[illegible]	44	431				67.0 (20)														
	LT																										
	TL																										
	ST	73	[illegible]	61	618	65	637											62									
	SL																										
7049-T73 DIE FORGING		(B)		(B)		(B)		(B)		10.6	136	.102									55	23	539	225	12.3	123	
4.0 to 5.0	L	71	71?	63	5?8	62	61?	[illegible]	[illegible]				66.0 (20)														
	LT																										
	TL																										
	ST	71	696	61	596	63	[illegible]											62									
	SL																										
7050-T73651 EXTRUSION		(B)		(B)		(B)		(B)		10.6	136	.102									55	23	539	225	(11)	127	17
.50 to 1.50	L	82	8.4	76	725	76	725						75.6 (20)														
	LT																										
	TL																										
	ST																	35									17
	SL														23												
7050-T76511 EXTRUSION		(B)		(B)		(B)		(B)		10.6	[illegible]	.102									55	23	539	225			17,21
.25 to .499	L	85	833	77	755	78	765						79.9 (20)												11.5	111	30
	LT	84	825	[illegible]	[illegible]	79	[illegible]							30			1.37										
	TL																										
	ST																										
	SL																										

[illegible]

( ) Estimated, B values based on Actual [illegible] Values

(20) Assumed values for [illegible] (0.7 secant stress calculated)

((B)) Estimated, B values based on estimated [illegible] values

TABLE XI PROPERTIES OF SELECTED STRUCTURE MATERIALS (CONCLUDED)

ALLOY		1	2	3	4	5	6	7	8	9	10	ρ	12	13	14	15	16	17	18	19	20	21	22	23	24	25	REFERENCES
7050-T73 DIE FORGING		((E))		((B))		((B))		((E))		(10.6)	134	102		(130)													SEE APPENDIX B
3.0	L	69	677	58	568	61	598	42	402												55	23	539	225	(16)	157	
	LT														(34)	334	.364										
	TL														(26)	255	.215										
	ST	65	647	56	549	58	568											(42)									
	SL														(22)	216	.154										

[illegible]

( ) Estimated, B values based on Actual [illegible] Values

(20) Assumed values for [illegible] (0.7 secant stress calculated)

((B)) Estimated, B values based on estimated [illegible] values comparable tempers will, therefore, be used for the candidate alloys other than sheet.

6. Correction factors for available $R \neq 0$ crack growth data to $R = 0$ conditions were determined using Forman's equations. However, data for some alloys were observed to deviate significantly from Forman's equation at da/dn of 10^{-5} and estimates were made where necessary.

7. The values for K_c and K_{I_c} have been listed at what is considered to be the limiting conditions for plane stress or plane strain to facilitate alloy evaluation. Specific values of fracture toughness for design calculations will give consideration to component thickness/width/crack length criteria.

8. The usefulness of fracture toughness, stress corrosion and crack propagation data must be considered in light of the present state-of-the-art for these properties. K_{I_c} properties have been determined from valid test data established by a standard ASTM procedure. Reliability for this parameter increases with the data base. Data values for K_c, $K_{I_{scc}}$ and ΔK are still unreliable or of uncertain quality due to lack of standard test procedures.

9. Directionality of tensile and compressive properties has been indicated by L (longitudinal), LT (long transverse), ST (short transverse), etc. in the tables. When no directionality is indicated, as occasionally occurred with some data sources, it will be assumed the values applies to any direction. Directionality of fracture toughness data has been indicated by the guidelines presented in Reference 11. Crack propagation data (da/dn) were considered inadequate to establish discreet values based on directionality.

3.2.1 Aluminum Alloys

The aluminum alloys selected for consideration are as follows:

2024-T3	Clad Sheet	7050-T736511	Extrusions
7075-T6	Clad Sheet	7050-T73	Forgings
7075-T7351	Plate	7050-T736	Forgings
7075-T6	Extrusions	7050-T73652	Forgings
7075-T6	Forgings	7175-T66	Forgings
7075-T73	Forgings	7175-T736	Forgings
7049-T73	Forgings	7475-T61	Sheet
7049-T76511	Extrusions	7475-T61	Clad Sheet
7050-T76	Sheet	7475-T761	Sheet
7050-T76	Clad Sheet	7475-T761	Clad Sheet
7050-T7651	Plate	7475-T651	Plate
7050-T73651	Plate	7475-T7651	Plate
7050-T76511	Extrusions	7475-T7351	Plate

The properties for these alloys are listed in Appendix B.

3.2.2 Titanium Alloys

The titanium alloys selected for consideration are as follows:

Ti-6AL-4V Ann (Ti-6-4)	Sheet, Plate, Extrusion
Ti-6-4 Sta	Sheet, Plate, Extrusion
Ti-6-4 Beta Ann	Plate
Ti-6AL-6V-2Sn Ann (Ti-6-6-2)	Sheet, Plate, Extrusion
Ti-6-6-2 Sta	Sheet, Plate, Extrusion
Ti-6-6-2 Beta Ann	Plate
Ti-3AL-8V-6CR-4MO-4Zr Sta (Ti-38-6-44)	Sheet, Plate
Ti-6AL-2Zr-2SN-2MO-2Cr Sta (Ti-6-22-22)	Plate
Ti-8AL-1MO-1V Mill Ann (Ti-8-1-1)	Sheet
Ti-8-1-1 Duplex Ann	Sheet
Ti-8MO-8V-2Fe-3AL Sta (Ti-8-8-2-3)	Strip, Plate
Ti-8-8-2-3 STOA	Strip

The bracketed terms shown above, e.g., (Ti-6-4), will be used as abbreviated designations for the alloy. The properties for these alloys are listed in Appendix B.

3.2.3 Steel Alloys

The steel alloys selected for consideration are as follows:

PH 15-7 Mo	Sheet, Plate
Marage 250	Sheet, Plate, Forgings, Extrusions
HP 9Ni-4Co-0.3C	Forgings, Extrusions
300M	Forgings, Extrusions
HP 310	Forgings, Extrusions

The properties for these alloys are listed in Appendix B.

3.2.4 Beryllium Alloys

The beryllium alloys selected for consideration are as follows:

PS 20 to SR 200E	Hot Rolled Sheet
(HIP) Pressed Block (No Specification)	Machined Sheet

The properties for these alloys are listed in Appendix B.

3.2.5 Advanced Composites

In general, unidirectional boron/epoxy will be used for stiffening structural elements. However, in the specific vertical tail spar cap case, which will be manufactured by the pultrusion process (Section 8.5), the raw materials utilized will be boron fibers and epoxy resin. These will be combined in situ during pultrusion. For the stringer reinforcement case, boron/epoxy laminated from prepreg will be used. The properties of the bare boron fiber are listed below.

BORON FILAMENT PROPERTIES

Tensile Strength	475 KSI
Tensile Modulus	58×10^6 PSI
Diameter	4.0 and 5.6 mils
Density	0.094 lbs/in^2

The expected properties of the boron/epoxy composite are shown in Table XII.

3.3 MATERIAL SELECTION

The material selection for the initial baseline aircraft is shown in Figure 30. This selection was based on state-of-the-art materials in use at the beginning of this study. However, due to weight increases required to meet the damage tolerance criteria for the study, an improved baseline material selection was made. This selection, Figure 31, became the basis for the baseline structural weight analysis.

The materials selected for thy airframe utilizing new structural concepts are summarized on Figure 32 for a honeycomb sandwich fuselage shell concept. The selection for the airframe having an isogrid fuselage shell design is presented in Volume II.

The principal alloy selected was 7050 with a few selective applications for 7049 and 7475. The alloys of beryllium, titanium or steel in the structural applications under study were found ineffective for either weight or cost consideration.

The following is a brief discussion of the principal characteristics of the selected materials and how they compare wth the other candidates for the various applications. The fatigue strengths, as defined by S/N curves for the aluminum alloys, except for sheet, are considered equal and so will not be discussed individually. The differences in static strength, fracture toughness, stress corrosion and crack propagation will be highlighted. Graphical comparisons of the various alloys, tempers and forms are shown in Figures 33 through 36. The crack propagation properties in Figure 37 have been synthesized by alloy and temper only, since the discordant data compiled from varying test procedures and influenced by an incomplete understanding of all test variables makes a rigorous display of the data unrealistic.

3.3.1 Wing Box

Alloy 7050-T76 and T7651 bare sheet and plate were selected for the upper wing skins for high strength, toughness, and exfoliation corrosion resistance. Alloy 7475-T7651 was chosen for the lower wing skin for its combination of higher toughness and good crack propagation resistance. Stress corrosion threshold is higher for the T76 tempers (25 KSI) than for either 7075-T6 or 2024-T3 (8 KSI) which are currently used on other aircraft wing skins. This higher threshold provides additional protection from occasional short transverse stress corrosion cracking on light gage plate.

Fracture toughness values K_{Ic} (Figure 35) are for heavy plate. For sheet or plate machined to thin sections, K_c and K_Q values will be necessary for

TABLE XII UNIDIRECTIONAL PROPERTIES OF BORON/EPOXY COMPOSITES

PROPERTIES (V_f = 0.50)				RT	350°F
Design strengths ["A" basis]	Longitudinal tensile ultimate	Ksi	F_L^{tu}	192.0	157.0
	Transverse tensile ultimate	Ksi	F_T^{tu}	10.4	6.0
	Longitudinal compression ultimate	Ksi	F_L^{cu}	353.0	116.0
	Transverse compression ultimate	Ksi	F_T^{cu}	40.0	11.0
	In-plane shear ultimate	Ksi	F_{LT}^{su}	15.3	5.5
	Interlaminar shear ultimate	Ksi	F^{isu}	13.0	7.0
	Ultimate longitudinal strain	μin./in.	ϵ_L^{tu}	6,500.0	5,400.0
	Ultimate transverse strain	μin./in.	ϵ_T^{tu}	4,000.0	7,600.0
Elastic properties [typical]	Longitudinal tension modulus	Msi	E_L^t	30.0	29.9
	Transverse tension modulus	Msi	E_L^t	2.7	1.13
	Longitudinal compression modulus	Msi	E_L^c	30.0	29.9
	Transverse compression modulus	Msi	E_T^c	2.7	1.13
	In-plane shear modulus	Msi	G_{LT}	0.7	0.32
	Longitudinal Poisson's ratio		ν_{LT}	0.21	0.21
	Transverse Poisson's ratio		ν_{TL}	0.019	0.008
Physical constants [typical]	Density	lb/in.^{3}	ρ	0.0725	0.0725
	Longitudinal coefficient of thermal expansion	μin./in./°F	α_L	2.3	3.0
	Transverse coefficient of thermal expansion	μin./in./°F	α_T	10.6	19.6

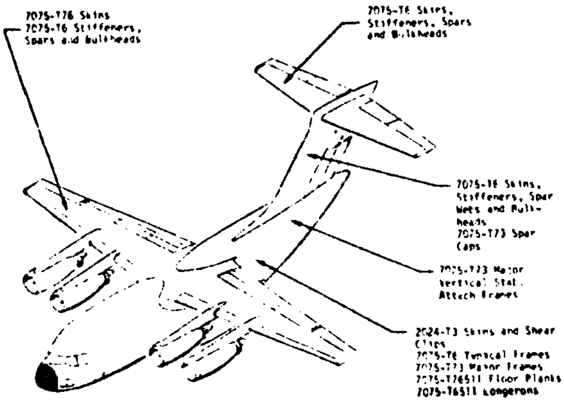

Figure 30 INITIAL BASELINE AIRFRAME MATERIAL SELECTION

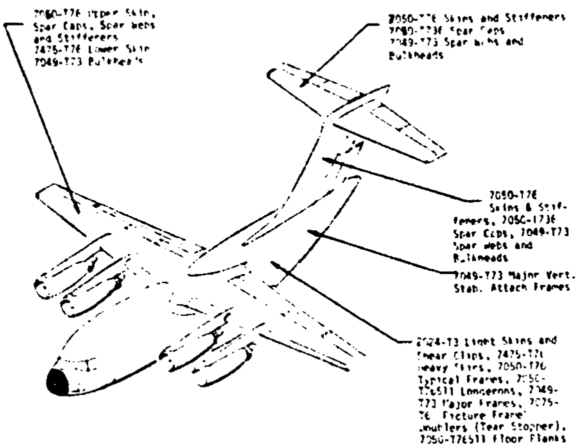

Figure 31 IMPROVED BASELINE AIRFRAME MATERIAL SELECTION

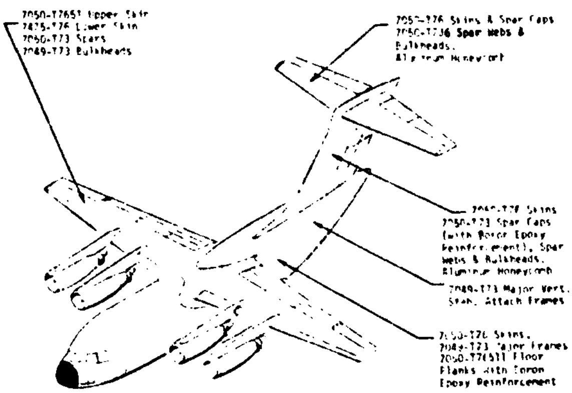

Figure 32 NEW CONCEPT AIRFRAME MATERIAL SELECTION (HONEYCOMB SANDWICH FUSELAGE)

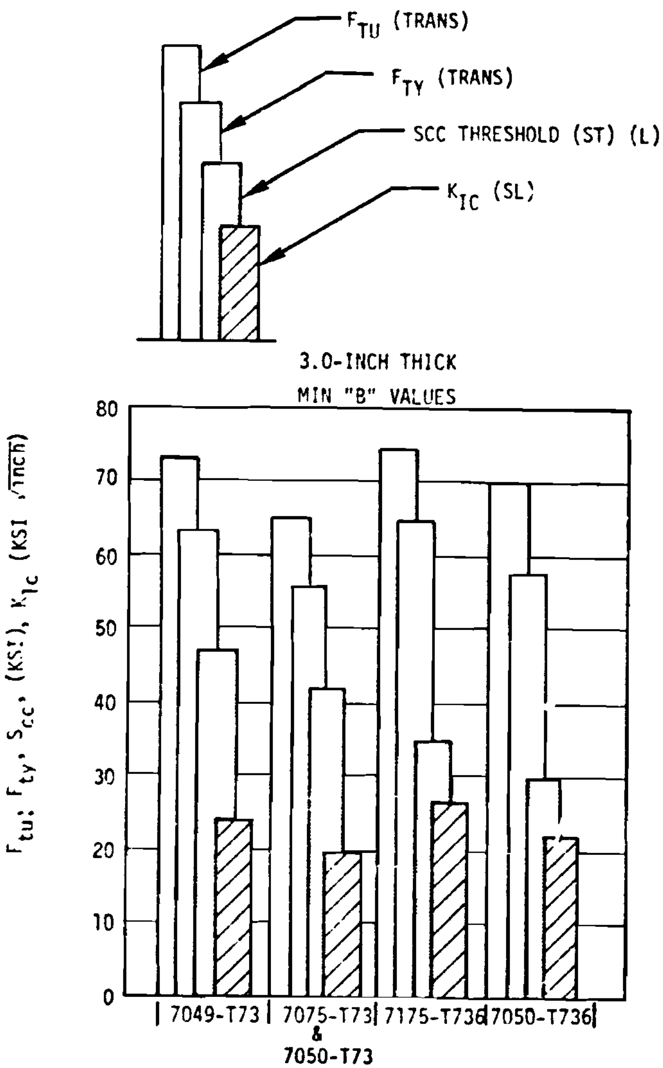

Figure 33 COMPARISON OF VARIOUS ALUMINUM ALLOYS' DIE FORGING DESIGN PROPERTIES

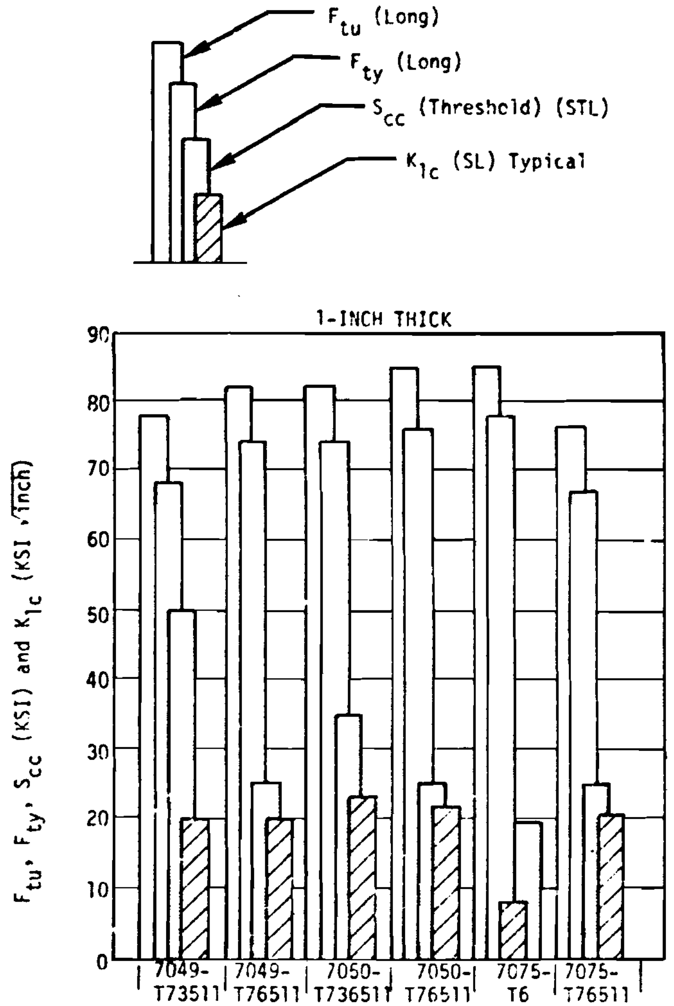

Figure 34 COMPARISON OF VARIOUS ALUMINUM ALLOYS' EXTRUSION DESIGN PROPERTIES

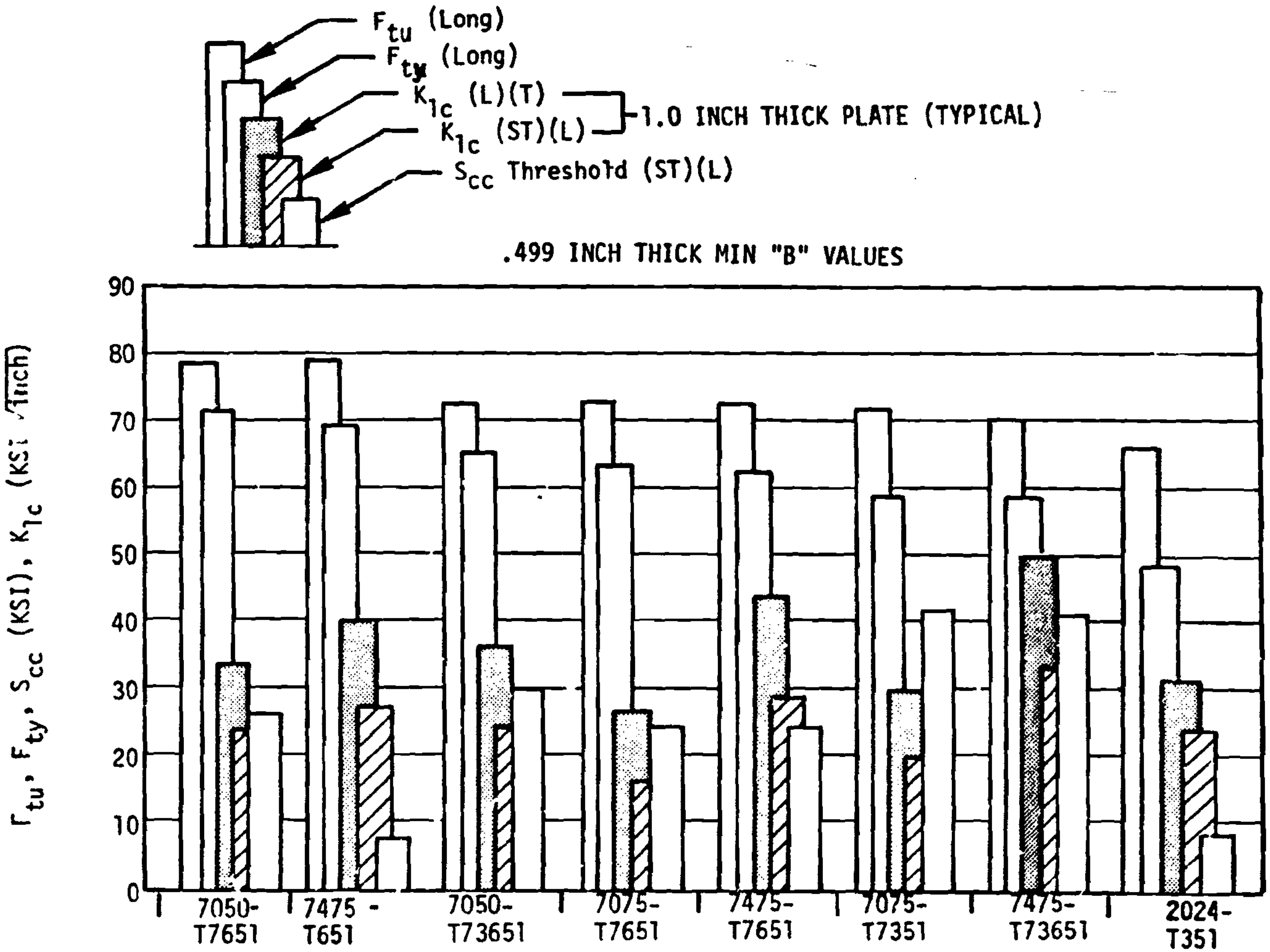

FIGURE 35 COMPARISON OF VARIOUS ALUMINUM ALLOYS' PLATE DESIGN PROPERTIES

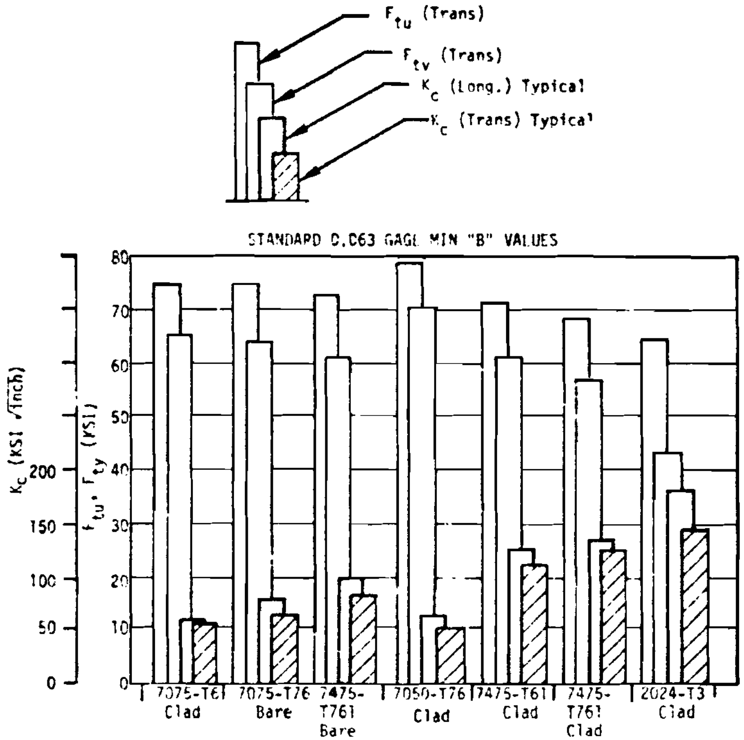

Figure 36 COMPARISON OF VARIOUS ALUMINUM ALLOYS' SHEET DESIGN PROPERTIES

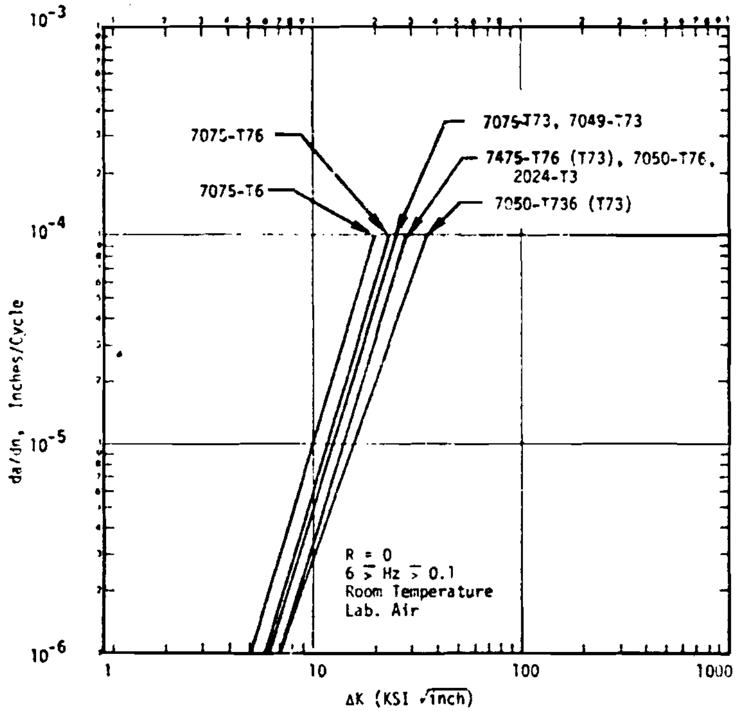

Figure 37 CRACK PROPAGATION CHARACTERISTICS OF ALUMINUM ALLOYS

completely valid comparisons and for damage tolerance analyses; however, preliminary data on thin section material indicates this method of ranking to be informative.

Alloy 7049-T73 was selected for large forgings to make the bulkheads. It is attractive for its high strength and stress corrosion resistance, as the latter property is necessary due to the extensive machining that will expose the short transverse grain to preloads. The alloy 7050-T73 was selected for the spar forgings. Although this temper has not been fully developed for forgings, it is technically feasible but with lower strength, probably equivalent to 7075-T73, and the same high crack propagation resistance exhibited by the other 7050 tempers.

3.3.2 Fuselage

For the Isogrid configuration, 7475-T7351 plate was selected for its high strength, toughness, corrosion resistance, and crack propagation resistance.

For the honeycomb sandwich shell, the alloy 7050-T76 clad was selected over 2024-T3 as it has higher strength, although somewhat lower fracture toughness, particularly at sub-zero temperatures.

For the cargo floor stringers, alloy 7050-T76511 was selected for its higher strength (equal to 7075-T6511), plus the advantages of higher stress corrosion, exfoliation corrosion resistance, toughness and crack propagation resistance. This alloy was selected for all other similar applications of thin extruded stiffeners or spar caps in wings and empennage where machining was minimal and fabrication preloads and other preloads were not above the threshold S_{cc} values.

3.3.3 Empennage

For its previously noted properties, 7050-T76 sheet was chosen for the horizontal and vertical stabilizer box covers. Alloy 7050-T73651 plate was chosen for the bulkheads. These will require substantial machining, and the higher strength compared to 7075-T73 will reduce weight while maintaining a reasonable stress corrosion threshold of 35 KSI and with better toughness.

3.4 MATERIAL DEVELOPMENT EFFORTS REQUIRED

During the course of this study program, several areas of insufficient data and incomplete material or process development were encountered. For the purposes of this study, the information required has been estimated and both this data and other needed developments are considered to be within the possibility of completion in the time frame for the aircraft design.

3.4.1 Beryllium

Serious consideration of beryllium materials in aircraft structure, no matter how attractive the weight reduction feature, is still restricted by the high cost of material and fabrication, and the unacceptability of the transverse ductility in cross-rolled sheet. Slabbed sheet from hot isostatic pressed block has improved ductility, but sheet size from current block is too small for the structural applications in this study.

3.4.2 Compressive Stress - Strain Data

The method of presenting compressive stress strain and tangent modulus curves in MIL-HDBK-5 should be revised to provide useful design information. The typical curves shown are not useful for design. They should be plotted so that the curve reflects the minimum allowable compressive yield stress. The variability of much of the observed data raises a question as to the validity of this information.

3.4.3 Fatigue Crack Retardation Data

Fatigue crack retardation mechanisms are an important aspect of fatigue life cycle characteristics. The properties of alloys vis-a-vis retardation must be known in order to apply it to analysis. Test procedures and data should be determined for this property.

3.4.4 Crack Propagation Tests

The use of current da/dn crack propagation data in damage tolerance analysis should be qualitative in respect to any conclusion. Test procedures have not been standardized, and knowledge of all variables is incomplete.

3.4.5 Resistance Curve Data

Calculations of residual strength by present methods will be overestimated to the extent that an alloy is subject to stable crack growth. Resistance (R) curve data, which is considered a material property, is needed for each alloy to correct the stress intensity factor of the more ductile materials influenced by stable crack propagation. (Resistance is defined as the level of available strain energy release rate required to grow a crack a given amount.)

3.4.6 Improved Fatigue Strength and Crack Propagation Properties

The current development efforts for aluminum alloys, i.e., powder metallurgy, thermo-mechanically working, etc., should be intensified to provide alloys with better fatigue strength and crack propagation properties. The fatigue and damage tolerant design analysis criteria presently being required may invoke weight and cost increases in order to satisfy the existing criteria in some structural design applications using available materials.

3.4.7 Stress Corrosion Resistant Tempers for 7050 Alloy

Current research work on alloy 7050 has ignored the T73 temper mainly because it did not appear to offer any strength advantage over 7075-T73. However, damage tolerance analyses indicate that crack propagation rates may be a limiting factor, in which case 7050-T73 appears to have lower rates than 7075-T73. This characteristic will be necessary for applications such as the forged wing spar which also requires high stress corrosion resistance.

3.4.8 Low Temperature Data for Damage Tolerance Analysis

Increased testing is required to obtain low temperature (-65°F) properties of aircraft structural alloys. Insufficient data is currently available to perform accurate damage tolerance analysis in this operational temperature range.

SECTION IV

STRUCTURAL GEOMETRIES

The basic parameter, other than material, influencing structural weight (and cost) is panel geometry where panel geometry, by definition, includes joining parameters. A broad spectrum of panel geometry options exists; these include the current state-of-the-art solutions and all new (and pertinent) concepts that ingenuity can devise. A geometry selection criteria, analogous to the material selection criteria and based on a consideration of each integrity mode is developed in Section 4.2. The selection criteria are implemented for selected geometry concepts for upper limit and representative geometry conditions in Section 4.3. These data were used for the new panel concept selection and demonstrated the parallelism and significance, relative to material, of the geometry parameter.

4.1 GEOMETRY SELECTION CRITERIA

As previously noted in Section 3.1, development of lighter structural concepts for fixed requirements relies on improved geometry and/or material characteristics for the critical integrity mode(s). For the case where requirements and material are held constant, geometry selection criteria are established directly from the analytical models defining structural capability for each mode. Geometry selection criteria results are summarized in Table XIII. The results are a function of the mode, the associated analysis model and the stipulated ground rules. The required important geometric properties are identified directly or indirectly from the selection criteria parameters. When implemented over a range of geometry candidates, the criteria parameters provide a direct comparison (by mode) of the candidates, e.g., their ranking one to another and the magnitude of weight improvement achieved.

4.2 PANEL GEOMETRY PROPERTIES

Geometry selection parameter limiting and representative characteristics are identified (Table XIV) for a range of readily available geometries associated with each mode. The parameter values calculated are indicative of the relative weight efficiencies (within integrity mode categories) of the geometry options. Additional geometry options (from the literature or other sources) may be added as necessary, this being analogous to additions to the materials list.

The results are generally classical in nature, being what every structural designer and analyst knows intuitively and practices informally. However, it does serve to formally highlight some of the more important geometry parameters, as identified by current analysis models. It should also be recognized that fundamental parameters identified, in many cases, are general in nature and represent a variety of subset geometric considerations. An example of this is K_t which can be influenced by many geometric variables, such as notch radius, specimen width, attachment interference, hole coining, etc., thus providing opportunity for ingenuity and innovation. Finally, the presence (or absence) and relative importance of the parameters are established from the analytical model, maximum model representativeness naturally being desirable.

TABLE XIII PANEL GEOMETRY SELECTION CRITERIA

INTEGRITY MODE		CRITERION (FOR MINIMUM WEIGHT)	REMARKS AND RATIONALE
Ultimate	Tension	$\dfrac{1}{[1 - K_o]_{max}}$	(1) Static strength mode $w = \rho \bar{t} = \rho N_x F = \rho N_x / (1 - K_o) F_{tu}$ w is unit weight = in.^{2} material characteristics ρ, F_{tu} = constant loading requirement N_x = constant failure stress $F = (1 - K_o) F_{tu}$ $f = F$ for margin of safety (M.S.) = 0 K_o = factor for hole out, notch, etc. $\therefore w_{min} \propto 1/(1 - K_o)_{max}$
	Compression	$[L^{\eta-1}/\epsilon]^{1/\eta}_{min}$	(2) Wide column mode plus local instability $w = \rho \bar{t} = [(\rho^{\eta} N_x L^{\eta-1})/(\bar{\eta} E \epsilon)]^{1/\eta}$ (Ref 31) ϵ = geometric efficiency factor η, ϵ = f (section type) L = pin-ended column type $\therefore w_{min} \propto [L^{\eta-1}/\epsilon]^{1/\eta}_{min}$
		$[b^{\eta-1}/\epsilon]^{1/\eta}_{min}$	(3) Panel mode plus local instability $w = \rho \bar{t} = [(\rho^{\eta} N_x b^{\eta-1})/(\bar{\eta} E \epsilon)]^{1/\eta}$ (Ref 31) b = panel width η, ϵ = f (section type) $\therefore w \propto [b^{\eta-1}/\epsilon]^{1/\eta}_{min}$
	Shear	$[b^{\eta-1}/\epsilon]^{1/\eta}_{min}$	(4) Same rationale as (3)

TABLE XIII PANEL GEOMETRY SELECTION CRITERIA (CONTINUED)		
INTEGRITY MODE	**CRITERION (FOR MINIMUM WEIGHT)**	**REMARKS AND RATIONALE**
Fatigue	$[1 + (K_t - 1)/(1 + \frac{\pi}{\pi - \omega}\sqrt{\rho'_f/r})]_{min}$	(5) Fatigue mode $w = \rho\bar{t} = \rho N_x/F_{1g} \propto 1/F_{1g}$ $F_{1g} = F_{max}/(1 + \Delta\eta) \propto F_{max} = S_{\eta_{K_t=x}}$ $S_{\eta_{K_t=x}} = S_{\eta_{K_t=1}}/K_f$ $K_f = 1 + (K_t - 1)/(1 + \frac{\pi}{\pi - \omega}\sqrt{\rho'_f/r})$ $S_{\eta_{K_t=1}}$ = constant (fixed corner edge geometry) ρ'_f = material constant ω, r = notch flank angle and radius $\therefore\ w_{min} \propto [1 + (K_t - 1)/(1 + \frac{\pi}{\pi - \omega}\sqrt{\rho'_f/r})]_{min}$
Flutter Rigidity: Torsion	$\frac{1}{[t_s/t]_{max}}$	(6) Torsion mode $w = \rho\bar{t}$ $\Delta J \propto \Delta A/(b/t_s) \propto t_s/b \propto (t_s/t)/(t/b)$ $G\Delta J$ = constant $\propto G\,(t_s/\bar{t})/(\bar{t}/b)$ $\bar{t} \propto$ (constant) $b/G\,(t_s/\bar{t}) \propto 1/(t_s/\bar{t})$ $w \propto 1/(t_s/\bar{t})$ $\therefore\ w_{min} \propto 1/(t_s/\bar{t})_{max}$
Flutter Rigidity: Bending	None	(7) Bending mode $w = \rho\bar{t}$ EI = constant $\propto E\bar{t}bh^2$ $\bar{t} = I/bh^2$ = constant$/bh^2$ = constant for b, h = constant (configuration geometry) $\therefore\ w$ = constant

TABLE XIII PANEL GEOMETRY SELECTION CRITERIA (CONCLUDED)		
INTEGRITY MODE	**CRITERION (FOR MINIMUM WEIGHT)**	**REMARKS AND RATIONALE**
Damage Tolerance	$[\lambda \sqrt{Aa_i}]_{min}$	(8) Damage tolerance mode $w = \rho \bar{t} = \rho N_{x_{1g}}/F_{1g} \propto 1/F_{1g} \propto 1/F_{max}$ For M.S. = 0, $F_{max} = \sigma_{max}$ $= (\Delta I)\, R_{ct}/(1 - R)\, \lambda \sqrt{Aa}$ initial crack growth conditions contribute the major portion of the period (T). Then $da/dN = C\Delta K^{\eta}/((1 - R)\, K_c - \Delta K)$ $\approx C\Delta K^{\eta}/(1 - R)\, K_c$ $\Delta K \approx [(da/dN)\,(1 - R)\, K_c/C]^{1/\eta}$ but $da/dN \propto 1/T$ $F_{max} \propto [(1 - R)\, K_c/TC]^{1/\eta}$ $[R_{ct}/(1 - R)\, \lambda \sqrt{Aa}]$ $(1 - R)$ = constant K_c = constant (Plane strain or stress) c = constant $F_{max} \propto R_{ct}/(T^{1/\eta})\, \lambda \sqrt{Aa}$ $T \propto T_{req'd}$ η = material constant $F_{max} \propto R_{ct}/\lambda \sqrt{Aa}$ representative initial condition $a = a_i + \Delta a = K_i a_i$ = constant $R_{ct} \approx 1.0,\ K_i$ = constant $\therefore\ w_{min} \propto (\lambda \sqrt{Aa_i})_{min}$

TABLE XIV PANEL GEOMETRY PROPERTIES

INTEGRITY MODE	REPRESENTATIVE OR LIMITING GEOMETRY CHARACTERISTICS	GEOMETRY PARAMETER	RELATIVE WEIGHT	REF
ULTIMATE TENSION	(1) No Holes	$\left(\frac{1}{(1 - K_o)}\right)_{max}$	1.0	
	(2) With Holes (No Pad) r=0.125", 1.25" o.c.		1.25	
	(3) With Holes & Pad (35" o.c.) 1.25t 4" t r=0.125", 1.25" o.c.		1.03	
ULTIMATE COMPRESSION	WIDE COLUMNS[1] (L = 30") (ϵ_{max}) (n)	$\left(\frac{L^{n-1}}{\epsilon}\right)^{1/n}_{min}$		31, 32
	(1) Unstiffened (.823) (3)		10.25	
	(2) Unflanged, Integrally Stiffened (.656) (2)		6.75	
	(3) Zee - Stiffened (.911) (2)		5.64	
	(4) Integral Zee (1.03) (2)		5.41	
	(5) Integral Tee (1.00) (2)		5.47	
	(6) "J" Stiffened (.793) (2)		6.12	
	(7) Straight Y-Tee Stiffened (1.23) (2)		4.94	
	(8) Straight Y Stiffened (.79) (2)		6.18	
	(9) Curved Y-Tee Stiffened (1.23) (2)		4.94	
	(10) Trap Corrugated Semisandwich (.685) (2)		6.60	
	(11) Truss Core Semisandwich (.686) (2)		6.60	
	(12) Semitrap Corrugated Sandwich (.72) (2)		6.42	
	(13) Hat Section Stiffened (.928) (2)		5.70	
	(14) Trapezoidal Corrugation (1.60) (2)		4.33	
	(15) Truss Core Corrugation (1.15) (2)		5.10	
	(16) Semicircle Corrugation Semi Sandwich (.706) (2)		6.50	
	(17) Truss Core Sandwich (.605) (2)		7.01	

TABLE XIV PANEL GEOMETRY PROPERTIES (CONCLUDED)				
INTEGRITY MODE	REPRESENTATIVE OR LIMITING GEOMETRY CHARACTERISTICS	GEOMETRY PARAMETER	RELATIVE WEIGHT	REF
ULTIMATE COMPRESSION	PANELS[2] (b = 30") (ϕ_{max}) (n)			
	(1) Unstiffened (3.62) (3)	$\left(\frac{b^{n-1}}{\epsilon}\right)^{1/n}_{min}$	6.28	
	(2) Unflanged Integral Stiffened (.97) (2.38)		7.22	31
	(3) Zee - Stiffened (1.03) (2.36)		7.00	32
	(4) Truss Core Sandwich (1.108) (2)		5.20	
	(5) Truss Core Semisandwich (.59) (2)		7.12	
	(6) 0°-90° Unflanged Grid (.302) (1)		3.31	
	(7) 0°-90° Tee-Flanged Grid (.88) (1)		1.14	
	(8) ± 45° Unflanged Grid (.628) (1)		1.59	
ULTIMATE SHEAR	PANELS (b = 30")			
	(1) Unstiffened (4.85) (3)		5.70	
	(2) Truss Core Sandwich (1.725) (2)		4.18	
	(3) Corrugated (1.17) (2)		5.06	
FATIGUE	(1) No Holes (K_t = 1)	$1+\left(\frac{K_t - 1}{1+\left(\frac{\pi}{\pi-w}\right)\sqrt{\rho'_f/r}}\right)_{min}$	1.0	
	(2) Notch Flank Angle w = 0, r = 0.125", K_t = 3.0 (i ≐ 0.002", Interference Attachments), p'f = 0.025"		2.38	
DAMAGE TOLERANCE	(1) Crack Arrest, No Holes, a_i = 0.06" (surface) $A = \frac{\pi}{2}$, $\lambda \doteq 1.1$	$\left(\lambda\sqrt{Aa_i}\right)_{min}$	0.34	
	(2) Crack Arrest, With Holes, a_i = 0.02" (through) $A = \pi$, $\lambda \doteq 3.0$		0.75	33
FLUTTER RIGIDITY TORSION	(1) Honeycomb (Core 7#/ft³) 1.5 t_f=0.150	$\left(t_{sk}/\bar{t}\right)_{max}$	1.21	19
	(2) Stiffened Skin		1.50	

1. Wide columns have loaded edges supported. 2. Panels have unloaded edges supported.

SECTION V

STRUCTURAL CONCEPT DEVELOPMENT

5.1 WING BOX STRUCTURE

A large contributor to the weight and cost of an airframe is the wing box structure. The high cost of this component is due to the fabrication of the cover panels and assembly of the structural box. Studies were conducted to develop new wing box structural design concepts with emphasis on the wing box upper and lower cover panels. The goal of the studies was to evolve new concepts which offer reduced weight and equivalent or reduced manufacture costs. The design concepts evaluated in the studies consisted primarily of new geometric arrangements utilizing new materials sized to the long fatigue life, damage tolerance and static strength criteria of the baseline wing box. Emphasis was placed on reducing the number of parts in order to reduce fabrication and assembly costs.

5.1.1 Baseline Design Concept

The baseline wing box structure (Figure 4) is a multi-rib stiffened cover panel design that carries wing bending and torque and serves as a fuel tank outboard to $X_W = \pm 520.00$ inches. The baseline wing upper and lower surfaces (Figures 38 and 39) consist of machine tapered cover skins and "J" section extruded stringers spliced chordwise at the airplane centerline and spanwise at the centerline of stringer number nine (upper surface) and stringer number twenty-nine (lower surface). The stringers are spaced six inches on center, parallel to the rear spar, and are mechanically attached to the skin. Skin material for the baseline design concept upper cover panel is 7050-T76 sheet. The material selected for the lower cover panel is 7475-T76 sheet. The stringer material is 7050-T76 aluminum extrusion. Spar caps are machined 7050-T76 extrusions that are spliced at the airplane centerline. Spars, bulkheads and ribs consist of machined extruded caps and stiffened sheet webs.

5.1.2 New Design Concepts

New design concepts involving different geometric arrangements of structure for the wing box were considered. Basic wing concepts investigated were the multi-rib and multi-shear web arrangements. The multi-rib box, such as the baseline component (Figure 4), utilizes chordwise ribs between spars for lateral support of the cover panels. The wing panel air loads and wing bending crushing loads from the cover panels are transferred to the ribs and transmitted by the ribs to the spars. The multi-shear web box (Figure 40) utilizes spanwise members between the upper and lower cover panels to stabilize the panels. Bulkheads or intercostals are required where: 1) high chordwise loads are introduced from the engine support pylon, flap, aileron; and 2) at fuel tank internal boundaries.

Initial layouts of the wing box for the C-15 indicated that, for weight efficiency, the most promising structural arrangement was the multi-rib wing box. The multi-shear web box was handicapped due to the large number of bulkheads or intercostals also required. Early studies also indicated steel and titanium

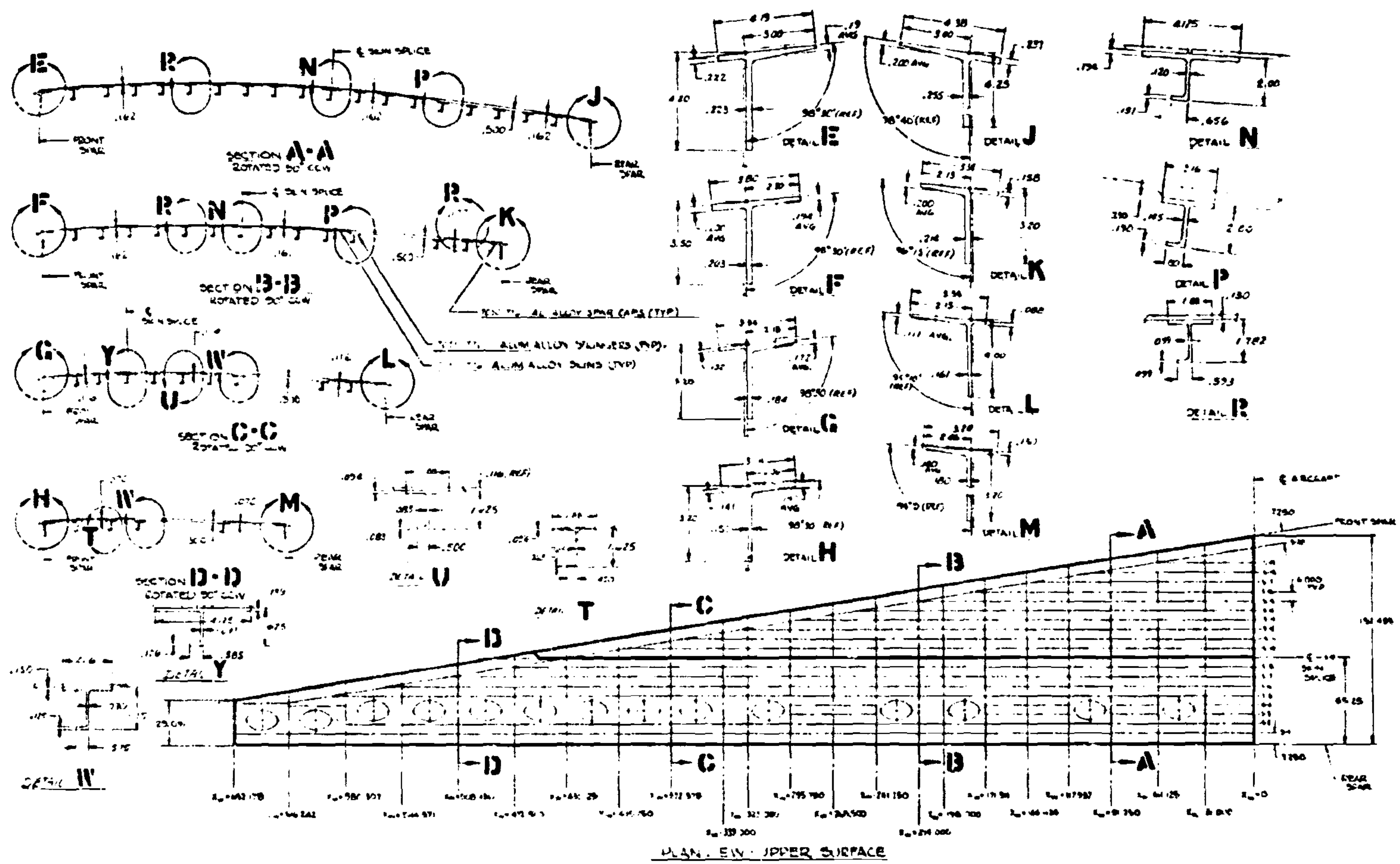

Figure 38 BASELINE WING UPPER COVER PANEL STRUCTURE

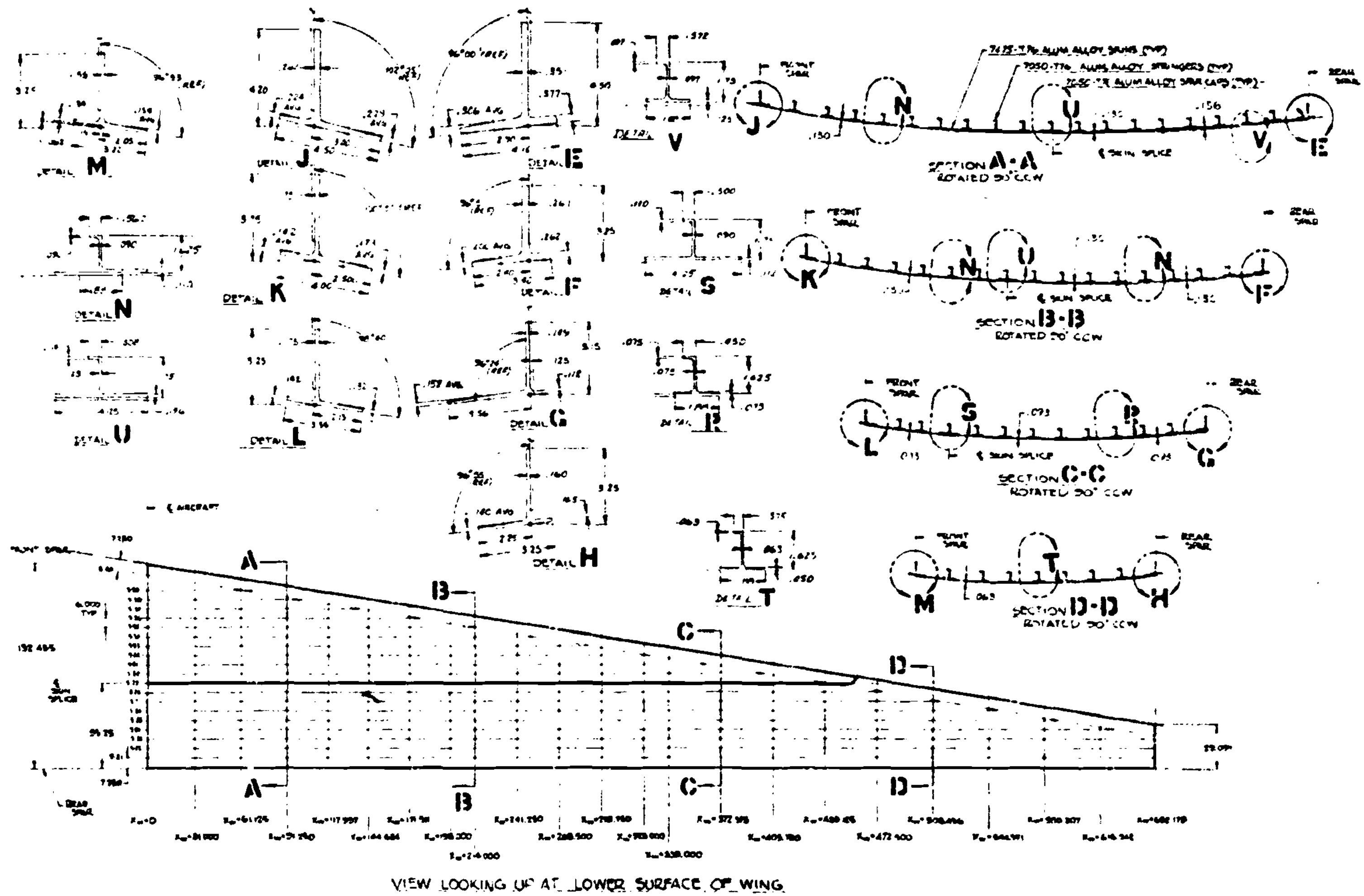

Figure 39 BASELINE WING LOWER COVER PANEL STRUCTURE

alloy materials were less efficient from a weight standpoint than the aluminum alloys because of the low load intensities and the moderate temperature environment on the wing. The advantage of steel and titanium alloys as wing box materials could be in the use of advanced joining techniques such as diffusion bonding, fusion welding, or other advanced welding tecnniques.

5.1.2.1 Wing Box Cover Panels - Emphasis was placed on the wing box upper and lower cover panels in the studies due to their influence on the total wing box cost and weight. Computer-aided parametric studies were conducted to evaluate weight efficiencies of the baseline design concept, and selected new design concepts for a load environment representative of the C-15 STOL Transport. The primary design concepts investigated were stiffened panels and honeycomb sandwich panels. Other concepts considered were: 1) corrugated unidirectional core sandwich panels, 2) integrally machined sandwich panels, 3) selective-reinforced stiffened panels, 4) stiffened honeycomb sandwich panels, and 5) beryllium "egg-crate" sandwich panels. Materials investigated were aluminum, titanium, stainless steel, and beryllium.

The materials and material combinations shown in Table XV were evaluated for weight efficiency at compressive load intensities starting with 2000 pounds per inch and ranging up to 16000 pounds per inch. Stress-strain-tangent modulus curves used in the studies were generated for the materials of Table XV by a modified Ramberg-Osgood equation. A typical computer drawn curve is shown in Figure 41 for 7050-T7651 aluminum alloy. The Ramberg-Osgood equation modification is in Appendix B along with all the compressive stress-strain-modulus curves for the materials considered in this study.

Integrally (flanged) and zee-stiffened skin panels were selected as the most efficient stiffened panel concepts in compression. In the studies, panel length was arbitrarily set at thirty (30) inches to provide accessibility for manufacture and repair. Stiffening ratio (area of skin-to-area of stiffener) was selected as 50 percent in order to provide adequate skin for resisting torsion and adequate stiffener to prevent rapid skin crack growth. A stringer spacing of 3.5 inches was selected as minimum for the integrally stiffened design concept in order to provide sufficient space to attach ribs and bulkheads to the cover panels. Parametric studies were conducted to evaluate the effect of constraining panel length, stiffening ratio, and stringer spacing on panel weight and on the overall wing box design.

Panel weight was determined for an integrally stiffened panel from the optimum design analysis presented in Reference 34. From this analysis, the structural index is determined to be

$$\frac{N_x}{L'} = 0.584 \left(\frac{[\sigma_g]^2}{4\sqrt{E E_T{}^3}} \right) \left(\frac{\left[1 + \frac{A_S}{A_{SK}} \right]^2}{\frac{A_S}{A_{SK}} \left[4.573 + \left(\frac{A_S}{A_{SK}} \right) \left(\frac{b_s}{b_e} \right) \right]^{1/2}} \right) \qquad (2)$$

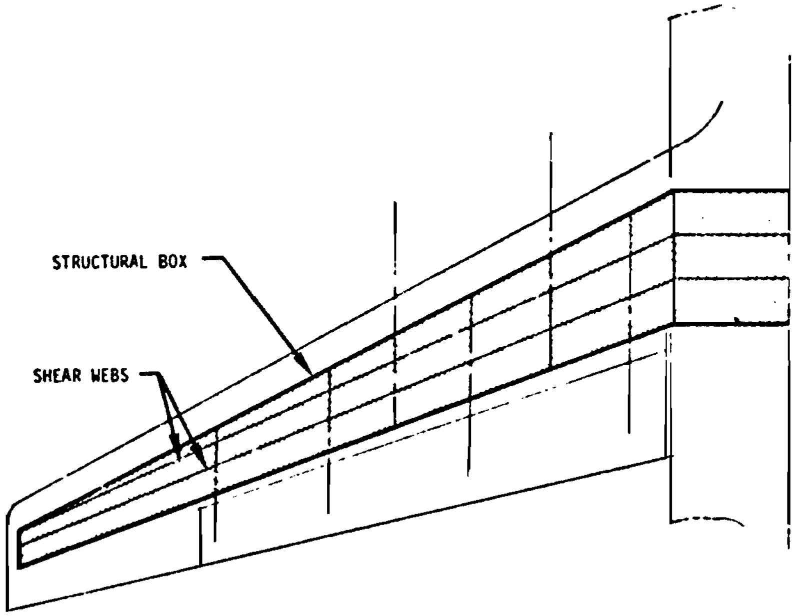

Figure 40 MULTISHEAR WEB WING BOX CONCEPT

TABLE XV WING COVER PANEL DESIGN CONCEPTS EVALUATED

Zee Stiffened Design Concepts	
Concept Number	**Materials**
1	7075-T76 Aluminum Skin 7075-T6511 Aluminum Extrusion
2	7475-T761 Aluminum Skin 7075-T6511 Aluminum Extrusion
3	7050-T76 Aluminum Skin 7075-T6511 Aluminum Extrusion
4	7050-T76 Aluminum Skin Ti-6Al-4V Annealed Titanium Extrusion
5	7075-T76 Aluminum Skin 9 Ni-4Co-.20C Steel Extrusion
6	Beryllium Cross Rolled Sheet Skin Beryllium Extrusion-
7	Beryllium Cross Rolled Sheet Skin Ti-6Al-4V Annealed Titanium Extrusion
8	Ti-6Al-4V STA Titanium Skin Beryllium Extrusion
9	Ti-6Al-4V STA Titanium Skin Ti-6Al-4V Annealed Titanium Extrusion
Integrally (Flanged) Stiffened Design Concept	
Concept Number	**Materials**
1	7050-T7651 Aluminum Plate
2	7475-T761 Aluminum Plate
3	Beryllium Plate
4	Ti-6Al-4V Titanium

This equation is derived based on the assumptions that at the applied stress level, local buckling and column buckling occur simultaneously. Maximum panel efficiency for fully effective skin ($b_s = b_e$) is obtained for a stiffening ratio $\frac{A_s}{A_{s_k}} = 1.25$. A non-optimum stiffening ratio of 0.4 was selected for integrally stiffened structure. With the assumption that $\frac{A_s}{A_{sk}} = 0.4$ and $b_s/b_e = 1.0$, the structural index is

$$\frac{N_x}{L'} = 1.28 \left(\frac{[\sigma_g]^2}{4\sqrt{EE_T{}^3}} \right) \tag{3}$$

For constant values of effective panel length, panel weight per unit or surface area can be plotted against load intensity since weight is a function of material density, stress level and load intensity, as defined by the equation

$$W = \left(\frac{N_x}{\sigma_g} \right) \rho \tag{4}$$

Intercostal weight added to their weight was obtained from stiffness criteria. These criteria are given in Reference 31 as

$$E_R I_R = 4 \left(\frac{N_x}{L'} \right) \left(\frac{B}{\pi} \right)^4 \tag{5}$$

For a channel type intercostal, the moment of inertia is given in terms of the caps and web by the approximate equations.

$$I_R = \frac{h^2}{2} \left(A_c + \frac{th}{6} \right) \tag{6}$$

Total intercostal area is determined as the sum of cap and web area,

$$A_R = 2\,A_c + th \tag{7}$$

Cap area from this equation is substituted into the moment of inertia equation to give the equation

$$I_R = \frac{h^2}{2}\left(\frac{A_R}{2} - \frac{th}{3}\right) \tag{8}$$

This equation is introduced into the stiffness criteria. Total intercostal area is determined to be

$$A_R = 16\left(\frac{N_x}{L'}\right)\left(\frac{B}{\pi}\right)^4\left(\frac{1}{E_R h^2}\right) + \frac{2th}{3} \tag{9}$$

For a bending section, maximum h/t ratio for the web is dictated by stability considerations. If h/t is assumed equal to 50, then intercostal area is

$$A_R = 16\left(\frac{N_x}{L'}\right)\left(\frac{B}{\pi}\right)^4\left(\frac{1}{E_R h^2}\right) \cdot \frac{h^2}{75} \tag{10}$$

Minimum intercostal area for constant N_x/L' and E_R is found by taking the derivative of this equation with respect to intercostal depth and setting the result equal to zero. Then, the resulting equation for the optimum intercostal depth is

$$h_{(opt)} = \left[1200\left(\frac{N_x}{L'}\right)\left(\frac{B}{\pi}\right)^4\left(\frac{1}{E_R}\right)\right]^{1/4} \tag{11}$$

Substituting this value of h into the rib area equation results in the following equation for minimum intercostal area

$$(A_R)_{min} = 0.0936\ (B)^2\left(\frac{N_x}{L'}\right)^{1/2}\left(\frac{1}{E_R}\right)^{1/2} \tag{12}$$

Intercostal $\bar{t}$ is obtained by spreading the area out over the entire panel length. Weight per unit of surface area is obtained as the product of $\bar{t}$ and intercostal material density,

$$W_R = \left(\frac{(A_R)_{min}}{L}\right) \rho_R \tag{13}$$

When this weight is added to panel weight, total compressive surface weight is obtained. These equations were used to investigate the effect of geometric and material constraints on panel weight.

Panel and intercostal weight, Figure 42, is shown as a function of compressive load intensity for representative materials from each family of materials investigated. The maximum axial load on the STOL aircraft is about 11,000 pounds per inch. Based on interaction, the equivalent uniaxial design load can be as high as 13,000 pounds per inch. In any case, aluminum and beryllium are shown to be the lightest materials for compression surface application as opposed to steel and titanium.

Figure 43 shows the panel and intercostal weight as a function of compressive stress for parametric variations of panel width, B. Panel load intensity was held constant at 15,000 pounds per inch. The curves are for integrally stiffened panels made from 7075-T76 aluminum sheet. Panel length as a function of panel stress is also shown on Figure 43. For ribs designed solely to support the cover panels, lightening holes are put in the ribs. Panel stiffness is provided by rib caps which bridge the lightening holes. Typical hole diameter runs between 20 and 30 inches. For a twenty inch diameter hole, B = 20 inches, minimum weight is shown in Figure 43 to correspond to a twenty inch panel length. For a thirty inch panel length constraint, there is a 2.0 percent increase in box weight.

Figure 44 is a plot of stress-to-density ratio for integrally stiffened panels made from 7075-T6 aluminum alloy. Stiffening ratio is held constant at 40%. The ratio of skin width-to-skin effective width, b_s/b_e, is varied along with structural index, P_1/L', and effective area stress, σ_e. For the STOL transport, structural index at the root is about 490. For a constant rib spacing of 30 inches (24.5 inches effective), the structural index decreases to 130 at X_w = 508 inches which corresponds to minimum gage load intensity, as shown by the shaded area of Figure 44. The average structural index over this span is about 360. The ratio, b_s/b_e, at this value of structural index is 1.3 for a 3.5 inch stringer spacing. Thus, on the average, a 6-7% weight penalty is paid for constraining the stringer spacing to 3.5 inches.

The compressive stiffening ratio of 50% is off of optimum based on analysis, which considers only local and Euler-Engesser buckling. As previously noted, the optimum stiffening ratio is 125%. However, when torsional buckling

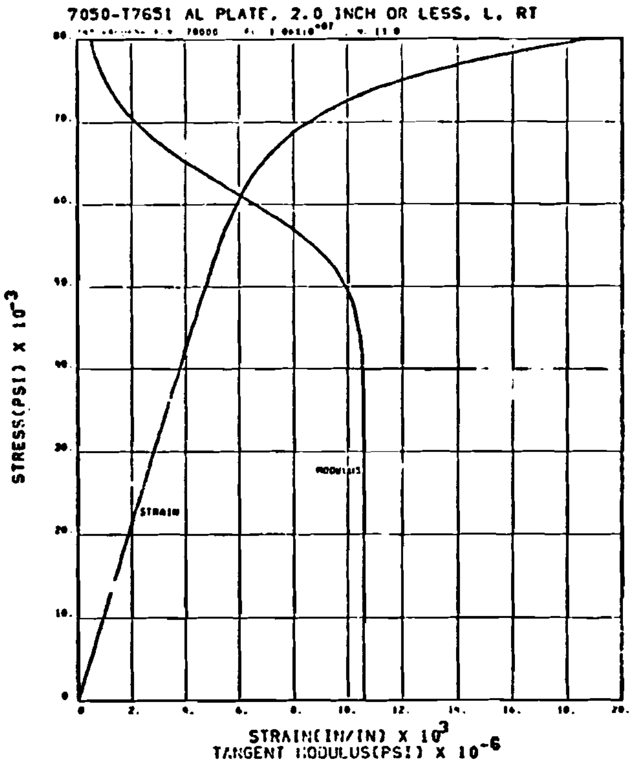

Figure 41 COMPUTER DRAWIN STRESS-STRAIN-TANGENT MODULUS CURVE FOR 7050-T7651 ALUMINUM ALLOY

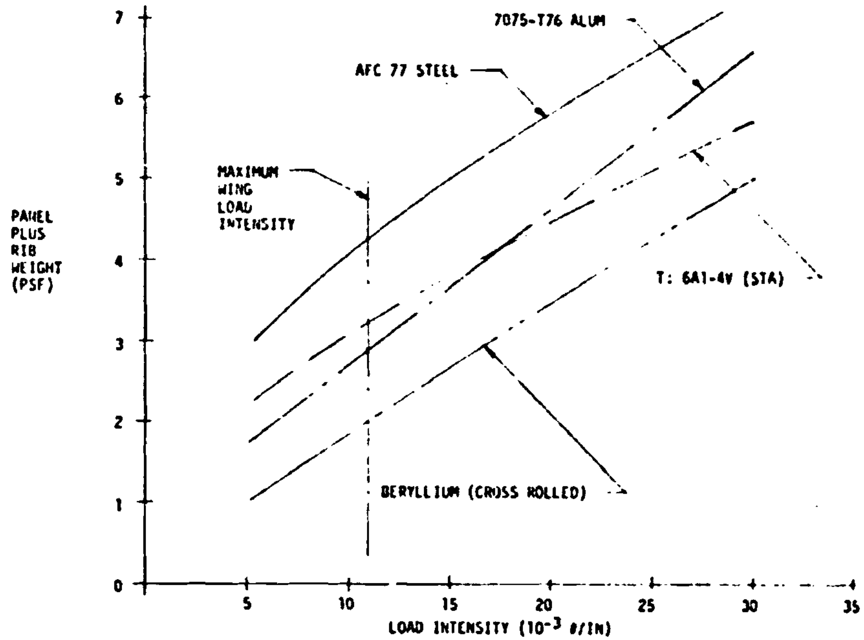

Figure 42 WEIGHT COMPARISON OF VARIOUS MATERIALS FOR INTEGRALLY STIFFENED SKIN PANELS

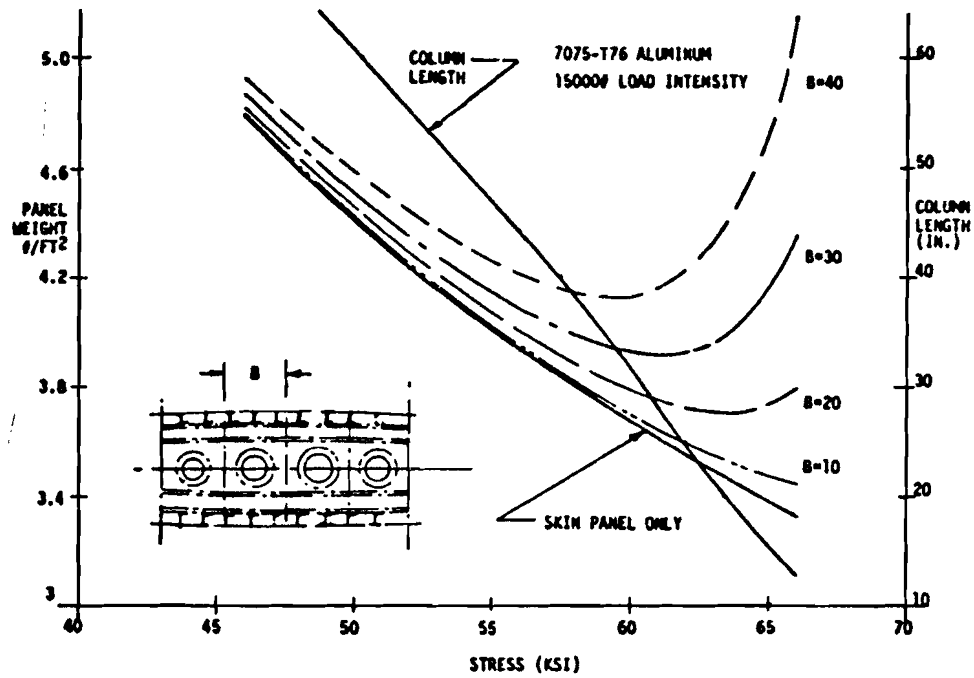

Figure 43 INTEGRALLY STIFFENED PANEL WEIGHT STUDY

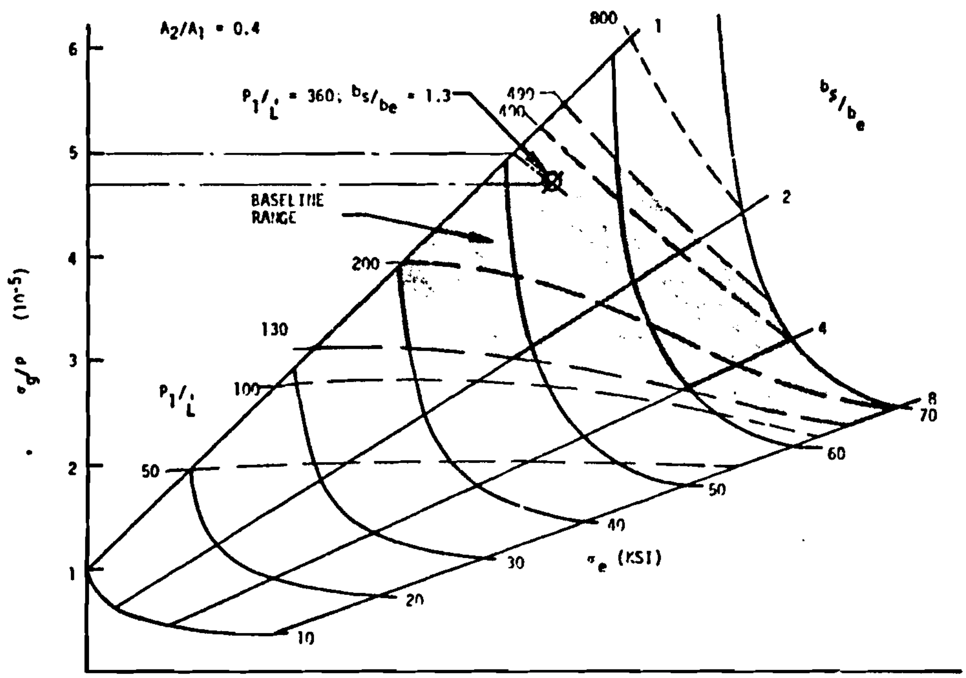

Figure 44 STRESS TO DENSITY RATIO FOR INTEGRALLY STIFFENED 7075-T6 PANELS

requirements are imposed on this optimum solution, the stiffening ratio for minimum weight is decreased. This is shown graphically in Figure 45 for an integrally stiffened panel under an applied load intensity of 12,000 pounds per inch and a constant stringer spacing of 3.5 inches. Panel weight is plotted as a function of stiffening ratio. When torsional buckling constraints are imposed, there is little penalty for a 50% stiffening ratio.

The weight curves of Figures 46, 47 and 48 show the effects of uniaxial compressive load intensity on integrally (flanged) stiffened and zee-stiffened skin panels when variations are made in material combinations and stringer spacing. The weight efficiency of the baseline J-stiffened skin panel design concept is also shown on the curves for comparison. The uniaxial results were obtained by computer programs, Reference 35, that are based on the assumptions that optimum design is obtained when the failure modes of local and panel instability occur simultaneously at the applied stress level. A constant strain approach is taken to account for variations in skin and stringer materials. Provisions are made in the program for non-optimum factors such as buckled skin, minimum skin gage, and minimum column length. The solution (section dimensions, section properties, material properties and panel weight) is graphically presented in Figure 49. The solution is for a compressive load intensity of 10,000 pounds per inch for: 1) the baseline design concept, 2) the integrally (flanged) stiffened design concept, and 3) the zee-stiffened design concept for skin panels of three different materials. They were also obtained for the remaining material combinations and load intensities.

Figure 50 shows a weight comparison for 7475-T761 aluminum alloy integrally stiffened skin panels at room temperature as a function of uniaxial compression stress. Weight includes the associated intercostal weight that is required for panel column support stiffness. This weight is based on the assumption that the intercostal has stiffeners spaced at 20 inches.

The effect of intercostal spacing on combined panel and intercostal weight is shown in Figure 51. Load intensity is varied from 2,000 to 12,000 pounds per inch. Optimum stress level ranges from 45,000 psi to 62,000 psi depending on the load intensity. Similarly, optimum panel spacing varies from about 10 to 20 inches. At 12,000 pounds per inch, there is little difference between the weight at optimum spacing and the weight at 30 inch spacing. The penalty becomes greater as the load intensity decreases when the skin is required to be fully effective. From a cost point of view, the maximum possible spacing with a small weight penalty should be chosen to eliminate parts. This spacing may be restricted, however, because of normal pressure caused by crash and overpressure fuel requirements in the wing.

Computer-aided analysis of honeycomb sandwich panels considered such items as: 1) adhesive system for the face to core joining of aluminum material, 2) dense core edge strips, and 3) mechanical fasteners along the edges. The weight of the adhesive material was assumed to be 0.13 pounds per square foot. Core density was set at 5 pounds per cubic foot. Fastener and edge strips were assumed to be 3/16 inch diameter aluminum and 1.5 inch wide aluminum core of 25 pounds per cubic foot, respectively. Basic panel core depths were established from an equation developed in Reference 36 for the design of infinitely long flat rectangular sandwich panels under edgewise compression.

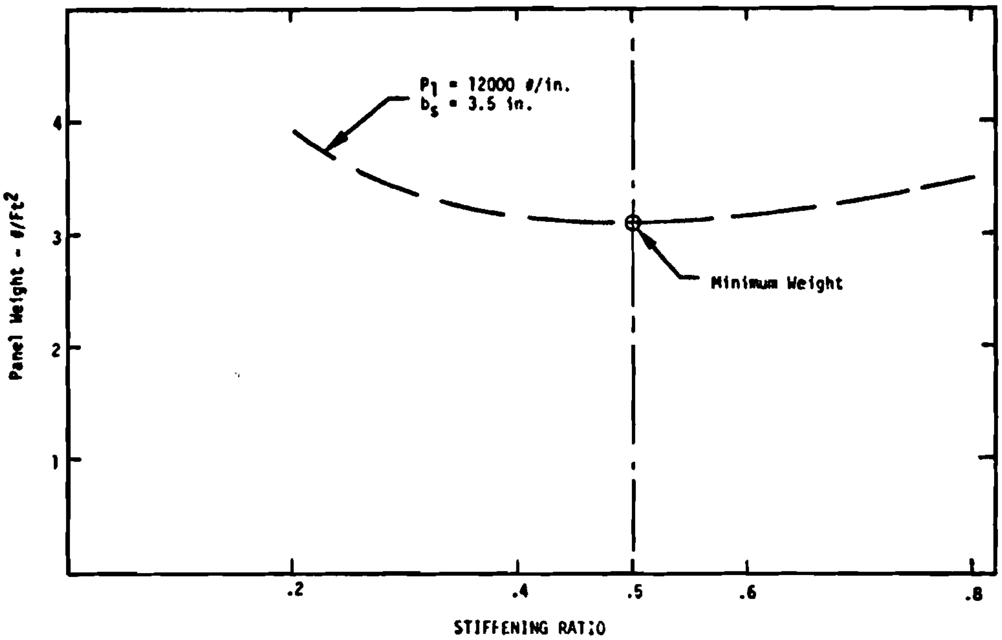

Figure 45 PANEL WEIGHT VS. STIFFENING RATIO

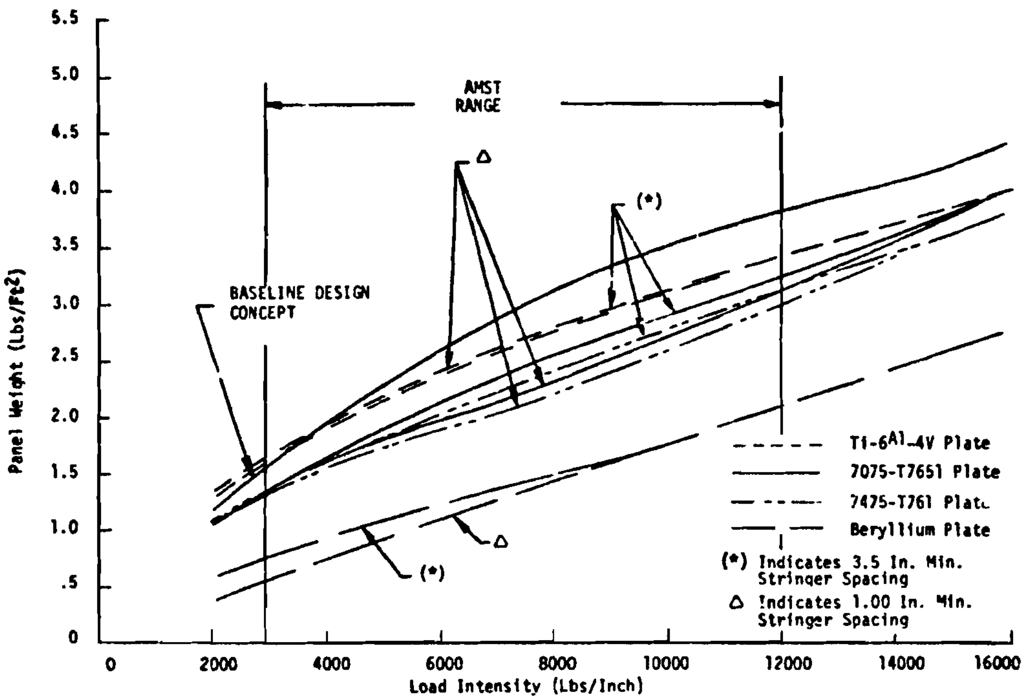

Figure 46 WEIGHT COMPARISON OF INTEGRALLY STIFFENED COMPRESSION PANEL CONCEPTS

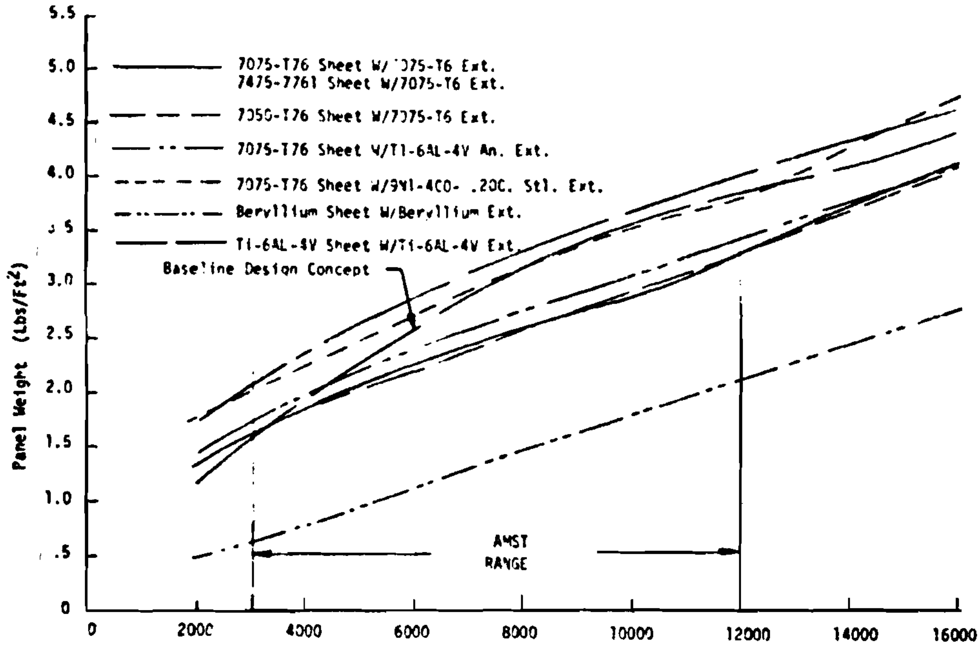

Figure 47 WEIGHT COMPARISON OF Z-STIFFENED COMPRESSION PANEL CONCEPTS (1.0 IN. MIN. SPACING)

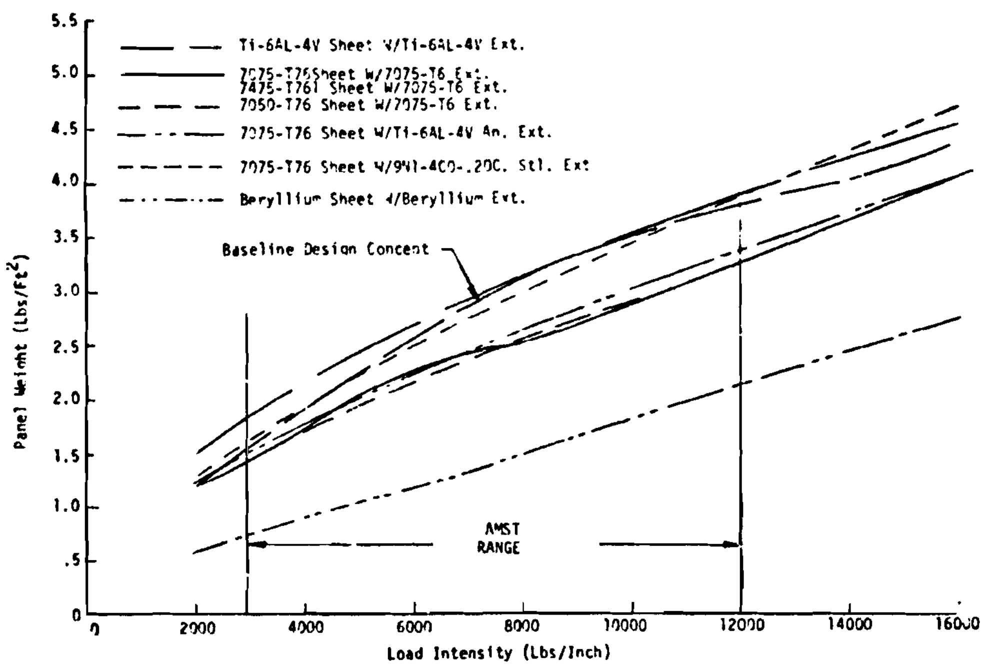

Figure 48 WEIGHT COMPARISON OF Z-STIFFENED COMPRESSION PANEL CONCEPTS (3.5 IN. MIN. SPACING)

NEW DESIGN CONCEPTS

ALUMINUM

Z-STIFFENED COMPRESSION PANEL

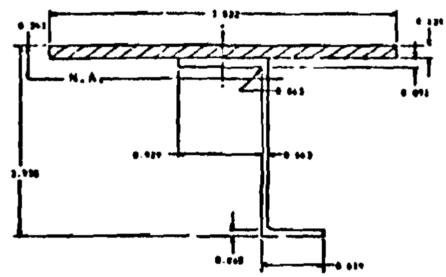

[illegible]	[illegible]	[illegible]	[illegible]
[illegible]	[illegible]	[illegible]	[illegible]
[illegible]	[illegible]		
[illegible]	[illegible]		
[illegible]		[illegible]	
[illegible]	[illegible]	[illegible]	[illegible]
[illegible]	[illegible]	[illegible]	[illegible]
[illegible]	[illegible]	[illegible]	[illegible]
[illegible]	[illegible]	[illegible]	[illegible]
[illegible]	[illegible]	[illegible]	[illegible]

* [illegible]

ALUMINUM

INTEGRAL (FLANGED) COMPRESSION PANEL

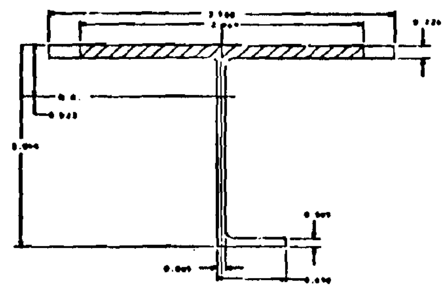

[illegible]	[illegible]	[illegible]	[illegible]
[illegible]	[illegible]	[illegible]	[illegible]
[illegible]	[illegible]		
[illegible]	[illegible]		
[illegible]		[illegible]	
[illegible]	[illegible]	[illegible]	[illegible]
[illegible]	[illegible]	[illegible]	[illegible]
[illegible]	[illegible]	[illegible]	[illegible]
[illegible]	[illegible]	[illegible]	[illegible]
[illegible]	[illegible]	[illegible]	[illegible]

* [illegible]

BASELINE DESIGN CONCEPT

J-STIFFENED COMPRESSION PANEL

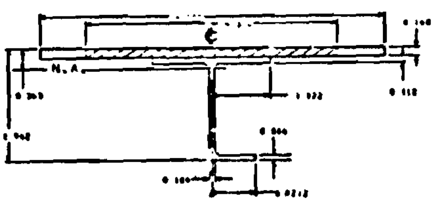

[illegible]	[illegible]	[illegible]	[illegible]
[illegible]	[illegible]	[illegible]	[illegible]
[illegible]	[illegible]		
[illegible]	[illegible]		
[illegible]		[illegible]	
[illegible]	[illegible]	[illegible]	[illegible]
[illegible]	[illegible]	[illegible]	[illegible]
[illegible]	[illegible]	[illegible]	[illegible]
[illegible]	[illegible]	[illegible]	[illegible]
[illegible]	[illegible]	[illegible]	[illegible]

* [illegible]

Figure 49 COMPRESSION PANEL DESIGN

NEW DESIGN CONCEPTS

BERYLLIUM
Z-STIFFENED COMPRESSION PANEL

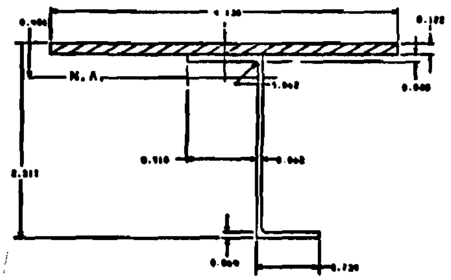

DESIGN REQUIREMENTS

LOAD INTENSITY (LBS/IN).....	[illegible]	GROSS AREA STIFFENING RATIO....	[illegible]
MAXIMUM STRAIN (IN/IN)......	[illegible]	COLUMN LENGTH (IN)............	[illegible]
SKIN.......	BERYLLIUM SHEET		
STRINGER...	BERYLLIUM [illegible]		

MATERIAL PROPERTIES		GEOMETRIC PROPERTIES	
WORKING STRAIN (IN/IN)......	[illegible]	MOMENT OF INERTIA..............	[illegible]
EFFECTIVE STRESS (PSI)......	[illegible]	EFFECTIVE AREA (SQ. IN)........	[illegible]
EFFECTIVE MODULUS	[illegible]	RADIUS OF GYRATION (IN)........	[illegible]
SKIN STRESS (PSI)...........	[illegible]	COLUMN LENGTH (IN).............	[illegible]
STRINGER STRESS (PSI).......	[illegible]	PANEL WEIGHT (LBS/SQ. FT).......	[illegible]

* FILLET AREA NOT INCLUDED IN ANALYSIS

TITANIUM
Z-STIFFENED COMPRESSION PANEL

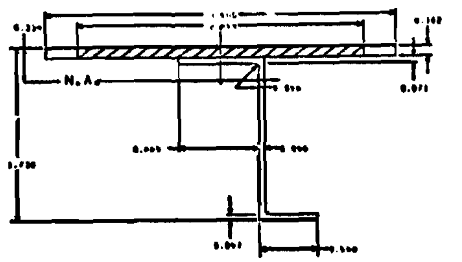

DESIGN REQUIREMENTS

LOAD INTENSITY (LBS/IN).....	[illegible]	GROSS AREA STIFFENING RATIO....	[illegible]
MAXIMUM STRAIN (IN/IN)......	[illegible]	COLUMN LENGTH (IN)............	[illegible]
SKIN.......	[illegible]		
STRINGER...	[illegible]		

MATERIAL PROPERTIES		GEOMETRIC PROPERTIES	
WORKING STRAIN (IN/IN)......	[illegible]	MOMENT OF INERTIA..............	[illegible]
EFFECTIVE STRESS (PSI)......	[illegible]	EFFECTIVE AREA (SQ. IN)........	[illegible]
EFFECTIVE MODULUS...........	[illegible]	RADIUS OF GYRATION (IN)........	[illegible]
SKIN STRESS (PSI)...........	[illegible]	COLUMN LENGTH (IN).............	[illegible]
STRINGER STRESS (PSI).......	[illegible]	PANEL WEIGHT (LBS/SQ. FT).......	[illegible]

* FILLET AREA NOT INCLUDED IN ANALYSIS.

BERYLLIUM
INTEGRAL (FLANGED) COMPRESSION PANEL

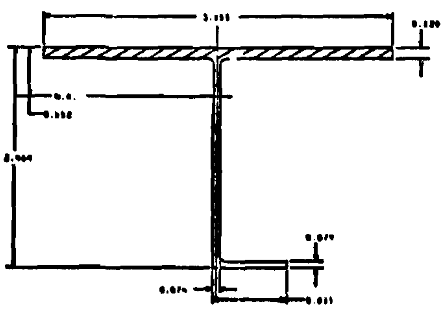

DESIGN REQUIREMENTS

LOAD INTENSITY (LBS/IN).....	[illegible]	STIFFENING RATIO...............	[illegible]
MAXIMUM STRAIN (IN/IN)......	[illegible]	COLUMN LENGTH (IN)............	[illegible]
SKIN.......BERYLLIUM PLATE			
STRINGER...BERYLLIUM PLATE			

MATERIAL PROPERTIES		GEOMETRIC PROPERTIES	
WORKING STRAIN (IN/IN)......	[illegible]	MOMENT OF INERTIA..........	[illegible]
EFFECTIVE STRESS (PSI)......	[illegible]	EFFECTIVE AREA (SQ. IN)....	[illegible]
EFFECTIVE MODULUS...........	[illegible]	RADIUS OF GYRATION (IN)....	[illegible]
SKIN STRESS (PSI)...........	[illegible]	COLUMN LENGTH (IN).........	[illegible]
STRINGER STRESS (PSI).......	[illegible]	PANEL WEIGHT (LBS/SQ. FT)....	[illegible]

* FILLET AREA NOT INCLUDED IN ANALYSIS.

TITANIUM
INTEGRAL (FLANGED) COMPRESSION PANEL

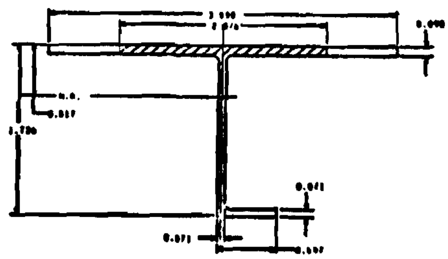

DESIGN REQUIREMENTS

LOAD INTENSITY (LBS/IN).....	[illegible]	STIFFENING RATIO...............	[illegible]
MAXIMUM STRAIN (IN/IN)......	[illegible]	COLUMN LENGTH (IN)............	[illegible]
SKIN.... [illegible]			
STRINGER...[illegible]			

MATERIAL PROPERTIES		GEOMETRIC PROPERTIES	
WORKING STRAIN (IN/IN).....	[illegible]	MOMENT OF INERTIA...........	[illegible]
EFFECTIVE STRESS (PSI).....	[illegible]	EFFECTIVE AREA (SQ. IN).....	[illegible]
EFFECTIVE MODULUS..........	[illegible]	RADIUS OF GYRATION (IN).....	[illegible]
SKIN STRESS (PSI)..........	[illegible]	COLUMN LENGTH (IN)..........	[illegible]
STRINGER STRESS (PSI)......	[illegible]	PANEL WEIGHT (LBS/SQ. FT)....	[illegible]

* FILLET AREA NOT INCLUDED IN ANALYSIS.

Figure 49 COMPRESSION PANEL DESIGN -- Concluded

$$\frac{F_c \lambda}{E'} = \pi^2 \left(\frac{h}{b}\right)^2 \tag{14}$$

A modified compression modulus was used for stress values above the proportional limit of the material

$$E' = (EE_T)^{1/2} \tag{15}$$

Figure 52 shows the weights of honeycomb sandwich panels at room temperature as a function of compressive face stress. Effects of variation in load intensity for a 40 inch panel width are shown. As stress is increased, face thickness decreases; but core depth increases for general instability requirements at constant width. At a stress of 60-65,000 psi, edge weight begins to dominate the weight equation due to excessive depth of core. Below this stress, the face weight is dominant. The optimum stress is shown to be about 65,000 psi · a 40 inch wide aluminum panel at 12,000 pounds per inch load intensity. The corresponding core depth is about 1.2 inches. At this stress, face wrinkling and dimpling are not critical failure modes for a core density of 5 pounds per cubic foot.

The honeycomb panel, shown in Figure 53, is a feasible concept for the wing box upper cover panel. This arrangement has two spanwise shear webs to reduce panel width and weight, as width is the critical dimension for panel stability.

The load intensities for the wing panel are above those for an efficient sandwich concept. Likewise, the spanwise shear webs are not compatible structure for the stiffened skin concept of the lower cover panel. Consequently, this concept was not considered as a prime candidate for the wing structure. However, this concept was found to be most efficient for the load intensities of the empennage structural boxes and is described in detail in paragraphs 5.3 and 5.4.

A design concept that was considered for the wing box cover panels is the corrugated unidirectional core concept shown in Figure 54. This design permits the core as well as the face sheets to resist the uniaxial loads in the panel. Parametric studies were conducted to evaluate the weight efficiency of this concept utilizing aluminum and titanium materials. However, only titanium could be utilized when considering the concept for flash welding (Figure 54).

Figure 55 compares the weight efficiency of the corrugated unidirectional core sandwich design concept with the honeycomb sandwich skin panels, and the zee-stiffened panels with the integrally (flanged) stiffened panel design concept. The unidirectional corrugated core and honeycomb sandwich represent multi-shear web design concepts and a valid comparison may be made between the two. The panels were sized for compressive load intensities starting at 2,000 pounds per inch and ranging up to 16,000 pounds per inch. Materials selected were 7075-T6 aluminum alloy sheet and Ti-6Al-4V titanium annealed sheet. Honeycomb core density was 5 pounds/ft^3. Panel width was 30 inches. The weight curves for the honeycomb sandwich concept reflect the additional weight of edge treatment (spanwise at the panel edges and chordwise across

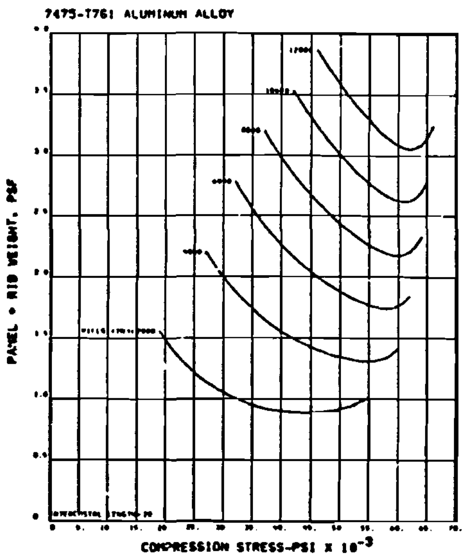

Figure 50 WEIGHT COMPARISON FOR 7475-T761 ALUMINUM ALLOY INTEGRALLY STIFFENED SKIN PANEL

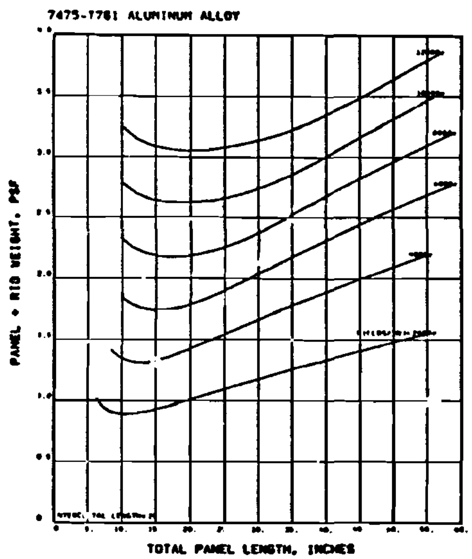

Figure 51 EFFECT OF INTERCOSTAL SPACING ON COMBINED PANEL AND INTERCOSTAL WEIGHT

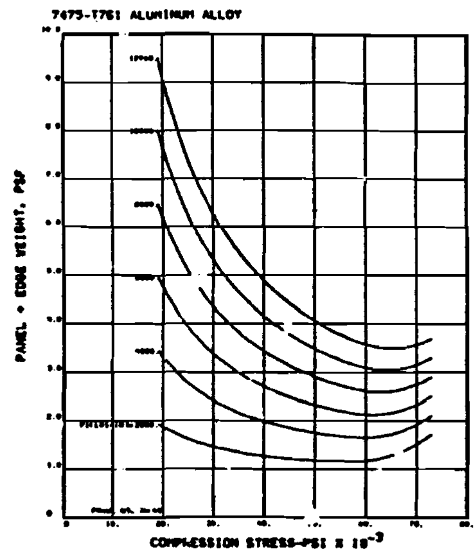

Figure 52 WEIGHTS OF HONEYCOMB SANDWICH PANELS AS A FUNCTION OF COMPRESSIVE FACE STRESS

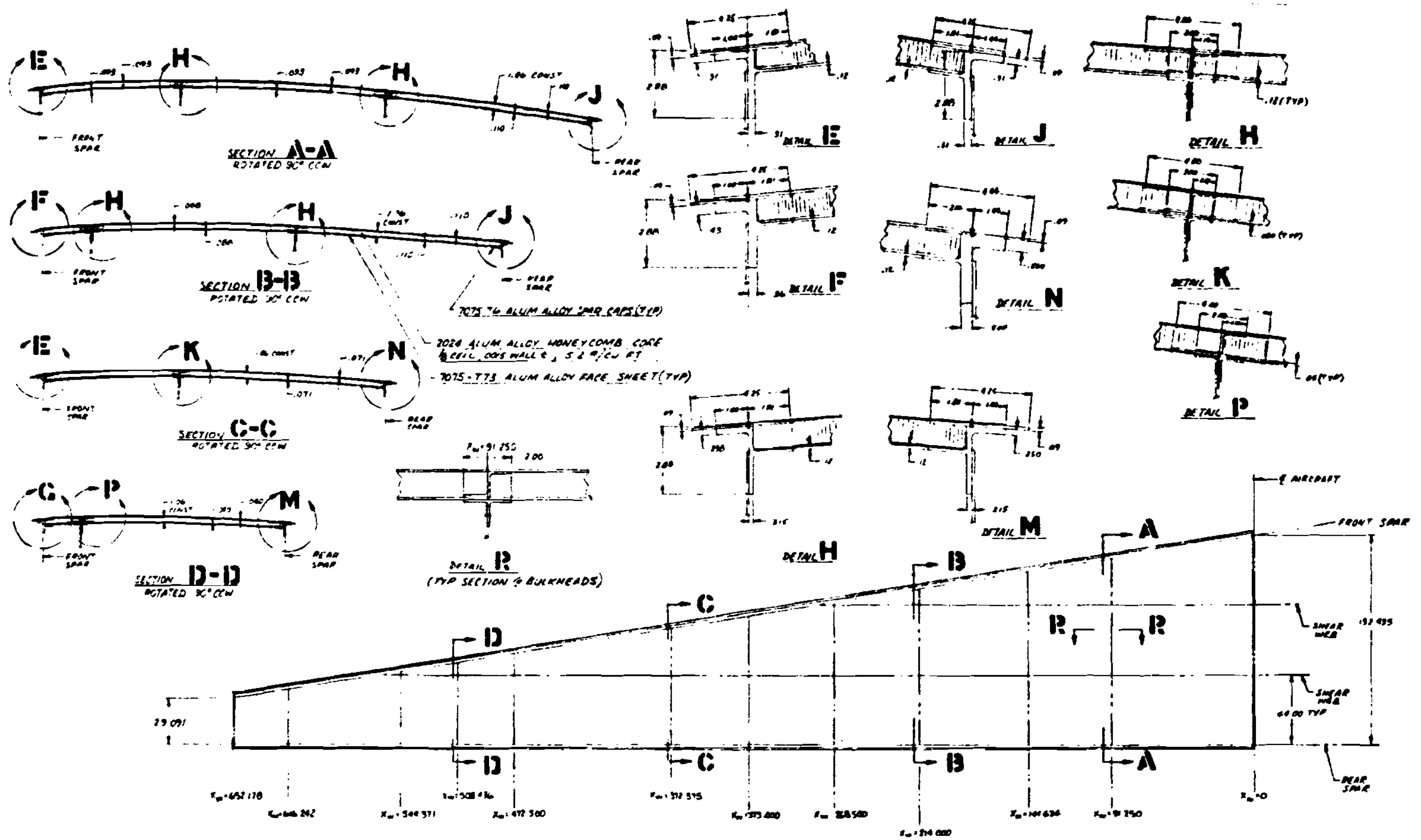

Figure 53 HONEYCOMB SANDWICH WING UPPER PANEL CONCEPT

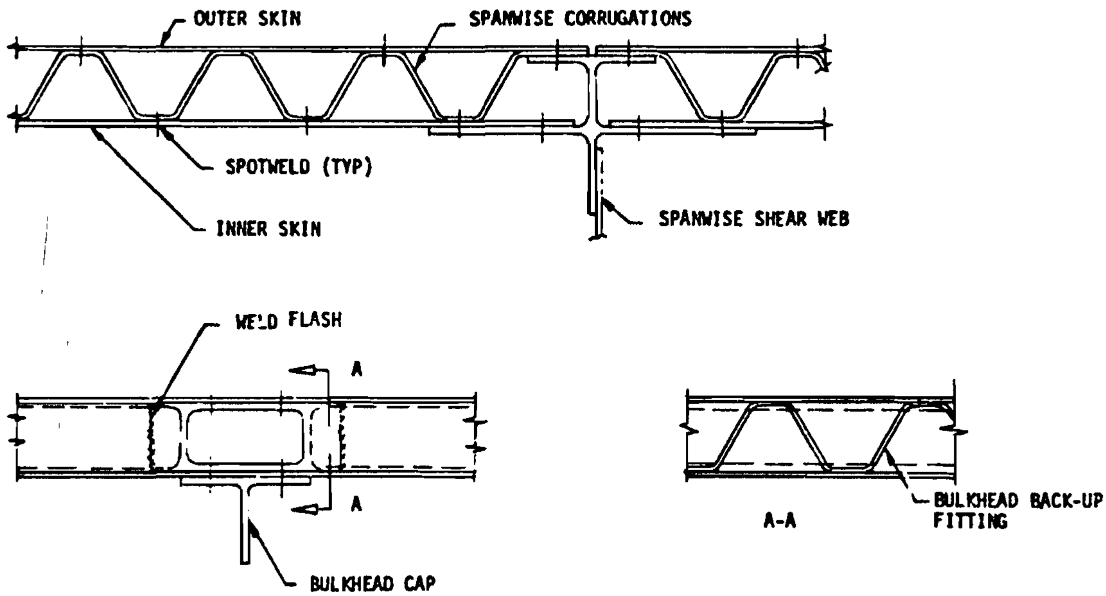

Figure 54 CORRUGATED CORE SANDWICH PANEL CONCEPT

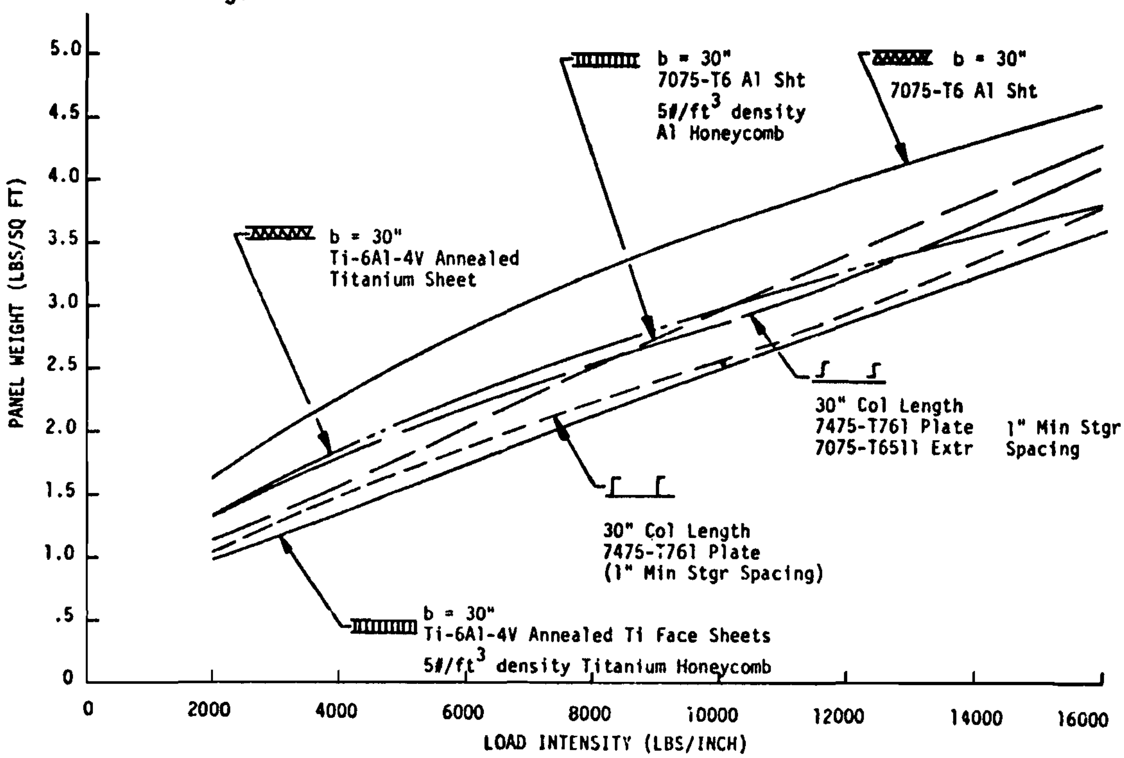

Figure 55 WEIGHT EFFICIENCIES OF VARIOUS DESIGN CONCEPTS

the panels at the required bulkhead locations). Edge treatment was assumed to be the addition of high density honeycomb core (25 pounds/foot^3) strips 1.5 inches wide. No weight was added to the unidirectional corrugated core concept weight curve for edge treatment. The weight curves for the integrally stiffened and zee-stiffened panels are for one-inch minimum stringer spacing which allows the skin to be fully effective for the compressive load. The integrally stiffened and zee-stiffened panels are multi-rib design concepts and a valid comparison can be made between the two. The weight curves are cover panel weight only and do not include rib or shear web weight.

Selective reinforced skin and stringer panels (Figure 56) are new design concepts that were studied for the wing box upper cover panel to increase the weight efficiency of the stiffened panel concept. Many variations of this technique were considered, and a computer program was used to aid in the evaluation of this concept. In general, the technique of selective reinforcement offers the following advantages:

(1) The concept takes maximum advantage of the composite properties and uses a minimum amount of the expensive reinforcement material.

(2) The metal portions use existing metal removal techniques and use standard manufacturing assembly procedures.

Figure 56(a) is an integrally (flanged) stiffened skin panel with selective reinforcement of graphite or boron-epoxy tape applied to the upstanding flange of the stiffener. This concept offers the following advantages:

(1) Integrally (flanged) stiffened skin panels are highly weight efficient and the skin thickness and stringer areas may be machine tapered to meet load requirements.

(2) The composite area may be reduced outboard by dropping off layers of tape as the compressive load decreases.

Disadvantages are:

(1) Advanced room-temperature setting adhesives are required for bonding the reinforcement to the stiffeners to reduce warpage and residual stresses induced during the cure cycle of the adhesive due to the mismatch of thermal coefficients of expansion of the materials.

(2) The composite reinforcement requires protection from the fuel tank environment.

(3) Expensive tooling is required to restrain the large skin panel to prevent warpage and residual stresses due to the mismatch of the thermal expansion coefficients during the cure cycle of the adhesive between the reinforcement and the stringer.

Figure 56(b) is a variation of the technique of selective reinforcement. This process was fostered by AVCO and consists of extruded hollow zee-section

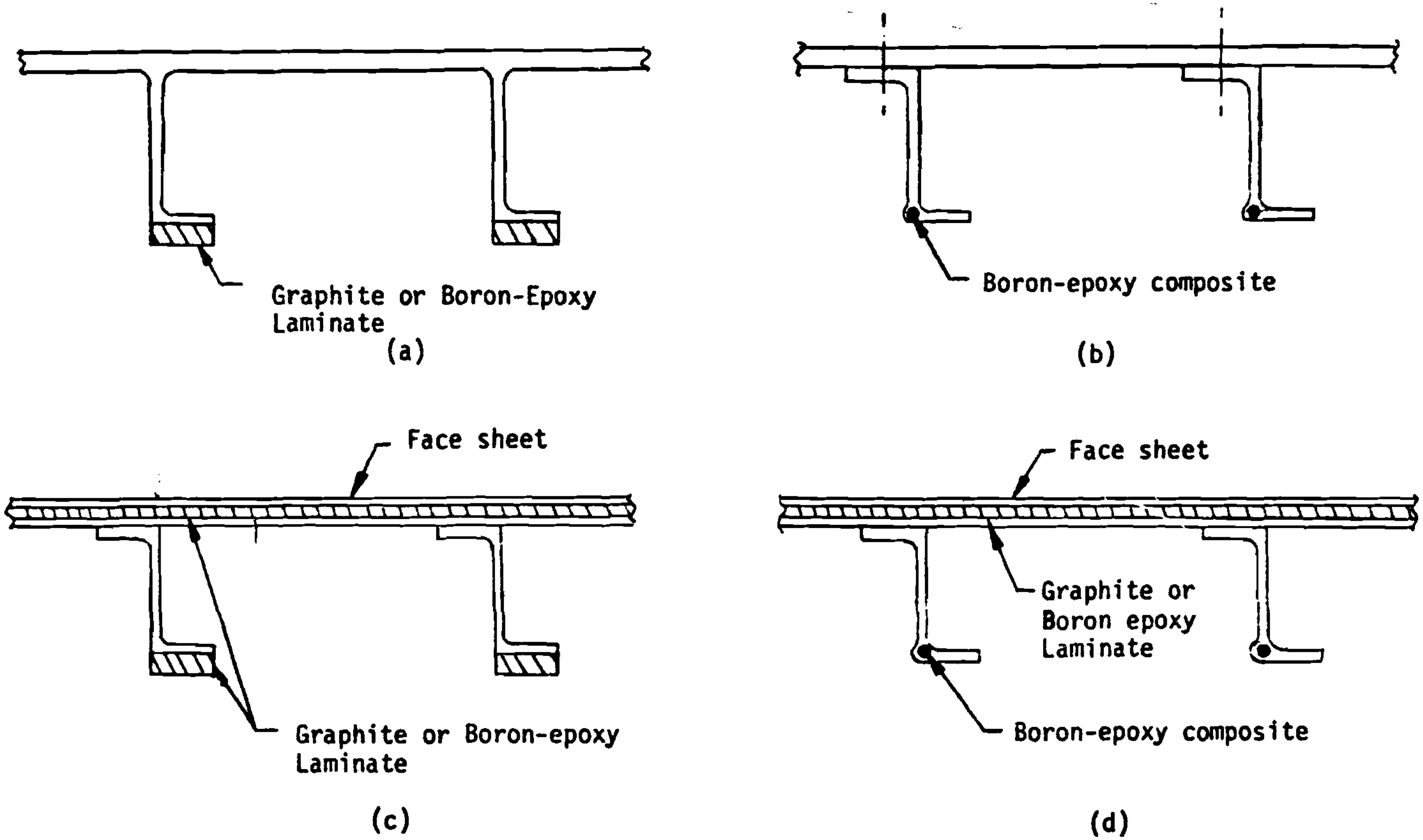

FIGURE 56 - SELECTIVE REINFORCED SKIN AND STRINGER PANEL CONCEPTS

aluminum stiffeners filled with boron/epoxy composite reinforcement. These reinforced stiffeners may be machine tapered and mechanically attached or bonded to a tapered aluminum skin. This infiltration technique offers increased weight efficiency and has the following additional advantages:

(1) Warpage of the stiffener due to the mismatch of the thermal expansion coefficients of the material and build-up of residual stresses is minimized. The technique of allowing the adhesive between the composite and the extrusion to cure at room temperature prior to the final cure cycle at elevated temperatures allows the composite to restrain the extrusion during the final cure cycle.

(2) The boron-epoxy composite is protected from the fuel tank environment.

(3) The metal portions use existing forming and metal removal techniques and use standard manufacturing assembly techniques.

(4) Concept utilizes existing adhesive and manufacturing processes.

(5) Laminate fabrication by using unidirectional construction is reduced to simplest form.

Some disadvantages are:

(1) The extruded hole in the stiffener is a constant diameter which requires a compromise in the amount of boron-epoxy composite which may be used as the area of the stiffener is reduced for decreasing load intensities. Technology should be developed to reduce the area of the boron-epoxy reinforcement as the stiffener is tapered.

(2) With present technology, the maximum length obtainable for boron-filled extrusions is in the area of 20 feet. Technology should be developed to increase the length of the reinforced extrusion to 55 feet and reduce the large number of splices (and resulting weight penalty) of the shorter lengths.

Figure 56(c) is another variation of the reinforcement technique. In this concept, the skin as well as the stiffener is reinforced. The stiffener is reinforced by the application of boron-epoxy or graphite-epoxy composite to the upstanding flange. Advantages of this concept include:

(1) The addition of reinforcement to the skin increases the skin thickness with small weight penalty and allows wider stiffener spacing, thus reducing the number of parts.

(2) The area of the stringer and reinforcement may be reduced as the load intensity decreases.

(3) The geometry of the stiffener may be revised to line up the centroids of the reinforcement with the upstanding leg to further reduce warpage due to thermal expansion coefficient mismatch between the two materials.

(4) The individual stiffeners may be restrained by common tooling as separate parts during the cure cycle of the adhesive between the reinforcement and the stringer cap.

Disadvantages are:

(1) Concept of reinforcing the skin is not feasible from a cost standpoint since the skin assembly requires:

   (a) layers of high cost composite reinforcement.

   (b) One constant thickness face sheet and one tapered face sheet or two tapered face sheets in order to be weight efficient.

   (c) Addition of high density core or filler at base of stiffeners for shear transfer between the face sheets and to prevent crushing of the laminate if attachments are used.

   (d) Expensive tooling is required to prevent warpage and residual stresses during the cure cycle due to the thermal coefficient of expansion mismatch between the materials.

(2) Attachment of stiffeners by mechanical means involves drilling through the reinforcement laminate.

(3) Means must be provided to protect the reinforcement laminate on the stiffener from the fuel tank environment.

Figure 56(d) shows a variation of the reinforcement technique and is another combination of the concepts already discussed.

The application of selective reinforcement increases the weight efficiency of stiffened wing box cover panels and is a recommended wing design concept for the upper cover panel. After considering the advantages and disadvantages of the variations discussed, the selective reinforcement concept recommended is shown in Figure 57(a). This design represents a combination of the various concepts which appear the most feasible from a cost and weight efficiency standpoint.

The concept consists of a machine tapered aluminum alloy extruded stiffener mechanically attached. The stiffeners are reinforced with boron-epoxy composite laminate bonded to the upper cap. The composite area is a percentage of the area of the stiffener. The boron-epoxy laminate and the adhesive are protected from the fuel tank environment by a protective coating.

The adhesive is precured at room temperature to eliminate residual stresses and warpage of the stiffener during the cure cycle. In the absence of a room temperature curing adhesive of adequate strength to bond the reinforcement to the stiffener, and/or satisfactory protective coating to resist the fuel tank environment, the stiffeners may be revised as shown in Figure 57(b). This will minimize the warpage and residual stresses due to the mismatch of thermal coefficients of expansion.

After the centroid of the reinforcement is lined up with the centroid of the upstanding leg of the stiffener, the stiffener may be restrained by common tooling from warpage on an individual basis during the higher temperature cure cycle of present adhesive systems. The reinforcement laminate and adhesive must now be protected from the fuel tank environment by application of a protective coating.

Another technique that eliminates the need for advanced adhesives and the protective coating is shown in Figure 58. This technique allows the fabrication of the reinforcement assembly to occur at the sub-assembly level and provides protection from the fuel tank environment with small weight penalty. Warpage and residual stress problems would be confined to the reinforcement assembly during the cure cycle. Another advantage of this technique is that the reinforcement is separated into two strands. In the event of the loss of one of the strands, the other would carry its portion of the load.

A computer-aided parametric study was conducted to evaluate the relative weight efficiency of selective reinforced stiffened panels when variations are made in the stringer spacing and composite reinforcement area. The panels were sized for compressive load intensities from 2,000 pounds per inch up to 16,000 pounds per inch. A compressive stiffening ratio of 0.50 was selected based on design experience and panel length was constrained to 30 inches. An end fixity of C = 1.5 was assumed as in the earlier studies.

Table XVI shows the relative weights of stiffened panels with variations in stringer spacing and composite area.

As a result of this study, the stringer spacing was set at 4.5 inches with a composite area of 30% of the stringer area for Wing Concept No. 2 upper cover panel. This combination of stringer spacing and composite reinforcement area allows adequate room for cover panel to bulkhead attachment and provides minimum stringer height required for attachment of shear clips in areas of low load intensity where the stringer is tapered to its minimum cross-sectional area.

Another concept considered for the wing box cover panels was the integrally machined sandwich design concept shown in Figure 59. This design concept features machined upper and lower skins spotwelded or bonded together. The inner skin has bulkhead caps integrally machined or bonded in place. Spanwise stiffeners are provided to make the skin fully effective for the compressive load. Chordwise gussets are provided for shear stability of the panels. The material considered for this concept is aluminum alloy. For weight efficiency, the skin and stiffeners are tapered spanwise.

This design concept was not considered feasible for the cover panels for the following reasons:

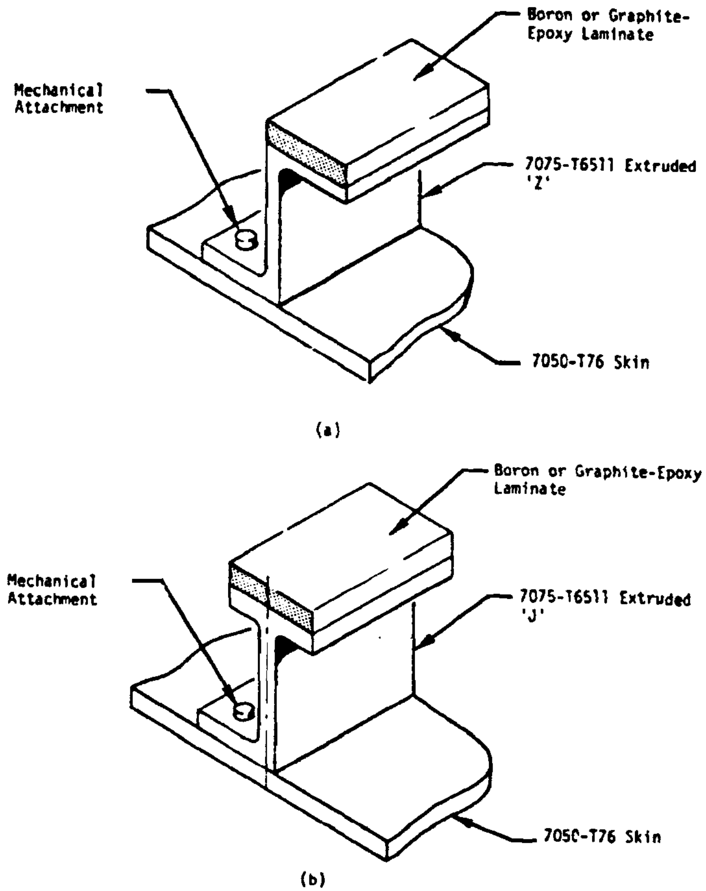

Figure 57 COMPOSITE REINFORCED STIFFENED PANEL CONCEPT

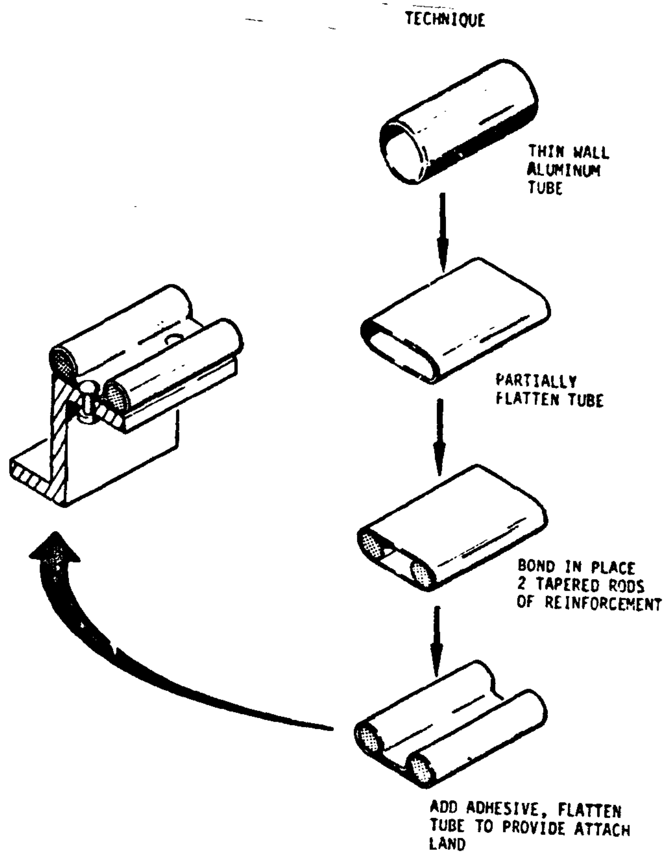

Figure 58 ENCAPSULATED COMPOSITE REINFORCED STIFFENER CONCEPT

TABLE XVI WEIGHT COMPARISON OF COMPOSITE REINFORCED STIFFENED PANELS								
PANEL LOAD (LB/IN)	COMPRESSION PANEL WEIGHT (LB/FT^2)							
	A_c/A_s = 0.1*			A_c/A_s = 0.2		A_c/A_s = 0.3		A_c/A_s = 0.4
	b_s (In.)°			b_s (In.)		b_s (In.)		b_s (In.)
	3.5	4.0	4.5	4.0	4.5	4.0	4.5	4.5
2000	1.022	0.992	0.990	0.924	0.924	0.901	0.894	0.904
4000	1.495	1.486	1.506	1.384	1.387	1.344	1.334	1.307
6000	1.900	1.934	1.980	1.809	1.836	1.737	1.750	1.697
8000	2.275	2.345	2.413	2.201	2.258	2.105	2.140	2.071
10000	2.620	2.718	2.814	2.574	2.640	2.459	2.519	2.428
12000	2.941	3.067	3.181	2.917	3.001	2.802	2.863	2.768
14000	3.243	3.396	3.527	3.237	3.341	3.117	3.197	3.098
16000	3.527	3.703	3.853	3.545	3.663	3.415	3.510	3.403

*A_c is composite area, and A_s is stiffener area; °b_s is stiffener spacing.

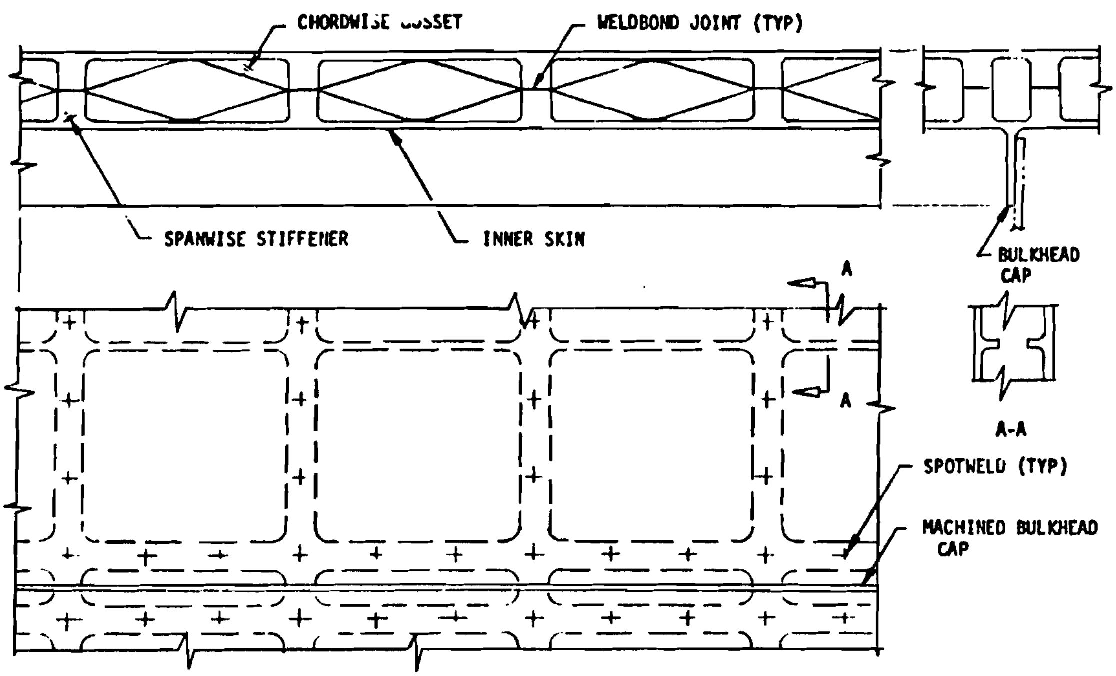

Figure 59 INTEGRALLY MACHINED SANDWICH PANEL CONCEPT

(1) Sizing studies have indicated that the required stiffener thickness, in areas of maximum load intensity, is too thick for spot welding.

(2) The depth of penetration required for spotwelding is too great for present welding technology.

(3) The stiffener locations of the two halves must match to be effectively joined by spotwelding or bonding.

Matching of the spanwise stiffeners of the two skin panels is very difficult due to adverse tolerance accumulation. The reduced stiffener cross-section in areas of low load intensities leaves little margin for mismatch between the stiffeners.

Extensive inspection procedures would be required to verify match-up of the spanwise stiffeners.

A design concept considered for the wing box cover panels is the stiffened honeycomb concept shown in Figure 60. This concept features integrally machined face sheets bonded to honeycomb core. The sandwich panels are zee-stiffened (Figure 60[a]) or stiffened by machined flanged stiffeners integral with the inner face sheet (Figure 60[b]). Inserts, machined pads, or high-density honeycomb core would be provided between the face sheets for shear transfer at the stiffeners, spanwise splices, bulkhead attachment and at panel attachment to the spar caps.

This concept has the advantages of:

(1) Reduced skin material thickness reducing the number of stringers and associated attachments required.

and some disadvantages of:

(1) Two machined skins are required per panel

(2) High manufacturing and assembly costs

A computer-aided parametric study was conducted to evaluate the weight efficiency of the stiffened honeycomb sandwich concept when compared to the integrally (flanged) stiffened skin panel. Figure 61 shows a weight comparison between the two skin panels for a compressive load intensity of 10,000 pounds per inch. The integrally (flanged) stiffened panel weight shown in Figure 61 is for a skin panel with fully effective skin at the compression stress. The effective panel length was set at 24.5 inches for the studies and the stiffening ratio was set at 0.40. The density of the honeycomb core was 5 pounds/foot^3. The weight of the stiffened honeycomb does not include the weight of inserts, machined pads, or high density core required along the stiffeners, at the bulkheads, the panel edges at the spar caps, and at spanwise splices. This additional weight would reduce the weight advantage. The lowered weight savings and additional manufacturing and assembly costs reduce the feasibility of this concept for the wing box cover panels.

Beryllium sandwich skin panels were considered for the wing box upper cover panel. This design concept, shown in Figure 62, features spanwise and chordwise stiffeners that are intermeshed through a series of machined cuts in the stiffeners joined by adhesive bonding at the stiffener intersections. The spanwise stiffeners are spaced to make the face sheets fully effective for the compressive load. The chordwise stiffeners are provided for shear stability of the panels. The edges of the panels are bonded to titanium edge members to eliminate holes in the beryllium skins. Titanium bulkhead caps and spanwise shear webs are also bonded to the panels. Additional stiffeners are provided between the face sheets for shear transfer between faces where bulkheads and shear webs are joined to the panel.

This concept was not considered feasible due to the high cost of the thin beryllium sheet and the high manufacturing and assembly costs associated with the concept.

5.1.2.2 Spars, Ribs and Bulkheads - The spars, ribs and bulkheads of the baseline wing box consist of machined extruded caps with stiffened sheet webs. The webs are 7050-T76 sheet and the stiffeners are machined from extrusions or plate stock. A typical flap bulkhead is shown in Figure 63. The shear clips which transfer the high axial load from the flap into the wing skins are machined 7049-T73 forgings. The butterfly clips, which support the wing crushing loads and fuel pressure loads, are also 7049-T73 forgings.

Several design concepts were investigated to determine the optimum structural arrangement for the spars, ribs and bulkheads for the Medium STOL Transport. Emphasis was placed on reducing the number of detail parts, thus reducing fabrication and assembly costs.

Critical loads for the spars and ribs are crushing loads due to wing bending and internal fuel tank overpressure. Critical loading for the bulkheads are the high loads introduced from engine support pylons, flaps and ailerons. Design concepts considered for the spars and fuel control bulkheads were: 1) closed isogrid, 2) honeycomb sandwich, 3) closed truss, and 4) one-piece integrally stiffened web. Closed-web designs are required to compartment the fuel. Design concepts considered for the ribs include: 1) open isogrid, 2) open truss, 3) one-piece web with mechanically attached stiffeners, and 4) one-piece integrally stiffened rib.

The honeycomb sandwich web (Figure 64) was considered for the spar and bulkhead webs.

This concept offers the advantage of eliminating the stiffeners required for a conventional stiffened web design. This concept was not considered feasible from a cost and weight standpoint due to:

(1) The weight efficiency is reduced due to the inserts required in areas where attachments are used.

(2) The face sheets of the sandwich must be tapered for the maximum weight efficiency.

(3) More detail parts and associated attachments are required

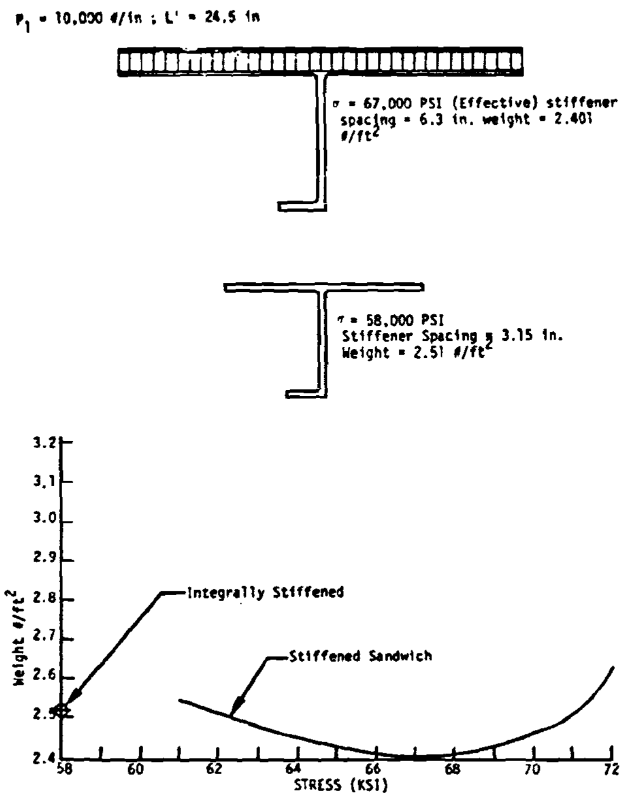

Figure 61 WEIGHT COMPARISON OF STIFFENED HONEYCOMB vs INTEGRALLY STIFFENED PANELS

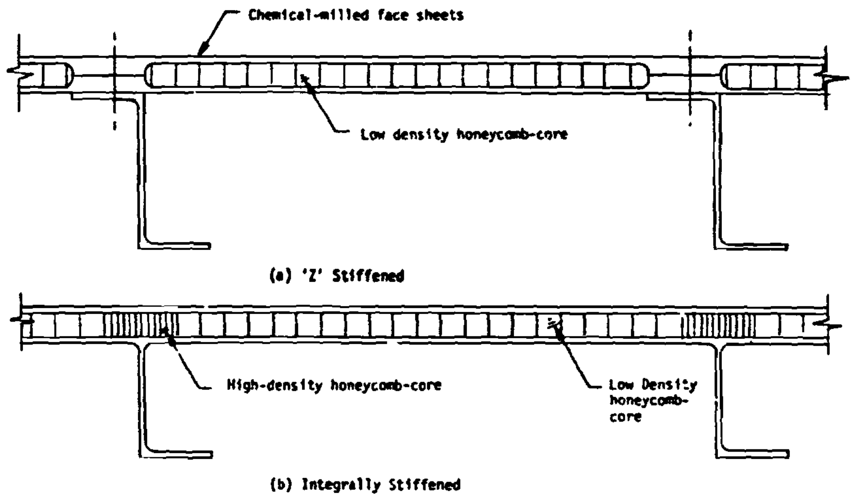

Figure 60 STIFFENED HONEYCOMB SANDWICH PANEL CONCEPTS

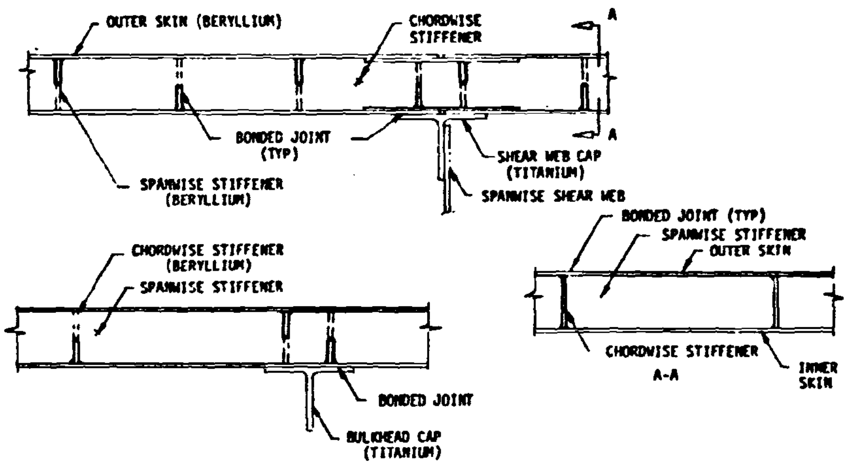

Figure 62 BERYLLIUM "EGGCRATE" SANDWICH PANEL CONCEPT

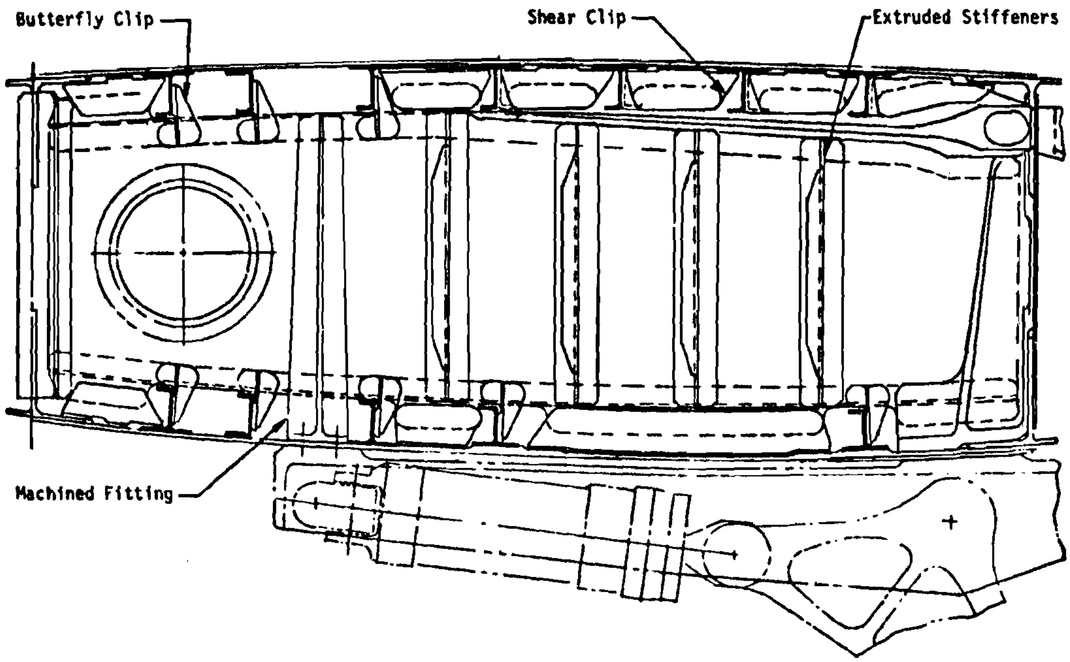

Figure 63 TYPICAL BASELINE WING BULKHEAD

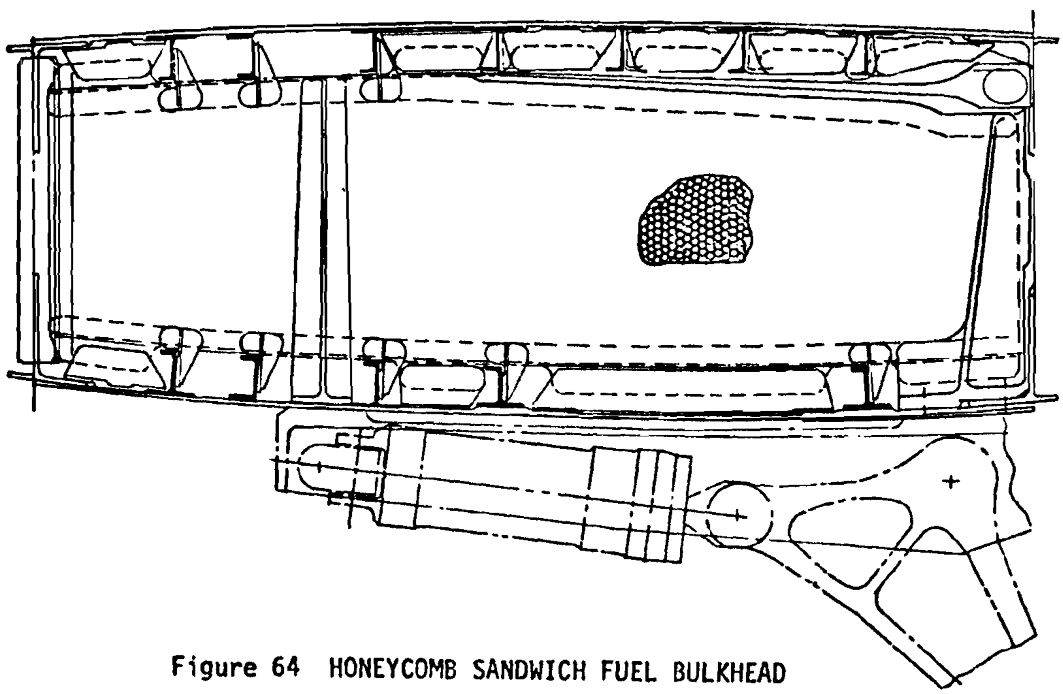

Figure 64 HONEYCOMB SANDWICH FUEL BULKHEAD

than for other design concepts.

(4) The sandwich web must be sealed to prevent exposure of the core to fuel due to leaks.

(5) The honeycomb core and face sheets are subject to corrosion and difficult to inspect.

The closed truss web concept (Figure 65) was considered for the spar and bulkhead webs. Parametric studies indicated that the open truss concept was weight efficient for the load intensities of the STOL Transport. The most efficient cross-members are thin-walled round tubes which are difficult to attach to the web and require separate fittings at the intersection of the cross-members. The weight penalty associated with the addition of a web to compartment the fuel also reduces the weight efficiency of this concept.

Other concepts considered for the spar webs and bulkheads were the closed isogrid web design and the one-piece-integrally stiffened web concept. A parametric study was conducted to compare the two concepts and their relative weight efficiency is shown in Figure 66. For the studies, the height of the bulkheads was set at 30 inches and the webs were sized for shear load intensities of 1,000 to 5,000 pounds per inch. Stiffening ratio for the integrally stiffened tension field webs was set at 50%.

5.1.3 Selected Wing Design Concepts

Two wing structural box design concepts were selected for complete weight studies. The concepts were selected for their relative weight efficiency and minimum number of parts.

The studies indicated that the most efficient structural arangement for the wing box substructure is the multi-rib concept. This was used for the two concepts.

The design concepts selected for the spars, ribs and bulkheads are integrally machined components. Parametric studies indicated these to be weight efficient and significantly reduce the number of parts required.

5.1.3.1 Wing Concept Number 1 - The design concept selected for the wing structural box upper and lower cover panels is shown in Figure 67. The panels are integrally (flanged) stiffened with a stiffener spacing of 3.5 inches which allows practical bulkhead to cover panel attachment between stiffeners. The forward stiffener of both upper and lower skin panels is parallel to the front spar. All other stiffeners are parallel to the rear spar and terminate at the forward stiffener or at the X_W 652.178 closing bulkhead. The skin thickness and stringer area are tapered both chordwise and spanwise to meet the load intensity requirements. Chordwise intercostals are integrally machined into the panels between the stiffeners to provide attach flanges for the ribs and bulkheads. This eliminates the need for shear clips, reduces the number of holes in the cover skins, and reduces the amount of fuel tank sealant required. The panels are spliced chordwise at the airplane centerline and spanwise at the centerline of stringer number 13 and 26 on the upper surface, and at the centerline of stringer number 49 and

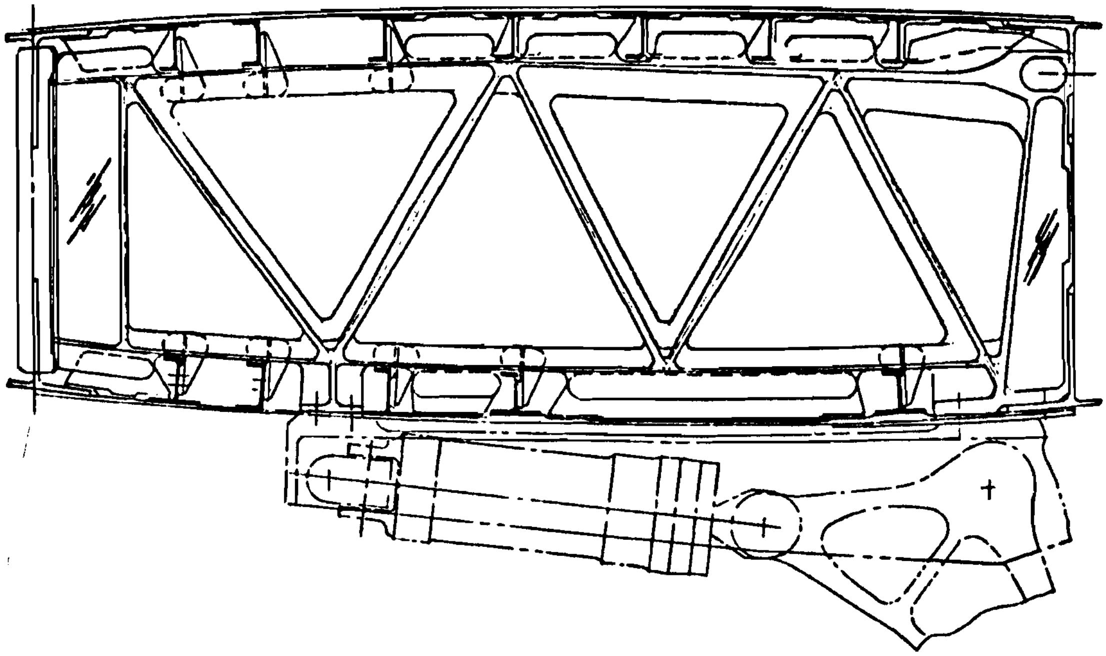

Figure 65 TRUSS WEB RIB CONCEPT

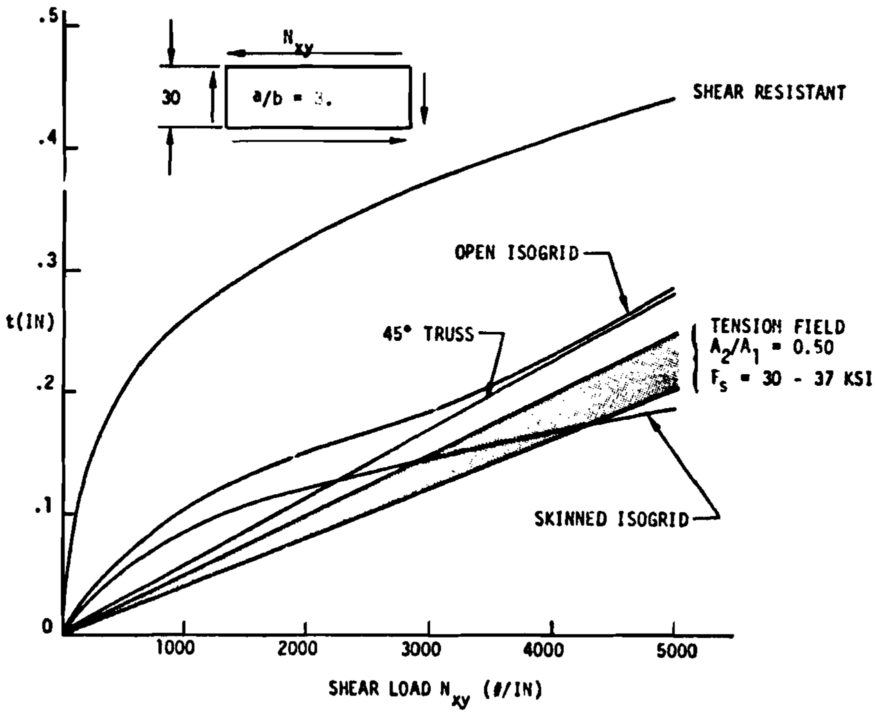

Figure 66 WEIGHT COMPARISON OF SHEAR WEB CONCEPTS

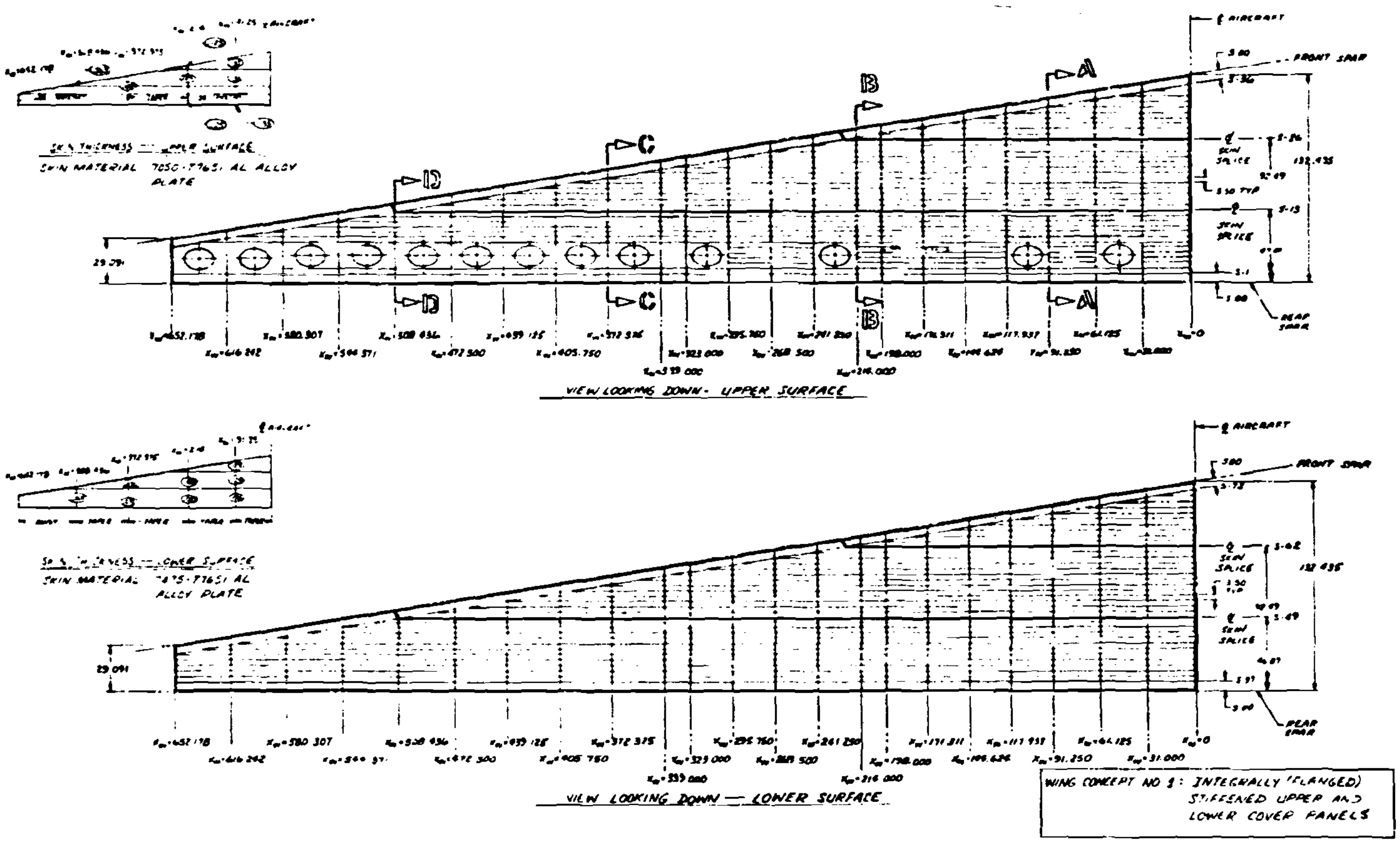

Figure 67 STRUCTURAL ARRANGEMENT FOR WING CONCEPT NO. 1 SHEET 1

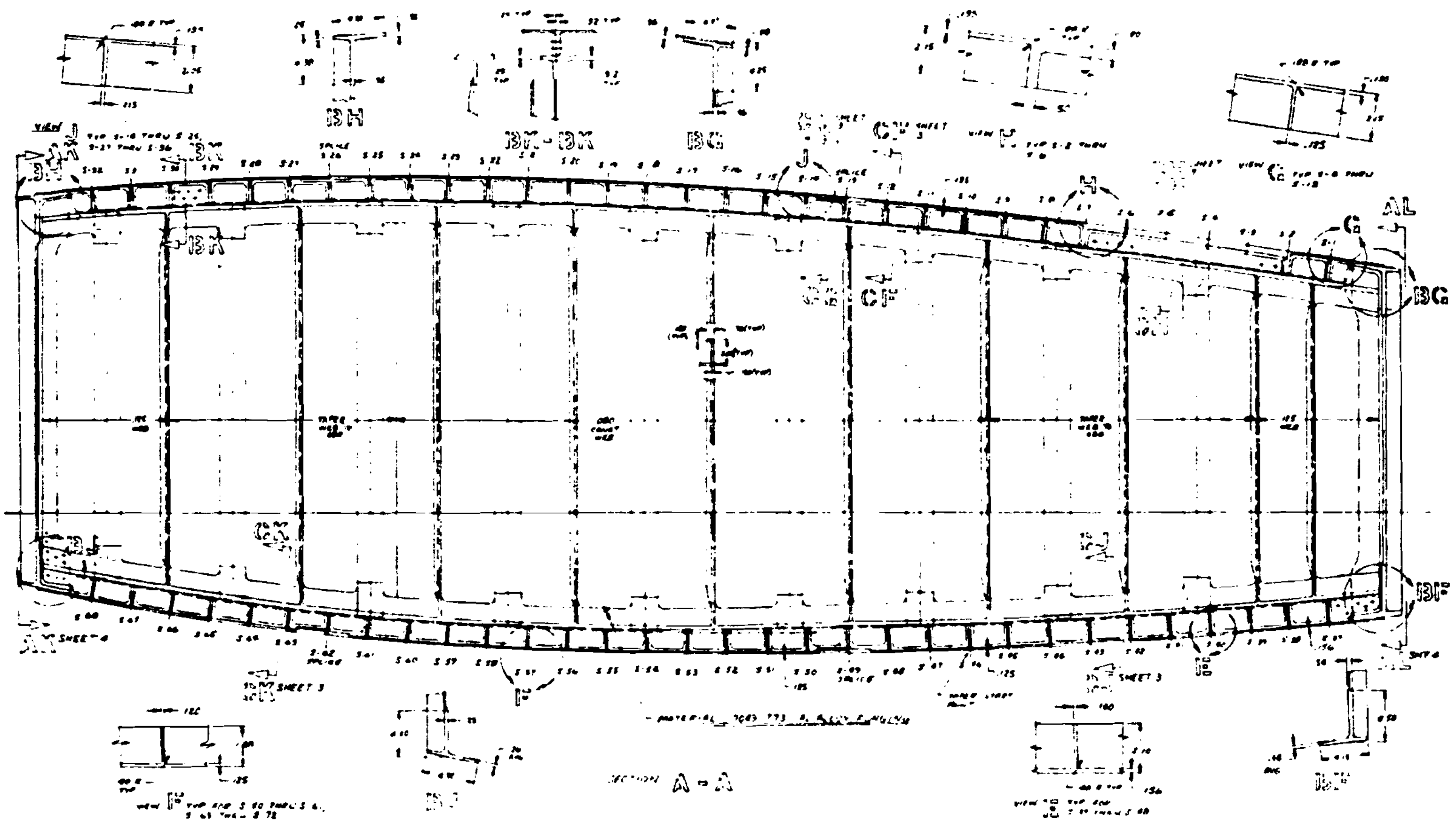

Figure 67 STRUCTURAL ARRANGEMENT FOR WING CONCEPT NO. 1 -- Continued SHEET 2

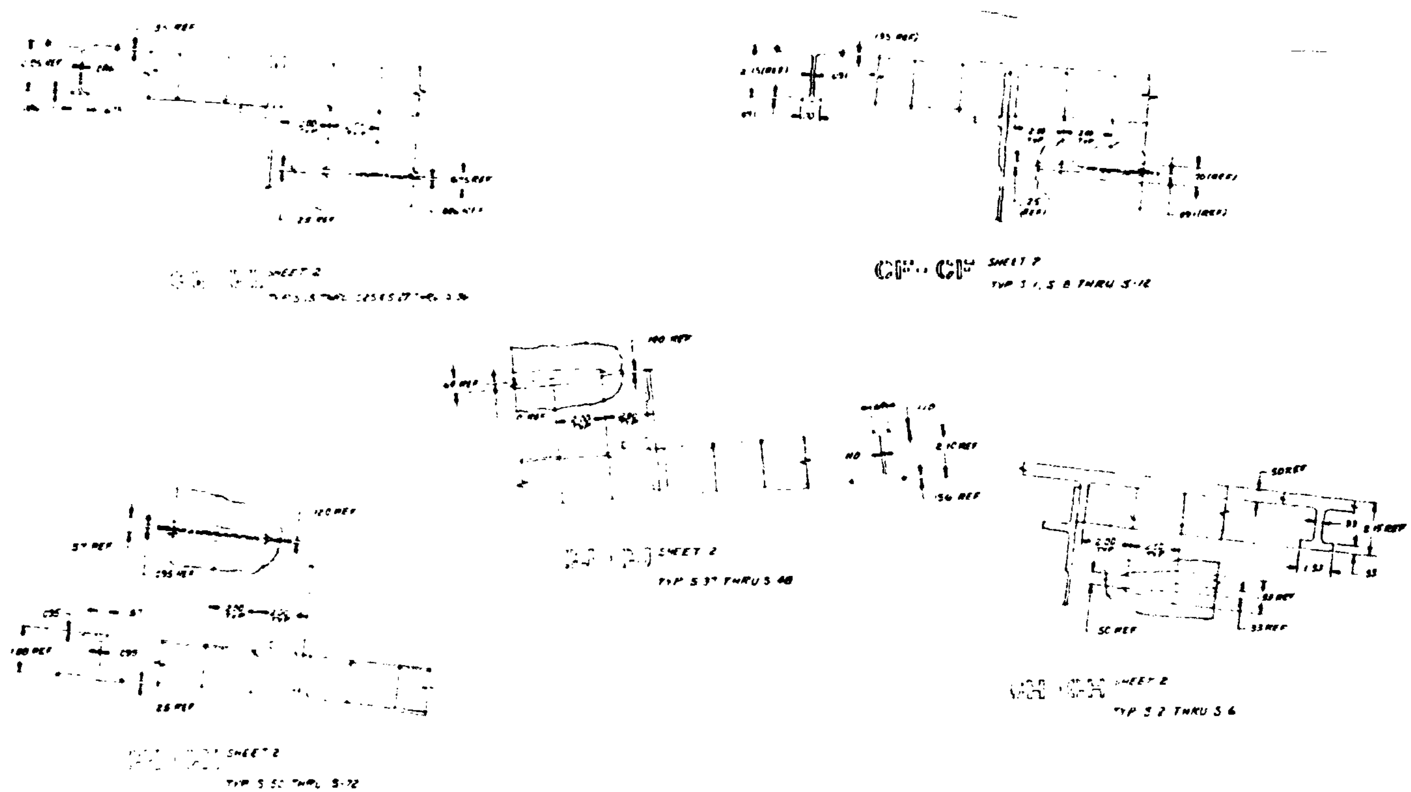

Figure 67 STRUCTURAL ARRANGEMENT FOR WING CONCEPT NO. 1 -- Continued SHEET 3

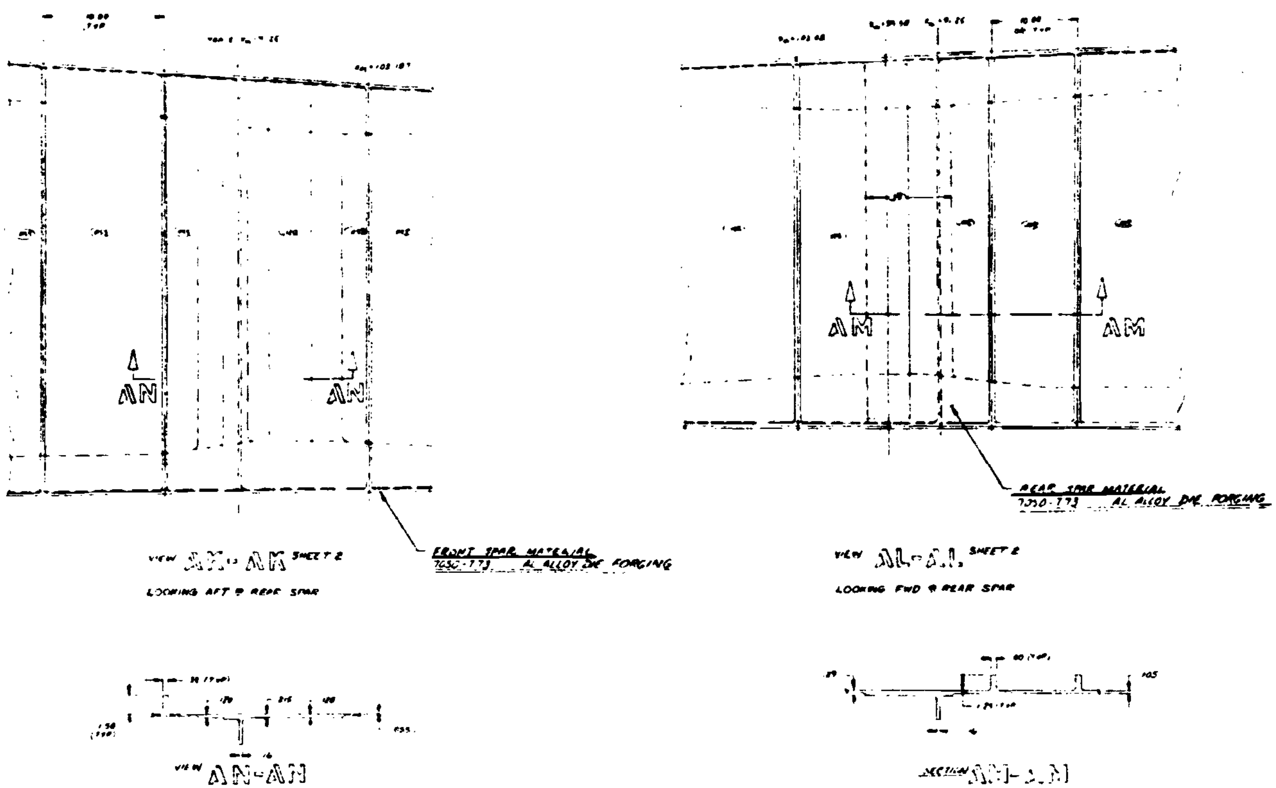

Figure 67 STRUCTURAL ARRANGEMENT FOR WING CONCEPT NO. 1 -- Continued SHEET 4

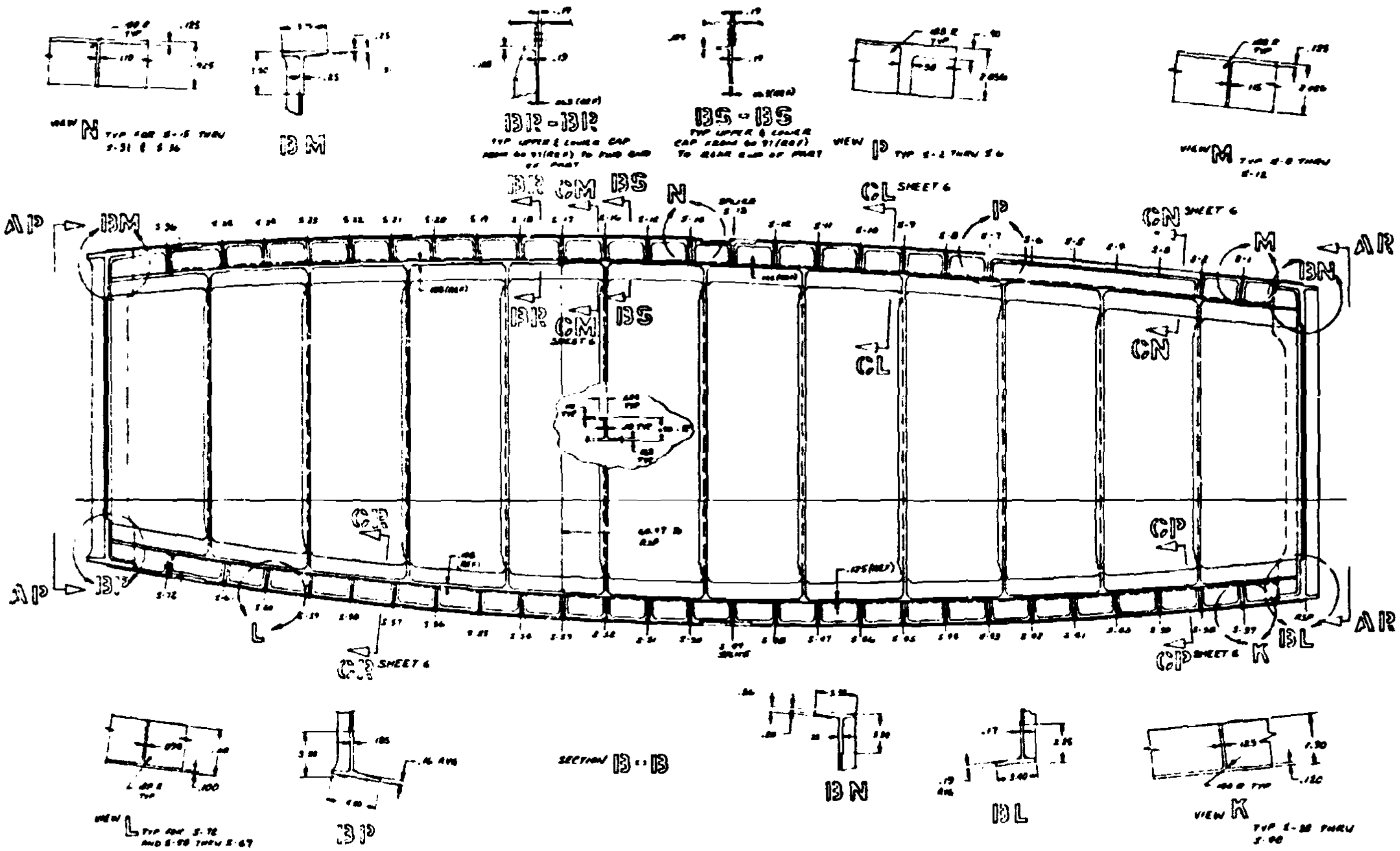

Figure 67 STRUCTURAL ARRANGEMENT FOR WING CONCEPT NO. 1 -- Continued SHEET 5

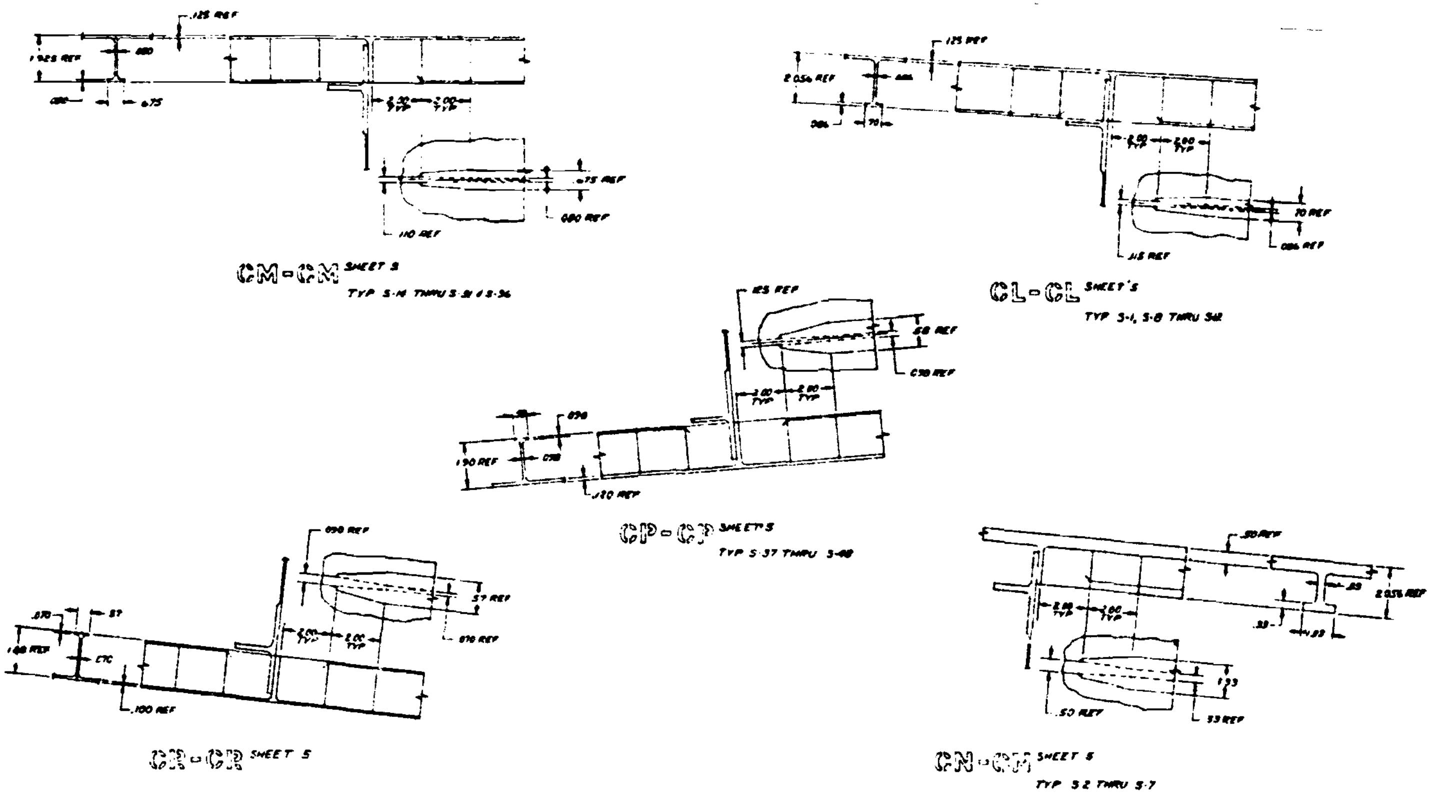

Figure 67 STRUCTURAL ARRANGEMENT FOR WING CONCEPT NO. 1 -- Continued SHEET 6

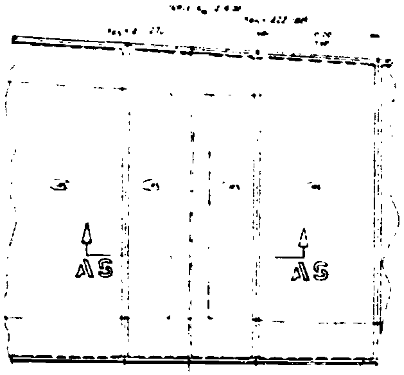

VIEW AP-AP

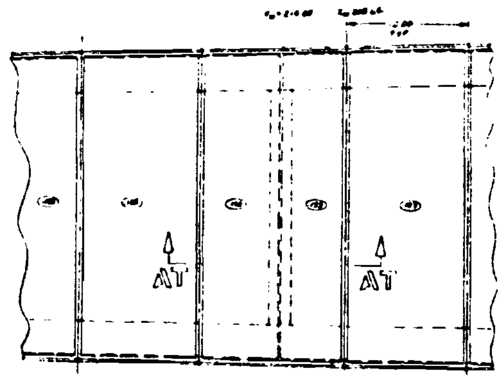

VIEW AR-AR

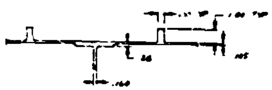

SECTION AS-AS

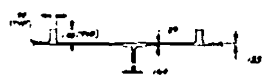

SECTION AT-AT

Figure 67 STRUCTURAL ARRANGEMENT FOR WING CONCEPT NO. 1 -- Continued SHEET 7

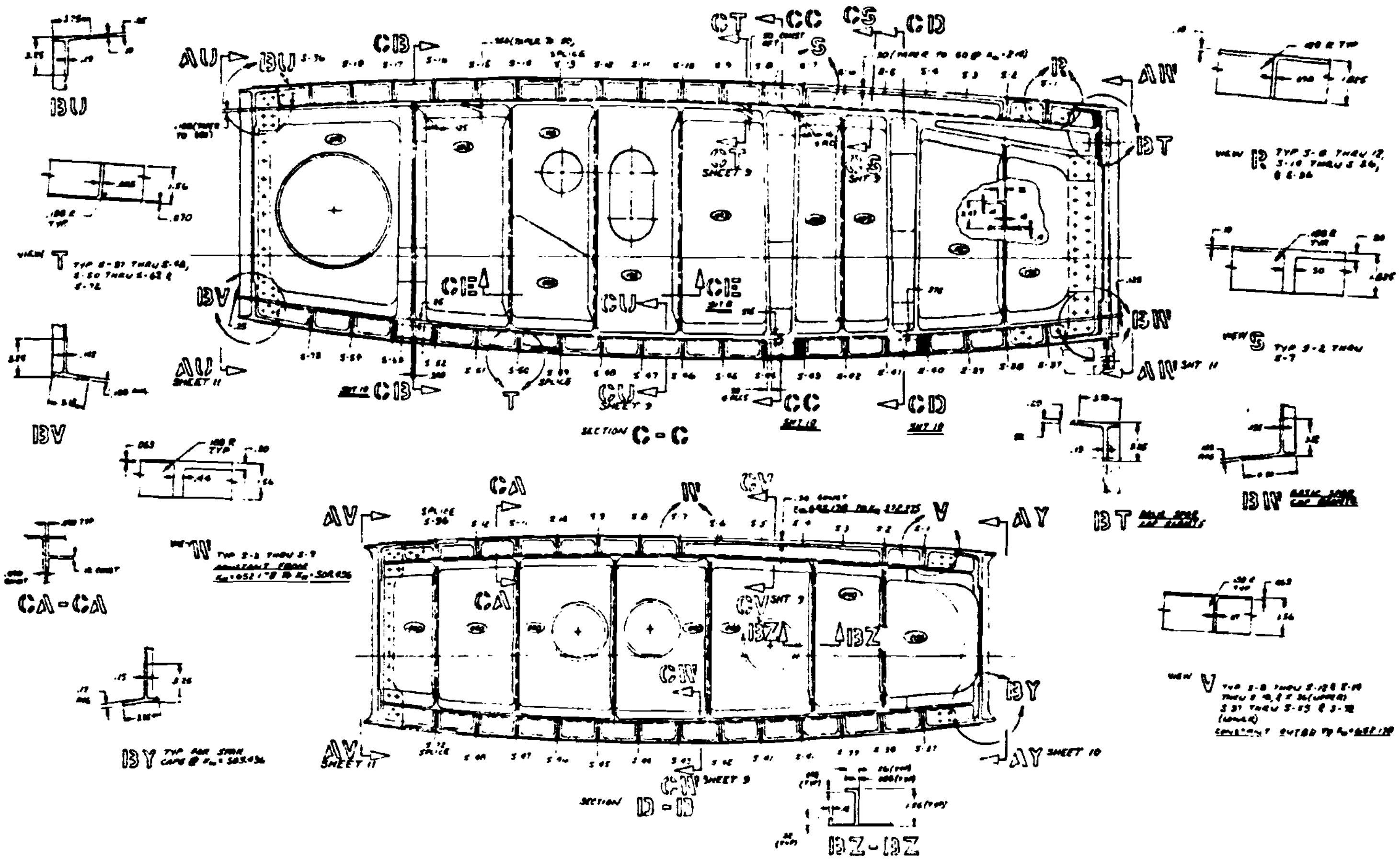

Figure 67 STRUCTURAL ARRANGEMENT FOR WING CONCEPT NO. 1 -- Continued SHEET 8

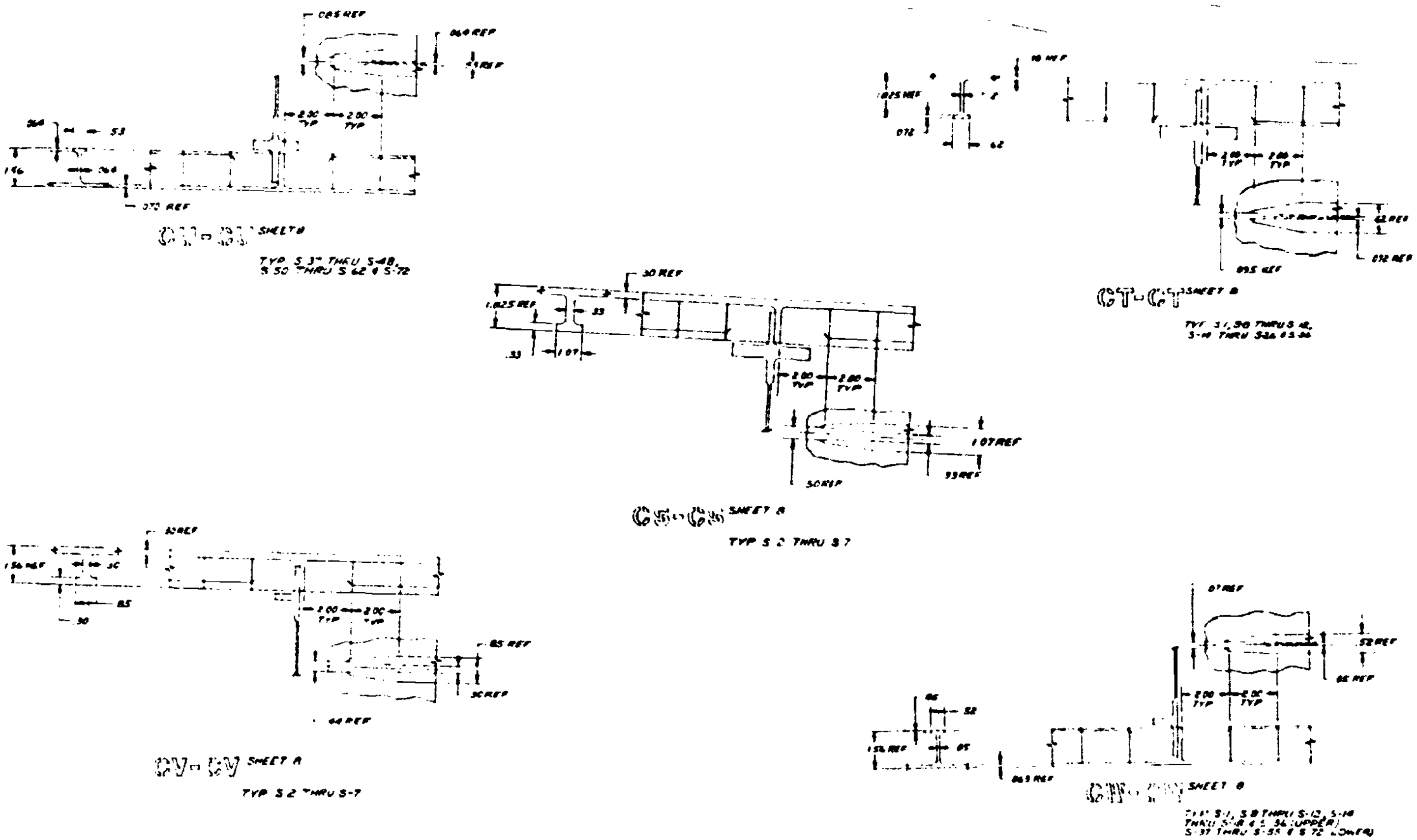

Figure 67 STRUCTURAL ARRANGEMENT FOR WING CONCEPT NO. 1 -- Continued SHEET 9

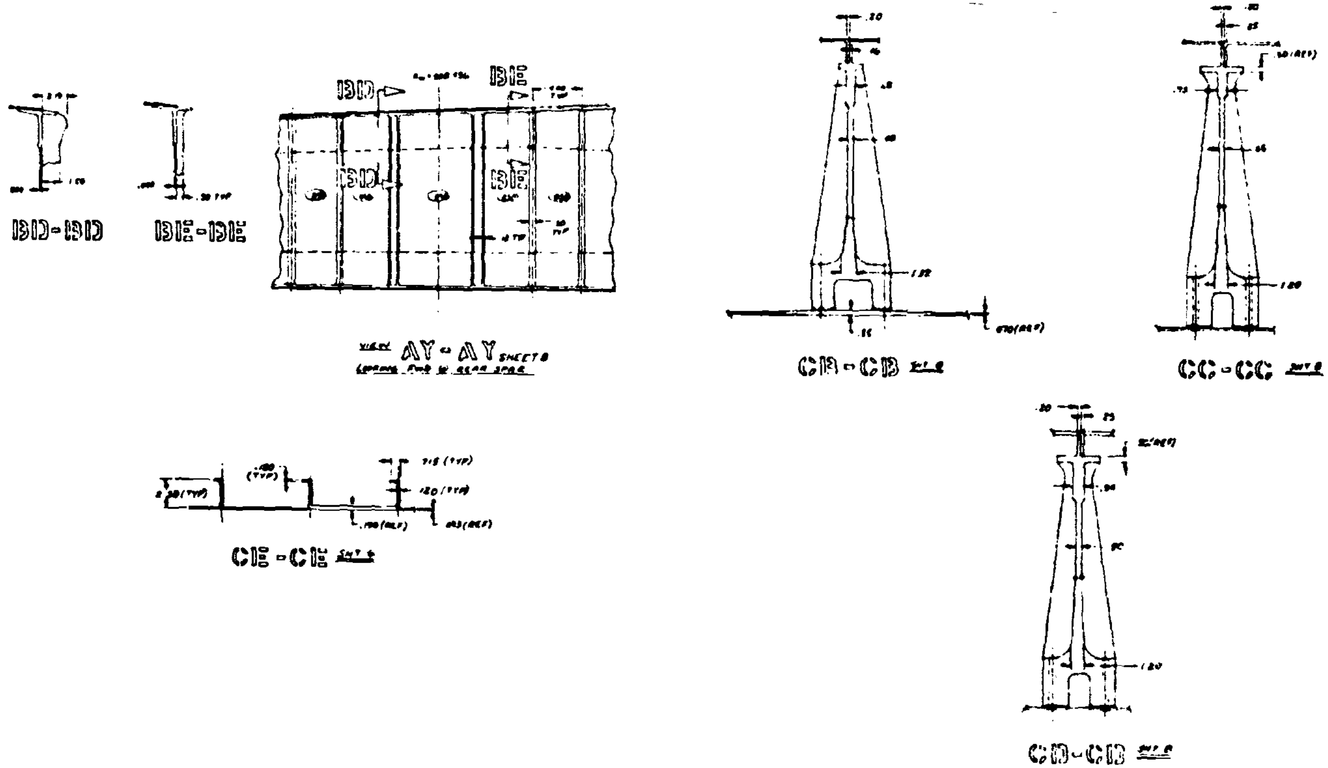

Figure 67 STRUCTURAL ARRANGEMENT FOR WING CONCEPT NO. 1 -- Continued

SHEET 10

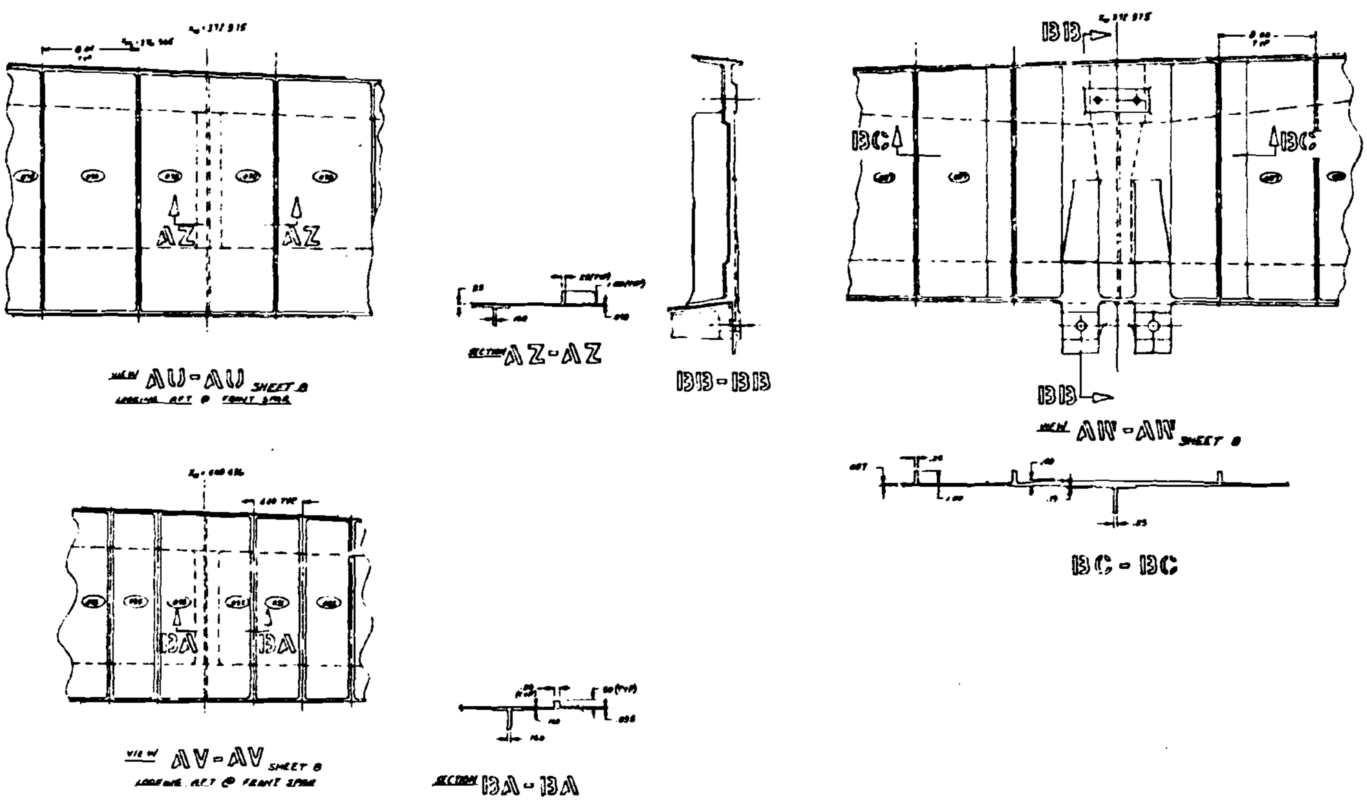

Figure 67 STRUCTURAL ARRANGEMENT FOR WING CONCEPT NO. 1 -- Concluded SHEET 11

62 on the lower surface. Fuel tank access doors are provided in the upper surface and the doublers required around the door openings are integrally machined into the skin panel. Fuel transfer slots are provided in the stringers of the lower skin panels. The only attachments through the cover skins are at the splices and cover panel to spar attachment. The reduced number of attachments permits the use of more expensive attachments and/or hole preparation techniques, with 100% inspection to improve fatigue life. The upper skin panel is machined from 7050-T7651 aluminum alloy plate and the lower skin panel is machined from 7475-T7651 aluminum alloy plate. One piece die forgings may be used to obtain increased material properties and reduce the amount of machining required. The inverted tee cross section of the integral stiffener (Figure 67, Sheet 3) was selected to allow maximum removal of material and simplify machining of bulkhead caps. The stiffener upper caps are eliminated near their intersection with the chordwise intercostals to allow maximum material removal.

5.1.3.2 Wing Concept Number 2 - The design concept recommended in Wing Concept Number 2 is identical to Wing Concept Number 1 with the exception of the upper wing cover panel. The concept selected for the upper panel consists of machine tapered 7050-T76 aluminum alloy skins with boron-reinforced zee-section stiffeners mechanically attached (Figure 68). The forward stringer is parallel to the front spar and the other stringers are parallel to the rear spar and terminate at the forward stiffener or at the X_W 652.178 bulkhead. Stiffener spacing is set at 4.5 inches on center to accommodate the addition of shear clips for cover panel to bulkhead attachment. The skin thickness and stringer cross-sectional area is tapered spanwise and chordwise to match the load intensity. The boron reinforcement area is set at 30% of the stiffener area and is tapered to match the stiffener. The boron reinforcement is tapered to an all metal stiffener cross-section in splice areas to allow splices to revert to conventional design. The panels are spliced chordwise at the aircraft centerline and spanwise at the centerline of stiffener number 41 and 54. The shear clips used for cover panel to bulkhead attachment are machined from aluminum alloy forgings and common shear clips are used in many areas due to the constant 4.5 inch stiffener spacing. Fuel tank access doors are provided in the upper skin and doublers required around the door cutout are integrally machined into the skin.

5.2 FUSELAGE SHELL STRUCTURE

Several innovative fuselage shell panel designs were studied. Two were selected as candidates for the complete airframe analysis. The following sections describe the baseline structure and the honeycomb sandwich concept. The second concept, Isogrid Shell, is more fully detailed in Volume II of this report. See Figure 69 for the baseline structure.

5.2.1 Baseline Design Concept

The fuselage is pressurized from the forward pressure bulkhead at fuselage station (FS) 269 to the aft pressure bulkhead (FS 1437) with the exception of the nose gear well, the wing center box, and the main gear wells. The constant section is 216 inches in diameter. The typical fuselage shell consists of 2024-T3 skin with 62 7050-T76511 extruded Z-section longerons spaced approximately 7.75 to 12.625 inches apart and transverse frames at 24 inch

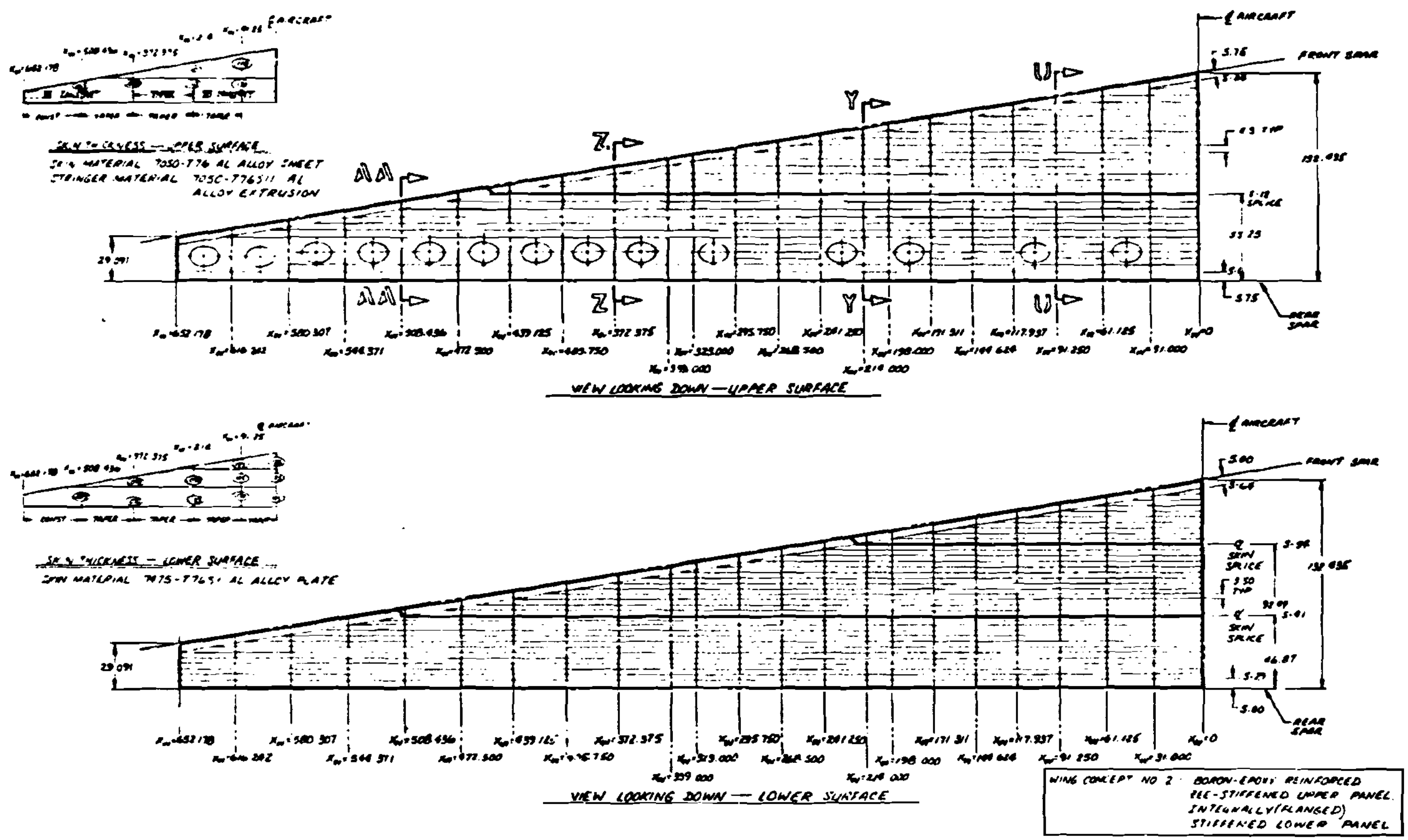

Figure 68 STRUCTURAL ARRANGEMENT FOR WING CONCEPT NO. 2 SHEET 1

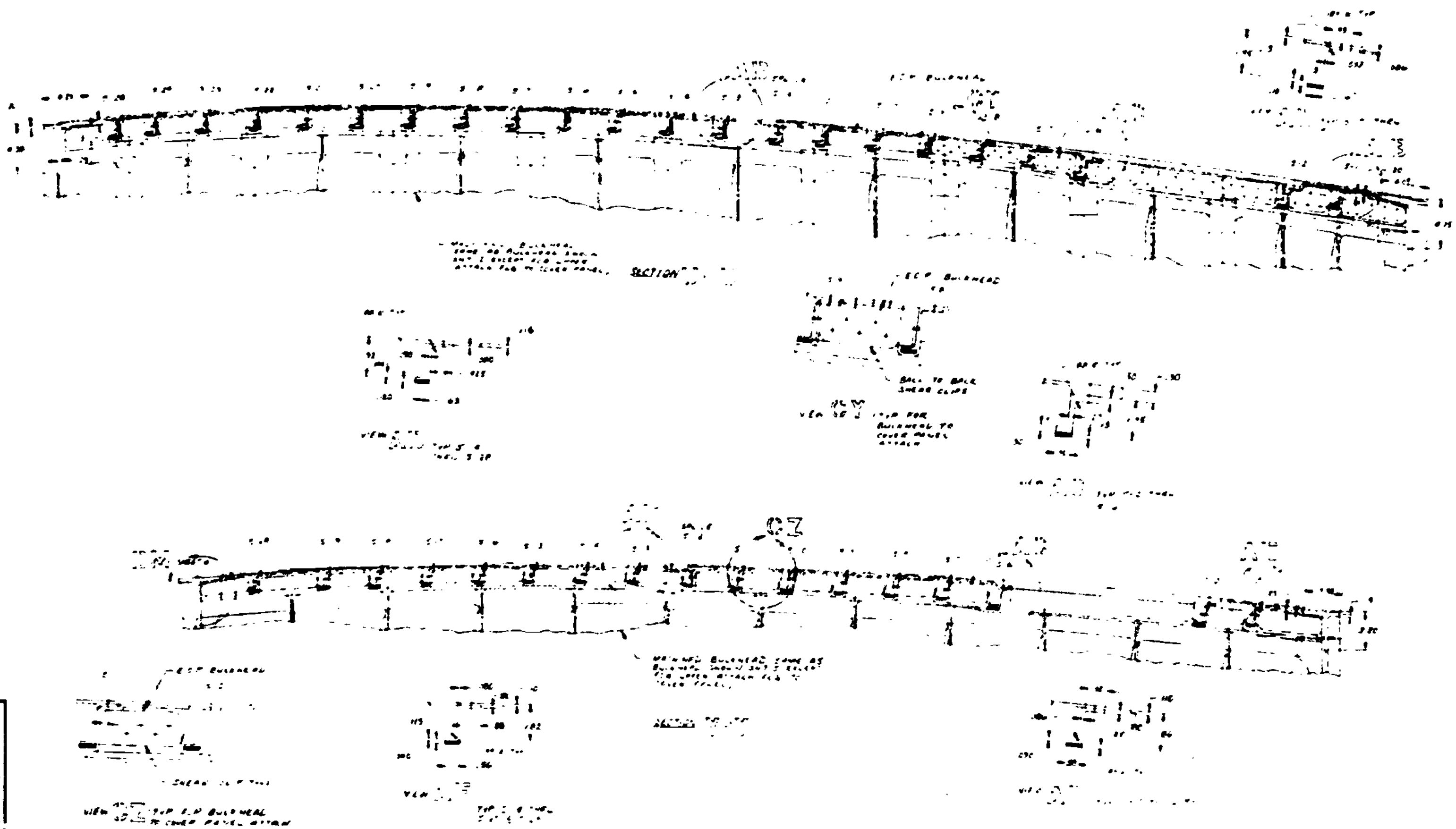

Figure 68 STRUCTURAL ARRANGEMENT FOR WING CONCEPT NO. 2 -- Continued SHEET 2

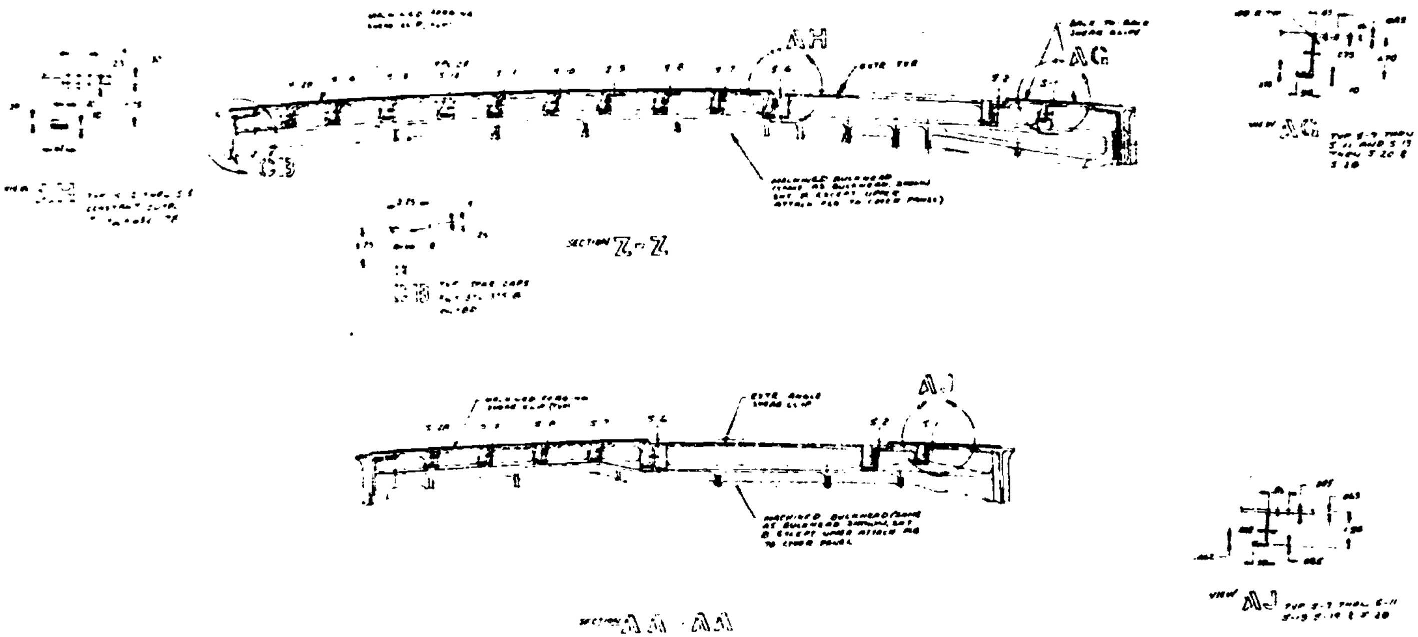

Figure 68 STRUCTURAL ARRANGEMENT FOR WING CONCEPT NO. 2 -- Concluded SHEET 3

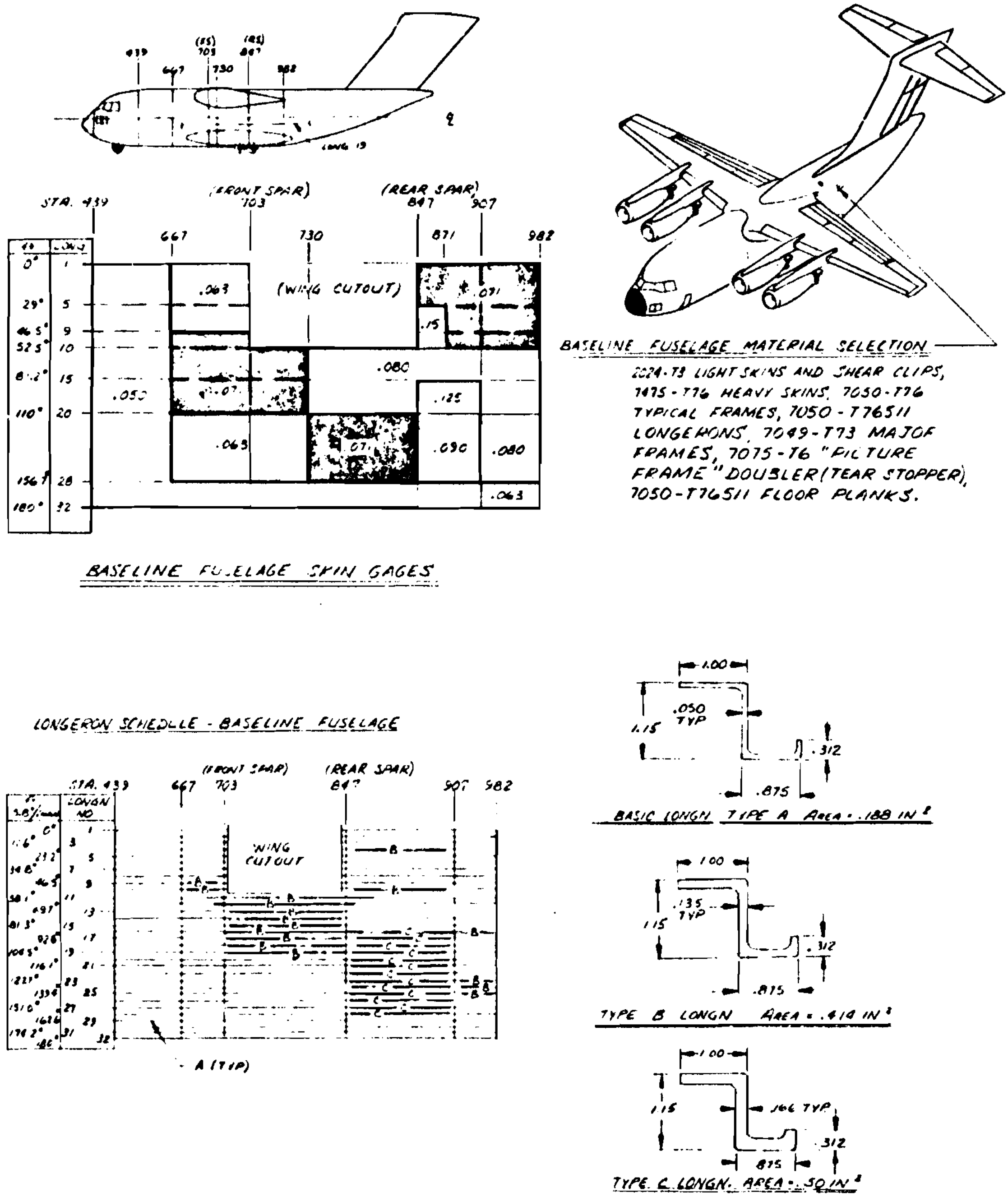

Figure 69 BASELINE FUSELAGE SHELL STRUCTURAL CONCEPT

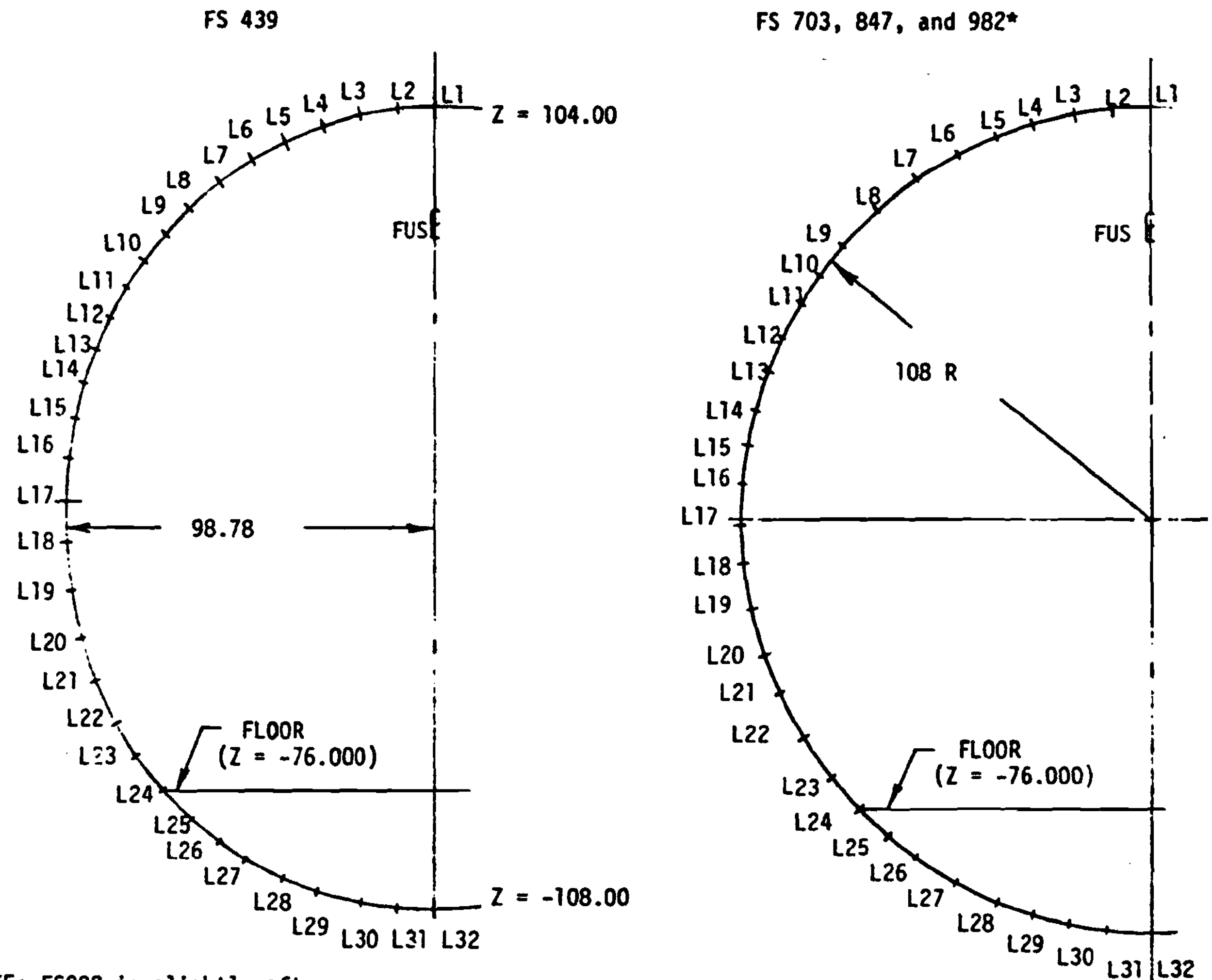

* NOTE: FS982 is slightly aft of the constant section

Figure 70 BASELINE FUSELAGE LONGERON LOCATIONS

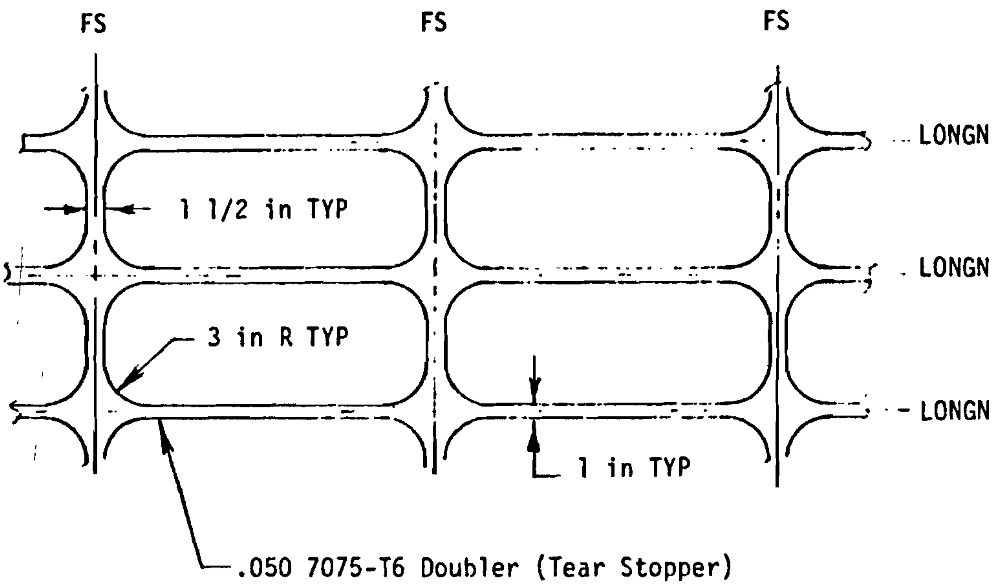

Figure 71 BASELINE FUSELAGE TYPICAL DOUBLER CONFIGURATION

TABLE XVII SUMMARY OF BASELINE FUSELAGE SKIN THICKNESSES

	FUSELAGE CONTROL STATIONS			
LONGERONS	FS439	FS703	FS847	FS982
1	.050	.063	.063	.063
9		.063	.063	.063
10				
		.071	.071	.071
20				
		.063	.080	.080
28				
32	.050	.050	.050	.050

spacing generally. See Figures 70, 71 and Table XVII. Tear stoppers consisting of 0.050 7075-T6 "picture-frame" doublers are used between the skin and longerons and skin and shear clips where the skin thickness is 0.063 inch or less (Figure 72). The extreme forward portion of the fuselage, ahead of FS 366, is stiffened only by frames at 9-inch spacing.

The skin thickness varies from 0.050 to 0.080 inches but the minimum skin gage in the pressure critical area is 0.050 inch per Table XVII. Typical frames are 7050-T76 rolled sheet metal Z-section members approximately 4.44 inches in depth. The side panels near the wing (FS 703, 847, and 907) are stiffened by machined, forged 7049-T73 frames (attached directly to the skin) and machined longerons between frames. The depth of the machined frame varies from 3 inches to about 10 inches. The longerons are mechanically attached to the frames by shear clips which join the upstanding leg of the longeron and web of the frame. Longeron depth is about 1.25 inch. In addition, bulkheads spaced 48 inches on center and parallel keel webs spaced 40.88 inches apart, i.e., 20.44 inches from the fuselage centerline, provide the necessary support for cargo floor loads. The baseline fuselage configuration is based on the best available loads information and projections for the fuselage structural design of the C-15.

The baseline fuselage shell panel geometry was established by using the C-15 as a reference geometry and modified by varying key parameters, such as skin thickness, longeron spacing, and thicknesses of the flanges on the longerons. Elements which were considered invariant for this purpose are the overall longeron height of 1.230 plus 0.020 inches and frame spacing of 24 inches.

The baseline cargo floor has fully recessed tiedown rings, integral roller conveyor system, guide restraint rails, and seat tracks. A powered cargo transfer system can be provided but is not included at this time (see Figure 73).

Three axial compressive load intensities (N_x = 1000, 2000, and 3000 lb./in.) were selected for the initial sizing studies. The axial loads at the four control stations are generally less than 1000 pounds per inch but longerons located at the rear spar and main gear station (FS847) are sized for axial loads above 3000 pounds per inch. For the studies the panels were sized based on the compressive load intensities noted and the initial weight curves do not reflect the relative effects of combined loads and non-optimum factors such as splices or joints. A minimum skin thickness of 0.050 inch was set for all of the design concepts, except honeycomb sandwich panels, based on consideration of the affects of panel shears, hoop tension stresses from pressurization, and the use of flush attachments.

Five fuselage structural shell concepts were evaluated for relative panel weights as a function of material and geometry.

5.2.2 New Fuselage Panel Concepts

Emphasis was placed on new fuselage shell panel concepts in this study due to the large impact of fuselage skin panels on total fuselage structural weight. The fuselage shell comprises 32.5 percent of the total fuselage structural weight and 80 percent of the fuselage shell weight is in the skin panels (see Figure 74).

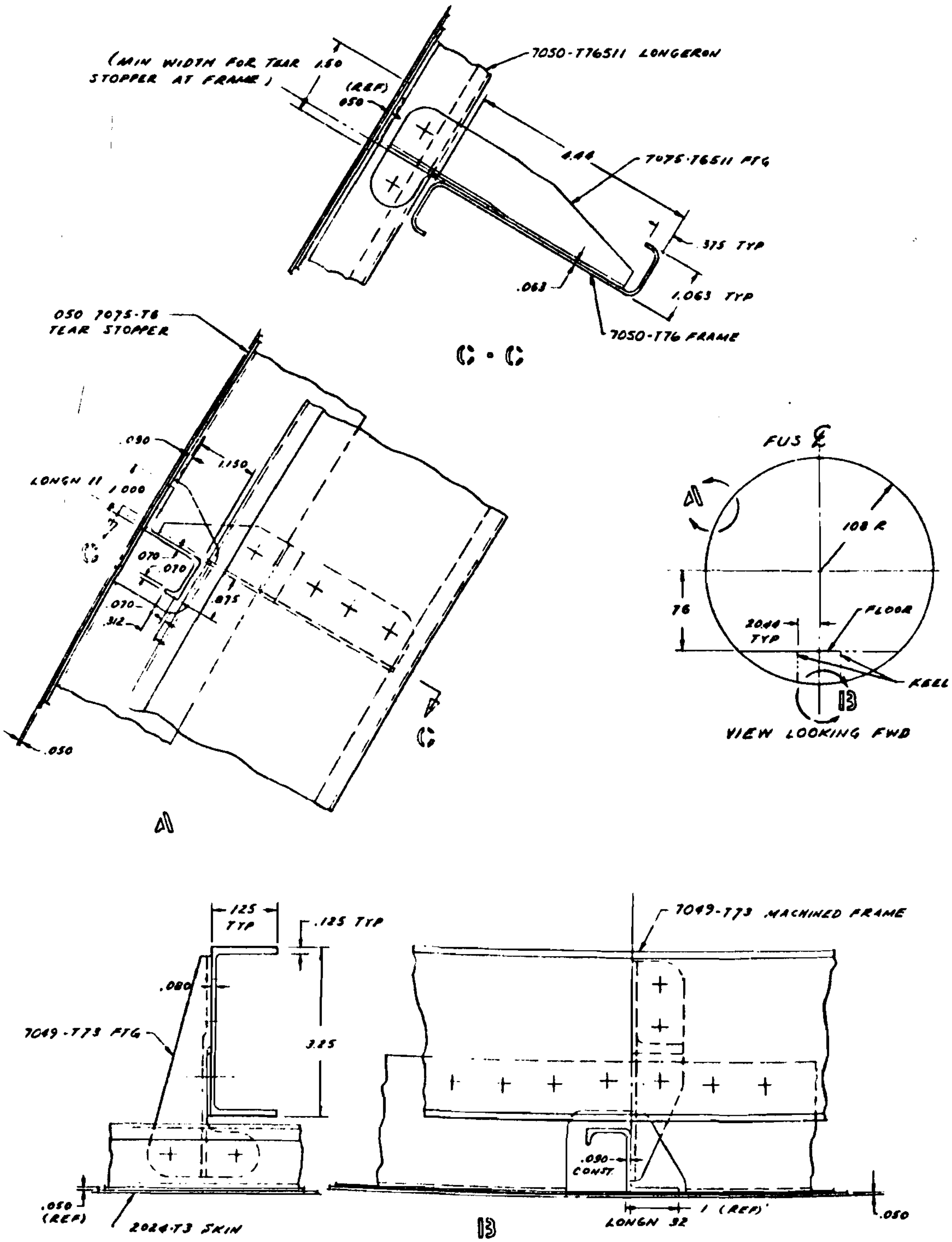

Figure 72 TYPICAL BASELINE FUSELAGE STRUCTURE

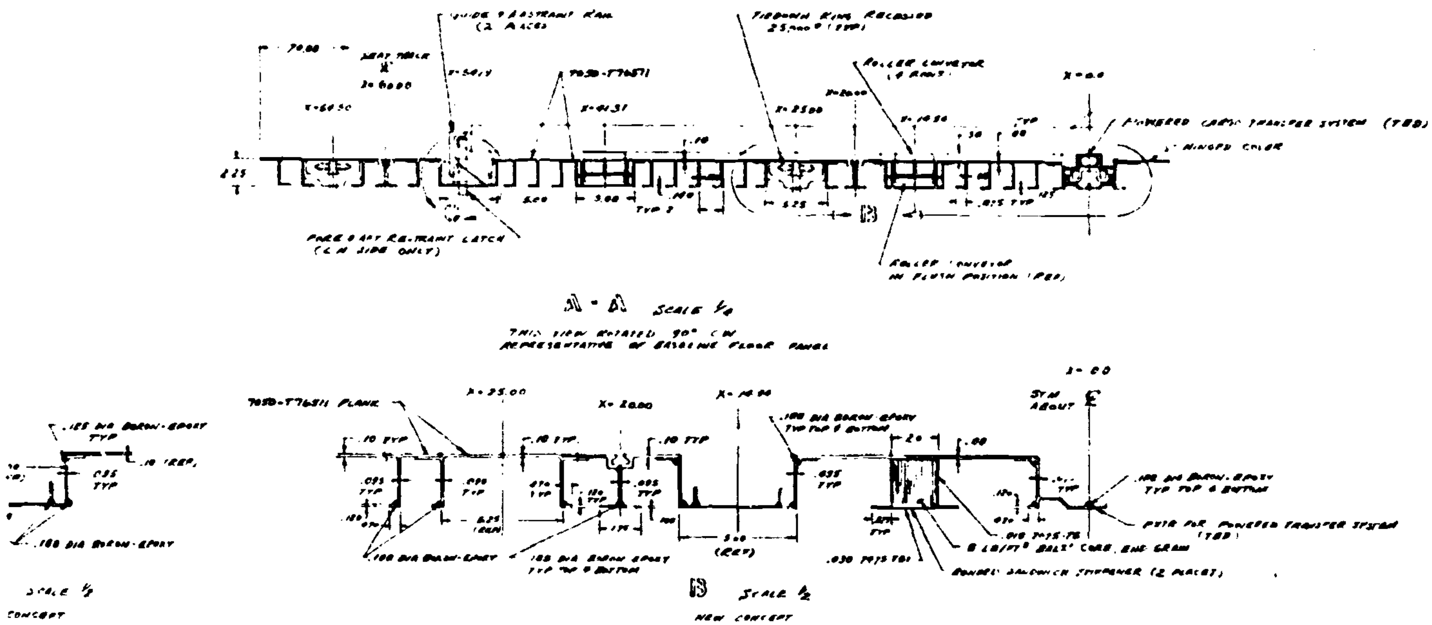

Figure 73 FUSELAGE CARGO FLOOR BASELINE AND NEW CONCEPT

5.2.2.1 Stiffened Panel Concepts - The first new concept, identified as IIA, was simply an increase in the spacing of the longerons around the circumference of the shell. Material combinations considered are: 1) baseline material combination, 2) 7475-T761 aluminum alloy skins with 7075-T6511 longerons, 3) S-200 grade beryllium skins and longerons, and 4) Ti-6Al-4V Ann titanium skins and longerons. The weight curves in Figure 75 show the relative weight efficiencies of the various material combinations and longeron spacing selected. The least efficient combination, Ti-6Al-4V Ann titanium skin and longerons, was about 0.4 $lbs./ft.^2$ heavier, while the most efficient for the load intensities selected was the combination of 7475-T761 aluminum alloy skin and 7075-T6511 aluminum alloy longerons.

A variation of concept IIA, identified as IIB, changes the frame spacing from 24 inches (baseline) to 96 inches. One significant result of this study, was that for a given N_x, the required frame bending stiffness decreases with increased frame spacing.

The weight efficiency (lower total frame weight) is essentially proportional to the increase in frame spacing. The material combination selected for this study was 2024-T3 aluminum alloy skins and 7050-T76511 aluminum alloy longerons. Longeron spacing was set at 11 inches. Two different frame gages (t_f = 0.063 and t_f = 0.080 inch) was considered. The most efficient geometry combination was 0.050 inch thick skin with 96-inch frame spacing.

5.2.2.2 Simple Isogrid Panel Concept - The second new concept selected for study is a simple integral isogrid panel (Figure 76). Three different materials, 7475-T761 aluminum, Ti-6Al-4V Ann titanium, and S-200 beryllium were evaluated for this concept and identified IIIA, IIIB, and IIIC. A parametric study was conducted to evaluate several configurations using the 7475-T761 material. Three different triangle heights (h = 3, 6, and 12 inches), four skin thicknesses (t_s = 0.050, 0.071, 0.090 and 0.125 inches), and four rib thicknesses (b = 0.5, 0.10, 0.15 and 0.20 inch) were evaluated. For the evaluation of beryllium isogrid h was set at h = 12, and b was set as b = 5, and three different skin thicknesses (t_s = 0.050, 0.071, and 0.090 inch) was considered. Titanium was evaluated with three different values of h (h = 3, 6, and 12 inches), two values of b (0.05 and 0.10 inch), and three skin thicknesses (t_s = 0.050, 0.071, and 0.090 inch). The relative weight efficiencies, based on the compressive load intensities selected, of the various material and geometry combinations are shown in Figure 77 through 79. At the low load intensities, a triangle height (h) of 3 inches is the most efficient, but the most efficient height at the higher load intensities is h = 5 inches.

5.2.2.3 Modified Isogrid Panel Concept - The third new concept is a modified isogrid concept (Figure 76) which is an array of small isogrids within a group of large isogrids. The large isogrids are sized for general instability buckling while the small isogrids are sized for the skin buckling failure mode. This geometric arrangement permits the basic triangle height (h) and the height of the smaller enclosed triangles (h') to be varied along with rib dimensions and skin thicknesses. Aluminum and titanium alloys (concept IVA and IVB, respectively) were compared with h values from 3 to 12 inches, h' values from 3 to 6 inches, t_s values from 0.050 to 0.090 inch, and four variations of rib

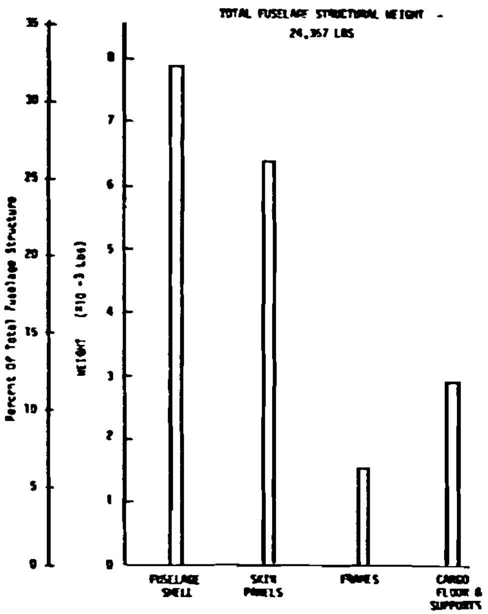

Figure 74 FUSELAGE STRUCTURAL WEIGHT DISTRIBUTION

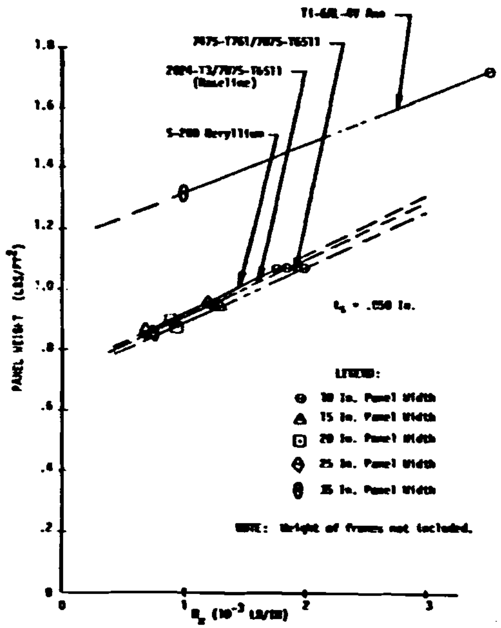

Figure 75 WEIGHT COMPARISON OF VARIOUS MATERIALS AND PANEL WIDTHS

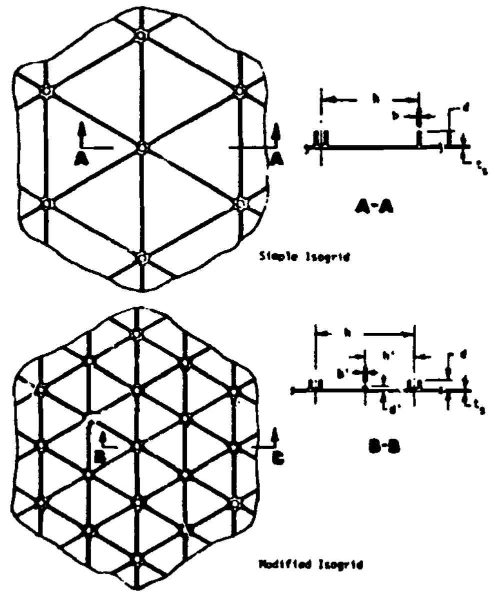

Figure 76 SIMPLE AND MODIFIED ISOGRID CONCEPTS

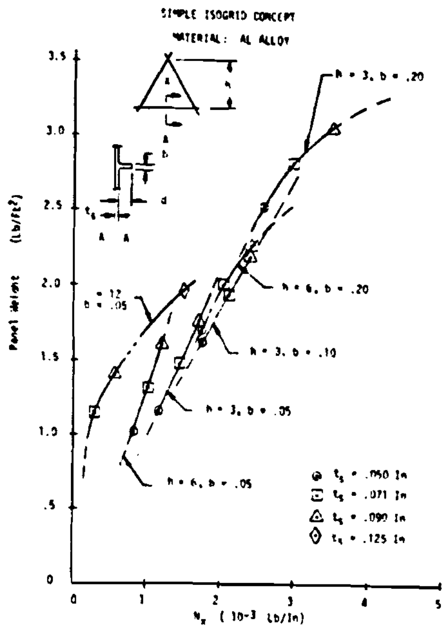

Figure 77 ALUMINUM ISOGRID PANEL WEIGHT COMPARISONS

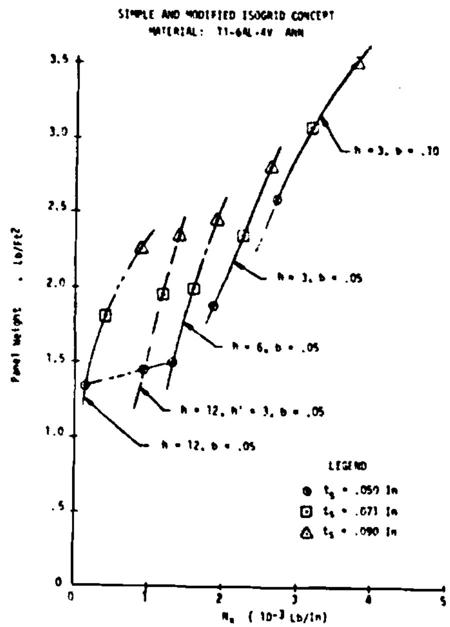

Figure 78 WEIGHT COMPARISON OF VARIOUS TITANIUM ISOGRID PATTERNS

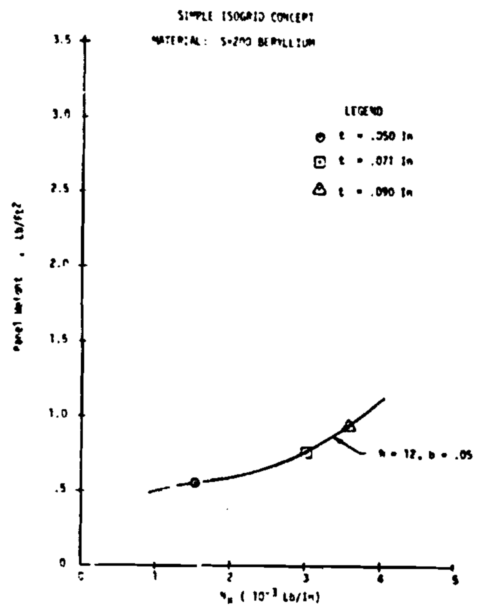

Figure 79 WEIGHT COMPARISON OF VARIOUS BERYLLIUM ISOGRID PATTERNS

width (b = 0.05, 0.10, 0.15, and 0.20 inch). The weight curves of Figure 78 and 80 show the relative weight efficiency of the material and geometric combinations. The panel weights shown are based on the assumption that intermediate frames are not required.

5.2.2.4 Honeycomb Sandwich Panel Concept - Another design concept evaluated is honeycomb sandwich panels. Materials evaluated are 7475-T761 aluminum alloy and Ti-6Al-4V Ann titanium (concepts VA and VB respectively). A minimum face sheet thickness of 0.020 inch was set for practical considerations of damage tolerance and fatigue associated with primary structure especially as related to pressurized shell design. The sandwich concepts are shown in Figure 81.

5.2.2.5 Integrally Stiffened Panel Concept - The fifth concept (VI) is an integrally stiffened panel utilizing 7475 aluminum alloy plate and incorporating J-section longerons spaced at 10, 15, 20, and 25 inches. The relative weight efficiencies of the various geometric arrangements is shown in Figure 82. Weight savings range from 7 percent to almost 12 percent.

Table XVIII is a summary of the relative weight efficiencies of the various fuselage panel concepts evaluated in the parametric studies. Figure 83 shows those design concepts which are more weight efficient than the baseline concept. Note that the weights in Table XVIII and Figure 83 are optimum based on compressive loads only and do not include such non-optimum factors as splices, joints, or window cutouts. The potential weight savings indicated here for the isogrid concepts are optimistic and were not realized in the isogrid fuselage design presented in Volume II due to the absence of the weight affects of shear, internal pressure, and combined loads.

5.2.3 Selected Fuselage Panel Design Concepts

The various components of the fuselage shell and cargo floor have been selected for the weight and cost studies of the complete airframe. These are described in the following paragraphs.

5.2.3.1 Honeycomb Sandwich Panel Concept - The honeycomb sandwich panel concept utilizes thin (0.020 to 0.033 inch) 7050-T76 clad aluminum faces adhesively bonded to 3.1 lb/ft^3 (1/8 -5056- .0007) honeycomb core. The core thickness varies from 0.19 inch at the most forward station (FS 366) to 1.00 inch at the front spar (FS 703). The variation between the stations is a straight taper. The core is a constant 1.00 inch thickness from FS 703 to FS 982. The sandwich panel dimensions at the four fuselage control stations are shown in Table XIX.

The fuselage shell has complete frame members at FS 366, 703, 847, and 982 only. The basic philosophy of retaining the cargo floor bulkheads at the baseline 48 inch spacing was retained so as not to degrade the load capability of the floor. The frame members at the bulkhead stations maintain full depth to the maximum half breadth location at the side of the fuselage and taper in depth and area to zero at the 45° position from the fuselage top center. The overall fuselage shell sandwich design, together with primary circumferential and longitudinal splices, are shown in Figure 84. Preliminary design details at the wing/fuselage and fuselage/floor intersections are also shown in Figure 84.

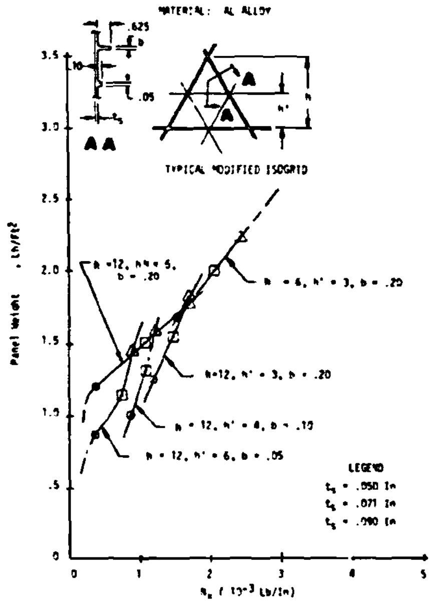

Figure 80 ALUMINUM MODIFIED ISOGRID PANEL WEIGHT COMPARISONS

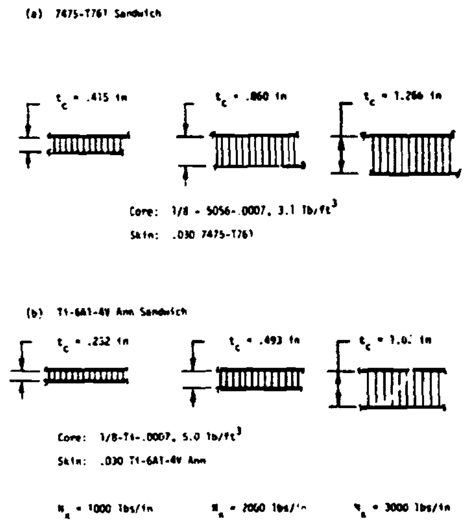

Figure 81 ALUMINUM AND TITANIUM SANDWICH PANEL CONCEPTS

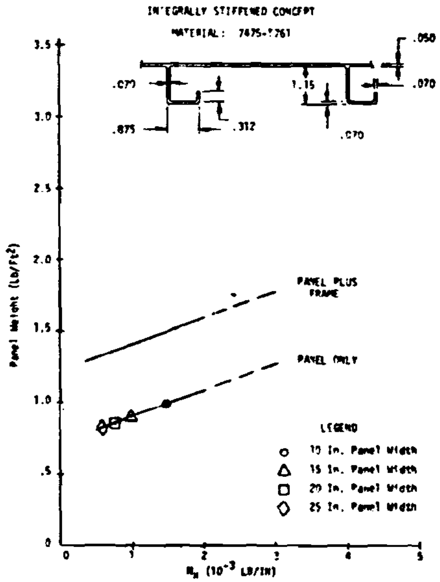

Figure 82 WEIGHT COMPARISON OF INTEGRALLY STIFFENED FUSELAGE SHELL PANEL CONCEPTS

TABLE XVIII - SUMMARY OF TYPICAL FUSELAGE STRUCTURAL PANEL CONCEPTS WEIGHTS

	Weight (lb/ft^2)		
	N_x=1000 lb/in	N_x=2000 lb/in	N_x=3000 lb/in
I Baseline 2024-T3 skin 7050-T76511 longerons, 7050-T76 frames	1.50	1.80	1.93

	Weight (lbs/ft^2)	Weight Saving	
		lbs/ft^2	Percent
IIA Increase Longeron Spacing, same material as Baseline	1.405	.095	6.33

	N_x = 1000 lbs/in			N_x = 2000 lbs/in			N_x = 3000 lbs/in		
	Weight (lbs/ft^2)	Weight Saving		Weight (lbs/ft^2)	Weight Saving		Weight (lbs/ft^2)	Weight Saving	
		lbs/ft^2	Percent		(lbs/ft^2)	(Percent		(lbs/ft^2)	Percent
IIB Increased Frame Spacing	1.28	.22	14.67	1.38	.42	23.33	1.44	.49	25.39
IIIA Simple Isogrid 7475-T761	1.18	.32	21.33	1.60	.20	11.11	2.04	-.11	-5.70
IIIB Simple Isogrid Ti-6Al-4V Ann	1.51	-.01	-.67	2.03	-.23	-12.78	2.92	-.99	-51.30
IIIC Simple Isogrid S-200 Beryllium	.50	1.00	66.67	.58	1.22	67.78	.75	1.18	61.14
IVA Modified Isogrid 7475-T761	1.18	.32	21.33	1.95	-.15	-8.33	2.57	-.64	-33.16
IVB Modified Isogrid Ti-6Al-4V Ann	1.58	-.08	-5.33	--	--	--	--	--	--
VA Sandwich 7475-T761	1.20	.30	20.00	1.30	.50	27.78	1.39	.54	27.98
VB Sandwich Ti-6Al-4V Ann	1.68	-.18	-12.00	1.78	0	0	2.02	-.09	-4.66
VI Integrally Stiffened 7475-T761	1.40	.10	6.67	1.60	.20	11.11	1.70	.23	11.92

TABLE XIX SUMMARY OF FUSELAGE SHELL SANDWICH PANEL DIMENSIONS					
Fuselage Control Station		FS 439	FS 703	FS 847	FS 982
t_c (in)		.363	1.00	1.00	1.00
t_f (in)	$\theta = 0°$	.020	.025	.025	.025
	$\theta = 30°$	.025	.021	.033	.020
	$\theta = 90°$	.020	.025	.033	.020
	$\theta = 150°$	.020	.020	.020	.020
	$\theta = 180°$				
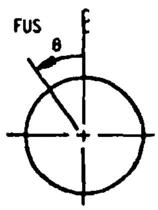 FUS θ ℄ FUSELAGE CROSS-SECTION					

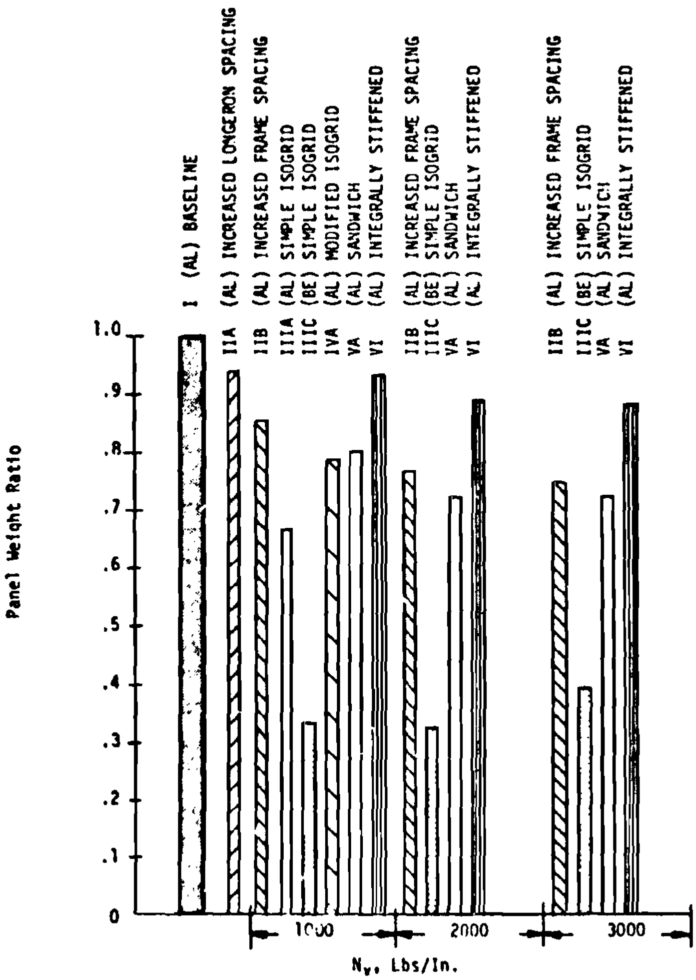

Figure 83 SUMMARY OF PANEL WEIGHT RATIOS

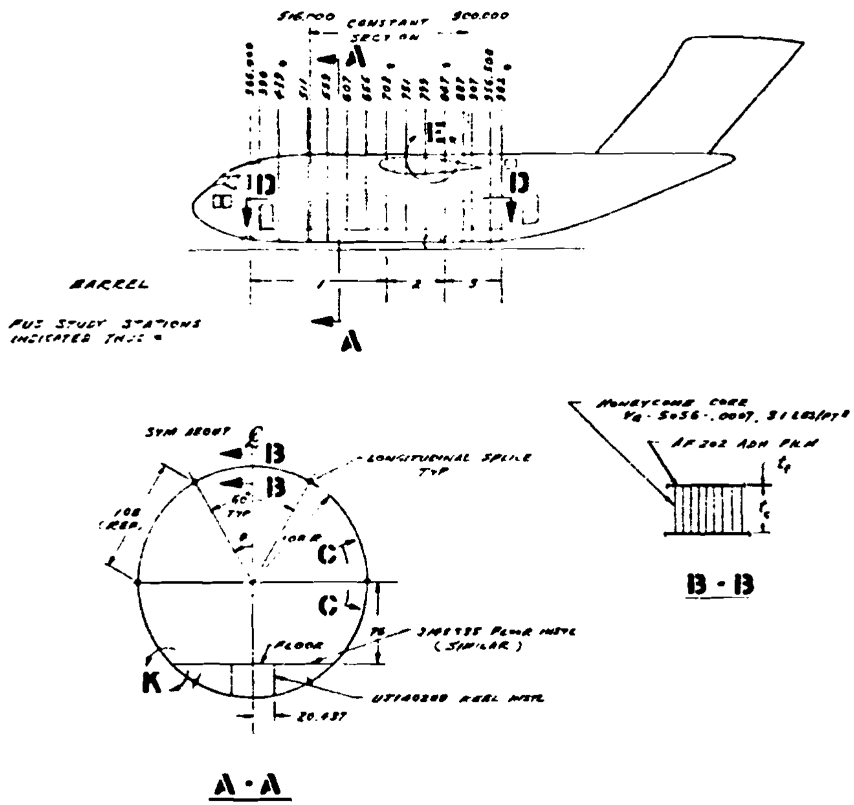

GENERAL NOTES

1. FUSELAGE SHELL FROM AFT OF THE COCKPIT (FS 366.000) TO AFT END OF CARGO FLOOR FS 982, TO BE SANDWICH PANEL CONCEPT
2. FUSELAGE SHELL FORWARD OF FS 366.000 TO BE BASELINE STRUCTURE
3. FUSELAGE SHELL AFT OF FS 982 TO BE BASELINE STRUCTURE
4. FRAME BULKHEADS FOR FLOOR SUPPORT TO BE SIMILAR TO AND LOCATED AT FUSELAGE STATIONS IDENTICAL TO BASELINE FRAME CROSS SECTION TO BE MAINTAINED FROM BOTTOM ℄ TO MAXIMUM HALF BREADTH WITH UNIFORM TAPER [illegible] OF FRAME DEPTH TO ZERO AT MIDPOINT BETWEEN MAX HALF BREADTH AND TOP ℄ (45° POSITION)
5. NO FRAMES BETWEEN BULKHEAD STATIONS
6. FS 703 AND 847 TO HAVE COMPLETE FRAMES FROM FUSELAGE TOP ℄ TO BOTTOM ℄
7. MATERIALS TO BE EVALUATED

   2024-T3 7475-T761
   7075-T6
   7475-T61
8. BOND HONEYCOMB TO ALUMINUM USING AF 202
9. BOND ALUM TO ALUM USING AF 32

FUS STUDY STA		633	703	847 982
BARREL		1	2	3
LENGTH		337	144	135
t_c		.200 1.00	1.00	1.00
t_F	θ = 0°			
		.020	.025	.025
7475-T6 CLAD	θ = 30°			
		.025	.021–.033	.033–.020
	θ = 90°			
		.020	.020–.033	.033–.020
	θ = 150°			
		.020	.020	.020
	θ = 180°			

Figure 84 HONEYCOMB SANDWICH FUSELAGE SHELL CONCEPT (Sheet 1)

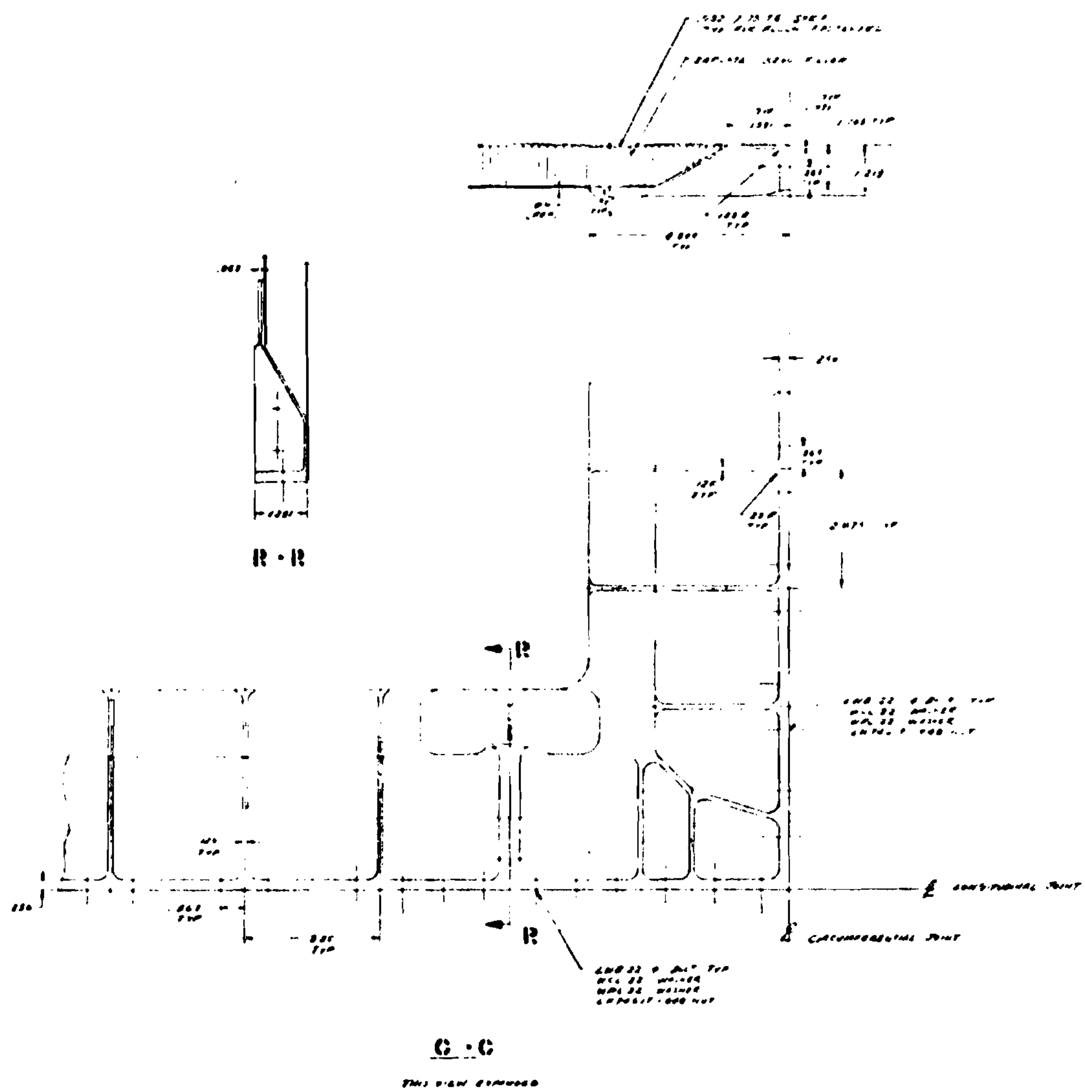

Figure 84 HONEYCOMB SANDWICH FUSELAGE SHELL CONCEPT -- CONTINUED (Sheet 2)

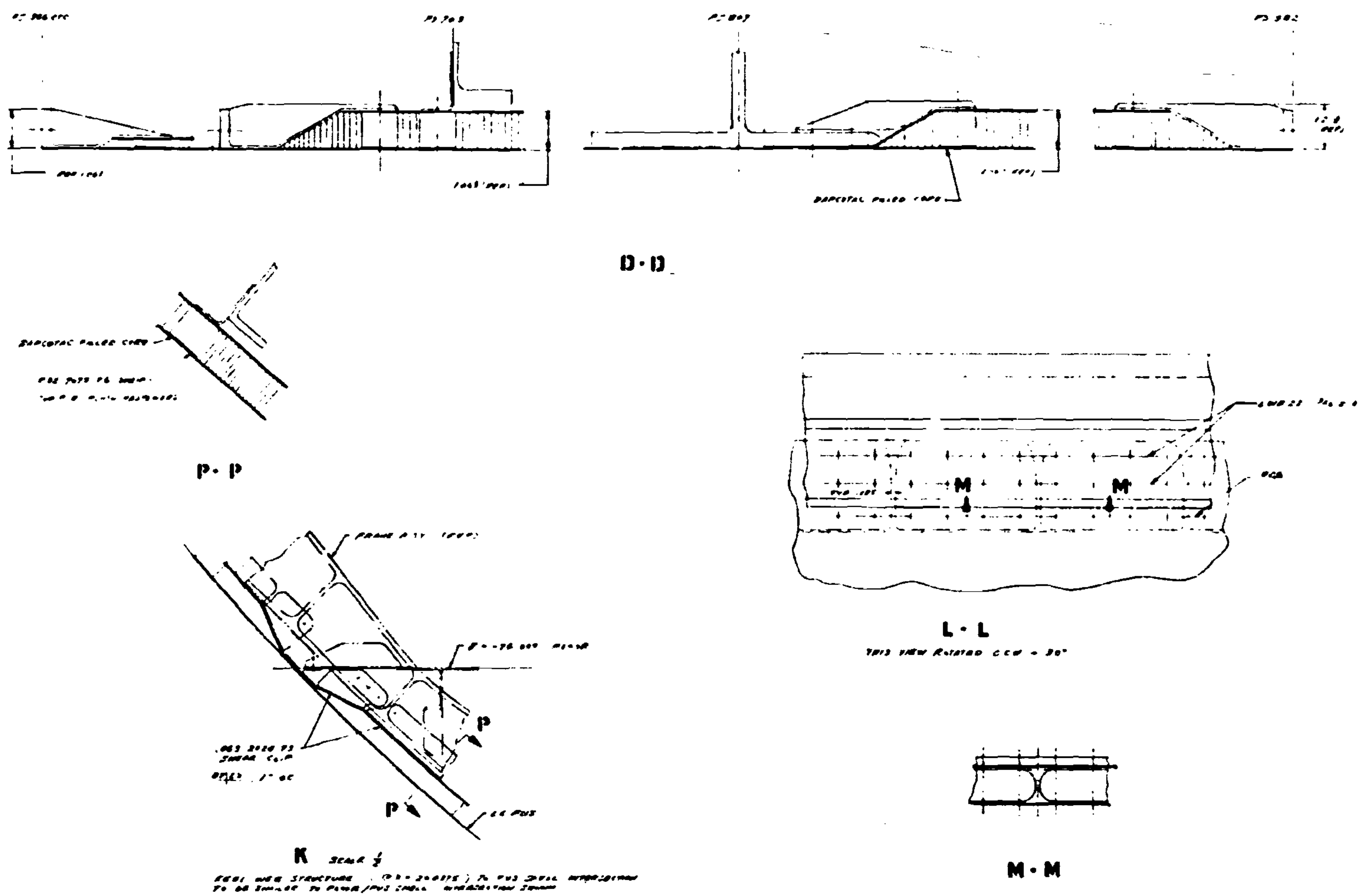

Figure 84 HONEYCOMB SANDWICH FUSELAGE SHELL CONCEPT -- CONTINUED (Sheet 3)

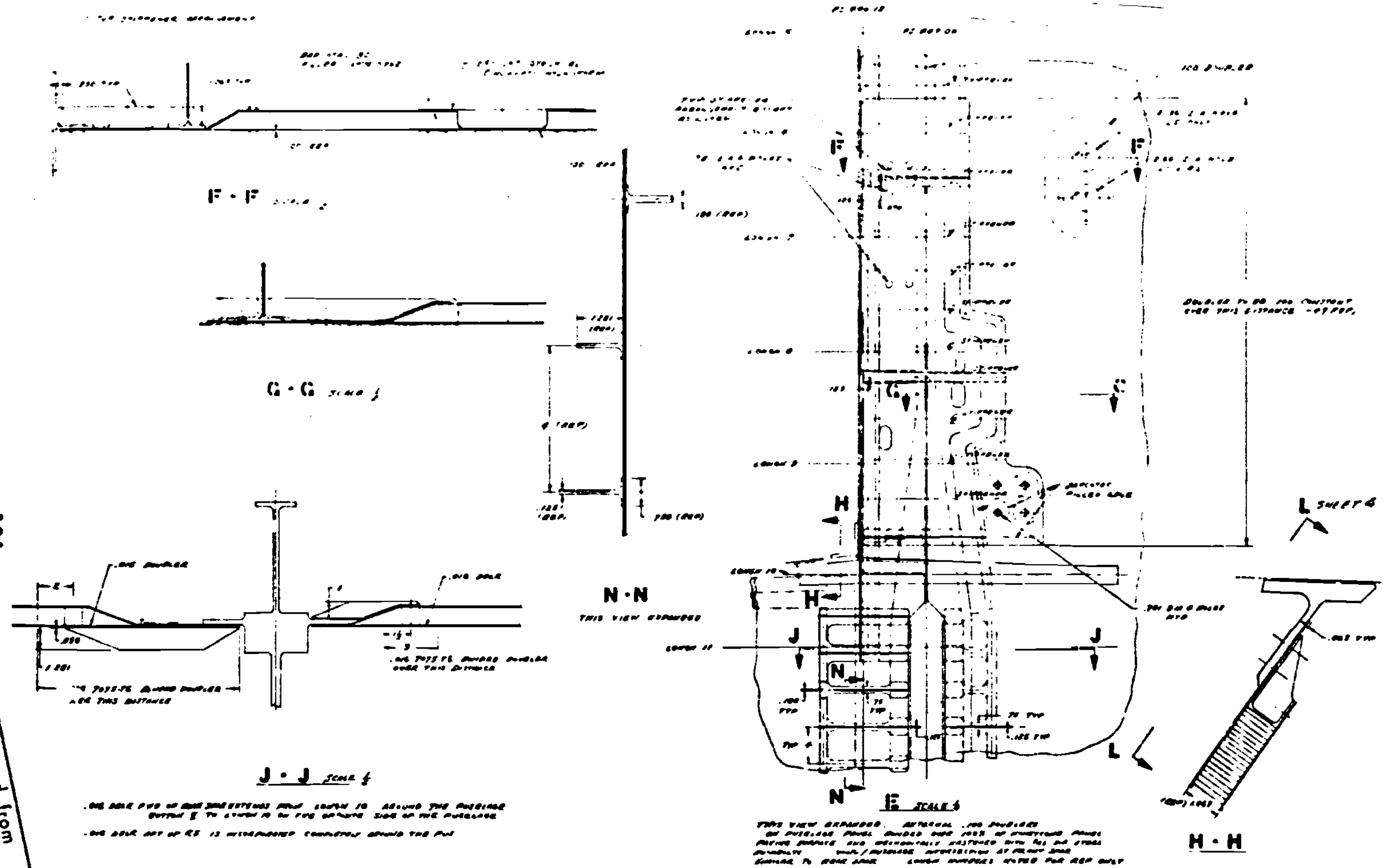

Figure 84 HONEYCOMB SANDWICH FUSELAGE SHELL CONCEPT -- Concluded (Sheet 4)

Each barrel assembly is divided longitudinally into 60° segments which are approximately 9 feet wide. The honeycomb panel assemblies are basically composed of an aluminum honeycomb core which is tapered at each of the four sides and enclosed within an aluminum picture frame member which incorporates integral end fittings on all sides. The aluminum edge member and the honeycomb sandwich are joined by a combination of adhesive bonding and mechanical fasteners. The honeycomb core at the fastener locations is filled with Dapcotac 3200 which provides the necessary strength for resisting fastener installation and service loads.

Doublers of 0.016 7075-T6 sheet are added locally in the high stress areas.

Strength requirements dictated the skin gages primarily to provide the necessary low stress level in tension resulting from fuselage pressurization and for shear. The second major consideration was compression stability which basically determined the core thickness or the overall panel thickness.

General instability failure mode was considered with frame spacing and stiffness as significant parameters. The equation for frame stiffness coefficient from Reference 37 was used.

$$C_f = \frac{(EI)_f L}{MD^2} \tag{16}$$

where

C_f = frame stiffness coefficient

$(EI)_f$ = frame bending stiffness

L = length of shell

M = bending moment

In addition, a value for C_f of 62.5×10^{-6} was used as a dividing line between panel failures and general instability failures, i.e., values of C_f no greater than the stated value would insure general stability with a high confidence level. A simplified analysis of the fuselage barrel section from FS 366 to FS 703 indicates a need for an $(EI)^f = .5 \times 10^6$ minimum for M_{max} of 55×10^6 inch-pound (ult) at FS 703. The baseline front spar frame was retained to insure adequate structural strength and stiffness in the new concept design.

The minimum I_f for the front spar frame occurs in the upper 90° (± 45° from top center) of the fuselage shell where the frame member is an .080 7075-T6 formed zee. The I_f is approximately 2.6 in^4 which provides an $(EI)_f$ approximately equal to 27.6×10^6 $lb\text{-}in^2$. Since the actual $(EI)_f$ is much greater than the theoretically required value, the simplified approach taken in this study should be satisfactory. The rear spar frame was treated in a manner similar to the front spar frame.

Weight savings for the new concept sandwich shell, bulkheads, and supporting structure of 330 lbs (3.1%) were achieved for the unresized configuration. See Table XX.

5.2.3.2 Isogrid Panel Concept - The final selected isogrid panel details are covered in Volume II of this report.

5.2.3.3 Selectively Reinforced Panel Concept for Cargo Floor - The selected floor panel concept is a hybrid structure which utilizes both the selectively reinforced (composite infiltrated extrusion) panel and sandwich panels. See Figure 73 and Table XX. The average weight saving for the new hybrid floor panel concept is 7.4%. The overall weight saving on the floor panel, support bulkheads, and keel structure is 4.8%. The new concept is a combination of sandwich structure utilizing 7475-T61 facings and 8 lbs/ft^3 balsa core in an adhesive bonded panel assembly and extruded 7050-T6511 planks. The aluminum extrusions are selectively reinforced with boron-epoxy composities, Figure 73. The channel for the integrated cargo handling system and the basic floor section are similar in that the configurations are comprised of small diameter rods of boron-epoxy oriented longitudinally. The section of floor extending to the fuselage shell is a continuation of the respective structural concepts, e.g., boron-epoxy infiltrated extruded planks and channels.

The selectively reinforced panel configuration has been successfully tested in many structural parts including an in-house DC-10 Passenger Floor Strut Test Program. Specifically, boron-epoxy composite reinforcement would be infiltrated into the hollow openings of 7050-T6511 extruded planks and channels. The epoxy matrix is room temperature cured and post cured at 250°F. The result is a composite reinforced aluminum member with no measurable distortion or locked-in residual stresses attributable to thermal mismatch.

TABLE XX SUMMARY OF RECOMMENDED HONEYCOMB SANDWICH PANEL AND COMPOSITE REINFORCED/SANDWICH CARGO FLOOR CONCEPTS

FUSELAGE COMPONENT	WEIGHT (lb/ft^2)	WEIGHT SAVING lb/ft^2	WEIGHT SAVING PERCENT
1. SHELL (includes joints and frames)			
a. Baseline	1.98	---	---
b. Honeycomb Sandwich	1.87	0.11	5.60
2. CARGO FLOOR PANEL			
a. Baseline	3.50	---	---
b. Composite Reinforced/Sandwich	3.24	0.26	7.40

A simplifying assumption was made at the outset based on the five different cases of cargo loading (various combinations of vehicles), that approximately four feet of floor width centered about the fuselage centerline would not be subjected to wheel loads. Based on intuitive engineering judgment, a second assumption was made that a sandwich type floor adequate for highly concentrated and cyclic loads, such as heavy vehicles, would not be competitive in terms of weight. Since a weight reduction with sandwich type structure appeared possible only in the narrow center portion of the floor, the use of this concept was restricted to this area.

5.3 HORIZONTAL STABILIZER STRUCTURE

The cover panel concept for the horizontal stabilizer evolved from the studies for the wing structure. The baseline and new concept discriptions are given in the following paragraph.

5.3.1 Baseline Design Concept

The baseline structure for the horizontal stabilizer consists of zee-stiffened aluminum skin panels, extruded aluminum spar caps and hat and "L" stiffened rib and spar webs. The basic structure is shown in Figure 85.

5.3.2 New Design Concept

The design concept selected and used for the weight and cost analyses is developed in the next few sections.

5.3.2.1 Cover Skin Panels - An investigation was conducted similar to that on the wing using 7075-T651 integrally stiffened skin planks. A local area taken on the lower surface of the horizontal stabilizer at X_H = 101 with a column length of 24.5 in. and a column load of 3,800 lb/in necessitated stringers at approximately 3.5 in. and gave a weight of 1.52 lb/sq. ft.

Due to the relatively low loads on the horizontal stabilizer, a honeycomb skin panel was then evaluated using 7050-T76 chem-milled tapered skin panels with an aluminum honeycomb core of 3.8 lb/cu. ft. density (Figure 86). To keep the honeycomb to a reasonable depth, the panel width was reduced by the addition of a lightweight center spar. This arrangement eliminated the need for stiffeners and intermediate ribs.

Taking the same local area at X_H = 101 as above, the weight was 1.26 lb/sq. ft., giving a weight saving of 17% over the integrally stiffened skin planks.

5.3.2.2 Spar Caps - The machined spar caps are made from 7050-T76511 aluminum extrusion and are bonded to the honeycomb skin panels during the same curing cycle, thus becoming an integral part (Figure 86) of the cover panel.

5.3.2.3 Ribs - The first concept investigated was the half rib and pin method (Figure 87). Due to the fact that the only ribs now remaining in the horizontal stabilizer pick up either hinge or actuator loads, the shear transfer through the pin joint was excessive and tension field ribs met the criteria more satisfactorily. To reduce assembly time, however, these are

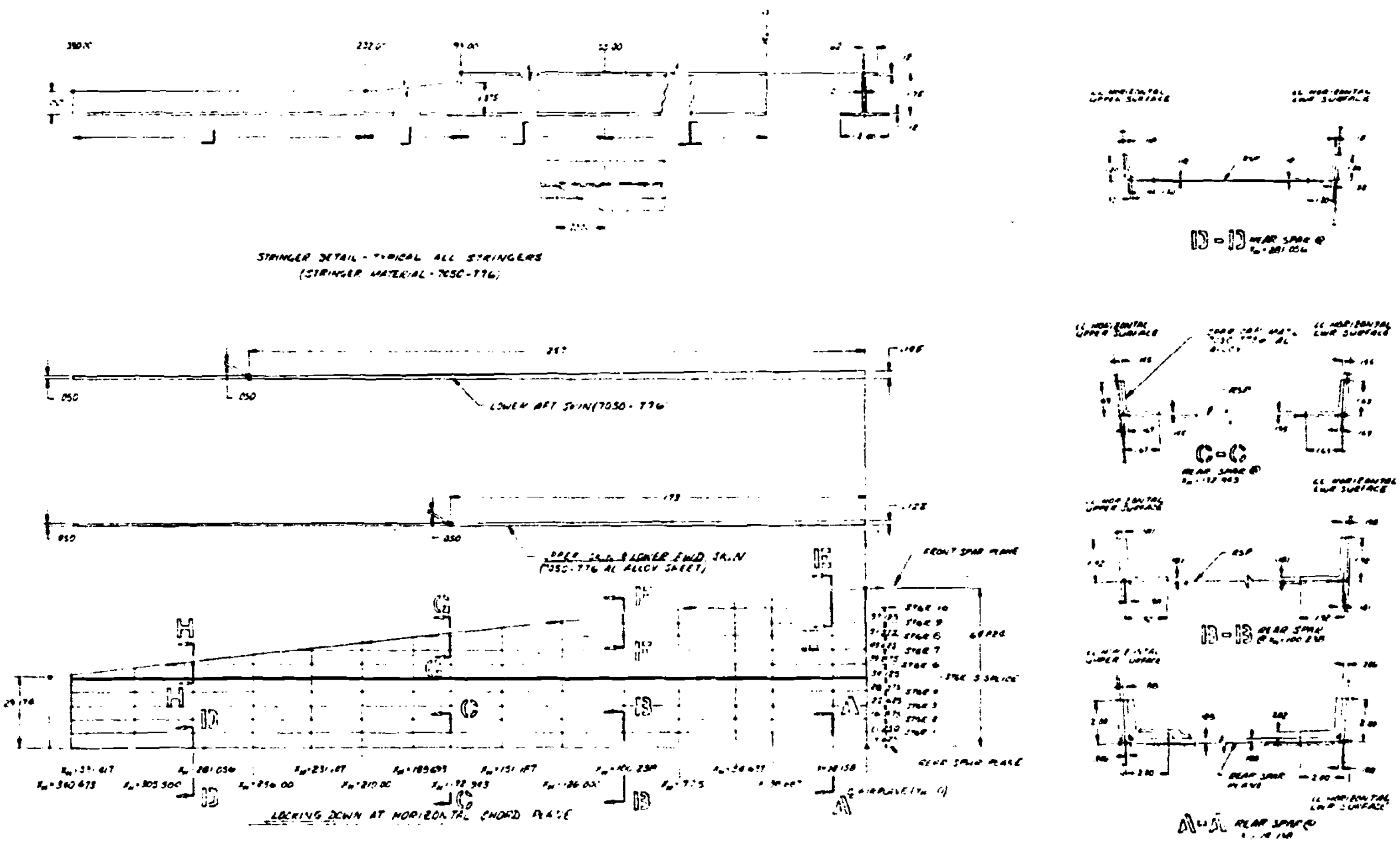

Figure 85 BASELINE HORIZONTAL STABILIZER STRUCTURE SHEET 1

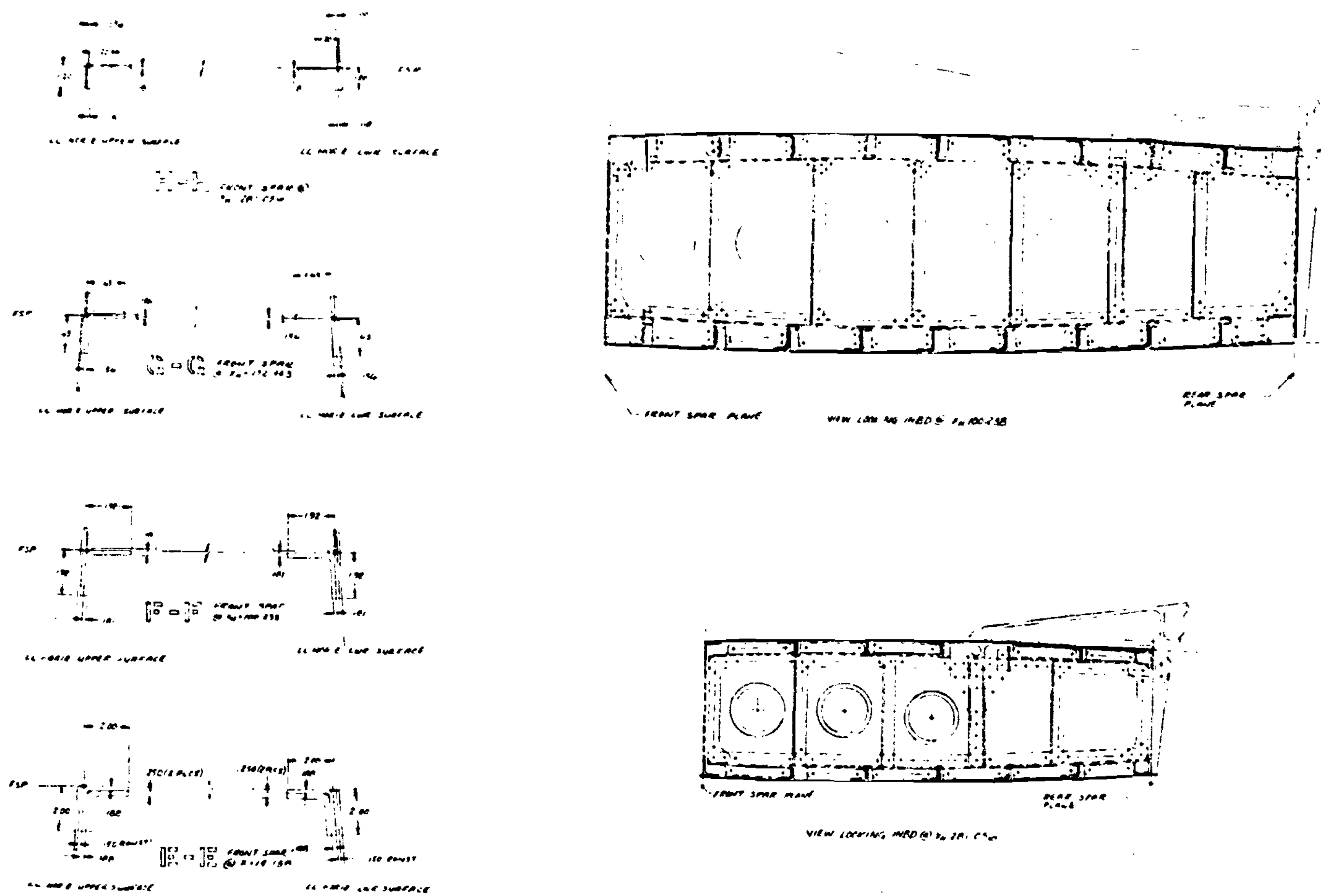

Figure 85 BASELINE HORIZONTAL STABILIZER STRUCTURE -- Concluded SHEET 2

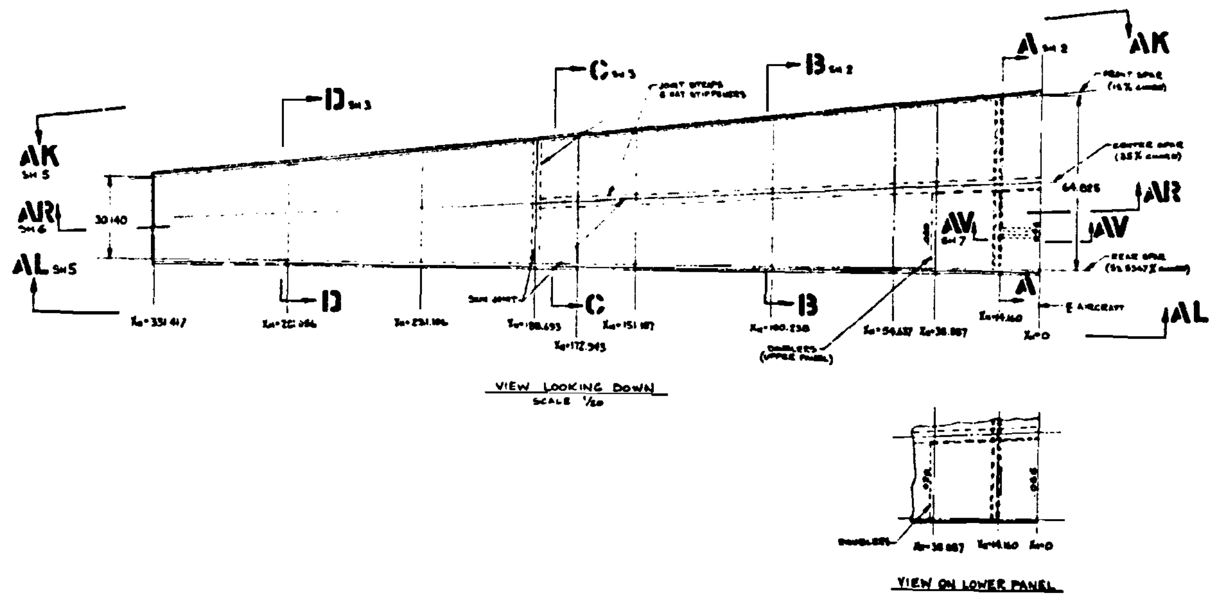

Figure 86 NEW HORIZONTAL STABILIZER STRUCTURAL DESIGN CONCEPT SHEET 1

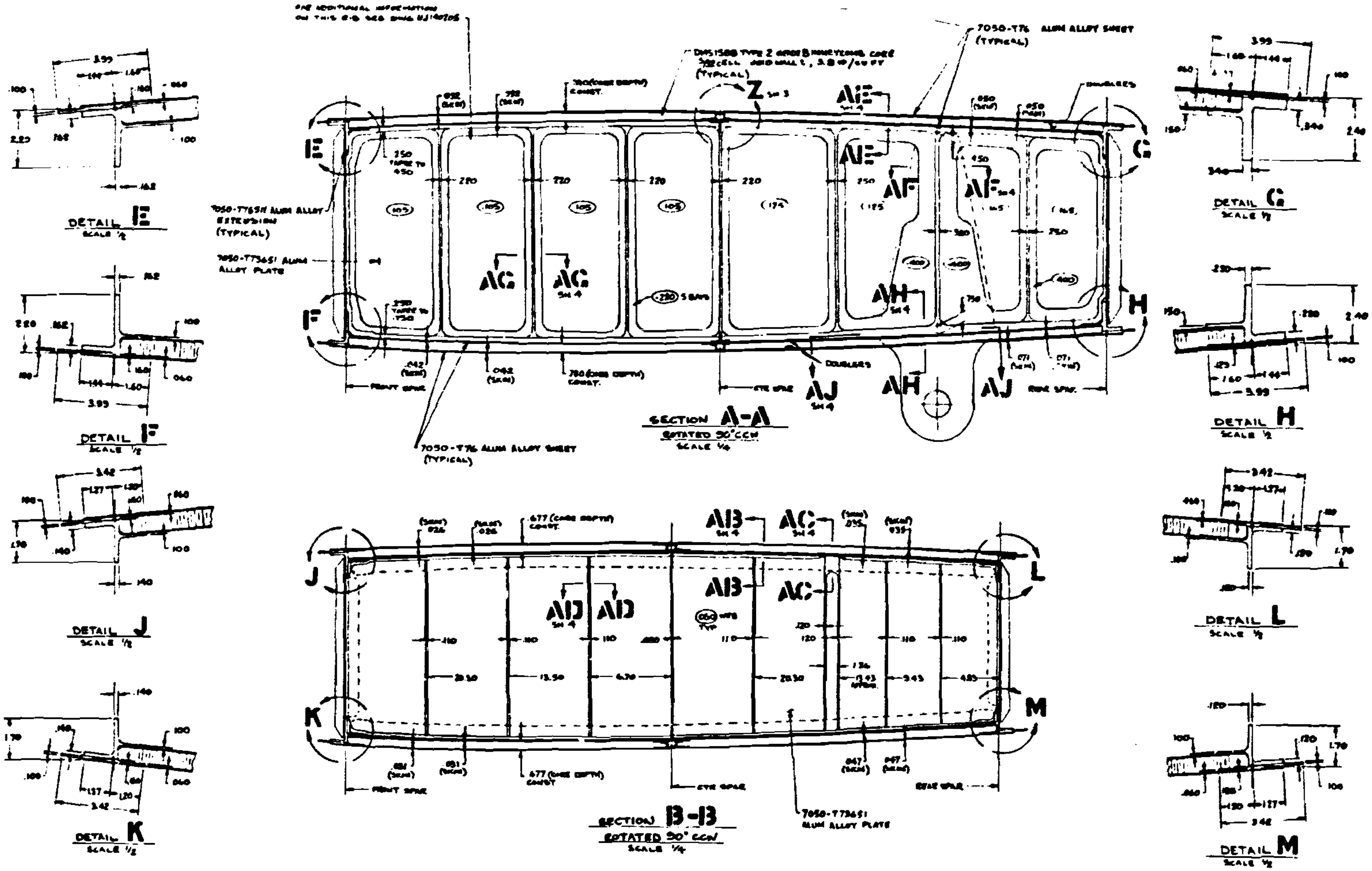

Figure 86 NEW HORIZONTAL STABILIZER STRUCTURAL DESIGN CONCEPT -- Continued SHEET 2

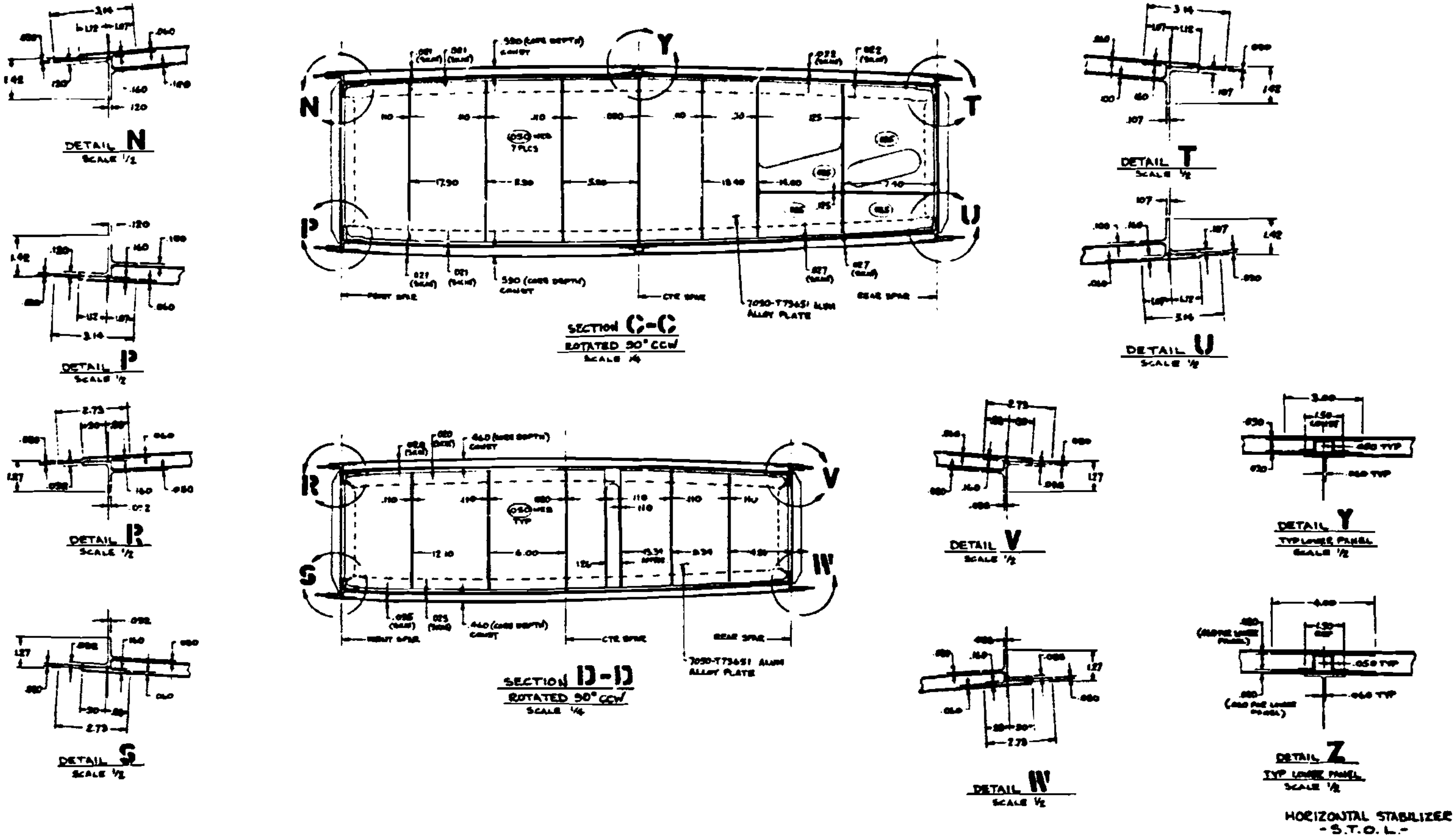

Figure 86 NEW HORIZONTAL STABILIZER STRUCTURAL DESIGN CONCEPTS -- Continued SHEET 3

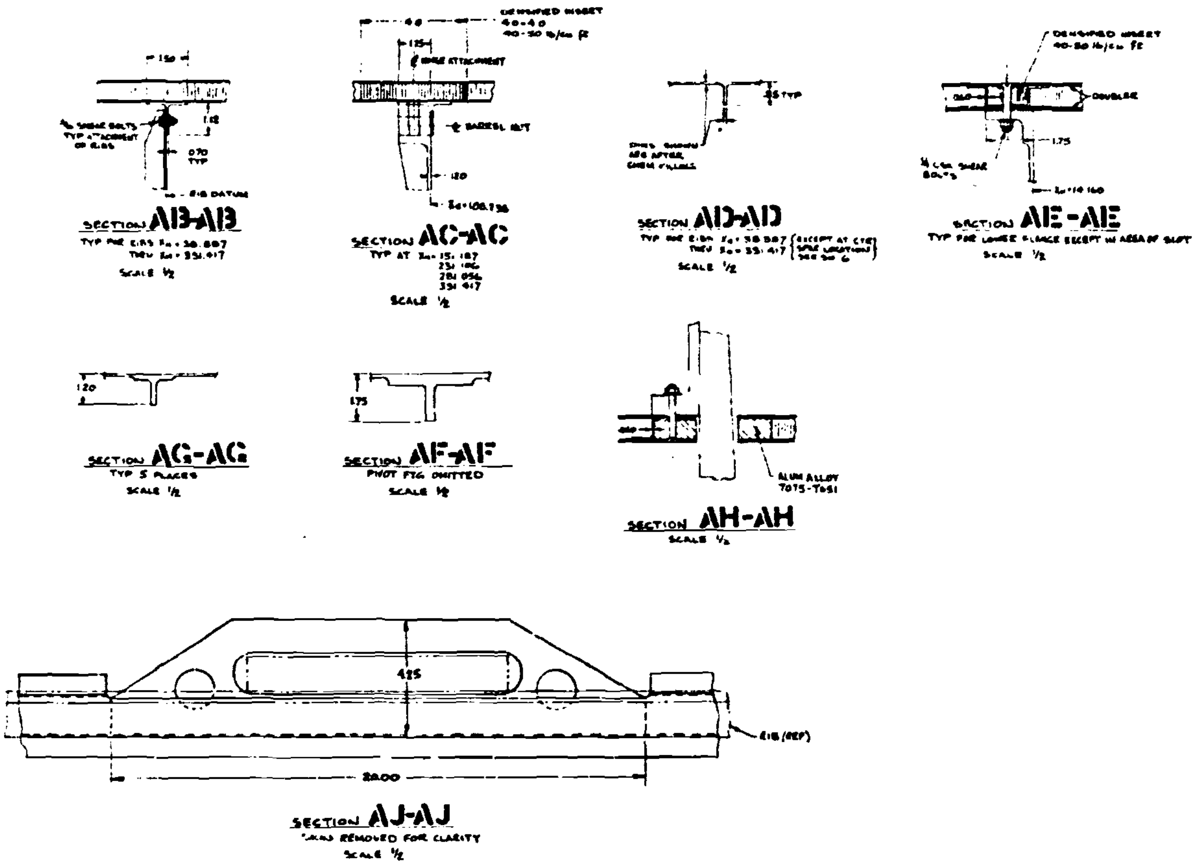

Figure 86 NEW HORIZONTAL STABILIZER STRUCTURAL DESIGN CONCEPTS -- Continued SHEET 4

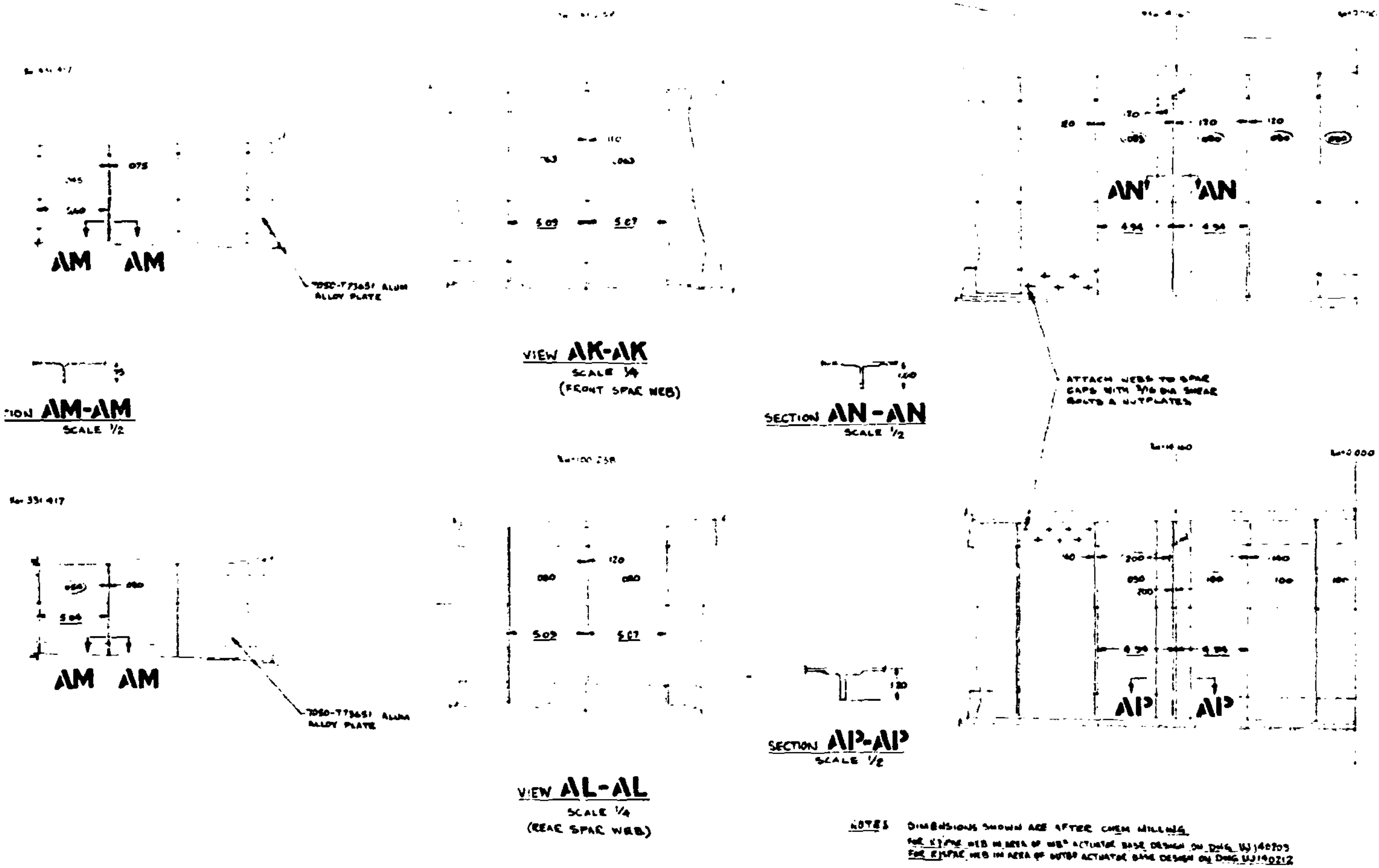

Figure 86 NEW HORIZONTAL STABILIZER STRUCTURAL DESIGN CONCEPTS -- Continued SHEET 5

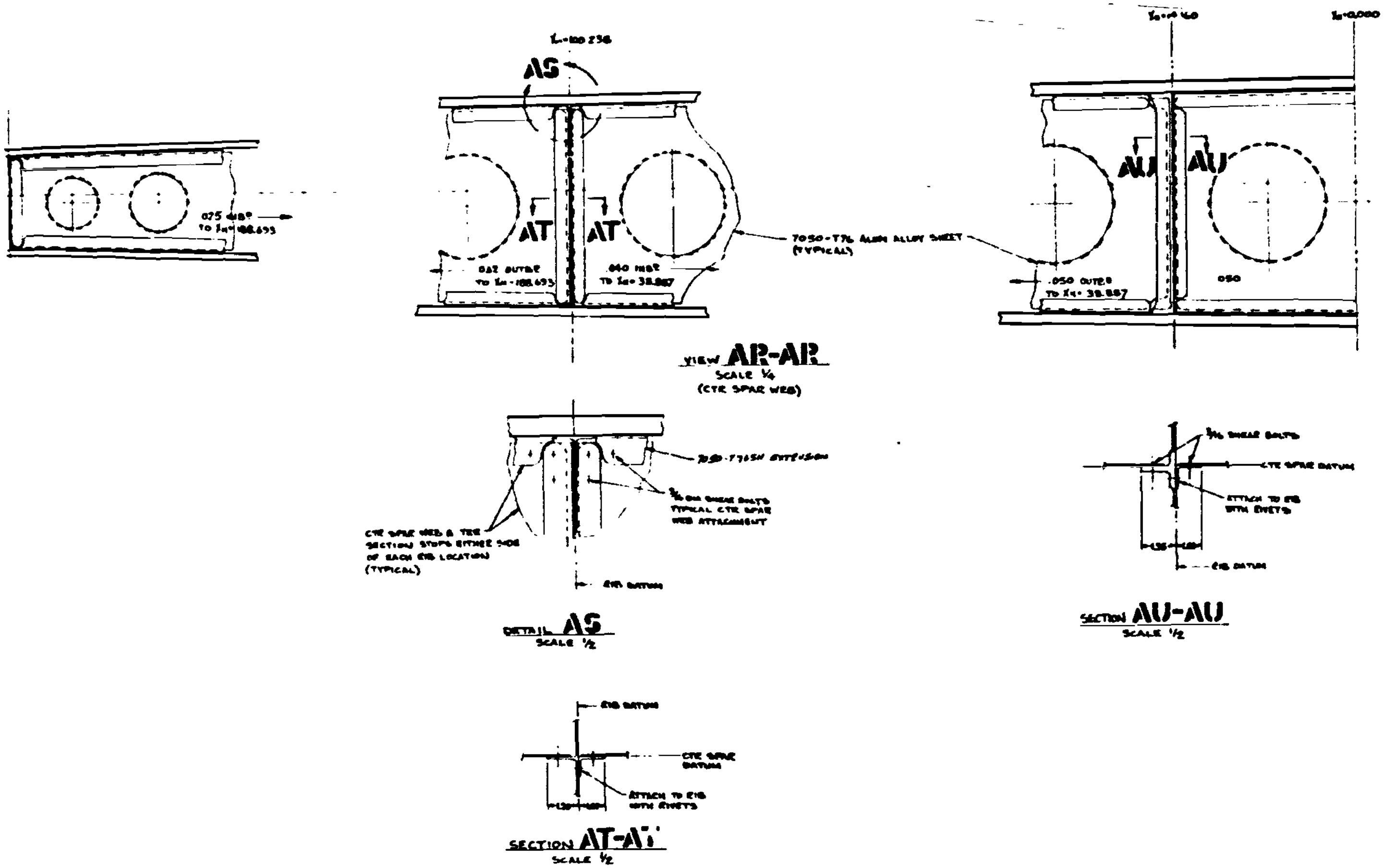

Figure 86 NEW HORIZONTAL STABILIZER STRUCTURAL DESIGN CONCEPTS -- Continued SHEET 6

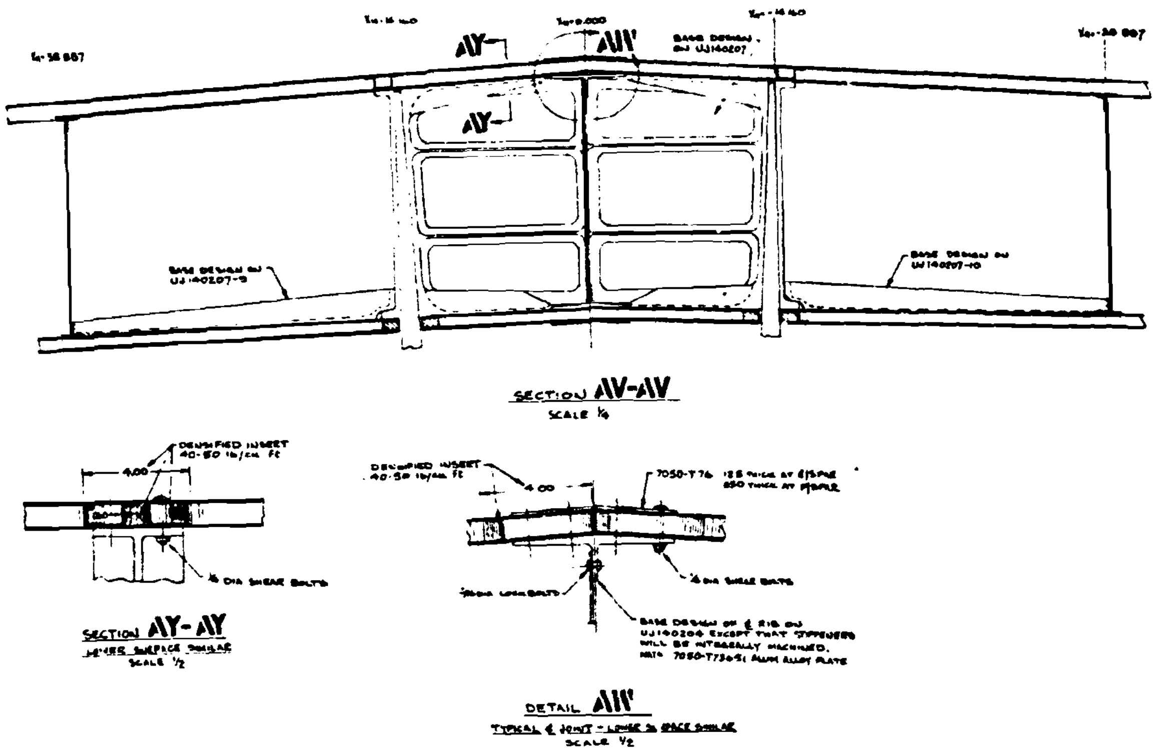

Figure 86 NEW HORIZONTAL STABILIZER STRUCTURAL DESIGN CONCEPTS -- Concluded SHEET 7

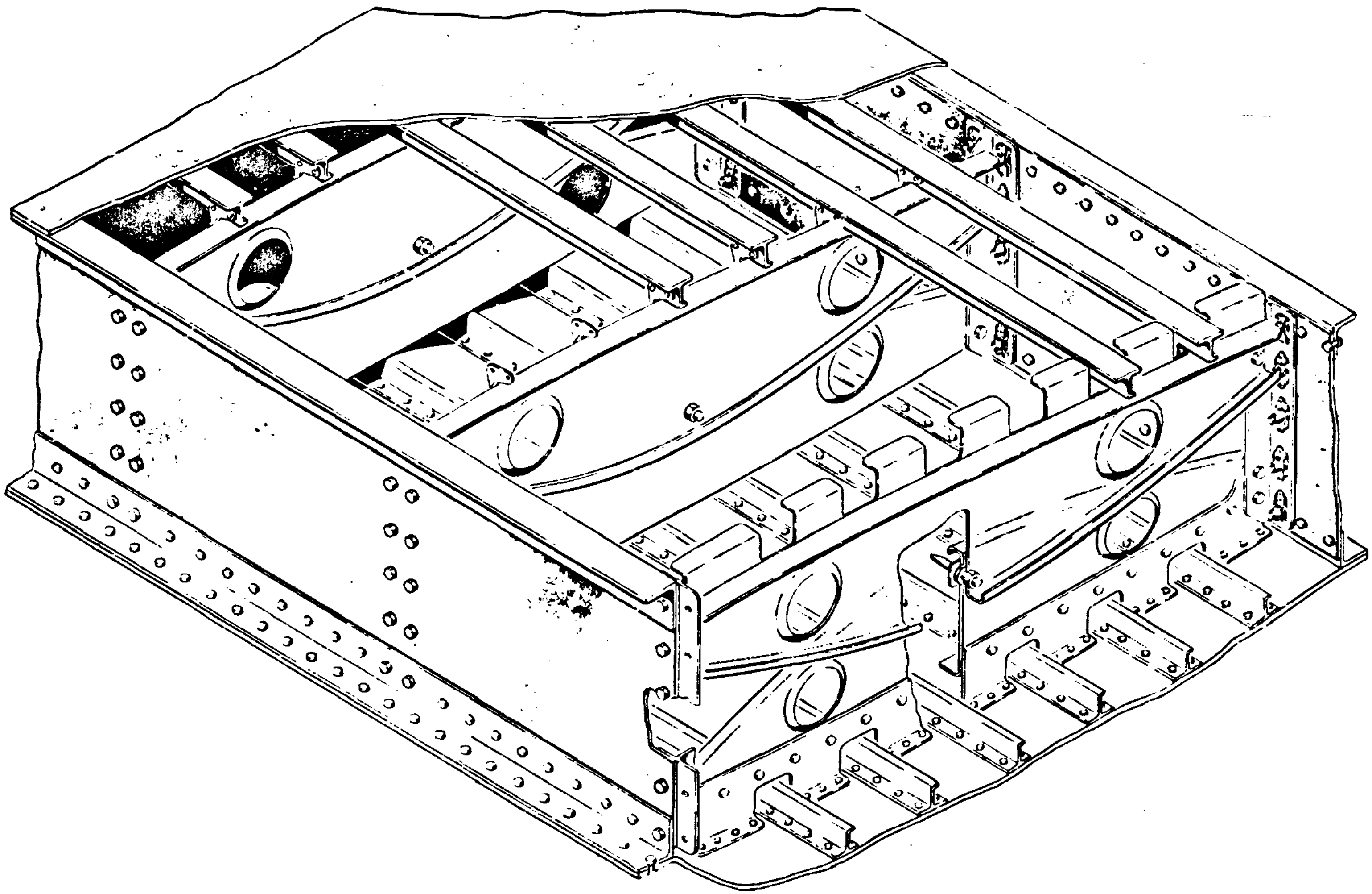

Figure 87 HALF-RIB DESIGN CONCEPT

integrally stiffened and made from 7050-T73651 aluminum plate (Figure 86). To keep web thickness to a minimum required chem-milling after machining as machining to 0.050 could produce varying web thickness due to distortion from relief of residual stresses. No masking off, however, will be required for chem-milling.

The ribs are attached to skin panels by bonding a rib cap to the skin panel during its curing cycle and bolting the ribs to the cap (Figure 86). The reason for bolts as opposed to rivets is due to the possibility of breaking the bond layer during impact assembly.

An exception to the above assembly method is the pivot ribs and bulkhead which are bolted through the skin panels using flush head bolts and local densified core inserts (Figure 86). This is due to the high boundary shears in these items.

5.3.2.4 Center Spar - This is a lightly loaded spar primarily for breaking up the skin panel widths as previously mentioned. It is made from 7050-T76 aluminum sheet with pressed flanged lightening holes and is attached to skin panels in a similar manner to the ribs, i.e., bonded caps with bolted web attachments (Figure 86).

5.3.2.5 Front and Rear Spars - These were investigated using an open iso-grid concept from 7050-T73651 aluminum plate. On comparison with a tension field spar web, the tension field method showed a weight saving as outlined in wing analysis (Section 5.1.2.2); and this method was adopted (Figure 86). The stiffeners are integrally machined into the web and the spar web then bolted to the spar caps.

As the spar webs are assembled last to close out the center box, access holes will not be necessary except at the actuator locations on the rear spar where access holes and panels will be provided for removal of actuators when servicing is required.

5.4 VERTICAL STABILIZER STRUCTURE

The same basic data from the wing studies were used to generate the cover panel and sub-structure concepts for the vertical stabilizer. The baseline and new concept descriptions follow.

5.4.1 Baseline Design Concept

The baseline structure for the vertical stabilizer consists of zee-stiffened skin panels, extruded aluminum spar caps and hat and "L" section stiffened rib and spar webs. The basic structure is shown in Figure 88.

5.4.2 New Design Concept

The design concept selected and used for the weight and cost analyses is described in the following sections.

5.4.2.1 Cover Skin Panels - Methods investigated and the honeycomb concept finally adopted is the same as for horizontal stabilizer (see 5.3.2.1). The center spar which stopped at Z_{RS} = 193.389 on the baseline concept now

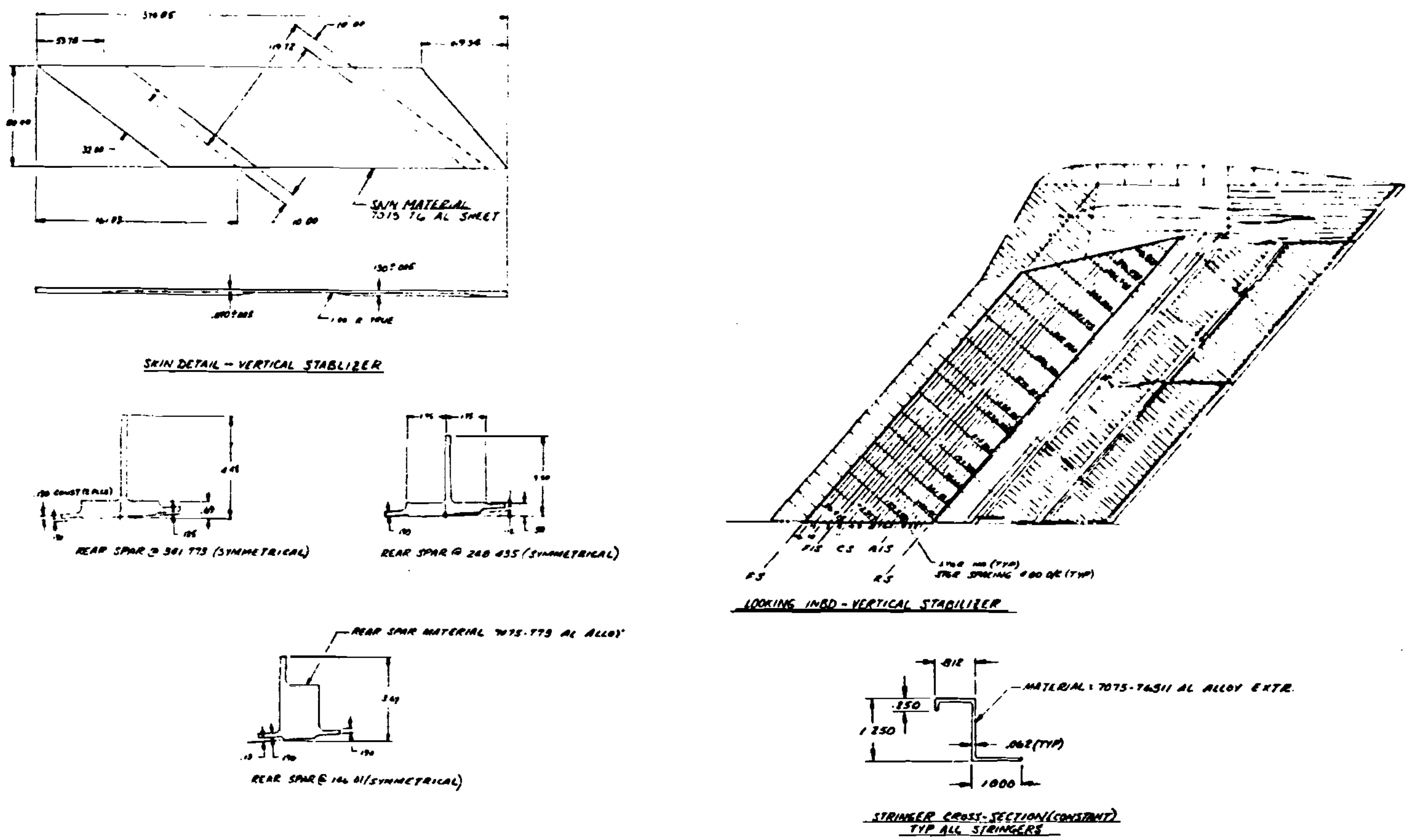

Figure 88 BASELINE VERTICAL STABILIZER STRUCTURE

SHEET 1

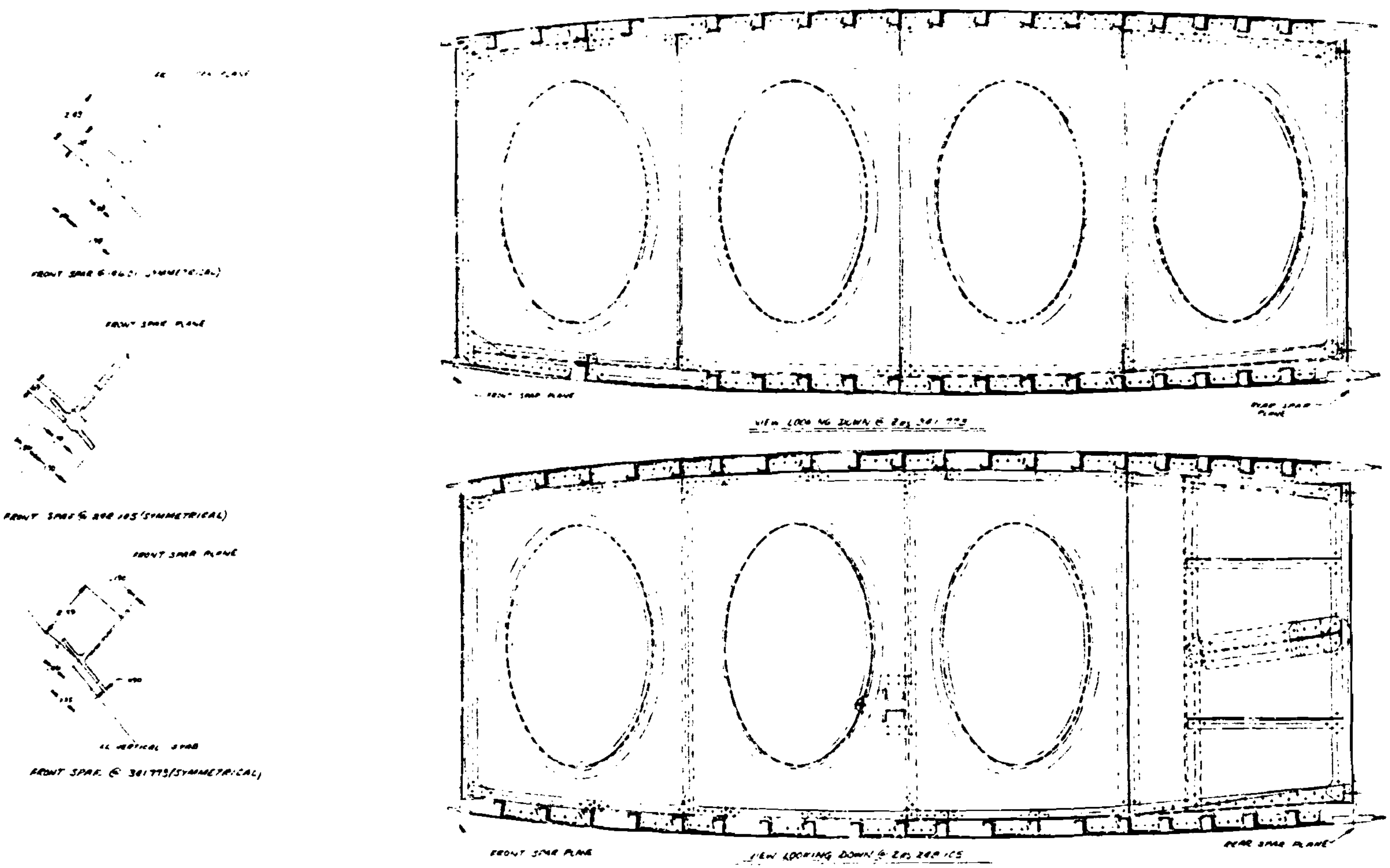

Figure 88 BASELINE VERTICAL STABILIZER STRUCTURE -- Concluded SHEET 2

extends to the top of the torque box (Figure 89), to break up the honeycomb panel width, thereby maintaining a reasonable depth of honeycomb. This method eliminates the need for stringers, intermediate full ribs and intermediate partial ribs.

5.4.2.2 Spar Caps - The forward center, center and rear center spar caps are machined from 7050-T76511 aluminum extrusion and bonded to the honeycomb skin panel during the curing cycle, thus becoming an integral part (Figure 89) of the panel. The forward and rear spar caps are machined from 7050-T736511 aluminum extrusion and filled with boron epoxy fibers (Figure 89). This is to add stiffness to the cap for meeting flutter requirements without adding excessive cap area, thereby keeping weight to a minimum. The boron inserts will be bonded to the caps by the method outlined in Section 8. During the honeycomb curing cycle the spar caps are bonded to the skin panels.

5.4.2.3 Ribs - Methods investigated and the integrally stiffened tension field rib concept finally adopted (Figure 89) is the same as for the horizontal stabilizer (Section 5.3.2.3).

5.4.2.4 Forward Center and Rear Center Spars - These are made from 7050-T76 aluminum sheet with pressed flanged lightening holes and attached to spar caps by means of bolts (Figure 89).

5.4.2.5 Center Spar - This is an integrally stiffened tension field spar web outboard to Z_{RS} = 193.389, made from 7050-T73651 aluminum plate. Outboard of Z_{RS} = 193.389, the web is made from 7050-T76 aluminum sheet with pressed flanged lightening holes. The web is attached to the spar caps by means of bolts (Figure 89).

5.4.2.6 Forward and Rear Spars - Methods investigated and the integrally stiffened tension field spar webs finally adopted (Figure 89) are the same as for horizontal stabilizer (Section 5.3.2.5).

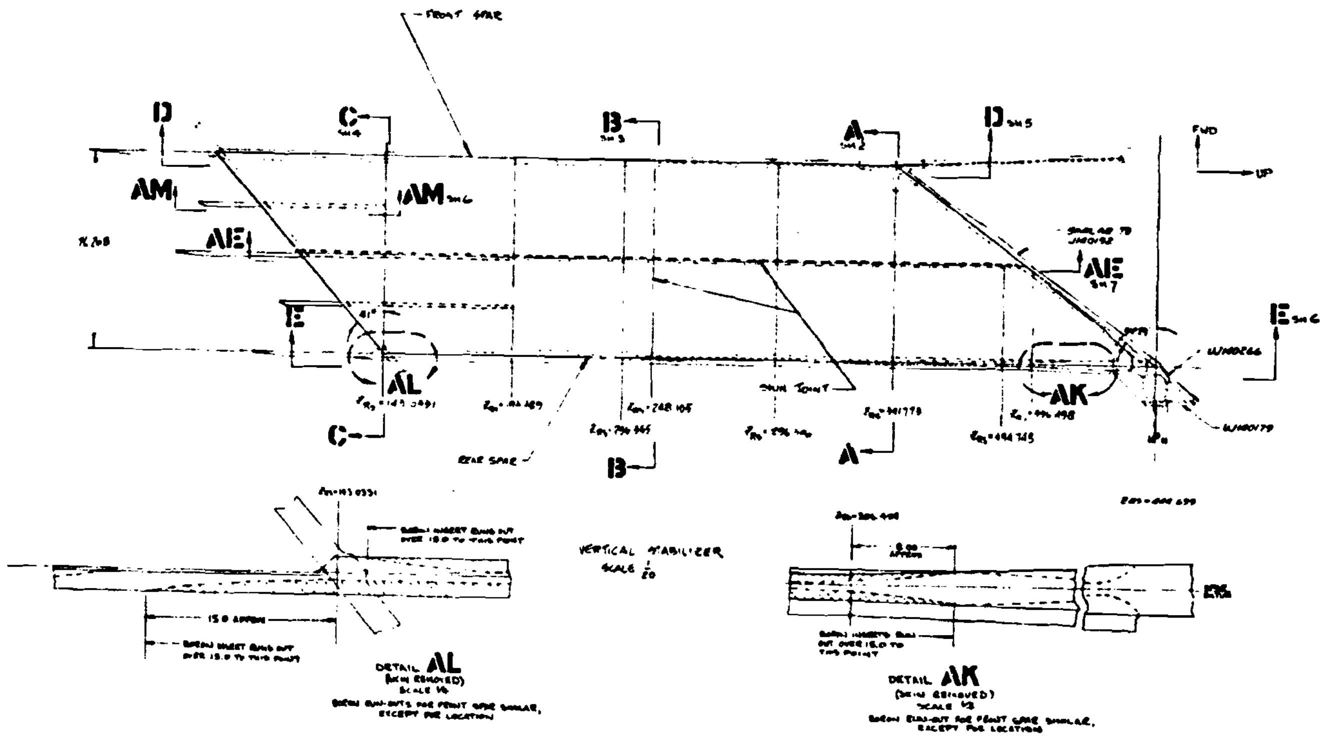

Figure 89 NEW VERTICAL STABILIZER STRUCTURAL DESIGN CONCEPT SHEET 1

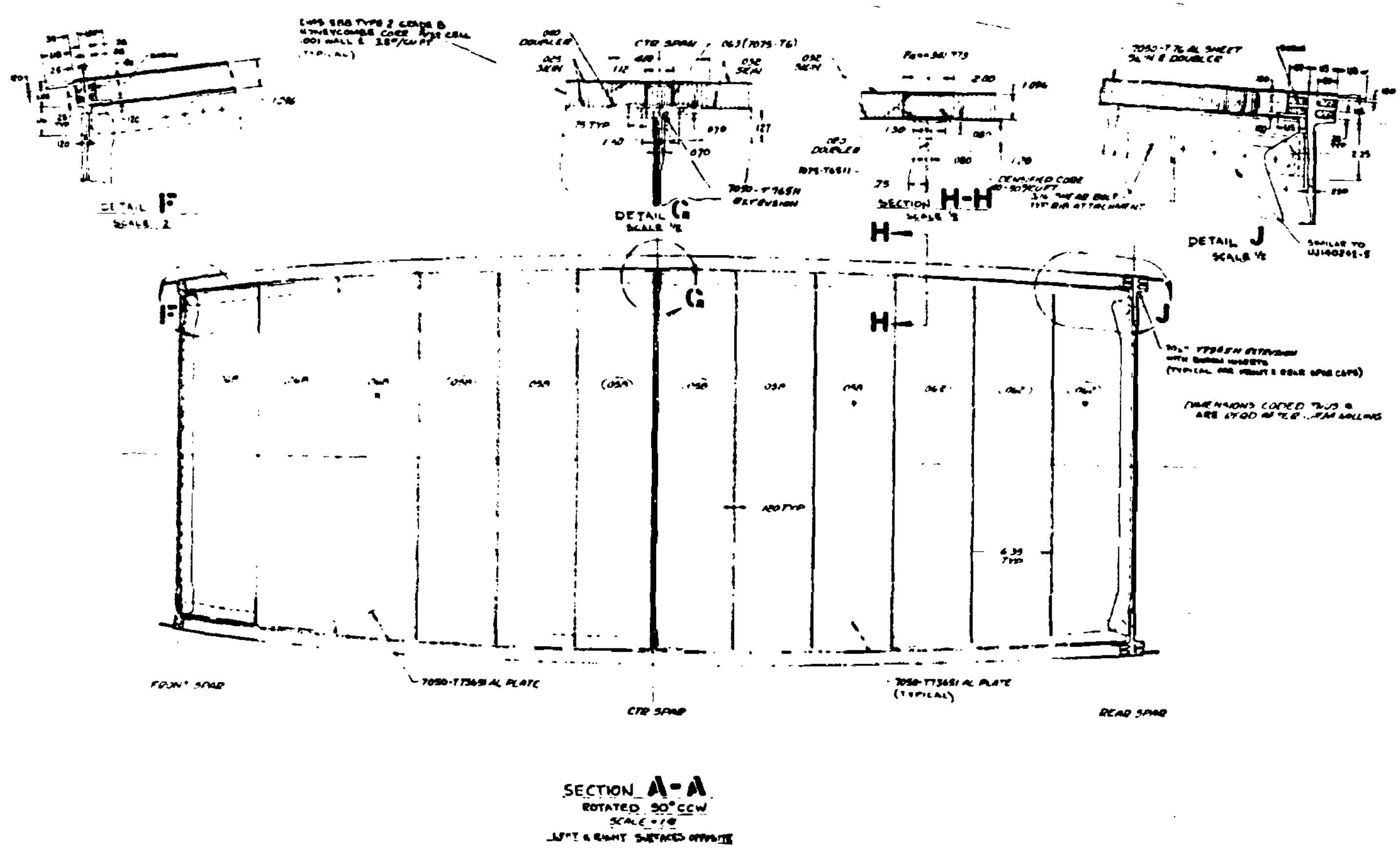

Figure 89 NEW VERTICAL STABILIZER STRUCTURAL DESIGN CONCEPT SHEET 2

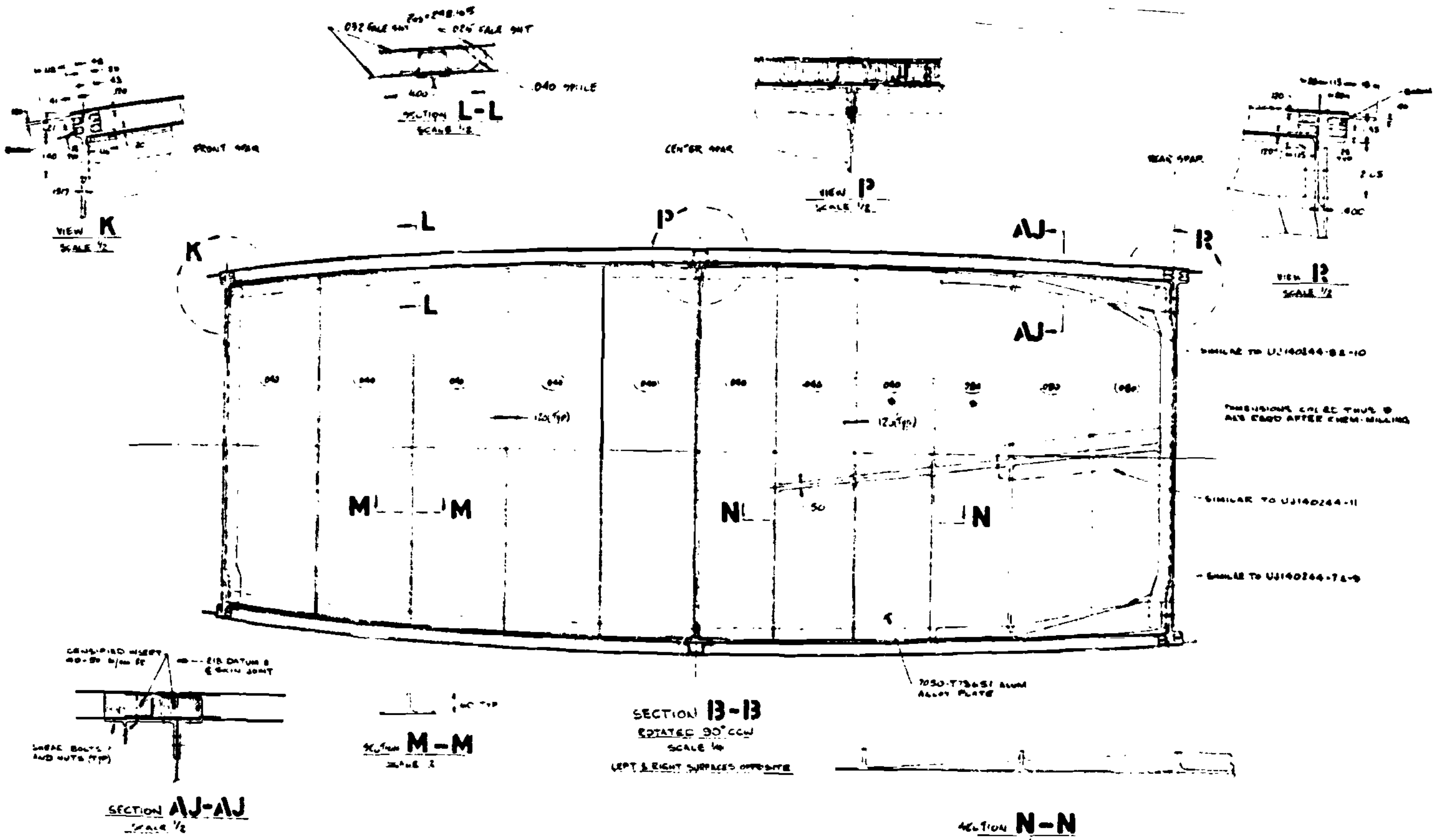

Figure 89 NEW VERTICAL STABILIZER STRUCTURAL DESIGN CONCEPT -- Continued

Sheet 3

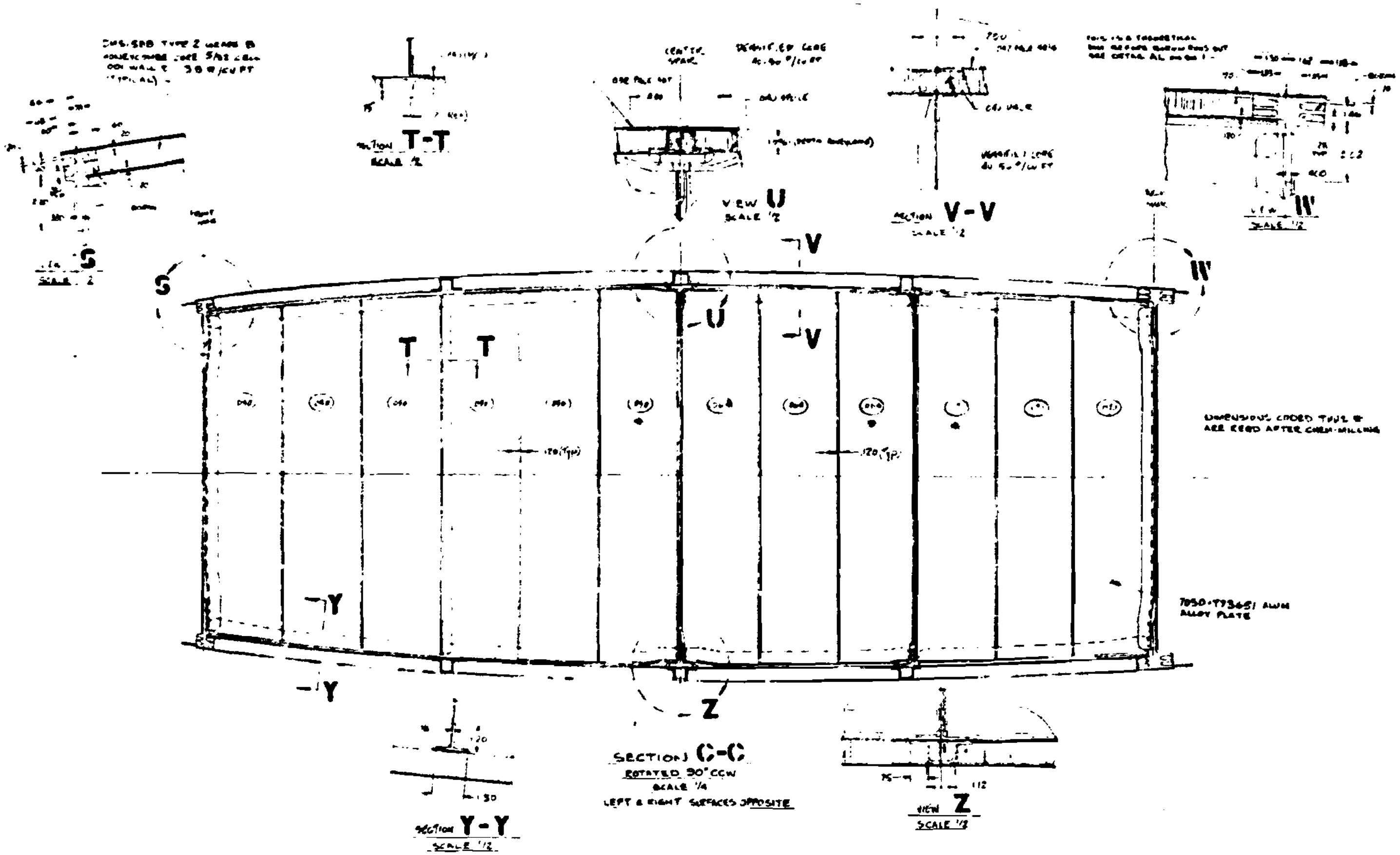

Figure 89 NEW VERTICAL STABILIZER STRUCTURAL DESIGN CONCEPT -- Continued

Sheet 4

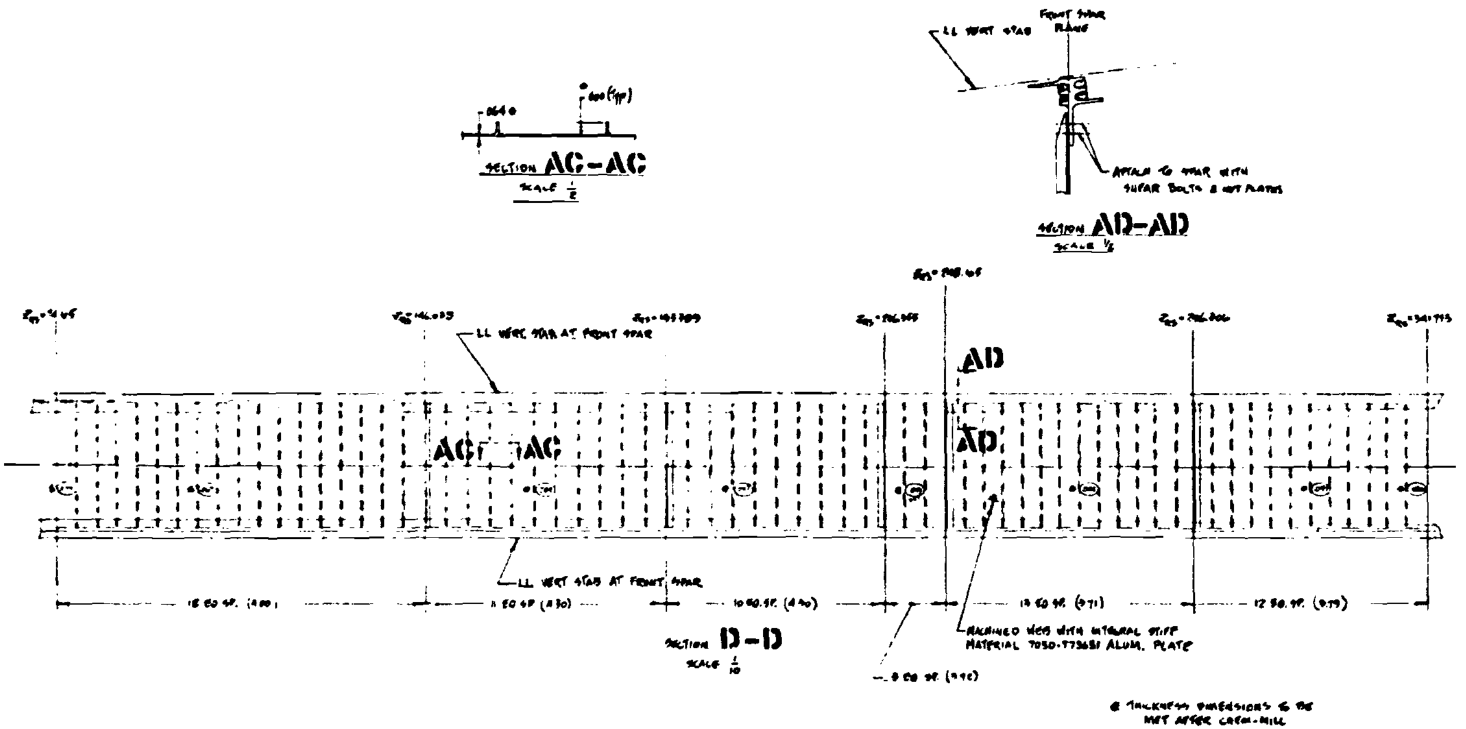

Figure 89 NEW VERTICAL STABILIZER STRUCTURAL DESIGN CONCEPT -- Continued SHEET 5

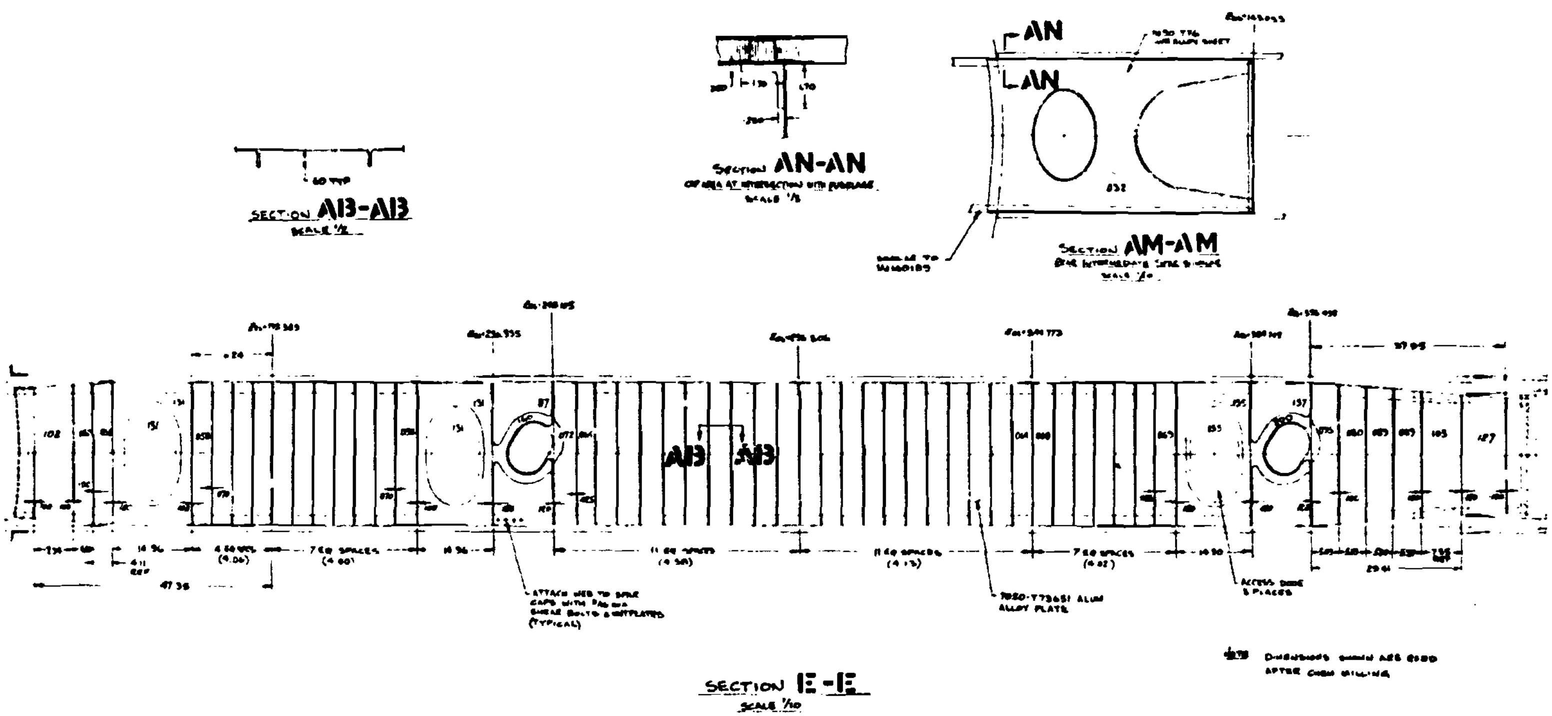

Figure 89 NEW VERTICAL STABILIZER STRUCTURAL DESIGN CONCEPT -- Continued SHEET 6

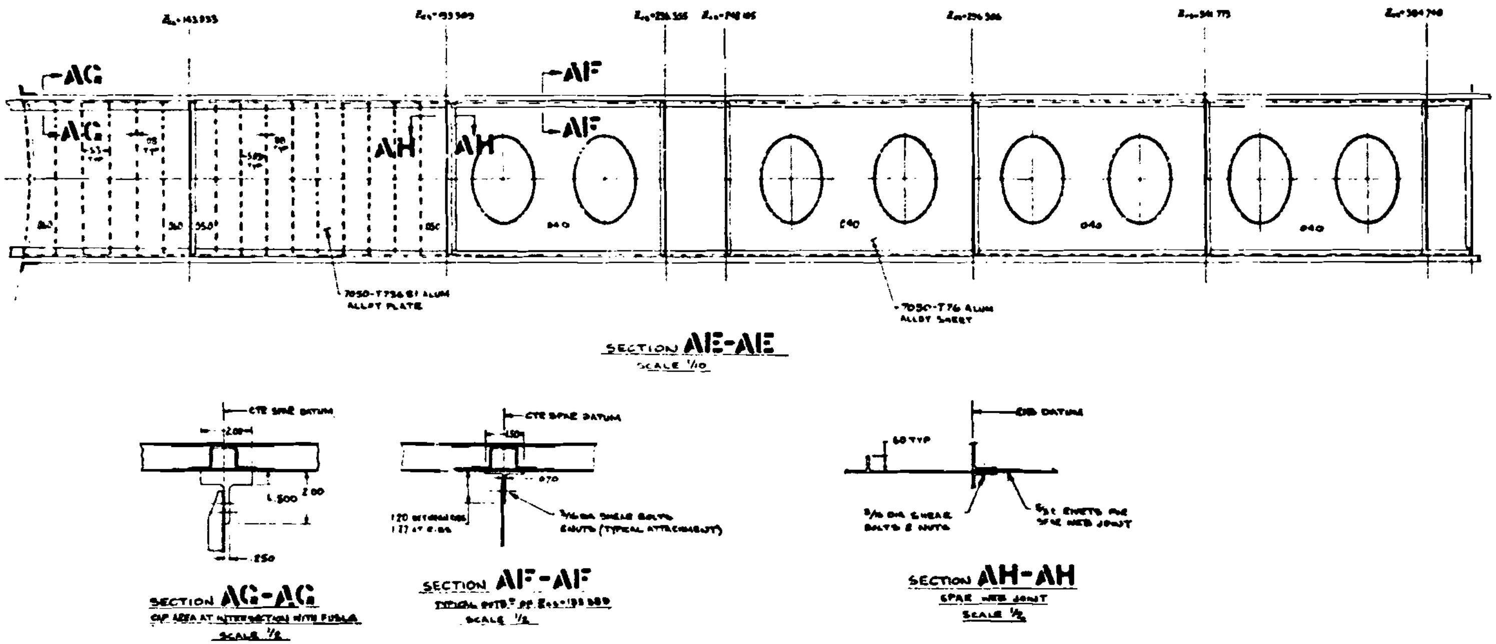

Figure 89 NEW VERTICAL STABILIZER STRUCTURAL DESIGN CONCEPT -- Concluded SHEET 7

SECTION VI

STRUCTURAL CONCEPT SELECTION

As indicated in Figure 1, the general (and primary) study objectives are to derive structural concepts of lower weight or cost or both, if possible, where "lower," by definition, is with respect to the state-of-the-art baseline concepts. Hence, the structural concept selection criteria are lower weight and lower cost.

From weight/unit area (ω) principles,

$$\omega_{min} \propto \frac{1}{(F/\rho)_{max}} \tag{17}$$

and the "lower weight" criterion is,

$$\frac{(F/\rho)_{B/L}}{(F/\rho)} \leq 1.0 \tag{18}$$

"Lower cost" criteria are selected to be "lower manufacturing cost" and "lower life cycle cost." From cost/unit area (C_S) principles,

$$(C_S)_{min} \propto (\omega C_{\#})_{min} = \frac{1}{(F/\rho C_{\#})_{max}} \tag{19}$$

where $C_{\#}$ = manufacturing cost per unit weight (\$/#). The "lower manufacturing cost" criterion is,

$$\frac{(F/\rho C_{\#})_{B/L}}{(F/\rho C_{\#})} \leq 1.0 \tag{20}$$

Similarly, for "life cycle costs" (C_{1c}), the criterion is,

$$\frac{(C_{1c})}{(C_{1c})_{B/L}} \leq 1.0 \tag{21}$$

From a fundamental standpoint, a structural concept is an unique combination of "material" and "geometry" defined by the imposed requirements. Aircraft functional and operational requirements for shape, volume, separation of environments, etc., dictate that the material be in a sheet (i.e., panel) geometry form, generally. Further, structural integrity requirements impose sufficient instability loads (shear and compression) to require stiffening to some degree for all sheet panels. Hence, the search basically is for combinations of materials and stiffened panel geometries meeting all the requirements and which have higher values of F/ρ and $(F/\rho C_{\#})$. "Geometry" includes the parameters introduced by the joining approach.

Recognized principles for improvement include the following:

- The multi-function principle, wherein a given structure performs more than one task. This principle has been generally applied to aircraft structures. As previously noted, a structural panel may provide shape, volume, separation of environments, structural integrity, etc. In this sense, aircraft panel structure may be thought of as weight efficient. The provision of this capability for less weight or the imposition of additional functions without commensurate weight increase is required to further enhance the overall efficiency. Aircraft landing gear, although necessary, are an example of low efficiency structure in this context. Wing and fuselage panels, on the other hand, are typical examples of higher efficiency structure.

- The superposition principle, wherein the "whole is greater than any individual part." In this approach, favorable (and unfavorable) characteristics are combined in a complementary manner such as to increase overall weight efficiency. An example of this is the "weld-bond" joining concept where, by a combination of spot-welding and bonding, the structural efficiency may possibly be enhanced beyond the value achievable by spot-welding or bonding individually. The desired goal, of course, is to identify pertinent combinations such that the "whole is greater than the sume of the parts."

- The separation principle, wherein unfavorable characteristics are not superimposed (opposite of superposition). An example of this is placement of required stress concentrations in low stress or high capability areas.

- The tradeoff principle, wherein excessive efficiency in one mode is reduced in order to enhance efficiency in a deficient mode, thereby achieving better overall efficiency. This is accomplished by appropriate choices of materials or geometries or both. Cost savings may thereby also result. An example of this is the "flattened stiffener" fuselage shell concept (Reference 19) where compressive efficiency was reduced to enhance fatigue efficiency.

- The repetitive principle, wherein through increasing standardization, manufacturing complexity is reduced and cost efficiency thereby increased. Standardization implies and includes reductions in the number of dissimilar parts and operations. A repetitive standardized operation can be more readily mechanized for even greater efficiency. The ideal goal is a reduction to one standard part and one standard operation for which a high volume is required. This ideal generally has not been achieved, even by the automobile industry, for example. The automobile "drive-away" price, nonetheless, is on the order of 1 $/# whereas the aircraft "fly-away" price is on the order of 110 $/#, a substantial differential. This indicates a potential for possible significant cost improvement in aircraft manufacture, e.g. by greater standardization.

Structural cost rate data ($C_{\#}$) for material and geometry variations are sumarized in Section 6.1. Concepts are evaluated and those concepts with improved weight or cost or both capability are identified in Section 6.2.

6.1 STRUCTURAL COST RATES

A preliminary design-for-cost method is required to directly support the concept selection process. Although development of a simple and reliable "bottom-up" method is beyond the scope of this study, such an approach should provide information which includes the following:

- Cost added during the various manufacturing stages, thus indicating where significant manufacturing cost increments occur. The method should correlate to existing experience.

- Costs for various material and geometry type combinations, thus identifying the relative importance of each to the total manufacturing cost.

- Life cycle costs, thus reflecting the relative importance of manufacturing versus life cycle costs in the total cost picture. Design dependent life cycle cost increments (such as for maintenance and repair) should be readily identifiable.

In support of the study (and in accordance with the approach), readily available manufacturing cost data are summarized in Table XXI. The data includes labor and material costs. Labor costs include manufacturing, quality control, tooling, planning and overhead; but exclude design development and test evaluation (DDTE) costs. Where necessary, the data were adjusted to 1972 rates and a 200 unit production run. Although the data are scattered, limited data (in most categories) and the estimated nature of some information elements undoubtedly qualify the results, the data (Figure 90) nonetheless provide a necessary preliminary estimate of manufacturing cost levels. As would be expected, most available data are for mechanically joined aluminum structure, which at the "major section" stage, is approximated at 45 $/# average. With aluminum mill product costs at less than 2 $/#, over 95% of this cost is associated with fabrication and assembly. Therefore, design concepts which encourage the mill product to be closer to the finished product, such as a panel for example, would appear to offer a potential for cost saving. Relative to aluminum, the higher cost levels of titanium and beryllium can only

CODE	MODEL	PRODUCT STAGE	GEOMETRY CONCEPT	MATERIAL	$C_\#$ (1)	REMARKS
1	-	Mill Product	Sheet, Plate & Extrusion	Aluminum	1-2	Vendor
2	-	Mill Product	Sheet, Plate & Extrusion	Titanium	6-10	Vendor
3	-	Mill Product	Sheet and Plate	Beryllium	250-300	Vendor
4	Δ	Wing Box Section	Riveted Plate & Extrusion	Aluminum	33	Ref. 38
5	Δ	Fuselage Section	Riveted Skin & Stiffener	Aluminum	40	Ref. 38
6	Δ	Airframe	Riveted Skin & Stiffener	Aluminum	77	Ref. 38
7	DC-10	Wing Box Section	Riveted Plate & Extrusion	Aluminum	38-62	Ref. 19
8	DC-10	Fuselage Section	Riveted Skin & Stiffener	Aluminum	39	Ref. 19
9	AST	Sections	Unspecified	Aluminum	50	In-House
10	AST	Sections	Unspecified	Titanium	95	In-House
11	Δ	Airframe	Welded Skin & Stiffener	Titanium	213	Ref. 38
12	DC-10	Wing Box Section	Honeycomb	Al + Ti	121	Ref. 19
13	DC-10	Wing Box Section	Riveted Plate & Extrusion	Titanium	88-130	In-House
14	General	Sections	Unspecified	Titanium	80-100	In-House
15	General	Sections	Riveted Skin & Stiffener	Aluminum	40-50	In-House
16	DC-10	Airframe	Riveted Skin & Stiffener	Aluminum	93	In-House
17	General	Wing Box Section	Riveted Plate & Extrusion	Aluminum	40-50	Ref. 39
18	General	Wing Box Section	Honeycomb	Aluminum	180	Ref. 39
19	General	Fuselage Section	Riveted Skin & Stiffener	Aluminum	40-50	Ref. 39
20	DC-10	Fuselage Section	Riveted Skin & Stiffener	Aluminum	54	Ref. 39
21	General	Empennage Section	Riveted Skin & Stiffener	Aluminum	40-55	Ref. 39
22	General	Panels	Riveted/Brazed/Welded Skin & Stiffener	Titanium	65-70	In-House
23	Δ	Airframe	Riveted Skin & Stiffener	Beryllium	780	Ref. 38
24	-	Mill Product	Sheet and Plate	Beryllium	415	Ref. 38
25	-	Mill Product	Honeycomb Core	Aluminum	4-8	Vendor
26	-	Mill Product	Honeycomb Core	Titanium	85	Vendor

Table: TABLE XXI MANUFACTURING COST DATA

(1)($/#) Adjusted to 1972 rates and [illegible] unit run. Δ Logistic Transport

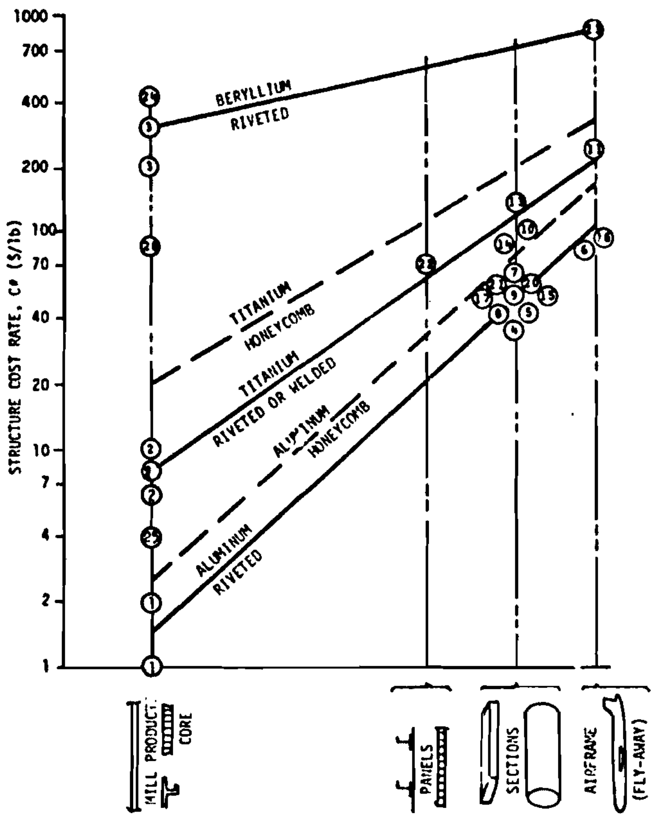

NOTE: (1) FOR $C_\#$ SEE TABLE 21.
(2) LABOR AND MATERIAL AT 1972 RATE FOR 200 AIRCRAFT

Figure 90 STRUCTURE COST RATE DATA

be offset by grea' r associated weight efficiencies. Within a material system, cost differences due to geometry variation also are evident with honeycomb, for example, estimated as being more costly than riveted construction.

The combined effect of structural weight and cost changes relative to the baseline is assessed during final study stages by life cycle cost analyses as indicated in the study approach (Figure 1). However, during the concept selection phase, a preliminary assessment of structural weight and cost variation impact on life cycle cost is desirable for selecting "cost effective" concepts. A preliminary evaluation tool is possible by relating new concept structural weight and cost with the system benefit required to not exceed baseline structural cost levels (Figure 91). Thus, for example, a concept relative weight and cost rate of .90 and 2.00, respectively, require a system benefit rate SBR > 300 $/# for cost effectiveness. Relative to a conservatively selected criterion value of 200 $/# upper limit for resized (or unresized) systems, the concept would not be cost effective. On the other hand, a concept relative weight and cost rate of .50 and 2.00, respectively, is obviously cost effective since concept initial cost equals baseline initial cost without SBR effects (hence, SBR required = 0) although SBR actual > 0 due to decreased weight benefits.

6.2 CONCEPT EVALUATIONS FOR WEIGHT AND COST

The general approach used to identify concepts for weight and cost improvements includes the following elements:

- Components (and subcomponents) are considered on an individual basis since varying requirements define different solutions.

- Emphasis is placed on major weight fraction subcomponents on the premise that a given percentage improvement on a larger weight item generates the greatest impact on overall system weight. Thus, the wing upper and lower covers and fuselage shell structure received the major attention (see Figures 5 and 6 for weight fraction data).

- Weight improvement is with respect to the baseline concept; therefore, a determination of the baseline concept critical integrity modes is performed to identify the "problem."

- Although the general problem is identified by the critical modes, the specific solution is not provided. To help identify pertinent solutions, a quantitative evaluation and screening procedure is introduced which permits a simple and systematic consideration of all material and geometry options and includes the influence of "requirements." This procedure is applied to the major subcomponents as described in the following subsections.

G.2.1 Wing Lower Panels

On the basis of past experience, wing lower panels are subject to constraints associated with ultimate tension and compression, fatigue, damage tolerance and flutter. Hence, the baseline panels were evaluated for these integrity modes. The baseline concept critical modes, as identified by minimum margins of safety, are shown on Figure 92. These data are most representative of the inboard panels including the rear spar cap and constitute a significant weight fraction. Fatigue and damage tolerance of the longitudinal skin and spar cap splices are the most critical modes.

[NOTE: The capability for each mode is expressed in terms of the critical ultimate mode design stress (tension, in this case), thereby establishing the mode comparisons on a common and convenient basis. The capabilities are plotted as a function of service life, since fatigue and damage tolerance capabilities vary with time. For this case, the ultimate mode capabilities are invariant with time.]

The capability stresses, F, for each mode M, are related to the ultimate mode reference condition as follows:

$$F_m = \frac{M_{tu}\, C\, \gamma}{(I_{req'd})_m} = \frac{N_x}{(\bar{t}_{req'd})_m} \tag{22}$$

where M_{tu}, N_x = ultimate mode design moment and associated loading (by FORMAT analysis)

γ = stress correlation factor (classical vs FORMAT)

$\frac{C}{(I_{req'd})_m}$, $(\bar{t}_{req'd})_m$ = section modulus and panel weight thickness required to meet the individual mode requirements

The actual ultimate mode tension stress, f_{tu}, is expressed similarly:

$$f_{tu} = \frac{M_{tu}\, C\, \gamma}{(I)_{actual}} = \frac{N_x}{(\bar{t})_{actual}} \tag{23}$$

Ultimate tension and compression stresses are related as follows:

$$K = \frac{M_{cu}}{M_{tu}} = \frac{N_{xcu}}{N_{xtu}} = \frac{f_{cu}}{f_{tu}} = 0.50 \text{ for the inboard wing.} \tag{24}$$

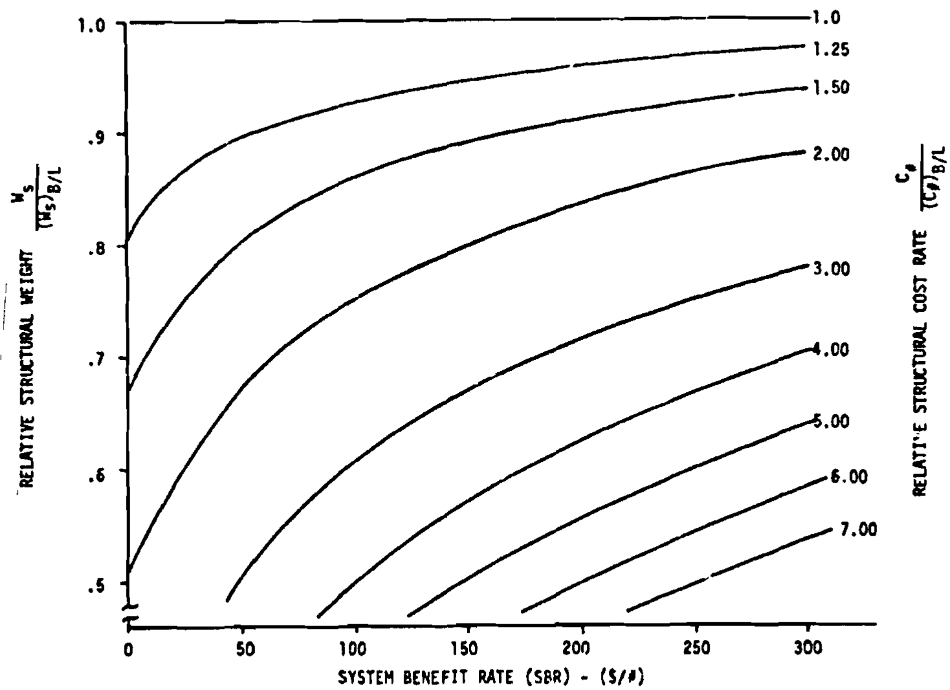

Figure 91 STRUCTURAL WEIGHT AND COST EFFECTS ON REQUIRED SYSTEM BENEFIT RATE

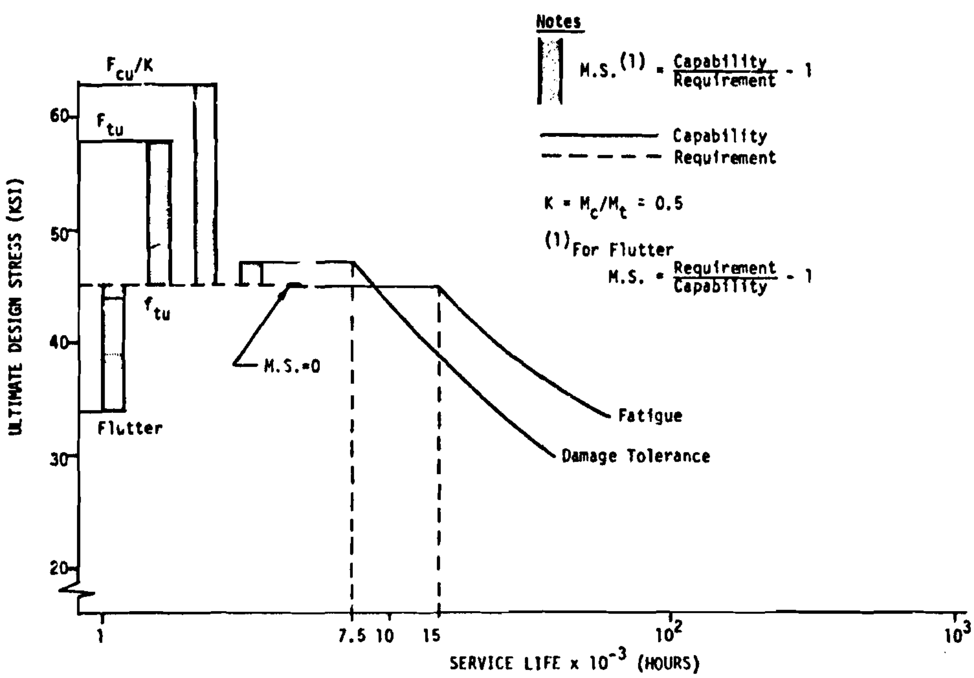

Figure 92 CRITICAL INTEGRITY MODES - BASELINE WING LOWER INBOARD PANELS

Therefore:

$$(F_{cu})_{eq} = \frac{F_{cu}}{K} \qquad (25)$$

The baseline panel margins-of-safety are developed in accordance with standard airframe analysis procedures as indicated in Table XXII. The same general analysis approach is also applied to new panel concepts. Detailed analyses are summarized in Section VII.

Achievement of a weight reduction goal requires an increase in critical capability stress (F), thereby permitting an increase in the requirement stress (f_{tu}). Increasing the "capability stress" for any mode depends on improvement of the panel material capability or geometry capability or both.

$$\begin{bmatrix}\text{Stress}\\ \text{Capability}\end{bmatrix}_{max} = f\begin{bmatrix}\text{Material} & & \text{Geometry}\\ \text{Capability} & X & \text{Capability}\end{bmatrix}_{max} \qquad (26)$$

An evaluation approach for "material" versus "geometry" options is to assume geometry constant and material variable and, alternately, material constant and geometry variable. The "geometry constant/material variable" evaluation is the classical "material selection criteria" approach for which materials data is summarized in Section III. Similarly, the "material constant/geometry variable" evaluation is the classical "structural geometric efficiency" approach for which geometry data is summarized in Section IV. Additional geometry effects data are provided by the study analyses, which are summarized in Section VII.

These two basic categories of information are integrated to define concept efficiency and capability charts for the various modes (see Figures 93 through 97). The material selection criteria data for each mode (summarized in Table 23 for convenience) are arranged along the abscissa according to numerical value. The panel capability F/ρ (ordinate) is set equal to the material capability for a selected upper limit geometric condition for each mode (denoted by $\varepsilon_g = 1$). The upper limit represents a geometric efficiency goal associated with the mode and corresponds to the maximum achievable capability for "material constant." Actual panels fall short of this goal in accordance with conflicting mode requirements, degradation due to the manufacturing process and cost constraints. Comparison of "actual-to-ideal" panel capability defines the geometric efficiency (ε_g):

$$\varepsilon_g = \frac{\text{actual panel capability}}{\text{ideal panel capability}} \qquad (27)$$

TABLE XXII BASELINE WING LOWER PANEL ANALYSIS APPROACH					
ELEMENT \ MODE	ULTIMATE TENSION	ULTIMATE COMPRESSION	FATIGUE	DAMAGE TOLERANCE	FLUTTER
MATERIALS AND GEOMETRY (REFERENCE SECTION V)	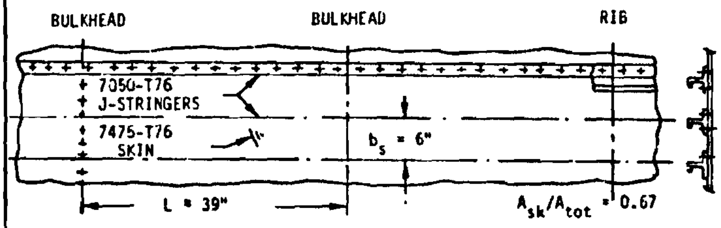				INTERFERENCE FASTENERS GEMCOR (Al) HI-LOK (Ti)
CAPABILITIES (REFERENCE SECTION VII)	•PANEL $F_{tu} = (1-K_0)\,F_{tu}$ •K_0 = CHORDWISE HOLE-OUT FACTOR = 0.20	•PANEL $F_{cu} = F_{co} - \left(\frac{F_{co}L'/\rho}{2\pi\sqrt{E}}\right)^2$ •$L' = \frac{L}{\sqrt{1.5}}$	•TEST S-N DATA (K_t = 3.0 to 4.0) 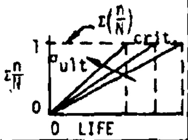	•TEST ΔK VS $\frac{da}{dN}$ DATA •$\frac{da}{dN} = \frac{C\Delta K^n}{(1-R)K_c - \Delta K}$ •$\Delta K = \sigma(1-R)\lambda\sqrt{a}$ 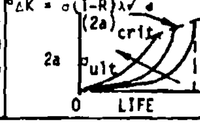	•$V_F \geq 1.15\ V_L$ $\geq$ 460KEAS @ S.L.
REQUIREMENTS (REFERENCE SECTION II)	•$N_x \leq$ 12,400 #/IN	•$N_x \leq$ 6,000 #/IN	•SIMPLIFIED SPECTRUM n_{GAG} = 95,020 ~/60,000 HOURS σ_{max}/σ_{1g} = 1 + Δn = 1.56, R = -0.99 n_{LLM+G} = 47,167 ~/60,000 HOURS σ_{max}/σ_{1g} = 1 + Δn = 1.75, R = 0.14		•V_F = 1.15 V_L •EI, GJ
MARGIN OF SAFETY	$\frac{\text{CAPABILITY}}{\text{REQUIREMENT}} - 1 \geq 0$				

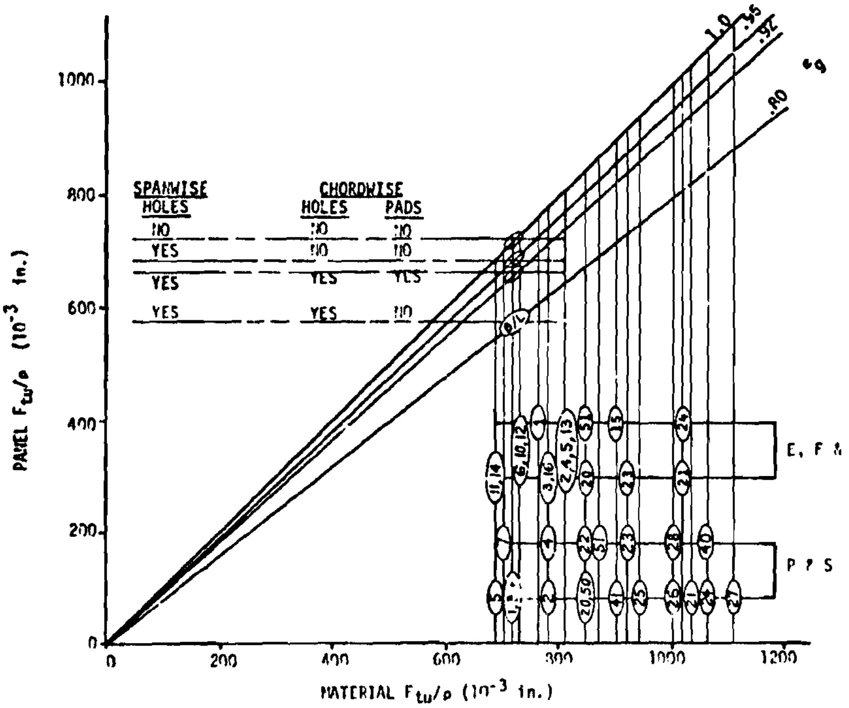

Figure 93 WING LOWER PANEL - CONCEPT EFFICIENCIES FOR ULTIMATE TENSION

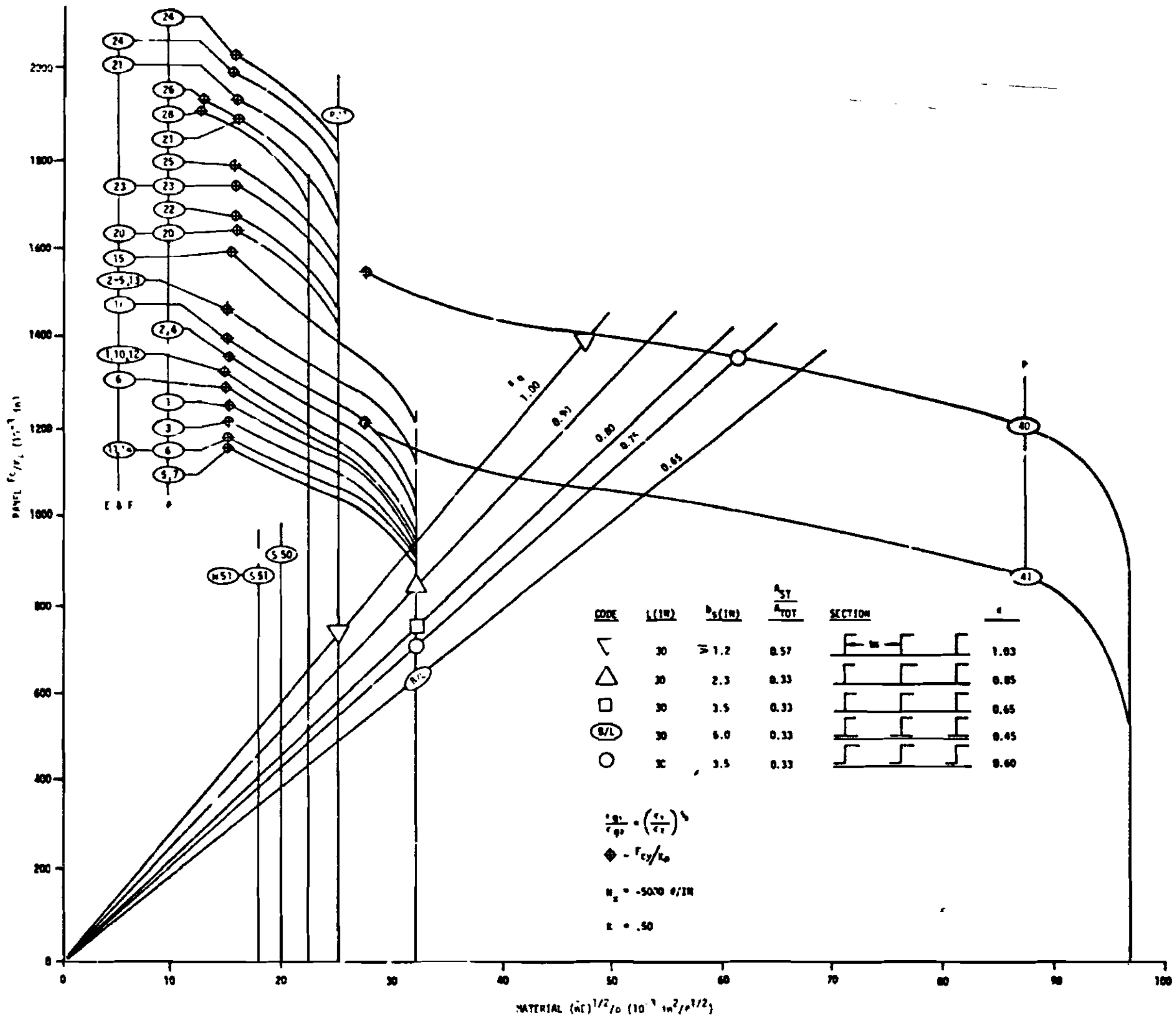

Figure 94 WING LOWER PANEL CONCEPT EFFICIENCIES FOR ULTIMATE COMPRESSION

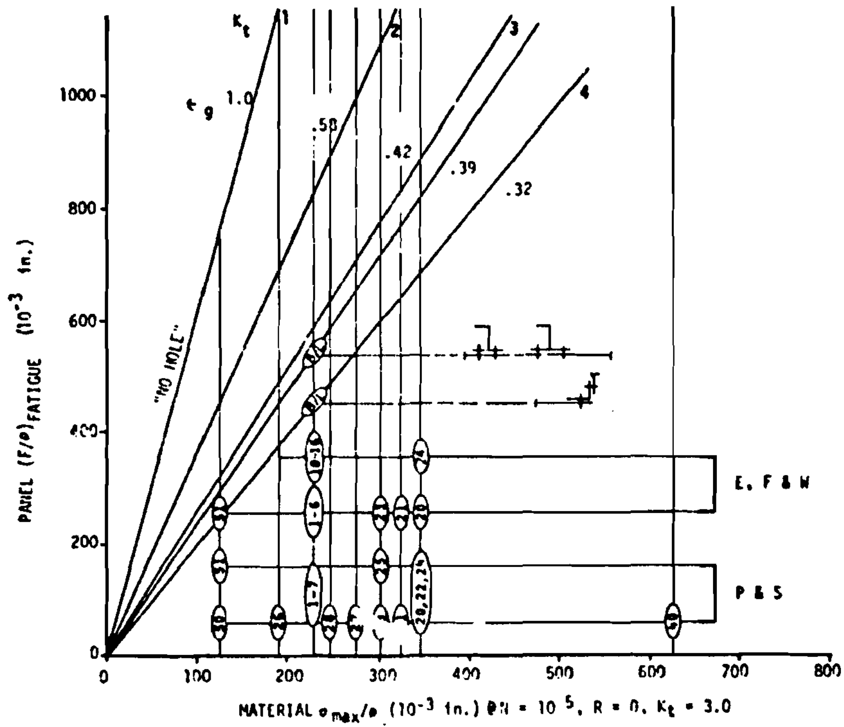

Figure 95 WING LOWER PANEL - CONCEPT EFFICIENCIES FOR FATIGUE

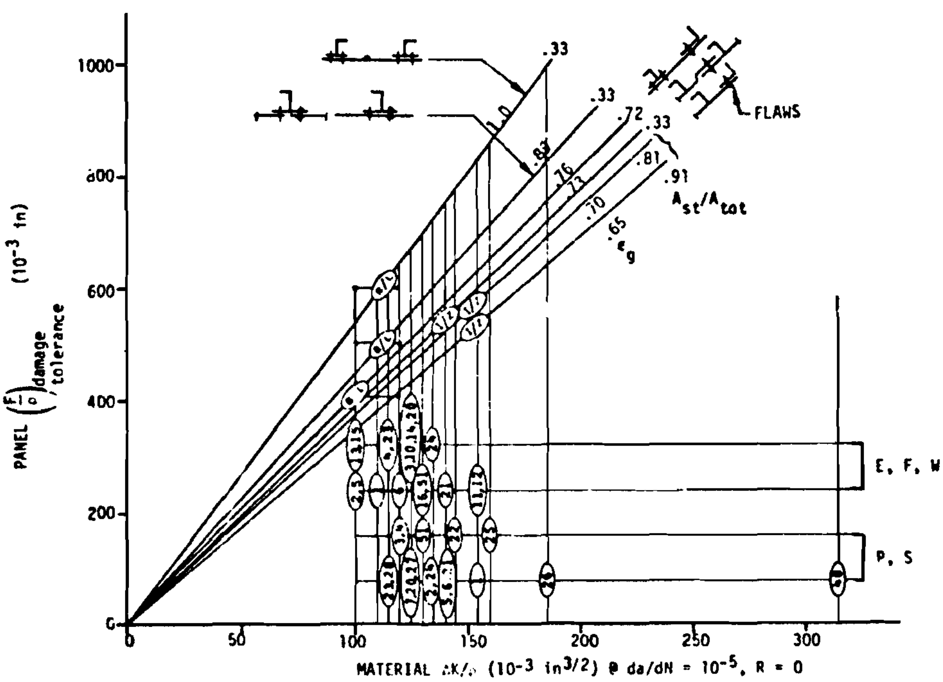

Figure 96 WING LOWER PANEL CONCEPT EFFICIENCIES FOR DAMAGE TOLERANCE

TABLE XXIII WING PANEL MATERIAL CAPABILITIES (1), (2)

CODE	FORM	MATERIAL	t	ρ	(3) ULTIMATE TENSION F_{tu}/ρ	(3) ULTIMATE COMPRESSION F_{cy}/ρ	(7) ULTIMATE COMPRESSION $\frac{(\hat{e}E)^{1/2}}{\rho}$	(4),(5) FATIGUE $\frac{\sigma_{max}}{\rho}$	(4),(6) DAMAGE TOLERANCE $\frac{\Delta K}{\rho}$	(4) FLUTTER $\frac{E}{\rho}$
			IN	#/IN³	10^{-3} IN	10^{-3} IN	$10^{-3}\left(\frac{IN^2}{\#^{1/2}}\right)$	10^{-3} IN	10^{-3} IN½	10^{-6} IN
P1		7050-T73651	>.25	.102	716	627	31.9	225	157	104
P2		7050-T7651		.102	775	686	31.9	225	137	104
P3	Aluminum	7075-T7651		.101	723	614	32.3	220	.19	105
P4	Plate	7475-T651		.101	782	683	32.3	220	119	105
P5		7475-T7351		.101	693	574	32.3	220	139	105
P6		7475-T7651		.101	713	594	32.3	220	139	105
P7		7075-T7351	>.25	.101	703	574	32.3	220	124	105
E1		7049-T73511	<.25	.102	765	667	31.9	225	108	104
E2		7049-T76511		.102	804	725	31.9	225	98	104
E3	Aluminum	7050-T736511		.102	775	716	31.9	225	127	104
E4	Extrusion	7050-T76511		.102	804	736	31.9	225	113	104
E5		7075-T6		.101	812	733	32.4	220	99	106
E6		7075-T76	<.25	.101	733	644	32.4	220	119	106
F10		7049-T73	>.25	.102	735	657	31.9	225	123	104
F11		7050-T73		.102	677	598	31.9	225	157	104
F12	Aluminum	7050-T736		.102	735	647	31.9	225	157	104
F13	Die	7075-T6		.101	802	723	32.0	220	99	103
F14	Forging	7075-T73		.101	683	604	32.0	220	123	103
F15		7175-T66		.101	881	802	32.1	220	99	104
F16		7175-T736	>.25	.101	782	693	32.4	220	129	106
P20		Ti-6-4 ANN	>.25	.160	844	819	25.4	340	125	103
P21		Ti-6-4 STA		.160	1031	756	25.4	325	138	103
P22		Ti-6-4 β ANN		.160	844	831	25.4	338	144	103
P23	Titanium	Ti-6-6-2 ANN		.154	915	866	25.7	305	116	107
P24	Plate	Ti-6-6-2 STA		.164	1067	1024	25.7	353	134	107
P25		Ti-6-6-2 β ANN		.164	945	896	25.7	305	159	107
P26		Ti-8-8-2-3 STA		.175	1000	972	22.2	188	183	86
P27		Ti-6-2-2-2-2STA		.162	1111	1123	26.1	270	123	110
P28		Ti-38-6-44 STA	>.25	.174	1006	960	22.1	247	116	85
E20		Ti-6-4 ANN	<.25	.160	856	825	25.4	338	125	103
E21	Titanium	Ti-6-4 STA		.160	1019	981	25.4	325	138	103
E23	Extrusion	Ti-6-6-2 ANN		.164	921	872	25.6	305	116	107
E24		Ti-6-6-2 STA	<.25	.164	1018	1006	25.6	353	134	107
P40	Beryllium	P S 20	>.25	.067	1045	776	97.0	627	317	627
P41	Sheet	Hip Pressed Bl	>.25	.067	896	597	97.0	-	-	627
S50	Steel	PH15-7(RH950)	<.25	.277	848	758	19.8	130	-	100
S51	Sheet	Marage 250	<.25	.300	867	833	17.8	120E	127E	95
W51	Wrought	Marage 250	-	.300	860	817	17.8	120	127	95
C1	0°	Boron Epoxy	-	.072	2660	4900	76.0	1810	-	415

(1) "L" Direction (2) Summarized From Tables in Appendix B (3) "B" Value (4) Typical Values

(5) $K_t=3$, R=0, N=10^5. (6) R=0, da/dn=10^{-5} (7) $\hat{e}=(E_t/E)^{.75}=1$ (Elastic Range)

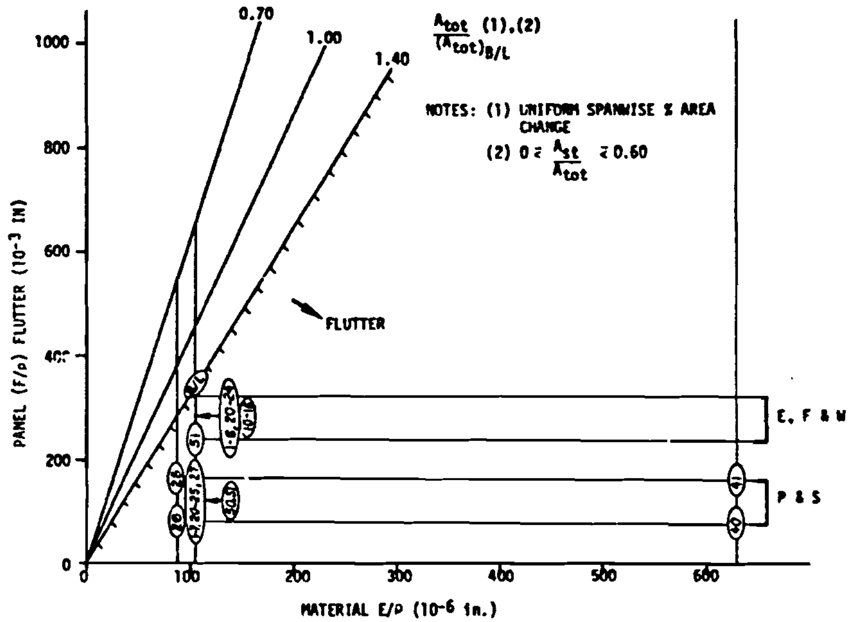

Figure 97 WING LOWER PANEL - CONCEPT EFFICIENCIES FOR FLUTTER

Baseline concept minimum geometric efficiencies are 0.80 for ultimate tension, 0.65 for ultimate compression, 0.32 for fatigue and 0.76 for damage tolerance. It should be recognized that the panel F/ρ values for each mode are established not only by the coupling of geometry and material efficiencies, but by the severity of the requirements relative to the reference mode.

For ultimate tension, geometric efficiency improvements may be achieved by eliminating attachment holes or by negating their effect through added local chordwise pads, for example, as indicated in Figure 93.

To establish a general format which applies to all ranges of compressive loadings, the ultimate compression mode material selection parameter has been revised to $(\bar{\eta}E)^{1/2}/\rho$ (Figure 94), thus encompassing both F_{cy}/ρ and E/ρ type selection parameters. $(\bar{\eta}E)^{1/2}$ values are established from basic stress/strain data (see Appendix B). This revision generalizes the chart format for any level of compressive loading and also correlates to the wide column analytical models of References 31 and 32. The "wide column" approach is selected over the "panel" approach because pylon and flap induced chordwise loadings and fuel tank boundaries require ribs and bulkheads irrespective of concept. Ribs and bulkheads are also required to provide necessary support for wide columns, hence, the overall efficiency of the wide column approach is enhanced. Data in References 19 and 31 also fail to establish any advantage for the "panel" approach over the "wide column" approach. The wide column data of Table XIV indicate integral zee, Z-stiffened and J-stiffened panel concepts provide high geometric efficiency, exterior smoothness for aerodynamic efficiency and open sections for inspectability and corrosion prevention. Therefore, these types are considered in Figure 94. Of these, the integral zee concept develops the highest levels of geometric efficiency. Because the load level N_x is relatively low, the full material capability of aluminum, titanium, and steel is not used. The slope of the geometric efficiency lines is proportional to $(N_{x_1}/N_{x_2})^{1/2}$, so that at $N_{x_1} = -20{,}000$ #/in., for example, the slope of the geometry lines would double and aluminum material capabilities would be fully exploited although titanium and steel material capabilities still would not. Beryllium capability, on the other hand, is fully utilized even at the lower -5000 #/in load level. Column length is selected at 30 inches, based on practical and near optimum rib spacing considerations (Figure 51).

The fatigue geometric efficiency is very sensitive to the stress concentration factor, K_t, reducing from $\varepsilon_g = 1$ at $K_t = 1$ to $\varepsilon_g = 0.32$ at $K_t = 4$; the latter corresponding to the baseline rear spar cap to skin splice case (Figure 95). Elimination of the attachment holes (i.e., "no hole" approach through integral, bonded or other joining procedures) dramatically improves the efficiency toward the limiting $\varepsilon_g = 1$, $K_t = 1$ level. Negation of hole effects through interference attachments, stress coining or other means provides another approach for efficiency improvement. However, this approach has been partially exploited to achieve the baseline level of efficiency, i.e., through interference fit attachments.

Similarly, for damage tolerance (Figure 96), elimination of the attachment hole and associated flaws provides a geometric efficiency improvement to the next limiting case, the "surface flaw", denoted by $\varepsilon_g = 1.0$. In regard to initial surface flaw size, a deviation to $a_i = 0.125$ in., based on current criteria levels, is used to preclude the "surface flaw" case from being more critical than the "hole flaw" case under depot level inspectability conditions. As with fatigue, a potential also exists for at least partially negating the hole flaw effect through interference fasteners, hole expansion stress coining, etc., as discussed in Reference 40. [NOTE: The damage tolerance material selection parameter for depot level inspectability, $\Delta K/\rho$, may require further upgrading to improve correlation to panel capability as indicated by limited analysis data (Figure 98). A more sophisticated parameter such as $\Delta K^{f(n)}/\rho$, where n is the slope of the da/dn curve, may provide a stronger correlation. Assuming verification through additional analysis data, implementation would require values of "n" for each material under consideration.]

Evaluation of the baseline flutter sensitivity criteria (Figures 24 and 25) for assumed uniform spanwise and chordwise percent rigidity changes identified section area ratio $A_{tot}/(A_{tot})_{B/L}$ as the major geometric parameter (Figure 97). Lower area ratios correspond to lower rigidity and improved flutter margin. Since this trend is compatible with the study objectives of reducing weight, flutter will not be a consideration normally. Weight increases (corresponding to area ratios > 1.0), if necessary, can also be accommodated by the existing flutter margin shown.

Panel capability improvements are also achievable through selection of "better" materials as indicated by the respective charts. However, as with geometry, materials that are better for one mode are not necessarily better for another mode. Identification of the best material and geometry combination(s) for all modes is required. A "geometry fixed/materials variable" analysis, using baseline geometry, is a logical first step for identifying better materials inasmuch as manufacturing cost increases are less likely through material substitution only. The effect of material substitution on panel capability F/ρ is established by the intersection of the material lines with the baseline geometric efficiency line for each mode. The results are summarized in Figure 99. The plate (P), extrusion (E), forging (F), and wrought (W) materials (for number code, see Table XXIII) become arrayed according to associated panel F/ρ values. For the "improved" baseline materials, denoted as B/L, $(F/\rho)_{B/L}$ relative to $(f_{tu}/\rho)_{B/L}$ identifies the most critical mode to be fatigue closely followed by damage tolerance. The rear spar cap to skin splice, the skin spanwise splices and the basic skin-to-stringer joints are the critical areas. Since all the aluminum materials are considered to have essentially the same fatigue capability, the baseline panel capability cannot be improved for fatigue by an aluminum material substitution only, as indicated. [NOTE: The "initial" study baseline materials, denoted as b/l, are indicated for reference only. Damage tolerance followed by fatigue were the most critical modes in this case.]

In the formal sense, use of the chart for better material selections involves identification of $(F/\rho)_{min}$ for each material and then selecting the best

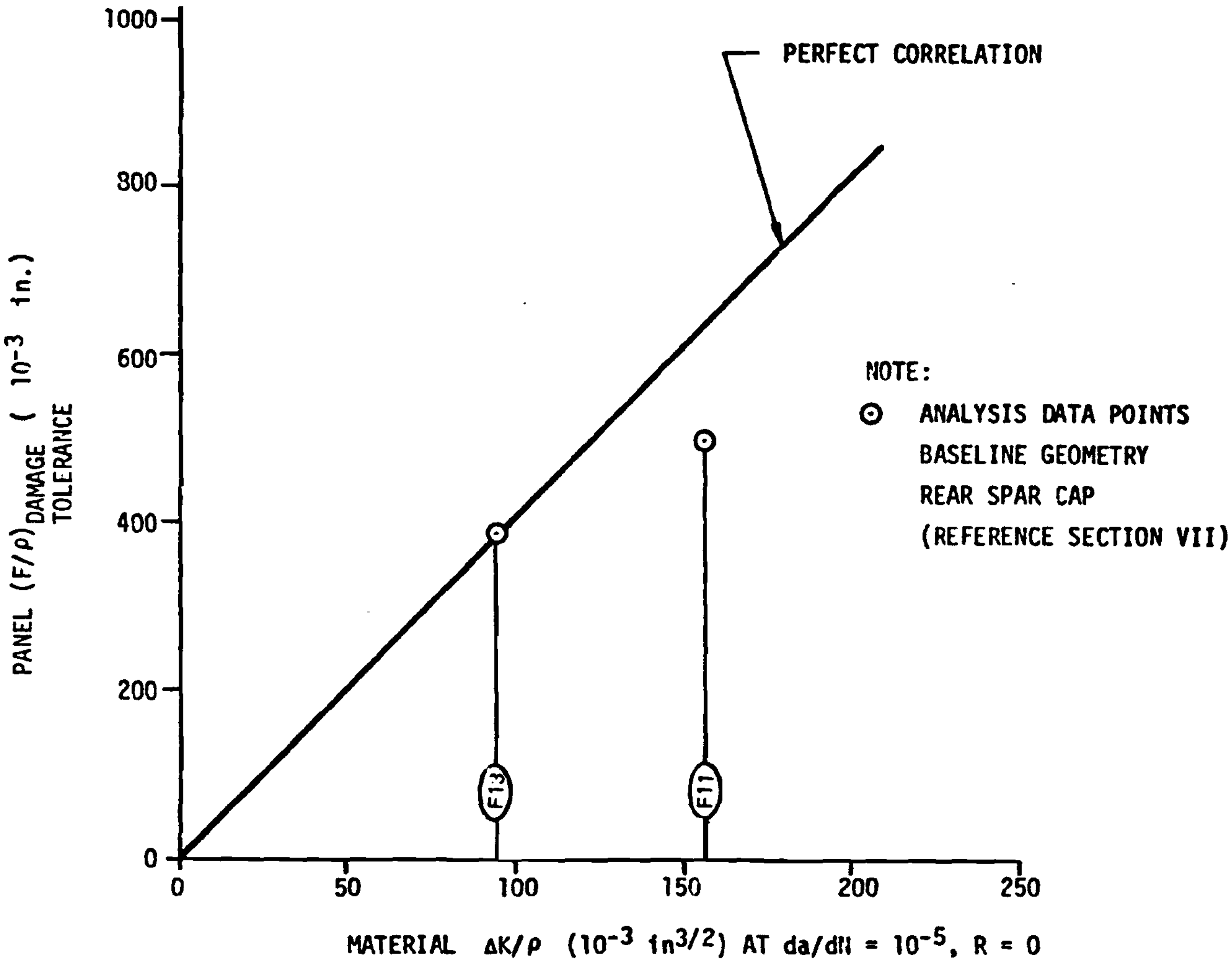

FIGURE 98 CORRELATION OF DAMAGE TOLERANCE DATA

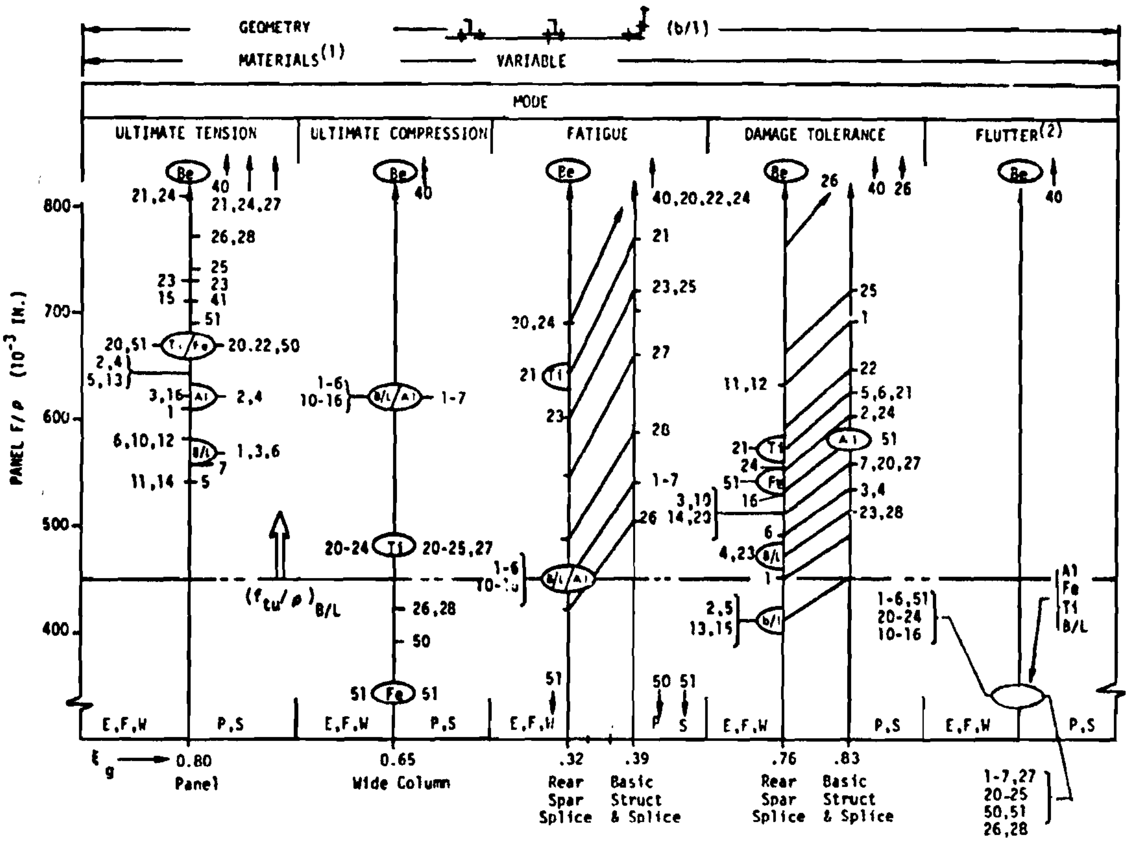

NOTES:

(1)

Code	Skin	Stringers	Spar Caps
b/1 (3)	P3 = 7075-T7651	E5 = 7075-T651	F13 = 7075-T6
B/L (4)	P6 = 7475-T7651	E4 = 7050-T76	E4 = 7050-T76
Al	P2 = 7050-T7651	E3 = 7050-T736511	F12 = 7050-T736
Ti	P22 = Ti-6-4 BETA ANN	E21 = Ti-6-4 STA	E21 = Ti-6-4 STA
Be	P40 = PS 20 Beryllium	P40 = PS 20 Beryllium	P40 = PS 20 Beryllium
Fe	S51 = MARAGE 250	W51 = MARAGE 250	W51 = MARAGE 250

(2) For "No Flutter" $f_{tu}/\rho \geq (F/\rho)_{flutter}$

(3) "Initial" Baseline Materials (Reference Only)

(4) "Improved" Baseline Materials (Study Basis)

Figure 99 WING LOWER PANEL NEW CONCEPT MATERIAL SELECTION material on the basis of maximum $(F/\rho)_{min}$. This is illustrated below for aluminum skin material selection (where F = Fatigue, T = Tension and D/T = Damage Tolerance, etc.).

P	$(F/\rho)_{min_1}$	$(F/\rho)_{min_2}$
1	450 F	570 T
2	450 F	600 D/T (Max)
3	450 F	535 D/T
4	450 F	535 D/T
5	450 F	540 T
6	450 F	570 T
7	450 F	560 T

Aluminum plate P2 (7050-T7651) is identified as a best choice for the wing lower panels on the basis of maximum $(F/\rho)_{min_2}$ capability since the maximum $(F/\rho)_{min_1}$ capability (defined by fatigue) is identical for all aluminum materials. [NOTE: Damage tolerance analyses of the baseline rear spar cap-to-skin splice show that the panel capability is established by failure of the spar car, hence, this mode area was omitted in the skin selection considerations.] In general, rules regarding panel element dependency are established from the analytical models and associated analysis results. Where the panel capability is defined by failure of one element, no element dependency exists. This generally is the case for ultimate tension and for fatigue. Where the panel capability is defined by failure of more than one element, then a degree of dependency exists which is defined by geometry and material mixture. This generally is the case for ultimate compression and for damage tolerance. Where these dependency relationships have not been completely developed, they are simulated for charting purposes by a simple area and material property ratio approximation. Given element areas A_1 and A_2, a panel capability $(F)_{eq}/(\rho)_{eq}$ and a material mixture m_1 and m_2, the equivalent material selection property characteristic $(FM)_{eq}/(\rho)_{eq}$ is defined in the following manner for the dependent case:

$$(Fm)_{eq} = \frac{Fm_1 A_1 + Fm_2 A_2}{A_1 + A_2} = Fm^* \tag{28}$$

$$(\rho)_{eq} = \frac{\rho_1 A_1 + \rho_2 A_2}{A_1 + A_2} = \rho^* \tag{29}$$

*for no material mixture, $m_1 = m_2 = m$

For the above relations to correlate exactly with the baseline spar cap damage tolerance analysis results, for example, would require $A_{cap}/A_{tot} = 1$, compared to the actual value of approximately 0.72.

Aluminum stiffener and spar cap materials (E and F) are selected in a manner similar to that for the skin. These are identified to be E3 (7050-T736511) and F12 (7050-T736). These "best" aluminums (Al) show no overall improvement relative to the baseline (B/L) due to the limiting fatigue mode although individual improvements for ultimate tension and for damage tolerance are realized.

Similarly, the best titanium materials (Ti) for skin and for stringer and spar cap, respectively, are P22 (Ti-6-4 β Ann) and E21 (Ti-6-4 STA). Relative to the baseline (B/L), considerable improvement in ultimate tension, fatigue, and damage tolerance is achieved; however, considerable degradation in the compression mode is also incurred. The overall improvement relative to the B/L nonetheless is 7 percent.

The best steel material (Fe), from a limited listing of candidates, is MARAGE 250 in sheet (S 51) and wrought (W 51) form. The panel capabilities of Fe for ultimate tension and damage tolerance are better relative to the B/L, however, serious capability reductions exist for compression and fatigue.

Beryllium (Be) substitution provides significant improvement for all strength modes. However, a basic incompatibility exists between the "no flutter" rigidity criterion $f_{tu}/\rho \geq (F/\rho)$ flutter (= 2000 for Be) and the strength criterion $f_{tu}/\rho \leq (F/\rho)$ strength ($\leq$ 1600 for Be). Unless sufficient offsetting rigidity decreases can be provided in other areas of the wing, beryllium cannot be used in this particular application. [NOTE: In cases such as this, where unusually large rigidity, weight, and rigidity-to-strength ratio changes from the baseline are involved, further flutter checks of serious candidates are required, eventually, to confirm these initial results.)

A summary comparison of the above material selections on a minimum weight $(F/\rho)_{max}$, total manufacturing cost $(F/\rho C_{\#})_{max}$ and life cycle cost (SBR) basis is shown in Table XXIV.

On the basis of initial cost as a primary criterion, Be, Ti, and Fe are eliminated from further consideration. This result is further supported on a life cycle cost basis as indicated by SBR values which exceed the conservative criterion value of 200 $/#. Therefore, only aluminum materials (Al) remain for further consideration, although no cost or weight improvement is achieved.

An "Al materials fixed/geometry variable" analysis is required to identify improvement potential (Figure 100). As indicated, for the baseline geometry (b/l), fatigue of the spanwise splices (spar cap-to-skin and skin-to-skin) and of the basic section (stiffener-to-skin) is constraining weight improvement. This constraint also applies to all other concepts with similar spanwise splices. Based on an improvement goal associated with achieving the

TABLE XXIV WEIGHT AND COST COMPARISONS OF WING LOWER PANEL CONCEPTS								
CODE	GEOMETRY	MATERIALS	F/ρ Fig. 99 (1)	$\frac{W_S}{(W_S)_{B/L}}$	C# Fig. 90	$\frac{C_\#}{(C_\#)_{B/L}}$	$\frac{F}{\rho C_\#}$	SBR REQUIRED Fig. 91
B/L	b/l	Aluminum	450 (F)	1.00	45	1.00	10.0	0
A1	b/l	Aluminum	450 (F)	1.00	45	1.00	10.0	0
Ti	b/l	Titanium	480 (C)	0.94	120	2.67	4.0	> 200
Fe	b/l	Steel	240 (C&F)	1.88	45 (2)	1.00	7.6	> 200
Be	b/l	Beryllium	840 (T)(3)	0.53	660	14.70	1.3	> 200

NOTES
(1) DT (Damage Tolerance); F (Fatigue); C (Compression); T (Tension)
(2) Assumed same as aluminum riveted
(3) Assumed no flutter constraint

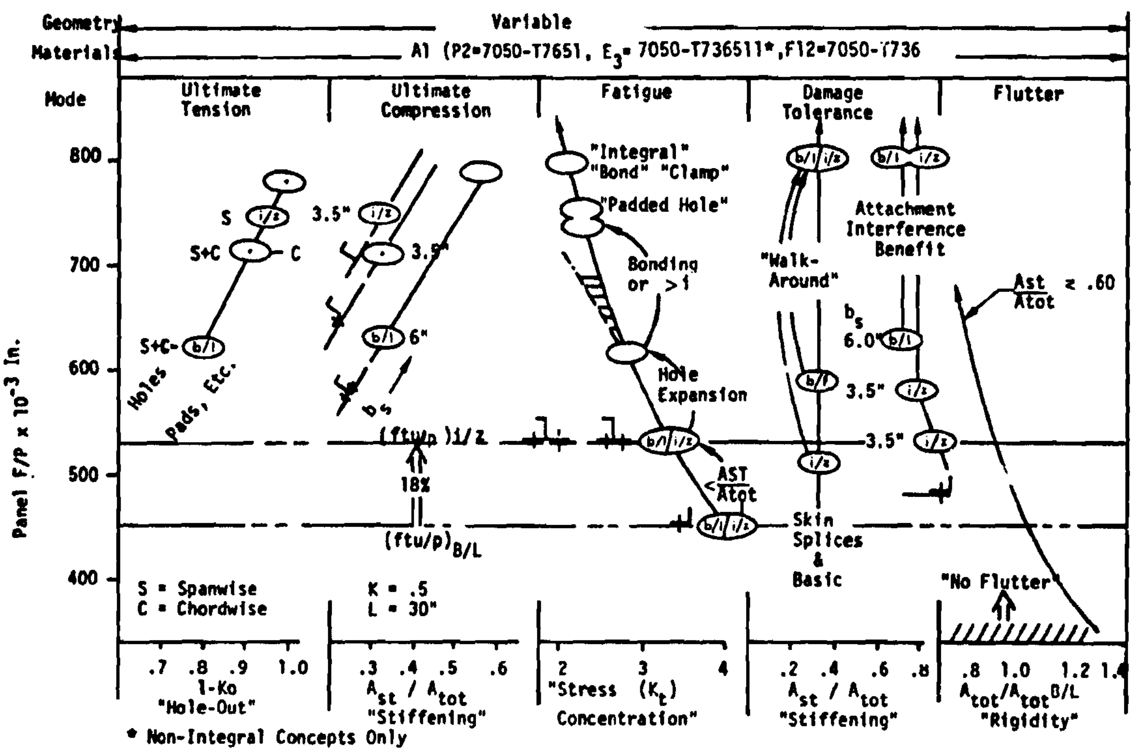

Figure 100 WING LOWER PANEL NEW CONCEPT GEOMETRY SELECTION

ultimate mode tension and compression capability limits ($F/\rho \approx 750$), a joining concept with $K_t \lesssim 2.3$ would be required. A listing of possible joining concepts and estimated associated geometric efficiencies (K_t) appears in Table XXV with several providing $K_t \lesssim 2.3$ potential. The various joining concepts are separated into "hole attachment" types and "no hole attachment" types in recognition of the known significance of attachment holes in fatigue geometric efficiency.

The hole attachment types are "internal clamping" with the discrete attachment acting as a tension and shear transfer device. This approach has been widely used in aircraft structure and likely will continue to be used in the future; hence, a consideration of the capability potential is justified. Past and current procedures to negate the effect of the hole include "interference fit" attachments, "stress coining," or a combination of the two. As shown in Figure 101, interference reduces cyclic amplitude without affecting maximum cyclic stress, while coining introduces favorable residual compressive stresses which reduce maximum cyclic stress without affecting cyclic range. The combination of interference and coining provides reductions in both maximum and cyclic stresses.

Attachment types providing a range of interference (i) include slug rivets ($\lesssim$ 0.006"), lockbolts and Taper-Loks ($\lesssim$ 0.004"), and bolts and screws ($\lesssim$ 0"). (Note: Interference dimensions shown apply to 0.25" diameter fasteners.) Due to decreased stress amplitude, fatigue capability improves with increasing interference level as indicated in Figures 102 and 103. However, at higher levels of stress, fretting, due to increased relative motion between rubbing surfaces, becomes an increasingly important constraint. This relative motion is accentuated with increasing load transfer ($\gamma \to 1$). Practical values of γ at critical points are estimated to be $\lesssim 0.5$ for tension splices (Reference 41) and $\lesssim 0.25$ for spanwise shear splices and for basic skin-to-stringer structure.

For the baseline spanwise skin splice, with conditions of $\gamma \approx 0.25$, near mixed mode regime (based on current surface treatments), countersink lockbolt attachments and $t/D \approx 2$, the fatigue capability σ_{max} is approximately 20 KSI at $N = 10^5$, $R = 0$. This corresponds to $K_t \approx 3.2$ as established from notched specimen data (Figure 104) and correlates with the analysis value ($K_t = 3.3$, Figure 100). Considering $t/D = 3$ for the baseline rear spar cap increases K_t to 3.8 (vs. 4.0, Figure 100). Further review, in conjunction with new concept spar cap area reduction for damage tolerance (subsequent discussion), justified $t/D \lesssim 2$, thereby making the rear spar cap splice equivalent to the skin splice at panel $F/\rho \approx 530$.

Per Figure 102, additional fatigue improvement is attained by stress coining (i.e., expansion cold working) of the attachment countersink area. This results in a significant panel capability increase to $F/\rho \approx 615$ (Figure 100). Fretting induced fatigue failures are estimated to become a consideration at panel capability levels above 615 as indicated. Fretting control through

TABLE XXV	ESTIMATED JOINING CONCEPT GEOMETRIC EFFICIENIES FOR FATIGUE				
APPROACH	CASE	JOINING CONCEPT	$\gamma^{(1)}$	K_t	REMARKS
HOLE ATTACHMENT	A	OPEN HOLE	0	3.0	Reference Case Only
	B	COUNTERSUNK AD SLUG RIVETS INTERFERENCE = 0.0015	0	2.2 (1.8)*	See Figures 103 and 104
			0.5	3.4 (2.7)*	*With Hole Expansion
			1.0	4.9 (3.6)*	
	C	COUNTERSUNK LOCKBOLTS INTERFERENCE = 0.002	0	2.4 (2.0)**	See Figures 102 and 104
			0.5	4.3 (3.2)**	**No Countersink or with Countersink Expansion
			1.0	6.0 (4.3)**	
	D	PADDED HOLE WITH COUNTERSUNK LOCKBOLTS INTERFERENCE = 0.002	0	1.0	Estimated from Preliminary Data
			0.5	2.4	and Case C for Attachment Effects
			1.0	3.6	
NO HOLE ATTACHMENT	E	INTEGRAL	0 - 1.0	1.0	Ideal Case (Reference)
	F	BOND	0 - 1.0	1.0	Transfer Loads Distributed by Bond
	G	SPOTWELD	0	2.4	MIL-HDBK-5, $\gamma = 1$ Data Correlates
			0.5	4.3	Approximately to Case C,
			1.0	6.0	$\gamma = 1$
	H	WELD BOND	0	2.4	See Case G, $\gamma = 0$
			0.5	3.6	Limited Preliminary Data
			1.0	4.7	
	I	MECHANICAL CLAMP	0 - 1.0	1.5	Shear Transfer through Low K_t Mechanical Interference

(1) γ = Transfer Load/Total Load $\lessapprox$ 0.25 for Basic and Spanwise Splice Structure

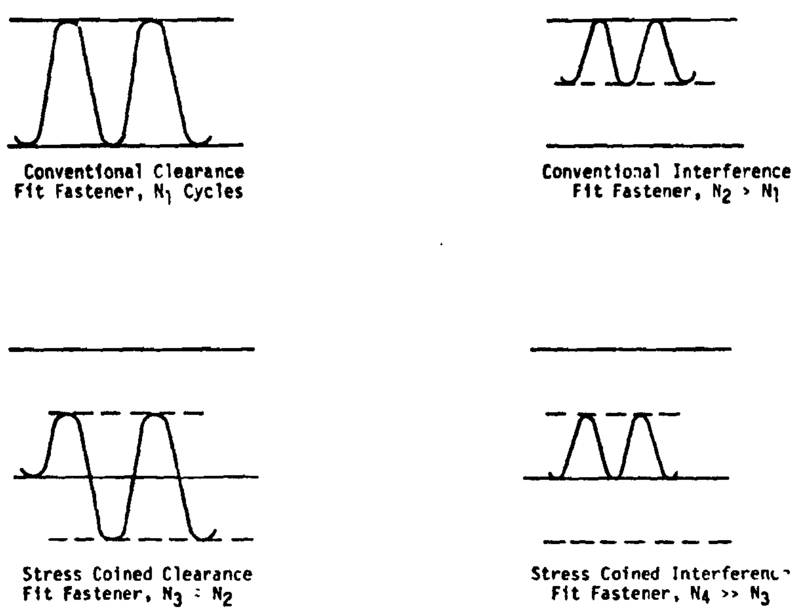

Figure 101 EFFECTS OF INTERFERENCE AND COINING ON FATIGUE STRESSES AND LIFE

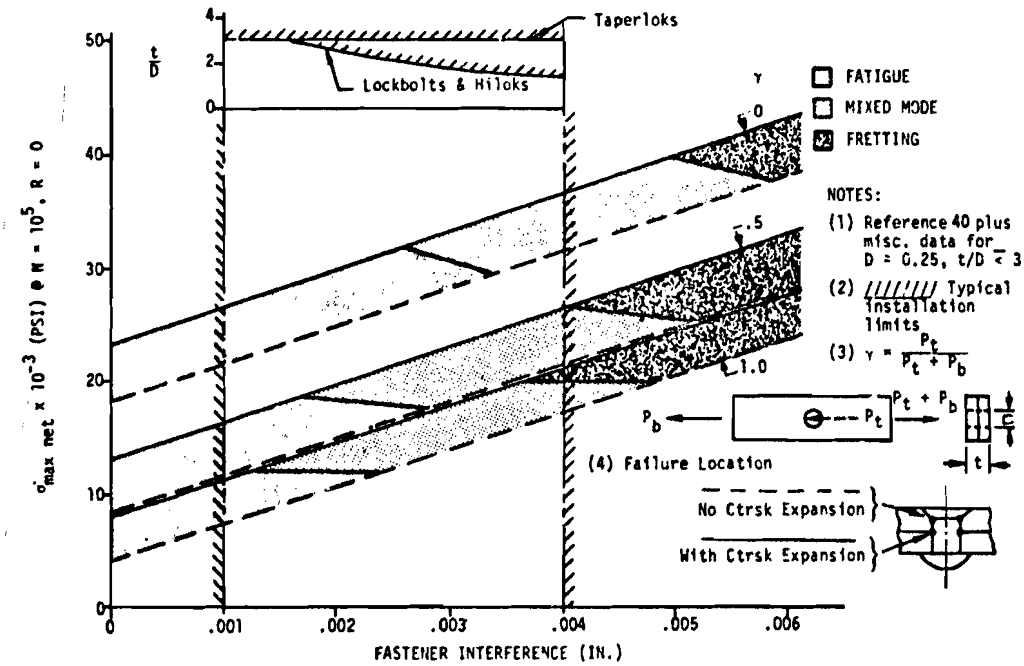

Figure 102 FATIGUE CAPABILITY OF LOCKBOLT, HILOK AND TAPERLOK JOINTS

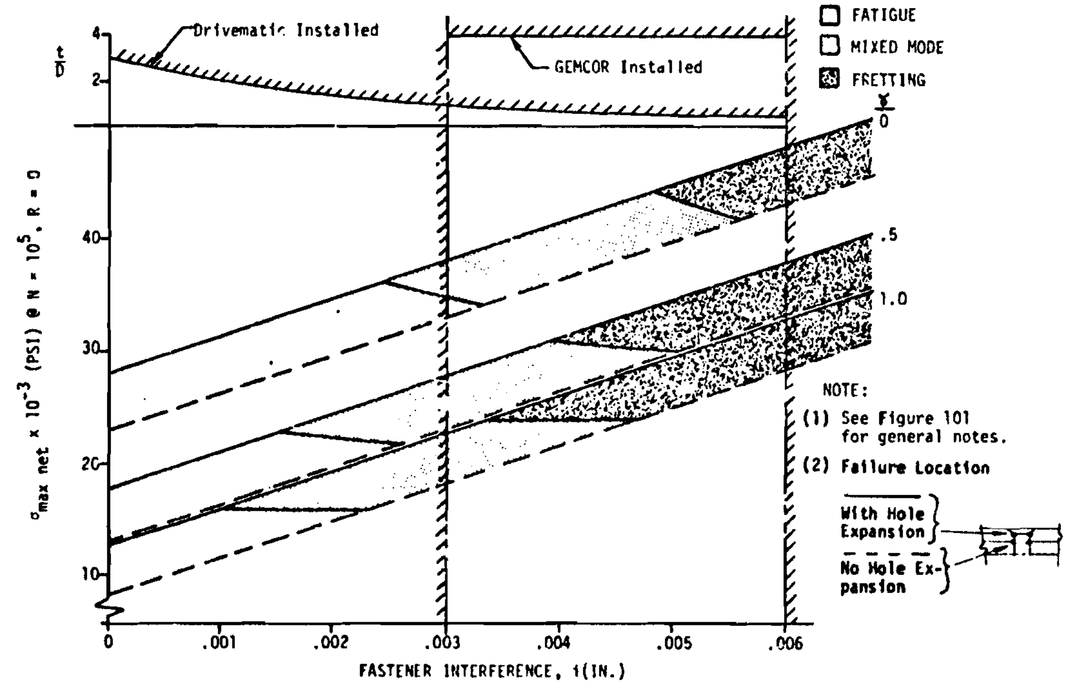

Figure 103 FATIGUE CAPABILITY OF "AD" SLUG RIVET JOINTS

faying surface coatings or fretting elimination through bonding (both of which require further development) could provide additional improvement opportunity. Bonding, for example, reduces attachment load transfer (assume $\gamma_{max} = 0.10$) and projects a further panel capability increase to $F/\rho \approx 740$ levels. Increased and controlled interference to 0.0035" levels through the use of taperlocks also provides a similar potential.

Similarly, for the baseline skin-to-stringer structure with $\gamma = 0.25$, countersink AD slug rivets "Drivematic" installed and $t/D \approx 2$, σ_{max} is equal to 20 KSI (Figure 103). This is identical to the skin splice value and corresponds to a panel $F/\rho \sim 530$. With hole expansion, an improvement is obtained to $F/\rho \approx 615$ levels. If further investigation indicates that $\gamma << 0.25$, then $F/\rho \approx 740$ levels can be projected (in lieu of 615) without bonding. Otherwise, bonding or an increase in interference through higher pressure installation equipment (such as Gemcor) is required to achieve 740. Another hole attachment approach, the "padded hole" concept (Table XXV, $K_t \leq 2$ @ $\gamma = 0.25$), also shows potential to $F/\rho = 750$ levels (Figure 100). Implementation of this concept to spanwise splice structure would likely be along the lines indicated in Figure 105, with "hole pads", used where required in lieu of hole expansion, increased interference, etc.

The no-hole attachment approach includes surface adhering types (such as bonding, spotwelding and weldbonding) and external clamping types (mechanical) as indicated in Table XXV. With the exception of spot welding concepts, these types are characterized by a continuous distributed attachment acting as a tension and shear transfer device, thereby achieving a low stress concentration factor and a corresponding high fatigue capability ($F/\rho > 750$) as indicated in Figure 100. Limited available data indicates that spotweld and weldbond concept fatigue quality approximates that of typical hole attachment concepts at low load transfer ratios (γ) with weldbond being better at higher load transfer ratios.

External clamping mechanical joints are of interest because of potentially higher fatigue and damage tolerance capability and lower cost relative to hole attachment types. Lower costs would accrue from elimination of the many discrete, close tolerance fasteners, holes and hole treatments through substitution of simple, continuous, close tolerance machined members, such as shown in Figure 106. The machining equipment required generally is available for other reasons, hence, no new equipment or technology is necessary. Spanwise mechanical interference (or bonding) is required to provide a positive non-friction dependent shear transfer capability.

Damage tolerance capabilities of the baseline and integral zee geometry concepts (Figure 100) identify the skin splices (and baseline skin-to-stringer) as slightly more critical than the spar cap splices on the basis of "depot level inspectability" requirements. However, the skin splices (and baseline skin-to-stringer) can also be qualified to the less stringent "walk-around inspectability" requirements, resulting in significantly higher F/ρ levels > 800 as shown.

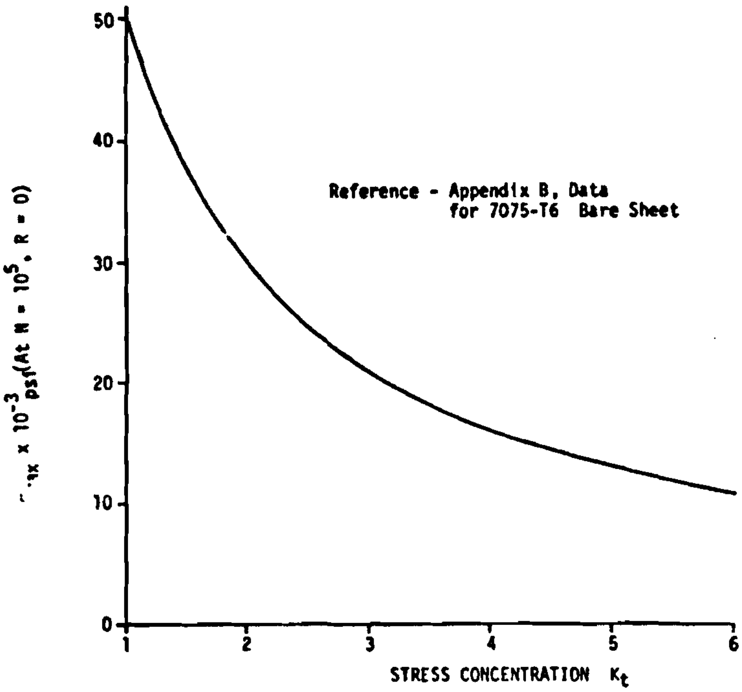

Figure 104 STRESS CONCENTRATION EFFECT ON FATIGUE STRENGTH

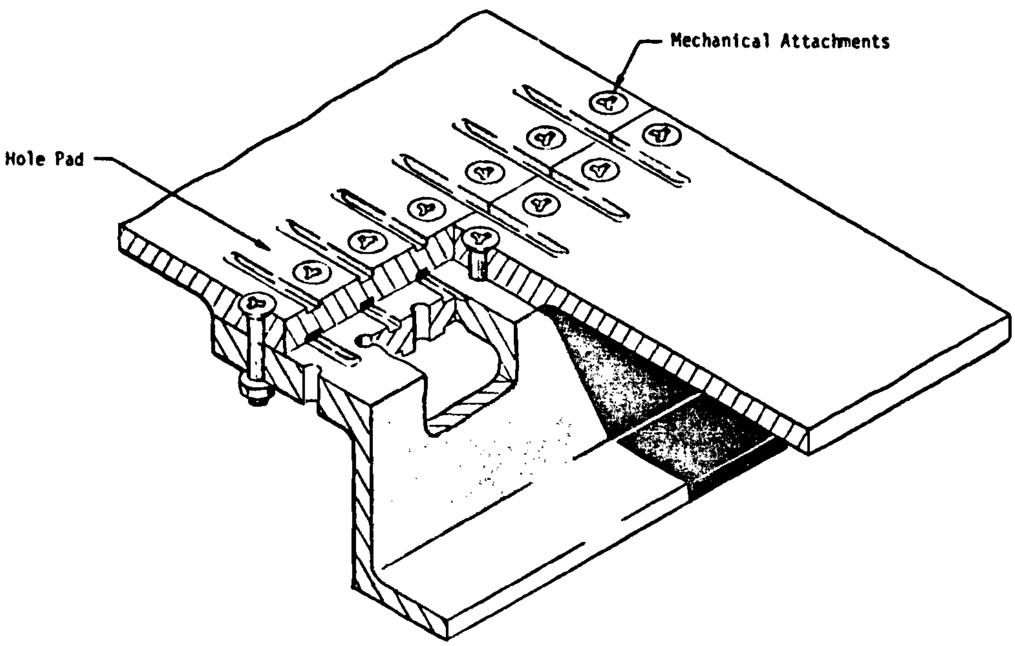

Figure 105 SPANWISE SPLICE "PADDED HOLE" CONCEPT

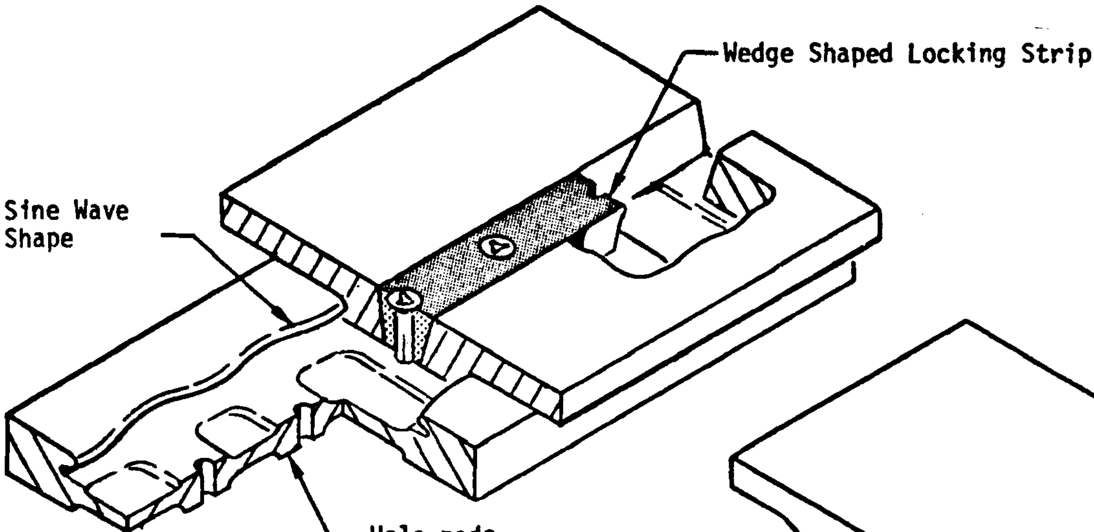

(a) Spanwise Skin Splice

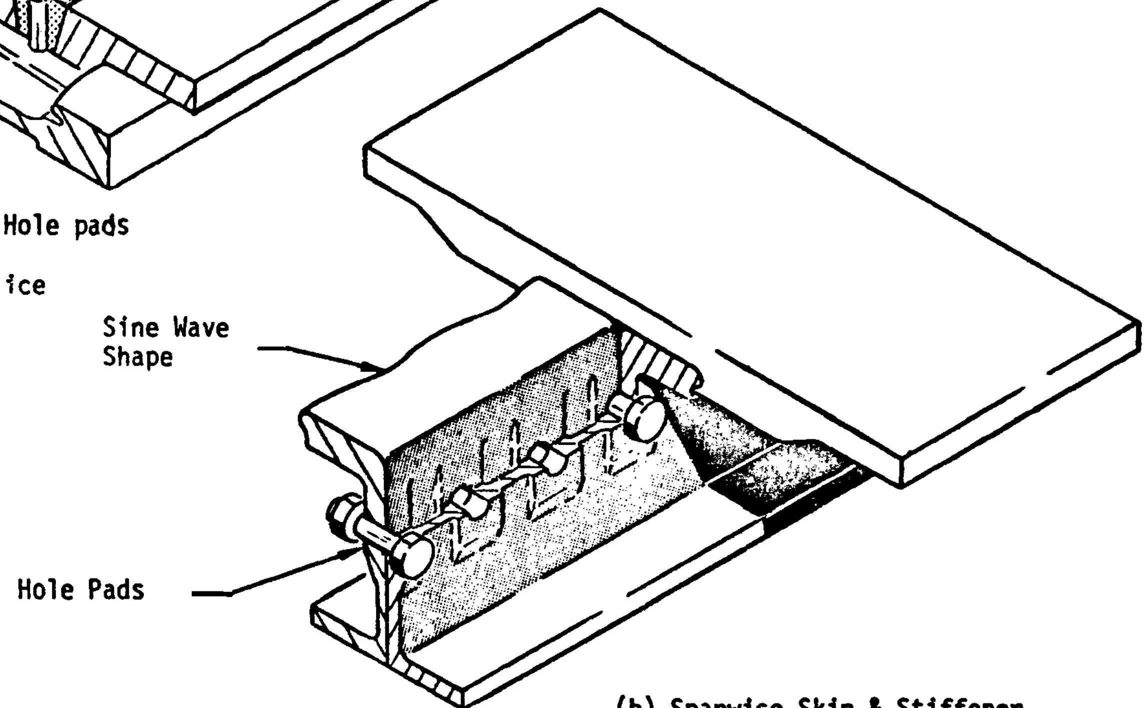

(b) Spanwise Skin & Stiffener

Figure 106 EXTERNALLY CLAMPED SKIN SPLICE AND STIFFENED SKIN CONCEPTS

An initial approach for improving the geometry of the wing lower panels is by examination of the analysis model that simulates damage tolerance behavior. For geometry variable/material fixed, da/dn vs ΔK is constant. Hence, the achieved period and associated panel F/ρ are controlled by the stress concentration factor $\Delta K/\Delta\sigma$ ($=\beta\sqrt{Aa}$). The factor β includes the influence of local stiffening and attachment rigidity conditions. For fixed attachment rigidity conditions, panel stiffening magnitude (A_{st}/A_{tot}) and distribution (spacing, b_s) are identified as potentially significant geometry parameters. For the spar cap, reduction of local stiffening ratio from 0.90 to 0.80 (minimum for shear transfer) provides a capability improvement to F/ρ = 580 for the integral zee concept (Figure 100). Also, an integral stiffener vs separate stiffener effect may also exist as indicated by the better performance of the baseline geometry. Additional analyses of this nature are required to fully define the influence of stiffening and attachment parameters. The preliminary trend indication to a lower stiffening ratio is rational in that, for the same total area, failure of a smaller separate stiffener releases less load to be supported locally by more available skin. Since the criteria "period" requirement is mostly achieved under small to moderate crack size conditions, the local stiffening ratio is important. Hence, the primary design implication is that the stiffening ratio should be minimized to some lower bound value established by alternate skin failure and compression considerations. Also, under small crack size conditions, cracks propagate at the same rate in thick stiffeners as they do in thin ones. Therefore, for a given minimum stiffening ratio and spacing, the stiffener thickness penetrated by a through hole flaw should also be minimized, i.e., the stiffener section periphery should be maximized to some upper bound value determined by compression stability and practical considerations. This provides more dispersion of the material along the crack growth path and, hence, more period before stiffener failure. This preliminary approach indication is most appropriate to "depot level inspectability" conditions where the emphasis is on large period, infrequent inspections and NDI methods suitable for high detectability rates of small crack sizes. For "walk-around" or "special visual" conditions, however, the emphasis is on more frequent inspections and on shorter periods defined by moderate to large crack sizes. Period achievement under moderate or large crack size conditions is determined by the high ΔK end of the da/dn curve and, hence, the period is increased by higher values of the fracture strength parameter K_c which is associated with lower structural element thicknesses. Therefore, for visual inspectability, the concept geometry can be influenced toward a "multi-skin" approach.

Beneficial effects also occur from attachment interference and hole cold working. Current proposed criteria allow for this through reduced initial hole flaw size (to corner radius flaw = 0.005 inch). Use of this reduced criteria to account for favorable attachment and hole conditions permits F/ρ > 800 levels for the spar cap splices also (Figure 100).

In summary, through the adoption of pertinent and beneficial geometry options, significant increases in design stress levels can be demonstrated analytically. For example, by thinning down the spar caps and including expansion cold working of the attachment holes for fatigue and damage tolerance improvement, a fatigue critical design stress level $f_{tu}/\rho = F/\rho \approx 615$ is achieved for either a separate or integral stiffened geometry concept (i.e., b/l or i/z). Relative to $(f_{tu}/\rho)_{B/L} = 450$, this is a 35% improvement. Also incorporating bonding, for example, increases the critical capability level to $F/\rho \approx 740$, a 65% improvement. Other options, such as increased "attachment interference," "padded hole," and "clamping" also offer similar attractive potentials, although additional data is required to fully establish the constraining influence of the fretting failure mode. In this regard, further data is also required to more fully validate most of the options and associated potentials indicated and the practicality thereof.

Two lower panel geometries, baseline (b/l) and integral zee (i/z) were studied in the concept sizing, weight and cost analyses. The capabilities of these geometries are indicated for each mode by the highest valued symbols b/l and i/z, (Figure 100). Although b/l geometry offers an overall F/ρ improvement potential similar to that for i/z, the integral concept was selected for further consideration for the wing lower panels because it offers a potential for cost reduction through the reduced parts count associated with fewer attachments, stiffeners, clips, etc. [NOTE: The availability of a simple and quantitative preliminary design type cost method for design engineer application at the concept selection phase would permit more confident, visible and quantitative design-for-cost decisions with respect to various geometry and material options. This would be a valuable and beneficial supplement to engineer intuition that is based on variable past experience.] In conjunction with Al materials, the i/z concept provides an overall 18% improvement relative to B/L.

However, since Al materials were identified using b/l geometry (Figure 100), an "i/z geometry fixed/materials variable" followup check is required to establish or verify the best material selection under the new geometry conditions. This is shown in Figure 107 using the data of Figures 93 to 97. The best materials are now identified as Al'and show a change of cover panel material to P1 (7050-T73651) from P2 (7050-T7651) associated with Al. The spar cap material remains unchanged as F12 (7050-T736). The material change occurs because of the i/z tension mode geometry improvement (chordwise holes are eliminated by integrally machined bulkhead shear clips). This deemphasizes the material tension capability requirements with respect to the other mode capability requirements. Materials actually selected for the integral concept design by conventional material selection procedures (and without benefit of the chart approach) are indicated as I/Z. The I/Z cover panel material selection is P6 (7475-T7651) with the spar cap material again being F12 (7050-T736). The differences in cover panel material selections do not result in differences in the minimum capability ($F/\rho = 530$ associated with fatigue) or in the overall achieved improvement (18% associated with Al, Al' and I/Z). The insensitivity, which in this case reflects the relative invariance of fatigue capability among the aluminum materials, does not necessarily extend to other situations, however.

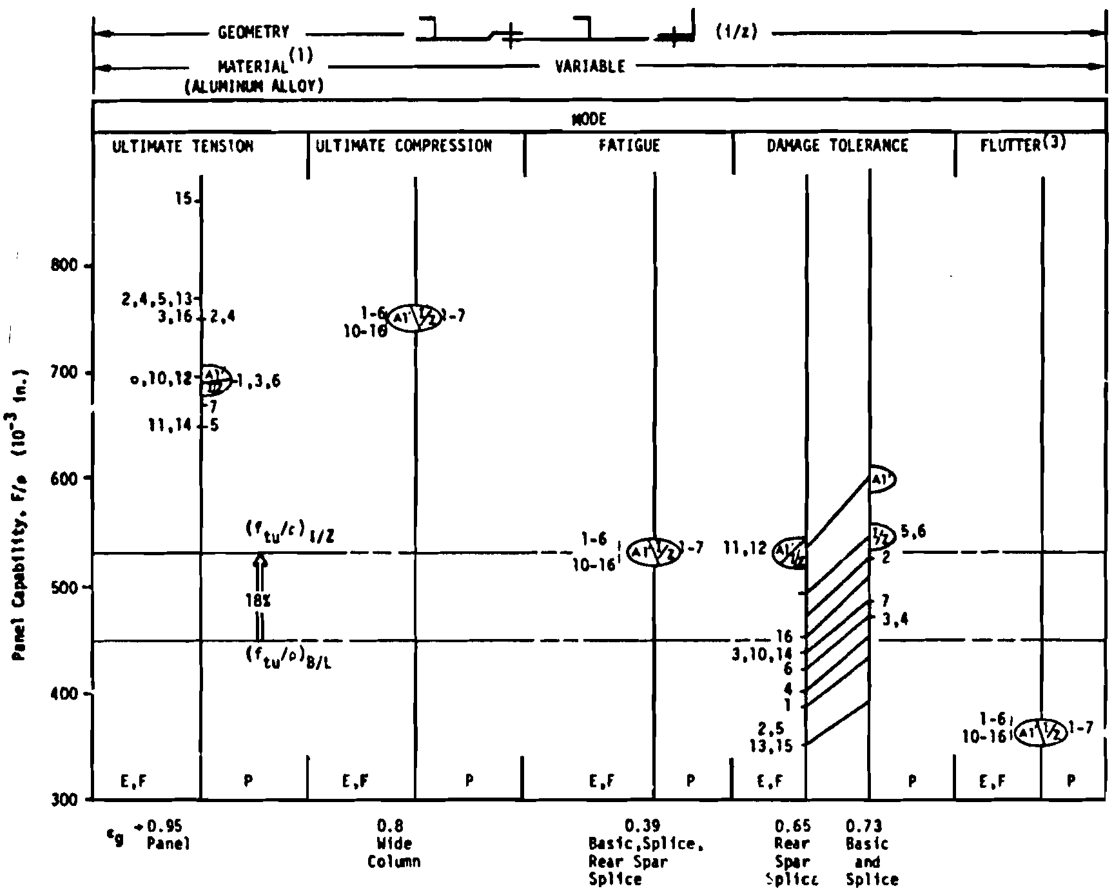

NOTES:

(1) CODE — INTEGRALLY STIFFENED SKIN — SPAR CAPS

CODE	INTEGRALLY STIFFENED SKIN	SPAR CAPS
A1'	P1 = 7050-T73651	F12 = 7050-T736
A1 (2)	P2 = 7050-T7651	F12 = 7050-T736
1/Z	P6 = 7475-T7651	F12 = 7050-T736

(2) REFERENCE FIGURE 99

(3) FOR "NO FLUTTER," $f_{tu}/\rho \leq (F/\rho)_{flutter}$

Figure 107 WING LOWER PANEL INTEGRAL CONCEPT ALUMINUM MATERIAL SELECTION

Comments with respect to the concept efficiency chart approach (Figures 93 through 97) include the following. The approach provides a means for directly relating available panel material, geometry and capability data, thereby better defining and integrating the goals and efforts of the structural material, design and analysis disciplines. By configuring the material selection parameter so as to establish a linear relationship between panel capability and material parameter, a singular material/geometry capability solution can be extended to all other materials, thus minimizing analytical effort. By using a "chart" format, visiblity and comprehension is improved, thus, also enhancing technical communication. By relating all mode capabilities to a common reference mode, direct and quantitative judgments and evaluations of material and geometry variation effects can be made, thereby aiding in the definition of a balanced and efficient structure from a capability, weight and cost standpoint. In addition, the procedure also provides a means of identifying material selection parameters that require improvement. A case in point is the material selection parameter for compression which was upgraded (Figure 94). Similarly, the damage tolerance material selection parameter for depot level inspectability, $\Delta K/\rho$, may require further upgrading (Figure 98). Thus, additional direction is provided to the materials data development and organization process.

In general, the procedure appears to be working properly, answering the basic "what, how much, why, etc." type design questions. Implementation requires only the engineering type data normally generated or available. Additional application experience and checks will further improve and verify the value of the approach.

6.2.2 Wing Upper Panels

The same failure modes are operative in the wing upper panels as in the lower panels even through the relative importance of each may be altered. Hence, the upper panel concept selection approach and considerations parallel those of the lower panels.

Upper inboard panel material and geometry options for ultimate compression and tension, fatigue, damage tolerance, and flutter are summarized in Figures 108 to 112. Baseline geometry and materials are included as a reference and point of departure for improvement. Materials data are taken from Table XXIII. Panel capability data is from Section VII. Design compression ultimate stress is used as a common reference for all modes.

A "geometry fixed/materials variable" check (using baseline geometry, Figure 113) identifies damage tolerance and compression as the most critical modes for the improved baseline (B/L) with $(F/\rho)_{B/L}$ = 410 and 430 respectively relative to (F_{cu}/ρ)B/L = 410. Since all the aluminum materials for this case have the same compression capability, the baseline geometry can be improved only slightly to (to F/ρ = 430 levels) by aluminum material substitution only. The "best" aluminum materials (Al) are determined to be P1 (7050-T73651), E3 (7050-T736511) and F12 (7050-T736) for the skin, stiffener and spar cap respectively. Relative to B/L Al shows a 5% overall improvement to the limiting compression mode capability F/ρ = 430.

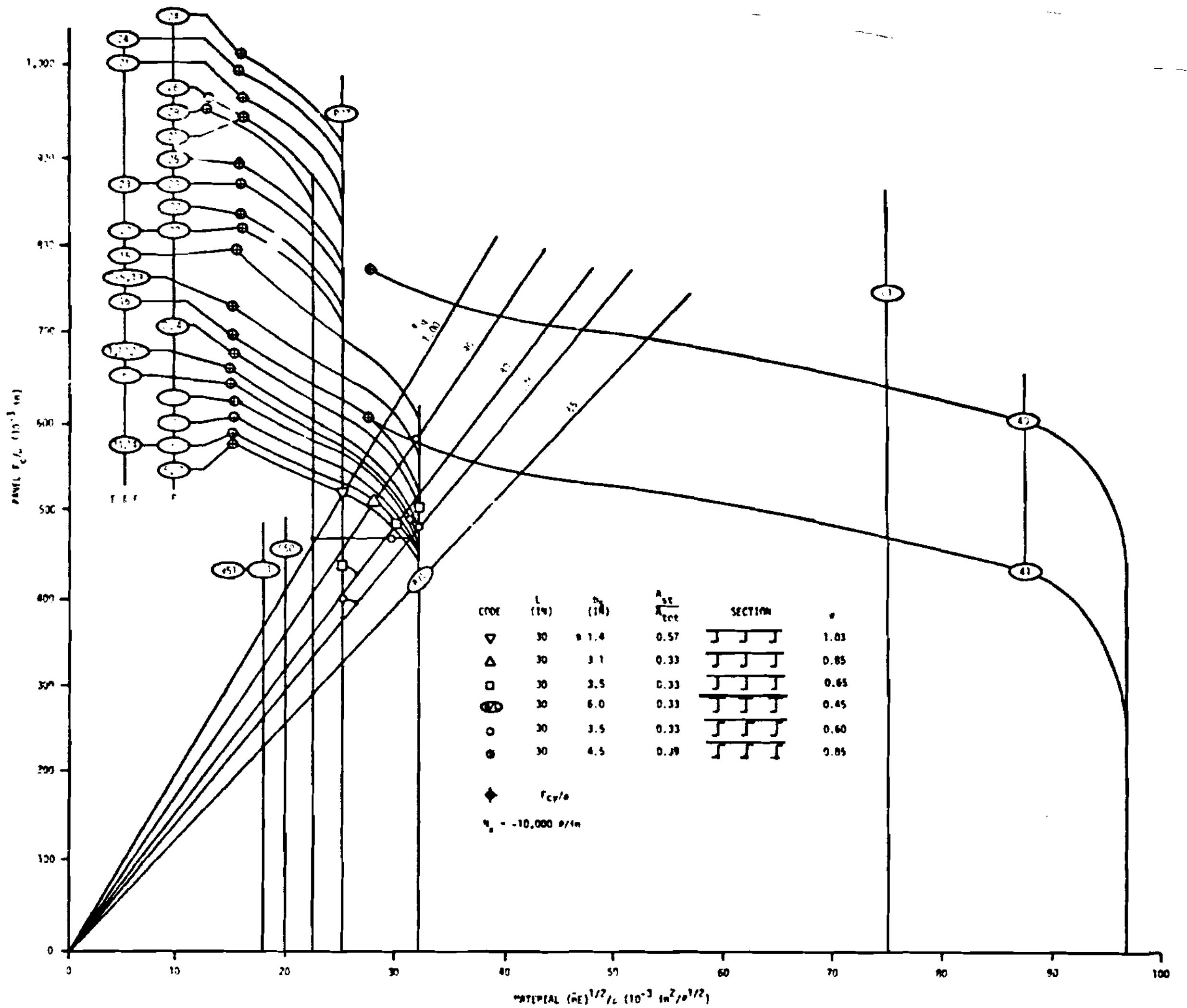

Figure 108 WING UPPER PANEL CONCEPT EFFICIENCEIES FOR ULTIMATE COMPRESSION

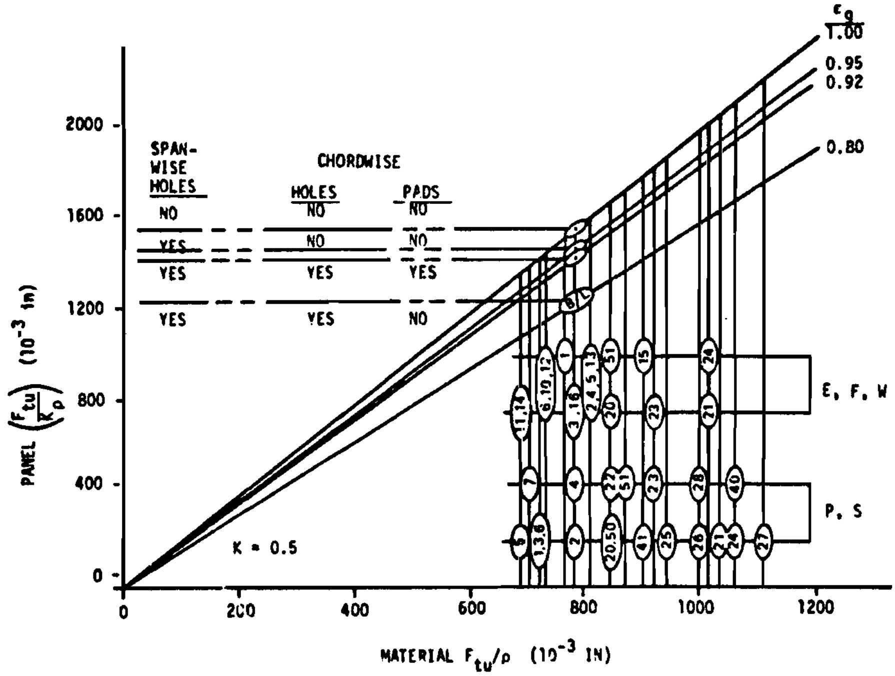

Figure 109 WING UPPER PANEL CONCEPT EFFICIENCIES FOR ULTIMATE TENSION

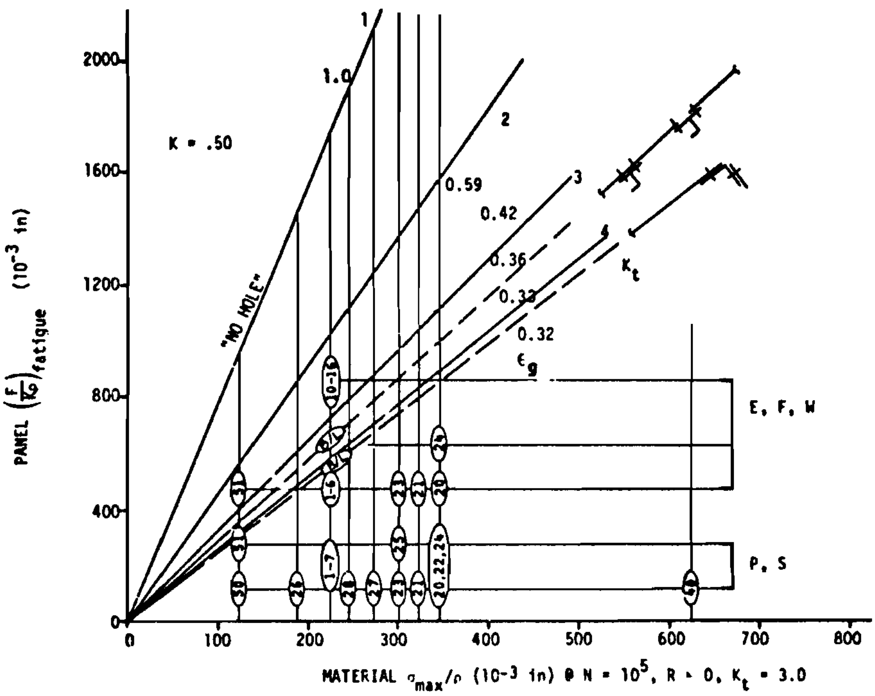

Figure 110 WING UPPER PANEL - CONCEPT EFFICIENCIES FOR FATIGUE

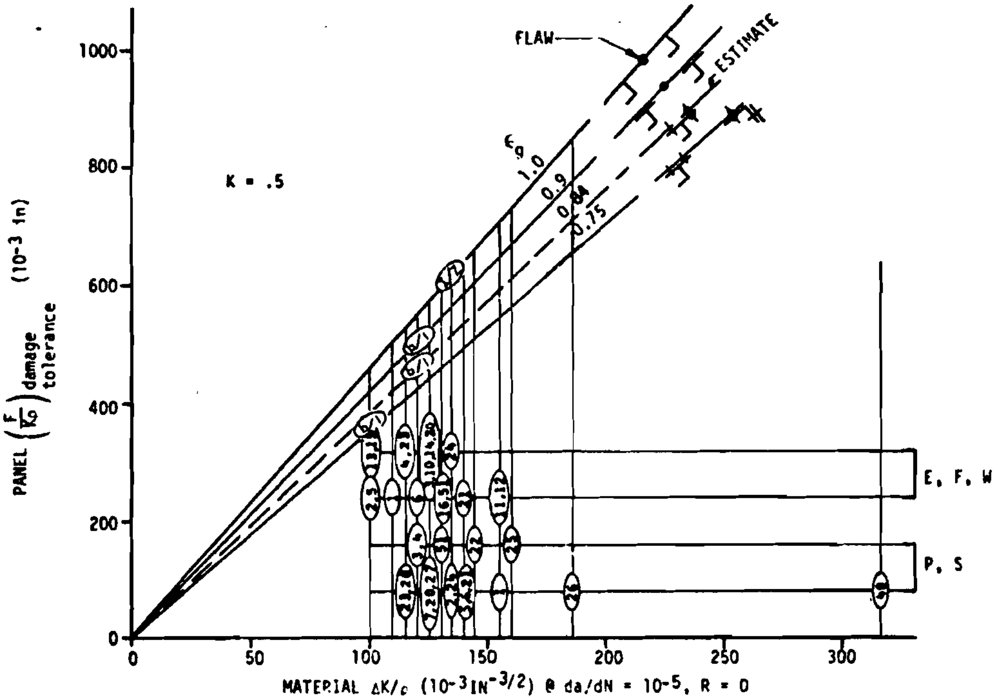

Figure 111 WING UPPER PANEL-CONCEPT EFFICIENCIES FOR DAMAGE TOLERANCE

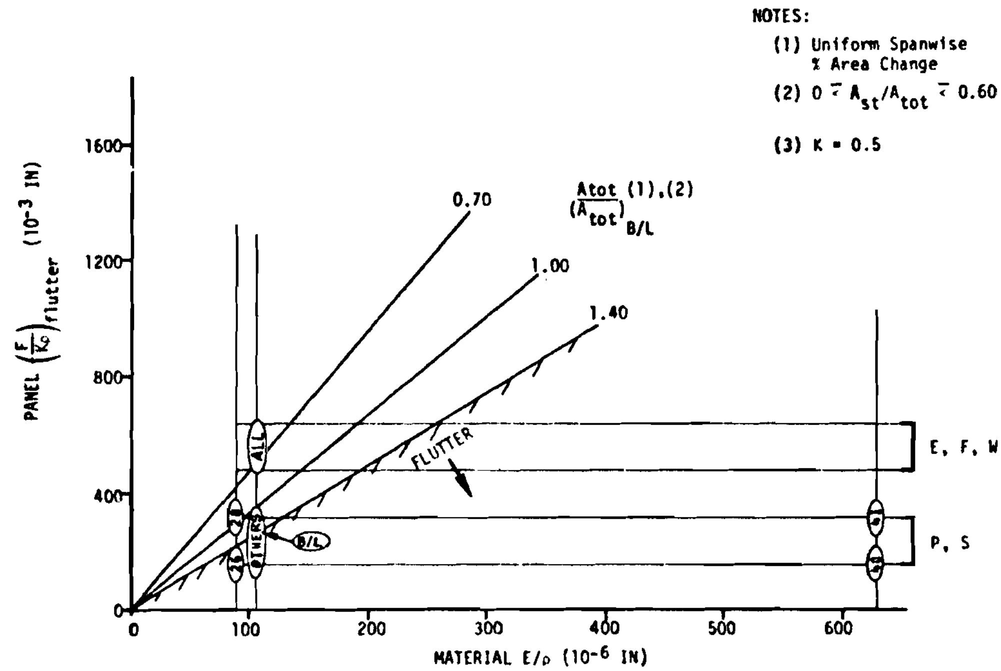

Figure 112 WING UPPER PANEL-CONCEPT EFFICIENCIES FOR FLUTTER

The best titanium materials (Ti) for the skin and for the stringer and spar cap, respectively, are P25 (Ti-6-6-2β Ann) and E21 (Ti-6-4 STA). Relative to the B/L, considerable improvement for damage tolerance and fatigue is achieved, however, considerable degradation in the compression mode is also incurred, resulting in an overall F/ρ degradation of -17%.

Similarly, the best beryllium (Be) and steel (Fe) materials are identified with overall and individual mode improvements (or degradations) relative to the B/L as indicated on Figure 113.

A summary comparison of the above material selections on an $(F/\rho)_{max}$, $(F/\rho C_{\#})_{max}$ and SBR basis is shown in Table XXVI. As with the lower wing panels, Be, Ti and Fe are eliminated from further consideration for the upper panels on the basis of $F/\rho C_{\#}$ and SBR. Therefore, only aluminum materials (Al) are retained for further consideration, although no cost rate and only a slight weight improvement is achieved.

An "Al materials fixed/geometry variable" analysis is performed to identify further improvement potential (Figure 114). As indicated for the baseline geometry (b/l), panel compression capability is constraining weight improvement. Capability improvement for compression to F/ρ = 520 levels is achievable with an integral zee (i/z) concept using a minimum practical stringer spacing b_s of 3.5 inches. Further improvement to F/ρ = 600 levels is also indicated by a composite reinforced zee stiffened (C/Z) concept. The combined effect of improved geometric efficiency (at least partly due to increased stiffening ratio) and improved material efficiency (due to improved material mixture) results in the higher overall capability. It should be recognized, however, that increased stiffening ratio and improved material mixture would likely increase the capabilities of the other concepts as well.

Considering F/ρ = 600 as a goal, examination of the other modes shows only fatigue and damage tolerance as potentially critical modes. The critical skin-to-spar cap splice fatigue capability can be improved to F/ρ > 600 (and equal to skin-to-stiffener joint and spanwise skin-to-skin splice levels) by reducing the spar cap thickness to $t/D \lesssim 2$ so that the required attachment interference $i \gtrsim 0.0025$ can be consistently attained (see Figure 102). Similarly, reduction of spar cap thickness also improves the capability for damage tolerance (shown in Figure 100 for the wing lower cover). Coupled with the "attachment interference benefit" of the proposed tentative March 1974 damage tolerance criteria, F/ρ>600 capability can be projected for all hole flaw cases. Calculations for the surface flaw case also show F/ρ>600 (again, for the March 1974 criteria). Hence, in conjunction with the above fatigue and damage tolerance options, composite reinforced concepts, such as the zee stiffener concept, offer a F/ρ improvement potential of 46% (= $\frac{600-410}{410}$ relative to $(f_{cu}/\rho)_{B/L}$ = 410.

Geometry options which are included in the subsequent concept sizing, weight, and cost analyses are indicated for each mode by the highest valued symbols b/l and i/z, denoting baseline and integral zee geometry, respectively. The

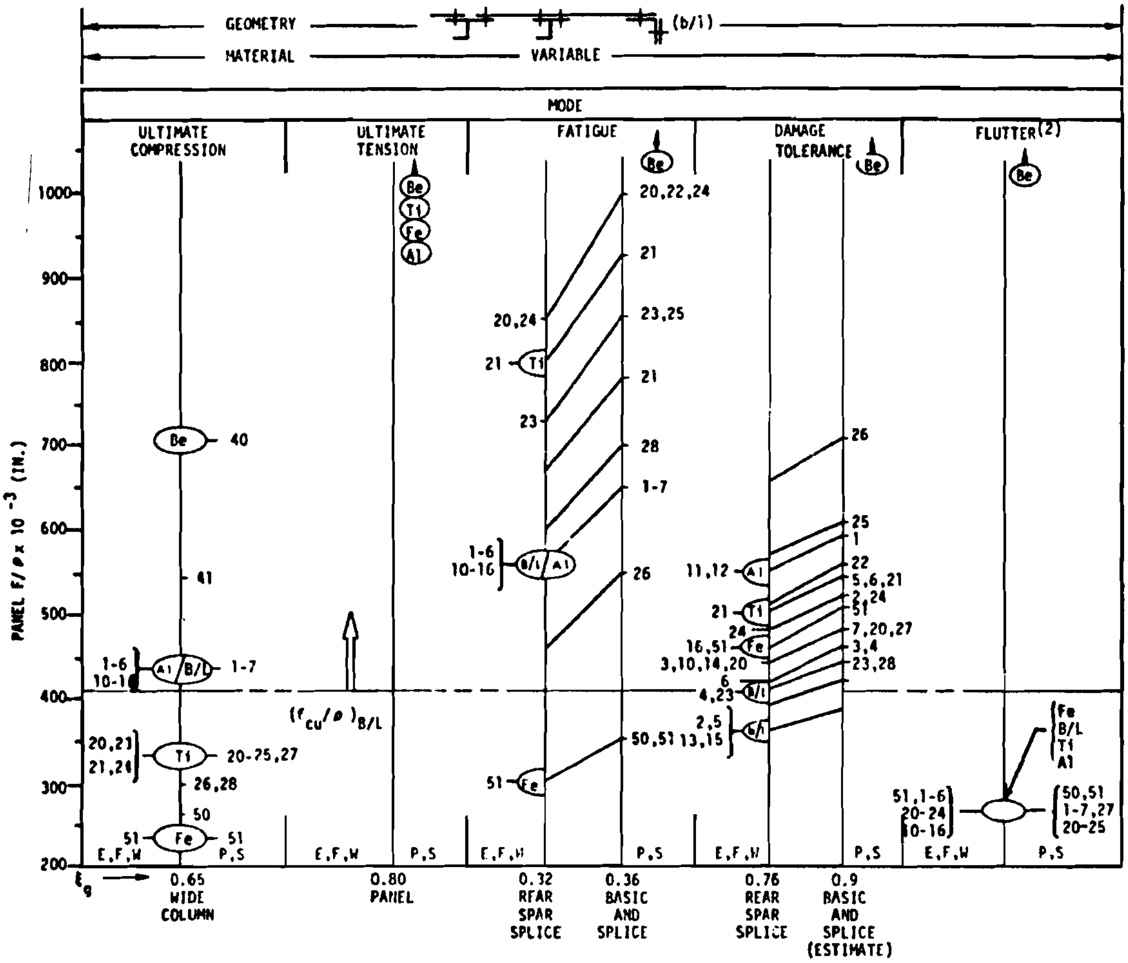

NOTES:

(1)

Code	Skin	Stringers	Spar Caps
b/L (3)	P3 = 7075-T7651	E5 = 7075-T651	F13 = 7075-T6
B/L (4)	P2 = 7050-T76	E4 = 7050-T76	E4 = 7050-T76
Al	P1 = 7050-T73651	E3 = 7050-T736511	F12 = 7050-T736
Ti	P25 = Ti-6-6-2 BETA ANN	E21 = Ti-6-4 STA	E21 = Ti-6-4 STA
Be	P40 = P.S. 20 BERYLLIUM	P40 = P.S. 20 BERYLLIUM	P40 = P.S. 20 BERYLLIUM
Fe	S50 = PH 15-7 (RH 950)	W51 = MARAGE 250	W51 = MARAGE 250

(2) For "No Flutter" $f_{tu}/\rho \leq (F/\rho)_{flutter}$

(3) "Initial Baseline" Materials (Reference Only)

(4) "Improved Baseline" Materials (Study Basis)

Figure 113 WING UPPER COVER NEW CONCEPT MATERIAL SELECTION

TABLE XXVI WEIGHT AND COST COMPARISONS OF WING UPPER PANEL CONCEPTS								
CODE	GEOMETRY	MATERIALS	$\frac{F}{\rho}$ (1) (FIGURE 113)	$\frac{Ws}{(Ws)_{B/L}}$	C# (FIGURE 90)	$\frac{C\#}{(C\#)_{B/L}}$	$\frac{F}{\rho C\#}$	$(SBR)_{req'd}$ (FIGURE 91)
B/L	b/1	ALUMINUM	410DT	1.00	45	1.00	9.11	0
A1	b/1	ALUMINUM	430C	0.95	45	1.00	9.56	0
Ti	b/1	TITANIUM	330C	1.24	110	2.44	3.00	>200
Fe	b/1	STEEL	240C	1.71	45 (3)	1.00	5.35	>200
Be	b/1	BERYLLIUM	710C (2)	0.58	660	14.70	1.08	>200

(1)DT (DAMAGE TOLERANCE; C (COMPRESSION)

(2)ASSUME NO FLUTTER RESTRAINT

(3)ASSUME SAME AS RIVETED ALUMINUM STRUCTURE

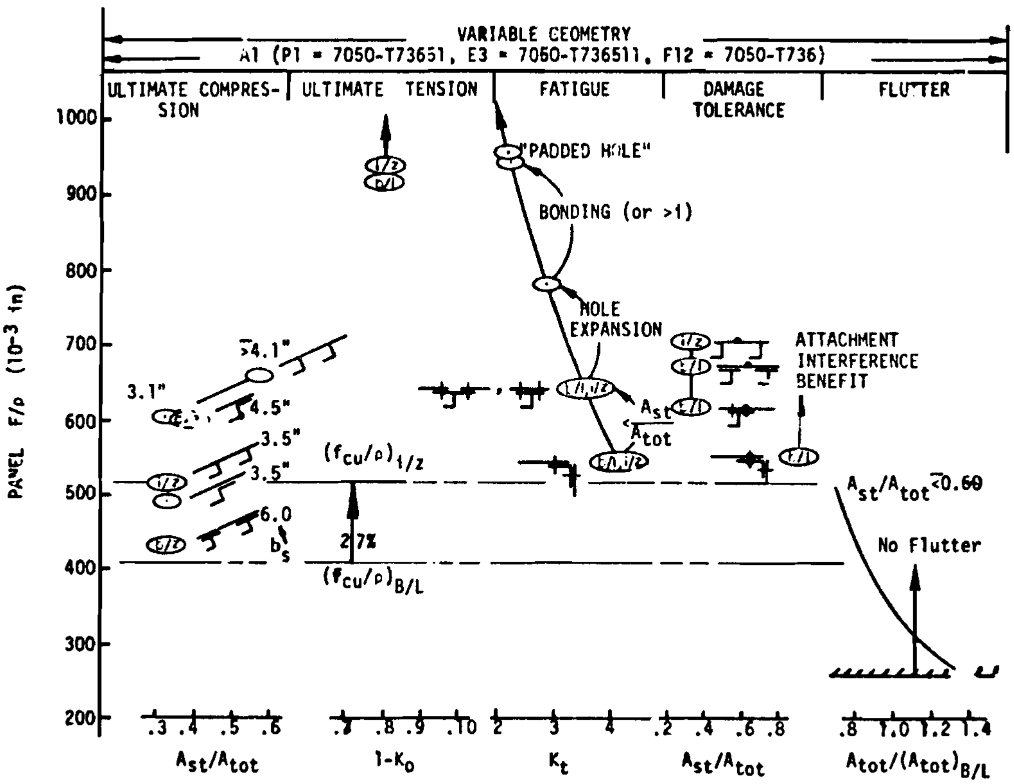

Figure 114 WING UPPER PANEL - NEW CONCEPT GEOMETRY SELECTION

integral zee concept was selected for further consideration, because of the cost reduction potential through reduced parts count and F/ρ improvement potential of 27% relative to $(f_{cu}/\rho)_{B/L}$. Since "Al" materials were identified using b/l geometry (Figure 113), an "i/z geometry fixed/materials variable" check is normally required to establish or verify the best material selection under the new geometry conditions. However, examination of Figure 114 identifies the critical modes, in order, as compression and fatigue, for which aluminum materials capabilities are equal for each mode (Figure 113). Hence, differences in material selection can have no influence on overall improvement potential and can only be the result of secondary mode considerations. Al materials are P1(7050-T73651) for the cover panels and F12(7050-T736) for the spar caps. The materials actually used for the I/Z concept are P2(7050-T7651) for the cover panels and F12(7050-T736) for the spar caps.

6.2.3 Fuselage Shell Panels

An evaluation of selected panel material and geometry options was performed at the fuselage top centerline (℄) area forward of the front spar (Station 703). The failure modes considered were ultimate tension and compression, fatigue and damage tolerance for longitudinal and transverse (hoop) loading modes. The basic data for this evaluation is summarized in Figures 115 to 121. Aluminum, titanium, beryllium and steel materials of sheet(S), plate (P) and extrusion (E) form are represented. The materials, material code and material properties are summarized in Table XXVII. The panel geometry options considered were limited to honeycomb, isogrid and baseline. Baseline geometry and materials are included as a reference and point of departure for improvement. Baseline and honeycomb panel capability data $F/K\rho$ are from Section VII and isogrid data from Volume II of this report, Section IV. All the panel capability data are related to a common reference stress, longitudinal tension f_{tu}, through factors, K, defined by compression and hoop loading ratios,

$$N_{xc}/N_{xt} \text{ and } N_{yt}/N_{xt}$$

respectively, where N_{xt} is the longitudinal tension loading.

The reference stress is further adjusted to reflect total panel weight ($\bar{t}$) by including the incremental $\bar{t}$'s associated with buckled skin, adhesive, core, nodes, etc., as appropriate to each panel concept. However, an allowance for panel edge weight is not included for honeycomb and isogrid. Also, in the case of honeycomb and isogrid, due to the circular section in this area, full frames are not required or included as for baseline.

A "baseline geometry fixed/material variable" analysis (Figure 122) identifies fatigue for longitudinal loading as the most critical mode for the baseline concept (B/L) at $(F/\rho)_{B/L} \approx 330$ relative to $(f_{tu}/\rho)_{B/L} \approx 215$. The B/L skin material S1(2024-T3) is also the best aluminum material. Reduction of the B/L 0.063" skin gage to 0.050" (minimum gage for countersink requirements) increases f_{tu}/ρ to approximately 245. Use of a minimum gage (0.050") titanium skin material such as S25 improves the capability F/ρ as shown but reduces

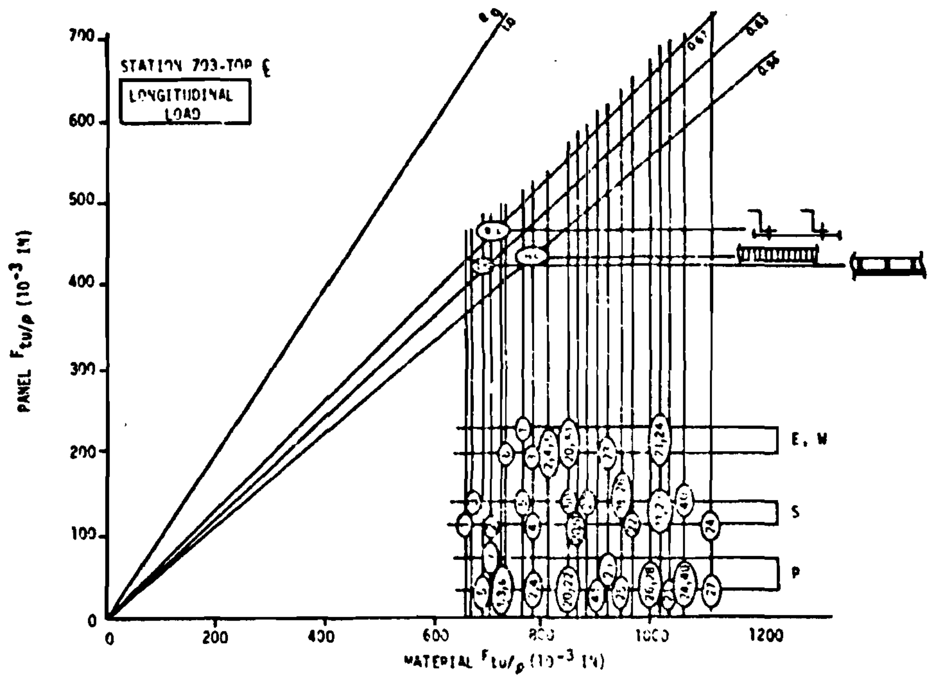

Figure 115 FUSELAGE CONCEPT EFFICIENCIES FOR ULTIMATE TENSION (LONGITUDINAL)

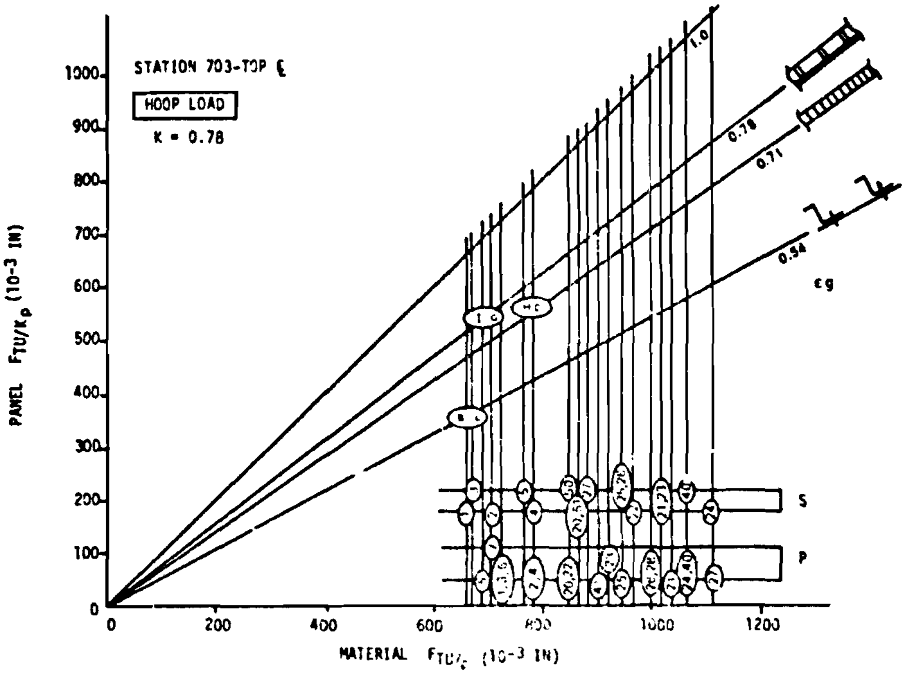

Figure 116 FUSELAGE CONCEPT EFFICIENCIES FOR ULTIMATE TENSION (HOOP)

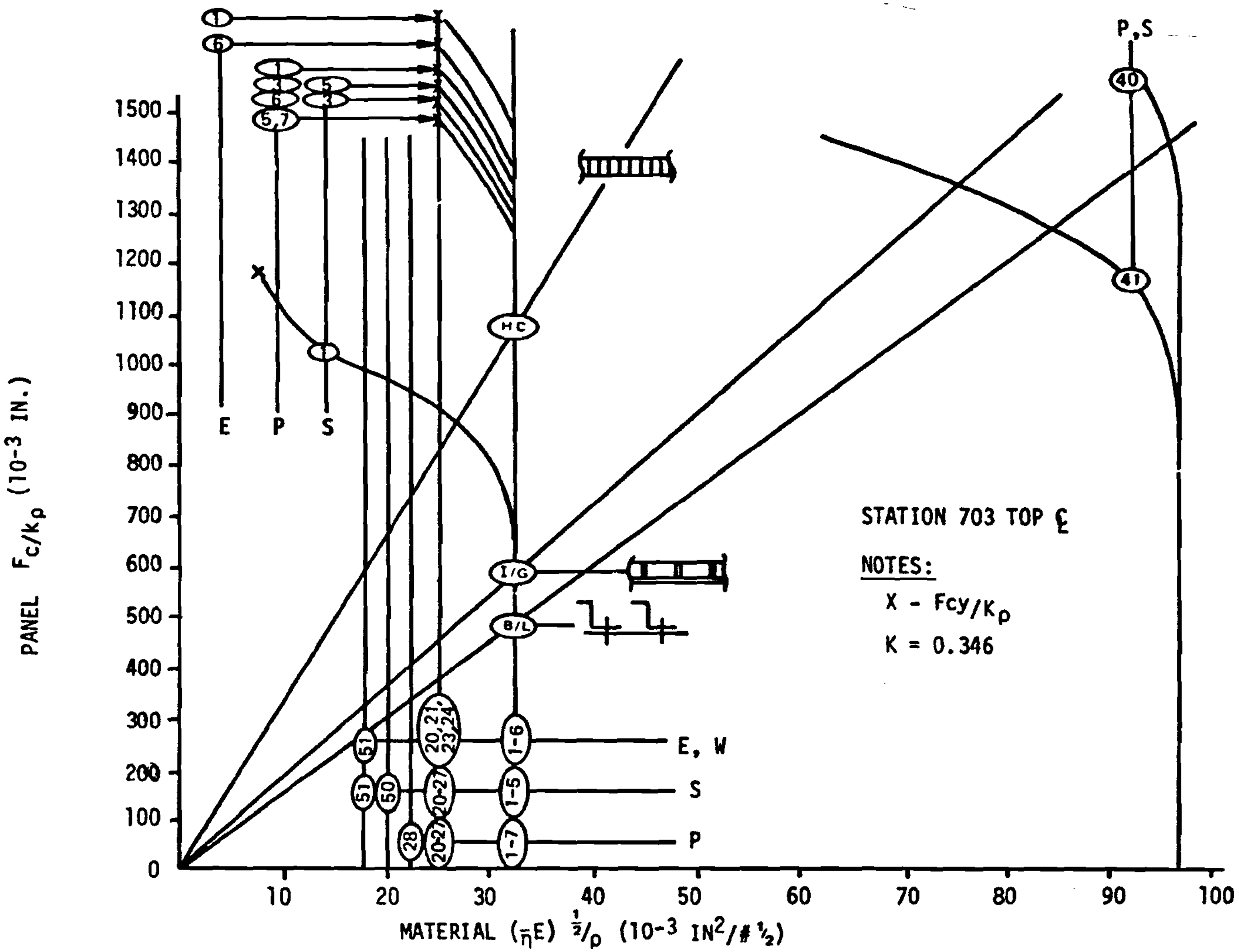

Figure 117 FUSELAGE CONCEPT EFFICIENCIES FOR ULTIMATE COMPRESSION

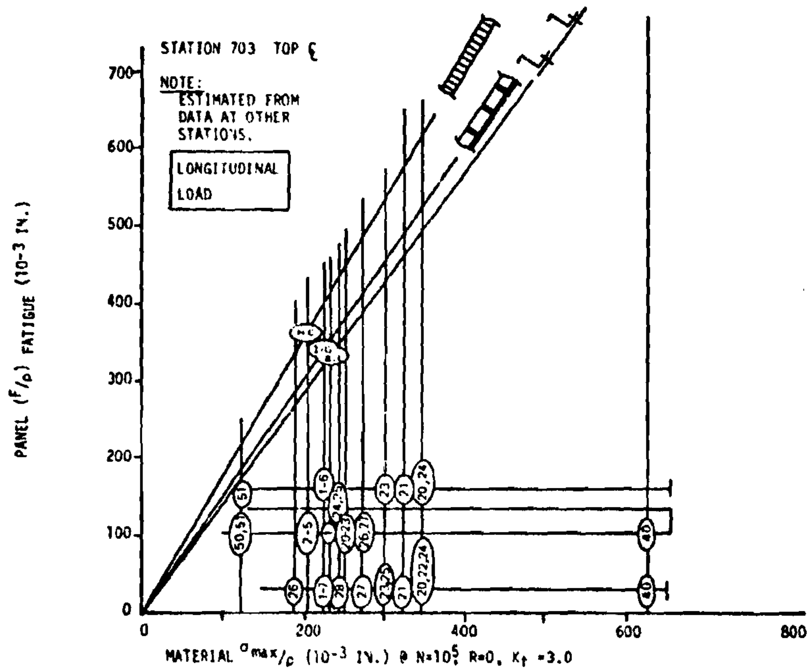

Figure 118 FUSELAGE CONCEPT EFFICIENCIES FOR FATIGUE (LONGITUDINAL)

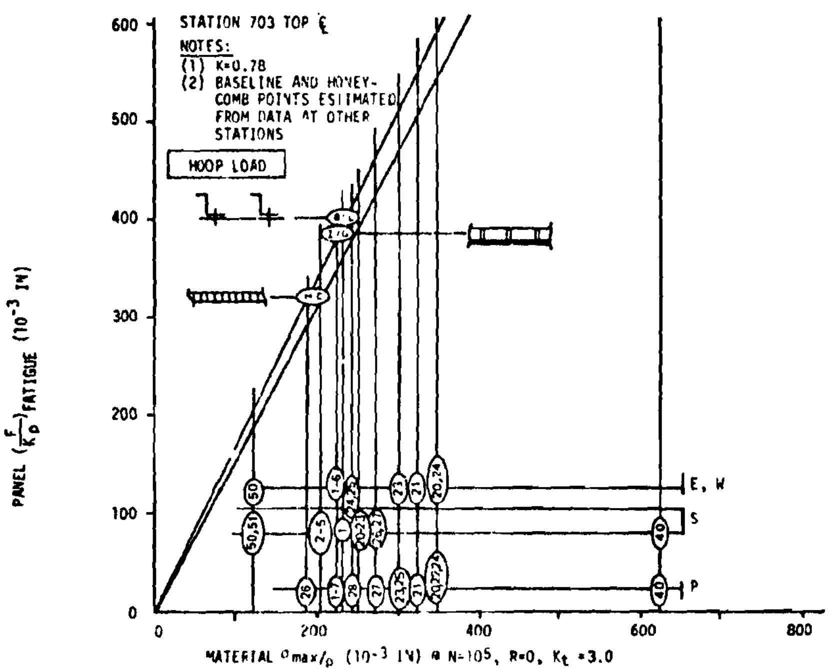

Figure 119 FUSELAGE CONCEPT EFFICIENCIES FOR FATIGUE (HOOP)

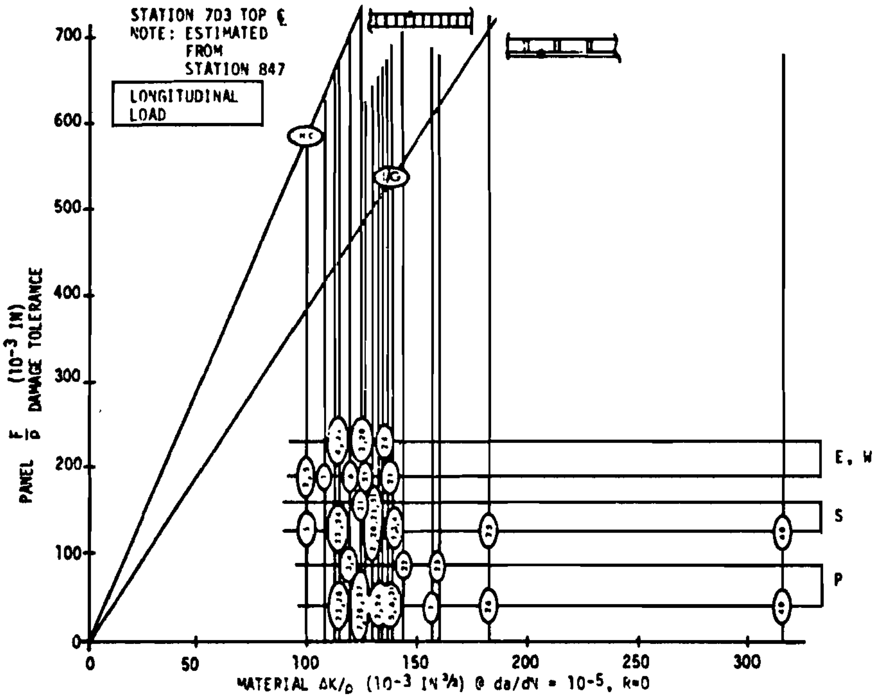

Figure 120 FUSELAGE CONCEPT EFFICIENCIES FOR DAMAGE TOLERANCE

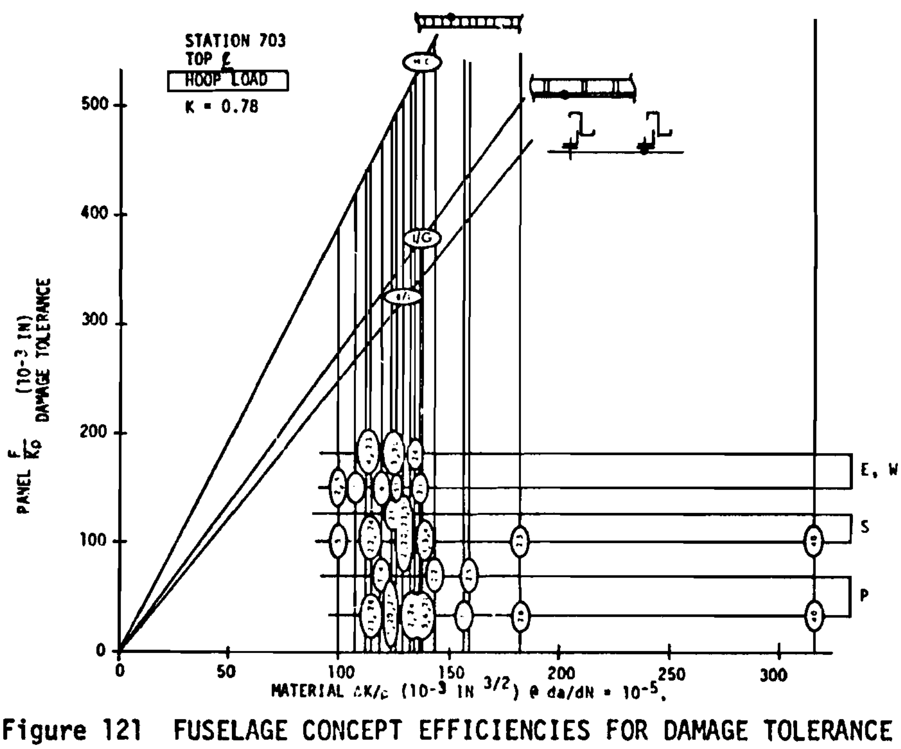

Figure 121 FUSELAGE CONCEPT EFFICIENCIES FOR DAMAGE TOLERANCE

					(3) ULTIMATE TENSION	(3) ULTIMATE COMPRESSION	(7)	(4);(5) FATIGUE	(4);(6) DAMAGE TOLERANCE	(4) FLUTTER
CODE	FORM	MATERIAL	t	ρ	F_{tu}/ρ	F_{cy}/ρ	$\frac{(\bar{\eta} E)^{1/2}}{\rho}$	$\frac{\sigma_{max}}{\rho}$	$\frac{\Delta K}{\rho}$	$\frac{E}{\rho}$
			IN	$\#/IN^3$	10^{-3} IN	10^{-3} IN	$10^{-3}\left(\frac{IN^2}{\# ^{1/2}}\right)$	10^{-3} IN	10^{-3} IN$^{1/2}$	10^{-6} IN
S1	Aluminum Sheet (Clad)	2024-T3	< .25	.100	660	410	32.7	230	140	109
S2		7475-T61	< .06	.101	703	614	32.1	208	129	105
S3		7475-T761	< .06	.101	673	564	32.1	208	139	105
S4		7050-T76	< .06	.102	774	716	31.5	206	137	104
S6		7075-T6	< .19	.101	762	673	32.1	208	99	105
P1	Aluminum Plate	7050-T73651	>.25	.102	716	627	31.9	225	157	104
P2		7050-T7651		.102	775	686	31.9	225	137	104
P3		7075-T7651		.101	723	614	32.3	228	119	105
P4		7475-T651		.101	782	683	32.3	228	119	105
P5		7475-T7351		.101	693	574	32.3	228	139	105
P6		7475-T7651		.101	713	594	32.3	228	139	105
P7		7075-T7351	>.25	.101	703	574	32.3	228	124	105
E1	Aluminum Extrusion	7049-T73511	<.25	.102	765	667	31.9	225	108	104
E2		7049-T76511		.102	804	725	31.9	225	98	104
E3		7050-T736511		.102	775	716	31.9	225	127	104
E4		7050-T76511		.102	804	735	31.9	225	113	104
E5		7075-T6		.101	812	733	32.4	228	99	106
E6		7075-T76	<.25	.101	733	644	32.4	228	119	106
S20	Titanium Sheet	Ti-6-4 ANN	<.19	.160	869	663	25.4	338	131	103
S21		Ti-6-4 STA		.160	1031	994	25.4	325	125	103
S22		Ti-6-6-2 ANN		.164	976	939	25.7	305	116*	107
S23		Ti-6-6-2 STA		.164	1067	1006	25.7	354	134*	107
S24		Ti-38-6-44 STA	<.19	.174	1128	1091	22.1	247	116*	85
S25		Ti-8-8-2-3 STA	<.06	.175	943	1046	22.2	171	183*	86
S26		Ti-8-1-1 MILL ANN	<.19	.158	949	917	26.5	278	-	112
S27		Ti-8-1-1 DUPL ANN	<.19	.158	868	835	26.5	278	-	112
P20	Titanium Plate	Ti-6-4 ANN	>.25	.160	844	819	25.4	338	125	103
P21		Ti-6-4 STA		.160	1031	956	25.4	325	138	103
P22		Ti-6-4 β ANN		.160	844	831	25.4	338	144	103
P23		Ti-6-6-2 ANN		.164	915	866	25.7	305	115	107
P24		Ti-6-6-2 STA		.164	1067	1024	25.7	353	134	107
P25		Ti-6-6-2 β ANN		.164	945	896	25.7	305	159	107
P26		Ti-8-8-2-3 STA		.175	1000	977	22.2	188	183	86
P27		Ti-6-2-2-2-2STA		.162	1111	1123	26.1	278	123	110
P28		Ti-38-6-44 STA	>.25	.174	1006	960	22.1	247	116	85
E20	Titanium Extrusion	Ti-6-4 ANN	<.25	.160	856	825	25.4	338	125	103
E21		Ti-6-4 STA		.160	1019	981	25.4	325	138	103
E23		Ti-6-6-2 ANN		.164	921	872	25.6	305	116	107
E24		Ti-6-6-2 STA	<.25	.164	1018	1006	25.6	353	134	107
S40 P40	Beryllium Sheet	P S 20	>.05	.067	1145	776	97.0	627	317	627
P41		Hip Pressed Blk	>.25	.067	896	597	97.0	-	-	627
S50	Steel Sheet	PH15-7(RH950)	<.25	.277	648	758	19.8	130	-	108
S51		Marage 250	<.25	.300	867	833	17.8	120E	127E	95
W51	Wrought	Marage 250	-	.300	850	817	17.8	120	127	95
C1	0.*	Boron Epoxy	-	.072	2660	4900	76.0	1810	-	415

Table title: TABLE XXVII FUSELAGE PANEL MATERIAL CAPABILITIES (1), (2)

(1) "L" Direction (2) Summarized From Tables in Appendix B (3) "B" Value (4) Typical Values

(5) $K_t=3$, $R=0$, $N=10^5$. (6) $R=0$, $da/dn=10^{-5}$ (7) $\bar{\eta}=(E_t/E)^{.75}=1$ (Elastic Range)

*Use plate values since sheet data is not available

f_{tu}/ρ to approximately 140 (= 245 x 0.1/0.175). This is a heavier structure due to the higher density and 0.050 minimum gage. Therefore, titaniums (and steels) are eliminated. Beryllium S40 results in a lighter structure due to the lower density; however, as for the wing (Section 6.2.1), it is eliminated on an initial and life cycle cost basis. Hence, the baseline geometry concept cannot be improved by a material substitution.

Examination of Figure 122 reveals that, with the exception of fatigue, the hoop loading mode is generally more critical than the longitudinal loading mode. This trend is further accentuated in the forward fuselage areas as longitudinal loadings decrease. This reflects the increasing importance of hoop loading relative to longitudinal loading as the fuselage diameter increases and suggests that the amount of longitudinally oriented material can be reduced, provided longitudinal fatigue efficiency on the top (and compression efficiency on the bottom) are improved. Further weight reduction requires a reduction in overall $\bar{t}$, including $t_{skin} < 0.050$ followed by improvement of the fatigue and then the damage tolerance capability for hoop loading.

A honeycomb concept was, therefore, selected for further study consideration. This concept, by eliminating attachment holes in the basic panel through bonding and by incorporating a core supported double skin approach, offered a potential for fatigue, compression and damage tolerance improvement. Elimination of the countersink requirement offers a skin gage reduction potential below0.050 minimum. The hoop-to-longitudinal area ratio is also increased.

A "honeycomb geometry fixed/materials variable" analysis (Figure 123) reveals fatigue for the hoop loading mode as most critical at $(F/\rho)_{H/C} \approx 320$ relative to $(f_{tu}/\rho)_{H/C} \approx 275$ which is established by the minimum skin gage (2t = 0.040). The honeycomb, H/C, skin material is S4(7050-T76). Substitution of S1(2024-T3), for example, would achieve a further capability improvement which only translates into a higher margin-of-safety (and higher reliability) since f_{tu}/ρ cannot increase due to the minimum gage constraint. A significant $(f_{tu}/\rho)_{H/C}$ increase of 28% over $(f_{tu}/\rho)_{B/L}$ is indicated. However, as previously noted, honeycomb panel edge weights are not reflected in these comparative results. Inclusion of edge weights as determined for the final design reduced the H/C weight improvement potential to approximately 0% in this area. A more efficient edge member concept is desirable for honeycomb, although it should be recognized that for a lower weight basic concept, edge weight constitutes a larger percentage of the total.

An isogrid concept was also selected for study. This concept eliminates attachment holes in the basic panel through integrally attached and relatively closely spaced stiffeners, and, based on preliminary fatigue data, effectively negates the node holes, thereby offering a potential for fatigue and damage tolerance improvement. The triangular stiffener grid and skin act as an isotropic panel for in-plane loads, similar to honeycomb. Orienting the same amount of material in the hoop direction as in the longitudinal direction offers a potential for improving the hoop loading modes.

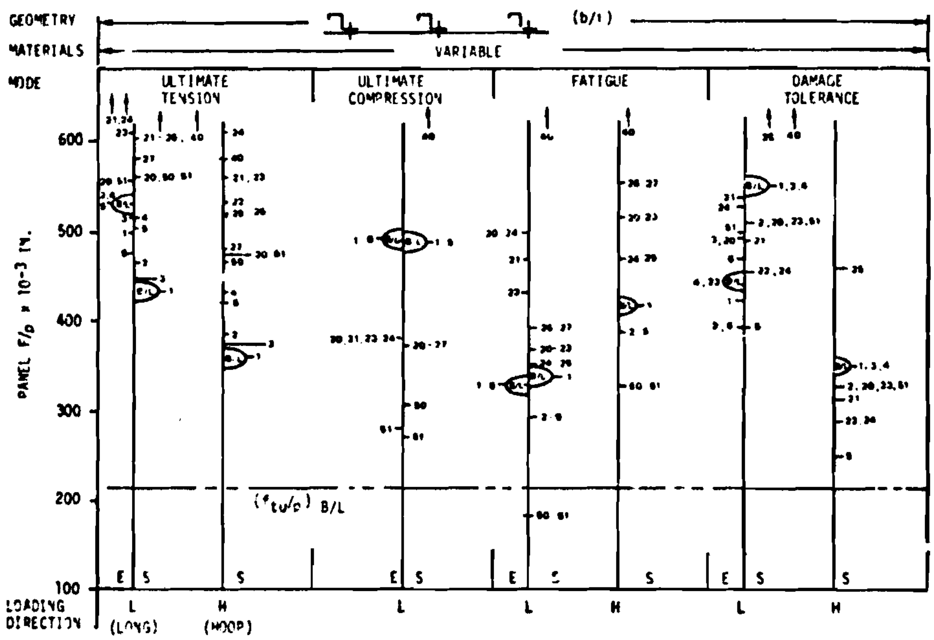

(1) CODE: B/L = S1 (2024 - T3) and E4 - (7050 - T76)

Figure 122 FUSELAGE MATERIAL SELECTION(1) (BASELINE GEOMETRY)

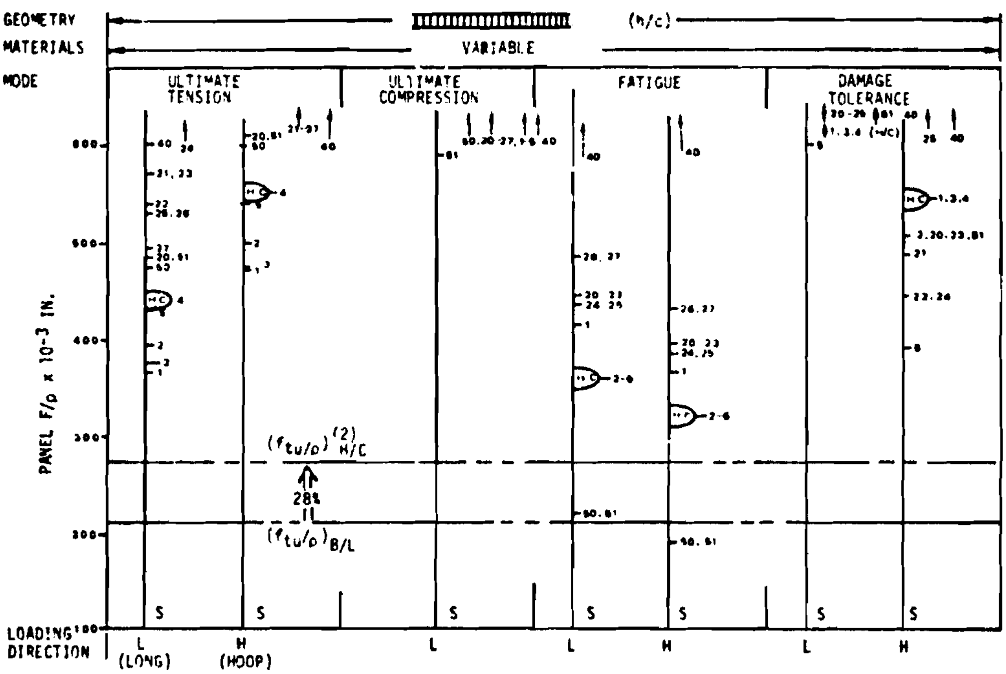

(1) CODE: H/C = S4 (7050-T76) (2) ESTABLISHED BY MINIMUM GAGE 2t = .040"

Figure 123 FUSELAGE MATERIAL SELECTION (1) (HONEYCOMB GEOMETRY)

An "isogrid geometry fixed/materials variable" analysis (Figure 124) shows fatigue for longitudinal loading to be critical, with a relatively high M.S. of 0.84 (= $\frac{340}{185}$ - 1). The relatively low value of $(f_{tu}/\rho)_{I/G}$ contributes to the high M.S. This low value at the top centerline is caused by the section requirement for general instability at the bottom centerline. Under the current analysis procedures, design for general instability requires axisymmetric material distribution around the section. Hence, at the top centerline, $(f_{tu}/\rho)_{I/G}$ is 14% less than $(f_{tu}/\rho)_{B/L}$, indicating a corresponding weight increase in this local area. Considering edge weights, the -14% increases to -20%. The I/G section at Station 703 is within 20% of being minimum gage, hence in the more lightly longitudinally loaded forward fuselage, the section minimum gage constraint in conjunction with edge weight may also be penalizing. Further, in the out-of-round forward fuselage, the isogrid concept requires frames for the pressure loads (as does honeycomb), thereby introducing an additional weight penalty. In the more heavily longitudinally loaded areas and along the bottom centerline in particular, the efficiency of the isogrid will increase.

Application of the chart procedure to other representative peripheral and station locations is desirable to identify efficient material and geometry options (or improvement potentials) from which an optimum integrated design (or overall improvement potential) can be defined.

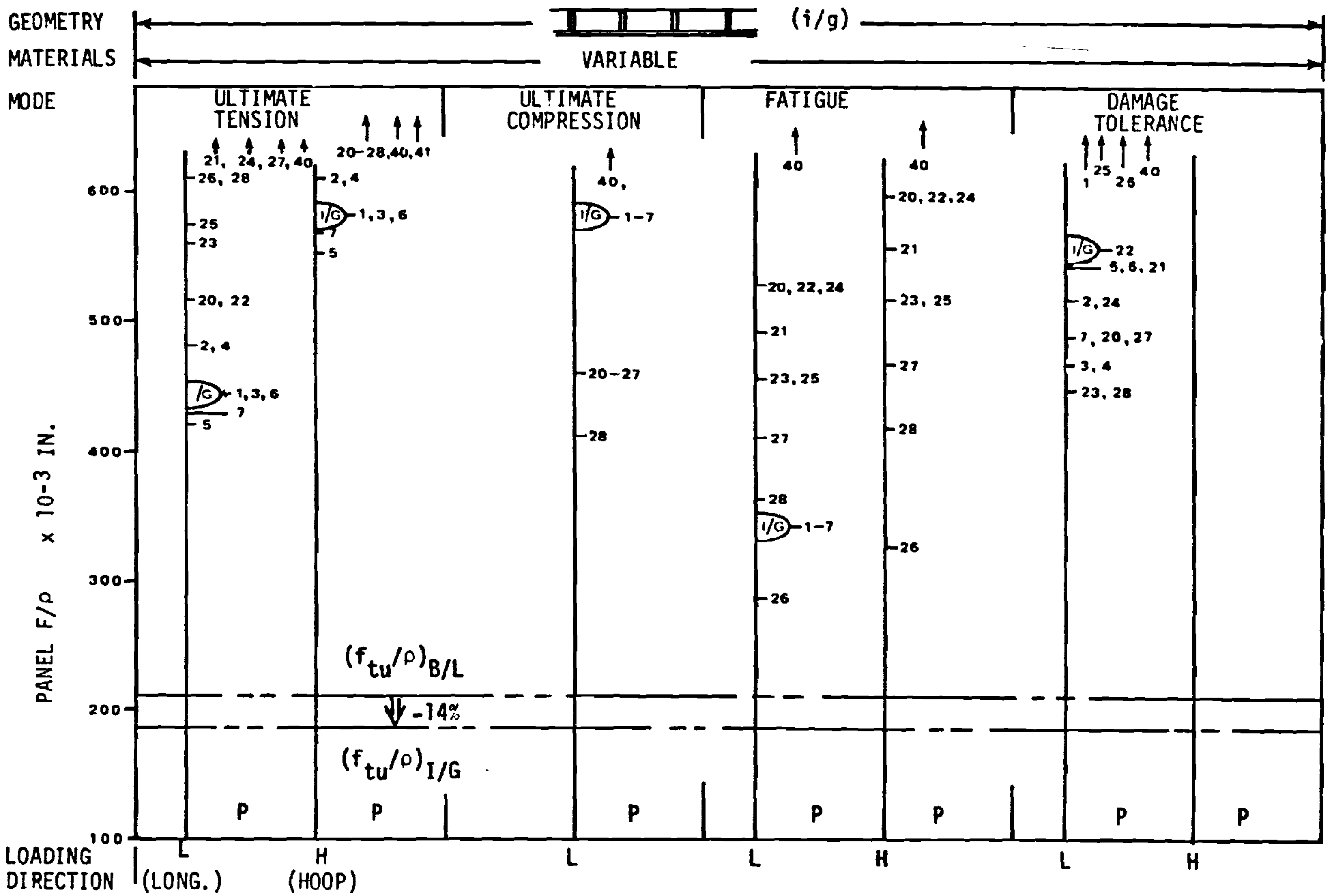

(1) CODE: I/G = P6 (7475-T7651)

Figure 124 FUSELAGE MATERIAL SELECTION (1) (ISOGRID GEOMETRY)

SECTION VII

STRUCTURAL ANALYSES

Structural analyses were performed in support of new concepts formulation and to size and verify the resulting design concepts. The analyses are in accordance with the classical margin-of-safety relationship, Equation 1. Structural integrity requirements are satisfied, and undesirable forms of structural behavior precluded, when the structural capability equals or exceeds the requirement. Minimum weight results when the capability equals the critical mode requirement. This is an objective of the sizing analyses. For the STOL aircraft of the study, the primary structural integrity modes considered are those for ultimate strength, fatigue life, damage tolerance, and flutter. The structures considered satisfy the requirements for each of these integrity modes. Support of the concept formulation and selection process required analyses of the baseline concept structural elements to identify the critical modes and parameters. Baseline data are included.

The structural elements of each concept were sized to the STOL requirements for the critical capability mode. The general sizing approach first identified the constraining local capability stresses for the ultimate strength, fatigue and damage tolerance modes, then checked the overall structure to the flutter mode requirements. The weight of the structure was then determined. In order to provide a valid basis for comparison of weights, the above approach was also applied to the baseline concept. The analysis methods generally used were simple and direct, consisting of classical principles and proven computer programs. The guidelines presented in Table XXVIII were used when analysis simplication was required. A description of the specific approach, methods, basic data used, and the results achieved are presented for each integrity mode.

7.1 FATIGUE ANALYSES

Fatigue analyses were performed on selected critical areas of the baseline and new concept components. In addition, the fuselage was checked for acoustic fatigue. The structures meet the design life (=4 x service life) specified in Section 2.2.2.

The analyses were primarily performed manually using two level truncated spectra, which were derived from and representative of the full load spectra of over 2000 stress levels, Section 2.3.2. Miner's Cumulative Damage Rule was used to determine the damage for a 60,000 hour design life caused by the cyclical loading. The total damage $\Sigma\frac{n}{N}$ was then used to calculate the service life, where $\Sigma\frac{n}{N} = 1$ at failure.

$$\text{Service life} = \frac{60{,}000 \text{ hours}}{4} \times \frac{1}{\Sigma\frac{n}{N}} \qquad (30)$$

The analysis S/N data shown in Figures 125 through 128 are based on tests of built-up aluminum structure and are considered applicable to all aluminum alloys. The S/N data represent the estimated "minimum fatigue quality" of the baseline and new concept designs, as appropriate.

TABLE XXVIII GENERAL GUIDELINES FOR ANALYSIS SIMPLIFICATION
Analysis emphasis to be on major weight, typical basic structure items.
Analysis simplification to provide accuracy within ± 5% in general on weight (or stress) with respect to the unsimplified approach.
Simplified analysis model(s) to retain the fundamental approach by retaining the important elements.
The important elements to be identified on the basis of preliminary (or existing) analysis data/experience using the "unsimplified" approach

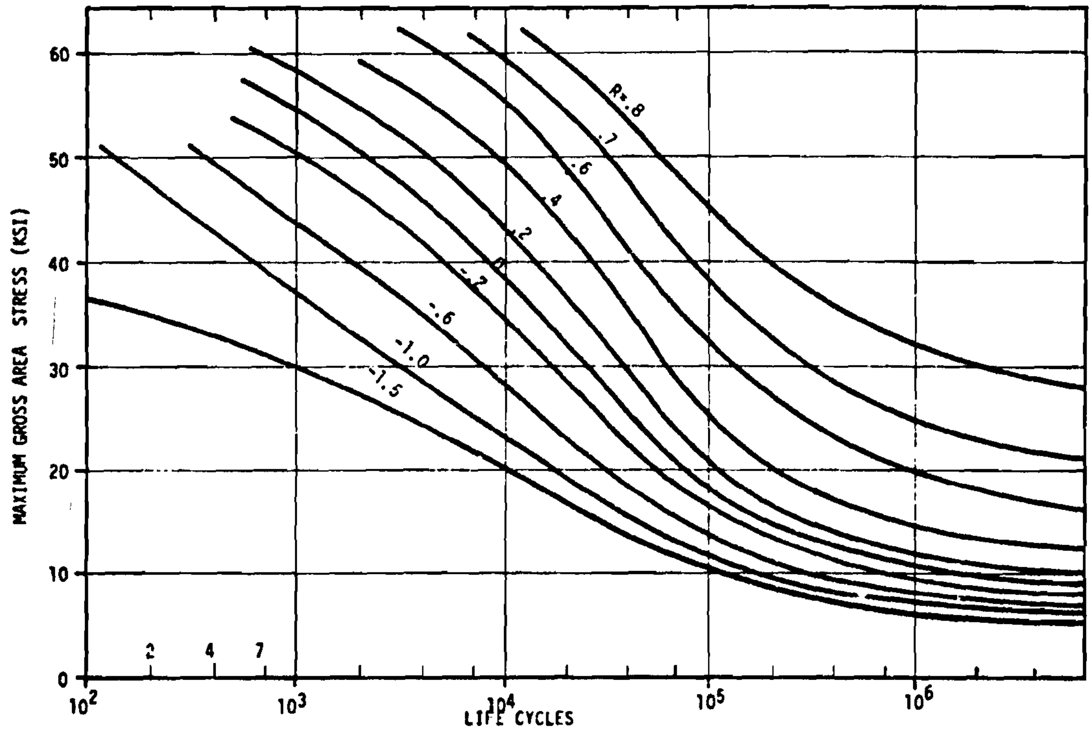

Figure 125 WING SPAR AND SKIN BASIC STRUCTURE S/N DATA FOR ALUMINUM

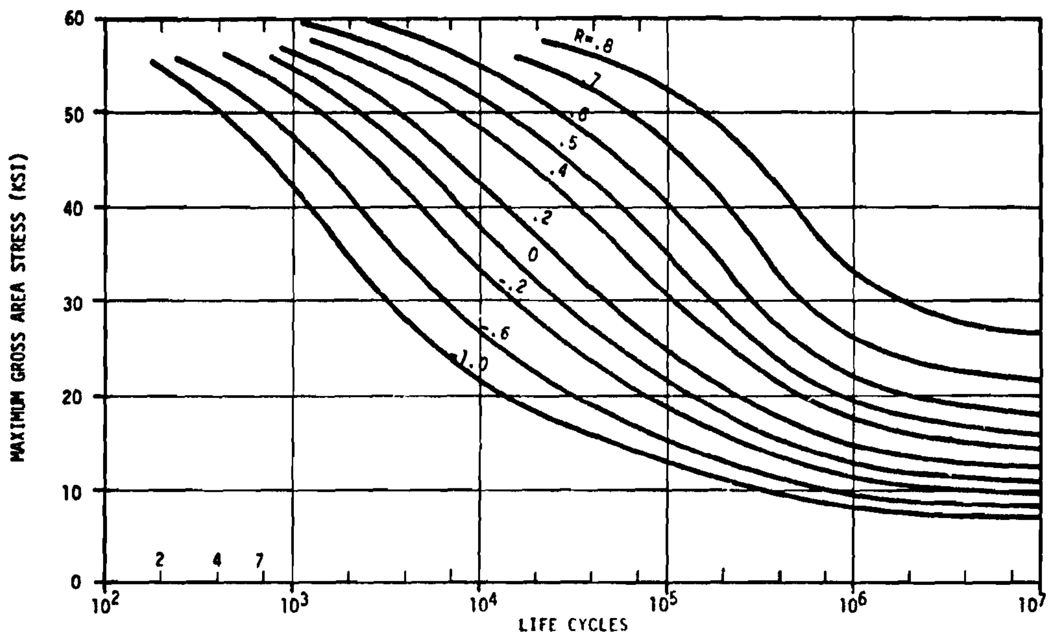

Figure 126 WING SKIN AND STIFFENER BASIC STRUCTURE S/N DATA FOR ALUMINUM

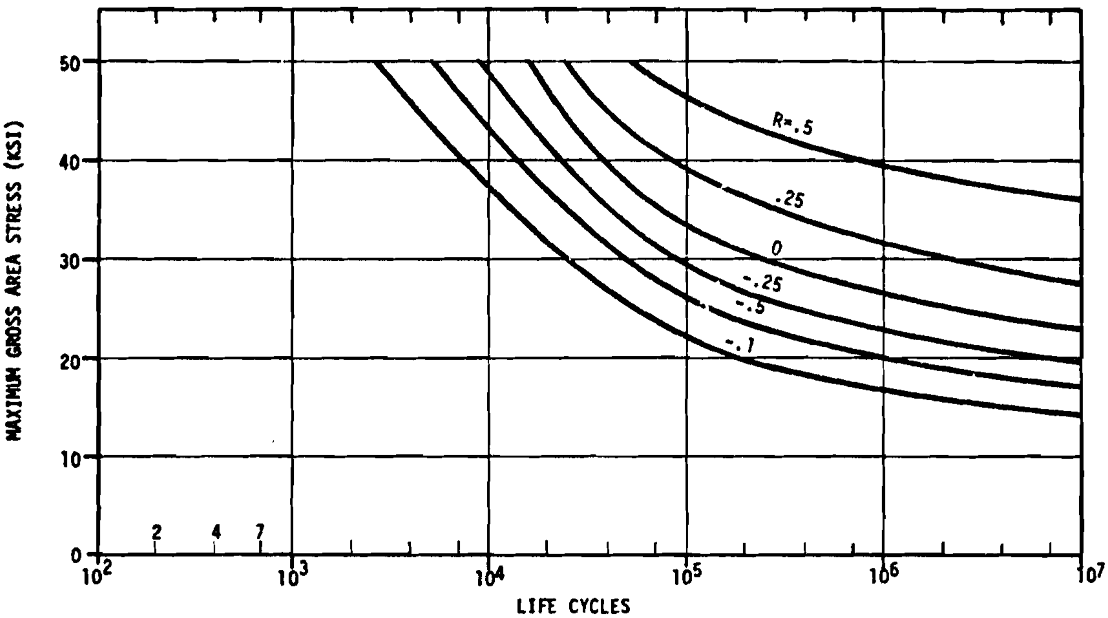

Figure 127 FUSELAGE SHELL STRUCTURE S/N DATA FOR ALUMINUM (NO HOLES, NOTCHES, ETC.)

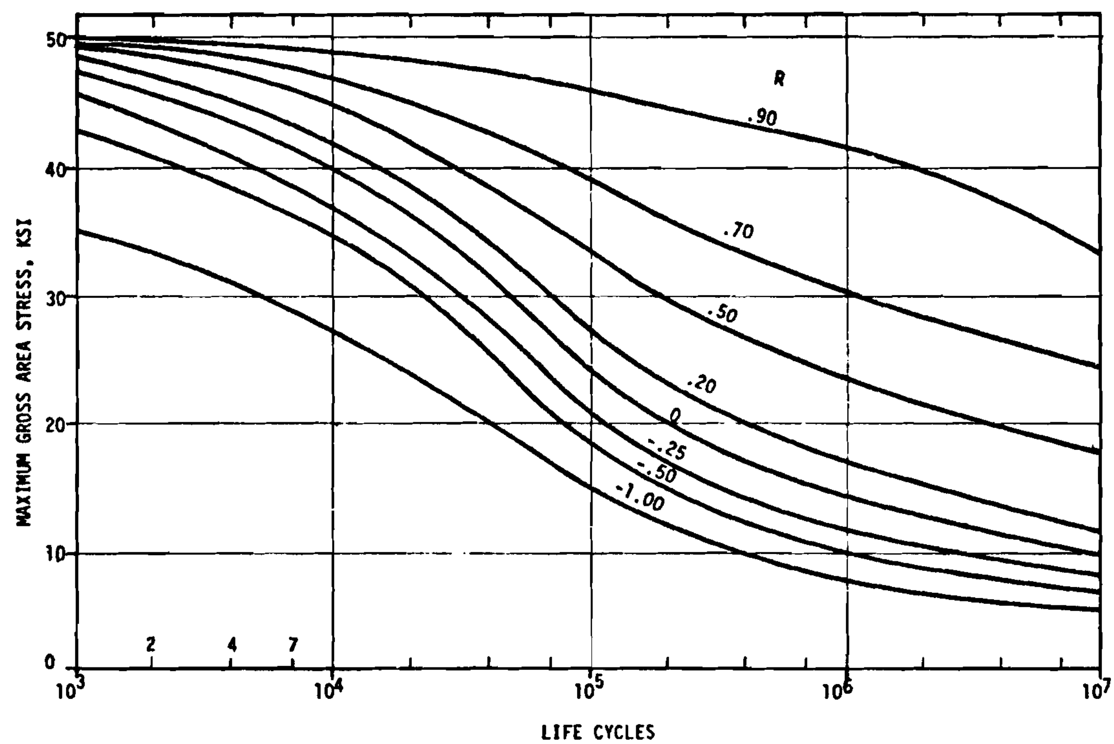

Figure 128 FUSELAGE BASIC STRUCTURE S/N DATA FOR 2024-T3 ALUMINUM

7.1.1 Wing Box Structure

Fatigue analyses were performed at wing stations 117.9 and 339.1. These stations were initially selected by the YC-15 project group as being representative of the basic structure and for which one-g bending moments, stresses and full spectra damage analysis for each mission segment were available. These data were used as a basis to derive representative two level spectra for the study analyses and to extend these spectra to the study check stations.

Due to the presence of significant flaps-down induced chordwise stress in conjunction with the primary spanwise stresses, a consideration of principal stress effects was required. Since the principal stress direction is constantly changing, this consideration was resolved in favor of using the primary spanwise stress component to establish fatigue damage at one critical point of the hole notch.

7.1.1.1 Wing Lower Cover - A two level spectra was used to analyze the wing lower cover. The two level spectra is composed of Ground-Air-Ground (GAG) and low level maneuver plus gust since the detailed computer analysis showed that the major part of the damage was caused by these sources, as shown in Figure 129.

For GAG, which is defined as "peak-to-peak," one cycle per flight, the cumulative frequency summary of peak flight and peak ground condition load factor excursions defines the full spectra. To reflect the fact that maximum load factor excursion is not always associated with maximum stress and that more than one large load factor excursion may occur per flight, only alternate peak excursions are used to define the GAG cycles and associated damage. A single equivalent GAG level is also defined to match the full GAG spectra damage. For the 95,020 landings (i.e., flights) per 60,000 flight hours, this equivalent average level occurs at Σf = 95,020 with flight $\Delta n \approx 0.56$ and ground Δn 0.47. (See Figure 23)

A similar matching of total spectra damage at a single most damaging load factor level is used to define the equivalent low level maneuver plus gust spectra element. The low level maneuver plus gust (LLM+G) spectra are given in Table XXIX.wherein the most damaging level is shown to occur in the region of Δn = 0.75. The one "g" bending moment and associated stress data are based on the mission midpoint and a section modulus $\sigma/M = 1200 \times 10^{-6}\ in^{-3}$. The full spectra in conjunction with the S/N data of Figure 125 were used to define the total damage. The two levels thus identified to give damage equivalent to that of the full spectra for stations 117.9 and 339.1 are summarized below:

Station	Spectra Element	Flight Δg	σ_{max}(KSI)	R	f/60,000 hrs.
117.9	GAG	.55	11	-.99	95,020
	LLM+G	.75	13	.14	47,167
339.1	GAG	.55	8.1	-.68	95,020
	LLM+G	.85	9.1	.08	9,066

A typical example of the accuracy of the simplification is shown in Figure

130. The sum of the damage ratios is 1.01 as compared to one for the full spectrum analysis. This is within the five percent limit specified in Table XXVIII.

For the Station 117.9 skin-spar cap joint, GAG and LLM+G damage were calculated for selected values of σ/M, from which corresponding service life and fatigue design stress values were established (Table XXX). From the service life-to-fatigue design stress relationship, a fatigue design stress = 47,000 psi is defined for the required service life of 15,000 hours. In a similar manner, the reference ultimate design stresses for fatigue of the skin-spar cap joint at Station 339.1 and of the skin splices at Stations 117.9 and 339.1 were determined. The same analysis results apply to both the baseline and concept designs since the spectra and the S/N data also apply to both.

The equivalent moments, associated with the equivalent GAG cycle stresses at Stations 117.9 and 339.1, closely corresponded to Mission 1, Segments 8 and 1, respectively, for flight and ground condition moments (Reference 42, Tables 5-1 & 5-2). This then provided a simple and direct means of establishing the equivalent GAG moments and stresses and hence damage at the other selected study stations, since Segments 8 and 1 "1g" moments were available at all other stations. Adding a similarly determined damage increment for LLM+G to that for GAG established the total damage and associated reference design stress level constraints for the study stations also (Figure 131). As indicated, the fatigue design stress levels increase significantly at the outboard wing stations. In the skin-spar cap case, the stress levels also increase with spar cap thickness reduction reflecting increased interference from the installed fasteners. Decreased spar cap thickness [from t/D $\approx$ 3 (baseline) to t/D $\leq$ 2] was selected for the new concepts.

7.1.1.2 Wing Upper Cover - A representative two level spectrum was also developed for the wing upper cover at Station 117.9 in a manner similar to that previously described for the lower cover. The predominant damage source is GAG, followed by taxi.

Station	Spectra Element	Ground Δg	$_{max}$(KSI)	R	f/60,000 hrs.
117.9	GAG	0.47	7.5	-0.99	95,020
	Taxi	0.75	8.9	0.14	827

Skin-spar cap joint and skin splice damage, service life, and reference design stress values were obtained, as before, on all check stations (Figure 132).

7.1.2 Fuselage Shell Structure

Fatigue analyses were performed on the baseline and on the honeycomb concept fuselage considering flight, landing and pressurization loadings. The detailed analysis work on the baseline configuration is covered in Reference 42. The detailed analysis of the honeycomb fuselage is summarized in Section 7.1.2.2.

The baseline vehicle was checked for longitudinal fatigue loading at Stations 703 and 847. It was further checked for hoop loading in a minimum skin gage

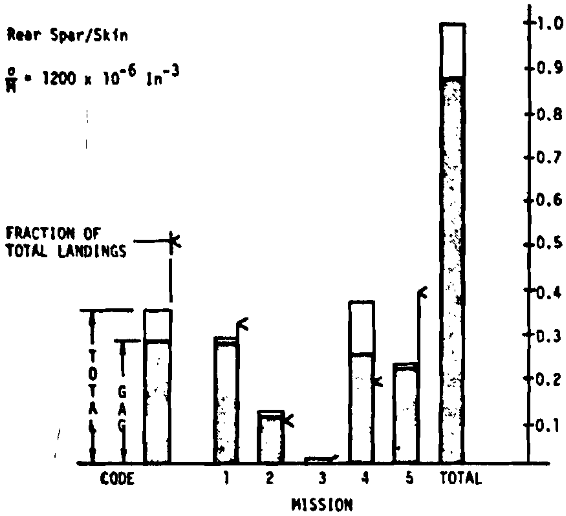

Figure 129 FULL LOAD SPECTRA FATIGUE DAMAGE DISTRIBUTION FOR BASELINE WING LOWER INBOARD PANEL

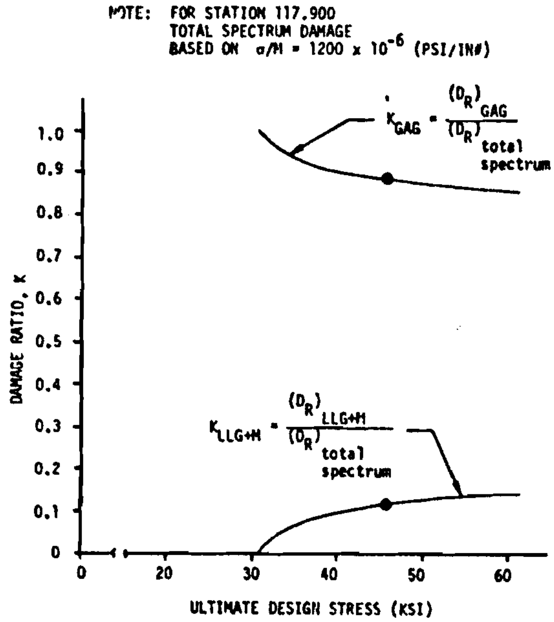

Figure 130 EXAMPLE OF SIMPLIFIED FATIGUE SPECTRA ACCURACY

TABLE XXIX DAMAGE DISTRIBUTION DUE TO LOW LEVEL MANEUVER PLUS GUST SPECTRUM FOR THE WING LOWER COVER

①	②	③	④	⑤	⑥	⑦	⑧	⑨	⑩
Δg *	n * $(\times 10^{-6})$	$1 + \Delta g$	$1 - g$	σ_{max} +	σ_{min} +	R	N $(\times 10^{-6})$	$\frac{n}{N}$	Damage Δ $(\Sigma \frac{n}{N})$
REFERENCE 1		1 + ①	1 - ①	③ K	④ K	⑥/⑤	Figure 124	②/⑧	
0.15	6.6004	1.15	0.85	8,563	6,329	0.74	---	---	---
0.25	1.9501	1.25	0.75	9,308	5,585	0.60	---	---	---
0.35	0.8100	1.35	0.65	10,052	4,840	0.48	---	---	0.1056
0.45	0.2625	1.45	0.55	10,797	4,095	0.38	140.00	0.00188	0.1037
0.55	0.0975	1.55	0.45	11,541	3,351	0.29	2.50	0.03900	0.0647
0.65	0.0090	1.65	0.35	12,286	2,606	0.21	0.83	0.01080	0.0539
0.75	0.0139	1.75	0.25	13,031	1,862	0.14	0.43	0.03230	0.0216
0.85	0.0071	1.85	0.15	13,775	1,117	0.081	0.33	0.02160	

* $\Delta g = \Delta N_{C.G.}$

\+ $K = (\sigma_{1g})_{LLG+M} = 7446$

Δ Damage based on 60,000 flight hours

• Occurrences of airplane incremental C.G. due to low level gust plus maneuver.

TABLE XXX STATION 117.900 SKIN-SPAR CAP JOINT FATIGUE CAPABILITY COMPUTATION

①	②	③	④	⑤	⑥	⑦	⑧	⑨
BM_{1g}	Δg	n	R	$d\sigma/dBM$	σ_{1g}	σ_{max}	N	$(D_R)_{GAG}$
STA. 117.9 GAG	GROUND-AIR-GROUND SPECTRUM			SELECTED ARBITRARILY	PSI	$(1 + \Delta g)\ \sigma_{1g}$ (PSI)		$\frac{n}{N}$
$\times 10^6$				$\times 10^{-6}$	⑤ x ①	(1 + ②)(⑥)	Figure 125	③ / ⑧
5.807	0.55	95,020	-0.989	1,600	9,291	14,401	47,000	2.02200
5.807	0.55	95,020	-0.989	800	4,646	7,201	1,000,000	0.09502
5.807	0.55	95,020	-0.989	900	5,226	8,100	420,000	0.22620
5.807	0.55	95,020	-0.989	1,000	5,807	9,001	250,000	0.38010

⑩	⑪	⑫	⑬	⑭	⑮	⑯	⑰	⑱
BM_{1g}	Δg	n	R	$d\sigma/dBM$	σ_{1g}	σ_{max}	N	$(D_R)_{LLG+M}$
STA. 117.9 LLG + M	LOW LEVEL GUST + MANEUVER SPECTRUM			SELECTED ARBITRARILY	PSI	$(1 + \Delta g)\ \sigma_{1g}$ (PSI)		$\frac{n}{N}$
$\times 10^6$				$\times 10^{-6}$	⑭ x ⑩	(1 + ⑪)(⑮)	Figure 125	⑫ / ⑰
6.205	0.75	47,167	0.14	1,600	9,928	17,374	140,000	0.33700
6.205	0.75	47,167	0.14	800	4,964	8,687	---	---
6.205	0.75	47,167	0.14	900	5,585	9,774	3,000,000	0.01570
6.205	0.75	47,167	0.14	1,000	6,205	10,859	1,250,000	0.03770

⑲	⑳	㉑	㉒	㉓
$\frac{d\sigma}{dBM}$	TOTAL DAMAGE BASED ON 60,000 FLIGHT HOURS	SERVICE LIFE (HOURS)	ULTIMATE FLIGHT BENDING MOMENT	$(F_{tu})_{Fatigue}$ AT SPAR CAP
$\times 10^{-6}$	⑨ x ⑱	60,000/(4 x ⑳)	REFERENCE 1	⑲ x ㉒
1,600	2.35900	6,359	38.4×10^6	61,440
800	0.09500	157,895	38.4×10^6	30,720
900	0.24190	62,009	38.4×10^6	34,560
1,000	0.41780	35,902	38.4×10^6	38,400

NOTE: Plotting Service Life vs $(F_{tu})_{Fatigue}$ at spar cap shows that the critical F_{tu} is 47000 PSI, i.e., at Total Damage = 1.0.

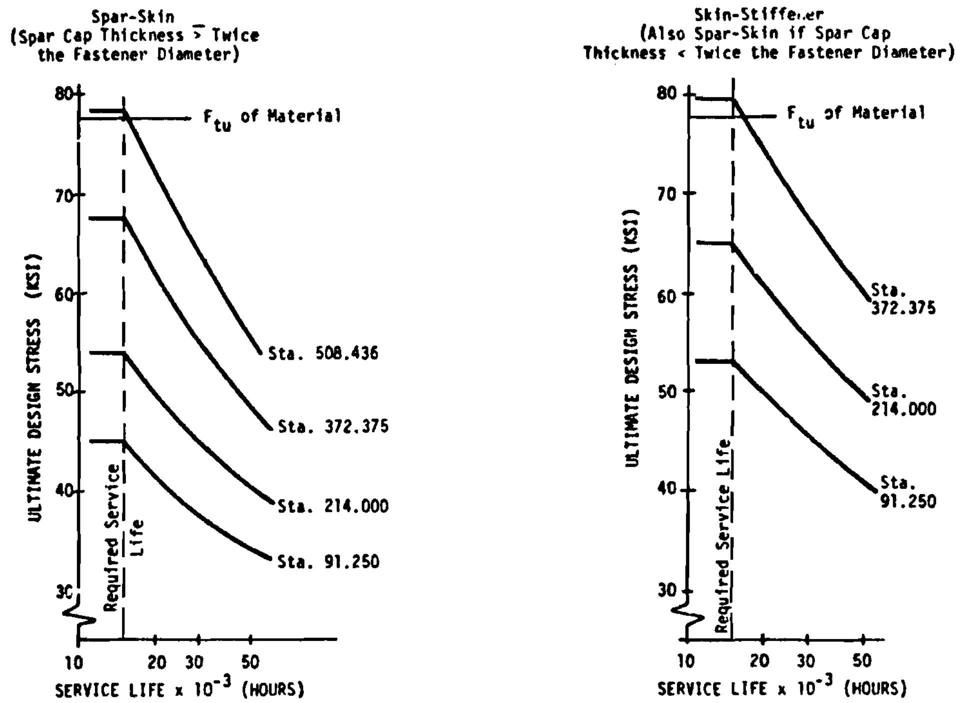

Figure 131 WING LOWER PANEL FATIGUE DESIGN STRESSES (INTEGRAL AND IMPROVED BASELINE CONCEPTS)

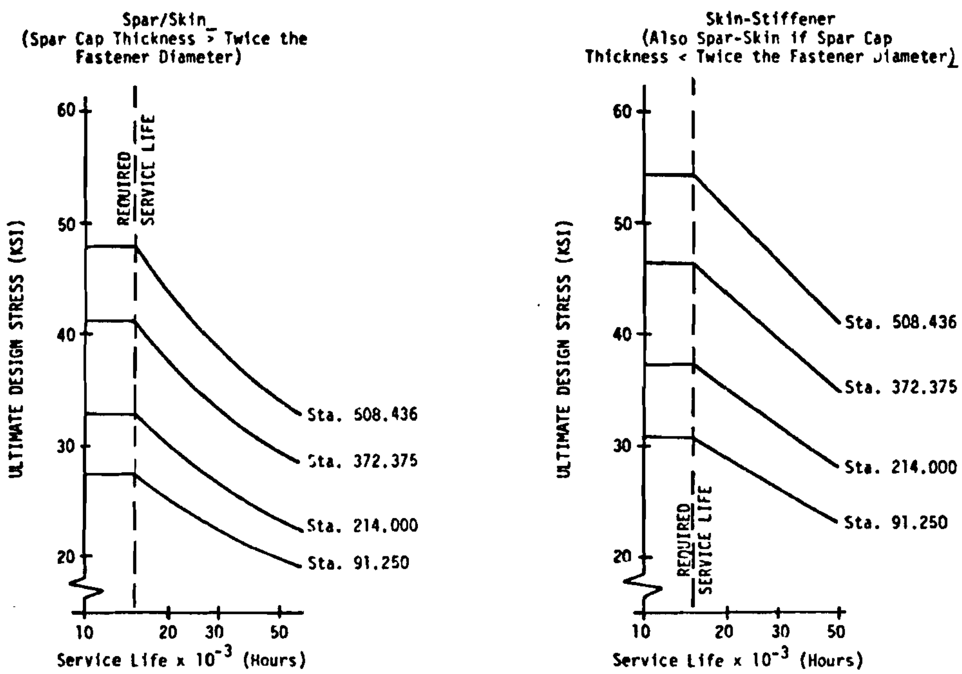

Figure 132 WING UPPER PANEL FATIGUE DESIGN STRESSES (INTEGRAL AND IMPROVED BASELINE CONCEPTS)

(.050") area. The service life projections of these analyses (shown in Table XXXI) relative to the service life requirement of 15,000 hours indicates high fatigue margins. The honeycomb fuselage analysis results also indicate ample margins, although lower than the baseline. The lower margins are due to the higher design stress levels associated with the honeycomb concept.

The baseline and honeycomb concepts were also checked for acoustic fatigue. The minimum margin of safety for the baseline vehicle panels was approximately zero, whereas the margins were high in the honeycomb concept.

The analyses leading to the above results are discussed in paragraphs 7.1.2.1 through 7.1.2.3.

7.1.2.1 Baseline Concept - Analyses of the baseline fuselage were accomplished using the DAC computer program A6PA (Reference 43). The program combines the full load spectra representing the environment with the S/N fatigue strength allowables to compute the damage. Two points, Station 703 in the forward fuselage, and Station 847, in the aft fuselage, were checked, Reference 42.

The forward fuselage is subjected to inertia loads, airloads, cabin pressurization and ground loads. The spectra defined incremental load factor excursions for the non-pressure load environments. The analysis then also defined and provided as input to computer program A6PA the following basic data.

Section modulus $\frac{\sigma}{M} = \frac{C}{I} = 198$ PSI/10^6 in lbs of applied moment,

One g stresses for each mission,

$d\sigma/dn$ (rate of change of stress for change in load factor)

for all mission segments, and

S/N data for the 2024-T3 fuselage basic structure.

The damage due to GAG was computed separately from that due to taxi, gust and maneuver, Table XXXII. The taxi, gust and maneuver loads do not generate any fatigue damage directly, although they do define the ground-air-ground (GAG) cycle which causes the damage. The predicted service life is 0.36×10^6 hours which is large relative to the service life requirement of 15,000 hours; hence, no fatigue problems are anticipated.

The fatigue analysis for the aft fuselage (Station 847), was conducted in a similar manner. The section modulus for this station was,

$\frac{\sigma}{M} = \frac{C}{I} = 184$ PSI/10^6 inch pounds of applied moment

The results are shown in Table XXXII. The computed service life is 1.92×10^6 hours, which is also high relative to the service life requirement so that no fatigue problem exists.

A fatigue check was also made for hoop stresses due to pressurization. The analysis in Reference 42, Page 62 was for a minimum gage of 0.063 inches.

TABLE XXXI FUSELAGE FATIGUE LIFE PREDICTIONS				
CONCEPT	LOADING	CHECK STATION	PREDICTED SERVICE LIFE (HOURS)	PAGE NUMBER FROM REFERENCE 42
BASELINE	LONGITUDINAL	703 (TOP ℄)	0.36×10^6	23
BASELINE	LONGITUDINAL	847 (TOP ℄)	1.92×10^6	23
BASELINE	HOOP	AREAS OF MINIMUM GAUGE	0.45×10^6	62
HONEYCOMB	LONGITUDINAL	703 (TOP ℄)	87,100	--
HONEYCOMB	HOOP	AREAS OF MINIMUM GAUGE	48,200	--

TABLE XXXII BASELINE FUSELAGE FATIGUE DAMAGE DUE TO LONGITUDINAL LOADING					
MISSION	FLIGHT HOURS	DAMAGE AT STA. 703		DAMAGE AT STA. 847	
		T, G & M*	G-A-G Δ	T, G & M*	G-A-G °
1(O)	16,000	0	0.01023	0	0.00146
1(R)	16,000		0.02460		0.00381
2(O)	4,800		0.00277		0.00006
2(R)	4,800		0.00316		0.00006
3	4,800		0.00065		0.00003
4	8,000		0		0.00238
5	5,600	0	0	0	0
TOTAL PER 60,000 FLIGHT HOURS			0.04141		0.00780

*TAXI, GUST AND MANEUVER SPECTRA

ΔSERVICE LIFE = $\frac{60,000}{4(0.04141)} = 0.36(10^6)$ HOURS

°SERVICE LIFE = $\frac{60,000}{4(0.0078)} = 1.92(10^6)$ HOURS

(1) REFERENCE 42, PAGES 23, 60 AND 61

The minimum gage of the study baseline vehicle is 0.050 inches, Reference Section 5.2.1. The Reference 42 analysis established the altitudes and maximum pressures reached during each mission, and defined the associated maximum hoop stresses and total damage. Duplication of the analysis for an 0.05 inch minimum gage shows a high predicted service life (0.45 x 10^6 hours, Table XXXIII.

7.1.2.2 Honeycomb Concept - The honeycomb fuselage was analyzed for both longitudinal and hoop loading. Longitudinal loading was considered at the four check stations--439, 703, 847 and 982. Hoop loading is critical in minimum face gage areas. Station 703 (forward) was selected as typical of these areas.

The longitudinal fatigue check assumed that 80% of all fatigue damage results from the ground-air-ground (GAG) cycle loads. This is slightly conservative in that the baseline fatigue analyses results (Table XXXII) show that practically 100% of the damage is due to the GAG cycles. The GAG cycle limits come from the C.G. load factor exceedance spectra, Figure 133. The number of design life GAG cycles is four times the number of service life landings, n = 4 x 23,755 = 95,020 cycles. The typical GAG cycle is 1.56g flight condition to 1.47 ground taxi condition. These loads are applicable to the fuselage forward of the wing. However, for the fuselage aft of the wing (Stations 847 and 982), the critical flight loads result from a flaps extended condition. The mission profile data (Reference 42) shows that the aircraft flies a total of 570 hours (out of 15,000) with flaps down. Flaps are extended during lower altitude operations which are associated with generally higher turbulence. Hence, the flaps down time was doubled, giving an equivalent flaps down time of 1140 hours, or 7.6% of the total flight time. The basic cumulative frequency curve was adjusted by the factor 0.076 to give the equivalent flaps down curve shown. This changed the GAG cycle flight load factor to 1.36 g's, while the ground taxi value remained unaltered.

One "g" inertia bending moments are presented in Reference 42, Pages 54 and 59, for Stations 725 and 871. The dead weight portion was rationally extended to the check stations. In addition, moments due to an average one "g" flaps down balancing tail load were added to inertia moments at Stations 847 and 982. The pressure loads corresponded to the maximum pressure differential for each mission defined by the maximum associated altitude and altitude lapse rate of Reference 42, Page 62.

The flight and ground condition moments defined the GAG cycle maximum and minimum moments at each check station. The checks were made at the fuselage top centerline, where maximum tension occurs. S/N data for the aluminum face sheets is from Figure 128. Section properties are summarized in Table XXXIV and the fatigue calculations for the critical Station 703 are shown in Table XXXV.

A fatigue check was also made for hoop pressure loading. The hoop stresses are maximum in minimum gage areas (minimum face skin gages = 0.02 inches), which exist over the top centerline area from Stations 366 to 703 and down the entire bottom centerline area. The hoop pressure loads are twice the longitudinal pressure loads (which are shown in Table XXXV) and have a cycle ratio R = C. The fatigue check, using Figure 128 S/N data, gives a predicted service life of 31,900 hours for the new concept design. The service life

TABLE XXXIII BASELINE FUSELAGE FATIGUE DAMAGE TO HOOP LOADING

MISSION	MAXIMUM ALTITUDE (10^3 FT)	σ_{max} (PSI)	N_1 CYCLES TO FAILURE	n_1	$\frac{n_1}{N_1}$
1(O)	34.20	14,000	1.2×10^6	15,240	0.0127
1(R)	37.80	15,100	1.0×10^6	15,240	0.0152
2(O)	31.57	12,900	1.9×10^6	4,572	0.0024
2(R)	33.09	13,500	1.8×10^6	4,572	0.0025
3	41.80	15,100	1.0×10^6	764	0.0007
4	1.00	400	-	4,324	0
5	15.00	6,100	-	9,336	0
TOTAL PER 60,000 FLIGHT HOURS				D_R =	0.0335

*R=D

*PREDICTED SERVICE LIFE = $\frac{60,000}{4(0.0335)}$ = $0.45(10^6)$ HOURS

TABLE XXXIV HONEYCOMB FUSELAGE SECTION PROPERTIES

STATION	I IN^4 (10^3)	C TOP (IN.)	C BOTTOM (IN.)	$(C/I)_{TOP}$ (IN^3)	$(C/I)_{BOT}$ (IN^3)
439	206.6	121.6	94.4	0.000589	0.000467
703	197.1	124.9	91.1	0.000633	0.000462
847	252.6	118.6	97.4	0.000469	0.000386
982	210.7	122.0	94.0	0.000578	0.000447

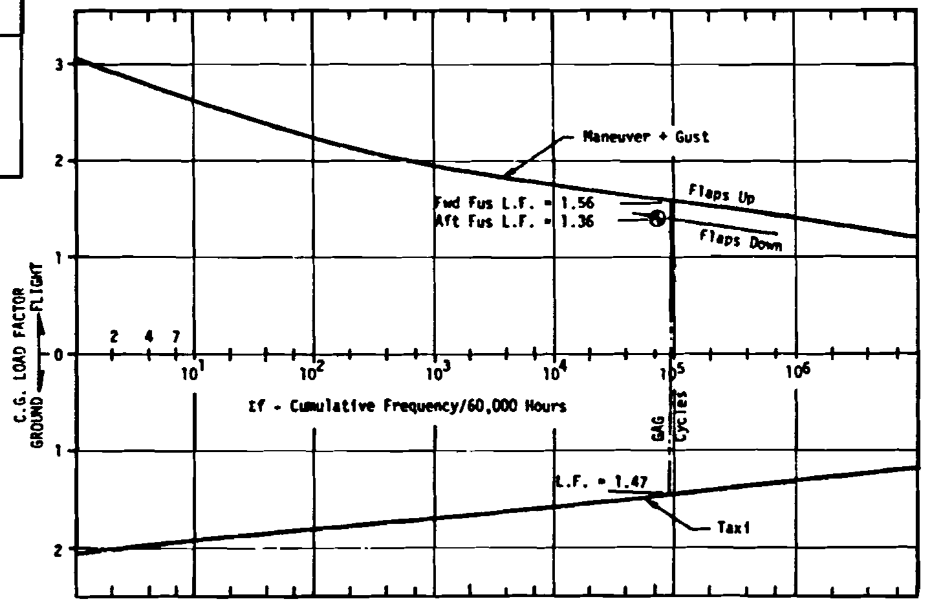

Figure 133 C. G. LOAD FACTOR EXCEEDANCE SPECTRA

TABLE XXXV FUSELAGE STATION 703 FATIGUE ANALYSIS (HONEYCOMB CONCEPT)

MISSION	ONE "g" MOMENTS (10^6 IN LBS)	1.56g FLIGHT MOMENTS (10^6 IN LBS)	1.56g FLIGHT STRESSES (KSI)	CABIN PRESSURE PSID	CABIN PRESSURE STRESS (KSI)	σ_{max} (KSI)
1(O)	-5.570	-8.689	5.5	6.83	9.2	14.7
1(R)	-5.585	-8.713	5.5	7.08	9.6	15.1
2(O)	-6.973	-10.878	6.9	6.64	9.0	15.9
2(R)	-6.988	-10.901	6.9	6.75	9.1	16.0
3	-3.114	-4.858	3.1	7.61	10.3	13.4
4	-5.585	-8.713	5.5	0.36	0.5	6.0
5	-3.133	-4.887	3.1	4.35	5.9	9.0

1g GROUND MOMENTS (10^6 IN LBS)	1.47g GROUND MOMENTS (10^6 IN LBS)	σ_{min} (KSI)	R	N_i (CYCLES TO FAILURE)	n_i	$\frac{n_i}{N_i}$
+0.257	+0.378	-0.2	-0.01	2.9×10^5	15,240	0.0526
-0.257	-0.378	+0.2	+0.01	2.4×10^5	15,240	0.0635
+0.520	+0.764	-0.5	-0.03	8.8×10^5	4,572	0.0052
-0.062	-0.091	0	0	1.8×10^5	4,572	0.0254
+2.813	+4.135	-2.6	-0.19	2.5×10^5	764	0.0031
+0.379	+0.557	-0.4	-0.07	∞	17,296	0
+1.462	+2.148	-1.3	-0.14	2.8×10^6	37,336	0.0133
				TOTAL	95,020	$D_R = 0.1632$

PREDICTED SERVICE LIFE IS 73,500 HOURS FROM $(60{,}000/4)(0.8)(1/[n_i/N_i])$ WHERE 0.8 ACCOUNTS FOR 80% DAMAGE DUE TO GAG versus design stress relationship (shown in Table XXXVI) is useful for identifying the design stress that exactly meets the service life requirement. This relationship is established through face skin gage variation where .02 inch gauge corresponds to 66,240 PSI maximum ultimate flight stresses at fuselage stations 703, top centerline (see Section 7.3.2).

7.1.2.3 Acoustic Fatigue for Baseline Fuselage - The acoustic fatigue analyses were limited to the baseline configuration skin panels. No analyses were required on the honeycomb concept because the effective panel sizes are so small that acoustic fatigue is not critical. The baseline concept is analyzed by a DAC design chart approach based on test data for skin and rib structure.

Estimated pressure spectrum levels on the fuselage during ground static operation at full takeoff power, with flaps at 0°, 23° and 55° curves are given in Reference 1. These data relate to fuselage zones, which are defined in Figure 134. Reductions from the estimated pressure spectra levels for fuselage zone and circumferential location are shown in Tables XXXVII and XXXVIII, respectively, where the reference points on Table XXXVIII refer to the locations on Figure 134. All skin panels were chosen to be 10.94 x 24 inch rectangles. The natural frequency of the panel is obtained from the DAC design chart. A plus and minus 25 CPS range is conservatively considered. The larger value is used to conservatively increase the number of applied (n) cycles. The smaller value is used on the design chart to establish the allowable life curve. All damage was assumed to occur at or near the ground, at or close to 100% thrust (Table XXXVII), and to be linearly cumulative.

Inspection of the skin gages and zone chart identified the critical panels, which are summarized in Table XXXIX along with the resulting margins of safety.

7.1.3 Horizontal Stabilizer Box Structure

Fatigue analyses of transport aircraft horizontal stabilizer box upper cover panels show, in general, that (1) fatigue is not a critical mode and (2) the ground-air-ground (GAG) cycle is the predominant fatigue damage mode. A preliminary check of the baseline cover panel spanwise splices using baseline wing lower panel GAG spectra and S/N data (Empennage spectra not available - hence this analysis qualified by spectra analysis) yielded a capability $F_{fatigue}$ > 90,000 PSI (expressed in terms of tension ultimate). This is greater than the panel tension ultimate capability .8 $F_{tu} \approx 62{,}000$ psi (7050-T76 skin material). Hence, it was concluded that fatigue is not a critical mode for the baseline horizontal box unless a reduction of fatigue geometric efficiency below baseline levels is considered for cost savings or other reasons.

A similar check of the bonded honeycomb concept on the basis of a "no hole" S/N curve ($K_t \lesssim 2$ assumed) yielded a fatigue capability significantly higher than that of the baseline.

TABLE XXXVI SUMMARY OF HOOP STRESS FATIGUE ANALYSIS	
DESIGN STRESS (PSI)	PREDICTED LIFE (HOURS)
59,600	78,400
66,240	31,900
72,900	19,700

TABLE XXXVII ACOUSTIC db REDUCTIONS FOR OPERATIONAL CONDITION					
NUMBER	CONDITION	FLAP SETTING	THRUST (%)	VELOCITY (KNOTS)	db REDUCTION
1	TAKEOFF	23°	100	0	0
2	TAKEOFF	23°	100	100	-7
3	3 ENGINE LANDING	55°	100	100	-7
4	4 ENGINE LANDING	55°	60	100	-11
5	TOUCH & GO LANDING	55°	100	80	-3
6	REVERSE THRUST	--	REVERSE	0	0

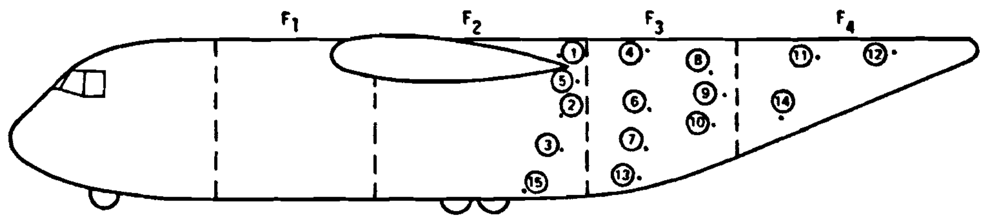

Figure 134 FUSELAGE ZONES OF ACOUSTIC NOISE

TABLE XXXVIII ACOUSTIC db REDUCTIONS FOR CIRCUMFERENTIAL LOCATION					
ZONE	REFERENCE POINT	OCTAVE BAND CENTER FREQUENCY			
		63	125	250	500
F2	1	-9	-5	-5	-5
F2	2	-1	0	0	-1
F2	3	-8	-4	-5	-3
F2	5	-2	0	0	-1
F2	15	-15	-13	-15	-10
F3	4	-8	-6	-6	-5
F3	6	0	-1	+1	-1
F3	7	-3	-5	-2	0
F3	8	-2	-1	-2	-3
F3	9	+1	+1	-1	-2
F3	10	-2	-1	-1	-2
F3	13	-8	-6	-5	-5
F4	11	-1	-1	-1	0
F4	12	-2	0	+1	-2
F4	14	-2	-2	-1	0

TABLE XXXIX SUMMARY OF ACOUSTIC FATIGUE ANALYSIS RESULTS						
CHECK POINT NUMBER	ZONE +	θ DEGREES FROM TOP ℄	SKIN GAUGE (IN)	RESONANCE FREQUENCY (CPS)	TOTAL DAMAGE $D_R = \Sigma \frac{n_i}{N_i}$	MARGIN OF SAFETY
1	F1	Any	0.050	70	0.0104	High
2	F2	0-52	0.063	90	0.3240	High
3	F3	52-110	0.080	130	~ 1.0	0
4	F4	110-157	0.071	110	~ 1.0	0
5	F5	157-180	0.050	70	0.0104	High

+See Figure 134 for zone locations

7.1.4 Vertical Stabilizer Box Structure

A preliminary check of the baseline cover panel-to-spar cap spanwise splice, using the baseline wing lower panel maneuver plus gust spectra and S/N data (See note in Section 7.1.3), yielded a capability $F_{fatigue} \approx 75{,}000$ PSI (expressed in tension ultimate), which is greater than the panel tension ultimate capability $.8\ F_{tu} = 62{,}000$ PSI (7050-T76 skin material). Hence, fatigue is not indicated to be a critical mode for the baseline vertical box unless a reduction of fatigue geometric efficiency below baseline levels is considered for cost saving or other reasons.

A similar check of the bonded honeycomb concept on the basis of a "no-hole" S/N curve ($K_t \lesssim 2.0$ assumed) yielded a fatigue capability significantly higher than that of the baseline.

7.2 DAMAGE TOLERANCE ANALYSES

Damage tolerance analyses were performed on critical wing and fuselage primary structure to identify design stress levels and to verify that the required unrepaired service usage period was being met. The criteria used was the USAF Damage Tolerance Criteria Revision D (18 August 1972), presented in Appendix A, except as noted in the following pages. Walk-around and depot inspectability were used for the wing lower covers. Special visual and depot inspectability were used for the wing upper covers, the critical upper quadrant of the fuselage, and the empennage.

Two level spectra applicable to the particular structure being investigated were determined from an evaluation of the full spectra which contained over 2000 stress levels (Reference 1). In each case, the truncated spectra consisted of a low frequency level (ground-air-ground, GAG) and a high frequency level (gust plus maneuver or taxi). The spectra values used are included in the subsections on the specific structural components.

The criteria used to select the structural members and locations for analysis are summarized in Table XL.

In general, hand analyses were used to account for a range of complex structural conditions including multiple members and associated interacting cracks, such as for the wing spar-skin joint, in a single analysis. The crack growth analyses were based upon linear elastic fracture mechanics wherein the crack growth rate and the residual strength of the structure are governed by the local stress conditions at the crack tip expressed as a stress intensity factor "K." A discussion of the method can be found in Reference 33. The general equation for the crack tip stress intensity factor is:

$$K = \beta\sigma\sqrt{\pi a} \qquad (31)$$

σ = gross area stress remote from the crack

a = crack half length

TABLE XL CRITERIA FOR SELECTION OF CRITICAL DAMAGE TOLERANCE ANALYSIS POINTS

LEVEL	FACTOR	CRITERION	REMARKS AND RATIONALE
Component or Area	Weight Fraction	$\left(\frac{\Delta W_S}{W_S}\right)_{max}$	(1) Study objective is to minimize structural weight fraction (W_S/W). For fixed study effort, enhanced quantitativeness of $W_{S_{min}}$ is achieved by placing analytical emphasis on maximum component weight fraction $(\Delta W_S/W_S)_{max}$.
Component or Area	$\left(\text{Achieved Period}\right)_{min}$		(2) Critical M.S. = $\left(\frac{\text{Achieved Period}}{\text{Required Period}}\right)_{min} - 1 \geq 0$ Minimum achieved period is a function of
	Stress Type	σ_t	(a) Tensile stresses (σ_t).
	Stress Magnitude	$\left(\frac{\sigma_{t1g}}{F_{tu}}\right)_{max}$	(b) Maximum positive cyclic stress range ($\Delta\ \sigma_{t_{max}} = \sigma_{t1g\ max}$) normalized for material $(\sigma_{t1g}/F_{tu})_{max}$.
	Section Geometry	$\left(\frac{A_{ST}}{A_{SK}}\right)_{max}$	(c) Maximum stiffener/skin area ratio (A_{ST}/A_{SK}) for maximum skin stress in presence of failed stiffener (internal and relatively uninspectable).
Point	Flaw Stress Concentration	λ_{max}	(d) Maximum stress intensity (K) per unit nominal stress (σ); i.e., $(K/\sigma)_{max} = \lambda_{max} \sqrt{\pi a} = \lambda_{max}$.
	Material	$K_{c_{min}}$	(e) Maximum crack growth rate @ $\Delta K << K_c$ $\left(\frac{da}{dn}\right)_{max} = \frac{C\ \Delta K^n}{(1-R)\ K_{c_{min}}} = \frac{1}{K_{c_{min}}}$.
	Initial Damage Size	$(2\ a_i)_{max}$	(f) Maximum start condition damage size = f (structure type)
Component, Area or Point	$\left(\text{Period Required}\right)_{max}$		(3) Maximum required period is a function of:
	Inspectability	I_{min}	(a) Minimum degree of inspectability (I_{min}).

β = modification factor for the effects of stiffener, finite width, holes, etc.

A = constant = π (for "through" flaw)

$= \frac{\pi}{Q}$ (for "part through" flaw)

Appropriate modification factors (β and A) were used to adjust the basic equation for structural conditions such as finite width sheet, asymmetric cracks, cracks starting from hole or surface flaws, through or part-through cracks, and the influence of stiffening members. The particular stress intensity factor formulations used are presented in the following analysis subsections.

For multiple cracks in stiffened structure, the influence of one cracking member on the crack growth of another member was also represented by a modification factor. The factor was assumed to be unity until the first member failed, at which time the factor increased to account for the load transfer and varied with the subsequent crack growth in the other member(s). The modification factors were determined using Douglas computer code N4BD (Reference 44), which requires a symmetric structure and crack. For asymmetric structures and cracks, e.g., wing skin-spar cap joint, the structure and its mirror image were input to provide a symmetric model approximation for the modification factor analysis.

Crack growth time-history calculations were based on experimentally determined curves of ΔK versus da/dN at room temperature and for lab air chemical environment conditions for the material of the structure being analyzed (Figures 135 through 140). The crack growth histories also did not account for crack retardation effects from crack tip plasticity. This is somewhat conservative, since literature and in-house test data indicate that time retardation factors as high as 1.5 are not unreasonable. More work, which is beyond the scope of this study, is required to calibrate existing retardation analysis models to test data. The study assumptions with respect to temperature, chemical and retardation effects are to some extent offsetting.

Failure (i.e., unarrested fast fracture) was determined from the criteria requirements for "one-time" load and a residual strength analysis of the particular structure. Residual strength was determined from the fracture mechanics principle that a partially cracked structure will fail completely when the crack tip stress intensity (K) reaches a critical value (K_c). The residual strength is then defined as:

$$\sigma_{res} = \frac{K_c}{\beta\sqrt{Aa}} \qquad (32)$$

The critical stress intensity, K_c, has been experimentally determined for many aircraft materials, Reference 11, and varies with material thickness.

The criteria specifies that the structure must be able to sustain the one-time load (or stress) that could occur in one hundred times the applicable inspection interval. This load requirement was established from cumulative frequency curves of σ_{max} derived from the full stress spectra associated

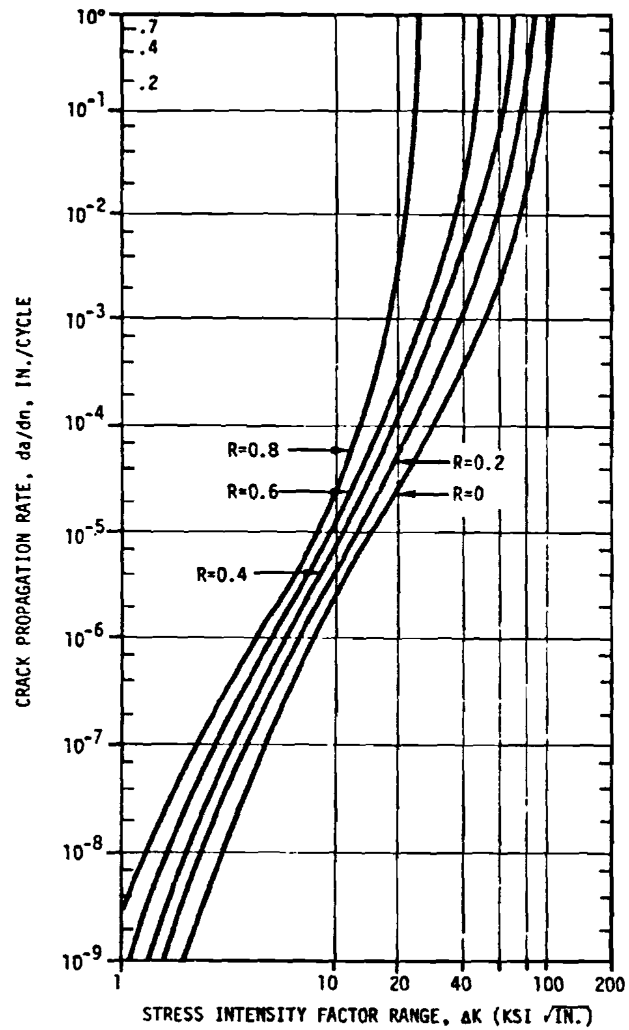

Figure 135 STRESS INTENSITY RANGE vs CR'.CK GROWTH RATE FOR 2024-T3 SHEET

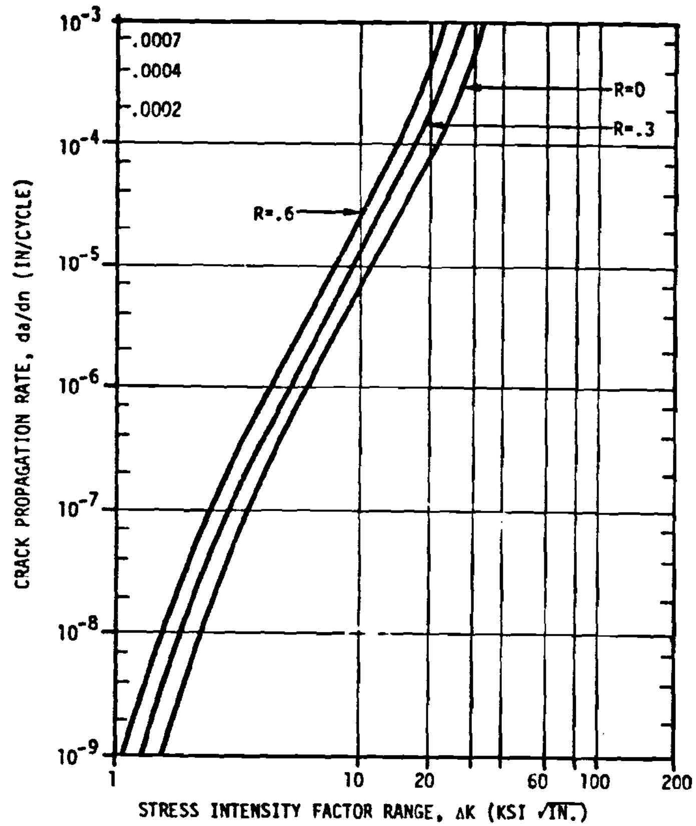

Figure 136 STRESS INTENSITY RANGE vs CRACK GROWTH RATE FOR 7049-T73 ALUMINUM DIE FORGING

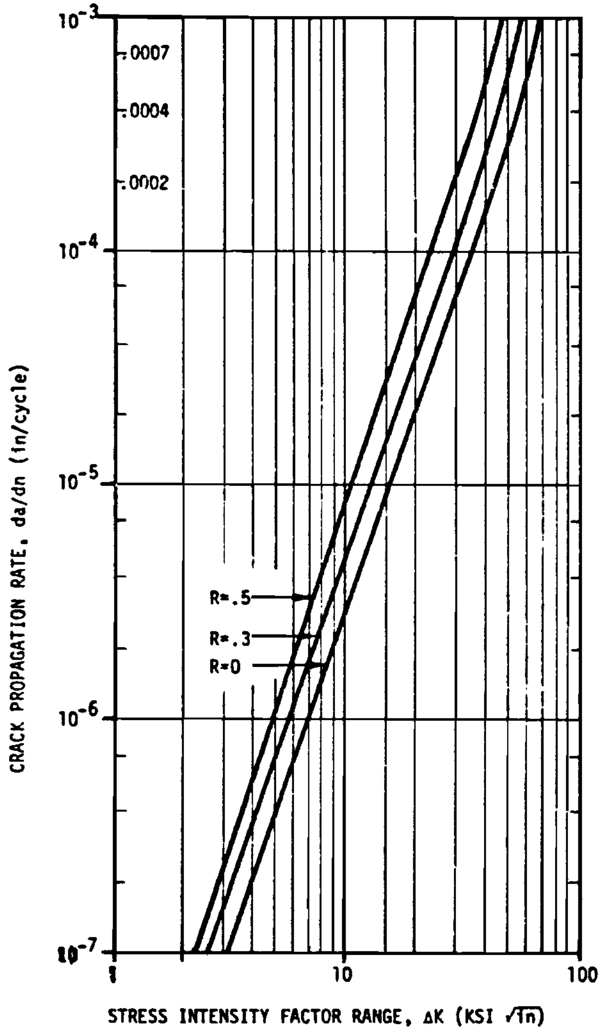

Figure 137 STRESS INTENSITY RANGE vs CRACK GROWTH RATE FOR 7050-T73651 ALUMINUM FORGING

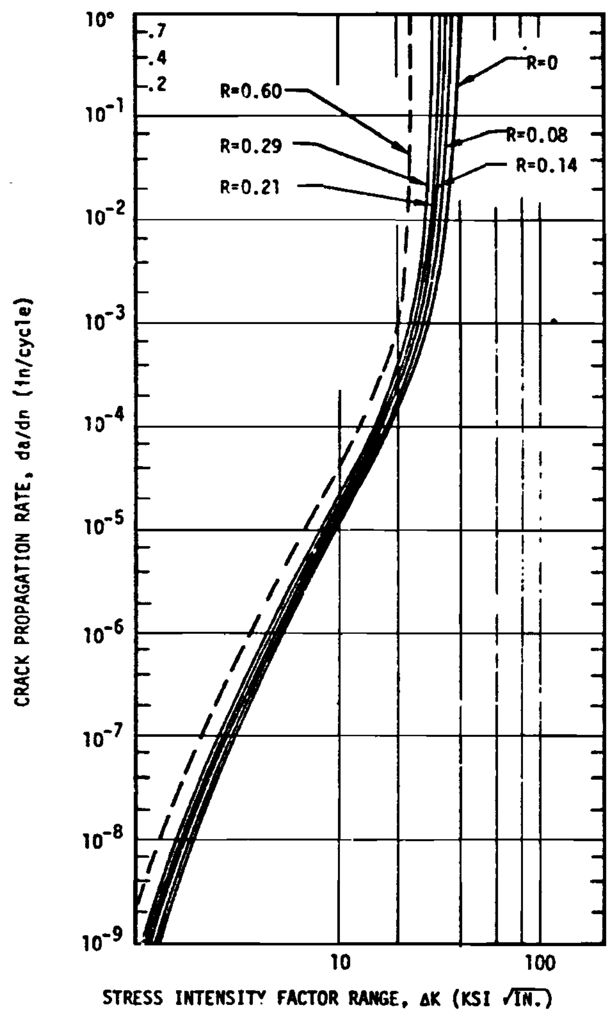

Figure 138 STRESS INTENSITY RANGE vs CRACK GROWTH RATE FOR 7075-T6 SHEET

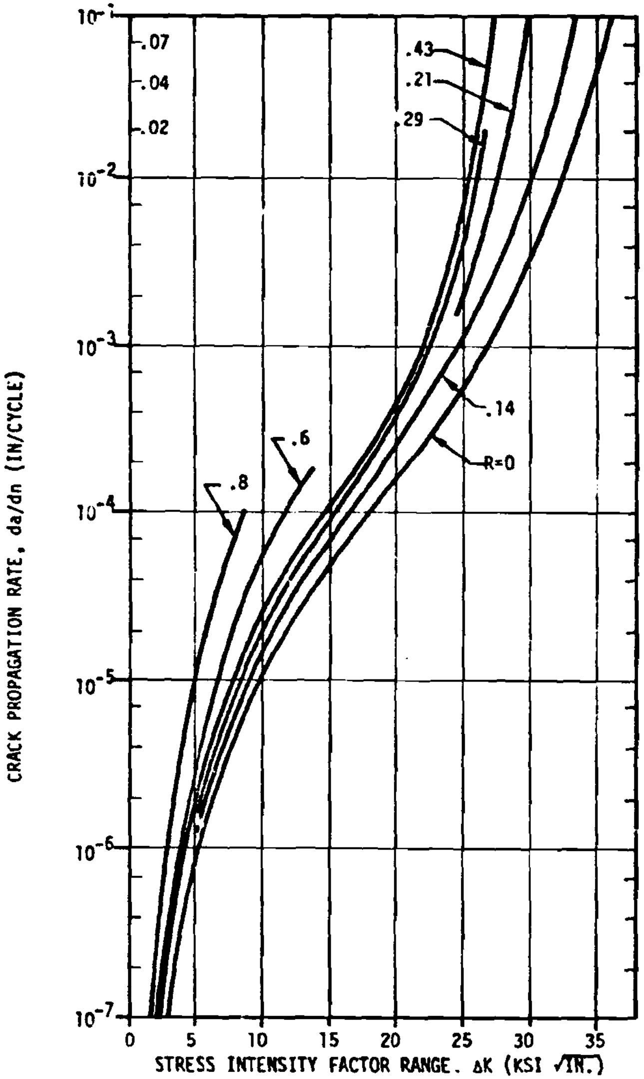

Figure 139 STRESS INTENSITY RANGE vs CRACK GROWTH RATE FOR 7075-T76 PLATE

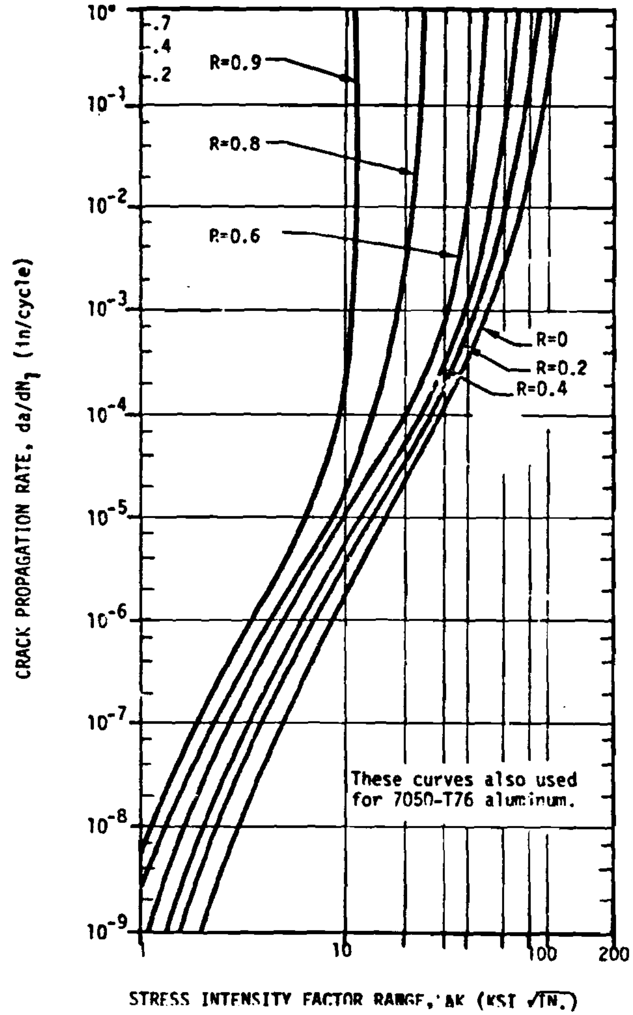

Figure 140 STRESS INTENSITY RANGE vs CRACK GROWTH RATE FOR 7475-T76 SHEET

with the structural component. An example derivation is given in Section 7.2.1 Structural failure starts at the crack size existing when the residual strength becomes less than the required load, thus defining the time period of safe crack growth.

As with fatigue, a reference design stress level is associated with the defined time period. Since, in the Forman equation, the time period is inversely proportional to da/dN and da/dN is proportional to $(\Delta K)^n$ in the region of primary period accumulation, a single time period and design stress solution (T_1, σ_1) can be extended to define other solutions (T_2, σ_2), $(\sigma_{req'd}, T_{req'd})$, etc.

$$\sigma_{required} = \sigma_1 \left(\frac{T_1}{T_{required}} \right)^{1/n} \tag{33}$$

The Forman equation exponent, n, is that of the critical structural member material which primarily determines the time period. For example, failure of the spar cap determined the life of the skin-spar cap structure in the baseline configuration. The constant, n, for the spar cap material was, therefore, used in that case. In the ensuing sections, results of the damage tolerance analyses are summarized and further described through numerical examples which illustrate more specifically the methods used.

7.2.1 Wing Box Structure

Damage tolerance analysis data and design stresses for the baseline and integral concept wing lower and upper covers are summarized in Tables XLI and XLII. The analyses were performed at Station 117.9 to make use of available data from the project group, e.g., the one "g" stress levels for the complete spectra. The Station 117.9 damage tolerance design stresses were then extended to the four check stations on the basis of the fatigue design stress variation developed in Section 7.1.1.

The damage tolerance analyses provided design stress levels for structural sizing and material, geometry, and criteria variation effects for concept selection guidance (Section 6.1). Both hole and surface flaws were investigated.

7.2.1.1 Wing Lower Cover - A representative two level spectra, developed from the complete spectra (Reference 1), was used in the wing lower cover analyses. An example of the two level spectra development method is shown in Section 7.2.1.2. The low frequency ground-air-ground (GAG) spectrum element, with the compression stress portion eliminated as non-damaging, was defined as follows:

$\Delta\sigma$ = 10,500 psi, R = 0, f = 23,800 cycles/15,000 hours

The high frequency $\pm$ maneuver and gust spectrum element (Reference 1) was defined as follows:

$\Delta\sigma$ = 4,400 psi, R = 0.48, f = 1,100,000 cycles/15,000 hours

(a) Spar-Skin Cap Joint - The baseline and integral concept skin-spar cap joints were analyzed for flaws at a fastener hole, (see Table XLI, Cases 1, 2, 3, 7, 8, 9, and 13). In an initial analysis, all of the initial flaws, Figure 141, were "grown" simultaneously until the failure crack length of points (2) through (5) in the region of the spar cap and point (1) in the skin were reached. Comparison of the crack growth time-histories established that the cracks of primary importance in determining the structural life and, therefore, the design stress, were the skin crack (1) and spar cap crack (2). Crack (1) growth was best represented with a symmetric model and crack (2) growth was an asymmetric model. The symmetry/asymmetry was determined by checking the slow crack growth history of cracks (3) and (5) relative to that of cracks (2) and (1), respectively. In the subsequent analyses, cracks (3), (4), and (5) were not considered since small structural elements were involved. Failure of the spar cap occurred when crack (2) reached the spar web. At spar cap failure, the skin crack tip stress intensity increased markedly due to the added spar cap load (Figure 142). (NOTE: The modification factor computer code currently does not account for the gradual spar cap load transfer to the skin during crack growth.) For the baseline, the separate non-integral stringers encountered were assumed to remain intact. However, for the integral concept, the skin crack branched and propagated into the stringers as well as the skin. In all cases, the influence of the local proximity of a stringer on the skin crack tip stress intensity was accounted for (Figure 143).

The stress intensity equation for the skin hole corner radius crack (1) growth through the thickness is as follows:

$$\Delta K = \Delta\sigma\sqrt{2a}\ \frac{a_b}{1.12}\ f\left(\frac{L}{r}\right)\beta_{spar\ cap} \quad \text{(Reference 45)} \tag{34}$$

where: $\beta_{spar\ cap}$ = modification factor accounting for the spar cap load transfer (Figure 142)

$L = \dfrac{a}{\sqrt{2}}$

a_b = back surface correction factor for a corner flaw from a hole (Reference 45, Page 176)

$f\left(\frac{L}{r}\right)$ = stress intensity factor coefficient for symmetric cracks at holes (Reference 33, Page 44)

The stress intensity equation used for skin "through" crack (1) growth is as follows:

$$\Delta K = \Delta\sigma\sqrt{\pi a}\ f\left(\frac{a}{r}\right)\beta_{spar\ cap}\,\beta_{stringer} \tag{35}$$

where: $\beta_{stringer}$ = modification factor for stringer load transfer, see Figure 143.

TABLE XLI WING DAMAGE TOLERANCE ANALYSIS SUMMARY LOWER COVER - STATION 117.900

CONCEPT	MATERIAL	STRUCTURE ELEMENT	A_{ST}/A_{TOT}	INITIAL FLAW TYPE AND CRITERIA	DEPOT INSPECTION: DESIGN STRESS	DEPOT INSPECTION: DAMAGE EXTENT AND BASIS	WALK-AROUND INSPECTION: DESIGN STRESS	WALK-AROUND INSPECTION: DAMAGE EXTENT AND BASIS	I AP	CASE NO.
NEW CONCEPT GEOMETRY INTEGRAL SKIN AND STRINGER	SKIN: 7475-T7651 STRINGERS: 7475-T7651 SPAR CAP: 7049-T73	SKIN-SPAR CAP JOINT	(FULL SIZE SPAR CAP) 0.91	FLAWS AT HOLE 0.01"R 0.05" CRITERIA REVISION D	47,739	SPAR CAP BREAKING. INTEGRAL STRINGER BREAKING. SLOW CRACK GROWTH.	37,233	SPAR CAP BREAKING. INTEGRAL STRINGER BREAKING. FAIL SAFE CRITERIA (INITIAL TIME AT a=2")	SKIN 15 CAP 11	1
	SKIN: 7475-T7651 STRINGERS 7475-T7651 SPAR CAP: 7050-T73		(FULL SIZE SPAR CAP) 0.91		53,038	SPAR CAP BREAKING. INTEGRAL STRINGER BREAKING. IMPROVED SPAR CAP MATERIAL. SLOW CRACK GROWTH	34,514	SPAR CAP BREAKING. INTEGRAL STRINGER BREAKING. FAIL SAFE CRITERIA (INITIAL TIME AT a=2")	SKIN 15	2
			(REDUCED SPAR CAP AREA) 0.81	FLAWS AT HOLE 0.01"R 0.02" CRITERIA REVISION D	59,812	SPAR CAP BREAKING. INTEGRAL STRINGER BREAKING. IMPROVEMENT DUE TO REDUCED SPAR CAP AREA. FAIL SAFE CRITERIA	93,778	SPAR CAP BREAKING. INTEGRAL STRINGER BREAKING. IMPROVEMENT DUE TO REDUCED SPAR AREA. FAIL SAFE CRITERIA	CAP 16	3
		SKIN-SPLICE	0.33	FLAWS AT HOLE CRITERIA REVISION D	58,151	STRINGER AT SPLICE AND 2 SUBSEQUENT INTEGRAL STRINGERS BREAKING. SLOW CRACK GROWTH	116,422	STRINGER AT SPLICE AND 2 SUBSEQUENT STRINGERS BREAKING SLOW CRACK GROWTH	15	4
		BASIC	0.33	SURFACE FLAW a/Q = 0.1 .20 CRITERIA REVISION D	53,269	INTEGRAL STRINGERS BREAKING. SLOW CRACK GROWTH.	116,592	INTEGRAL STRINGERS BREAKING. SLOW CRACK GROWTH	15	5
			0.33	0.125 0.25 CRITERIA MARCH 1974	71,516	INTEGRAL STRINGERS BREAKING EFFECT OF MAR. 1974 CRITERIA SLOW CRACK GROWTH	116,572	INTEGRAL STRINGERS BREAKING. SLOW CRACK GROWTH.	15	6
BASELINE GEOMETRY - RIVETED SKIN AND STRINGER	SKIN 7075-T76 STRINGER 7075-T651 SPAR CAP 7075-T6	SKIN - SPAR CAP JOINT	(FULL SIZE SPAR CAP) 0.72	FLAWS AT HOLE 0.01 R .05 CRITERIA REVISION D	39,092	SPAR CAP BREAKING AND STRINGER INTACT	TIME PERIOD = 0		9.5	7
			(REDUCED SPAR CAP AREA) 0.67		37,092	SLOW CRACK GROWTH	13,409	SPAR CAP BREAKING AND STRINGER INTACT. SLOW CRACK GROWTH	9.5	8
			(FULL SIZE SPAR CAP) 0.72	FLAWS AT HOLE 0.01 SIMILAR TO MARCH 1974 CRITERIA [illegible] WITH INTERFERENCE FIT FASTENERS.	49,421 (ESTIMATE BASED ON OTHER CASES)	SPAR CAP [illegible] AND STRINGER INTACT. REDUCED INITIAL FLAW SIZE.	TIME PERIOD = 0		9.5	9
		SKIN - SPLICE	0.33	FLAWS AT HOLE 0.01 R .06 CRITERIA REVISION D	42,511	STRINGER AT SPLICE BREAKS. NEXT STRINGER REMAINS INTACT. SLOW CRACK GROWTH	96,257	STRINGER AT SPLICE BREAKS NEXT STRINGER REMAINS INTACT. SLOW CRACK GROWTH	9.5	10
		BASIC	0.33	SURFACE FLAW .20 CRITERIA REVISION D	33,5[illegible]	STRINGER ENCOUNTERED BY SKIN CRACK REMAINS INTACT SLOW CRACK GROWTH	[illegible],630	STRINGER ENCOUNTERED BY SKIN CRACK REMAINS INTACT. SLOW CRACK GROWTH	9.5	11
				0.125 0.25 CRITERIA [illegible] 1974	[illegible],771	STRINGER ENCOUNTERED BY SKIN CRACK REMAINS INTACT EFFECT OF [illegible] 1974 CRITERIA [illegible]	[illegible]	STRINGER ENCOUNTERED BY SKIN CRACK REMAINS INTACT. EFFECT OF [illegible] 1974 CRITERIA. SLOW CRACK [illegible]	9.5	12
	SKIN 7475-T7651 STRINGER 7475-T7651 SPAR CAP 7050-T73	SKIN SPAR CAP JOINT	(FULL SIZE SPAR CAP) 0.72	FLAWS AT HOLE 0.01 R .06 CRITERIA REVISION D	48,537	SPAR CAP BREAKING AND STRINGER INTACT EFFECT OF MATERIAL [illegible] SLOW CRACK GROWTH	53,106	SPAR CAP BREAKING AND STRINGER INTACT. EFFECT OF MATERIAL [illegible] SLOW CRACK GROWTH	SKIN 15 CAP 16	13

TABLE XLII WING DAMAGE TOLERANCE ANALYSIS SUMMARY - UPPER COVER - STA 117.900

CONCEPT	MATERIAL	STRUCTURE ELEMENT	AST A_{TOT}	INITIAL FLAW TYPE AND CRITERIA	DEPOT INSPECTION		SPECIAL VISUAL INSPECTION		ΔK [1]	CASE NO.
					DESIGN STRESS	DAMAGE EXTENT AND BASIS	DESIGN STRESS	DAMAGE EXTENT AND BASIS		
BASELINE GEOMETRY RIVETED SKIN AND STRINGER	SKIN: 7075-T76 STRINGERS: 7075-T651 SPAR CAP: 7075-T6	SKIN-SPAR CAP JOINT	(FULL SIZE SPAR CAP) 0.72	FLAWS AT HOLE 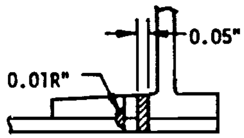 CRITERIA: REVISION D	16475	SPAR CAP BREAKING AND STRINGER INTACT. SLOW CRACK GROWTH.	NOT APPLICABLE. TIME PERIOD=0		9.5	14
		BASIC	0.33	SURFACE FLAW 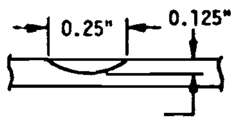 CRITERIA: MARCH 1974	20128	STRINGERS INTACT. MARCH 1974 CRITERIA. SLOW CRACK GROWTH	13418	STRINGERS INTACT. MARCH 1974 CRITERIA. SLOW CRACK GROWTH.	9.5	15
	SKIN: 7050-T76 STRINGER: 7050-T76 SPAR CAP: 7050-T73	SKIN-SPAR CAP JOINT	(FULL SIZE SPAR CAP) 0.72	FLAWS AT HOLE 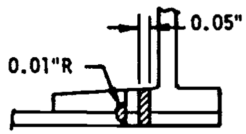 CRITERIA: REVISION D	18636	SPAR CAP BREAKING AND STRINGER INTACT. SLOW CRACK GROWTH.	NOT APPLICABLE. TIME PERIOD=0		16.0	16
BEST NEW CONCEPT GEOMETRY INTEGRAL SKIN AND STRINGER	SKIN: 7050-T7651 STRINGER: 7050-T7651 SPAR CAP: 7050-T73	BASIC	0.33	SURFACE FLAW 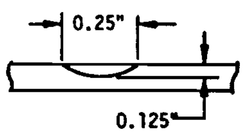 CRITERIA: MARCH 1974	33937	INTEGRAL STRINGERS BREAKING. MARCH 1974 CRITERIA. SLOW CRACK GROWTH.	19023	INTEGRAL STRINGERS BREAKING. MARCH 1974 CRITERIA. SLOW CRACK GROWTH.	16.0	17

1. ΔK at $da/dN = 10^{-5}$ at $R = 0$

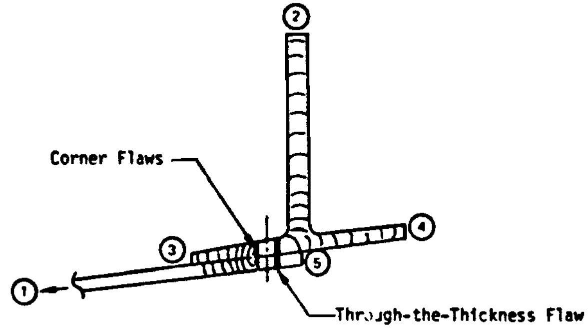

Figure 141 SKIN-SPAR CRACK GROWTH MODEL

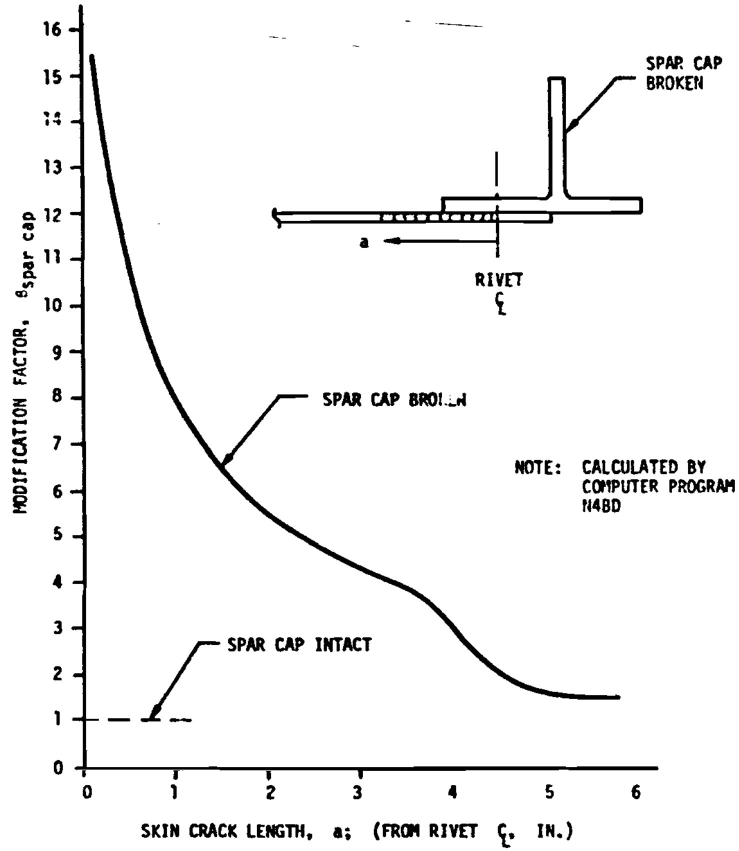

Figure 142 SKIN CRACK TIP STRESS INTEGRITY MODIFICATION FACTOR DUE TO BROKEN SPAR CAP

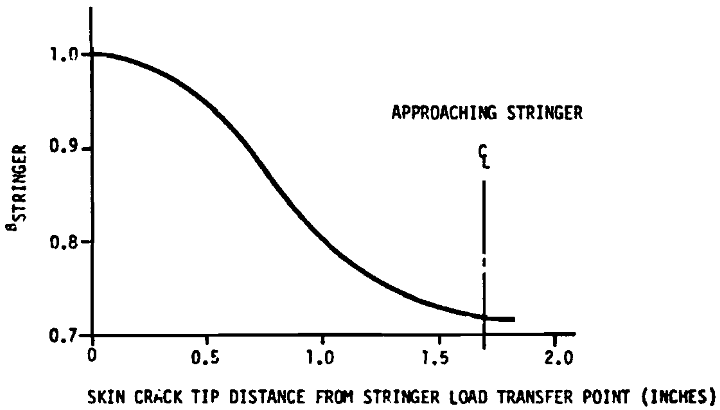

Figure 143 SKIN CRACK TIP STRESS INTENSITY MODIFICATION FACTOR DUE TO STRINGER LOAD TRANSFER

Similarly, the stress intensity equation for spar cap "through" crack (2) growth is as follows:

$$\Delta K = \Delta\sigma\sqrt{\pi a_{equivalent}}\ \lambda \tag{36}$$

where: $a_{equivalent} = a\left[f\left(\frac{a}{r}\right)\right]^2$

= equivalent Griffith crack length (Reference 33, Page 74)

λ = finite width correction (Reference 33)

$f\left(\frac{a}{r}\right)$ = stress intensity factor coefficient for asymmetric cracks at holes (Reference 33)

A numerical example of the methods used in shown in Table XLIII and Figure 144 for the skin crack (1) growth (Case 2, Table XLI). Using slow crack growth criteria, the skin crack (1) growth history was first computed for the spar cap intact (i.e., $\beta_{spar\ cap} = 1$). A similar but separate calculation for spar cap crack (2) growth (with the skin intact) established spar cap failure at 10,460 hours. (NOTE: For the spar cap cases, cap failure was defined at $\frac{da}{dN} \rightarrow \infty$ or the crack reaching the end of spar cap leg, whichever came first.) Skin and integral stringer growth subsequent to spar cap failure is precipitous and provides only a small additional period prior to final failure.

The corner crack and through crack formulations for ΔK were used to calculate the residual strength of the skin, Table XLIV. The residual strength variation is shown in Figure 145. When the required one-time-stress level (determined at 100 times the depot or walk around inspection intervals per Appendix A) equals the residual strength, the maximum safe crack length and, hence, time period is defined.

The one-time-stress levels were derived from the maximum stress versus cumulative frequency data for the complete load spectra of the wing lower panel at Station 117.9 (Figure 146). A cross plot of the data readily identifies the one-time-stress values for the inspection periods considered (Figure 147). For depot inspection, Figure 145 shows no crack arrest since the residual strength curve does not recross above the one-time stress line. Use of slow crack growth criteria to define the initial flaw sizes was, therefore, justified. However, crack arrest does occur for walk-around inspection at a crack length of 5.75 inches, since the dynamic factor requirement was exceeded.

$$\frac{\sigma_{res\ max}}{\sigma_{one\text{-}time}} = \frac{23{,}000}{18{,}750} > 1.15$$

However, the initial flaw sizes were kept unchanged, since the period for walk-around inspection starts at a two-inch crack and therefore is assumed to be relatively unaffected by initial conditions.

TABLE XLIII NUMERICAL EXAMPLE OF SKIN CRACK GROWTH CALCULATIONS FOR WING SKIN-SPAR CAP JOINT WITH SPAR CAP INTACT[1]

TABLE XLIII: NUMERICAL EXAMPLE OF SKIN CRACK GROWTH CALCULATIONS FOR WING SKIN-SPAR CAP JOINT WITH SPAR CAP INTACT[1]

1	2	3	4	5	6	7	8
a	SKIN GAUGE t	a/t	a_b	$\frac{L}{r} = \frac{a}{r\sqrt{2}}$	f(L/r)	$\sqrt{2a}$	$\frac{\Delta k}{\Delta \sigma}$
	STA. 117.9	1/2	REF. 45 p.175	r = 0.125	REF. 33 p. 44	$\sqrt{2 (1)}$	4 6 7/1.12
0.01=a_i	0.162	0.0617	1.0	0.0566	3.0	0.1414	0.3788
0.04	↕	0.247	1.001	0.2262	2.4	0.2828	0.6066
0.07		0.432	1.006	0.3959	2.0	0.3742	0.6722
0.1		0.6173	1.016	0.5656	1.775	0.4472	0.7201
0.16	0.162	0.9877	1.25	0.905	1.51	0.5657	0.9534

1	10	11	12	13	14	15	16	17
a	Δσ	R	f**	Δk	da/dN	fda/dN*	Σfda/dN	$\frac{da}{dt} \times 10^3$
	2 LEVEL SPECTRA			8 10	FIG 140	12 14	Σ 15	16 / 15,000
0.01	10,500	0	23,810	3977	4.2×10^{-8}	0.001	0.00815	0.000543
	4,400	0.48	1,100,000	1677	6.5×10^{-9}	0.00715		
0.04	10,500	0	23,810	6369	2.8×10^{-7}	0.00667	0.07817	0.005211
	4,400	0.48	1,100,000	2669	6.5×10^{-8}	0.0715		
0.07	10,500	0	23,810	7056	4.1×10^{-7}	0.009762	0.1253	0.00835
	4,400	0.48	1,100,000	2958	1.05×10^{-7}	0.1155		
0.1	10,500	0	23,810	7561	5.5×10^{-7}	0.01310	0.1506	0.01004
	4,400	0.48	1,100,000	3168	1.25×10^{-7}	0.1375		
0.16	10,500	0	23,810	10011	1.8×10^{-6}	0.04286	0.4059	0.02706
	4,400	0.48	1,100,000	4195	3.3×10^{-7}	0.363		

1	18	19	20	21	22
a	Δa	a MIDPOINT	$\frac{da}{dt} \times 10^{-3}$	Δt	TIME, HOURS
REFERENCE	Δ1	1 AVERAGE	17 @ $a_{MIDPT.}$	18 / 20	Σ 21
0.01					0
	0.03	0.025	0.003	10,000	
0.04					10,000
	0.03	0.055	0.0065	4,615	
0.07					14,615
	0.03	0.085	0.0093	3,225	
0.1					17,840
	0.06	0.13	0.017	3,295	
0.16					21,134

[1]CASE 2, TABLE XLI *PER 15,000 HOURS **7475-T76

TABLE XLIV NUMERICAL EXAMPLE OF SKIN CRACK RESIDUAL STRENGTH[1] CALCULATIONS

CORNER CRACK

1	2	3	4	5	6	7	8	9	10	11
a (in)	SKIN GAUGE (IN.)	a/t	a_b	$\frac{L}{r} = \frac{a}{r\sqrt{2}}$	$f(\frac{L}{r})$	$\sqrt{2a}$	β SPAR CAP	$\Delta K/\Delta\sigma$	K_c	SKIN σ_{max} RESIDUAL STRENGTH
	STA. 117.9	1/2	REF 45 PAGE 175	r = 0.125	REF 43 PAGE 44	$\sqrt{2}$ 1	FIG. 100	4 6 7 8 / 1.12	7475-T76	10 / 9
0.01	0.162	0.0617	1.000	0.0566	3.000	0.1414	1.0	0.3788	145,000	382,788
0.04	0.162	0.2470	1.001	0.2262	2.400	0.2628	1.0	0.6066	145,000	239,037
0.07	0.162	0.4320	1.006	0.3959	2.000	0.3742	---	---	145,000	---
0.10	0.162	0.6173	1.016	0.5656	1.775	0.4472	15.3	11.018	145,000	13,160
0.16	0.162	0.9877	1.250	0.9050	1.510	0.5657	14.7	14.015	145,000	10,346

THROUGH CRACK

1	2	3	4	5	6	7	8	9
a	a/r	$f(\frac{a}{r})$	$\sqrt{\pi a}$	β SPAR CAP	β STRINGER	$\Delta K/\Delta\sigma$	K_c	SKIN σ_{max} RESIDUAL STRENGTH
	r = 0.125	REF 43P44	$\sqrt{\pi (1)}$	FIG. 142	FIG. 143	3 4 5 6	7475-T76	8 / 7
0.5	4.0	1.100	1.2533	11.00	1.00	15.165	145,000	9,561
1.0	8.0	1.035	1.7725	8.00	1.00	14.676	145,000	9,882
1.5	12.0	1.015	2.1713	6.45	1.00	14.215	145,000	10,200
2.0	16.0	1.000	2.5063	5.50	1.00	13.783	145,000	10,520
2.5	20.0	1.000	2.8023	4.80	1.00	13.450	145,000	10,780
3.0	24.0	1.000	3.0700	4.30	1.00	13.201	145,000	10,984
3.5	28.0	1.000	3.3163	3.85	1.00	12.766	145,000	11,358
4.0	32.0	1.000	3.5450	3.05	0.985[2]	10.650	145,000	13,615
4.5	36.0	1.000	3.7595	2.05	1.00	7.708	145,000	18,812
5.0	40.0	1.000	3.9633	1.60	1.00	6.341	145,000	22,867
5.5	44.0	1.000	4.1565	1.50	1.00	6.236	145,000	23,252
7.0	56.0	1.000	4.6900	1.50	1.00	7.035	145,000	20,611

(1)CASE 2, TABLE XLI (2)The skin crack a = 4.4" at stringer failure

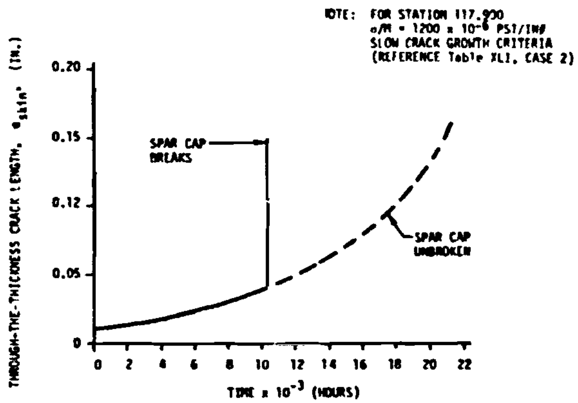

Figure 144 EXAMPLE SKIN CRACK-HISTORY FOR WING SKIN-SPAR CAP JOINT

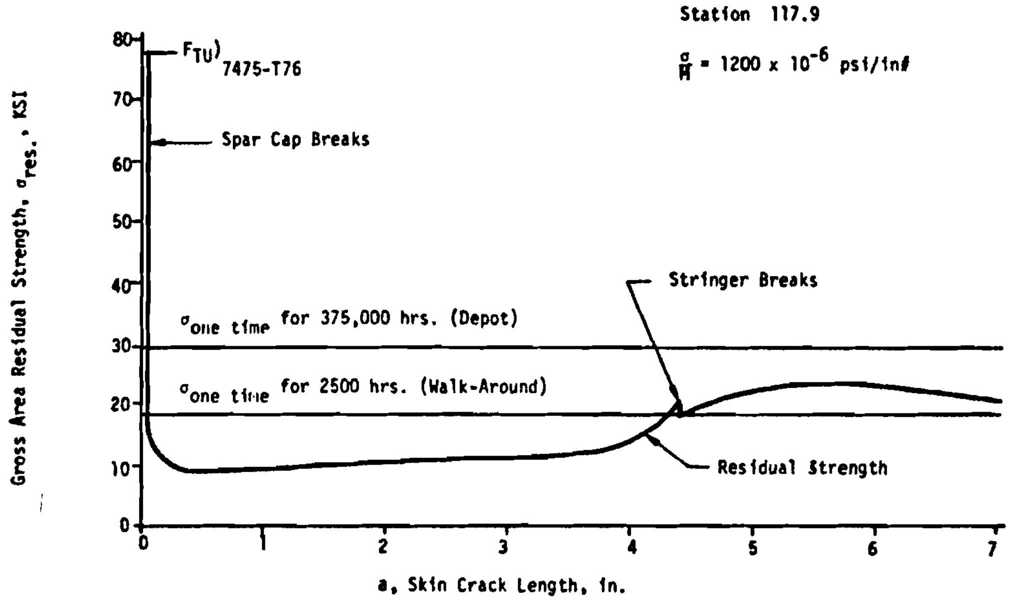

Figure 145 EXAMPLE SKIN RESIDUAL STRENGTH VARIATION FOR THE SKIN-SPAR CAP JOINT

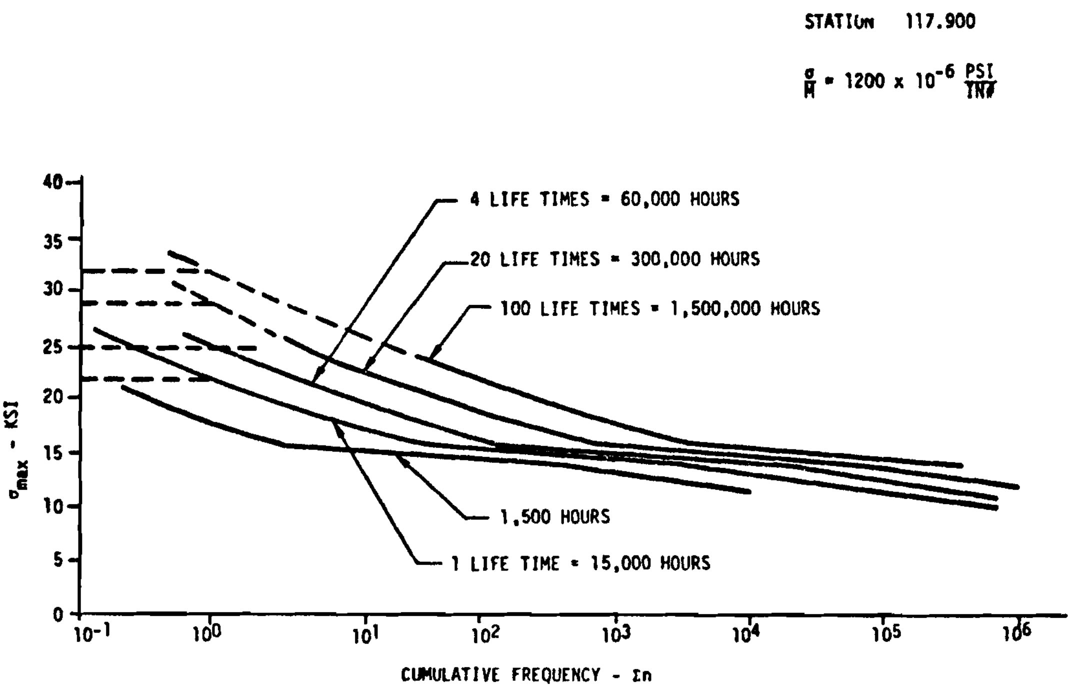

Figure 146 MAXIMUM STRESS vs CUMULATIVE FREQUENCY FOR THE WING

For depot inspection, the safe time period was approximately 10,460 hours (Figure 145). The associated reference design stress (σ_1) corresponding to the design bending moment (Reference 1) was 46,080 psi. The critical element was the 7050-T73 cap, for which the Forman equation exponent n = 2.376. Using the stress/period relation developed in Section 7.2.,

$$\sigma_2 = \sigma_1 \left(\frac{T_1}{T_2} \right)^{1/n} \tag{37}$$

where: T_2 = 7500 = 2x Depot Inspection Interval (Appendix A)

$$\sigma_2 \approx 46{,}080 \left(\frac{10{,}461}{7{,}500} \right)^{1/2.376} = 53{,}038 \text{ psi} = F_{T_{\text{Damage Tolerance}}}$$

For walk-around inspection, the crack is in an arrested state from 4.5 inches to 7.25 inches (Figure 145). The time period for the arrested portion was calculated to be 63 hours using the method for the corner radius crack shown previously. The minimum crack size for walk-around inspection is 2 inches; therefore, the total period was also 63 hours since the crack was fast running between 2 inches and 4.5 inches, i.e., zero time. The design stress was calculated as:

$$\sigma_1 \approx 46{,}080 \left(\frac{63}{125} \right)^{1/2.376} = 37{,}233 \text{ psi} = F_{T_{\text{Damage Tolerance}}}$$

where: T_1 = 5 x walk around interval = 125 hours (Appendix A)

T_2 = 63 hours

Therefore, the lightest structure for the skin-spar cap joint for the wing lower cover (Case 2, Table XLI) was obtained using the higher capability level associated with depot inspection (Figure 148).

A summary of the skin-spar cap joint damage tolerance analysis results appears in Table XLI, Cases 1, 2, 3, 7, 8, 9 and 13.

(b) Skin-Splice - The baseline and integral concept spanwise skin splices were analyzed for flaws at a fastener hole (Figure 149). Skin crack (1) and stringer crack (2), shown in the figure, determined the time period and, hence, the design stress for the splice structure. The crack growth model symmetry/asymmetry selection was guided by the skin-spar cap joint analysis previously discussed. The residual strength and design stress calculation methods were also the same as those used for the skin-spar cap joint. The baseline "approaching" stringer was assumed to remain intact. The integral concept "approaching" stringer was subject to crack growth as shown in Figure 149. The results of the skin-splice analyses are summarized in Table XLI (Cases 4 and 10).

(c) Surface Flaws - The baseline and integral concept wing skins were analyzed for the surface flaw geometry shown in Figure 150. The crack was

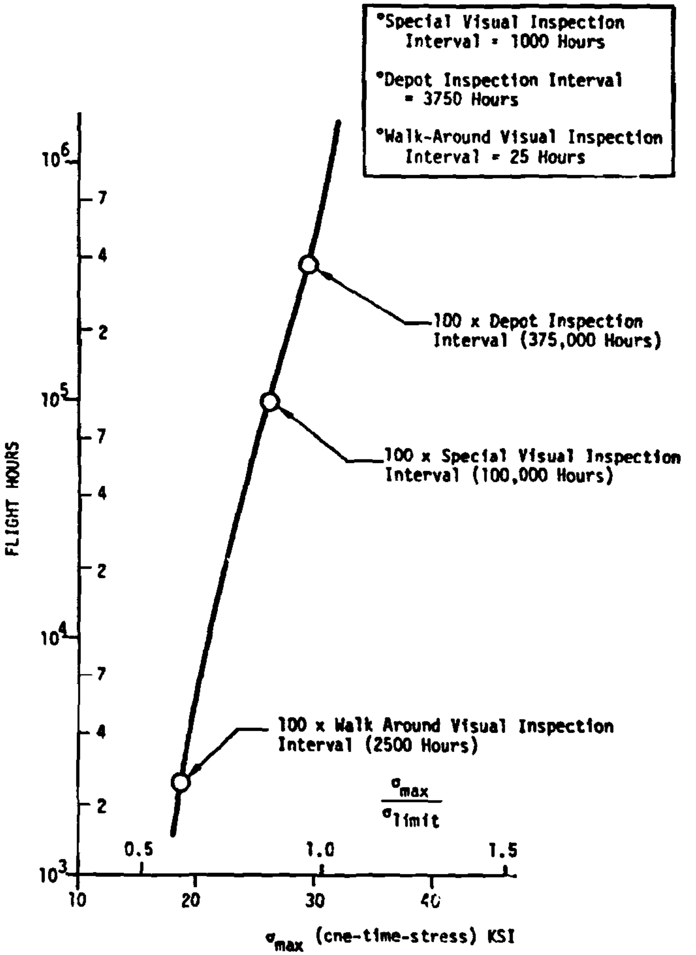

Figure 147 ONE-TIME-STRESS vs FLIGHT HOURS FOR THE WING

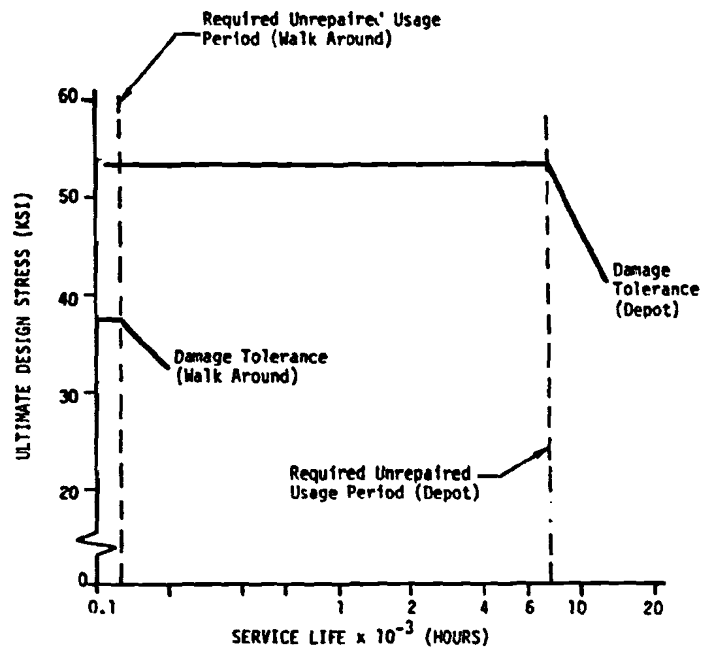

Figure 148 DAMAGE TOLERANCE DESIGN STRESSES FOR THE WING INTEGRAL CONCEPT (LWR SKIN REAR SPAR CAP JOINT - STA 117.900)

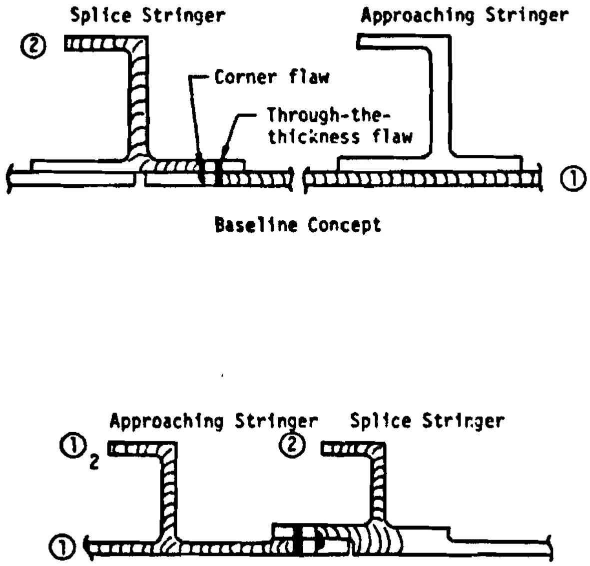

Crack Tip Stress Intensity Relations:

<u>Skin Crack ①</u>

$$\Delta K = \frac{\Delta\sigma\sqrt{\pi a}_{\text{equivalent}}\ \beta_{\text{approaching stringer}}\lambda}{\beta_{\text{splice stringer}}}$$

<u>Spar Cap Crack ②</u>

Corner Crack:

$$\Delta K = \Delta\sigma\sqrt{2a}\left(\frac{a_b}{1.12}\right)\left[\left(f\ \frac{L}{r}\right)_{\text{symmetric}}\right]\lambda$$

Through Crack:

$$\Delta K = \Delta\sigma\sqrt{\pi a}\left[f\left(\frac{a}{r}\right)_{\text{symmetric}}\right]\lambda$$

where: the terms are as described for the skin-spar cap joint.

Figure 149 WING SKIN-SPLICE CRACK GROWTH MODELS

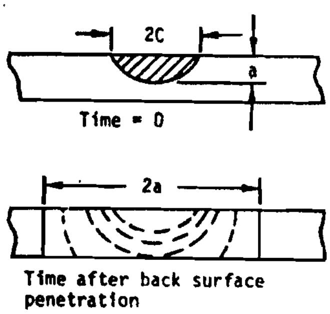

Crack Tip Stress Intensity Relations:

<u>Part-through Crack</u>

$$\Delta K = 1.1\ \Delta\sigma M_K\left(\frac{\pi a}{Q}\right)^{1/2}$$

<u>Through Crack</u>

$$\Delta K = \Delta\sigma\sqrt{\pi a}\ \beta_{\text{stringer}}$$

where:

M_K = Elastic stress magnification factor for deep surface discontinuities in tension (Ref. 33, p 121)

Q = Flaw shape parameter (Ref. 33, p 120)

All other terms are as described for the skin-spar cap joint.

Figure 150 WING STRUCTURE SURFACE FLAW CRACK GROWTH MODEL "grown" through the thickness to back-surface-penetration and then continued as a through-the-thickness crack to failure. The calculation methods used for crack growth, residual strength and design stress were the same as previously described in the skin-spar cap numerical example. The surface flaw analysis results are tabulated in Table XLI (Cases 5, 6, 11, and 12).

7.2.1.2 Wing Upper Cover - A two level spectra based on ground-air-ground (GAG) and taxi elements was developed for the wing upper cover analysis. The low frequency equivalent-spectrum-element was defined from the full GAG spectrum with the compression stresses eliminated:

$$\Delta\sigma = 7491 \text{ psi}, \; R = 0, \; f = 23{,}800 \text{ cycles/15,000 hours}$$

The high frequency equivalent-spectrum-element was defined from the full taxi spectrum (Reference 1).

$$\Delta\sigma = 2{,}548 \; R = 0.6, \; f = 5{,}115{,}232 \text{ cycles/15,000 hours}$$

The taxi equivalent-spectrum-element calculation is shown in Table XLV to illustrate the method used in computing all of the truncated damage tolerance spectra used in the study.

On the basis of wing lower cover data, the baseline and integral concept skin-spar cap joints were identified as the most critical location for upper cover analysis. The results of the analysis, using the methods and models described in Section 7.2.1.1, are presented in Table XLII.

7.2.1.3 Parameter Sensitivity Studies - Damage tolerance was the critical mode for much of the inboard upper and lower cover structure of the initial baseline (7075 aluminum) wing. Information on the effect of material, geometry, and criteria changes on damage tolerance was therefore developed, which in conjunction with the concept selection charts (Section 6.2.1), provide design guidance for improving the wing concept. Crack growth resistance was increased in the new concepts by incorporating material and geometry changes and in the initial baseline by material changes only.

Damage tolerance analyses of the initial baseline wing are described in Tables XLI and XLII (Cases 7, 10, 11 and 14). As indicated, use of walk-around inspection (in lieu of depot inspection) criteria eliminated surface flaws and skin-splice hole flaws in the wing lower cover from being critical for design. For the upper surface, however, special visual inspection criteria applied instead of walk-around, so that surface flaws could be critical and, hence, were considered (Table XLII, Cases 15 and 17). The skin-spar cap joint was a critical flaw location for both the lower and upper covers.

Spar cap thickness (hence, area) reduction was studied (Table XLI, Case 8 vs Case 7) to define the effect on the skin crack tip stress and period. The associated load reduction effect under broken spar cap conditions is seen in the residual strength diagram (Figure 151) where the residual strength improvement also improves the walk-around inspection period and hence the design stress. The effect is more pronounced under improved material conditions (Table XLI, Case 3 versus 2).

The effect of changing materials was also studied (Table XLI, Case 13 vs 7).

TABLE XLV TAXI SPECTRUM TRUNCATION (TYPICAL)

1	2	3	4	5	6	7	8	9	10	11	12	13	14	15	16	17	18
									$a = 3.0$, $\Delta K/\Delta\sigma = 3.07$			$a = 0.3$, $\Delta K/\Delta\sigma = 0.97$			$a = 0.05$, $\Delta K/\Delta\sigma = 0.3963$		
GROUND Δn_{cg} * $\Delta\sigma$	n (TAXI) *	$1 + \Delta\sigma$	$1 - \Delta\sigma$	σ_{max} **	σ_{min}	R	f	$\Delta\sigma$	ΔK	da/dN @ R = 0	f(da/dN)	ΔK	da/dN @ R = 0	f da/dN	ΔK	da/dN @ R = 0	f da/dN
MID-POINT	REFERENCE 1	MID-POINT	MID-POINT	5096 (3)	5096 (4)	(6) / (5)	(2) / (4)	(5) - (6)	3.07 (9)	7050-T73	(8) (11)	0.9703 (9)	7050-T73	(8) (14)	0.3963 (9)	7050-T73	(8) (17)
0.15	24,796,000	1.15	0.85	5,860	4,332	0.739	6,199,000	1,528	4,691	3.30×10^{-7}	2.04570	1,483	1.40×10^{-8}	0.086800	606	1.60×10^{-9}	0.0099180
0.25	6,964,000	1.25	0.75	6,370	3,822	0.600	1,741,000	2,548	7,822	1.40×10^{-6}	2.43740	2,474	6.00×10^{-8}	0.104500	1,010	5.00×10^{-9}	0.0087100
0.35	1,928,000	1.35	0.65	6,880	3,312	0.481	482,000	3,568	10,954	3.70×10^{-6}	1.78340	3,464	1.35×10^{-7}	0.065100	1,414	1.35×10^{-8}	0.0065100
0.45	309,466	1.45	0.55	7,389	2,803	0.379	77,367	4,586	14,070	7.10×10^{-6}	0.54930	4,452	2.70×10^{-7}	0.020900	1,817	2.60×10^{-8}	0.0020100
0.55	46,615	1.55	0.45	7,899	2,293	0.290	11,654	5,606	17,210	1.25×10^{-5}	0.21510	5,442	5.00×10^{-7}	0.005830	2,222	4.40×10^{-8}	0.0005130
0.65	6,070	1.65	0.35	8,408	1,784	0.212	1,518	6,624	20,336	2.05×10^{-5}	0.03110	6,431	8.10×10^{-7}	0.001230	2,625	6.40×10^{-8}	0.0000970
0.75	827	1.75	0.25	8,918	1,274	0.143	207	7,644	23,467	3.10×10^{-5}	0.00642	7,421	1.20×10^{-6}	0.000250	3,029	9.60×10^{-8}	0.0000200
0.85	122	1.85	0.15	9,428	764	0.081	31	8,664	26,598	4.40×10^{-5}	0.00136	8,411	1.65×10^{-6}	0.000051	3,434	1.35×10^{-7}	0.0000041
0.95	17	1.95	0.05	9,937	255	0.030	4	9,682	29,724	5.70×10^{-5}	0.00023	9,399	2.35×10^{-6}	0.000009	3,837	1.85×10^{-7}	---
1.05	3	2.05	-0.05	10,447	-255	-0.020	1	10,702	32,855	8.00×10^{-5}	---	10,390	2.90×10^{-6}	---	4,241	3.00×10^{-7}	---
											$\Sigma = 0.28467$			$\Sigma = 0.28467$			$\Sigma = 0.0277824$

*Per 60,000 hours; ** 1g = 5096 PSI; *Per 15,000 hours

<u>Calculation For Equivalent Taxi Spectrum</u>

(a) Most damaging level is @ $\Delta n_{cg} = 0.25$; $R = 0.6$; $\Delta\sigma = 2{,}548$

(b) Adjust frequency to give same total damage using

$$f_{eg} = \frac{\Sigma f\,(da/dn)}{f\,(da/dn)_{\Delta g = 0.25}} \times f_{\Delta g = 0.25}$$

a	$f_{eg}/f_{\Delta g = 0.25}$
3.0	2.9006
0.3	2.7241
0.05	3.1897
Average	2.9381

(c) Use average factor to obtain equivalent frequency,

$$f_{eg} = 1{,}741{,}000 \times 2.9381 = 5.115 \times 10^6 \text{ cycles/15000 hours.}$$

(d) Resulting Equivalent Taxi Spectrum For 15000 hours is.

$R = 0.6$; $\Delta\sigma = 2{,}548$ psi; $f_{eg} = 5.115 \times 10^6$ cycles.

The skin and stringers were changed to 7475-T7651 and the spar cap to 7050-T73 from 7075-T651 and 7075-T6, respectively. The improvement is shown in Figure 152. One of the material change effects was to improve the residual strength capability such that walk-around inspection criteria provided a higher allowable design stress than depot inspection.

The effect of a criteria change was also investigated (Table XLI, Case 9 vs 7). The March 1974 tentative USAF Damage Tolerance Criteria (Table XLVI) includes an initial flaw size of 0.005" R for holes with interference fit fasteners which is much less severe than the Revision D criteria requirement of a 0.05" through-the-thickness initial flaw (Slow Crack Growth). Extrapolating data for a 0.01" R initial corner flaw and for 0.02" and 0.05" initial through-the-thickness flaws, the design stress for a 0.005" R initial corner flaw was estimated to be 51,750 psi, a 33% improvement for an initial baseline skin-spar cap joint.

A comparison of March 1974 tentative USAF surface flaw criteria (Table XLVI) to that of Revision D (Appendix A) was also made using the lower wing cover (Table XLI, Cases 11 and 12). As indicated in the Table, although a considerable improvement was achieved for the depot inspection design stress, the design stress for walk-around inspection did not change since the criteria change affected only the time period occurring before the specified 2" minimum crack size. For the upper wing cover, where walk-around inspection is not applicable, the tentative March 1974 surface flaw criteria was used to compute the upper cover design stress (Table XLI, Cases 15 and 17).

7.1.2.4 Wing Damage Tolerance Summary - As previously stated, all damage tolerance calculations for the wing were made at Station 117.9 to take advantage of existing project group data. Damage tolerance design data for the four wing check stations were then obtained by extending the Station 117.9 data as described. Improved baseline and integral concept design stresses for the check stations are plotted in Figures 153 thru 155. These stresses are based on the March 1974 tentative USAF Damage Tolerance Criteria (Table XLVI) for surface flaws and for holes (interference fasteners required everywhere). These stresses were compared to the allowable tensile stresses for the other integrity modes and the most critical values used for design.

7.2.2 Fuselage Shell Structure

Damage tolerance analyses were also performed on the baseline and on the honeycomb concept fuselages. These analyses included both flaws at rivet holes and surface flaws. The analysis procedures followed the approach presented in Section 7.2.1. As in that approach, modification factors were obtained which, for the baseline, were for a cracked center longeron (longitudinal loads) and for a cracked center frame rip stopper (hoop loads). The honeycomb concept required a modification factor to account for the effect of the uncracked sheet.

Development of the equivalent spectra followed the approach indicated in Section 7.2.1. The various environmental modes were considered for longitudinal loads and for hoop loads. For the longitudinal loads, these included: low level maneuver plus gust, flight maneuver, fuselage pressurization, flaps down flight (for aft fuselage only), and ground taxi. Preliminary work indicated that almost all the damage was due to low level maneuver plus gust and

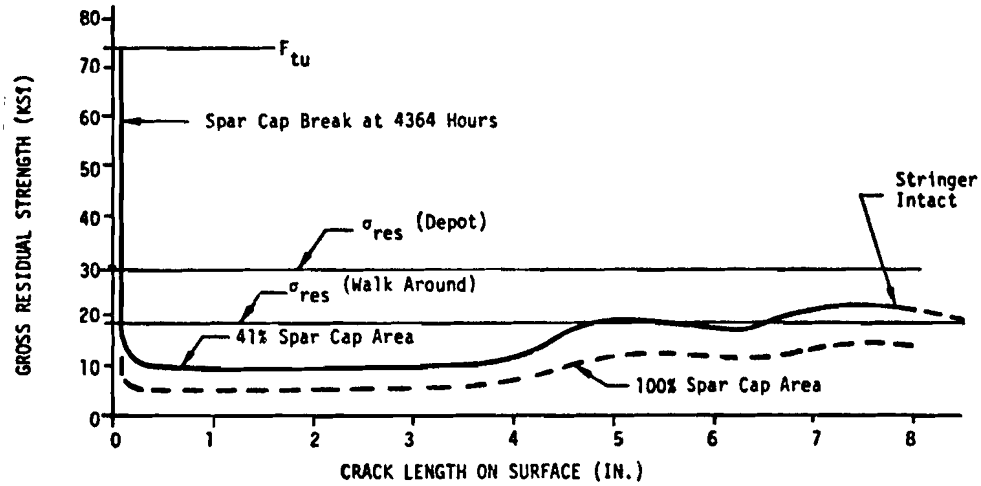

Figure 151 EFFECT OF SPAR CAP AREA REDUCTION ON WING SKIN RESIDUAL STRENGTH

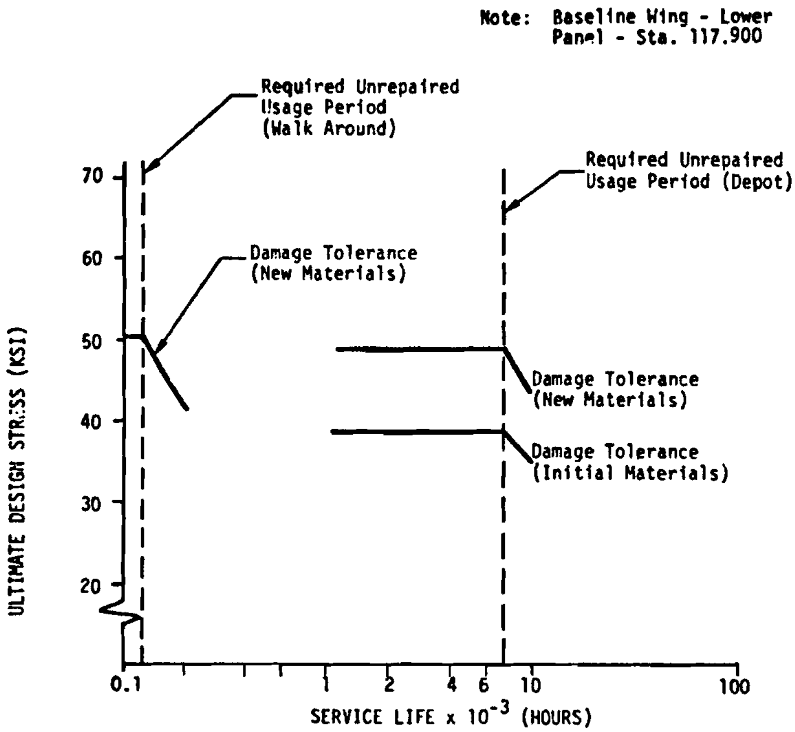

Figure 152 EFFECT OF NEW MATERIALS ON WING DAMAGE TOLERANCE CAPABILITY

TABLE XLVI		TENTATIVE (MARCH 1974) USAF DAMAGE TOLERANCE CRITERIA	
CATEGORY		MARCH 1974 TENTATIVE INITIAL FLAW SIZES	
SLOW CRACK GROWTH STRUCTURE	AT HOLES	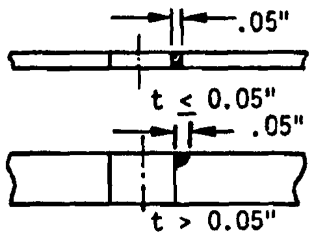	
	OTHER THAN AT HOLES	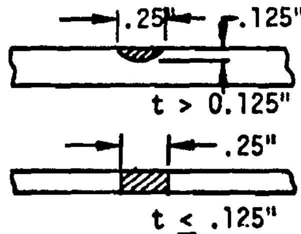	
FAIL SAFE STRUCTURE	AT HOLES	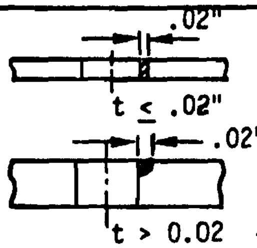	Not defined in present version, but these will be the most likely sizes in the issued version after discussion with Air Force Review team.
	OTHER THAN AT HOLES	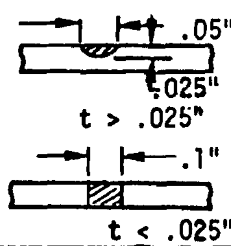	
Initial flaws at every hole from Day 1		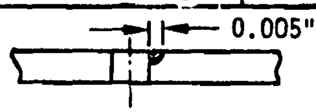	
Initial flaws at holes with interference fit fasteners			

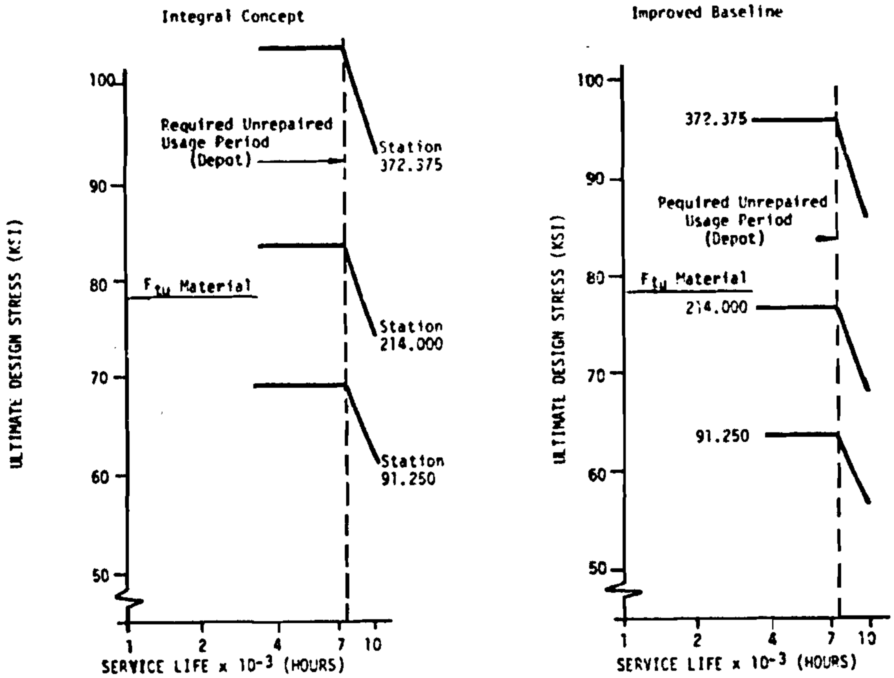

Figure 153 DAMAGE TOLERANCE DESIGN STRESSES FOR THE WING LOWER SKIN-SPAR CAP JOINT (HOLE FLAW CASE)

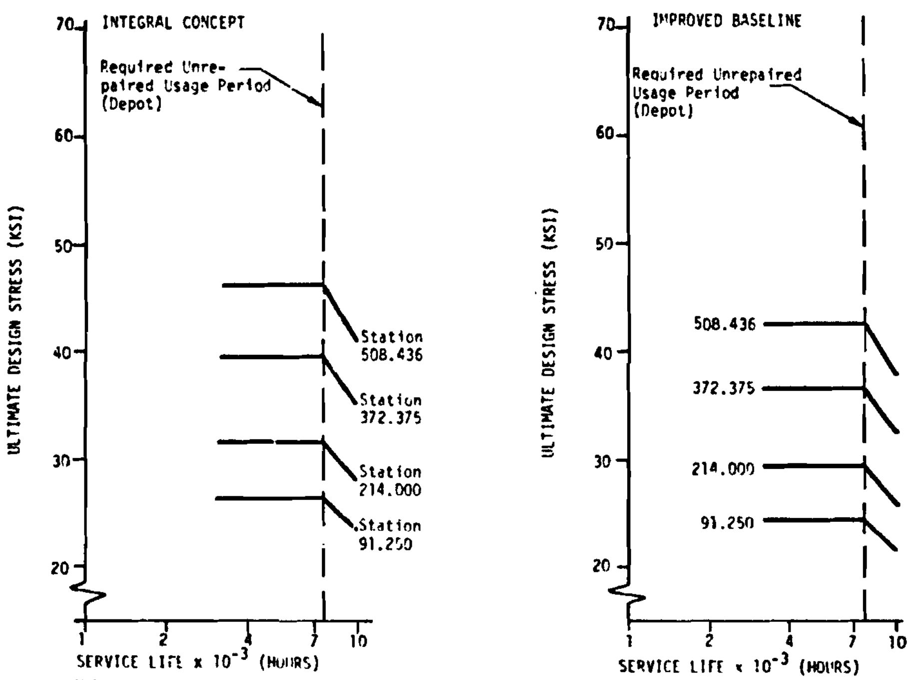

Figure 154 DAMAGE TOLERANCE DESIGN STRESSES FOR THE WING UPPER SKIN-SPAR CAP JOINT (HOLE FLAW CASE)

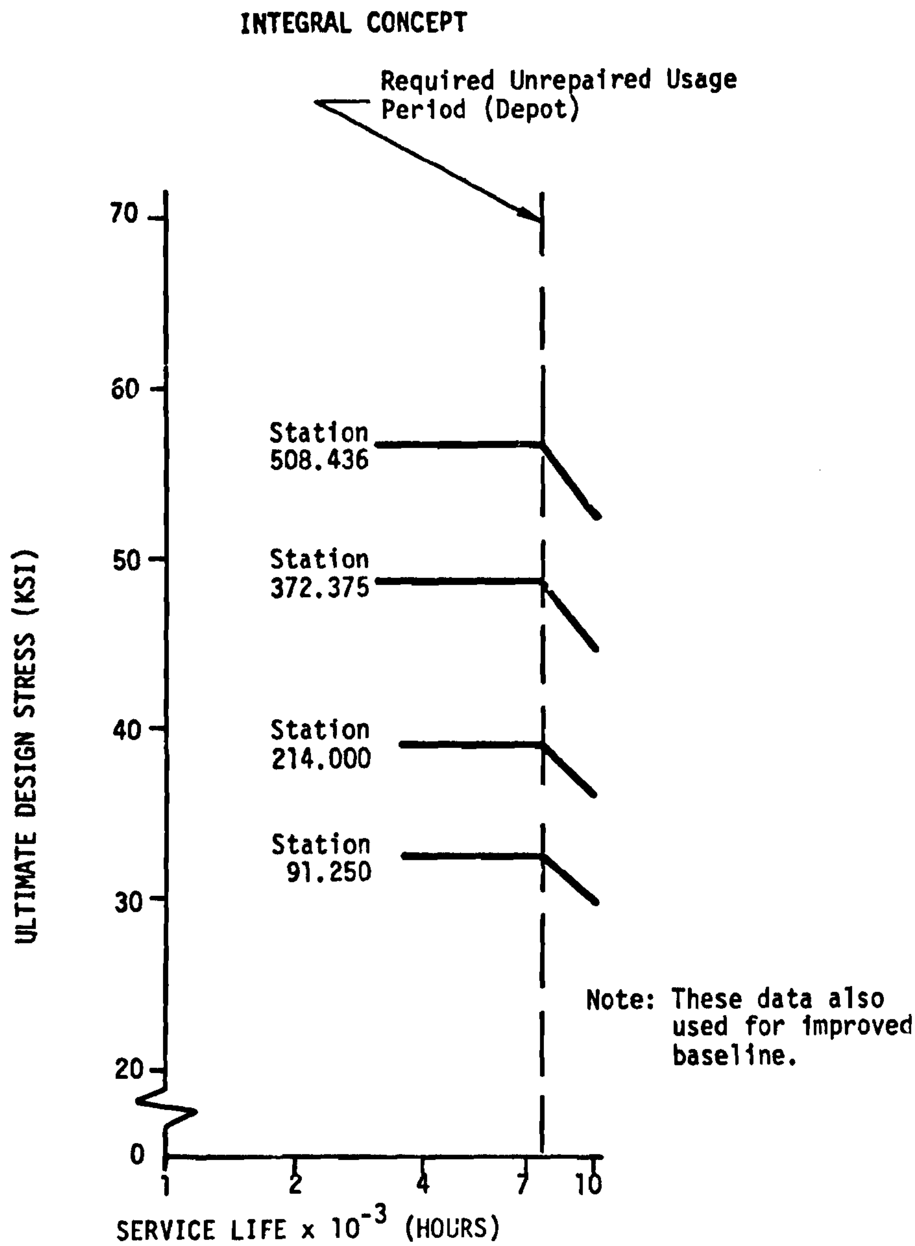

Figure 155 DAMAGE TOLERANCE DESIGN STRESSES FOR THE WING UPPER PANEL (SURFACE FLAW CASE)

ground taxi, so only these were included in the final simplified spectra. Hoop loads were limited to fuselage pressurization.

These analyses established that the critical damage tolerance mode resulted from hoop loading. Positive margins of safety based on stress are:

Concept	Station	M.S.	Inspectability
Baseline	667	+0.54	Depot
Honeycomb	703*	+0.97	Special Visual

(*Note: Analysis point is typical of station 703 forward)

7.2.2.1 Baseline Fuselage - The baseline fuselage concept is described in Section 5.2.1. The analyses are based on initial baseline materials. The initial baseline included three basic sizes of 7075-T6511 extruded stringers 0.05 to 0.08 inches thick, 2024-T3 clad skins, 1.0 inch wide by .05 inch thick 7075-T6 crack stopper under each longeron and frame; and a heavy floor structure designed for vehicle loads. The section properties for use with the damage tolerance analysis are based on fully effective skin because of the relatively low stresses involved. The floor is included and also considered fully effective. These section properties are presented in Table XLVII for the four check stations--439, 703, 847 and 982.

One g inertia bending moments for each mission at stations 725 and 847 are in Reference 42. These were extrapolated to the four check stations. The moments at stations 847 and 932 were further increased by the effect of an average one g down balancing tail load of 3800 pounds, and the final moments were used with the section properties of Table XLVII to get one g flight stress levels. Maneuver plus gust cumulative frequency data in conjunction with 1g flight stress levels for each mission were used to get the average one g stress flight level shown in Table XLVIII.

On the basis of maximum one g flight stress levels, Station 847 was identified as the critical area. A two level spectra comprised of low level maneuver plus gust and ground taxi was derived for this station, in the manner shown in Section 7.2.1 for the wing upper cover. The resulting spectra are shown in Table XLIX.

(a) Hoop Crack Analysis For Station 847 - Hoop cracks were grown simultaneously in the longeron and in the sheet. When the longeron failed, the skin growth rate was accelerated by the modification factor $\beta_{1 \text{longeron}}$ (Figure 156). The load spectra of Table XLIX, however, resulted in very low da/dn rates, such that the hoop crack case was obviously not critical and the crack history calculations therefore were not completed. The residual strength requirement, however, was defined from fuselage maximum stress exceedance versus cumulative frequency of occurrence data for the baseline (Figure 157). The one time occurrence maximum stress values are plotted on Figure 158 with the required residual strength corresponding to the maximum expected load in 100 times the applicable inspection interval (Table L).

(b) Longitudinal Crack Analysis for Station 667 - Longitudinal cracks result

TABLE XLVII BASELINE FUSELAGE SECTION PROPERTIES

STATION	CONDITION	I $(IN^4)(10^3)$	C_{UPPER} (IN)	C_{LOWER} (IN)	$C_{UPR/I}$ (IN^{-3})	$C_{LWR/I}$ (IN^{-3})
439	For	428.7	140.8	75.2	0.000328	0.000175
703 (FWD)	Damage	488.8	136.4	79.6	0.000279	0.000163
847 (AFT)	Tolerance	408.8	139.7	76.3	0.000275	0.000150
982	Analysis	508.8	139.7	76.3	0.000275	0.000150

TABLE XLVIII SUMMARY OF AVERAGE ONE "g" FLIGHT STRESSES

MISSION	σ_{1g} (KSI)				Σf
	STA 438	STA 703	STA 847	STA 982	
1(0)	0.7	1.6	3.4	2.3	142,497
1(R)	0.7	1.6	3.4	2.3	152,001
2(0)	0.9	1.9	3.5	2.4	25,224
2(R)	0.9	1.9	3.5	2.4	26,411
3	0.4	0.9	3.2	2.2	7,741
4	0.7	1.6	3.4	2.3	2,437,645
5	0.4	0.9	3.2	2.2	979,977
$(\sigma_{1g})_{ave}$	0.7	1.4	3.4	2.3	

NOTE: $(\sigma_{1g})_{ave} = \frac{\Sigma(\sigma_{1g})(\Sigma f)}{\Sigma(\Sigma f)}$

TABLE XLIX STA. 847 LONGITUDINAL LOAD SPECTRA

MODE	f (CYCLES)	$\Delta\sigma$ (PSI)	R
LOW LEVEL MANEUVER PLUS GUST	3.56×10^6	1360	+0.67
GROUND TAXI	8.00×10^6	1290	+0.68

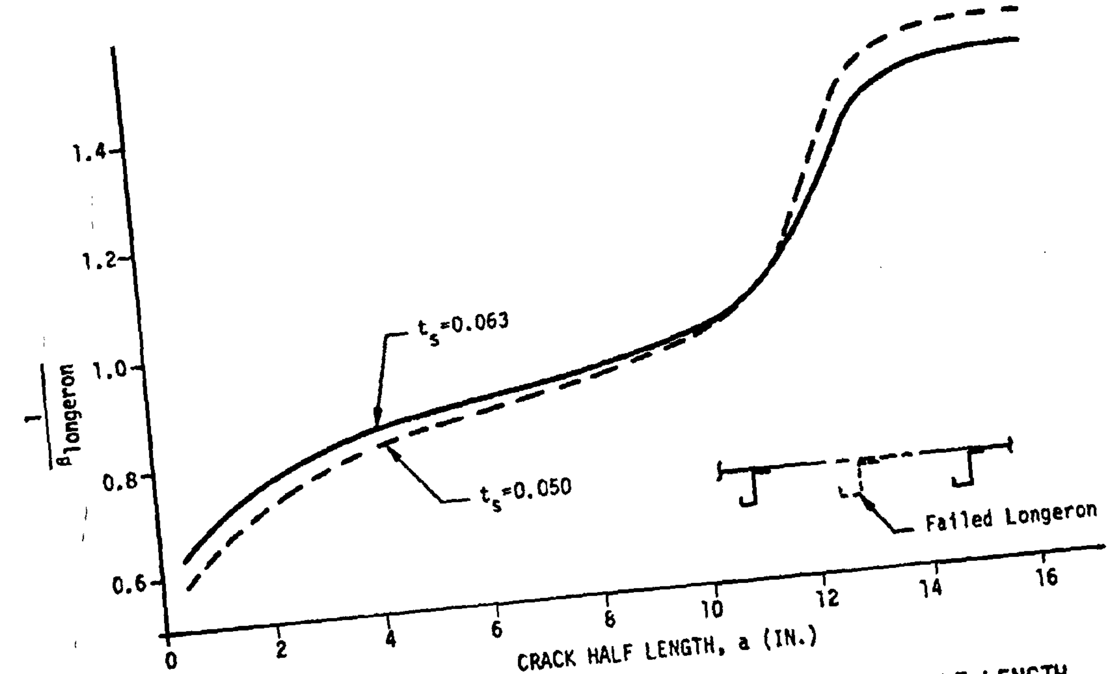

Figure 156 MODIFICATION FACTOR ($\beta_{longeron}$) VS CRACK HALF LENGTH (a) FOR FAILED CENTER LONGERON

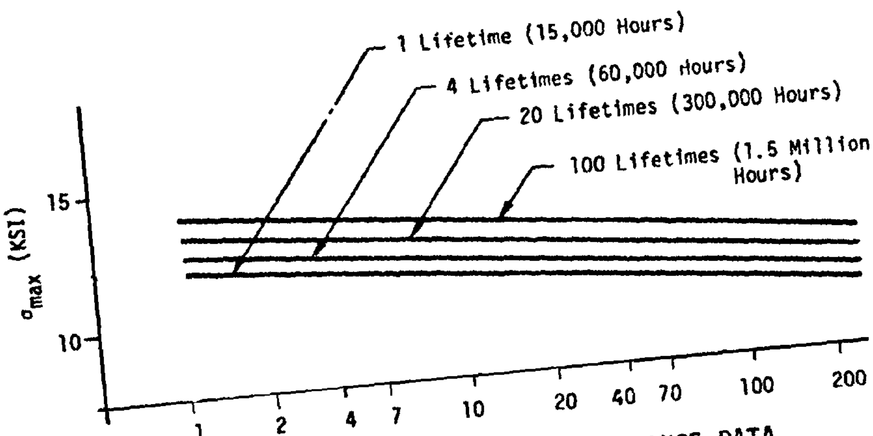

Figure 157 FUSELAGE MAXIMUM STRESS EXCEEDANCE DATA

from cyclic pressure loads. The maximum hoop stress is in the .050 minimum gage area of the forward barrel including Station 667, top centerline. The nominal operating pressure is 7.5 psid, giving a hoop stress of 7.5 x 108/.05 = 16200 psi. The number of pressure cycles was defined by including all missions except the low altitude flights of Mission 4 (23,944 - 4,324 = 19,431; Reference 42, Page 24) giving approximately 19,500 cycles. The resulting load spectrum was:

$\Delta\sigma = \sigma_{max} = 16200$ psi,

$R = 0$, and
$n_i = 19{,}500$ cycles.

The analysis considered a crack growing simultaneously in a crack stopper (1 x 0.05 inch thick, 7075-T6 sheet) and in the skin. The failure effect of the crack stopper on the skin growth rate was accounted for by the modification factor, $\beta_{crack\ stopper}$, (Figure 159). Fast fracture in the skin occurred at the half crack length a, equal to approximately 7.5 inches at 19,000 flight hours, as defined by the residual strength level falling below the requirements level. The minimum residual strength requirement in this case is the maximum pressure stress $\sigma_{max} = 16{,}200$ psi.

For study and design convenience, the damage tolerance capability is expressed in terms of the maximum ultimate tensile stress at Station 667 top centerline. The critical external loads (Section 2.2.1) show a maximum bending moment of 45.5×10^6 inch pounds ultimate, tension top centerline. Ultimate cabin pressure differential is 11.25 psid. Section properties at Station 667 are similar to those at Station 439 (see Table XLVII). Then, the maximum ultimate tensile stress is:

$$f_{t_{(ult)}} = Mc/I + PR/2t_{eff} \approx 23{,}600 \text{ PSI} \tag{38}$$

Only special visual and depot inspections apply to the top of the fuselage. The reference tensile stress (F) corresponding to the associated unrepaired usage period ($T_{req'd}$) was established through the following relation developed in Section 7.2.1

$$\sigma_{req'd} = \sigma_1 \left(t_1/T_{req'd}\right)^{1/n} = F \tag{39}$$

where: σ_1 is the maximum ultimate tensile stress = 23,600 psi,

T_1 is the corresponding period = 19,000 hours, and

n = 3.666 is the slope of the da/dn curve for 2024-T3 sheet in the region of 10^5 cycles.

Depot inspection gave the lightest structure with a design allowable stress (F) of 30,400 psi corresponding to the 7500 hour period of unrepaired service usage. This is equivalent to a margin of safety of (30,400/23,600) - 1 = 0.20, Table LI.

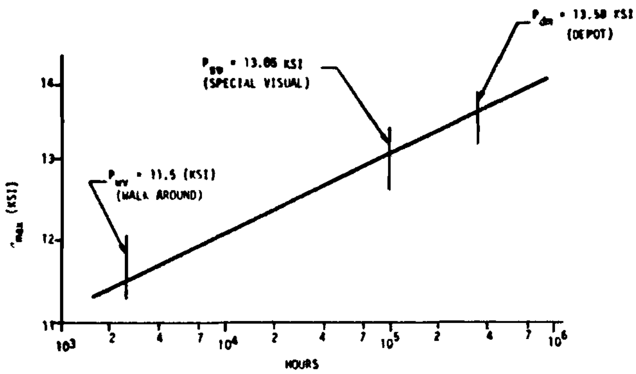

Figure 158 MINIMUM REQUIRED RESIDUAL STRENGTH CORRESPONDING TO "ONE-TIME" LOAD OCCURRENCE IN 100 X APPLICABLE INSPECTION INTERVAL

TABLE L SUMMARY OF MINIMUM RESIDUAL STRENGTH REQUIREMENTS

INSPECTION	WALK AROUND	SPECIAL VISUAL	DEPOT
SYMBOL FOR FREQUENCY	f_{wv}	f_{sv}	f_{DM}
FREQUENCY (HOURS	25	1,000	3,500
MINIMUM PERIOD OF UNREPAIRED SERVICE USAGE (HOURS)	125	2,000	7,500
"ONE-TIME" OCCURRENCE LOAD INTERVAL (HOURS)	2,500	100,000	350,000
P_{XX} - MINIMUM REQUIRED RESIDUAL STRENGTH FOR "ONE-TIME" LOAD OCCURRENCE IN 100 X APPLICABLE INSPECTION INTERVAL (KSI)	P_{wv} 11.5	P_{sv} 13.05	P_{DM} 13.58

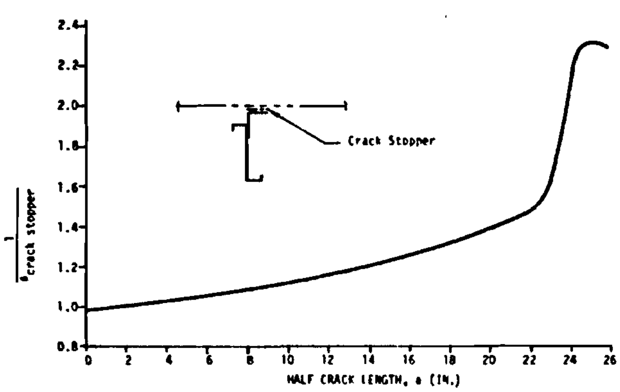

Figure 159 MODIFICATION FACTOR ($\beta_{crack\ stopper}$) vs CRACK HALF LENGTH (a) FOR FAILED CENTER CRACK STOPPER

7.2.2.2 Honeycomb Fuselage - The honeycomb fuselage was originally designed with 7075-T6 clad face sheets. The first damage tolerance analyses were, therefore, with this alloy. The results indicated that the minimum 0.02 inch gage, 7075-T6 face sheets were not adequate. An alternate alloy, 7050-T76, with improved resistance to crack propagation, was substituted resulting in a positive margin of safety.

The damage tolerance analysis results (summarized in Table LII) demonstrate the superior capability of the 7050 alloy relative to 7075. The analysis procedures paralleled those of Sections 7.2.1 and 7.2.2. The modification factor (β_{skin}) associated with a crack in one face of a honeycomb panel was defined per Douglas computer program N4BD. These analyses are discussed in the following paragraphs.

(a) Hoop Crack Analysis for Station 847 Aft - The honeycomb concept design, which is described in Section 5.2.2.1, consists of honeycomb panels with core thickness tapering from 0.363 inches at Station 439 to 1.0 inch at Station 703, and remaining at 1.0 inch back to Station 982. Face sheets are from 0.02 to 0.033 inches thick; both faces are the same thickness; and tapered sheets have been used.

Certain basic data are required for the analysis. First, the section properties for the check stations are in Table XXXIV. These properties, in conjunction with the baseline vehicle one g bending moments, reference Section 7.2.2.1, established the mission one g stresses, from which the station top centerline average one g stresses were defined (Table LIII). The crack modification factor, β_{skin}, versus half crack length (a) is shown in Figure 160. This figure shows that the uncracked face progressively relieves the stresses in the cracked face.

The primary load spectra modes were established to be low level maneuver plus gust and fuselage pressurization. These are summarized in Table LIV. Inspection of the table indicated that the critical spectra are at Station 847.

The hoop crack was grown at Station 847 aft. The face sheets were assumed to be 7075-T6, 0.025 inches thick. The crack became fast when it reached a half length (a) of 14.4 inches, at a total of 14,000 hours.

Load exceedance data were estimated for the honeycomb fuselage by scaling the baseline data (Figure 157) by $(C/I)_{honeycomb}$ divided by $(C/I)_{baseline}$ to reflect the change in stress levels. Minimum required residual strengths corresponding to one time load occurrence in 100 times the applicable inspection interval were defined. These were: for walk-around inspection, P_{WA} = 23.4 KSI; for special visual inspection, P_{SV} = 26.9 KSI; and for depot inspection, P_{DM} = 28.1 KSI. Again, only special visual and depot were applicable for a crack at the top centerline of the vehicle. The evaluations showed that depot inspection permitted higher design stresses.

The damage tolerance capability, expressed in terms of the maximum ultimate tensile stress at Station 847, is 71,100 PSI. The design allowable stress at the 7500 hour minimum period of unrepaired service usage is 97,270 psi, giving a margin of safety of 0.37.

TABLE LI STA 669 DAMAGE TOLERANCE CAPABILITY FOR HOOP LOADING

T (HOURS)	F (PSI)	M.S. (MARGIN OF SAFETY)
MINIMUM REQUIRED HOURS OF UNREPAIRED SERVICE USAGE	DESIGN ALLOWABLE STRESS	MAXIMUM ULTIMATE APPLIED STRESS = 23,600 PSI
6,000	32,300	-
7,500 (DEPOT)	30,400	0.29
10,000	28,100	-
19,000	23,600	-

TABLE LII SUMMARY OF DAMAGE TOLERANCE ANALYSES FOR FUSELAGE HONEYCOMB CONCEPT

CHECK	FACE SKIN ALLOY	CRACK ORIENTATION	STATION	FACE SKIN GAUGE (IN)	MARGIN OF SAFETY
1	7075-T6	HOOP	847	0.020	+0.37
2	7075-T6	LONGITUDINAL	703 (FWD)	0.020	-0.16
3	7050-T76*	LONGITUDINAL	703 (FWD)	0.020	+0.97

*THIS MATERIAL ADOPTED

TABLE LIII SUMMARY OF AVERAGE ONE "g" FLIGHT STRESSES FOR THE FUSELAGE HONEYCOMB CONCEPT

MISSION	ONE "g" FLIGHT STRESSES (KSI)				Σf
	STA 439	STA 703	STA 847	STA 982	
1(O)	1.3	3.5	5.8	4.8	142,947
1(R)	1.3	3.5	5.8	4.8	152,001
2(O)	1.6	4.4	6.0	5.0	25,224
2(R)	1.6	4.4	6.0	5.0	26,411
3	0.7	2.0	5.4	4.5	7,741
4	1.3	3.5	5.8	4.8	2,437,645
5	0.7	2.0	5.4	4.5	978,977
$(^1g)_{avg}$	1.1	3.1	5.7	4.7	-

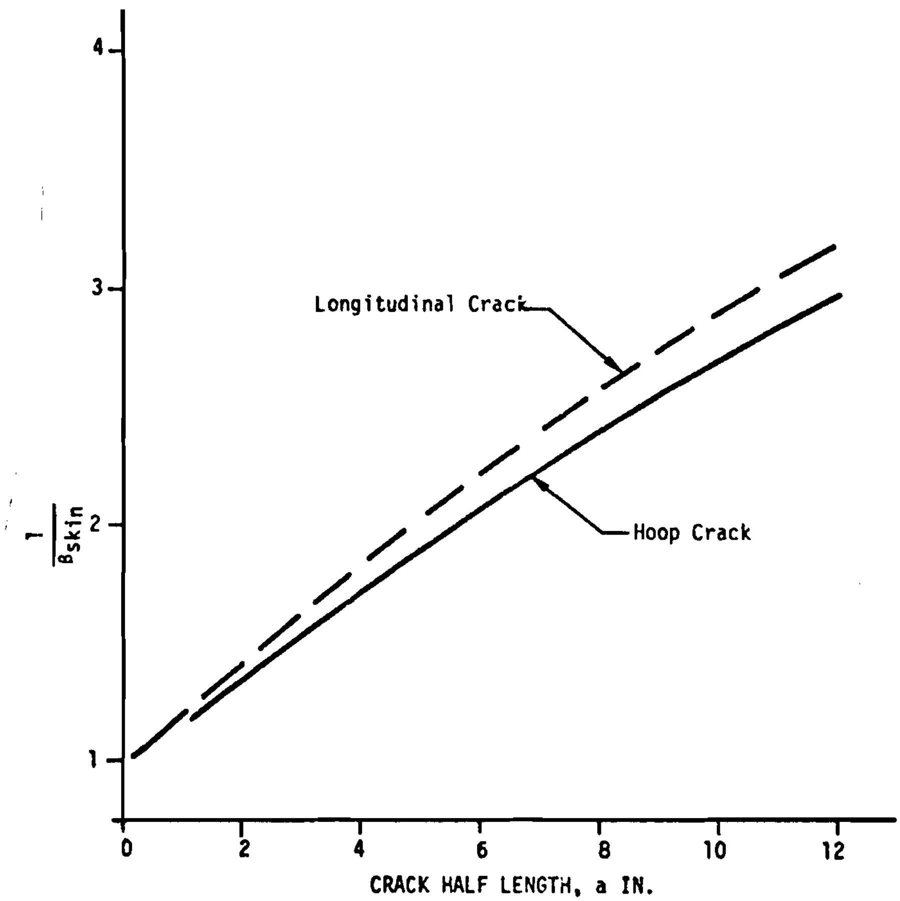

Figure 160 MODIFICATION FACTOR (β_{skin}) VS CRACK HALF LENGTH
(a) FOR HONEYCOMB PANEL WITH ONE 0.020 INCH SKIN CRACKED

TABLE LIV LONGITUDINAL LOADING SPECTRA FOR HONEYCOMB FUSELAGE						
Station	LOW LEVEL MANUEVER PLUS GUST SPECTRUM			PRESSURE SPECTRUM		
	$\Delta\sigma$ (PSI)	R	n_i ($\times 10^6$)	$\Delta\sigma$ (PSI)	R	n_i
439	260	0.70	4.56	10,130	0	19,500
703	1470	0.62	0.99	10,130	0	19,500
847	3400	0.54	2.20	8,100	0	19,500
982	2240	0.60	2.88	8,100	0	19,500

(b) Longitudinal Crack Analysis for Station 703 Forward - An initial damage tolerance check for a longitudinal crack was made in the 0.02" thick 7075-T6 face sheets just forward of Station 703. The primary loading was hoop pressure. The operating stress was equal to PR/2t or 7.5 x 108/2 x 0.02 = 20,250 psi which is also equal to $\Delta\sigma$. The number of cycles is the same as for the baseline hoop crack pressure case (19,500 cycles). The final spectrum, therefore, was $\Delta\sigma$ = 20,250 psi, n_i = 19,500 and R = 0.

The crack was grown to this environment in the basic panel. The crack became fast when it reached a half length (a) of approximately 4.0 inches at 4,216 hours. The minimum required residual strength in this case is the maximum pressure stress $\sigma_{max} \approx$ 20,250 psi. Depot level inspection was determined to provide the maximum design stress. The corresponding maximum ultimate tensile stress at Station 703 is 49,675 psi, reference Section 7.1.2. The design allowable stress of 48,500 psi corresponding to the depot level period of 7,500 hours gave a negative margin of safety of -0.16.

7050-T76 clad sheet with better damage tolerance capability was therefore selected. The face sheet thickness was 0.02 inches; hence, the loading spectrum was $\Delta\sigma$ = 20,250 psi, n_i = 19,500 and R = 0. This analysis showed the special visual inspection to give a slightly lighter structure than depot inspection. The design allowable stress was 97,710 psi giving a margin of safety of 0.97.

7.2.3 Horizontal Stabilizer Box Structure

A load spectra was not available for the baseline horizontal tail from the project group; therefore, damage tolerance analyses were not performed on the horizontal upper surface panels. However, a comparison of estimated upper surface geometry, material and spectra characteristics to the corresponding wing lower surface characteristics provided an estimate of relative capability and criticality (Table LV).

For the baseline concept, the horizontal tail basic panels and spanwise splices, by virtue of equal or better geometry, material and spectra characteristics, will have damage tolerance capabilities F/ρ equal to or better than the corresponding wing elements. Significant additional capability improvement above the levels indicated results from attachment interference benefits (tentative March 1974 criteria). Therefore, on a comparative evaluation basis, the baseline horizontal structure is not indicated to be critical for damage tolerance.

For the honeycomb concept, the horizontal basic panels have improved geometry and material characteristics which result in improved capability. The March 1974 surface flaw criteria likely will not provide significant additional improvement because of the relatively thin face skin gauges involved. The projected capability improvement relative to the also higher requirement (defined by the ultimate mode) indicates that the basic panels may possibly be marginal for damage tolerance.

The honeycomb concept spar cap geometry, material and spectra characteristics are similar to those of the wing spar caps; hence, no capability improvement can be projected. The March 1974 "attachment interference benefit" criteria

TABLE LV COMPARATIVE DAMAGE TOLERANCE ESTIMATES FOR EMPENNAGE BOX STRUCTURE[1]

CONCEPT	COMPONENT	GEOMETRY		MATERIAL		SPECTRA	CAPABILITY	REQUIREMENT
		ELEMENT	ε_g	CODE	$\Delta K/\rho$	G + M (CYCLES)	F/ρ (3)	F/ρ
B/L	WING BOX LOWER SURFACE	STRINGER	0.83	E4(7075-T76)	113 } 129	f_1	580	450
		SKIN		P6(7475-T76)	139			
		SPAR CAP	0.76	E4(7050-T76)	113	f_1	460	450
B/L	HORIZONTAL AND VERTICAL	STRINGER	0.83 (2)	E4(7050-T76)	113 } 128	f_1 (2)	580 (2)	450 (2)
		SKIN		P2(7050-T76)	137			
		SPAR CAP	0.76 (2)	E3(7050-T736)	127	f_1 (2)	> 460 (2)	450 (2)
HONEY-COMB	STABILIZER BOX COVER PANELS	OUTER SKIN	0.83 (2)	P2(7050-T76)	137 } 137	f_1 (2)	> 580 (2)	$\lessapprox$ 700 (2)
		INNER SKIN		P2(7050-T76)	137			
		H SPAR CAP	0.76 (2)	E4(7050-T76)	113	f_1 (2)	460 (2)	$\lessapprox$ 700 (2)
		V SPAR CAP	0.76 (2)	E3(7050-T736)	127	f_1 (2)	> 460 (2)	$\lessapprox$ 650 (2)

(1) REFERENCE SECTION 6.2.1

(2) ESTIMATED

(3) DEPOT LEVEL (REVISION D OF DAMAGE TOLERANCE CRITERIA)

will provide significant improvement. The capability improvement relative to the also higher stress requirement indicates that the spar caps may well be critical for damage tolerance. If verified by analysis, significant additional capability could be achieved by material substitutions such as E3(7050-T736) or F12(7050-T736) with $\Delta K/\rho$ = 127 or 157, respectively.

7.2.4 Vertical Stabilizer Box Structure

The damage tolerance discussion provided for the horizontal stabilizer in Section 7.2.3 also applies to the vertical stabilizer cover panel structure.

7.3 ULTIMATE STRENGTH ANALYSES

Ultimate strength analyses were performed to establish the wing box, fuselage shell and empennage box structural component capabilities at discrete check stations. Design stress level constraints imposed by the fatigue and damage tolerance modes were also included in the sizing and verification process. Critical loadings at each check station investigated are shown in Reference 1. These were obtained from a Format analysis of a highly idealized discrete element model of the appropriate STOL prototype airplane structure. These loads were distributed over the appropriate bar element spacing to obtain the critical N_x and N_{xy} loading. Structural capabilities used in sizing are given under each structure subsection.

7.3.1 Wing Box Structure

The integral wing concept was sized for the critical modes. The wing upper panels were critical in compression and shear, and the lower panels were designed by either tension and shear (outboard) or fatigue (inboard) as shown in Figure 161. Deviation to tentative March 1974 damage tolerance requirements for surface flaws and for hole flaws, reflecting interference fit attachment benefits, eliminated damage tolerance as a critical design mode. The required compression, tension, and shear loads for the check stations are summarized in Figure 14 and presented as detail chordwise load distributions in Reference 1.

Compression panel design was in conformance with classical principals and standard aircraft practices to preclude both local and general instability. Given the design requirements, optimum panel geometry properties were derived using Douglas Computer Code K3BF, as shown in Table LVI. A compression only sizing chart for pertinent panel concepts investigated was constructed from the computer data as shown in Figure 162. Sizing for compression or tension in conjunction with shear was based on the interaction relations

$$R_T^2 + R_S^2 = 1 \text{ and } R_C + R_S^{1.75} = 1 \qquad (40)$$

For the wing integral concept, this is shown as example sizing charts (Figures 163 and 164). The fatigue and damage tolerance constraints, as developed in Sections 7.1.1 and 7.2.1, respectively, are also included. The charts define the minimum $\bar{t}$'s for design. However, practical manufacturing and cost considerations, such as straight line tapering, may result in higher $\bar{t}$'s in the final design.

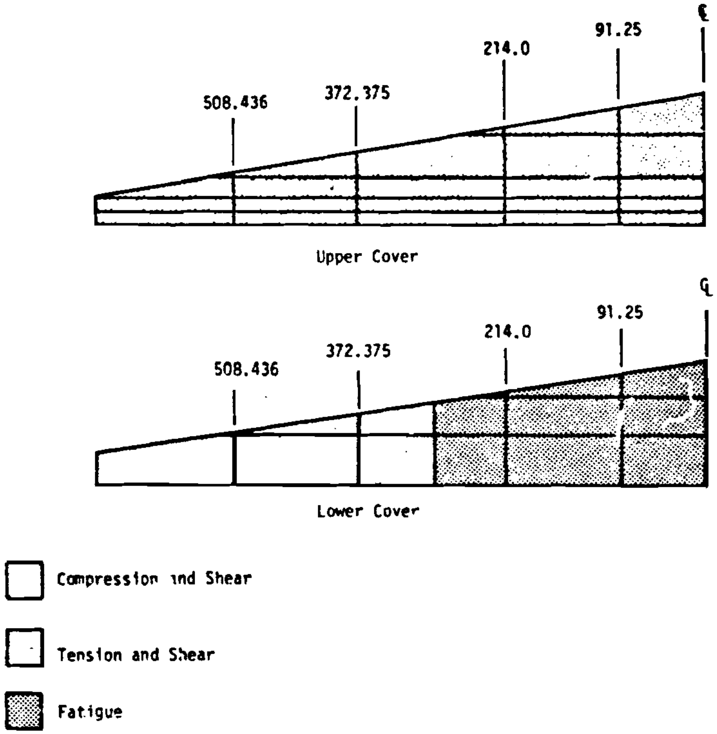

Figure 161 CRITICAL INTEGRITY MODES FOR THE INTEGRAL WING CONCEPT

TABLE LVI EXAMPLE OF WING COVER PANEL SIZING DATA

INTEGRAL (FLANGED) COMPRESSION PANEL

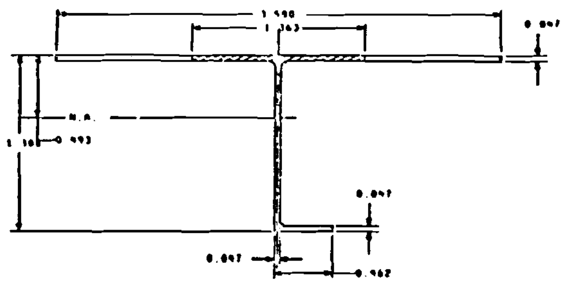

DESIGN REQUIREMENTS

LOAD INTENSITY (LBS/IN).....	2000.000	STIFFENING RATIO..............	0.500
MAXIMUM STRAIN (IN/IN)......	0.00900	COLUMN LENGTH (IN)............	29.500
SKIN ......7050-T7651 PLATE			
STRINGER ..7050-T7651 PLATE			

MATERIAL PROPERTIES		GEOMETRIC PROPERTIES	
WORKING STRAIN (IN/IN)......	0.00455	MOMENT OF INERTIA...........	0.042
EFFECTIVE STRESS (PSI)......	46839.63	EFFECTIVE AREA (SQ. IN)......	0.149
EFFECTIVE MODULUS	10299413.	RADIUS OF GYRATION (IN)......	0.531
SKIN STRESS (PSI).....	46839.59	COLUMN LENGTH (IN)	29.751
STRINGER STRESS (PSI).......	46839.59	PANEL WEIGHT (LBS/SQ. FT)....	1.057

* FILLET AREA NOT INCLUDED IN ANALYSIS.

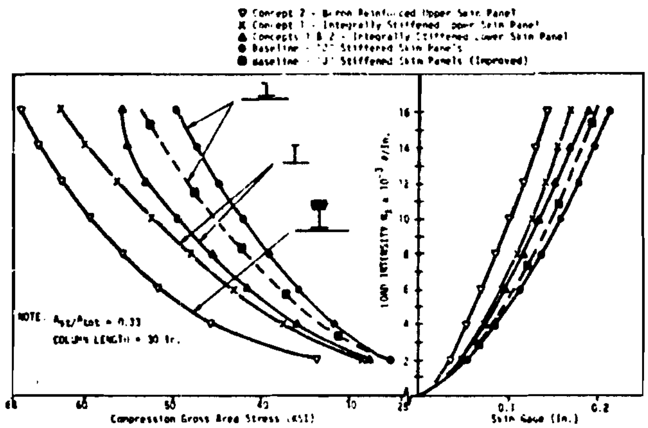

Figure 162 WIDE COLUMN COMPRESSION ALLOWABLE STRESSES FOR WING PANELS

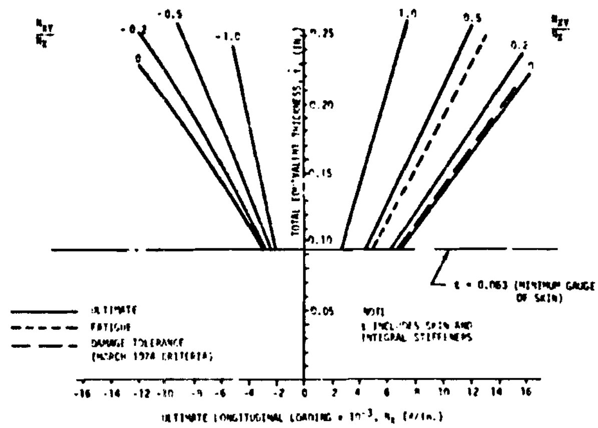

Figure 163 WING STA. 91.250 LOWER COVER PANEL SIZING CHART FOR INTEGRAL CONCEPT

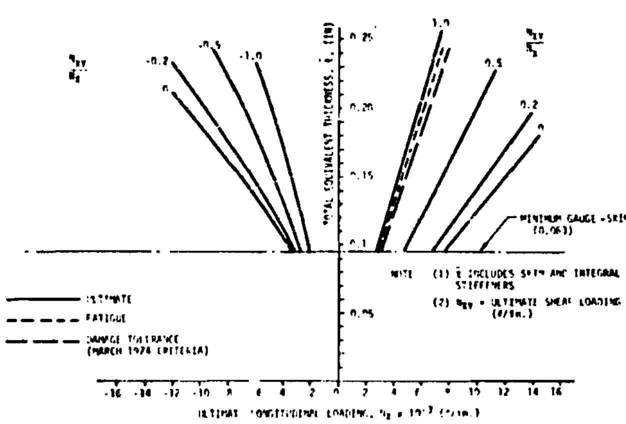

Figure 164 WING STA. 91.250 UPPER COVER PANEL SIZING CHART FOR INTEGRAL CONCEPT

The final design was checked for both strength and flutter requirements. Strength margins of safety for the lower and upper cover panels for the integral wing concept are shown in Tables LVII and LVIII, respectively. The analysis approach and methods used are similar to those subsequently described for the horizontal stabilizer in Section 7.3.3. Zero or low margins of safety are generally associated with the critical modes at the chord and station check points except for the lower wing cover panel at Station 508.436, where minimum gage prevails. Flutter checks and margins are described in Section 7.4.

The integral concept spar caps were sized for the tension and compression loads and the spar webs for the shear flows and fuel pressures presented in Reference 1. Standard classical analysis methods were used. In the spar cap analysis, strain compatibility was maintained with the attached skin. Tension, compression, fatigue, and damage tolerance modes were checked. A tension field analysis was made of the spar webs. Web stiffeners were designed and analyzed to resist the bending loads induced by the out-of-plane fuel pressure loads. The resulting spar cap and web sizes were included in the wing rigidity used in the flutter check.

The bulkheads at the check stations were analyzed for the in-plane shear and axial loads (including crushing) and for the out-of-plane bending moments resulting from the fuel pressure loads (Reference 1). Standard analysis methods were used, with the webs being sized for tension field. All four bulkheads were designed for flight shear and axial loads. In addition, the bulkhead sizing at: (1) Stations 91.25 and 214.0 accounted for fuel pressure (including over pressure); (2) Station 214.0 accounted for pylon loads; (3) Station 372.375 included flap loads; and (4) Station 508.436 included aileron loads.

The baseline concept sizing and design check approach paralleled that described above for the integral concept.

7.3.2 Fuselage Structure

Sizing and verification analyses for ultimate strength were performed on both the baseline and the honeycomb fuselage shell and floor beam structure. Similar checks for fatigue and damage tolerance on the shell were accomplished in Sections 7.1.2 and 7.2.2, respectively. A summary of the ultimate mode analysis approach and results is presented in the subsequent subsections.

7.3.2.1 Baseline Fuselage Shell Structure - The ultimate stress analysis of the baseline fuselage shell duplicated the methods used by the YC-15 project group. The analysis approach included Format derived panel axial and shear loadings and the use of existing test and experience based panel tension, compression and shear allowables. The development of panel allowables was also supported by classical and standard aircraft structural analysis procedures. Curved panel shear allowables and attendant longeron loadings, however, also used a DAC developed curved web diagonal tension field analysis. The interaction equations to obtain margins of safety were:

$$R_T^{2} + R_S^{2} = 1 \text{ (tension and shear)} \quad (41)$$

$$R_C^{1.4} + R_S^{1.45} = 1 \text{ (compression and shear)} \quad (42)$$

TABLE LVII WING LOWER COVER INTEGRAL CONCEPT MARGINS OF SAFETY

STATION	PANEL LOCATION	ULTIMATE APPLIED STRESS, PSI				ULTIMATE ALLOWABLE STRESS, PSI					MARGIN OF SAFETY			
		TENSION	SHEAR	COMP.	SHEAR	TENSION	COMP.	SHEAR	FATIGUE	DAMAGE TOLER.	TENSION	COMP.	FATIGUE	DAMAGE TOLER.
91.25	FWD.	52,667	15,420	34,667	8,000	73,000	42,100	47,000	53,000	72,800	0.31	0.16	0	0.37
	CENTER	53,000F 50,273T	9,316	29,508	3,689		46,900				0.43	>1	0	0.37
	AFT	52,980F 50,331T	11,589	26,711	6,623		52,800		53,000	72,800	0.41	0.91	0	0.37
214.0	FWD.	64,725	16,990	30,421	23,165		42,900		65,000	87,604	0.05	0	0	0.35
	CENTER	64,744	2,644	28,205	12,125		43,000				0.12	0.38	0	0.35
	AFT	64,857	4,496	26,549	5,195		45,000		65,000	87,604	0.11	0.66	0	0.35
372.375	CENTER	61,904	25,000	---	---		---		79,500	109,182	0	--	0.28	0.76
	AFT	67,677	11,364	24,828	5,924		33,600		79,500	109,182	0.05	0.32	0.17	0.61
508.436	AFT	31,746	9,683	13,757	16,159	73,000	32,600	47,000	$>F_{TU}$	$>F_{TU}$	>1	>1	--	--

TABLE LVIII WING UPPER COVER INTEGRAL CONCEPT MARGINS OF SAFETY

STATION	PANEL LOCATION	ULTIMATE APPLIED STRESS, KSI				ULTIMATE ALLOWABLE STRESS, KSI					MARGIN OF SAFETY			
		TENSION	SHEAR	COMP.	SHEAR	TENSION	COMP.	SHEAR	FATIGUE	DAMAGE TOLER.	TENSION	COMP.	FATIGUE	DAMAGE TOLER.
91.250	FWD.	26,065	8,271	43,108	18,939	80,000	53,800	48,000	32,349	32,409	>1	0	0.24	0.24
	CENTER	29,268	3,252	50,943	3,252		51,500				>1	0	0.11	0.11
	FWD OF DOORS	23,810	5,357	51,319	11,679		55,700				>1	0	0.36	0.36
	DOOR AREA	---	---	59,023	5,732		60,400				--	0	--	--
	AFT OF DOORS	---	---	36,915	23,140		50,900		32,349	32,409	--	0	--	--
214.000	FWD.	25,185	17,674	49,382	12,373		54,700		39,690	38,990	>1	0	0.58	0.55
	CENTER	21,667	9,325	50,000	3,033		50,700				>1	0	0.83	0.80
	FWD OF DOORS	37,500	7,047	52,063	4,297		53,000				>1	0	0.59	0.56
	DOOR AREA	---	---	42,185	25,989		64,100				--	0	--	--
	AFT OF DOORS	--	---	41,667	10,417		44,500		39,690	38,990	--	0	--	--
372.375	CENTER	11,333	2,580	41,667	10,700		45,500		48,668	48,594	>1	0	>1	>1
	FWD OF DOORS	15,000	[illegible]	44,333	1,000		45,500				>1	0	>1	>1
	DOOR AREA	---	---	44,666	8,692		47,400				--	0	--	--
	AFT OF DOORS	---	---	31,689	15,507		36,800		48,668	48,594	--	0	--	--
508.436	FWD OF DOORS	12,698	[illegible]	33,545	2,476		34,600		56,563	56,682	>1	0.03	>1	>1
	DOOR AREA	---	---	33,333	11,765		36,400				--	0	--	--
	AFT OF DOORS	---	---			80,000	36,400	45,000	56,563	56,682	--	>1	--	--

The ratios R represent the applied loading (or stress) divided by allowable loading (or stress).

The baseline vehicle fuselage design (described in Section 5.2.1) incorporates only three basic longeron sizes. The basic cross section areas are $0.188\ in^2$, $0.414\ in^2$, and $0.500\ in^2$. A routed out 7075-T6 sheet doubler strip, 0.05 inch thick by 1.0 inch wide, is sandwiched between the 7075-T6 longerons (and frames) and 2024-T3 skin. For analysis, the total longeron area, including the doubler area, was 0.238, 0.464 and 0.550 in^2, respectively. The skin gages vary from 0.05 to 0.15 inches.

The baseline fuselage was checked at Stations 439, 703 (wing front spar forward), 847 (wing rear spar aft), and 982 (ahead of the aft door). From the Format analysis results, ten or more critical loadings were compiled for each check station at selected circumferential locations. These loadings reflect both the general gross vehicle loads and the significant local redistribution effects for structural discontinuities and arrangements.

The section analyses showed: (1) generally high margins at Station 439; (2) margins of 0.11 or better at Station 703, except for a zero margin at longerons 17 through 19; (3) margins of 0.10 or better at Station 847 except for small or zero margins at longerons 9, 10 and 17 through 19; and (4) margins of 0.13 or greater except for small or zero margins at longerons 16 through 18, 23, and 25 through 30.

7.3.2.2 Honeycomb Fuselage Shell Structure - The ultimate stress analysis approach for the honeycomb concept is similar to that used for the baseline concept (Section 7.3.2.1). Format derived panel loadings for the baseline fuselage (Reference 1) were also applied to the honeycomb fuselage.

Margins of safety are obtained by using the interaction equations in Reference 5. General buckling of panels under compression and shear is described by the interaction equation $R_c + R_S^2 = 1$ and the margin of safety is given by

$$M.S. = \frac{2}{(R_T^2 + R_S^2)^{1/2}} - 1 \qquad (43)$$

Basic allowables are also established in accordance with Reference 5. For tension, the ultimate allowable F_{tu} of the 7075-T76 clad sheet is 79,000 PSI. The compression allowable is the lesser of the material compression yield, the sandwich panel general instability or the wrinkling stress of the face sheets. The compression yield F_{cy} is 73,000 PSI. For equal facing thicknesses of 0.020, the general instability allowable is 67,700 PSI; and, for 0.033 inch thick face sheets, 66,100 PSI. The wrinkling allowable is 78,200 PSI minimum for the 0.02 inch thick face sheets. General instability then establishes the minimum compression allowable. The ultimate shear allowable F_{su} of the face sheets is 47,000 PSI. These allowables are summarized in Table LIX.

Minimum margin of safety calculations at Stations 439, 703, 847 and 982 are shown in Table LX. Margins for combined tension and shear and for combined

TABLE LIX HONEYCOMB FUSELAGE SHELL ALLOWABLE STRESSES		
MODE		ALLOWABLE (PSI)
TENSION ULTIMATE - F_{tu}		79,000
COMPRESSION YIELD - F_{cy}		73,000
GENERAL INSTABILITY	$t_f = 0.020$	67,700
	$t_f = 0.033$	66,100
FACE WRINKLING		78,200
SHEAR ULTIMATE - F_{su}		47,000

TABLE LX HONEYCOMB FUSELAGE SHELL MINIMUM MARGINS OF SAFETY

STATION	MODE*	θ (DEGREES)*	FACE GAUGE ($2 \times t_f$)	N_x (#/in.)	N_{xy} (#/in.)	F_u (t or c) (PSI)	f_{su} (PSI)	R_c $\frac{f_{cu}}{F_c}$	R_T $\frac{f_{tu}}{79,000}$	R_S $\frac{f_{su}}{47,000}$	M.S.
439	T/S	97	.040	+1114	508	+27,850	12,700	-	.36	.27	1.22
439	C/S	97	.040	-393	364	-9,825	9,100	.14	-	.19	2.67
703	T/S	51.4	.042	+2782	928	+66,240	22,100	-	.86	.47	.02
703	C/S	51.4	.042	-1222	280	-29,100	6,700	.43	-	.14	1.12
847	T/S	16.7	.050	+3555	883	+71,100	17,700	-	.92	38	.005
847	C/S	102.9	.066	-2345	2091	-35,500	31,700	.52	-	.67	.02
982	T/S	0	.050	+3052	107	+61,000	2,100	-	.79	.05	.26
982	C/S	128.2	.040	-1419	1010	-35,500	25,300	.52	-	.54	.16

*T = TENSION; C = COMPRESSION AND S = SHEAR;

*CHECK POINT IN DEGREES FROM TOP ℄

compression and shear are shown for each check station. For the design, the minimum margins of safety are 0.005 in combined tension and shear, and 0.02 in combined compression an/ shear at Station 847. A face skin sizing chart (Figure 165) summarizes the defined relationship between loading, strength, design and weight. Additive weight thickness $\bar{t}$ increments for core and adhesive are also indicated.

The panel joints were checked for discontinuity stresses through the splice area. The results of one such analysis are presented here. Inspection of Table LX indicates that the maximum tension loads occur at F.S. 847 at Θ=16.7°. At this point, there is an ultimate tension loading of 3555 lbs per inch with an associated ultimate shear loading of 883 pounds per inch. The splice cross section is shown in Figure 166. Checks were made at critical sections A-A and B-B. The stresses and margins of safety for these sections are adequate as shown in Table LXI.

7.3.2.3 Fuselage Cargo Floor - The baseline floor plank members are similar in cross section to those used in the YC-15. The weight saving modifications are proposed to this basic member. The first is to substitute, for a major portion of the lower cap, boron filaments which are infiltrated into a 0.188 inch diameter hole in the basic extrusion (see Figure 73). Since stresses in the plank members are functions of C/I and cross section areas, these values are presented in Table LXII for the baseline and new concept floor plank members. The table shows that the stresses in the new concept will be somewhat less than in the baseline. The new concept is therefore acceptable by inspection.

The second modification is based on the determination that the centerline four foot strip of the floor would not be subjected to wheel loadings, reference Section 5.2.3.3. The floor FORMAT analysis was searched for a maximum nose wheel loading. This was Case LX, the 300 psf bulk load over one bay between bulkheads, at N_z = 10.1 ultimate. Maximum loads were:

In bar 12 at centerline of floor,

P = -20,198 lbs, V = -5,018 lbs, and M = -60,826 in lbs

In bar 33 at 15 inches from centerline,

P = -13,499 lbs, V = -3,391 lbs, and M = -40,292 in lbs

A check was made of the floor panel from the fuselage centerline to X = 14.94 from the fuselage (see Figure 73). Bar 12 is a strip 7.5 inches on each side of the centerline, while bar 33 runs from 7.5 inches to 17.75 inches off the fuselage centerline. Hence, the load on the check section is half of the bar load plus 73% of the bar 33 load. The check load is then

P = -19,980 lbs, V = -5,065 lbs, and M = -59,895 in lbs

The section properties of the check section included the composite section as well as half the sections at the fuselage centerline (x = 0) and x = 14.94. These properties were I = 2.411 in^4, A = .007 in^2, C_{bottom} = 1.379 in and C_{top} = 0.871 in. The section check showed stresses of -28.2 KSI in the upper

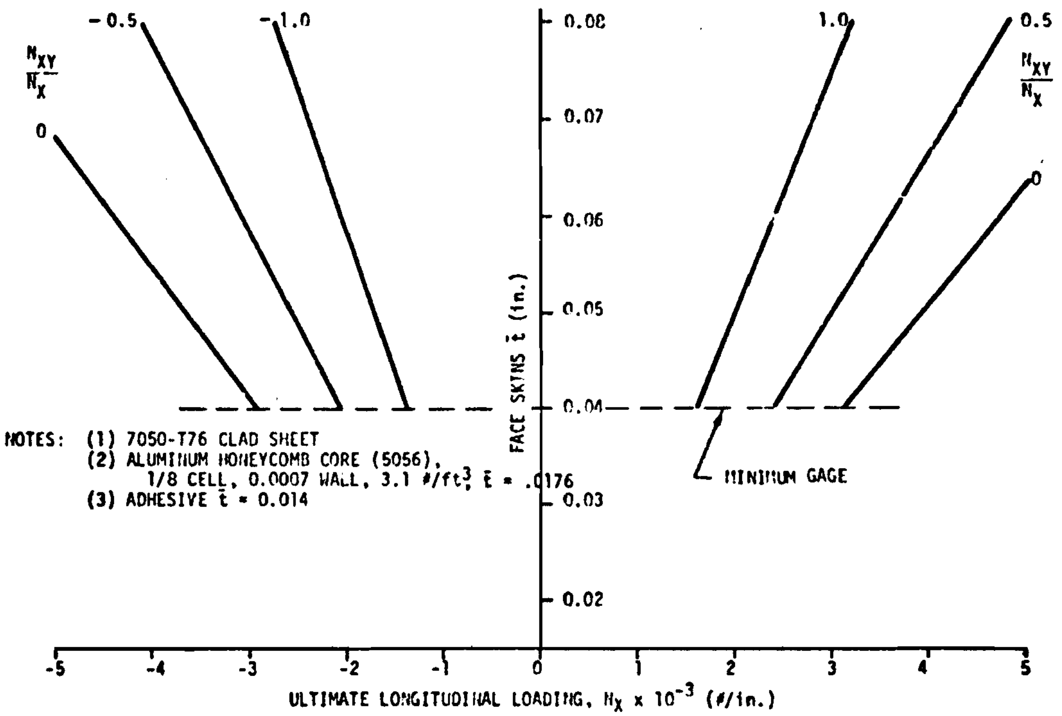

Figure 165 FUSELAGE SHELL HONEYCOMB PANEL SIZING CHART

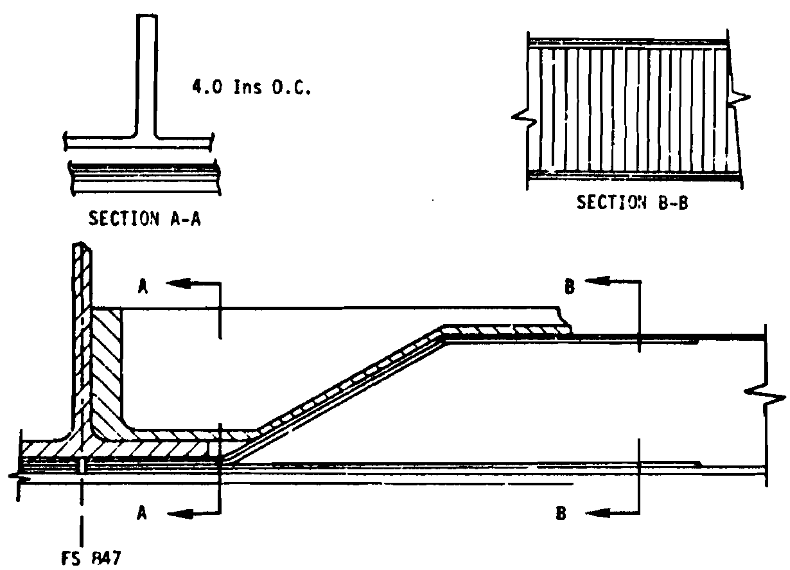

Figure 166 STATION 847 FUSELAGE SHELL JOINT (HONEYCOMB CONCEPT)

TABLE LXI STA. 847 SPLICE STRESSES AND MARGINS OF SAFETY					
SECTION (FIGURE 166)	MAXIMUM STRESSES (PSI)		ALLOWABLE STRESSES (PSI)		M.S.
	INB'D	OUTB'D	INB'D	OUTB'D	
A-A	+59,500	+6000	79,000	79,000	0.13
B-B	+77,100	+9600	79,000	79,000	0.10

TABLE LXII CARGO FLOOR PLANK SECTION PROPERTIES				
CONFIGURATION	$\frac{C_{BOTTOM}}{I}$ (in^{-3})	$\frac{C_{TOP}}{I}$ (in^{-3})	EQUIVALENT ALUMINUM AREA (in^2)	
			STRESS	WEIGHT
BASELINE	2.95	2.28	0.529	0.529
NEW CONCEPT	2.64	2.20	0.545	0.483

TABLE LXI STA. 847 SPLICE STRESSES AND MARGINS OF SAFETY					
SECTION (FIGURE 166)	MAXIMUM STRESSES (PSI)		ALLOWABLE STRESSES (PSI)		M.S.
	INB'D	OUTB'D	INB'D	OUTB'D	
A-A	+59,500	+6000	79,000	79,000	0.13
B-B	+77,100	+9600	79,000	79,000	0.10

TABLE LXII CARGO FLOOR PLANK SECTION PROPERTIES				
CONFIGURATION	$\frac{C_{BOTTOM}}{I}$ (in^{-3})	$\frac{C_{TOP}}{I}$ (in^{-3})	EQUIVALENT ALUMINUM AREA (in^2)	
			STRESS	WEIGHT
BASELINE	2.95	2.28	0.529	0.529
NEW CONCEPT	2.64	2.20	0.545	0.483

surface and +27.2 KSI in the lower surface; hence, no stress problem exists.

7.3.3 Horizontal Stabilizer Box Structure

The horizontal stabilizer box new concept structure consists of upper and lower cover panels of aluminum tapered face skins and aluminum honeycomb core. The face skins are chem-milled with a straight taper spanwise from $X_H = 0$ to $X_H = 182$. The face skins outboard of $X_H = 182$ are of minimum gauge thickness equal to the $X_H = 182$ thickness. Conventional aluminum extrusions are used for front and rear spar caps with chem-milled integrally stiffened spar webs. The bulkheads are also chem-milled and integrally stiffened. The four check stations investigated represented maximum stabilizer internal loads ($X_H = 15$), inboard elevator hinge station ($X_H = 101$), an intermediate station ($X_H = 173$), and outboard elevator hinge station ($X_H = 292$). Critical loadings at each of the horizontal stabilizer check stations are shown in Reference 1.

Material allowables used for sizing the horizontal stabilizer box structure are summarized below. "B" value allowables for all materials are used for ultimate strength mode checks. Honeycomb surface paneling is generally bonded to the spar caps and bulkheads; therefore, no hole-out factor was applied to the allowable. Where mechanical fasteners are used to attach the honeycomb paneling to the bulkhead (Station $X_H = 15$), the facing skins are reinforced with bonded doublers and the core densified. Mechanical fasteners are used to attach the spar cap flange to the spar web; therefore, a hole-cut factor was used for the tension mode analyses.

Structure	Material	F_{tu} (PSI)	F_{cy} (PSI)	F_{su} (PSI)
Honeycomb Face Panel	7050-T76 Sheet	80,000	74,000	48,000
Spar Cap	7050-T76511 Ext.	82,620	72,400	
Spar & Bulkhead Webs	7050-T73651 Plate	73,400		

7.3.3.1 Honeycomb Panel Face Skins - The upper and lower honeycomb surface panel skins were sized for the more critical of tensile or compressive loadings in combination with corresponding shear loading. [NOTE: Fatigue and damage tolerance are less critical, see Sections 7.1.3 and 7.2.3]. For axial loading and shear loading, the design stress level was determined by standard $\frac{N_x}{2t}$ and $\frac{N_{xy}}{2t}$ formulas, respectively, where N_x and N_{xy} are applied running loads in pounds per inch and 2t is the combined thickness of the fully effective outside and inside face skins. Interaction of "shear and compression" and "shear and tension," which was used to design the honeycomb face skins, was established on the basis of standard interaction relationships. For shear and compression, $R_S^2 + R_C = 1$ and for shear and tension $R_S^2 + R_T^2 = 1$.

An example of the panel face skin ultimate strength check is as follows: check panel at station 15 between front and center spars ($t = 0.032$). The critical loading between 29.9 and 35.7 inches from leading edge is from Condition 4.

$$N_x = 4497 \text{ lbs/in} \qquad N_{xy} = 1389 \text{ lbs/in}$$

$$f_t = \frac{N_x}{2t} = \frac{4497}{2(0.032)} = 70{,}265 \text{ PSI} \qquad f_s = \frac{N_{xy}}{2t} = \frac{1389}{2(0.032)} = 21{,}703 \text{ PSI}$$

$$R_T = \frac{f_t}{F_T} = \frac{70{,}265}{80{,}000} = 0.878 \qquad R_S = \frac{f_s}{F_S} = \frac{21{,}703}{48{,}000} = 0.452$$

R_{TA} = allowable tensile stress ratio for design shear stress

$$= \sqrt{1 = R_S^2} = \sqrt{1 = (0.452)^2} = 0.892$$

F_{TS} = allowable tensile stress for design shear stress = $R_{TA} \times F_T$

$$= (0.892)(80{,}000) = 71{,}355 \text{ PSI}$$

$$M.S. = \frac{1}{\sqrt{R_T^2 + R_S^2}} - 1 = \frac{1}{\sqrt{(0.878)^2 + (0.452)^2}} - 1 = 0.01$$

Similarly, for compressive loading, the core of the honeycomb panels was sized (Reference 36) such that general instability of the panel at compressive yield stress was critical.

$$R_C = \frac{f_c}{F_{CY}} \qquad F_{CS} = R_{CA} \times F_{CY}$$

$$R_{CA} = 1 - R_S^2 \qquad M.S. = \frac{2}{R_C + \sqrt{R_C^2 + 4R_S^2}} - 1 \tag{44}$$

Tables LXIII and LXIV summarize the horizontal stabilizer upper and lower surface panel face skin minimum margins of safety. Further lowering of these margins of safety by reducing the skin thickness would also adversely influence the rigidity mode (see Section 7.4.2).

The above strength criteria are also reflected in the sizing chart (Figure 167) to establish the relationship between loading, design and weight. In addition to the face skin $\bar{t}$, incremental additive t's for core and adhesive are also indicated.

7.3.3.2 Front and Rear Spar Caps - Spar caps of the honeycomb concept are bonded to the surface panels and mechanically fastened to the spar web. A hole-out reduction factor of 0.87 was applied to the material ultimate tension allowable. No hole-out reduction was used for compression loading. Ultimate strength margins of safety for the front and rear spar caps for specified check

TABLE LXIII SUMMARY OF HORIZONTAL STABILIZER UPPER PANEL FACE SKIN MARGIN OF SAFETY

PANEL LOCATION	Loading Type	STA	COND NO	SKIN GAUGE (2t) (IN.)	N_x (#/IN)	f_t OR f_c (PSI)	R_T OR R_C	N_{xy} (#/IN)	f_s (PSI)	R_S	R_{TA} OR R_{CA}	f_{ts} OR f_{cs} (PSI)	M.S.
FRONT SPAR TO CENTER SPAR	Tensile	15	4	.064	4,497	70,265	.88	1,389	21,703	.45	.89	71,355	.01
		101	5	.052	3,513	67,558	.84	1,111	21,365	.45	.90	71,638	.05
		173	6	.042	552	13,143	.16	1,195	28,452	.59	.81	64,431	.63
		282	1	.040	413	10,325	.13	222	5,550	.12	.99	79,463	4.77
	Compressive	15	3	.064	-3,415	-53,359	.72	1,404	21,938	.46	.79	-58,543	.06
		101	2	.052	-3,269	-62,865	.85	465	8,769	.18	.97	-71,530	.13
		173	2	.042	-1,890	-45,000	.61	161	3,833	.08	.99	-73,528	.62
CENTER SPAR TO REAR SPAR	Tensile	15	5	.172	10,283	59,784	.75	5,167	30,040	.63	.78	62,396	.03
		101	5	.070	3,378	48,257	.60	1,849	26,414	.55	[illegible]	66,797	.22
		173	5	.044	2,295	52,159	.65	1,354	30,773	.64	.77	61,397	.09
	Compressive	15	2	.172	-9,001	-52,331	.71	4,436	25,791	.54	.71	-52,636	.00
		101	2	.070	-3,353	-47,900	.65	713	10,186	.21	.95	-70,668	.41
		173	2	.044	-1,806	-41,045	.55	964	21,909	.46	.79	-58,583	.23
		282	6	.040	-111	-2,775	.04	719	17,975	.37	.86	-63,623	1.64

(a) Face skins are 7050-T76 aluminum alloy sheet.

(b) No face s' n splice at Station 282.

TABLE LXIV SUMMARY OF HORIZONTAL STABILIZER LOWER PANEL FACE SKIN MARGIN OF SAFETY

PANEL LOCATION	Loading Type	STA.	COND NO.	SKIN GAUGE (2t) (IN.)	N_x (#/IN)	f_t OR f_c (PSI)	R_T OR R_C	N_{xy} (#/IN)	f_s (PSI)	R_S	R_{TA} OR R_{CA}	f_{ts} OR f_{cs} (PSI)	M.S.
FRONT SPAR TO CENTER SPAR	Tensile	15	2	.084	4,367	51,988	.64	3,094	36,833	.76	.65	51,994	.00
		101	2	.062	3,769	60,790	.76	418	6,742	.14	.99	79,207	.29
		173	2	.042	1,942	46,238	.58	333	7,929	.17	99	78,901	.66
		282	2	.050	416	8,320	.10	214	4,280	.09	.99	79,364	6.30
	Compressive	15	1	.084	-4,697	-55,917	.76	1,347	16,036	.33	.89	-65,741	.13
		101	5	.062	-3,528	-56,902	.77	1,220	19,677	.41	.83	-61,564	.06
		173	5	.042	-1,950	-46,429	.63	908	21,619	.45	.80	-58,989	.16
		282	6	.050	-123	-2,460	.03	670	13,400	.28	92	-68,233	2.38
CENTER SPAR TO REAR SPAR	Tensile	15	2	.240	---	33,533	.42	4,972	20,717	.43	.90	72,165	.66
		101	2	.094	3,332	35,447	.44	871	9,266	.19	.98	78,495	1.07
		173	2	.054	1,829	33,870	.42	629	11,648	.24	.97	77,609	1.05
	Compressive	15	5	.240	-7,364	-30,683	.41	2,782	11,592	.24	.94	-69,684	.90
		101	5	.094	-3,646	-38,787	.52	1,909	20,309	.42	.82	-60,753	.32
		173	5	.054	-1,989	-36,833	.50	1,418	26.259	.55	.70	-51,853	.18

(a) Face skins are 7050-T76 aluminum alloy sheet.

(b) No face skin splice at Station 282.

stations are shown in Table LXV. Integrally stiffened spar webs were designed for tension field action when stressed to the ultimate tensile strength of the material. The classical equation for allowable web buckling shear stress and Wagner's equation for tension field action were used with sheet edge restraint midway between clamped and simply supported. Figure 168 shows the spar web margins of safety. A reduction of spar cap areas or spar web thicknesses would adversely influence the rigidity mode (see Section 7.4.2).

7.3.3.3 Bulkhead Webs - Integrally stiffened chem-milled bulkhead webs were designed for tension field action when stressed to the ultimate tensile strength of the web material. Each of the check station bulkheads contained from 8 to 10 chordwise panels extending from the upper surface to the lower surface. Table LXVI shows the minimum margin of safety for the most critically loaded panel of each bulkhead. Internal design shear loadings for the panels (in pounds) were derived from Reference 1 where panel member loads are tabulated in pounds per inch and designed by a "P" panel number. The sum of three tabulated panel shear flows is converted to shear load in pounds to obtain the true bulkhead shear from the upper to the lower surface.

7.3.4 Vertical Stabilizer Box Structure

The vertical stabilizer box structure concept consists of cover panels made from aluminum constant thickness face skins and aluminum honeycomb core. Face skin thicknesses between front and rear spars below vertical stabilizer station Z_{RS} = 248.105 are 0.032, above Z_{RS} = 248.105 between front spar and center spar, 0.025; and between center spar and rear spar, 0.032. Front and rear spar caps are aluminum tapered extrusions reinforced with boron epoxy. Spar webs and bulkheads are chem-milled and integrally stiffened. The three check stations investigated represent maximum vertical stabilizer bending load (Z_{RS} = 143.1), an intermediate station (Z_{RS} = 250.5), and the upper end of the front spar (Z_{RS} = 343.1). Critical loads at each of the vertical stabilizer check stations are shown in Reference 1.

Allowables used for the sizing of the vertical stabilizer box structure are summarized below. "B" value allowables of all materials are used for ultimate strength mode checks. Honeycomb surface panels are bonded to the spar caps and bulkheads; therefore, no hole-out factor was applied to the material allowable. Mechanical fasteners are used to attach the spar cap flange to the spar web. There, a hole-out factor was used for tension mode analyses.

Structure	Material	F_{tu} (PSI)	F_{cy} (PSI)	F_{su} (PSI)
Honeycomb Face Panels	7050-T76 Sheet	80,000	74,000	48,000
Spar Cap	7050-T736511 Ext.	79,560	69,360	
Spar Cap	Boron-Epoxy	186,000		
Spar & Bulkhead Webs	7050-T73651 Plate	73,400		

7.3.4.1 Honeycomb Panel Face Skins - The left and right side honeycomb panel skins were sized for the more critical of tensile or compressive loading in combination with corresponding shear loading identical to the method

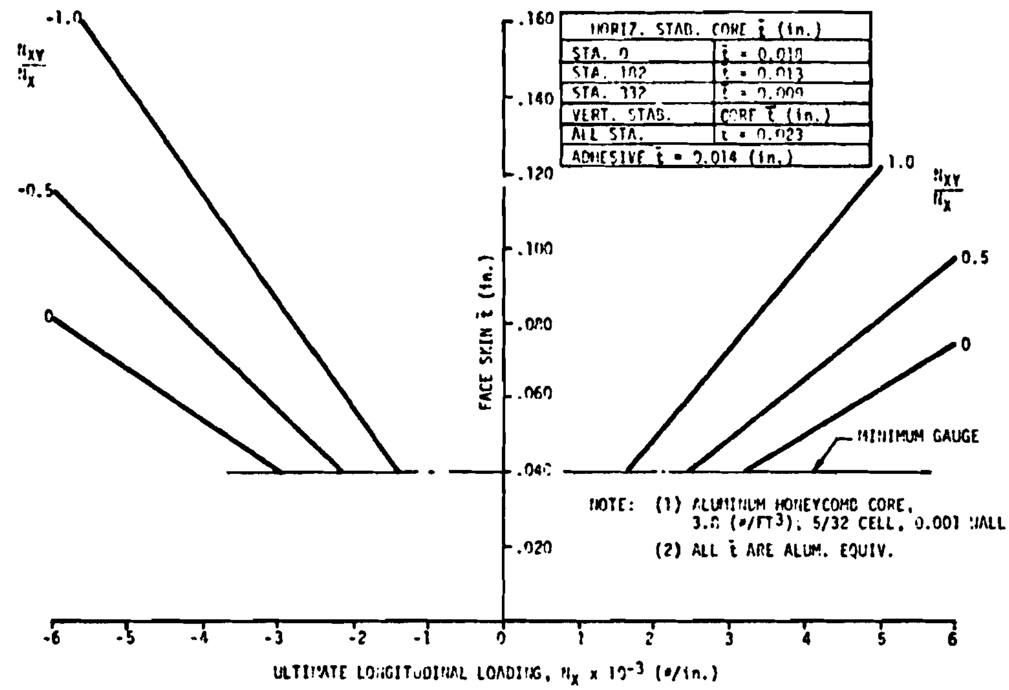

Figure 167 SIZING CHART FOR EMPENNAGE COVER PANELS

TABLE LXV SUMMARY OF HORIZONTAL STABILIZER SPAR CAP MARGINS OF SAFETY

ITEM		STA.	CAP AREA (IN^2)	COND NO.	TENSION LOAD (LBS)	F_t (PSI)	M.S.	COND NO.	COMPRESSION LOAD (LBS)	f_c (PSI)	M.S.
FRONT SPAR	Upper Cap	15	0.95	4	61,407	64,639	0.11	3	47,759	50,273	N.C.
		101	0.71	5	48,979	69,985	0.04	2	39,582	55,749	N.C.
		173	0.57	5	30,285	53,132	0.36	2	21,491	37,704	N.C.
		282	0.40	5	6,988	17,470	3.12	2	2,567	6,418	N.C.
	Lower Cap	15	0.95	2	65,190	68,621	0.05	1	63,224	66,552	N.C.
		101	0.71	2	38,024	53,555	N.C.	5	39,550	55,704	0.30
		173	0.57	2	19,828	34,786	N.C.	5	21,007	36,854	0.95
		282	0.40	2	2,521	6,303	N.C.	5	4,523	11,308	5.40
REAR SPAR	Upper Cap	15	1.66	5	114,863	69,195	0.04	2	109,077	65,709	N.C.
		101	0.66	5	35,987	54,526	0.32	2	34,078	51,633	N.C.
		173	0.54	1	17,248	31,941	1.25	2	17,136	31,733	N.C.
		282	0.40	7	1,927	4,818	13.94	3	1,404	3,510	N.C.
	Lower Cap	15	1.17	2	55,369	47,324	N.C.	5	84,519	72,238	0.002
		101	0.63	2	28,232	44,813	N.C.	5	35,699	56,665	0.270
		173	0.52	2	16,585	31,894	N.C.	5	26,394	50,758	0.430
		282	0.40	3	1,242	3,105	N.C.	7	2,044	5,110	13.170

(a) Cap material is 7050-T76511 aluminum extrusion
(b) F_{tu} = 72,000 PSI (87% of 82,620); F_{cy} = 72,400 PSI

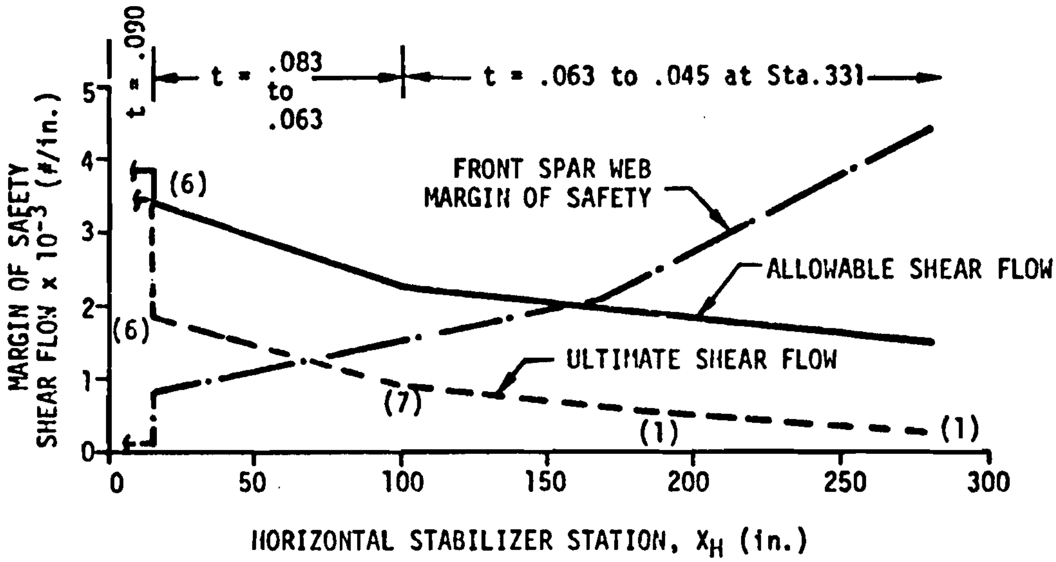

NOTE: 1. 7050-T73651 ALUMINUM PLATE
2. LOAD CONDITION NUMBERS DENOTED THUS ( )

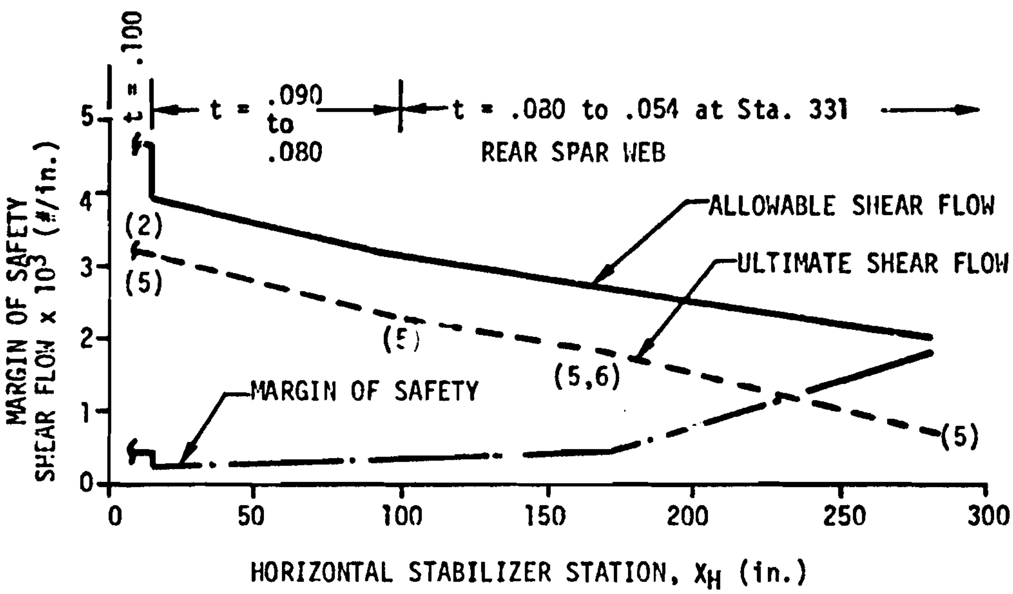

Figure 168 HORIZONTAL STABILIZER SPAR WEB MARGINS OF SAFETY

described in Section 7.3.3.1. Table LXVII shows a summary of the vertical stabilizer side surface panel face skin minimum margins of safety. Further lowering of the margins of safety by reducing the skin thickness would also adversely influence the rigidity mode (see Section 7.4.2). A face skin sizing chart relating loading, strength, design and weight is shown on Figure 167.

7.3.4.2 Front and Rear Spars - Spar caps of the honeycomb concept are bonded to the surface panels and mechanically fastened to the spar web. A hole-out reduction factor of 0.87 was applied to the material ultimate tension allowable. No hole-out reduction was used for compression loading. In order to increase the chordwise stiffness required by the rigidity mode and still maintain minimum weight, the front and rear spar caps incorporate composite reinforcement. An aluminum extruded tapered cap with slots impregnated with boron epoxy is used. A typical section is shown in Table LXVIII. The aluminum portion of the cap is sized to carry limit loads without yielding and the boron epoxy portion sized to obtain the desired total chordwise moment of inertia. For strength checks, the boron epoxy is considered 90% effective. Minimum margins of safety for the front and rear spar caps are shown in Table LXIX.

Integrally stiffened spar webs were designed to tension field action when stressed to the ultimate tensile strength of the material. The classical equation for allowable web buckling shear stress and Wagner's equation for tension field action were used with sheet edge restraint midway between clamped and simply supported. Figure 169 shows the spar web margins of safety.

7.3.4.3 Bulkhead Webs - Integrally stiffened chem-milled bulkhead webs were designed for tension field action when stressed to the ultimate strength of the web material. Each of the check station bulkheads contained 12 chordwise panels extending from the left surface to the right surface. Table LXX shows the minimum margin of safety for the most critically loaded panel of each bulkhead. Internal design shear loading for the panels was derived from Reference 1 where panel member loads are tabulated in pounds per inch and defined by a "P" panel member. Three tabulated panel shears in pounds must be added to obtain the true panel shear from left to right surfaces of the bulkhead.

7.4 RIGIDITY ANALYSES

Rigidity for flutter is a primary consideration for wing and empennage. The rigidity requirements of Section 2.2.3 were applied to the sizing process and in the subsequent rigidity checks of the wing and empennage box structure designs.

7.4.1 Wing

The effect of wing local rigidity changes on the flutter damping parameter g is shown in Figures 25 and 26 for the two most critical frequencies. Analysis of the data established section area as an important geometric parameter affecting flutter (Figure 170). A relative insensitivity to stiffening ratio change is also shown.

A flutter check of the baseline and integral concept wing designs was also made. For this analysis, improved baseline and integral concept wing proper-

TABLE LXVI SUMMARY OF HORIZONTAL STABILIZER BULKHEAD MARGINS OF SAFETY

BULKHEAD STATION	WEB t (in.)	PANEL LOCATION(5)	ALLOWABLE SHEAR LOAD (lbs.)	DESIGN SHEAR LOAD (lbs.)	COND. NO.	M.S.
X_H = 15	.165	AT R.S.	95,832	86,542(1)	2	.11
X_H = 101	.050	BETWEEN C.S. AND R.S.	20,797	17,062(2)	5	.22
X_H = 173	.050	BETWEEN C.S. AND R.S.	12,255	4,360(3)	6	1.81
X_H = 282	.050	AT R.S.	12,510	12,472(4)	5	.00

MATERIAL: 7050-T73651 ALUMINUM PLATE

(1) DESIGN SHEAR LOAD FROM P22, P23, AND P24 = (3354)(1.77) + (6118)(14.46) + (-4441)(1.77) = 86,542 lbs.

(2) DESIGN SHEAR LOAD FROM P13, P14, AND P15 = (-807)(1.75) + (-515)(12.9) + (-648)(1.75) = -9190 x 1.86 = -17,062 lbs.

FORMAT ANALYSIS COVERED LOADING FROM MID-STA. 87.75 and 113.75 = 26 in.
CONCEPT STUDY COVERED LOADING FROM MID-STA. 77.44 and 125.71 = 48.27 in. INCREASE LOADS BY 48.27 ÷ 26 = 1.86

(3) DESIGN SHEAR LOAD FROM P11, P20, AND P13 = (-326)(1.75) + (-209)(10.7) + (-337)(1.75) = -4360 lbs.

(4) DESIGN SHEAR LOAD FROM P19, P20, AND P21 = (-300)(1.75) + (-743)(6.4) + (-529)(1.75) = -6205 x 2.01 = -12,472 lbs.

FORMAT ANALYSIS COVERED LOADING FROM MID-STA. 269.5 and 294.5 = 25 in.
CONCEPT ANALYSIS COVERED LOADING FROM MID-STA. 256.08 and 306.24 = 50.16 in. INCREASE LOADS BY 50.16 ÷ 25 = 2.01

(5) P22 = PANEL 22, etc. FROM REF. 1

TABLE LXVII SUMMARY OF VERTICAL STABILIZER SURFACE PANEL FACE SKIN MARGINS OF SAFETY

	STA. LOCATION	COND. NO.	SKIN 2t (in.)	N_X (lbs/in)	f_t or f_c (PSI)	R_T or R_C	N_{XY} (lbs/in)	f_s (PSI)	R_S	R_{TA} R_{CA}	F_{TS} or F_{CS} (PSI)	M.S.
TENSILE LOADING	143.1 at C.S.	10	.064	4520	70,625	.88	650	10,156	.21	.98	78,189	.10
	250.5 aft F.S.	5	.050	3010	60,200	.75	560	11,200	.23	.97	77,791	.27
	343.1 aft F.S.	5	.050	2460	49,200	.62	360	7,200	.15	.99	79,095	.58
COMPRESSIVE LOADING	143.1 at C.S.	10	.064	-4180	-65,313	.88	810	12,656	.26	.93	-68,855	.05
	250.5 fwd R.S.	5	.064	-3050	-47,656	.64	1300	20,313	.42	.82	-60,746	.17
	343.1 aft F.S.	2	.050	-1610	-32,200	.44	870	17,400	.36	.87	-64,276	.56

(1) MATERIAL: 7050-T76 ALUMINUM ALLOY SHEET

TABLE LXVIII VERTICAL STABILIZER COMPOSITE SPAR CAP AREAS							
COMPONENT		ALUM. AREA (IN^2)	BORON AREA (IN^2)	ALUM. EQUIVALENT OF BORON AREA		TOTAL ALUM. EQUIV. AREA	
				100% EFFECTIVE	90% EFFECTIVE	BORON 100%	BORON 90%
FRONT SPAR	Sta. 74.0	1.88	0.92	2.58	2.32	4.46	4.20
	Sta. 143.1	1.41	0.64	1.79	1.61	3.20	3.02
	Sta. 250.5	1.08	0.44	1.23	1.11	2.31	2.19
	Sta. 330.0	0.80	0.28	0.79	0.71	1.56	1.51
	Sta. 343.1	1.03	--	--	--	--	--
REAR SPAR	Sta. 143.1	2.62	1.12	3.14	2.83	5.76	5.45
	Sta. 250.5	1.82	0.85	2.38	2.14	4.20	3.96
	Sta. 343.1	1.82	0.85	2.38	2.14	4.20	3.96
	Sta. 430.0	1.82	0.85	2.38	2.14	4.20	3.96

ALUM. EQUIV. OF BORON AREA = $\frac{E_{BORON}}{E_{ALUM.}} \times A_{BORON}$

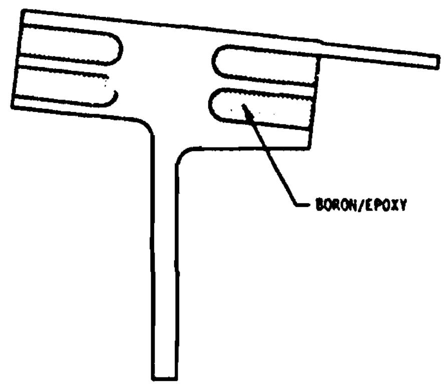

TABLE LXIX SUMMARY OF VERTICAL STABILIZER SPAR CAP MARGINS OF SAFETY								
COMPONENT STATION		COND. NO.	EQUIV ALUM AREA (in^2)	TENSION LOAD (LBS)	f_t (PSI)		M.S. (TENSION)	
					ALUM.	BORON	ALUM.	BORON
FRONT SPAR	143.1	5	3.02	124,542	41,240	115,620	0.68	0.61
	250.5	5	2.19	91,290	41,680	116,870	0.66	0.59
	343.1	5	1.03*	55,634	54,010	---	0.28	---
REAR SPAR	143.1	2	5.45	162,521	29,820	83,610	1.32	1.22
	250.5	5	3.96	107,978	27,270	76,450	1.54	1.43
	343.1	2	3.96	129,859	32,790	91,940	1.11	1.02
*CAP IS ALL ALUMINUM ABOVE STATION 330.0				COMPRESSION LOAD (LBS)	f_c (PSI)		M.S. (COMPRESSION)	
					ALUM.	BORON	ALUM.	BORON
FRONT SPAR	143.1	2	3.02	-86,703	-28,710	-80,500	1.42	1.31
	250.5	2	2.19	-63,917	-29,190	-81,830	1.38	1.27
	343.1	2	1.03*	-36,765	-35,690	---	0.94	---
REAR SPAR	143.1	5	5.45	-221,198	-40,590	-113,790	0.71	0.63
	250.5	5	3.96	-141,062	-35,620	-99,870	0.95	0.86
	343.1	5	3.96	-156,316	-39,470	-110,670	0.76	0.68

(1) 7050-T736511 ALUM. AND BORON EPOXY

(2) BORON STRESS = $\frac{E_{BORON}}{E_{ALUM}} \times f_{ALUM}$

(3) ALLOWABLES:

ALUM: F_{tu} = 0.87 (79,560) = 69,200 PSI
F_{cy} = 69,360 PSI

BORON: F_{tu} = 186,000 PSI

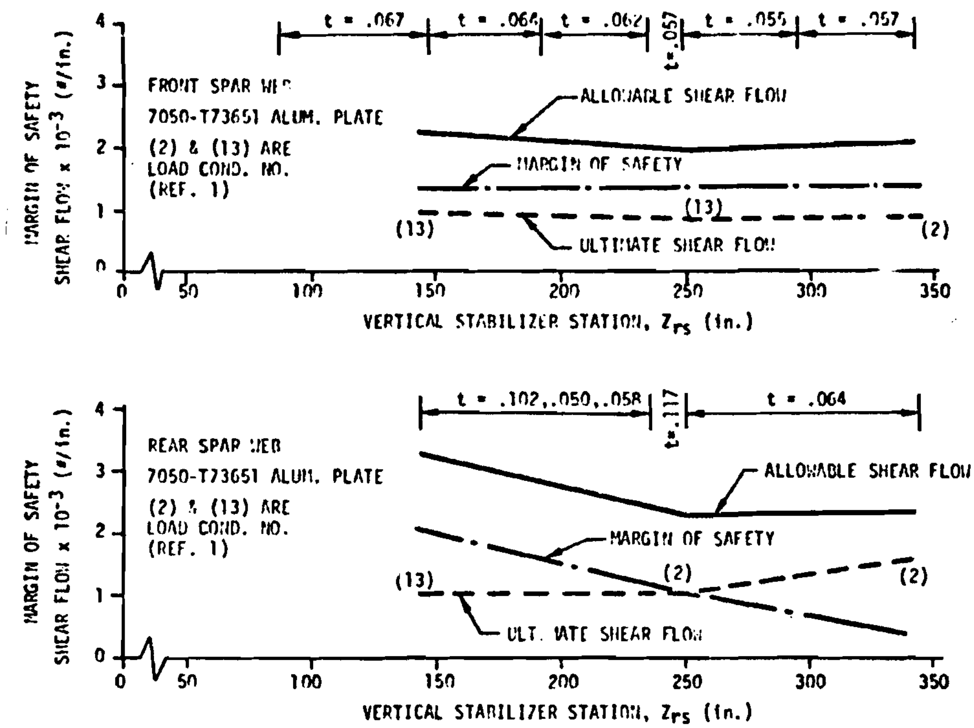

Figure 169 VERTICAL STABILIZER SPAR WEB MARGINS OF SAFETY

TABLE LXX SUMMARY OF VERTICAL STABILIZER BULKHEAD MARGINS OF SAFETY

BULKHEAD STATION	WEB* t (in.)	PANEL LOCATION (4)	ALLOWABLE SHEAR FLOW (#/in.)	DESIGN SHEAR FLOW (#/in.)	COND. NO.	M.S.
143.1	0.070	AT REAR SPAR	2,249	654 (1)	2	2.44
250.5	0.080	AT REAR SPAR	2,210	812 (2)	14	1.71
343.1	0.068	AT FRONT SPAR	2,132	-530 (3)	2	3.03

(1) DESIGN SHEAR FLOW FROM SHEAR LOAD IN P_4, P_8, AND P_{12} = (713 + 16,930 + 653) ÷ 28 = 654 lbs./in.

(2) DESIGN SHEAR FLOW FROM SHEAR LOAD IN P_4 AND P_8 = (188 + 12,058) ÷ 15 = 816 lbs./in.

(3) DESIGN SHEAR FLOW FROM SHEAR LOAD IN P_1, P_5, AND P_9 = (-540 -13,603 -555) ÷ 27.75 = -53[illegible] lbs./in.

(4) P4 = PANEL 4, ETC. FROM REFERENCE 1

*7050-T73651 ALUMINUM PLATE

ties were computed based on the drawings shown in Sections 5.1.1 and 5.1.3 and the rigidity changes relative to the initial baseline wing rigidity established (Figure 24). From Figures 25 and 26, the equation for the change in damping, as shown below, defined the incremental damping change Δg.

$$\Delta g = \int \left(\frac{\Delta g}{\%\Delta EI}\right)\left(\frac{\Delta EI}{EI_o}\right) \times 100\, dx + \int \left(\frac{\Delta g}{\%\Delta GJ}\right)\left(\frac{\Delta GJ}{GJ_o}\right) \times 100\, dx \tag{45}$$

where: $\frac{\Delta g}{\%\Delta EI}$ and $\frac{\Delta g}{\%\Delta GJ}$ are given in Figures 25 and 26.

$\frac{\Delta EI}{EI_o}$ = the change in the wing EI

$\frac{\Delta GJ}{GJ_o}$ = the change in the wing GJ

Both the improved baseline and the integral concept wings are flutter free as can be seen in the results tabulated below.

Frequency	Allowable Δg	Calculated Δg	Calculated Δg
Figures 25 and 26		Improved Baseline	Integral Concept
2.8	+0.18 $-\infty$	-0.0001752	-0.001163
3.5	+0.43 $-\infty$	-0.01235	-0.02898

7.4.2 Horizontal Stabilizer

The honeycomb concept horizontal stabilizer box structure was evaluated in conjunction with the vertical stabilizer box structure to verify that the empennage symmetric flutter requirements were met. The flutter free requirement is met if the change of empennage flutter speed (ΔV) relative to the baseline empennage is equal to or greater than zero. Change of empennage flutter speed is related to the rigidity changes as follows:

$$\Delta V = \int \left(\frac{\Delta V}{\%\Delta GJ}\right)\left(\frac{\Delta GJ}{GJ_o}\right)_{H.S.} \times 100\, dx + \int \left(\frac{\Delta V}{\%\Delta EI}\right)\left(\frac{\Delta EI}{EI_o}\right)_{H.S.} \times 100\, dx$$

$$+ \int \left(\frac{\Delta V}{\%\Delta EI}\right)\left(\frac{\Delta EI}{EJ_o}\right)_{V.S.} \times 100\, dx$$

where: $\left(\frac{\Delta GJ}{GJ_o}\right)_{H.S.}$ = the change of the horizontal stabilizer GJ

$\left(\frac{\Delta EI}{EI_o}\right)_{H.S.}$ = the change of the horizontal stabilizer EI

$\left(\frac{\Delta EI}{EJ_o}\right)_{V.S.}$ = the change of the vertical stabilizer EI

J_o, I_o = baseline torsional and bending moments of inertia

$\left(\frac{\Delta V}{\%\Delta GJ}\right)$ and $\left(\frac{\Delta V}{\%\Delta EI}\right)$ are given in Figure 171 for the horizontal and vertical stabilizers

For the minimum weight honeycomb sandwich panel concept (based on ultimate mode requirements only), the horizontal stabilizer portion of the integral had a ΔV equal to -7.34 KEAS and the vertical stabilizer portion of the integral had a ΔV equal to -30.32 KEAS. A parametric study was conducted to determine the minimum weight changes to either or both horizontal and vertical stabilizer box structure in order to obtain stiffness characteristics that would yield a ΔV equal to zero or greater.

A minimum weight increase was accomplished by changing only the vertical stabilizer spar caps to increase chordwise bending stiffness. The aluminum front and rear spar caps, therefore, are designed with a boron epoxy fill as shown in Table LXVIII.

Plots of the baseline and honeycomb concept rigidity values used in the empennage flutter speed evaluation are shown in Figures 172 and 173. An example evaluation is given in Table LXXI. Evaluation of the three integrals gives the following change of empennage flutter speed:

$$\Delta V = -52.19 + 44.85 + 7.56 = 0.22 \text{ KEAS}$$

Since ΔV is greater than zero, the honeycomb concept empennage is flutter free.

7.4.3 Vertical Stabilizer

The rigidity requirement of the honeycomb concept vertical stabilizer box structure is evaluated in conjunction with the horizontal stabilizer as described in Section 7.4.2.

7.5 WEIGHT ANALYSIS

The weight analysis for the baseline structure and the new structural concepts are presented in the following sections.

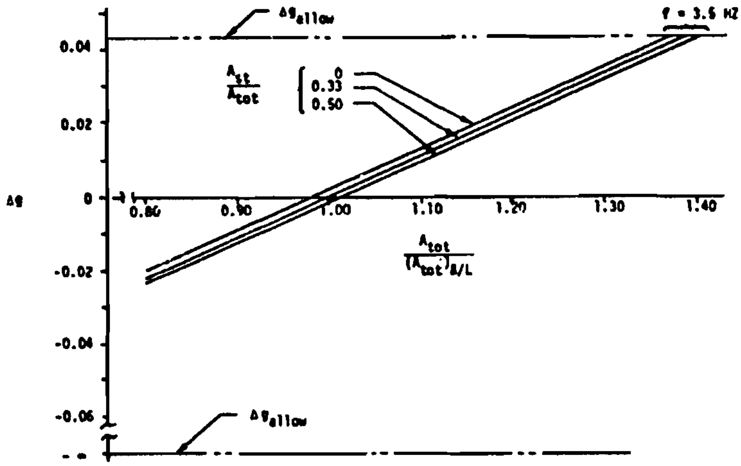

Figure 170 EFFECT OF WING PANEL GEOMETRY ON FLUTTER DAMPING PARAMETER

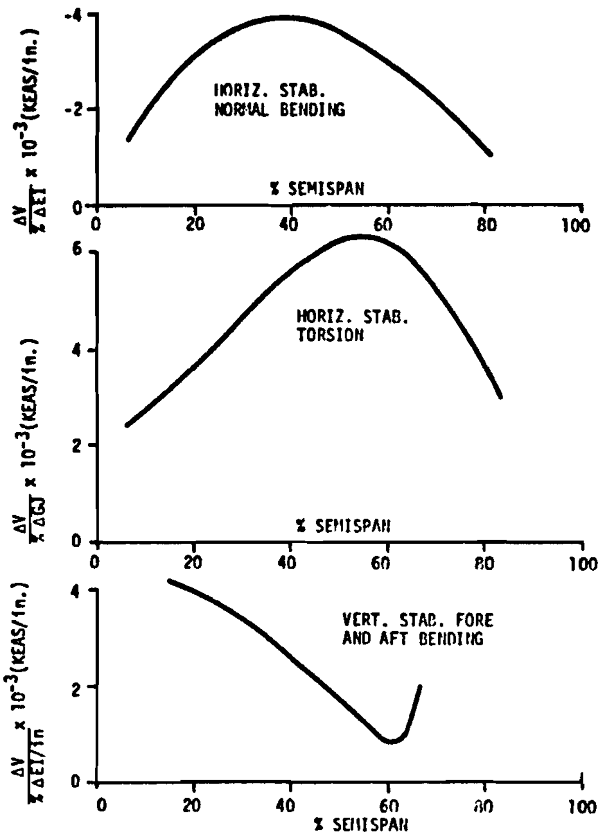

Figure 171 CHANGE IN EMPENNAGE FLUTTER SPEED WITH HORIZONTAL AND VERTICAL STABILIZER STIFFNESS VARIATIONS

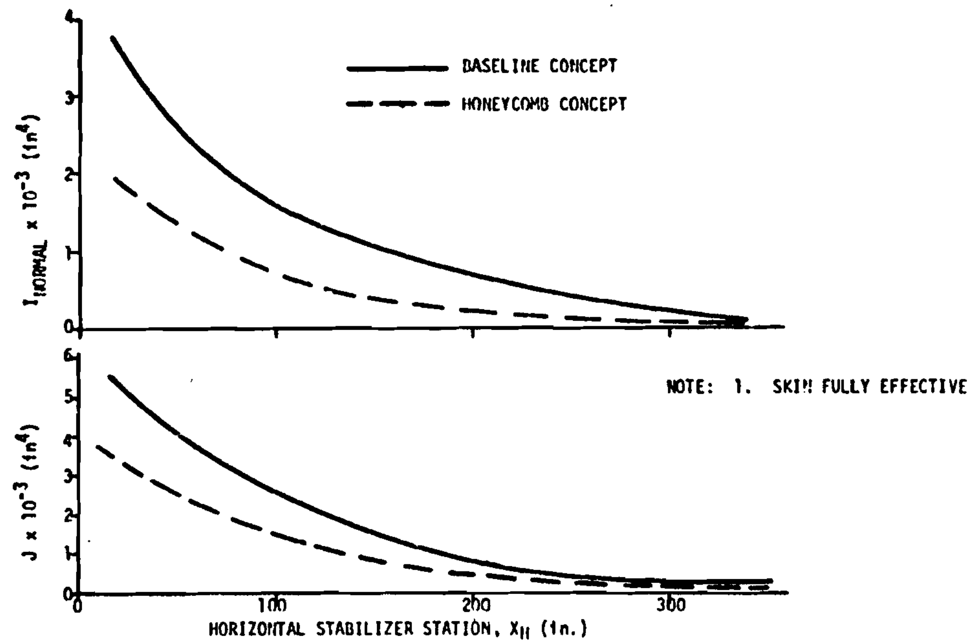

Figure 172 HORIZONTAL STABILIZER I_{NORMAL} AND J CURVES

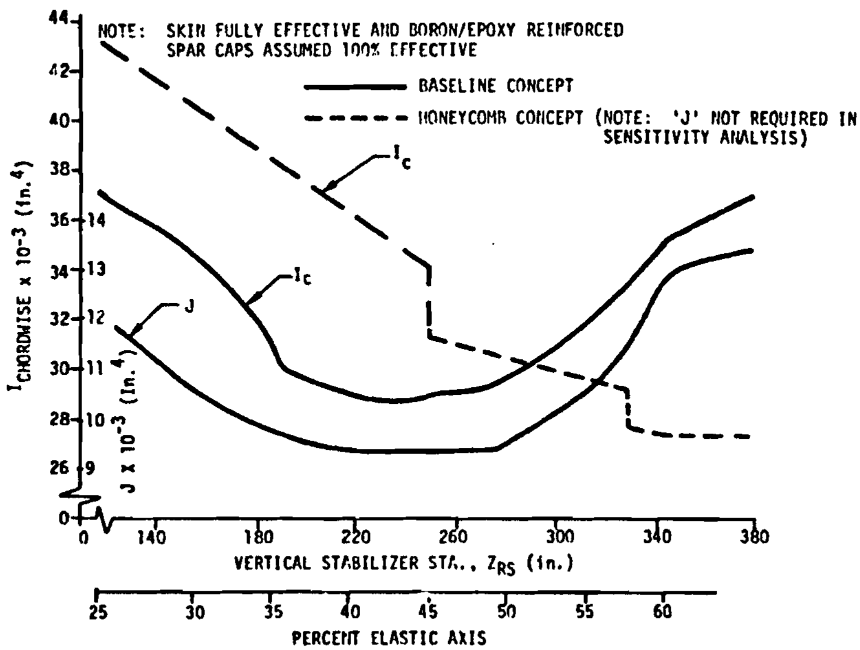

Figure 173 VERTICAL STABILIZER I_c AND J CURVES

TABLE LXXI CHANGE OF EMPENNAGE FLUTTER SPEED RESULTING FROM A CHANGE OF HORIZONTAL STABILIZER TORSIONAL STIFFNESS

% SEMI SPAN	MID % SEMI SPAN	STA. X_H (IN.)	d_X (IN.)	$\frac{\Delta V}{\% \Delta GJ}$ (KEAS/IN.)	J HONEYCOMB (IN^4)	J_o BASELINE (IN^4)	ΔJ $(J-J_o)$ (IN^4)	$\frac{\Delta J}{J_o}$	$\left(\frac{\Delta V}{\% \Delta GJ}\right)\left(\frac{\Delta J}{J_o}\right) \times 100 d_X$ (KEAS)
6									
	8.0	27.3	13.64	0.00253	3,180	4,930	-1750	-0.355	-1.225
10									
	12.5	42.6	17.05	0.00295	2,720	4,300	-1580	-0.367	-1.848
15									
	17.5	59.7	17.05	0.00342	2,300	3,700	-1400	-0.378	-2.206
20									
	22.5	76.7	17.05	0.00392	1,950	3,200	-1250	-0.391	-2.611
25									
	27.5	93.8	17.05	0.00442	1,600	2,730	-1130	-0.414	-3.119
30									
	32.5	110.8	17.05	0.00492	1,300	2,300	-1000	-0.435	-3.647
35									
	38.5	131.3	23.87	0.00548	1,000	1,850	-850	-0.459	-6.010
42									
	46.0	156.9	27.28	0.00605	750	1,420	-670	-0.472	-7.787
50									
	52.5	179.0	17.05	0.00632	600	1,070	-470	-0.439	-4.733
55									
	57.5	196.1	17.05	0.00630	500	860	-360	-0.419	-4.496
60									
	62.5	213.1	17.05	0.00605	400	700	-300	-0.429	-4.421
65									
	67.5	230.2	17.05	0.00555	340	580	-240	-0.414	-3.916
70									
	76.0	259.2	40.92	0.00431	260	400	-140	-0.350	-6.173
82									

$\Delta V = -52.192$ (KEAS)

7.5.1 Baseline Concept Weights

Table LXXII presents a summary of the design weights, geometry, and empty weights for the AMST baseline aircraft. The vehicle is sized for a 400 n-mi radius at the initial takeoff gross weight. STOL performance is achieved at the midpoint weight which includes fuel for the 400 n-mi return mission. The aircraft is configured with four JT8D-17 engines.

Detailed structural weight breakdowns are given in Tables LXXIII and LXXIV for the wing, empennage, and fuselage. These tabulations represent both the primary and secondary structure for the baseline vehicle. These values are for comparison with the weights from the structural concepts study.

The results of reducing the aircraft size due to the weight reductions provided by the advanced structural concepts are shown. Two resizing configurations are investigated. For the first resized configuration (completely resized), no restrictions are placed on the resizing; and, in the second case, the engine size is fixed (partially resized).

7.5.2 Advanced Concepts Structural Weights

Table LXXV presents the structural weight savings achieved through application of advanced structural concepts. Two concepts were investigated for the wing box structure. Concept No. 1 has integral stringers and rib attach flanges on the upper surface panel, while the Concept No. 2 upper panel employs non-integral construction with boron caps on the stringers. Both concepts have integrally stiffened lower panels. The use of 95 lb. of boron did not offset the weight savings due to integral construction, and Concept No. 2 is 64 lb. heavier than Concept No. 1. Concept No. 1 was chosen for the resizing study.

Concept No. 1 has a 1,002 lb. weight reduction prior to resizing, and further weight savings when resized.

The horizontal tail box utilizes integrally stiffened spar webs and bulkheads and sandwich construction on the box covers. The covers have linearly tapered core with face sheets that are tapered in most areas. Most of the weight savings shown in Table LXXV can be attributed to the cover design.

The vertical tail box also has integrally stiffened spar webs and bulkheads, and sandwich covers. However, most of the weight savings (approximately 150 lb.) is obtained by using a significant amount of boron in the front and rear spar caps.

The fuselage shell utilizes sandwich construction from fuselage station 366 to 982, which results in a 330 lb. weight reduction. The structure remains unmodified forward of station 366 and aft of station 982.

Boron infiltrated aluminum extrusions provide weight reduction in the cargo floor. Structural weight savings can also be translated into significant weight and size reductions in other aircraft components when resizing is employed. Table LXXVI has a summary of the vehicle description for the resize study. The group weight statement for the various aircraft sizes is presented in Table LXXVII. Resizing was performed by the "Parametric Weight Sensitivity Program," M5BA.

TABLE LXXII AMST WEIGHT SUMMARY

VEHICLE DESCRIPTION	BASELINE PRODUCTION A/P
Initial TOGW (lbs)	166,500
Midpoint TOGW (lbs)	150,000
Wing Area (Ft^2)	1,740
Engine Designation	JT8D-17
Engine Thrust (SLS/Eng)(103°F)	14,900
Sound Suppression	None
Horiz/Vert Tail Area (Ft^2)	643/462
Horiz/Vert Tail Length (In.)	743/616
Horiz/Vert Tail Volume	1.323/.1235
Wing Loading-Initial/MP (PSF)	95.7/86.2
Thrust Ratio-Initial/MP	.358/.397
Fuel Fraction-Initial/MP	.218/.132
Fuselage Dia/Length (In.)	216/1318
Cargo Compt. (Ft)	11.3x11.7x46.7
Fuel Capacity-Usable (lbs)	77,970
WEIGHTS	
1. Wing	18,765
2. Fuselage	24,367
3. V-Tail	3,460
4. H-Tail	3,234
5. Landing Gear	7,741
6. Flight Controls	3,966
7. Propulsion	21,709
8. Fuel System	768
9. Aux. Power Unit	966
10. Instruments	1,453
11. Hydraulics	1,436
12. Pneumatics	340
13. Electrical	1,736
14. Avionics	2,045

TABLE LXXII -- Concluded

WEIGHTS (Continued)	BASELINE PRODUCTION A/P
15. Furnishings	5,4[illegible]7
16. Air Conditioning	837
17. Ice Protection	254
18. Handling Gear	150
MANUFACTURER'S WEIGHT EMPTY	98,724
19. Operator's Items	4,510
Operator's Empty Weight	103,234
Payload	27,000
Fuel	19,766
TOGW - MIDPOINT	150,000
COST WEIGHTS	
Mfg. Empty Weight	98,724
Less: Rolling Assy	- 3,[illegible]9
Engines	-13,320
Cost Weight	82,055
Less Items Peculiar to AMPR	(- 3,039)
Starters	- 105
APU	- 410
Instruments	- 578
Battery & A.C. Supply	- 450
Avionics (Black Boxes)	- 1,183
Air Condition Units	- 242
Hydraulics (Drop-out Gen.)	- 71
AMPR WEIGHT	79,016

TABLE LXXIII BASELINE AERODYNAMIC SURFACE WEIGHTS

	COMPONENT	WEIGHT (lb)
WING	Wing Box	9118
	Wing/Fuselage Attach	516
	Leading Edge (Fixed)	482
	Trailing Edge (Fixed)	515
	Wing Tips	37
	Wing Fuselage Fairings	786
	Aileron Structure, Supports & Balance Wts.	405
	L.E. Flaps	460
	Slats & Support	776
	T.E. Flaps	2326
	Spoilers & Support	612
	Flap Hinge Fairings	119
	Main Flap Links & Support	2009
	Aft Flap Links & Support	604
	TOTAL	18765
HORIZONTAL TAIL	Horizontal Stabilizer Box	1749
	Leading Edge Structure	356
	Trailing Edge Structure	227
	Tips	10
	Elevators	772
	Elevator Hinges & Supports	120
	TOTAL	3234
VERTICAL TAIL	Vert. Stab. Box	1475
	Pivot Installation	410
	Leading Edge Structure	110
	Trailing Edge Structure	170
	Fairing & Dorsal	358
	Rudder Structure	830
	Rudder Hinges & Supports	107
	TOTAL	3460

TABLE LXXIV BASELINE FUSELAGE WEIGHTS

COMPONENT	WEIGHT (lb)
Fuselage Shell	7897
Wing & Main Landing Gear Support	1409
Nose Landing Gear Support	49
Vertical Stabilizer Support	1277
Cockpit Enclosure	981
Pressure Panels (Primary Structure)	470
Cockpit Floor & Support	322
Cargo Floor & Support	2892
Vehicle Loading Curb	402
Main Landing Gear Doors	747
Nose Landing Gear Doors	183
Aft Loading Door	1297
Ramp	2638
Pressure Panels & Bulkheads (Secondary Structure)	144
Main Landing Gear Pods	1306
Radome	142
Tailcone	161
Sealant	83
Cockpit Ladder & Stairs	13
Misc. Cargo Handling Provisions	125
Cockpit Down Vision Windows	250
Troop Door	212
Jump Door & Deflector	854
Misc. & Life Raft Doors	513
TOTAL	24367

TABLE LXXV ADVANCED CONCEPT STRUCTURAL WEIGHTS

COMPONENT	BASELINE	UNRESIZED	% SAVED	COMPLETELY RESIZED	% SAVED	PARTIALLY RESIZED	% SAVED
Wing*	(18,765)	(17,763)	5.3	(17,257)	8.0	(16,991)	9.5
Box Structure	9,118	8,116	11.0	7,876	13.6	7,763	14.9
Remainder	9,647	9,647	0	9,381	2.8	9,228	4.3
Horiz.	(3,234)	(3,031)	6.3	(2,978)	7.9	(2,948)	8.8
Box Structure	1,749	1,546	11.6	1,519	13.2	1,504	14.0
Remainder	1,485	1,485	0	1,459	1.8	1,444	2.8
Vert.	(3,460)	(3,288)	5.0	(3,231)	6.6	(3,249)	6.1
Box Structure	1,475	1,303	11.7	1,280	13.2	1,287	12.7
Remainder	1,985	1,985	0	1,951	1.7	1,962	1.2
Fuselage Δ	(24,367)	(23,899)	1.9	(23,802)	2.3	(23,809)	2.3
Shell, (366-982)	5,730	5,539	3.3	5,500	4.0	5,500	4.0
Floor (366-982)	1,841	1,702	7.6	1,702	7.6	1,702	7.6
Remainder	16,796	16,658	0	16,600	0	16,607	0

*Wing Concept with Integral Skins Δ Honeycomb Fuselage Shell

TABLE LXXVI SANDWICH FUSELAGE AIRCRAFT DESCRIPTION°

VEHICLE DESCRIPTION	BASELINE	UNRESIZED	COMPLETELY RESIZED	PARTIALLY RESIZED
Takeoff Wt. - STOL (Lb)	150,000	150,000	146,312	146,570
Wing Area (Ft^2)	1,740	1,740	1,697	1,671
Engine Description	JT8D-17	JT8D-17	JT8D-17 Type	JT8D-17
Engine Thrust (Lb/Eng)	14,900	14,900	14,532	14,900
Horiz. Tail Area (Ft^2)	643	643	632	626
Vert. Tail Area (Ft^2)	462	462	454	457
Horiz. Tail Length (In.)	743	743	743	743
Vert. Tail Length (In.)	616	616	616	616
Horiz. Tail Volume	1.3234	1.3234	1.3500	1.3680
Vert. Tail Volume	0.1235	0.1235	0.1260	0.1297
Wing Loading (PSF)	86.2	86.2	86.2	87.7
Thrust Ratio	0.3973	0.3973	0.3973	0.4066
Fuel Fraction	0.1318	0.1441*	0.1330	0.1329
Fuselage Diameter (In.)	216	216	216	216
Fuselage Length (In.)	1,318	1,318	1,318	1,318

°With Wing Concept #1 *Extended Mission

TABLE LXXVII GROUP WEIGHT STATEMENT FOR ADVANCED STRUCTURE

ITEM	BASELINE	UNRESIZED	% SAVED	COMPLETELY RESIZED	% SAVED	PARTIALLY RESIZED	% SAVED
Wing (Concept #1)	18,765	17,763	5.3	17,257	8.0	16,991	9.5
Horizontal Tail	3,234	3,031	6.3	2,978	7.9	2,948	8.8
Vertical Tail	3,460	3,288	5.0	3,231	6.6	3,249	6.1
Fuselage (Sandwich)	24,367	23,899	1.9	23,802	2.3	23,808	2.3
Landing Gear	7,741	7,741	0	7,551	2.5	7,564	2.3
Flight Controls	3,966	3,966	0	3,905	1.5	3,875	2.3
Propulsion	21,709	21,709	0	21,173	2.5	21,709	0
Fuel System	768	768	0	759	1.2	752	2.1
APU	966	966	0	966	0	966	0
Instruments	1,453	1,453	0	1,453	0	1,453	0
Hydraulics	1,436	1,436	0	1,414	1.5	1,415	1.5
Pneumatics	340	340	0	340	0	340	0
Electrical	1,736	1,736	0	1,736	0	1,736	0
Avionics	2,045	2,045	0	2,045	0	2,045	0
Furnishings	5,497	5,497	0	5,497	0	5,497	0
Air Conditioning	837	837	0	837	0	837	0
Ice Protection	254	254	0	254	0	254	0
Handling Gear	150	150	0	150	0	150	0
Structural Weight (No. L.G.)*	53,922	52,077	3.4	51,263	4.9	51,092	5.2
Structural Weight (With L.G.)*	61,663	59,818	3.0	58,814	4.6	58,656	4.9
Manufacturer's Empty Weight	98,724	96,879	1.9	95,348	3.4	95,589	3.2
Operator's Items	4,510	4,510	0	4,505	---	4,501	---
Operator's Empty Weight	103,234	101,389	1.8	99,853	3.3	100,090	3.0
Payload	27,000	27,000	0	27,000	---	27,000	---
Return Segment Fuel	19,766	21,611**	0	19,459	1.6	19,480	1.4
Takeoff Weight - STOL	150,000	150,000	0	146,312	2.5	146,570	2.3

*Includes Nacelle & Pylon Structure (4096 Lb. for Baseline); **Extended Mission.

7.5.3 Growth Factors

The term "growth factor" defines the total weight effect on a vehicle due to resizing as a result of a weight increase or decrease to the unresized vehicle. The numerical value of a growth factor is the number by which the initial weight increment is multiplied to obtain the total vehicle weight change. The mission performance of the vehicle is usually held constant.

Growth factors are especially pertinent to the medium STOL transport structural concepts studies. For example, if a new structural concept produced a weight savings of 1,000 pounds to the fuselage, the takeoff gross weight could be reduced by an amount greater than 1,000 pounds while retaining the same payload, range, and field length performance. This additional reduction in takeoff weight would result from decreases in wing size, tail size, and mission fuel, plus the corresponding reduction in structures and systems weights (i.e., reduced gear weight, reduced wing structure and flight controls weight due to change in wing size, etc.). The sum of the initial weight reduction plus the reductions due to resizing divided by the initial reduction is the growth factor.

Table LXXVIII presents growth factors for the AMST baseline based on initial reductions of 1,000 pounds to the unresized vehicle. Two cases are shown. Case I represents a constant wing loading and thrust-to-weight ratio (completely resized) to maintain constant field length performance. Fuel fraction is increased slightly in order to maintain a constant 400-nautical mile return mission. This case assumes a "rubber" engine with the characteristics of the JT8D-17, since the baseline engine is a fixed JT8D-17 installation. Case II (partially resized) presents the growth factors for constant field length and range for the fixed JT8D-17 installation. As the gross weight is reduced, the thrust-to-weight ratio increases (constant thrust) and, therefore, the wing loading is increased to maintain constant field length. Fuel fraction is also increased slightly, as in Case I, in order to maintain constant range.

As an example of how to use the growth factor tables, assume that 2,800 pounds, 1,000 pounds, and 3,600 pounds could be saved in the unresized wing, empennage and fuselage, respectively. The total savings to OEW and TOGW, using Case II values, for the vehicle resized to constant performance is as follows:

Component	(1) Initial Weight Reduction	(2) Growth Factor	(3) OEW (1 x 2)	(4) Growth Factor STOGW	(5) STOGW (1 x 4)
Wing	2,800	1.80	5,040	2.01	5,628
Empennage	1,000	1.79	1,790	2.00	2,000
Fuselage	3,600	1.83	6,588	2.05	7,380
Total Change	7,400		13,418		15,008

Therefore, for a total initial weight reduction of 7,400 pounds, 13,418 pounds can be saved in OEW and 15,008 pounds in TOGW.

All growth factors are based on constant tail volume and tail length. Parametric weight values for aerodynamic sizing and growth factor derivation are obtained from the "Parametric Weight Sensitivity Program," M5BA.

The growth factors obtained in this study are shown in Table LXXIX. The Table LXXIX values are about 95 percent as large as those presented in Table LXXVIII. There are two reasons for the small difference between the two tables. Table LXXVIII assumed a constant tail volume, whereas the tail volume tends to increase slightly as aircraft size is reduced. The second reason is that growth factor decreases (partially resized), most noticeably as the magnitude of the weight saving increases.

7.5.4 Material Description

Material descriptions were developed for the baseline aircraft, and the completely resized advance structural concept aircraft (see Tables LXXX and LXXXI).

7.5.5 Cost Weight and AMPR Weight

The cost weights and AMPR weights for the baseline, unresized, partially resized (fixed engine size) and the completely resized aircraft are found in Table LXXXII.

TABLE LXXVIII GROWTH FACTORS - AMST PRODUCTION - JT8D-17 ENGINE									
ITEM	WING LOADING (PSF)	THRUST (SLS) TO WEIGHT RATIO	FUEL TO WEIGHT RATIO	OEW (LBS)	Δ OEW (LBS)	GROWTH FACTOR OEW	STOL TOGW (LBS)	Δ TOGW (LBS)	GROWTH FACTOR STOGW
CASE I - Vary Wing Area and Thrust									
Base Case	86.21	.3973	.1317	103,234	----	----	150,000	----	----
Wing - 1000#	86.21	.3973	.1322	101,357	-1877	1.88	147,908	-2092	2.09
Tail - 1000#	86.21	.3973	.1322	101,365	-1869	1.87	147,917	-2083	2.08
Fuselage - 1000#	86.21	.3973	.1322	101,323	-1911	1.91	147,869	-2131	2.13
Landing Gear - 1000#	86.21	.3973	.1322	101,351	-1883	1.88	147,901	-2099	2.10
Engines - 1000#	86.21	.3973	.1322	101,379	-1855	1.86	147,934	-2066	2.07
Systems* - 1000#	86.21	.3973	.1322	101,337	-1897	1.90	147,886	-2114	2.11
CASE II - Vary Wing Area at Constant Thrust									
Base Case	86.21	.3973	.1317	103,234	----	----	150,000	----	----
Wing - 1000#	86.93	.4027	.1321	101,439	-1795	1.80	147,993	-2007	2.01
Tail - 1000#	86.93	.4027	.1321	101,449	-1785	1.79	148,005	-1995	2.00
Fuselage - 1000#	86.93	.4028	.1321	101,401	-1833	1.83	147,950	-2050	2.05
Landing Gear - 1000#	86.93	.4028	.1321	101,421	-1813	1.81	147,973	-2027	2.03
Engines - 1000#	86.93	.4028	.1321	101,422	-1812	1.81	147,975	-2025	2.03
Systems* - 1000#	86.93	.4028	.1321	101,417	-1817	1.82	147,969	-2031	2.03

* Systems are those items that vary with wing area, TOGW, and thrust: Surface controls, fuel system, hydraulics and ice protection; other systems (i.e. Avionics) have the same growth factors as the fuselage.

TABLE LXXIX GROWTH FACTORS FOR ADVANCED AIRFRAME					
ITEM	INITIAL WEIGHT REDUCTION	CASE I COMPLETELY RESIZED		CASE II PARTIALLY RESIZED	
		ΔOEW	ΔTOGW	ΔOEW	ΔTOGW
WING	1002	1508	1508	1774	1774
HORIZONTAL TAIL	203	256	256	286	286
VERTICAL TAIL	172	229	229	211	211
FUSELAGE (SANDWICH)	468	565	565	559	559
MISCELLANEOUS	0	823	823	314	314
FUEL	0	0	307	0	286
TOTAL WEIGHT REDUCTION	1845	3381	3688	3144	3430
GROWTH FACTOR	-	1.83	2.00	1.70	1.86

TABLE LXXX BASELINE STRUCTURE MATERIAL WEIGHT BREAKDOWN

COMPONENT	GLASS, FIBER-GLASS	FILLER, ATTACH, PAINT	ADHESIVES	ALUMINUM FORGING	ALUMINUM NON FORGING	STEEL	TITANIUM	ALUMINUM HONEYCOMB	HIGH DENSITY METAL	BORON-ALUMINUM	TOTAL
Wing Structure			NONE					NONE		NONE	(18,765)
Box		543		165	8,410						9,118
Remainder	786	95		3,197	1,811	681	2,930		147		9,647
Horizontal Tail Structure											(3,234)
Box		85		55	1,609						1,749
Remainder		44		307	1,134						1,485
Vertical Tail Structure											(3,460)
Box		79		61	1,335						1,475
Remainder		52		384	1,455	94					1,985
Fuselage Structure											(24,367)
Shell (Forward of 366)		20			251						271
Shell (366 to 982)		182			4,980						5,162
Shell (Aft of 982)		95			2,369						2,464
Other Primary Structure	681	80		2,295	1,524						4,580
Cargo Floor, Ramp and Supports	402	180		320	4,830	200					5,932
Remainder	232	263	NONE	247	4,889	327		NONE		NONE	5,958
TOTAL	2,101	1,718	0	7,031	34,597	1,302	2,930	0	147	0	49,826

TABLE LXXXI RESIZED STRUCTURE MATERIAL WEIGHT BREAKDOWN (#1 WING - SANDWICH FUSELAGE)

COMPONENT	GLASS, FIBER-GLASS	FILLER, ATTACH, PAINT	ADHESIVES	ALUMINUM FORGING	ALUMINUM NON FORGING	STEEL	TITANIUM	ALUMINUM HONEY-COMB	HIGH DENSITY METAL	BORON* / BORON ALUMINUM	TOTAL
Wing Structure											(17,257)
Box		175			7,701						7,876
Remainder	764	93		3,109	1,761	662	2,849		143		9,381
Horizontal Tail Structure											(2,978)
Box		112	109		1,185			113			1,519
Remainder		43		302	1,114						1,459
Vertical Tail Structure											(3,231)
Box		15	59	110	909			132		55*	1,280
Remainder		51		378	1,430	92					1,951
Fuselage Structure											(23,802)
Shell (Forward of 366)		20			251						271
Shell (366 to 982)		211	561	609	2,710			769			4,860
Shell (Aft of 982)		95			2,369						2,464
Other Primary Structure	681	76		2,190	1,508						4,455
Cargo Floor, Ramp and Supports	402	180		320	2,990	200				1,702	5,794
Remainder	232	263		247	4,889	327					5,958
TOTAL =	2,079	1,334	729	7,265	28,817	1,281	2,849	1,014	143	55* / 1,702	47,268

TABLE LXXXII ADVANCED CONCEPT AIRFRAME (HONEYCOMB FUSELAGE) COST WEIGHT AND AMPR WEIGHT

ITEMS		BASELINE	ADVANCED CONCEPT		
			UNRESIZED	COMPLETELY RESIZED	PARTIALLY RESIZED
MANUFACTURE'S EMPTY WEIGHT		98,724	96,879	95,348	95,589
LESS	ROLLING ASSEMBLY	-3,349	-3,349	-3,267	-3,272
	ENGINES	-13,320	-13,320	-12,991	-13,320
COST WEIGHT		82,055	80,210	79,090	78,997
LESS	STARTERS	-105	-105	-102	-105
	APU	-410	-410	-410	-410
	INSTRUMENTS	-578	-578	-578	-578
	BATTERY & A.C. SUPPLY	-450	-450	-450	-450
	AVIONICS (BLACK BOXES)	-1,183	-1,183	-1,183	-1,183
	AIR CONDITIONING UNITS	-242	-242	-242	-242
	HYDRAULICS (DROP-OUT GENERATOR)	-71	-71	-71	-71
AMPR WEIGHT		79,016	77,171	76,054	75,958

SECTION VIII

MANUFACTURING METHODS

8.1 METAL PROCESSING

Advanced design concepts for the stol transport evolved from studies emphasizing reduction in the number of parts required in an effort to reduce cost. The resulting designs utilize large integrally machined or honeycomb sandwich structural components with relatively few mechanical attachments. Fabrication of the large components utilizes existing conventional processes, and no special problems are expected except for the double curvature forming of isogrid. The unique feature of the advanced design concepts is the large size of many of the structural components. Larger facilities are required for such processes as heat treatment, penetrant inspection, ultrasonic inspection, check and straighten operations, and the curing of honeycomb sandwich components.

8.2 METAL REMOVAL

Precision machining of complex geometric patterns from thick plate and forging stock with dimensional conformance and required surface finish is necessary for the success of the advanced design concepts. The machining of the integrally stiffened wing cover and fuselage isogrid panels from aluminum plate stock involves the removal of a large volume of material. Die forgings were selected as the stock material for structural components where possible to reduce the machining required.

8.2.1 Machining

The two primary machining techniques proposed are numerically controlled machining and chemical milling. Multiple-spindle N/C machines to be used to machine the large structural components, wherever possible. For surface finishes required, cutters using replaceable lockable carbide inserts to be used. These cutters offer the additional advantage of lower tool replacement cost when compared to the use of brazed carbide inserts. The cutters to have the capability to end cut, side cut, and undercut to accommodate the flanged stiffeners of the design concepts. The machining to be accomplished with the stock material in "AQ" condition to increase tool life, and minimize heat treatment and check and straighten operations.

Surface finishes to be controlled by optimizing feeds and speeds and designing pockets with radii that permit correct tool loading. Float-passes to be used where feeds arc decreased and surface speeds increase to generate fine finishes. Hand finishing to be used to spot touch areas where machined finishes do not meet engineering requirements. The use of float-pass and hand finish techniques to be minimized to reduce cost.

Three types of numerically controlled machines--direct computer controlled, magnetic tape, and punched tape--were evaluated to determine the most effective. For production applications, direct computer control provides the most rapid response in verifying and modifying programs to reflect engineering design changes. Magnetic tape or punched tape methods are inflexible in that changes must be programmed separately, then processed into the controller for function checks. Direct computer control eliminates this intermediate step.

Conventional machining techniques can be used to machine honeycomb cores used in the sandwich panels with no special problems expected. Bevel edges of the core can be provided by standard band saw type operations.

Boron/epoxy reinforced aluminum extrusions were considered for extra stiffness in wing, floor, and vertical stabilizer assemblies. The high ratio of aluminum to boron in a typical extrusion cross-section complicates the machining of the extrusion because of the diverse cutting properties of the aluminum and boron fibers. Boron can only be cut with diamond tooling, as the high hardness of boron precludes the use of conventional steel or carbide cutting materials. Cutting through the aluminum extrusion tends to fill the diamond wheel and stop the cutting action of the diamonds. Present in-house machining efforts are treating this problem by using special metal matrix wheels at high surface speeds to minimize filling. Special oscillating grinding wheel operations can be used to grind off the excess boron reinforcement on the outside surface of the vertical stabilizer spar caps. Boron-reinforced extrusions could be purchased to net lengths from proven suppliers to eliminate machining operations on assembly.

8.2.2 Chemical Milling

The ribs of the wing and horizontal and vertical stabilizer, and the wing spars, are integrally stiffened members with large, flat webs between stiffeners. Web thicknesses are generally .040 to .10 inch thick with variations in thickness along the longitudinal rib dimension. The wing cover panels are integrally stiffened and are tapered spanwise and chordwise. Skin thicknesses range from .063 up to approximately .156 inch thick. Stringer cross-sectional areas are tapered spanwise.

After numerical control machining to a minimum thickness of approximately .090, the chemical milling process will be used to obtain the final thickness required. By masking and withdrawing the structural components at a controlled rate, the web and stiffener thicknesses may be tapered to engineering requirements. No special problems are expected in chemical milling the structural components, but facilities must be provided to accommodate the large wing cover panels and spars.

8.3 FORMING

The use of integrally stiffened panels, especially those with an isogrid network, requires some special forming techniques. The forming of integrally stiffened panels has been performed on brake presses and creep apparatus. These methods have certain limitations: brake forming is limited to simple contours only and creep forming is expensive and constrained by part size.

The rapid growth in shot peening among manufacturers over the past decade, and advancements through research and development have made this process a highly favorable candidate for forming these large panels. Research and development in the shot peening of panels to simple and compound contours support peening techniques as being both economical and reliable. However, additional development is required for double contouring.

Conventional forming methods will be utilized for the horizontal and vertical stabilizer honeycomb sandwich panels and conventionally constructed fuselage components. No special problems are expected in these areas. Large autoclaves are required to accommodate the large honeycomb panels.

8.4 JOINING

The large size of the structural components of the advance design concepts reduces the number of mechanical attachments required in the advanced STOL transport. There are several types of mechanical attachments that offer advantages over conventional types. Crown flush rivets eliminate rivet shaving and the associated skin rivet marking problems. Aerodynamic smoothness is maintained provided the tolerances on the rivet head and countersink are held. Other crown flush attachments 1) prevent structural damage when driving interference fasteners, 2) provide increased head tension strength, and 3) insure full head seating prior to the nut or collar installation.

A Rivbolt fastening system should be considered for attachments up to 3/8 inch diameter and 4D grip in fatigue critical areas where permanent attachments are required. Stationary and portable installation equipment is available. Taperloks should also be considered for use in fatigue critical areas. Stress-coining techniques with 100% inspection can be used.

Improved coatings and lubricants for interference fit attachments should be used to expand the use of straight shank fasteners in areas of greater than 4D material thickness to prevent adhesion upon installation.

In honeycomb sandwich panels where attachments are installed, densified core inserts or "potting" can be used to prevent the core from crushing and to transfer the load into the panel. No special problems are expected.

Adhesive bonding is a joining technique that is used extensively in the advanced concepts. The honeycomb sandwich cover panels of the horizontal and vertical stabilizer, and the honeycomb fuselage shall all use conventional adhesive systems. Large autoclaves are required to fabricate these components. The spar caps and splice doublers of the horizontal and vertical stabilizer are bonded to the cover panels. Accurate tolerance control is a requirement in these areas.

Adhesives are used to bond the boron reinforcement to the stringers of the wing, to the vertical stabilizer spar caps, and to the cargo floor panels. Cold setting adhesives that are environmentally resistant are required for this operation, and several candidates should be evaluated to determine their efficiency. Development of a suitable new adhesive system may be required.

8.5 BORON/EPOXY REINFORCEMENT

The spar caps of the vertical stabilizer will be reinforced by infiltrating with boron/epoxy reinforcement. Figure 174 shows a schematic of the operation. The 7050-T6511 aluminum alloy "T" spar caps will be infiltrated with boron/epoxy composite by pultrusion. The pultrusion die is approximately 30 inches long, and the filler plugs are aligned with the aluminum T's after the boron/epoxy filaments and resin are bonded onto the front end of the aluminum "T." The pultrusion die temperature is maintained at 350°F. The pull rate of the infiltrated "T" is 1 to 3 inches per minute. The boron/epoxy infiltrated aluminum "T" will be sufficiently cured going through the pultrusion

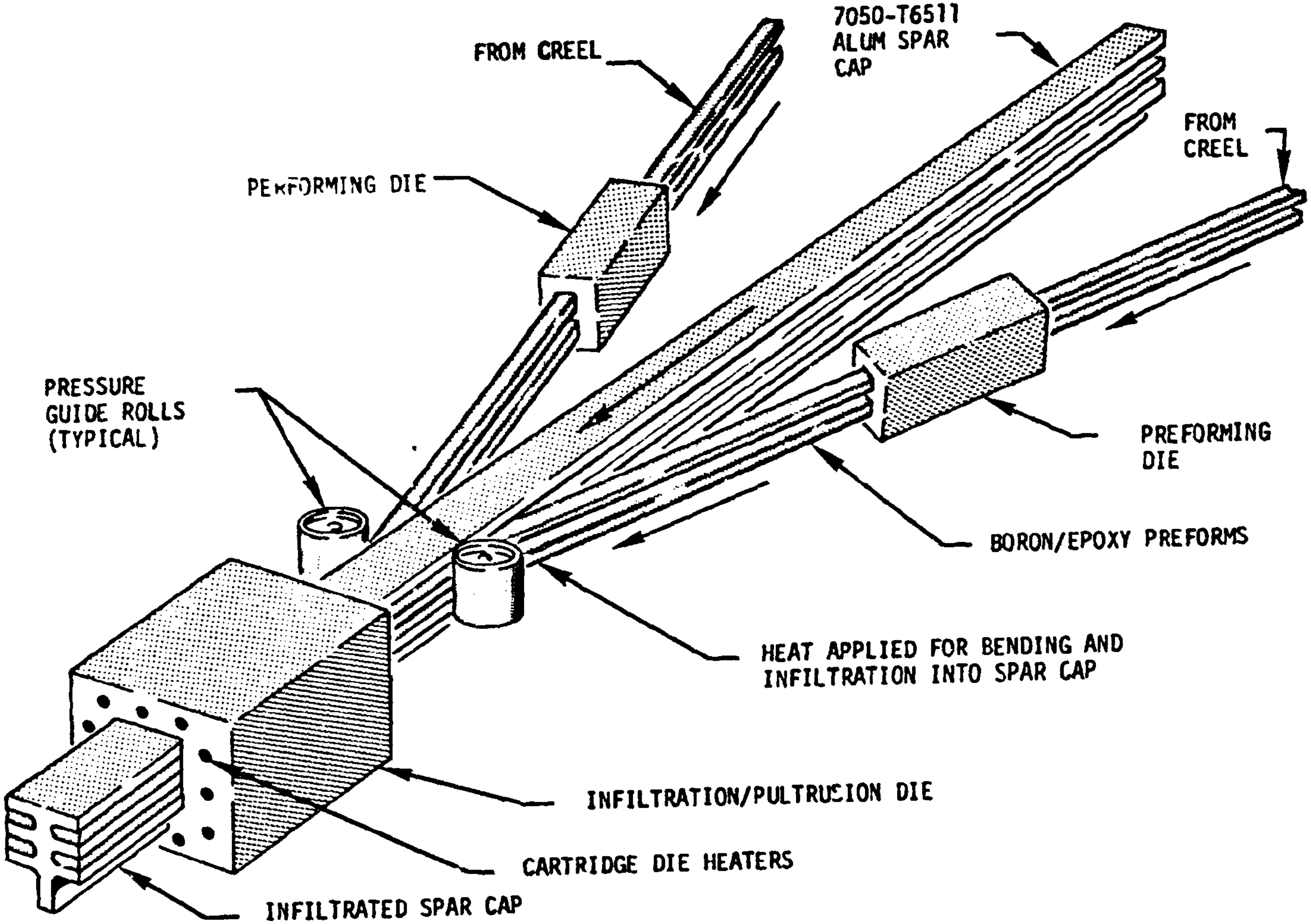

Figure 174 SCHEMATIC OF METHOD FOR INFILTRATING SPAR CAP WITH BORON-EPOXY COMPOSITE

die to allow an oven post cure without mold pressurization. After the 30 foot long double length infiltrated "T" leaves the pultruder, the boron/epoxy irregular filaments existing beyond the aluminum "T" surface are ground off with an aluminum oxide wheel. The grinding wheel oscillates while rotating to ensure a smooth outside surface.

The cargo floor planks are reinforced by infiltrating the aluminum extrusions with boron filaments. This method offers many advantages, but it's limited by the inability to obtain infiltrated extrusions longer than approximately 20 feet in length, and the lack of an effective method of reducing the amount of boron reinforcement if the area of the stringer is reduced.

8.6 MANUFACTURING METHODS DEVELOPMENTS REQUIRED

The advanced design concepts for the AMST transport require development of techniques to provide: 1) infiltrated reinforced extrusions between 50 and 60 feet in length, 2) suitable methods of reducing reinforcement area along the length of the infiltrated extrusion, 3) cost-effective techniques for reinforcing extrusions by pultrusion, 4) effective environmentally resistant adhesive systems that cure at room temperature, 5) further capability in the area of shot peen forming of double contours in isogrid panels and with determination of the degree and effects of stress distribution between peened and unpeened areas, and 6) large die forgings between 50 and 60 feet in length.

8.6.1 Boron/Epoxy Infiltrated Extrusions

Continuous pieces of infiltrated boron extruded metal of 50 foot lengths for floor supports have not been produced to date. Somydevelopment and analysis will be necessary to confirm that the part can be made and that the bond of resin to metal will withstand thermal expansions and contractions and repeated loadings during service environment.

8.6.2 Boron/Epoxy Pultrusion

Development work is essential to establish the economics of pultruding the boron/epoxy into place. Analysis to confirm that the bond of resin to metal will withstand thermal expansions and contractions and loadings during service is necessary for the proposed stiffening of spar caps.

8.6.3 Shot Peen Forming

In support of the concept of shot peen forming of isogrid fuselage skin panels, Douglas has a development program in progress to evaluate and demonstrate the shot peen forming capability for contouring isogrid panels with stiffeners approximately one inch in height. Consideration must also be given to node areas and the degree and effect of stress distribution between peened and unpeened areas.

8.6.4 Large Forgings

The wing box concept has incorporated the use of large single piece die forged front and rear spars. Die forged upper and lower wing cover panels may be used to reduce the amount of machining required and for increased material properties. The 50 foot lengths proposed exceed the current state-of-the-art of approximately 30 feet. Discussions with the large die forgers indicate the limited size of the current die platens could be circumvented by the use of overlapping segmented dies to produce the longer forged lengths.

SECTION IX

NONDESTRUCTIVE INSPECTION

9.1 NDI INSPECTION SENSITIVITY

Fracture critical parts will require inspections for material and fabrication defects per NDI process specifications and per damage tolerance requirements. A planar discontinuity, sharply terminated, and oriented normal to the predominant tensile stress is most effective in reducing performance and is most easily accommodated in fracture mechanics calculations. In most designs, this orientation will also be transverse to the long axis of the part and perpendicular to the surface. For most NDI procedures, this type of discontinuity is readily detectable.

9.1.1 Material Inspection

Minimum initial defect sizes are specified in MIL-A-XXXXXX (Appendix A). Smaller initial flaw sizes may be assumed subsequent to a demonstration that all flaws larger than these assumed sizes have at least a 90% probability of detection with a 95% confidence level. The results of demonstration tests, as reported in References 46 and 47 are shown in Figure 175. Recent results, as noted in Reference 48, are shown in Figure 176. These results indicate that radiography should not be used during production inspection of fracture critical parts. Test methods should be confined to penetrant, magnetic-particle, eddy-current, and ultrasonic shear or surface wave inspections.

The most recent and realistic NDI demonstration program was conducted at the B-1 Division of Rockwell International, at Los Angeles, in conjunction with Dr. Packman of USAF Materials Laboratory at Dayton. The results, obtained using optimum inspection techniques on different materials, are shown in Table LXXXIII. The minimum detectable flaw size was for cracks a/2c = 1/2; where a = crack depth, and 2c = crack length. For the AMST program, it is assumed that equal results will be demonstrated with a 90% probability at a 95% confidence level using production conditions, equipment, and personal.

9.1.1.1 At Locations Other than Holes - The assumed initial damage size shall be (a/Q) = .10 where (a) is measured in the principal direction of crack growth, and Q is the flaw shape parameter. The (a/Q) values must be determined for the material and temper finally selected for the design concepts. However, for the purpose of analysis, a hypothetical flaw size curve is shown in Figure 177. The shape is based on the assumption that the longer the flaw, the shallower it can be and still be found and vice-versa. In general, different NDI methods will have different detectability limits. For each flaw depth (a), with its corresponding length (2c), a depth to length ratio (a/2c) can be calculated as shown in Figure 178. In the available literature, there are few data relating detectability to flaw size, especially data relating depth and length. The study, in Reference 49, took data from References 46 and 50 for penetrant inspection of 7075-T651 and plotted detectable flaw size data as shown in Figure 179. While several flaw sizes were studied, only a (a/2c ≈ .5) was represented. When the data is sparse as in this case, some assumption must be made regarding the real curve. The intuitive curve would be hyperbolic through the known point and one such curve is

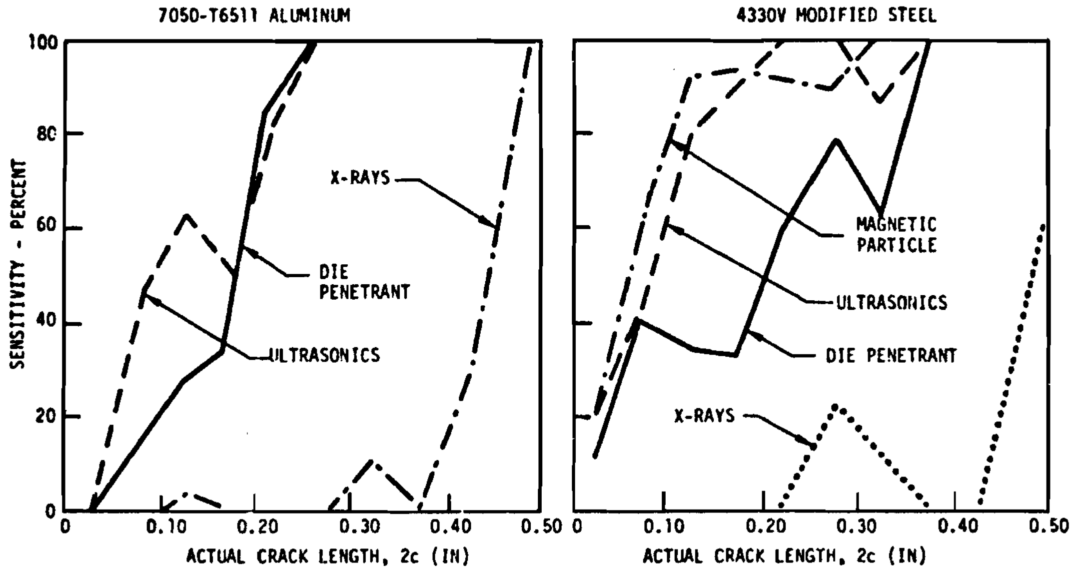

Figure 175 SENSITIVITY OF NDT INDICATIONS IN DETECTING SURFACE FATIGUE CRACKS

REF. 46 & 47

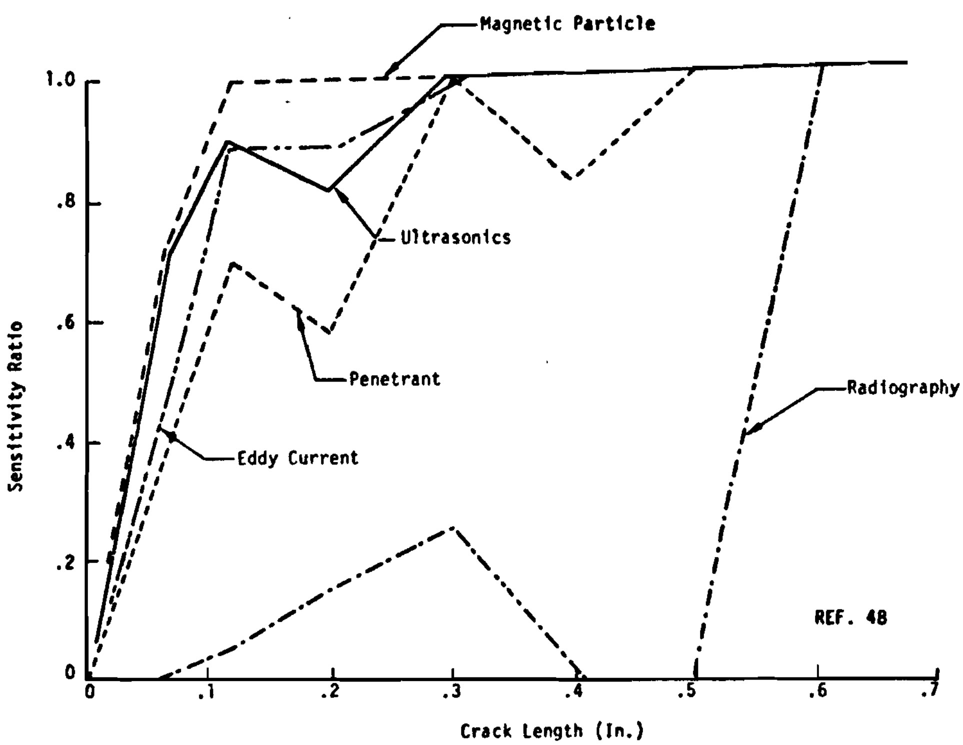

Figure 176 SENSITIVITY OF THE FIVE NDT METHODS TO SURFACE FLAWS

TABLE LXXXIII NDI DEMONSTRATION PROGRAM FOR B-1 BOMBER

ITEM	NDI METHOD	MIN. FLAW LENGTH (2C) (INCH)	PRODUCT	R.I. B-1 DIV. REPORT NO.
1	Penetrant (P5F-2.5)	0.025 - 0.050 △1	Titanium Extrusion, Plate, Sheet	TFD-72-793
2	Penetrant (P5F-2.0)	0.030 - 0.075 △1	Titanium Forgings or Diffusion Bonded	TFD-72-1005 TFD-72-1515
3	Penetrant (P5F-2.0)	0.049 - 0.080 △1	PH13-8Mo Steel	TFD-73-496
4	Penetrant (P5F-2.5)	0.037 - 0.068 △1	Aluminum	TFD-72-767
5	Magnetic Particle (fluorescent)	0.070 - 0.100 △1	Steel	TFD-72-768
6	Ultrasonic (shear wave)	0.076 - 0.100 △1	Welded steel	TFD-79-372
7	Ultrasonic (shear wave)	0.048 - 0.090 △1	Wrought or Welded Titanium	TFD-73-371
8	Ultrasonic (shear wave)	0.108 - 0.126 △1	Wrought Steel	TFD-73-140
9	Eddy Current (hole probe)	0.048 - 0.060 △2	Stacked steel, Aluminum and Titanium	TFD-73-27
10	Ultrasonic (long wave)	0.046 dia. (3/64) △3	Titanium Wrought or Diffusion Bonded	TFD-72-677-1

△1 Flaw

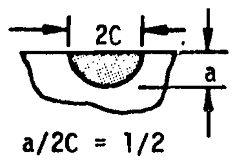

a/2C = 1/2

△2

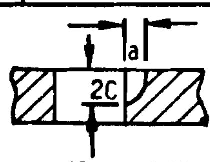

a/2C = 1/2

△3

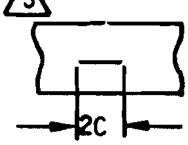

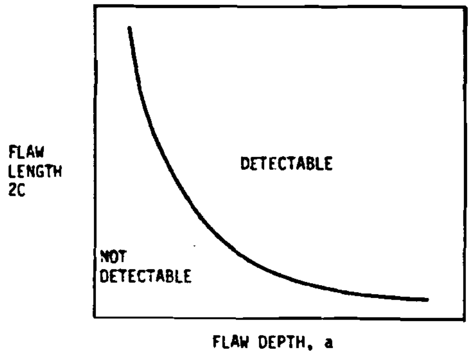

Figure 177 INTUITIVE LIMITS OF FLAW SIZES DETECTABLE BY NDT

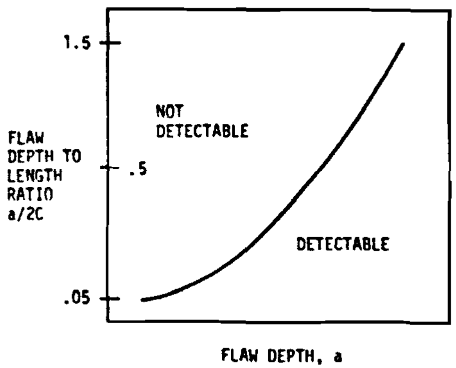

Figure 178 INTUITIVE LIMITS OF FLAW DEPTH TO LENGTH RATIO DETECTABLE BY NDT

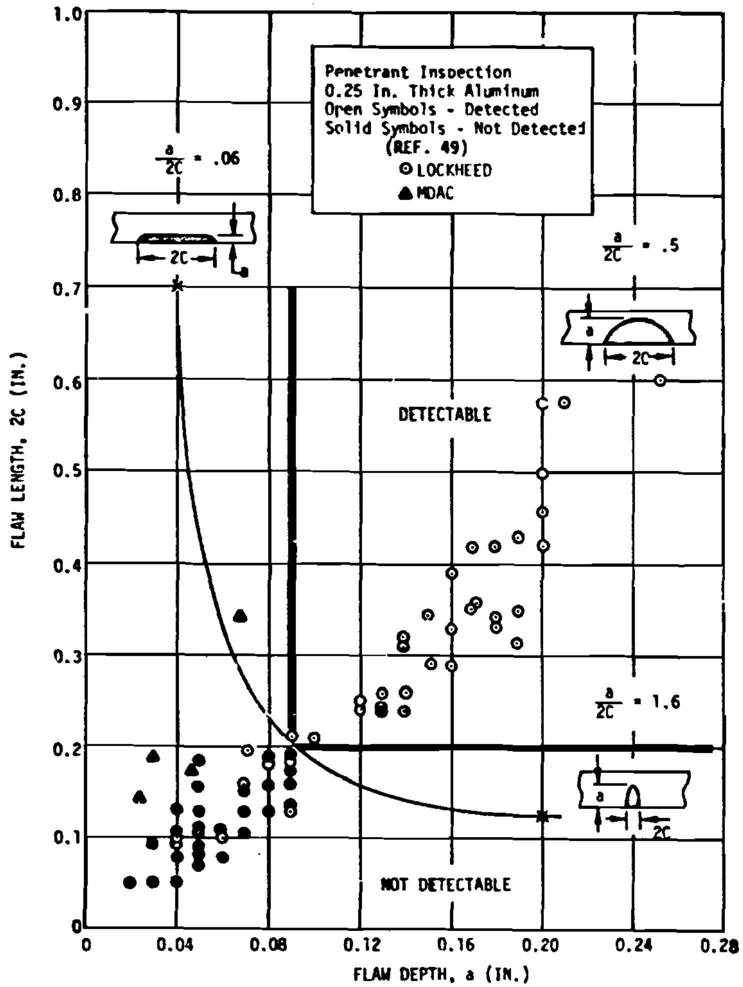

Figure 179 DETECTABLE FLAW SIZE DATA

shown. There is, however, no real basis for such a curve and a more defensible approach would be to use the known point as the limits of both (a) and (2c) giving the linear curve as shown. In fact, the latter could be considered the limiting case of the hyperbolic form. Once a detectable flaw size curve has been established for the conditions of interest, the appropriate (a/2c) ratios can be obtained. Figure 180 shows (a/2c) as a function of (a) for Figure 179 limit points. Once the limits of (a/2c) have been established, then for any given stress, the factor Q can be calculated for each value of (a) by Irwin equation Reference 49. Looking at Figure 179, an (a/2c) of .06 represents a long shallow defect like a scratch, gouge, or machine mark whereas an (a/2c) of 1.6 represents a pit. Therefore, it appears that for cracklike defects, the (a/2c) hyperbolic limits range between 0.05 to 1.5 as illustrated in Figure 178.

Reference 51 has a report on flaw detection in .060 and .225 with thick 2219-T87 by various NDT methods. Figure 181 is a plot of these detectable data points for (a) as a function of (2c) for penetrant and eddy current inspection. The limiting curve from Reference 49 is included in the plot to show the improvement in detectable limits. An effort was tried to make flaws with (a/2c) ratios of 0.1, 0.25, and 0.5 in all specimens. However, the flaw depth (a) to thickness (t) ratio influenced the (a/2c) ratio as illustrated in Figure 182. This figure shows that low values of (a) or (a/t) require large (a/2c) values and vice versa with the range being different for the various thicknesses.

Based on the data presented, it is obvious that fatigue crack standards for NDT detection capabilities always produce defects with an (a/2c) ratio of 0.10 to 0.50 which was a consequence of their crack initiation and growing techniques. Other types of defects [with (a/2c) ratio less than 0.1 or greater than 1.0] may not be detectable. In view of these problems, it may be necessary to either establish detectable flaw size curves for each metal thickness and flaw shape as well as for each detection method. Further theoretical studies are required to explain the relationship between the real data in Figures 181 and 182 to the intuitive limits of Figures 177 and 178.

9.1.1.2 At Locations Adjacent to Holes - Figure 183 shows a typical wing-box lower-surface concept for integral stiffened panels and also the baseline design. Illustrated is a through the thickness crack of 0.02 inch and a corner crack of 0.01 inch at a 0.25 inch hole. The corner crack with a radius of 0.01 inch (a=2c=1.0) is the minimum level of detectability for penetrant and eddy current during fabrication inspection. The through-the-thickness crack (0.020 inch deep) has a (a/2c) ratio slightly greater than 0.12 which is also the minimum level of detectability for penetrant and eddy current.

9.1.2 Fabrication Inspection

Inspection of fracture critical parts during fabrication is required in order to insure a crack-free structural component. A discussion of the areas of inspection for various concepts is presented in the following sections.

9.1 2.1 Wing Box Structure - The wing concepts 1 and 2 are shown in Figure 184. The integral stiffened wing concepts, upper and lower, require ultrasonic inspection of the plate stock, prior to machining, to a Grade-A (3/64 in. dia.) level. The finished machined parts require penetrant inspection

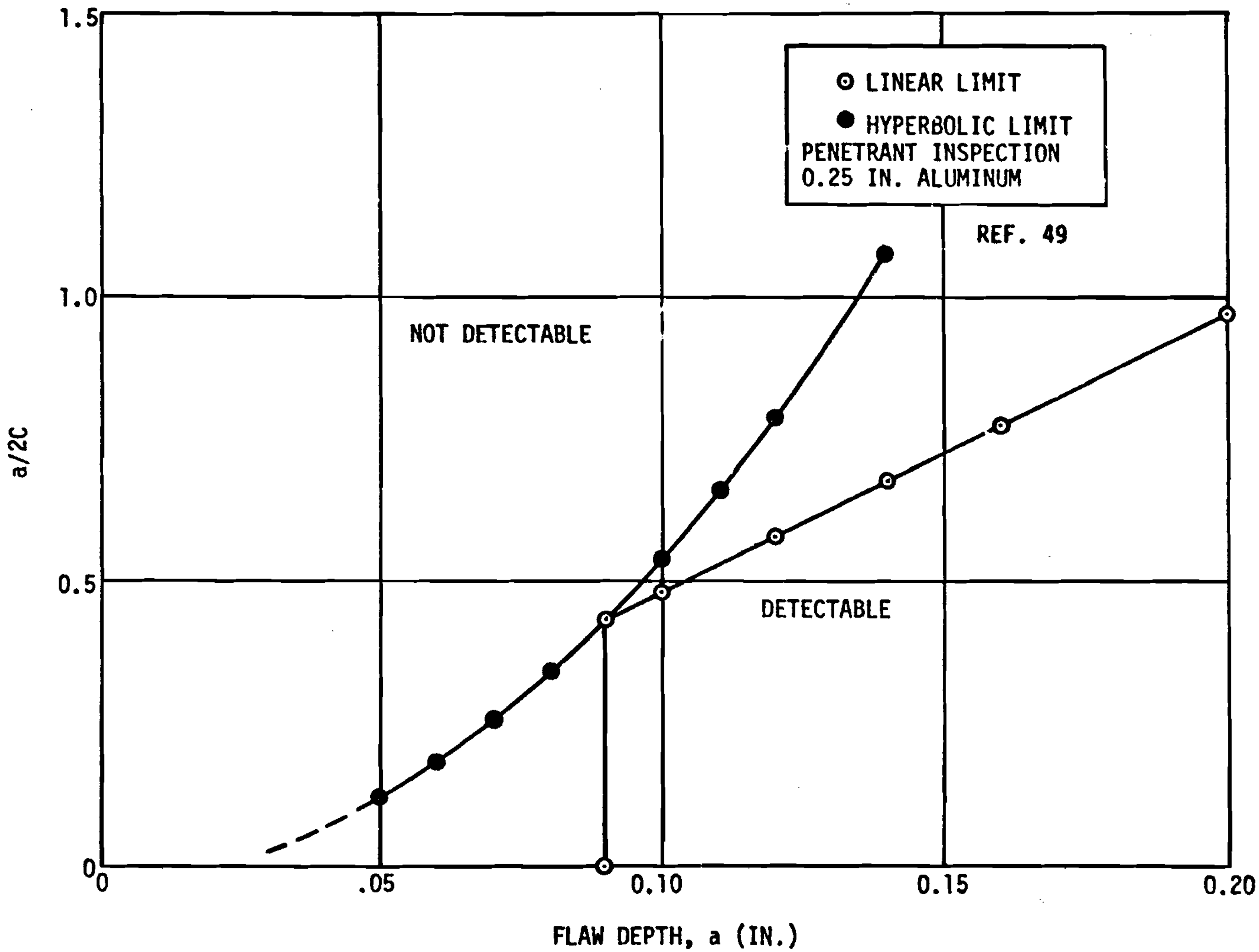

Figure 180 THEORETICAL FLAW DEPTH TO LENGTH RATIO

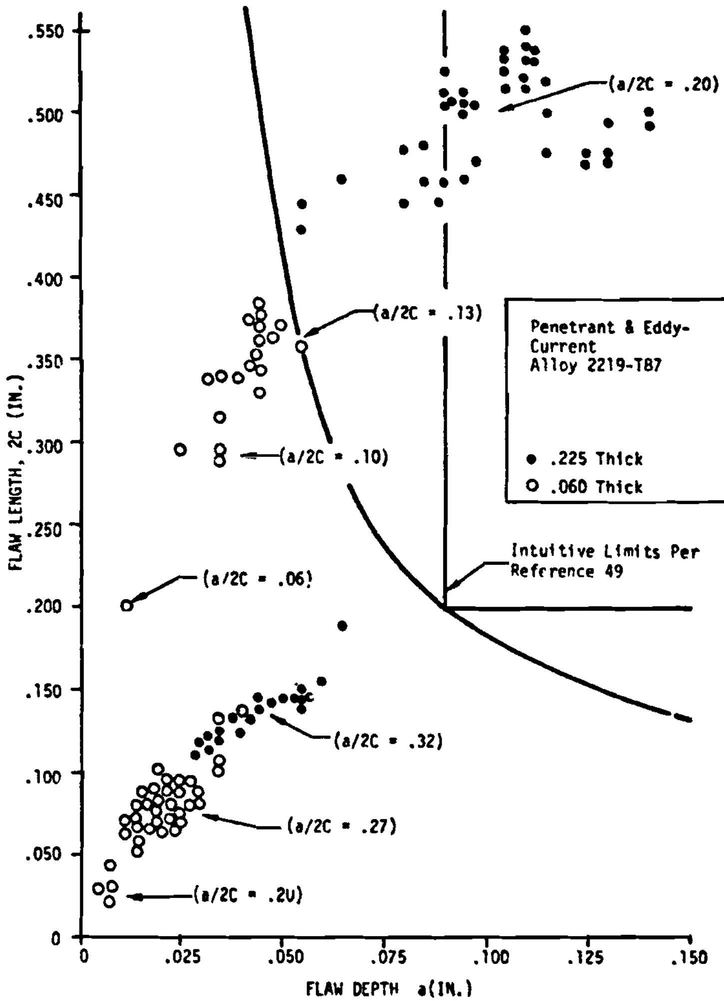

Figure 181 DETECTABLE FLAW SIZE DATA (EDDY-CURRENT)

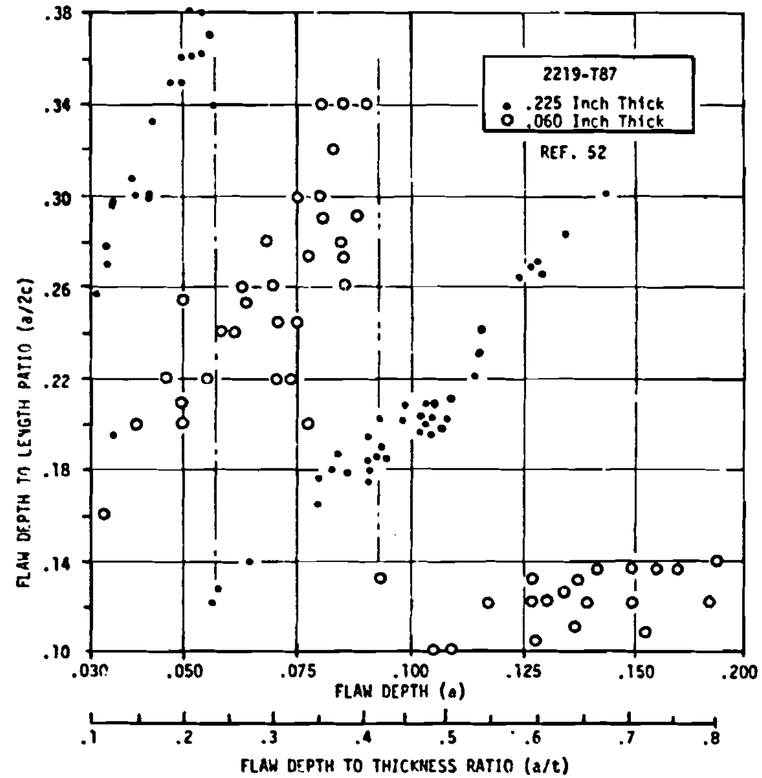

Figure 182 DETECTABLE FLAW SIZE RATIO DATA

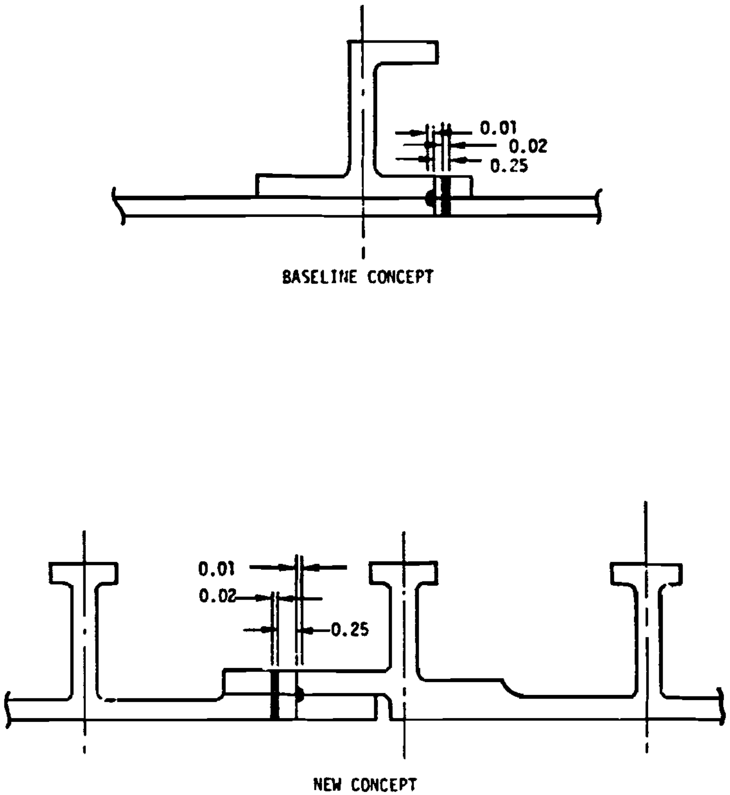

Figure 183 INITIAL FLAW SIZE AT HOLE LOCATIONS

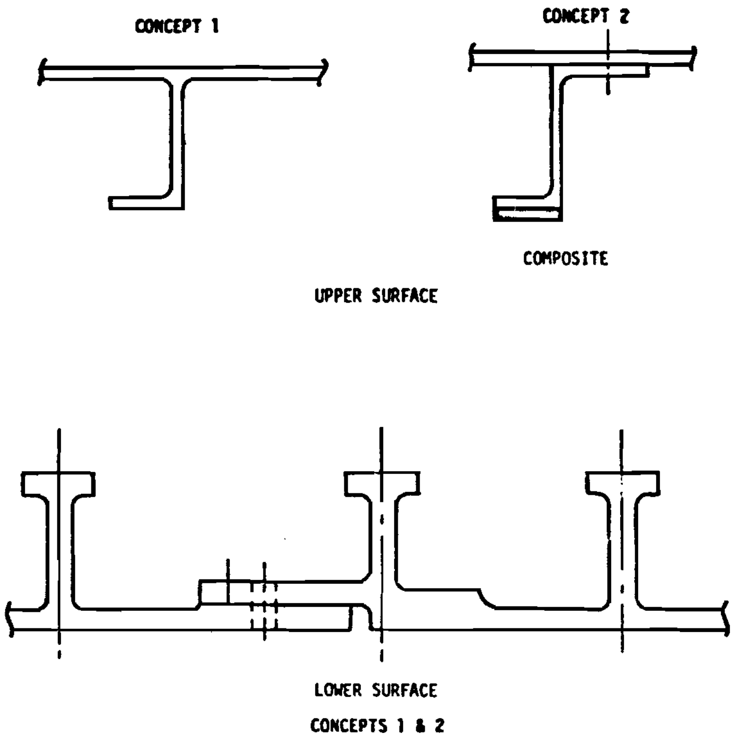

Figure 184 WING COVER PANEL CONCEPTS

using a MIL-I-25135 Group-V or better penetrant and non-aqueous spray developer. Critical holes are to be checked by penetrant or eddy-current (whichever is most applicable). The foregoing statement also applies to wing spar-caps and wing to fuselage attach fittings. The integral stiffened machined wing skins and machined spar caps require an ultrasonic or mechanical thickness check because of the variations in thickness due to tapering.

Wing concept 2, with the boron-reinforced stringers at the upper panel, should be handled as follows: 1) The skin material will not be ultrasonically inspected, 2) The stringer extrusions to be ultrasonically inspected before machining, 3) The finished machined stringers to be penetrant inspected, 4) Critical holes to be penetrant or eddy-current inspected, 5) The boron-epoxy laminate to be radiographed or ultrasonic C-scanned for voids and delaminations before bonding and (6) The bond quality between the boron-epoxy laminate and the stringer caps to be evaluated by contact pulse-echo ultrasonic or Fokker bond test.

9.1.2.2 Empennage Box Structure - The horizontal and vertical stabilizer box sections are fabricated from adhesive bonded aluminum honeycomb (Figure 185).

Clealiness of panels prior to bonding is determined by water-break test. Other surface analysis methods such as contact angle measurement, electron micrographs, electron emission energy measurement, surface impedance measurement are still being analyzed to control adhesive bond strength. However, no one method or combination of methods has yet been established for production inspection prior to bonding.

Considerable work has been done, at DAC, to establish NDI methods and acceptance criteria for adhesive bonded honeycomb panels. Based on these studies, the application of NDI methods in the production cycle for honeycomb sandwich panels generally includes the following: (Ref. 52)

- material property tests
- cleaning method checks (pre-bond)
- verifilm (pre-bond) tooling check
- visual inspection
- hot water leak test
- radiographic check for water, core damage, fit-up, and other internal discontinuities
- ultrasonic inspection for voids and lack of bond
- nondestructive and destructive testing of first assembly for correlation of findings and thorough evaluation.

To avoid unwarranted inspection costs, engineering drawings should be zoned with quality limits based on stress analysis or criticality of part function. A typical example of a zoned drawing for a vertical stabilizer is shown in Figure 186. A definition of inspection zone letters vs allowable adhesive void sizes is shown in Figure 187. Reference standards should contain discontinuities of the required minimum sizes as specified by the applicable zones of inspection for any given part.

The configuration of the standard must be representative of the test article with respect to skin thickness, material type, adhesive type and underlying structure.

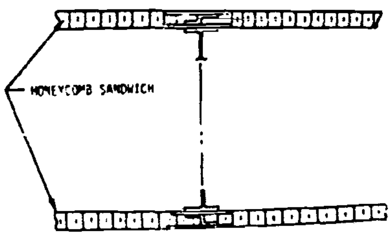

Figure 185 HORIZONTAL & VERTICAL STABILIZER DESIGN CONCEPT

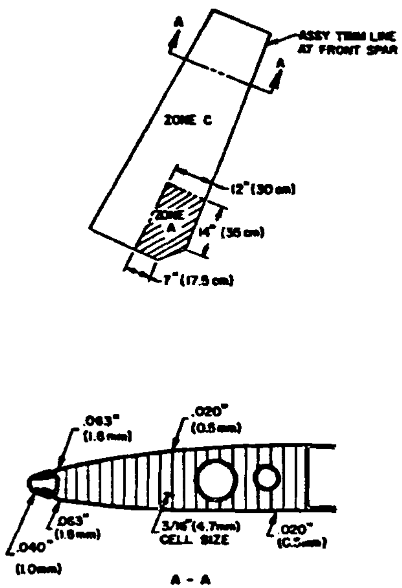

Figure 186 QUALITY ZONING FOR VERTICAL TAIL LOWER FORWARD BOX ASSY

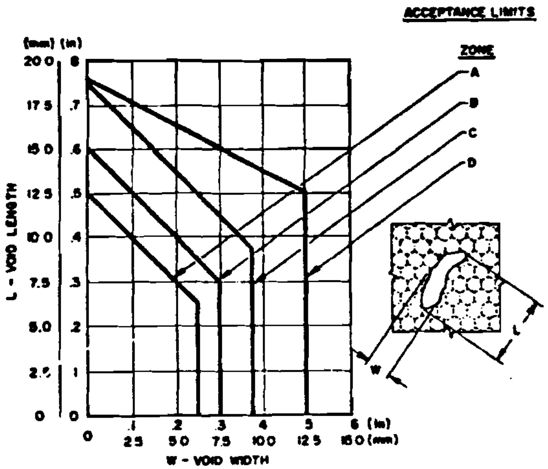

NOTE: W IS THE MAXIMUM PROJECTED VOID WIDTH, MEASURED ACROSS THE VOID IN THE "NARROW" DIRECTION AS SHOWN IN THE SKETCH. L IS THE PROJECTED VOID LENGTH MEASURED PERPENDICULAR TO W.

Figure 187 DEFINITION OF INSPECTION ZONES AND ALLOWABLE ADHESIVE VOID SIZES

Quality assurance of production parts can only be obtained by: 1) preparing specifications for each NDT method, 2) preparing technique charts for each NDT method as applicable to a specific part, and 3) recording test results on mylar overlay of each part.

9.1.2.3 Honeycomb Fuselage Shell - The NDI discussion for the empennage box structure is applicable to the honeycomb fuselage shell concept. In addition, the plate stock for the "picture frame" edge member (Figure 84), would require an ultrasonic inspection of the plate stock and penetrant inspection of the finished machine parts.

9.2 IN-SERVICE INSPECTION

This section discusses Special Visual Inspectable and Depot or Base Level Inspectable structures during service. To be consistent with the damage tolerance criteria (Appendix A), the discussion will only cover on-aircraft inspections of fracture critical structure. The frequency of inspection associated with the inspection plan element is as follows:

Inspection Plan Element	Inspection Interval (Hours)
Walk Around Visual	25
Special Visual	1,000
Depot or Base Level	3,750

9.2.1 Special Visual Inspectable

Structure is special visual inspectable if the nature and extent of damage being considered is unlikely to be overlooked by personnel conducting a detailed visual inspection of the aircraft for the purpose of finding damaged structure. The procedure may include removal of access panels and doors, and may permit simple visual aids such as mirrors and magnifying glasses. MIL-M-38780A specifies: "Special cases may be included at the request of the using command(s) based on the component criticality. . ."

Problems of accessibility or removal of access panels could be minimized by locating small access holes near critical structure for endoscope inspections. Holes approximately 1/4 inch dia. could be provided at selected locations. Quick removal fasteners could be used to plug the holes when the aircraft is in service (see Figure 188).

The smallest damage which can be presumed to exist in the structure after completion of special visual inspection shall be an uncovered open 2-inch through the thickness crack. This limit does not agree with demonstrated tests (Reference 53) for through the thickness fatigue cracks generated in 1/2 in. thick 7075-T651 anodized specimens with organic coatings. Table LXXXIV shows the results for fatigue cracks generated under organic coatings from a 3/8 in. dia. hole.

The word "open" crack is difficult to define because a crack may not be visible at a no-load or compressive-load condition, but becomes visible if a static tensile load is applied as illustrated in Figure 189. In Figure 189 we see that the real length of the crack was not indicated until the tensile load reached 60 percent of maximum. Table LXXXIV clearly indicates that cracks

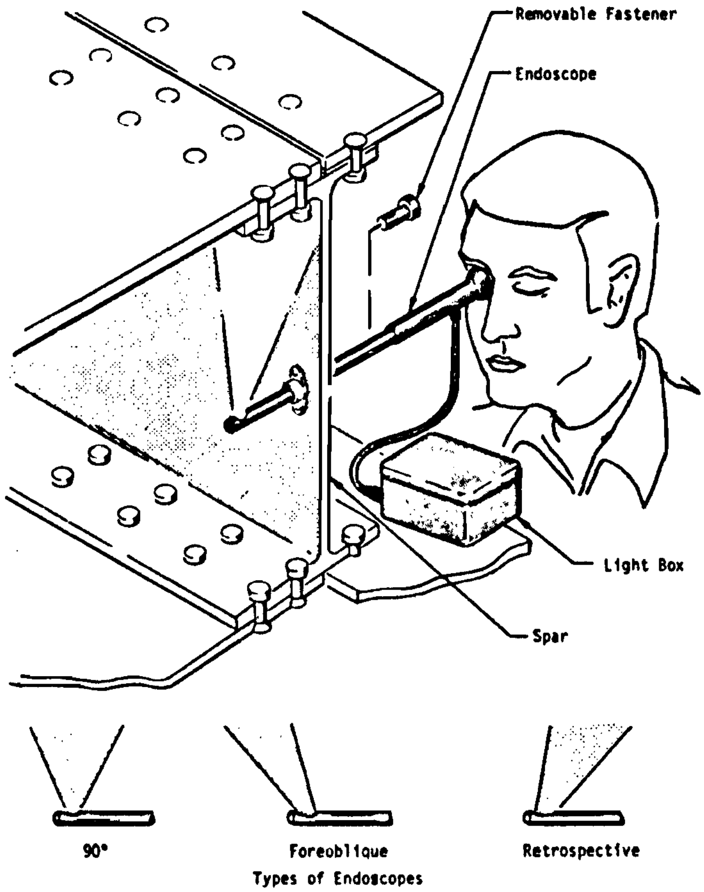

Figure 188 INSPECTION HOLES FOR IN-SERVICE INSPECTION

TABLE LXXXIV MINIMUM DETECTABLE CRACK LENGTH UNDER ORGANIC COATINGS (VISUAL INSPECTION)

SPECIMENS	TYPE OF COATING	CRACK LENGTH (NO LOAD) (IN)		CRACK LENGTH (LOADED) (IN)*	
		LENGTH	CYCLES	LENGTH	CYCLES
1	FUEL TANK	1.20	63K	0.250	57K
2	FUEL TANK-PRIMER TOP-COAT	1.43	97K	0.090	82K
3	F.R. PRIMER CORUGARD SYSTEM	>3.25	61K	0.125	45K

*CRACK DETECTABLE ON ONE SIDE OF HOLE ONLY on the order of 1.0 inch long may be found in anodized aluminum. Cracks less than 2.0 inch may be found in aluminum coated with anodize, fuel tank coating, primer, and topcoat. However, for surfaces coated with F.R. primer, and Corogard system cracks must be at least 3.5 inch long to be visually detected with a no-load or compressive load condition. Hence, NDI methods must be used to locate possible cracks. X-ray and visual (from the anodized side) were used to follow the crack growth (with and without load) in the study.

9.2.2 Depot Level Inspectable

The Damage Tolerance Criteria (Appendix A) state: where NDI techniques such as penetrant, eddy-current or ultrasonics are applied to a component installed in the aircraft, the minimum assumed size shall be a through the thickness crack emanating from a fastener hole, having 0.25 inch of uncovered length. At other locations, the minimum assumed damage size shall be a/Q = 0.20 inch. Appendix A also states that smaller sizes may be specified subsequent to a demonstration to a 90% probability and 95% confidence using in-service inspection procedures.

MIL-M-38780A states that the primary inspection method be backed-up by a secondary verification procedure where initial results do not provide uncontestable data for determination of the serviceability of the item inspected. It is desirable to perform the verification procedure by a method employing direct visual observation (optical, magnetic-particle, or penetrant) when the initial procedure is performed by an instrumented method (X-ray, eddy-current or ultrasonic) providing it does not result in extensive disassembly. In reality, the NDI engineer, selecting the test methods, does not have many options to choose from. The methods selected are more generally governed by the structural configuration, defect location, and defect orientation, than by any other reasons as illustrated in Figure 190.

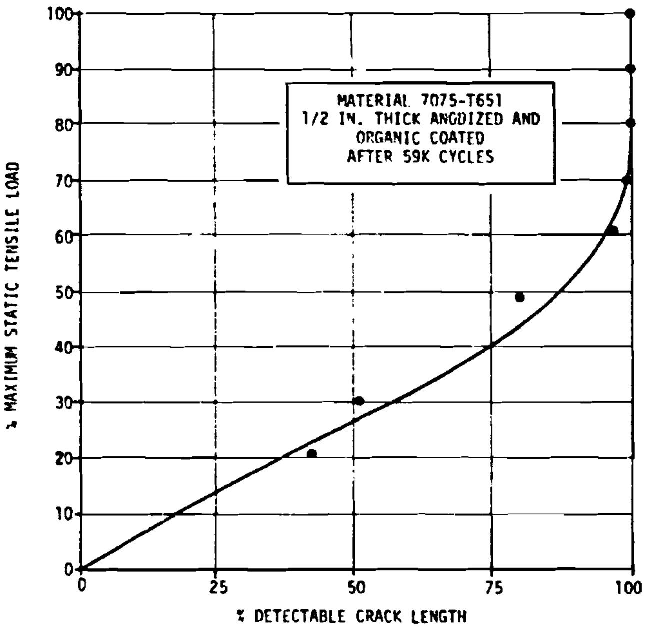

Figure 189 MINIMUM DETECTABLE CRACK LENGTH (UNDER ORGANIC COATING) vs PERCENT STATIC LOAD

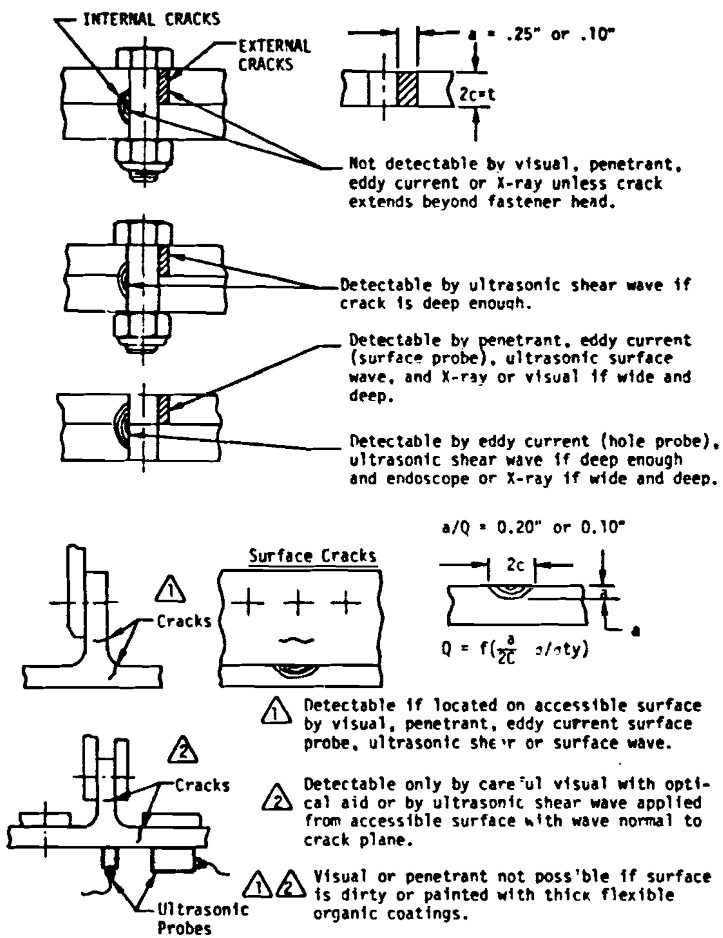

Figure 190 IN-SERVICE NDI FASTENER HOLE CRACK DETECTION CAPABILITIES

SECTION X

COSTS

In studies of this type involving new design concepts, new materials, and new manufacturing methods, there is an inherent minimum of historical experience upon which to base development, production, and life cycle cost estimates. In general, some experience does however exist to draw upon from completed or ongoing research and development or smaller scale applications to past and present aircraft or spacecraft of similar concepts, materials, and manufacturing processes. This historical experience and production cost data together with a comparatively detailed examination of each component were used to estimate projected costs for each of the elements necessary to the development, production and operation of the AMST aircraft.

The baseline aircraft and two new concept aircraft (incorporating the selected new concepts and materials in the primary structure) were analyzed in parallel to the same detail to produce directly comparable data. The two new concept aircraft had the same wing and empennage box structure but different fuselage shell concepts. The first of these utilized a honeycomb sandwich fuselage shell and all detailed data is presented in this section. The second new concept aircraft incorporated an isogrid concept fuselage shell. Detailed data for this configuration is contained in Volume II with only summary results presented in this section. Each new concept aircraft was considered unresized and again, as resized to take maximum advantage of the reduced weight of the new concepts. The baseline aircraft incorporated new metallic materials but not new design concepts and is referred to as the "improved baseline" in Section V. The resized aircraft costs were calculated using a scaled engine based on the off-the-shelf baseline JT8D-17 engine.

Acquisition and life cycle costs were generated for the baseline and the new concept aircraft. The acquisition cost is the total of development and production phase costs with all the necessary supporting elements. The life cycle costs include the projected operations and support costs. Aircraft production quantities of 100, 300 and 500 were considered. The production rates postulated for the three quantity programs were 3, 6, and 9 aircraft per month, respectively.

The information available on the baseline aircraft and generated for the new concept aircraft during the study made possible a much more detailed analysis than is usually possible in a program of this type. Not only were precise structural materials and concepts defined but also the manufacturing processes for fabrication and assembly. The overall analytical process is illustrated in Figure 191 beginning with the requirements and engineering data and ending with the costs.

10.1 ACQUISITION COSTS

The acquisition costs are made up of the following resource elements within the two program phases:

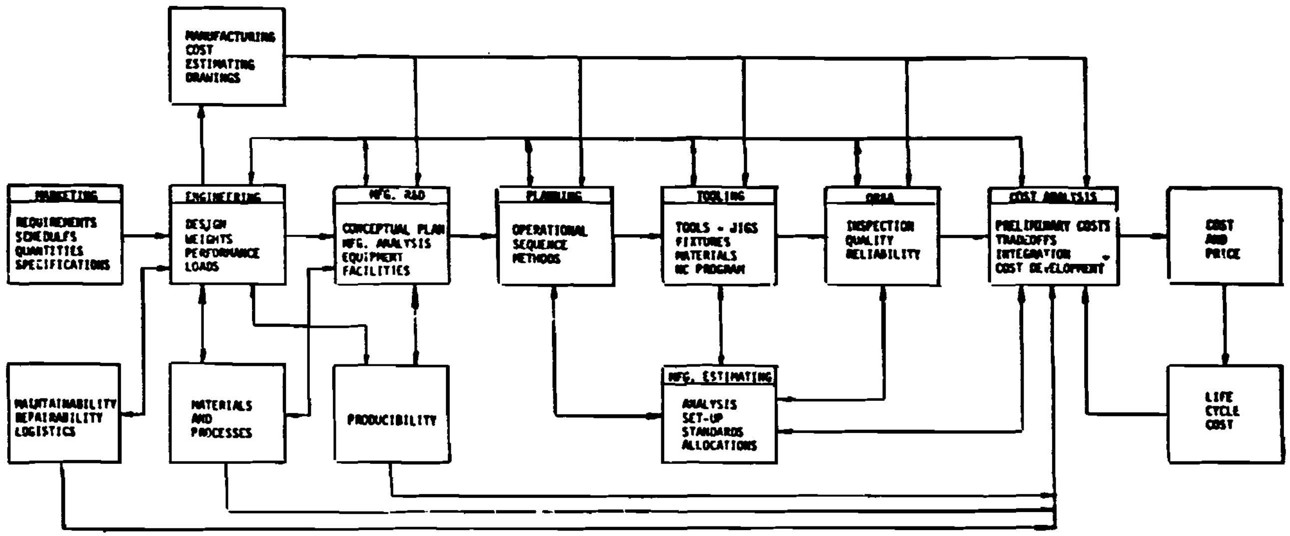

Figure 191 COST ANALYSIS INFORMATION FLOW

Development	Production
Air Vehicle	Air Vehicle
Project Management	Project Management
Product Support	Product Support
Test Spares	Initial Spares
Packaging, Marking, Shipping	Packaging, Marking, Shipping
ECPS	ECP
Training/Trainers	Training/Trainers
AGE	AGE

Each of these elements was addressed separately during the study.

The air vehicle production costs were estimated using the engineering drawings produced for each selected component concept (see Section V) as the basis. A detailed industrial engineering approach was then made to estimate the costs of major part fabrication and assembly. All costs reflect the analyses of the detailed shop standards, the detailed definition of materials and gages, the historical relationships between standard and anticipated actual hours, and the 1973 cost base used, which held direct labor, overhead and G&A rates constant.

10.1.1 Labor Hours

Bid worksheets were created which reflected the manufacturing concepts and processes selected, including the specification of material, equipment and facilities required. The bid worksheets (Figures 192 and 193) accumulated the detailed planning, tooling, quality assurance and manufacturing manhour estimates made for each sequenced operation. This information was then collected on a structural component by component basis so that at the end of the analysis it was possible to compare the total fabrication and assembly costs for the various portions of the wing, horizontal tail, vertical tail, fuselage, and the remainder of the aircraft. All information was prepared in a manner to ensure cost compatibility. It should be noted that the bid worksheet requires separate consideration of set-up time and operating time and permits traceability on a part basis through to the final total estimate. When the estimating process is conducted in parallel at this level upon the actual work to be performed, rather than by cost or labor hour ratio, more accurate comparative estimates are obtained. In addition, the relationship of manhours between fabrication, assembly, tooling, planning, and quality assurance is much better defined.

The cumulative average direct production manhour estimates are summarized in Tables LXXXV, LXXXVI, and LXXXVII for the 100, 300, and 500 baseline aircraft programs, respectively. The primary structural components subject to application of the new concepts are listed separately. The corresponding direct labor estimates for the resized new concept aircraft with the honeycomb sandwich fuselage are contained in Tables LXXXVIII, LXXXIX, and XC. Planning estimates considered the significant reductions in numbers of parts for the new concept components compared to the baseline and the magnitude of the manufacturing and tooling estimated hours. As noted in the tables, the fabrication and assembly hours reflect this reduction in parts for each of the structural components.

BID WORK SHEET

PART NO.: PLAN NO. 1
CHG. LET.:
PART NAME: UPPER WING SKINS, SPARES, AND BULKHEAD ASSEMBLY
MAT'L.:
SIZE:
SPEC.:
TOTAL NO. REQ.:
NEXT ASSEM.:
END ITEM:
PLAN:
Q.C.:
MAT'L.:
PROC.:
TOOL EST.:
MFG. EST.:

PART ILLUSTRATION:

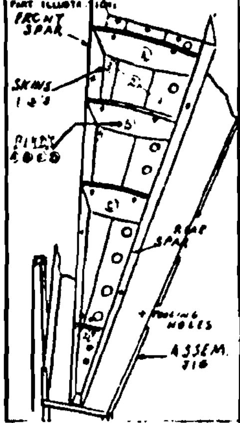

NO.	OPERATION	TOOL	EQUIPMENT	DEPT.	UNIT COST SET-UP	UNIT COST FAB.	UNIT COST ASSEM.	TOOL COST DES.	TOOL COST FAB.
1	LOCATE SKIN #1	A.J.	HOIST						
2	LOCATE SKIN #2	A.J.	HOIST						
3	LOCATE SKIN #3	A.J.	HOIST						
	#1, #2, #3 + TOOLING								
	HL INDEX								
4	LOCATE FRONT SPAR	A.J.	HOIST						
5	LOCATE BULKHEAD A,B,C,D	A.J.	HAND						
	#4 & #5 + T.H. INDEX	A.J.							
6	LOCATE REAR SPAR	A.J.	HOIST						
	T.H. INDEX								
7	DRILL, SEAL & RIVET PER								
	PROCESS STANDARDS								
	NOTE: DESIGN A.J. TO LOCATE ABOVE PARTS BY TOOLING HL INDEX - HEIGHT OF A.J. SHOULD BE HIGH ENOUGH TO ENABLE MECHANIC TO COMPLETE FINAL BOTTOM SKIN ATTACH THROUGH TOP SKIN ACCESS HOLES IN STANDING POSITION. PART OF A.J. THAT LOCATES A, B, C & D BULKHEADS MUST BE REMOVABLE TO ALLOW FOR BOTTOM SKIN INSTALLATION.								
8	INSPECT								
9	OK TO INSTALL BOTTOM SKIN								

UNIT COST SUMMARY

SET-UP		HRS
FAB.		HRS
ASSEM.	10716.0	HRS
MAT'L.	$	
CYCLE		DAYS

BID WORK SHEET

PART NO.: PLAN NO. 1
CHG. LET.:
PART NAME: BOTTOM WING SKINS TO UPPER
MAT'L.:
SIZE:
SPEC.:
TOTAL NO. REQ.:
NEXT ASSEM.:
END ITEM:
PLAN:
Q.C.:
MAT'L.:
PROC.:
TOOL EST.:
MFG. EST.:

PART ILLUSTRATION:

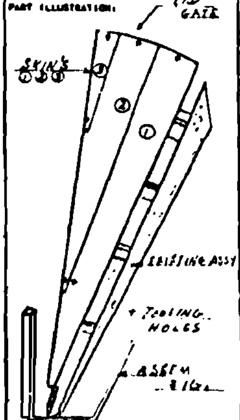

NO.	OPERATION	TOOL	EQUIPMENT	DEPT.	UNIT COST SET-UP	UNIT COST FAB.	UNIT COST ASSEM.	TOOL COST DES.	TOOL COST FAB.
10	LOCATE SKIN #1	A.J.	HOIST						
	INDEX TOOL HL'S	A.J.							
	DRILL, SEAL & RIVET								
11	LOCATE SKIN #2	A.J.	HOIST						
	INDEX TOOL HL'S	A.J.							
	DRILL, SEAL & RIVET								
12	LOCATE SKIN #3	A.J.	HAND						
	INDEX TOOL HL'S	A.J.							
	DRILL, SEAL & RIVET								
13	COMPLETE WING ASSEMBLY								
14	2ND INSPECTION								
	NOTE: DESIGN REMOVABLE END GATE WITH TOOLING HOLE INDEX 3 EACH FOR TOP & BOTTOM SKINS. OTHER TOOLING HOLE INDEX FOR BOTTOM SKIN #2 & #3 MUST BE CONTROLLED BY BULKHEAD INDEX & OR A.J. THROUGH TOP SKIN ACCESS HOLES.								

UNIT COST SUMMARY

SET-UP		HRS
FAB.		HRS
ASSEM.		HRS
MAT'L.	$	
CYCLE		DAYS

Figure 192 TYPICAL BID WORKSHEET FOR WING COST ANALYSIS

ESTIMATOR ANALYSIS SHEET

ASSEMBLY NO. PLAN NO. 1 — LEADMAN
ASSEMBLY NAME UPPER & LOWER WING SKINS — CHART
NEXT ASSEMBLY SPAR FRONT & REAR & BULKHEADS — LINE NO

Oper. No.	Estimator Description	Qty.	Man Load	Rate Per Min.	Total Man Hrs.
1	LOCATE FRONT SPAR USING HOIST				22
2	LOCATE 9 BULKHEAD IN A.J. A, B, C, D, E, F, G				39
3	LOCATE REAR SPAR IN A.J. USING HOIST				31
4	LOCATE SKIN PANEL #1 ON STRUCTURE (HOIST)				37
5	LOCATE SKIN PANEL #2 ON STRUCTURE (HOIST)				22
6	LOCATE SKIN PANEL #3 ON STRUCTURE (HOIST)				17
7	DRILL THROUGH BULKHEAD CAP TO SPAR CAP				189
	APPROX: 225 TABS 1150 HOLES				
8	DRILL WING SKIN SPLICES APPROX. 2092 HOLES				350
9	REMOVE SKINS CLEAN & REPLACE				154
10	INSTALL FASTENERS				840
11	INSTALL LWR WING PANEL #1 LOCATE (HOIST)				31
12	INSTALL LWR WING PANEL #2 LOCATE (HOIST)				22
13	INSTALL LWR WING PANEL #3 LOCATE (HOIST)				17
14	DRILL THROUGH BULKHEAD CAP TO SPAR CAP				189
	APPROX: 225 TABS 1150 HOLES				
15	DRILL WING SKIN SPLICES APPROX. 2092 HOLES				350
16	REMOVE SKINS CLEAN & REPLACE				154
17	INSTALL FASTENERS				840
18	DRILL & INSTALL FASTENER AT STA. BULKHEAD				420
	SIDE FLANGES ATTACH TO FRONT & REAR SPAR VIEW AV & BV,				
	ETC.				
19	REAM ATTACH BEAMS AT VIEW C-B, C-C, D-C				84
20	BOLT AS REQUIRED TORQUE				35
21	SEAL PER DPS				210

Accessibility	Type of Work	No. of Oper.		
Good	Light		Total Basic Time	T100
Fair	Medium		% Allowance	
Poor	Heavy		Total Standard at Unit #	
Extra Poor	Extra Heavy		Time Per Unit #	

Date	Analyst	Reason for Restudy	Units Per Airplane	Tot. Std. Man Hours Per Airplane #
		TOTAL WING &	JOIN T100	- Man Hours 10716.0

ESTIMATOR ANALYSIS SHEET

ASSEMBLY NO. PLAN NO. 1 — LEADMAN
ASSEMBLY NAME — CHART
NEXT ASSEMBLY — LINE NO.

Oper. No.	Estimator Description	Qty.	Man Load	Rate Per Min.	Total Man Hrs.
22	COMPLETE WING PICKUP				420
					4467
	NORMAL ALLOWANCE				491
	TOTAL ACTUAL ASSEMBLY HOURS AT T100				4958
	THIS IS FOR 1/2 WING ONLY L.H.				
	R.H.				4958
	TOTAL R & L.H. WING				9916
	WING JOINING (NO PAPER AVAILABLE)				
	REAMING, INSTALLING BOLTS, TORQUE				800
					10716

Accessibility	Type of Work	No. of Oper.		
Good	Light		Total Basic Time	
Fair	Medium		% Allowance	
Poor	Heavy		Total Standard at Unit #	
Extra Poor	Extra Heavy		Time Per Unit #	

Date	Analyst	Reason for Restudy	Units Per Airplane	Tot. Std. Man Hours Per Airplane #
		TOTAL WING &	JOIN T100	- Man Hours 10716.0

Figure 192 TYPICAL BID WORKSHEET FOR WING COST ANALYSIS -- CONCLUDED

BID WORK SHEET

MAT'L: ALUMINUM CORE	TOTAL NO. REQ.	PART NO: ALUM H-CORE PANEL ASSEMBLY	CHG. LET.
SIZE: .125 CELL/5056 ALLOY - .0007 FOIL		PART NAME: SEGMENT 1-6 SANDWICH - STRUCTURE	
SPEC: ALUMINUM HOBE NOTE PG. 2		NEXT ASSEM: STA. #695-#847	
		END ITEM:	

PLAN	
Q.C.	
MAT'L.	
PROC.	
TOOL EST.	
MFG. EST.	

PART ILLUSTRATION:

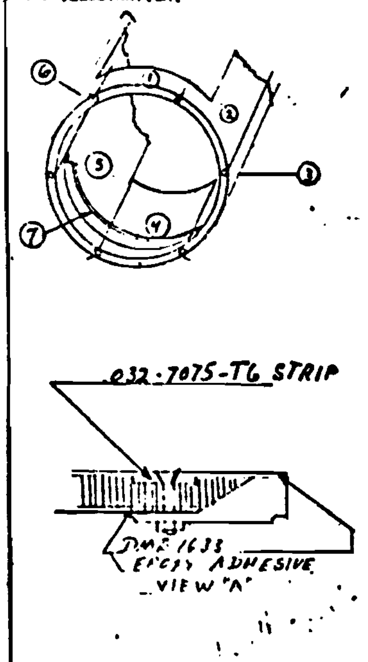

NO.	OPERATION	TOOL	EQUIPMENT	DEPT.	UNIT COST SET-UP	UNIT COST FAB.	UNIT COST ASSEM.	TOOL COST DES.	TOOL COST FAB.
*1	SET UP ALUM H/C HOBE ON				1.0	-	-		
	MILL. MILL (4) FOUR								
	SEGMENTS AS ON PG. 2 -								
	MAKE FROM 4 HOBES AS								
	NOTED.								
2	FOUR (4) HOBES WILL MAKE				-	-	-		
	CORES FOR ALL SIX PANELS								
	(PG. 2) CORE SPLICE								
	REQUIRE FOR # (1) & (4)								
	PANELS NOTED PG. 2 VIEW								
	"C".								
3	MACHINE (4) HOBES AS				-	1.300	-		
	NOTED TO 1.00 SIZE.								
4	EXPAND THE HOBES (4)				-	2.320	-		
	REQUIRE MAKES 110" x								
	151" AS NOTED. VIEW "C".								
*	NOTE: ALUM EXPANDED H-CORE MAY BE PURCHASED IN LIEU OF HOBE.								

UNIT COST SUMMARY

SET-UP	2.5/15.0	HRS
FAB.	34.328	HRS
ASSEM.		HRS
MAT'L.	$	
CYCLE		DAYS

Figure 193 TYPICAL BID WORK SHEET FOR FUSELAGE COST ANALYSIS

BID WORK SHEET

MAT'L:	TOTAL NO. REQ.	PART NO: ALUM H-CORE PANEL ASSEMBLY	CHG. LET.
SIZE:		PART NAME: SEGMENTS 1-6 SANDWICH - STRUCTURE	
SPEC:		NEXT ASSEM: STA. #696-84"	
		END ITEM:	

PLAN | Q.C. | MAT'L. | PROC. | TOOL EST. | MFG. EST.

PART ILLUSTRATION:

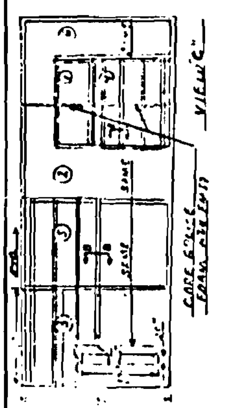

NO.	OPERATION	TOOL	EQUIPMENT	DEPT.	UNIT COST SET-UP	UNIT COST FAB.	UNIT COST ASSEM.	TOOL COST DES.	TOOL COST FAB.
5	MAKE CORE SPLICE IN				-	.780	-		
	SEGMENT (2) & (6). CUT								
	OUT SEGMENTS (1) & (4)								
	FROM SEGMENTS (2) & (6)								
	AS NOTED.								
6	BAND SAW PERIMETER PER				-	1.716	-		
	TEMP., SAW TAPERED								
	EDGES 1, 2, 3, 4, 5, 6.								
7	MILL CUT CORE 032 FOR								
	STRIP FOR BOLT ATTACH								
	(SEE VIEW "B") AROUND								
	PERIMETER FA PANEL, FOR								
	FRAME ATTACH ANGLE (4)								
	REQUIRE PANELS 3, 5 & 4								
	ITEM # 7								
8	INSTALL EPOXY POTTING				-	-	.498		
	COMPOUND.								

UNIT COST SUMMARY		
SET-UP		HRS
FAB.		HRS
ASSEM.		HRS
MAT'L.	$	
CYCLE		DAYS

BID WORK SHEET

MAT'L:	TOTAL NO. REQ.	PART NO: ALUM H-CORE PANEL ASSEMBLY	CHG. LET.
SIZE:		PART NAME: SEGMENTS 1-6 SANDWICH - STRUCTURE	
SPEC:		NEXT ASSEM: STA. #696-847	
		END ITEM:	

PLAN | Q.C. | MAT'L. | PROC. | TOOL EST. | MFG. EST.

PART ILLUSTRATION:

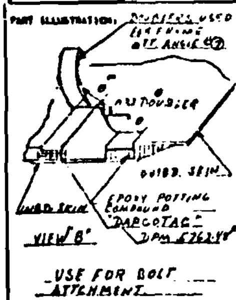

NO.	OPERATION	TOOL	EQUIPMENT	DEPT.	UNIT COST SET-UP	UNIT COST FAB.	UNIT COST ASSEM.	TOOL COST DES.	TOOL COST FAB.
8	CONT.				-	-	-		
	"DAPCOTAC"								
	DMS 5762-48 CU. FT.								
	AROUND PERIMETER OF								
	EACH PANEL & WHERE .052								
	MILL CUT IS MADE FOR								
	DOUBLER.								
9	ADD PROTECTIVE FILM TO				-	-	.300		
	CORE SHEET & TRANSFER								
	TO THE BOND FIXTURE.								
10	MAKE OUTER SKINS TO L.T.				.5	.900	-		
	TEMP. MATERIAL 7075 T6								
	1, 2, 3, 4, 5 & 6.								
11	MAKE INNER SKIN TO L.T.				-	.900	-		
	TEMP. 7075 T6								
	1, 2, 3, 4, 5 & 6								

UNIT COST SUMMARY		
SET-UP		HRS
FAB.		HRS
ASSEM.		HRS
MAT'L.	$	
CYCLE		DAYS

Figure 193 TYPICAL BID WORKSHEET FOR FUSELAGE COST ANALYSIS -- Continued

BID WORK SHEET

MAT'L.:	TOTAL NO. REQ.	PART NO.: ALUM H-CORE PANEL ASSEMBLY	CHG. LET.:
SIZE:		PART NAME: SEGMENTS 1-6 SANDWICH - STRUCTURE	PLAN
SPEC.:		NEXT ASSEM.: STA. #696-847	Q.C. / MAT'L. / PROC. / TOOL EST. / MFG. EST.
		END ITEM:	

PART ILLUSTRATION:

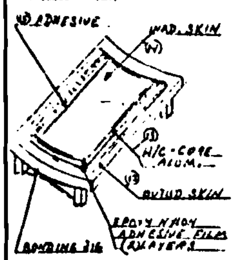

* NOTE - PRE FIT OF MATED PARTS, OPER. ITEMS IS REQ IN ALL SEGMENTS TO CHECK TOLERANCE

NO.	OPERATION	TOOL	EQUIPMENT	DEPT.	UNIT COST SET-UP	UNIT COST FAB.	UNIT COST ASSEM.	TOOL COST DES.	TOOL COST FAB.
12	PREPARE BONDING FIXTURE FOR SEGMENT (4). USE UPS 1.99-102 BONDING PROCEDURE ADHESIVE BOND PER DMS 1673. ADD A DICHROMATE SEAL PRIMER TO THE ALUM SURFACE PRIOR TO THE ADHESIVE BOND OPERATION. USE ADHESIVE TAPE FOR THE ALUM - HONEYCOMB CORE BOND TO THE ALUM SKIN.				-	-	.050		
13	PLACE THE OUTBOARD ALUM SKIN ON THE PLP (TOOL). ADD LAYER OF DMS 1633 & AF202 ADHESIVE FILM ON INBOARD SURFACE OF SKIN.	BJ			-	-	.116		
14	PLACE HONEYCOMB CORE ON OUTBOARD SKIN. ADHESIVE MUST BE BETWEEN MATING SURFACE.	BJ			-	-	.130		

UNIT COST SUMMARY		
SET-UP		HRS
FAB.		HRS
ASSEM.		HRS
MAT'L.	$	
CYCLE		DAYS

BID WORK SHEET

MAT'L.:	TOTAL NO. REQ.	PART NO.: ALUM H-CORE PANEL ASSEMBLY	CHG. LET.:
SIZE:		PART NAME: SEGMENTS 1-6 SANDWICH - STRUCTURE	PLAN
SPEC.:		NEXT ASSEM.: STA. #696-847	Q.C. / MAT'L. / PROC. / TOOL EST. / MFG. EST.
		END ITEM:	

PART ILLUSTRATION:

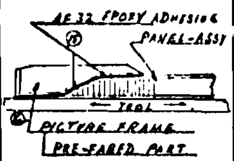

NO.	OPERATION	TOOL	EQUIPMENT	DEPT.	UNIT COST SET-UP	UNIT COST FAB.	UNIT COST ASSEM.	TOOL COST DES.	TOOL COST FAB.
	ADD 2ND LAYER OF EPOXY/ NYLON FILM ADHESIVE ON TOP OF HONEYCOMB CORE.				-	-	-		
15	PLACE THE INBOARD ALUM SKIN ON THE HONEY CMB CORE. (ADHESIVE MUST BE BETWEEN MATING SURFACE).	BJ			-	-	.080		
16	PLACE DMS 1633 AF32 EPOXY ADHESIVE TAPE ON THE 4 EDGES OF THE PANEL WHERE THE MACHINED METAL IS TO BE ATTACHED TO THE PANEL.	HAND			-	-	.143		
17	POSITION & INDEX THE ALUM PICTURE FRAME ON TOP OF HONEYCOMB LAYUP & HOLD DOWN WITH STOP & INDEX POINTS.	BJ			-	-	.060		

UNIT COST SUMMARY		
SET-UP		HRS
FAB.		HRS
ASSEM.		HRS
MAT'L.	$	
CYCLE		DAYS

Figure 193 TYPICAL BID WORKSHEET FOR FUSELAGE COST ANALYSIS -- Continued

BID WORK SHEET

MAT'L:		PART NO:	ALUM H-CORE PANEL ASSEMBLY
SIZE:	TOTAL NO. REQ.	PART NAME:	SEGMENTS 1-6 SANDWICH - STRUCTURE
SPEC:		NEXT ASSEM:	STA. #696-847
		END ITEM:	

CHG. LTR.	
PLAN	
Q.C.	
MAT'L.	
PROC.	
TOOL EST.	
MFG. EST.	

PART ILLUSTRATION:

NO.	OPERATION	TOOL	EQUIPMENT	DEPT.	UNIT COST SET-UP	UNIT COST FAB.	UNIT COST ASSEM.	TOOL COST DES.	TOOL COST FAB.
18	APPLY VACUUM BAG & CHECK	BJ			-	-	.809		
	HOLD DOWN POINTS.								
19	PLACE ASSEMBLY & B.J.				-	-	2.000		
	IN AUTOCLAVE CURE THE								
	EPOXY ADHESIVE - 1.5 HRS								
	AT 300°F. PER DPS 1.99-								
	102 STD. BONDING								
	PROCEDURE.								
20	REMOVE ASSEMBLY FROM				-	-	.178		
	AUTO CLAVE & B.J. CLEAN								
	& INSPECT.								
21	USE NTD B.J. FOR ALL				-	-	-		
	SEGMENTS 1, 2, 3, 4, 5								
	& 6.								

UNIT COST SUMMARY		
SET-UP		HRS
FAB.		HRS
ASSEM.		HRS
MAT'L.	$	
CYCLE		DAYS

BID WORK SHEET

MAT'L:		PART NO:	ALUM H-CORE PANEL ASSEMBLY
SIZE:	TOTAL NO. REQ.	PART NAME:	SEGMENTS 1-6 SANDWICH - STRUCTURE
SPEC:		NEXT ASSEM:	STA. #696-847
		END ITEM:	

CHG. LTR.	
PLAN	
Q.C.	
MAT'L.	
PROC.	
TOOL EST.	
MFG. EST.	

PART ILLUSTRATION:

NOTE: THE MACHINED ALUM FRAME STRUCTURE HAS BEEN ANODIZED FOR CORROSIVE PROTECTION & REQUIRES A DICHROMATE SEAL PRIMER TO BE ADDED TO THE ANODIZED METAL SURFACE OF THE FRAME THAT GET ADHESIVE BONDED TO THE ALUM SKIN OF THE HONEYCOMB CORE PANEL ASSEMBLY - PRIOR TO THE ASSEMBLY OF BONDED OPERATION.

NO.	OPERATION	TOOL	EQUIPMENT	DEPT.	UNIT COST SET-UP	UNIT COST FAB.	UNIT COST ASSEM.	TOOL COST DES.	TOOL COST FAB.
*22	OPERATION 11-20 SAME FOR				-	-	17.834		
	ALL SEGMENTS EXCEPT FOR								
	SIZE.								
23	MACHINE PERIMETER OF	M.F.			.5	1.200	-		
	SEGMENT NET PER B/P		M.F. REQUIRED FOR SEGMENT						
	TOLERANCE.		1, 2, 4, 3 & 5.						
24	DRILL F/S ATTACH HOLES	D.J.			-	1.110	-		
	IDENTIFYING INDEX SIDE		D.J. REQUIRED FOR SEGMENT						
	OF SEGMENT FOR NEXT		1, 2, 3, 4 & 5						
	ASSEMBLY REQUIREMENTS.								
	*USE 3.566 STD. FOR								
	OPERATION 11-20 ON EACH								
	REMAINING SEGMENT.								

UNIT COST SUMMARY		
SET-UP		HRS
FAB.		HRS
ASSEM.		HRS
MAT'L.	$	
CYCLE		DAYS

Figure 193 TYPICAL BID WORKSHEET FOR FUSELAGE COST ANALYSIS -- Concluded

TABLE LXXXV DIRECT PRODUCTION LABOR ELEMENT ESTIMATES BASELINE - 100 AIRCRAFT PROGRAM

AIRCRAFT COMPONENT	DIRECT LABOR HOURS PER AIRCRAFT[1]			
	MANUFACTURING	QUALITY ASSURANCE	TOOLING	PLANNING
WING				
Wing Box	55,050	4,517	2,860	3,853
Remainder (Includes also Flaps, Ailerons, Balance Weights)	71,968	6,235	7,979	5,038
Subtotal	127,018	10,752	10,830	8,891
HORIZONTAL TAIL				
Horizontal Box	9,136	760	731	640
Remainder	9,641	842	1,291	675
Subtotal	18,777	1,602	2,022	1,315
VERTICAL TAIL				
Vertical Box	7,031	589	618	492
Remainder	11,751	1,033	1,660	823
Subtotal	18,782	1,622	2,278	1,315
FUSELAGE				
Fuselage Shell (Station 366-982)	34,326	2,964	3,191	2,402
Remainder	76,153	6,575	7,078	5,332
Subtotal	110,479	9,539	10,269	7,734
REMAINDER OF AIRCRAFT[2]	98,435	14,340	9,031	6,889
TOTAL	373,491	37,855	34,460	26,144

[1] Cumulative average recurring estimated actual hours

[2] Includes the following airframe systems:

- landing gear (less rolling assembly)
- flight controls
- propulsion (less engine)
- fuel system
- auxiliary power unit
- instruments
- hydraulics
- pneumatics
- electrical
- avionics
- furnishings
- air conditioning
- ice protection
- handling gear

TABLE LXXXVI DIRECT PRODUCTION LABOR ELEMENT ESTIMATES BASELINE - 300 AIRCRAFT PROGRAM

AIRCRAFT COMPONENT	DIRECT LABOR HOURS PER AIRCRAFT[1]			
	MANUFACTURING	QUALITY ASSURANCE	TOOLING	PLANNING
WING				
Wing Box	39,499	3,210	1,651	2,765
Remainder (Includes also Flaps, Ailerons, Balance Weights)	51,638	4,379	4,601	3,615
Subtotal	91,137	7,589	6,252	6,380
HORIZONTAL TAIL				
Horizontal Box	6,594	540	422	462
Remainder	6,958	593	745	487
Subtotal	13,552	1,133	1,167	949
VERTICAL TAIL				
Vertical Box	5,075	418	357	355
Remainder	8,402	727	958	594
Subtotal	13,557	1,145	1,315	949
FUSELAGE				
Fuselage Shell (Station 366-982)	24,203	2,058	1,842	1,694
Remainder	53,693	4,565	4,086	3 758
Subtotal	77,896	6,623	5,928	5,452
REMAINDER OF AIRCRAFT[2]	68,520	9,838	5,231	4,796
TOTAL	264,659	26,328	19,893	1[illegible],526

[1] Cumulative average recurring estimated actual hours

[2] Includes the following airframe systems:

- landing gear (less rolling assembly)
- flight controls
- propulsion (less engine)
- fuel system
- auxiliary power unit
- instruments
- hydraulics
- pneumatics
- electrical
- avionics
- furnishings
- air conditioning
- ice protection
- handling gear

TABLE LXXXVII DIRECT PRODUCTION LABOR ELEMENT ESTIMATES, BASELINE - 500 AIRCRAFT PROGRAM

AIRCRAFT COMPONENT	DIRECT LABOR HOURS PER AIRCRAFT[1]			
	MANUFACTURING	QUALITY ASSURANCE	TOOLING	PLANNING
WING				
Wing Box	33,889	2,745	1,305	2,372
Remainder (Includes also Flaps, Ailerons, Balance Weights)	44,303	3,739	3,637	3,101
Subtotal	78,192	6,484	4,942	5,473
HORIZONTAL TAIL				
Horizontal Box	5,673	463	334	397
Remainder	5,987	506	539	419
Subtotal	11,660	969	923	816
VERTICAL TAIL				
Vertical Box	4,366	358	282	306
Remainder	7,297	620	757	511
Subtotal	11,663	978	1,039	817
FUSELAGE				
Fuselage Shell (Station 366-982)	20,596	1,742	1,455	1,442
Remainder	45,690	3,865	3,230	3,199
Subtotal	66,286	5,607	4,685	4,641
REMAINDER OF AIRCRAFT[2]	57,951	8,282	4,134	4,056
TOTAL	225,752	22,320	15,723	15,603

[1] Cumulative average recurring estimated actual hours

[2] Includes the following airframe systems:

- landing gear (less rolling assembly)
- flight controls
- propulsion (less engine)
- fuel system
- auxiliary power unit
- instruments
- hydraulics
- pneumatics
- electrical
- avionics
- furnishings
- air conditioning
- ice protection
- handling gear

TABLE LXXXVIII DIRECT PRODUCTION LABOR ELEMENT ESTIMATES, RESIZED NEW CONCEPTS, HONEYCOMB FUSELAGE -- 100 AIRCRAFT PROGRAM

AIRCRAFT COMPONENT	DIRECT LABOR HOURS PER AIRCRAFT[1]			
	MANUFACTURING	QUALITY ASSURANCE	TOOLING	PLANNING
WING				
Wing Box	36,153	3,755	2,360	1,808
Remainder (Includes also Flaps, Ailerons, Balance Weights)	69,973	6,140	7,752	4,898
Subtotal	106,126	9,895	10,112	6,706
HORIZONTAL TAIL				
Horizontal Box	4,589	514	754	229
Remainder	9,467	824	1,228	663
Subtotal	14,056	1,338	1,982	892
VERTICAL TAIL				
Vertical Box	4,087	449	579	204
Remainder	11,549	1,016	1,642	809
Subtotal	15,636	1,465	2,221	1,012
FUSELAGE				
Fuselage Shell (Station 366-982)	40,927	4,380	3,423	2,046
Remainder	75,264	5,498	6,995	5,268
Subtotal	116,191	10,878	10,418	7,314
REMAINDER OF AIRCRAFT[2]	97,409	7,254	9,032	6,817
TOTAL	349,418	30,830	33,765	22,741

[1] Cumulative average recurring estimated actual hours

[2] Includes the following airframe systems:

- landing gear (less rolling assembly)
- flight controls
- propulsion (less engine)
- fuel system
- auxiliary power unit
- instruments
- hydraulics
- pneumatics
- electrical
- avionics
- furnishings
- air conditioning
- ice protection
- handling gear

TABLE LXXXIX DIRECT PRODUCTION LABOR ELEMENT ESTIMATES, RESIZED NEW CONCEPTS, HONEYCOMB FUSELAGE - 300 AIRCRAFT PROGRAM

AIRCRAFT COMPONENT	DIRECT LABOR HOURS PER AIRCRAFT[1]			
	MANUFACTURING	QUALITY ASSURANCE	TOOLING	PLANNING
WING				
Wing Box	24,808	2,547	1,319	1,240
Remainder (Includes also Flaps, Ailerons, Balance Weights)	50,206	4,318	4,448	3,514
Subtotal	75,014	6,865	5,767	4,754
HORIZONTAL TAIL				
Horizontal Box	3,374	364	412	169
Remainder	6,834	580	704	478
Subtotal	10,208	944	1,116	647
VERTICAL TAIL				
Vertical Box	3,043	323	309	152
Remainder	8,336	714	942	584
Subtotal	11,379	1,037	1,251	736
FUSELAGE				
Fuselage Shell (Station 366-982)	29,280	3,111	2,227	1,464
Remainder	53,066	4,511	4,038	3,715
Subtotal	82,346	7,622	6,265	5,179
REMAINDER OF AIRCRAFT[2]	67,801	9,740	5,183	4,746
TOTAL	246,748	26,208	19,582	16,062

[1] Cumulative average recurring estimated actual hours

[2] Includes the following airframe systems:

- landing gear (less rolling assembly)
- flight controls
- propulsion (less engine)
- fuel system
- auxiliary power unit
- instruments
- hydraulics
- pneumatics
- electrical
- avionics
- furnishings
- air conditioning
- ice protection
- handling gear

TABLE XC DIRECT PRODUCTION LABOR ELEMENT ESTIMATES RESIZED NEW CONCEPTS HONEYCOMB FUSELAGE - 500 AIRCRAFT PROGRAM

AIRCRAFT COMPONENT	DIRECT LABOR HOURS PER AIRCRAFT[1]			
	MANUFACTURING	QUALITY ASSURANCE	TOOLING	PLANNING
WING				
Wing Box	20,836	2,132	1,028	1,042
Remainder (Includes also Flaps, Ailerons, Balance Weights)	43,075	4,318	3,528	3,015
Subtotal	63,911	6,450	4,556	4,057
HORIZONTAL TAIL				
Horizontal Box	2,927	308	270	146
Remainder	5,879	496	559	412
Subtotal	8,806	804	829	558
VERTICAL TAIL				
Vertical Box	2,655	278	235	133
Remainder	7,172	610	747	502
Subtotal	9,827	868	982	635
FUSELAGE				
Fuselage Shell (Station 366-982)	25,087	2,648	1,730	1,254
Remainder	45,158	3,820	3,192	3,161
Subtotal	70,245	6,468	5,922	4,415
REMAINDER OF AIRCRAFT[2]	57,340	8,610	4,110	4,014
TOTAL	210,129	23,220	15,399	13,679

[1] Cumulative average recurring estimated actual hours

[2] Includes the following airframe systems:

- landing gear (less rolling assembly)
- flight controls
- propulsion (less engine)
- fuel system
- auxiliary power unit
- instruments
- hydraulics
- pneumatics
- electrical
- avionics
- furnishings
- air conditioning
- ice protection
- handling gear

For engineering hours, the initial design, sustaining design and manufacturing liaison engineering, and the engineering laboratory efforts were considered. A group by group discipline evaluation of the total tasks was made which accounted for the impact of the structural concepts. Labor for engineering laboratory and flight test are assumed to be constant for baseline and new concept aircraft and within a given aircraft quantity. These labor elements reflect a full scale test program for compliance with military standards, specifications and requirements for airworthiness. Product support represents the manufacturer's participation in developing the integrated logistics support system and includes the requirements for the three major subsystems - airframe, engines and avionics. Examples of the product support expenditures are developing a maintenance concept, maintainability plan, initial training, etc. Product support costs for the new concepts are lower reflecting fewer parts. However, logistics costs increase with increases in the fleet size due to increased numbers of aircraft and bases. Also, included in these costs are subsystem technical representatives for the various bases and depot. While these are direct estimates they are based on past experience.

10.1.2 Material Costs

Raw material costs for the airframe structure are dependent on the quantities of each material, the mill forms, and the cost per pound of those materials. Table XCI is the listing of materials, mill forms, and costs for each that were used in this study. Also shown is the material utilization factor for each as an average value used in the study considering the concepts. The utilization factor is the weight ratio of the material in the aircraft to the purchased material.

The detailed raw material estimates are listed in Tables XCII through XCIX for the baseline aircraft and the resized new concept aircraft. Each table is for one of the major structural components of the study. The purchased weights were determined by dividing the calculated design weights by the utilization factors shown in Table XCI. These tables are for the production cumulative average in the 300 aircraft program and illustrate the calculation procedure.

Tables C and CI list the raw materials and purchased parts costs summary by component for the 100, 300, and 500 aircraft programs and for the baseline and resized new concept aircraft. The costs of Tables XCII through XCIX for 300 aircraft were multiplied by learning curve factors for the 100 and 500 aircraft programs. The "Remainder of Aircraft" is the cost for the various onboard systems, such as pneumatics, hydraulics, landing gear, instruments, etc. For each aircraft quantity, the unit cost of these items was held relatively constant to account for small configurational variations in the size of the systems. The cost per pound for all structural components and for the remainder of the aircraft are summarized as follows:

TABLE XCI MATERIAL UNIT COST		
Material Type	$/Lb	Utilization Factor
Fiberglass & Glass	2.78	0.59
Adhesive	25.66	0.83
Aluminum - 7075 Forging	2.46	0.25
Aluminum - 2024, 7075 Sheet, Plate, Extrusion	1.64	0.81
Aluminum - Honeycomb	8.17	0.83
Aluminum - 7050 Sheet & Plate (Mostly Sheet)	1.78	0.81
Aluminum - 7050 Extrusion	2.05	0.81
Aluminum - 7050 Forging	3.07	0.25
Aluminum - 7049 Forging	2.64	0.25
Aluminum - 7475 Sheet & Plate	1.81	0.81
Steel	1.43	0.35
Titanium	9.19	0.37
Boron - Aluminum (With 7050 Extrusion)	7.72	0.67
Boron	88.88	0.71
Other (Filler, Attachments, Paint, Balance Weights)	4.87	1.00

January 1973 Dollars

TABLE XCII WING COMPONENT RAW MATERIAL COST ESTIMATE, BASELINE - 300 AIRCRAFT PROGRAM

MATERIAL CATEGORY	MATERIAL WEIGHT - LB		COST[1] JANUARY 1973 DOLLARS
	DESIGN	PURCHASED	
Fiberglass & Glass	786	1,336	3,714
Adhesive	-	-	-
Aluminum - 7075 Forging	3,197	12,788	31,458
Aluminum - 2024, 7075 Sheet, Plate, Extrusion	1,811	2,228	3,654
Aluminum - 7050 Sheet & Plate (Mostly Sheet)	3,111	3,827	6,812
Aluminum - 7475 Sheet & Plate	1,987	2,444	4,424
Aluminum - 7049 Forging	1,731	6,924	18,279
Aluminum - 7050 Forging	1,746	6,984	21,441
Aluminum - 7050 Extrusion	-	-	-
Boron - Aluminum (With 7050 Extrusion)	-	-	-
Aluminum - Honeycomb	-	-	-
Steel	681	974	2,747
Titanium	2,930	7,911	72,702
Boron	-	-	-
Other (Filler, Attachments, Paint, Balance Weights)	785	785	3,823
Total	18,765	46,201	169,054

[1] Cumulative Average Estimate

TABLE XCIII HORIZONTAL TAIL COMPONENT RAW MATERIAL COST ESTIMATE, BASELINE - 300 AIRCRAFT PROGRAM

MATERIAL CATEGORY	MATERIAL WEIGHT - LB		COST[1] JANUARY 1973 DOLLARS
	DESIGN	PURCHASED	
Fiberglass & Glass	-	-	-
Adhesive	-	-	-
Aluminum - 7075 Forging	307	1,228	3,021
Aluminum - 2024, 7075 Sheet, Plate, Extrusion	1,134	1,395	2,288
Aluminum - 7050 Sheet & Plate (Mostly Sheet)	1,073	1,320	2,350
Aluminum - 7475 Sheet & Plate	-	-	-
Aluminum - 7049 Forging	55	220	581
Aluminum - 7050 Forging	-	-	-
Aluminum - 7050 Extrusion	536	659	1,351
Boron - Aluminum (With 7050 Extrusion)	-	-	-
Aluminum - Honeycomb	-	-	-
Steel	-	-	-
Titanium	-	-	-
Boron	-	-	-
Other (Filler, Attachments, Paint, Balance Weight)	129	129	628
Total	3,234	4,951	10,219

[1] Cumulative Average Estimate

TABLE XCIV VERTICAL TAIL COMPONENT, RAW MATERIAL COST ESTIMATE BASELINE - 300 AIRCRAFT PROGRAM

MATERIAL CATEGORY	MATERIAL WEIGHT - LB		COST[1] JANUARY 1973 DOLLARS
	DESIGN	PURCHASED	
Fiberglass & Glass	-	-	-
Adhesive	-	-	-
Aluminum - 7075 Forging	384	1,536	3,779
Aluminum - 2024, 7075 Sheet, Plate, Extrusion	1,455	1,790	2,936
Aluminum - 7050 Sheet & Plate (Mostly Sheet)	890	1,094	1,947
Aluminum - 7475 Sheet & Plate	-	-	-
Aluminum - 7049 Forging	61	244	644
Aluminum - 7050 Forging	-		-
Aluminum - 7050 Extrusion	445	547	1,121
Boron - Aluminum (With 7050 Extrusion)	-	-	-
Aluminum - Honeycomb	-	-	-
Steel	94	134	378
Titanium	-	-	-
Boron	-	-	-
Other (Filler, Attachments, Paint, Balance Weight)	131	131	638
Total	3,460	5,476	11,443

[1] Cumulative Average Estimate

TABLE XCV FUSELAGE COMPONENT RAW MATERIAL COST ESTIMATE BASELINE - 300 AIRCRAFT PROGRAM

MATERIAL CATEGORY	MATERIAL WEIGHT - LB		COST[1] JANUARY 1973 DOLLARS
	DESIGN	PURCHASED	
Fiberglass & Glass	1,315	2,236	6,216
Adhesive	-	-	-
Aluminum - 7075 Forging	-	-	-
Aluminum - 2024, 7075 Sheet, Plate, Extrusion	12,679	15,595	25,576
Aluminum - 7050 Sheet & Plate (Mostly Sheet)	-		-
Aluminum - 7475 Sheet & Plate	644	792	1,434
Aluminum - 7049 Forging	2,862	11,448	30,223
Aluminum - 7050 Forging	-	-	-
Aluminum - 7050 Extrusion	5,280	6,494	13,313
Boron - Aluminum (With 7050 Extrusion)	-	-	-
Aluminum - Honeycomb	-	-	-
Steel	527	754	2,126
Titanium	240	648	5,935
Boron	-	-	-
Other (Filler, Attachments, Paint, Balance Weights)	820	820	3,994
Total	24,367	38,787	88,837

[1] Cumulative Average Estimate

TABLE XCVI WING COMPONENT RAW MATERIAL COST ESTIMATE RESIZED NEW CONCEPT - 300 AIRCRAFT PROGRAM

MATERIAL CATEGORY	MATERIAL WEIGHT - LB		COST[1] JANUARY 1973 DOLLARS
	DESIGN	PURCHASED	
Fiberglass & Glass	764	[illegible]	3,611
Adhesive	--	--	--
Aluminum - 7075 Forging	3,109	12,436	30,593
Aluminum - 2024, 7075 Sheet, Plate, Extrusion	1,761	2,166	3,552
Aluminum - 7050 Sheet & Plate (Mostly Sheet)	2,849	3,504	6,237
Aluminum - 7475 Sheet & Plate	1,819	2,237	4,049
Aluminum - 7049 Forging	1,434	5,736	15,143
Aluminum - 7050 Forging	1,599	6,396	19,636
Aluminum - 7050 Extrusion	--	--	--
Boron - Aluminum (With 7050 Extrusion)	--	--	--
Aluminum - Honeycomb	--	--	--
Steel	662	947	2,671
Titanium	2,849	7,692	70,689
Boron	--	--	--
Other (Filler, Attachments, Paint, Balance Weights)	411	411	2,001
Total	17,257	42,824	158,182

[1]Cumulative Average Estimate

TABLE XCVII HORIZONTAL TAIL COMPONENT RAW MATERIAL COST ESTIMATE RESIZED NEW CONCEPT - 300 AIRCRAFT PROGRAM

MATERIAL CATEGORY	MATERIAL WEIGHT - LB		COST[1] JANUARY 1973 DOLLARS
	DESIGN	PURCHASED	
Fiberglass & Glass	--	--	--
Adhesive	109	131	3,361
Aluminum - 7075 Forging	302	1,208	2,972
Aluminum - 2024, 7075 Sheet, Plate, Extrusion	1,114	1,370	2,247
Aluminum - 7050 Sheet & Plate (Mostly Sheet)	922	1,134	2,019
Aluminum - 7475 Sheet & Plate	--	--	--
Aluminum - 7049 Forging	--	--	--
Aluminum - 7050 Forging	--	--	--
Aluminum - 7050 Extrusion	263	323	662
Boron - Aluminum (With 7050 Extrusion)	--	--	--
Aluminum - Honeycomb	113	136	1,111
Steel	--	--	--
Titanium	--	--	--
Boron	--	--	--
Other (Filler, Attachments, Paint, Balance Weights)	155	155	754
Total	2,978	4,457	13,126

[1]Cumulative Average Estimate

TABLE XCVIII VERTICAL TAIL COMPONENT RAW MATERIAL COST ESTIMATE RESIZED NEW CONCEPT - 300 AIRCRAFT PROGRAM

MATERIAL CATEGORY	MATERIAL WEIGHT - LB		COST[1] JANUARY 1973 DOLLARS
	DESIGN	PURCHASED	
Fiberglass & Glass	--	--	--
Adhesive	59	71	1,822
Aluminum - 7075 Forging	378	1,512	3,720
Aluminum - 2024, 7075 Sheet, Plate, Extrusion	1,430	1,759	2,885
Aluminum - 7050 Sheet & Plate (Mostly Sheet)	792	974	1,734
Aluminum - 7475 Sheet & Plate	--	--	--
Aluminum - 7049 Forging	--	--	--
Aluminum - 7050 Forging	--	--	--
Aluminum - 7050 Extrusion	227	279	572
Boron - Aluminum (With 7050 Extrusion)	--	--	--
Aluminum - Honeycomb	132	158	1,291
Steel	92	132	372
Titanium	--	--	--
Boron	55	77	6,844
Other (Filler, Attachments, Paint, Balance Weights)	66	66	321
Total	3,231	5,028	19,561

[1]Cumulative Average Estimate

TABLE XCIX HONEYCOMB FUSELAGE COMPONENT RAW MATERIAL COST ESTIMATE RESIZED NEW CONCEPT - 300 AIRCRAFT PROGRAM

MATERIAL CATEGORY	MATERIAL WEIGHT - LB		COST[1] JANUARY 1973 DOLLARS
	DESIGN	PURCHASED	
Fiberglass & Glass	1,315	2,236	6,216
Adhesive	561	673	17,269
Aluminum - 7075 Forging	--	--	--
Aluminum - 2024, 7075 Sheet, Plate, Extrusion	10,733	13,202	21,651
Aluminum - 7050 Sheet & Plate (Mostly Sheet)	3,319	4,082	7,266
Aluminum - 7475 Sheet & Plate	--	--	--
Aluminum - 7049 Forging	2,757	11,028	29,114
Aluminum - 7050 Forging	--	--	--
Aluminum - 7050 Extrusion	1,162	1,429	2,929
Boron - Aluminum (With 7050 Extrusion)	1,702	2,553	19,709
Aluminum - Honeycomb	769	923	7,541
Steel	527	754	2,126
Titanium	112	302	2,775
Boron	--	--	--
Other (Filler, Attachments, Paint, Balance Weights)	845	845	4,116
Total	23,802	38,027	120,712

[1]Cumulative Average Estimate

TABLE C RAW MATERIALS AND PURCHASED PARTS SUMMARY BASELINE

AIRCRAFT COMPONENT	DESIGN COST WEIGHT LB	JANUARY 1973 DOLLARS		
		100 ACFT. PROGRAM	300 ACFT. PROGRAM	500 ACFT. PROGRAM
WING				
Wing Box	9,118	63,342	53,600	49,596
Remainder (Includes also Flaps, Ailerons, Balance Weights)	9,647	136,437	115,454	106,828
Subtotal	18,765	199,779	169,054	156,524
HORIZONTAL TAIL				
Horizontal Box	1,749	5,549	4,696	4,345
Remainder	1,485	6,327	5,523	5,110
Subtotal	3,234	1[illegible],076	10,219	9,455
VERTICAL TAIL				
Vertical Box	1,475	4,836	4,097	3,791
Remainder	1,985	8,681	7,346	6,797
Subtotal	3,460	13,517	11,443	10,588
FUSELAGE				
Fuselage Shell (Station 366-982) & Floor Panels	7,571	30,471	25,785	23,859
Remainder	16,796	74,511	63,052	58,341
Subtotal	24,367	104,982	88,837	82,200
REMAINDER OF AIRCRAFT[2]	32,229	588,817	498,260	461,035
TOTAL	82,055	919,171	777,813	719,802

[1]Cumulative average estimate

[2]Includes the following airframe systems:

- landing gear (less rolling assembly)
- flight controls
- propulsion (less engine)
- fuel system
- auxiliary power unit
- instruments
- hydraulics
- pneumatics
- electrical
- avionics
- furnishings
- air conditioning
- ice protection
- handling gear

TABLE CI RAW MATERIALS AND PURCHASED PARTS SUMMARY RESIZED ADVANCED CONCEPT, HONEYCOMB FUSELAGE

AIRCRAFT COMPONENT	DESIGN COST WEIGHT LB	JANUARY 1973 DOLLARS[1]		
		100 ACFT. PROGRAM	300 ACFT. PROGRAM	500 ACFT. PROGRAM
WING				
Wing Box	7,[illegible]76	54,262	45,917	42,487
Remainder (Includes also Flaps, Ailerons, Balance Weights)	9,381	132,669	112,265	102,878
Subtotal	17,257	186,931	158,182	146,365
HORIZONTAL TAIL				
Horizontal Box	1,519	9,097	7,698	7,123
Remainder	1,459	6,415	5,428	5,022
Subtotal	2,978	15,512	13,126	12,143
VERTICAL TAIL				
Vertical Box	1,280	14,580	12,336	11,416
Remainder	1,951	8,539	7,225	6,685
Subtotal	3,231	23,118	19,561	18,101
FUSELAGE				
Fuselage Shell (Station 366-982) And Floor Panels	7,202	70,398	59,571	55,121
Remainder	16,700	72,253	61,141	56,573
Subtotal	23,802	142,651	120,712	111,694
REMAINDER OF AIRCRAFT[2]	31,822	581,381	491,968	455,213
TOTAL	79,090	949,593	803,549	743,516

[1]Cumulative average estimate

[2]Includes the following airframe systems:

- landing gear (less rolling assembly)
- flight controls
- propulsion (less engine)
- fuel system
- auxiliary power unit
- instruments
- hydraulics
- pneumatics
- electrical
- avionics
- furnishings
- air conditioning
- ice protection
- handling gear

Concept	Costs Per Pound		
	Structural Components	Remainder	Total
Baseline	\$5.61	\$15.46	\$9.48
Resized New Concept	\$6.59	\$15.46	\$10.16

The structural material cost per pound increased by 17.5 percent but the total material and purchased parts cost per pound increased by only 7.2 percent for the resized new concept.

The above raw materials and purchased parts identify all raw stock procured for fabrication as well as fabricated parts purchased which are classified as "low-value" items. Another material classification, instruments and special equipment, excludes the raw materials category and considers only "high-value" items or purchased parts and equipment such as landing gear, etc. Estimates for parts and equipment are based on historical data applicable to this type of aircraft.

Tooling materials that are used for jigs and fixtures, etc. (except capital equipment and facilities) are related to the estimated tool design and fabrication labor and are estimated using historical factors. Product support materials are related to the effort described in 10.1.1.

All of the material costs and raw material cost factors include an overlay for internal handling, distribution, and warehousing. The functional relationship varies with the type of material.

10.1.3 Subcontracts

The third major element of air vehicle costs is the engine and avionics costs. The baseline engine costs are for the JT8D-17 engines with these costs scaled down by the ratio of thrust required for the resized new concept aircraft. The avionics costs are for the units which make up the system complement in the baseline. Both of these are considered as constant unit cost with quantity.

10.1.4 Research, Development, Test and Evaluation

The air vehicle costs for the 100, 300, and 500 aircraft programs were apportioned to research, development, test and evaluation (RDT&E) on the basis of five aircraft being produced utilizing RDT&E funds for each program. Table CII summarizes these costs. These estimates are constant for each of the three aircraft except for peak production rate variation effects on non-recurring tooling and non-recurring planning. A profit of 8 percent has been applied to all the material and labor elements of cost for both the development and production phases. Because engines and avionics are usually considered as GFE, no profit is applied to them.

TABLE CII AIR VEHICLE RDT&E COST ESTIMATE COMPARISON (NEW CONCEPTS - HONEYCOMB FUSELAGE)

RESOURCE ELEMENT	100 AIRCRAFT PROGRAM			300 AIRCRAFT PROGRAM			500 AIRCRAFT PROGRAM		
	BASELINE	UNRESIZED NEW CONCEPT	RESIZED NEW CONCEPT	BASELINE	UNRESIZED NEW CONCEPT	RESIZED NEW CONCEPT	BASELINE	UNRESIZED NEW CONCEPT	RESIZED NEW CONCEPT
LABOR									
MANUFACTURING	83.0	79.5	78.4	83.0	79.5	78.4	83.0	79.5	78.4
TOOLING	51.0	51.6	50.8	75.5	76.0	74.9	91.5	93.8	92.5
PLANNING	10.2	8.8	8.6	16.3	14.9	14.7	21.8	20.1	19.6
QUALITY ASSURANCE	9.4	8.0	7.8	19.5	19.4	19.2	27.2	27.7	27.4
ENGINEERING DESIGN	153.9	143.6	141.6	153.9	143.6	141.6	153.9	143.6	141.6
ENGINEERING LABORATORY	45.0	45.0	45.0	45.0	45.0	45.0	45.0	45.0	45.0
FLIGHT TEST	33.8	33.8	33.8	33.8	33.8	33.8	33.8	33.8	33.8
PRODUCT SUPPORT	14.5	13.4	13.4	14.5	13.4	13.4	14.5	13.4	13.4
SUBTOTAL	400.8	383.7	379.4	441.5	425.6	421.0	472.7	456.9	451.7
MATERIAL									
MANUFACTURING - RAW MATERIALS AND PURCHASED PARTS	17.5	18.3	18.0	17.5	18.3	18.0	17.5	18.3	18.0
EQUIPMENT - INSTRUMENTS AND SPECIAL EQUIPMENT	16.8	16.8	16.8	16.8	16.8	16.8	16.8	16.8	16.8
TOOLING	4.2	3.8	3.8	5.5	5.0	4.9	6.5	5.9	5.8
FLIGHT TEST	5.3	5.3	5.3	5.3	5.3	5.3	5.3	5.3	5.3
PRODUCT SUPPORT	12.3	11.5	11.4	12.3	11.5	11.4	12.3	11.5	11.4
SUBTOTAL [2]	56.1	55.7	55.3	57.4	56.9	56.4	58.4	57.8	57.3
SUBCONTRACTS									
ENGINES	7.5	7.5	7.3	7.5	7.5	7.3	7.5	7.5	7.3
AVIONICS	2.2	2.2	2.2	2.2	2.2	2.2	2.2	2.2	2.2
SUBTOTAL	9.7	9.7	9.5	9.7	9.7	9.5	9.7	9.7	9.5
TOTAL PRICE	466.6	449.1	444.2	508.6	492.2	486.9	540.8	524.4	518.5
JANUARY 1973 DOLLARS, MILLIONS									

[1] INCLUDES OVERHEAD, G&A, OVERTIME PREMIUM, DIRECT CHARGES, PROFIT

[2] INCLUDES DIRECT CHARGES, PROFIT

10.1.5 Air Vehicle Production Costs

The air vehicle production cost estimates for the baseline, unresized new concept, and resized new concept aircraft are shown in Table CIII. The total procurement subtotal is for the program aircraft quantities noted minus the RDT&E costs for the five aircraft included in Table CII. The unit prices shown are the flyaway cumulative average prices for each production quantity.

10.1.6 Other Acquisition Costs

Deployment of an aircraft system also requires initial spares, ground equipment, manuals, training, and development changes. In addition, the program must be supported by the manufacturer's organization to coordinate with, and be responsive to, field experience.

Table CIV summarizes the total acquisition costs for the baseline and new concept aircraft. The costs for each element for both the development and production phases, were determined from historical experience. For the new concept aircraft, the costs of program management, spares, product support, and engineering change proposals (ECP's) were proportioned by air vehicle costs. Cost of spares required consideration of various major portions of the aircraft. Engine spares were proportioned to engine costs, avionics were held constant, and airframe spares were proportioned to airframe costs. Training/trainers and AGE were computed as a function of the Prime Mission Equipment (PME) with consideration given to the numbers of aircraft and an assumed basing concept.

10.2 LIFE CYCLE COSTS

10.2.1 Operating Factors and Maintenance Manpower

The operational costs of the system were projected using the Air Force "Planning Aircraft Cost Estimating" (PACE) model (Reference 54) for forces of 100, 300, and 500 aircraft operating for 20 full force years without any phase-in or phase-out phenomenon. In the 100 aircraft case, 15 aircraft were withheld for pipeline advanced attrition and command and support purposes. 44 aircraft were withheld for the 300 case, and 73 aircraft for the 500 case. The remaining unit equipment (UE) aircraft were organized into squadrons of 16 aircraft each. Since full squadrons could not be held for the 100 and 500 aircraft cases, fractional squadrons were used for these two cases to maintain data comparability. Each UE aircraft operates 900 hours per year.

The most significant single component of operating costs is the personnel required to operate the system. The determination of personnel begins with establishing the anticipated maintenance manhours per flying hour for the aircraft under consideration in the operating environment. Table CV displays the estimated maintenance manhours per flight hour for the baseline aircraft and the unresized and resized new concept configuration. The airframe maintenance function manpower requirements shown vary in response to the changed maintenance requirements as a result of the new concept structure.

TABLE CIII AIR VEHICLE PRODUCTION COST ESTIMATE COMPARISON (NEW CONCEPTS - HONEYCOMB FUSELAGE)

RESOURCE ELEMENT	100 AIRCRAFT PROGRAM			300 AIRCRAFT PROGRAM			500 AIRCRAFT PROGRAM		
	BASELINE	NEW CONCEPT		BASELINE	NEW CONCEPT		BASELINE	NEW CONCEPT	
		UNRESIZED	RESIZED		UNRESIZED	RESIZED		UNRESIZED	RESIZED
LABOR									
MANUFACTURING	549.2	521.3	513.8	1,260.0	1,192.5	1,175.2	1,825.8	1,725.6	1,700.6
TOOLING	131.2	132.6	130.7	194.0	195.5	192.6	240.5	241.3	237.8
PLANNING	79.1	68.3	66.9	126.0	114.9	113.4	168.7	155.1	151.5
QUALITY ASSURANCE	58.0	48.9	47.7	118.9	119.4	117.9	167.0	170.4	168.3
ENGINEERING DESIGN	116.1	111.9	110.3	145.1	139.9	137.9	163.4	160.1	157.9
ENGINEERING LABORATORY	3.1	3.1	3.1	5.1	5.1	5.1	5.5	5.5	5.5
FLIGHT TEST	3.1	3.1	3.1	5.1	5.1	5.1	5.5	5.5	5.5
PRODUCT SUPPORT	4.0	3.8	3.7	5.7	5.4	5.3	6.3	6.0	5.9
SUBTOTAL[1]	944.4	893.0	879.3	1,861.5	1,777.8	1,752.5	2,585.1	2,469.5	2,433.0
MATERIAL									
MANUFACTURING - RAW MATERIALS AND PURCHASED PARTS	84.0	87.8	86.7	239.8	250.6	247.7	379.2	396.3	391.7
EQUIPMENT - INSTRUMENTS AND SPECIAL EQUIPMENT	97.9	97.9	96.6	304.0	304.0	300.1	510.1	510.1	503.6
TOOLING	7.4	7.1	7.0	11.0	10.1	10.0	13.7	12.4	12.2
FLIGHT TEST	0.0	0.0	0.0	0.0	0.0	0.0	0.0	0.0	0.0
PRODUCT SUPPORT	5.7	5.4	5.3	8.1	7.6	7.5	9.0	8.4	8.3
SUBTOTAL[2]	195.0	198.2	195.6	562.9	572.3	565.3	912.0	927.2	915.9
SUBCONTRACTS									
ENGINES	142.5	142.5	139.0	442.5	442.5	431.6	742.5	742.5	724.2
AVIONICS	42.5	42.5	42.5	131.9	131.9	131.9	221.3	221.3	221.3
SUBTOTAL	185.0	185.0	181.5	574.4	574.4	563.5	963.8	963.8	945.5
TOTAL PROCUREMENT	1,324.5	1,276.2	1,256.4	2,998.8	2,924.5	2,881.3	4,460.9	4,360.5	4,294.4
UNIT PRICE[3]	13.942	13.434	13.225	10.165	9.914	9.767	9.012	8.809	8.675
RDT&E	466.6	449.1	444.2	508.6	492.2	486.9	540.8	524.4	518.5
TOTAL AIR VEHICLE	1,791.1	1,725.3	1,700.6	3,507.4	3,416.7	3,368.2	5,001.7	4,884.9	4,812.2

[1] INCLUDES OVERHEAD, G&A, OVERTIME PREMIUM, DIRECT CHARGES, PROFIT
[2] INCLUDES DIRECT CHARGES, PROFIT
[3] FLYAWAY PRICE ONLY

JANUARY 1973 DOLLARS, MILLIONS

TABLE CIV ACQUISITION COST COMPARISON (NEW CONCEPTS - HONEYCOMB FUSELAGE)

RESOURCE ELEMENT	100 AIRCRAFT PROGRAM			300 AIRCRAFT PROGRAM			500 AIRCRAFT PROGRAM		
	BASELINE	UNRESIZED NEW CONCEPT	RESIZED NEW CONCEPT	BASELINE	UNRESIZED NEW CONCEPT	RESIZED NEW CONCEPT	BASELINE	UNRESIZED NEW CONCEPT	RESIZED NEW CONCEPT
DEVELOPMENT									
AIR VEHICLE	439.8	424.2	419.4	481.8	467.3	462.1	514.0	499.5	493.7
PROJECT MANAGEMENT	28.8	27.8	27.5	31.6	30.7	30.3	33.7	32.8	32.4
PRODUCT SUPPORT	26.8	24.9	24.8	26.8	24.9	24.8	26.8	[illegible]	24.8
TEST SPARES	28.3	27.4	27.1	30.8	30.0	29.6	32.8	31.9	31.5
PKG. MRKG. SHPG.	.9	.8	.8	.9	.9	.9	1.0	1.0	.9
ECPS	17.6	17.0	16.8	19.3	[illegible]	18.5	20.6	20.0	19.7
TRAINING/TRAINERS	16.8	16.2	16.0	27.5	[illegible]	26.4	39.1	38.2	37.7
AGE	15.8	15.2	14.9	40.3	39.3	38.7	66.6	[illegible]	64.1
SUBTOTAL	574.8	553.5	547.3	659.0	638.5	631.3	734.6	713.4	704.9
PRODUCTION									
AIR VEHICLE (PME)	1,314.8	1,267.0	1,247.4	2,985.0	2,911.5	2,868.5	4,445.6	4,346.1	4,280.2
PROJECT MANAGEMENT	23.9	22.2	21.8	[illegible]	51.0	50.2	77.8	76.1	74.9
PRODUCT SUPPORT	9.7	9.2	9.0	13.8	13.0	12.8	15.3	14.4	14.2
INITIAL SPARES	116.2	113.3	111.4	294.8	290.4	285.8	460.9	455.0	447.6
PKG. MRKG. SHPG.	3.5	3.4	3.3	8.9	8.7	8.6	13.8	13.6	13.4
ECP	52.6	50.7	49.9	119.4	116.4	114.7	177.9	173.8	171.2
TRAINING/TRAINERS	25.2	24.3	24.0	41.2	40.2	39.6	58.7	57.4	56.5
AGE	23.7	22.8	22.5	60.5	59.0	58.1	99.9	97.7	96.2
SUBTOTAL	1,568.7	1,512.9	1,489.3	3,575.8	3,490.2	3,438.3	5,349.9	5,234.1	5,154.2
ACQUISITION TOTAL	2,143.5	2,066.4	2,036.6	4,234.8	4,128.7	4,069.6	6,084.5	5,947.5	5,859.1

JANUARY 1973 DOLLARS, MILLIONS

While these estimates are preliminary, they are based upon detailed considerations of the structural problems and advantages associated with the various new concepts used in the major structural portions of the airplane wing, horizontal stabilizer, vertical stabilizer, and fuselage. As shown in the table, the maintenance manhours for propulsion are a function of the thrust level. Avionics maintenance was, of course, held constant.

These seemingly small variations in maintenance manhours per flying hour, together with the associated changes in spares costs as a result of design simplification and, to a lesser extent, resizing yield rather large changes in total maintenance costs over the life of the system, Table CVI. The total spares and material costs for the new concept resized aircraft are $60 million less than for baseline case, or a savings of six percent. Maintenance labor costs for the resized aircraft are $33 million less than the baseline maintenance labor costs, or a savings of almost 2.5 percent. The total maintenance savings amount to 4 percent of total maintenance cost with most of this (3 percent) due to the new structural design concept.

Since the new concept structures influence not only maintenance manhours per flying hour but also aircraft structural spares and modifications/spares, there is an impact upon the total maintenance of the system. Table CVI assembles the various components of total maintenance to provide a comparison of the new concept and the baseline aircraft total maintenance cost. The final line of this table shows the ratios which would be anticipated on the basis of an unresized and resized new concept aircraft as compared with the baseline aircraft design.

10.2.2 Total Life Cycle Costs

The total life cycle costs for the baseline and the unresized and resized new concept aircraft are shown in Table CVII for 100, 300, and 500 aircraft in the total procurement period. The acquisition costs displayed here are from Table CIV. The operations and support costs displayed were calculated using the PACE model for the various quantities of aircraft at a 900-hour per aircraft per year utilization level. The POL (petroleum, oil, and lubricant) costs shown here were taken on the basis of 15 cents per gallon for fiscal year 1973, as reported in AFM 173-10. These cost levels were used despite the fact that current fuel prices have advanced very significantly. However, to maintain comparability between these and other similar studies, the January 1973 cost level was held constant.

10.3 New Concept Economic Benefits

The various areas of cost changes resulting from the use of the new structural design concepts can best be highlighted through the derivation of cost complexity factors. These cost factors, since they are developed as a result of the detailed analysis of this study, are referred to as implicit complexity factors.

TABLE CV MAINTENANCE MAN-HOURS PER FLIGHT HOUR COMPARISON (NEW CONCEPTS - HONEYCOMB FUSELAGE)			
MAINTENANCE FUNCTIONS	BASELINE	NEW CONCEPT	
		UNRESIZED	RESIZED
AIRFRAME	3.13	3.11	2.99
PROPULSION	3.62	3.62	3.55
AVIONICS	1.77	1.77	1.77
SUBTOTAL	8.52	8.50	8.31
SERVICING	2.70	2.70	2.70
CLEANING/ CORROSION CONTROL	0.28	0.28	0.28
SUPPORT OTHER	0.45	0.45	0.45
SUBTOTAL	3.43	3.43	3.43
PRE/POST FLIGHT	0.57	0.57	0.57
PHASE (PH) INSPECTION (LOOK)	0.98	0.98	0.98
SUBTOTAL	1.55	1.55	1.55
TOTAL	13.50	13.48	13.29

TABLE CVI COMPARISON OF MAINTENANCE COSTS FOR 300 AIRCRAFT PROGRAM (NEW CONCEPTS - HONEYCOMB FUSELAGE)			
MAINTENANCE COST ELEMENT	BASELINE	NEW CONCEPT	
		UNRESIZED	RESIZED
REPLENISHMENT SPARES	290.3	284.7	280.0
MODIFICATION/SPARES	233.5	228.1	224.7
COMMON AGE/SPARES	31.7	31.7	31.7
SYSTEM SUPPORT MATERIAL	290.3	284.8	280.2
GENERAL SUPPORT MATERIAL	188.9	185.1	181.5
SUBTOTAL	1,034.7	1,014.4	998.1
MAINTENANCE PERSONNEL	588.1	562.8	555.2
DEPOT MAINTENANCE	753.9	753.9	753.9
SUBTOTAL	1,342.0	1,316.7	1,309.1
TOTAL	2,376.7	2,331.1	2,307.2
COMPARISON WITH BASELINE	1.00	0.98	0.97

JANUARY 1973 DOLLARS, MILLIONS
256 OPERATING AIRCRAFT

The implicit factors are defined as follows:

$$C_F = \frac{C_N}{C_{BL}} = C_c \times S_F \tag{47}$$

where C_F = Complexity Factor

C_N = Cost of New Concept Component

C_{BL} = Cost of Baseline Component

C_c = Cost Coefficient

S_F = Scale Factor = Ratio of the Weights of the New Concept Component to the Baseline Component

The labor complexity factors for manufacturing, quality assurance, tooling, and planning for each of the four components and the remainder of the aircraft are shown in Table CVIII for the 300 aircraft quantity. The corresponding material complexity factors are presented in Table CIX. The labor factors range from 0.448 for wing box planning to 1.512 for fuselage shell quality assurance. The material factors range from 0.857 for the wing box structure to 3.010 for the vertical stabilizer box structure. Although these factors are very specific because of the detailed methodology used, these factors may be applied for cost analysis of similar design concepts and components when transformed into cost coefficients. The scaling factors may be calculated from the weight data for the components.

The economic benefits of the new concepts in dollars, are listed in Table CX for each structural component of the resized aircraft together with the weight and change in cost divided by the change in weight. All of the components were reduced in weight and all were reduced in cost except the fuselage shell and floor. The new concept fuselage component was 26.2% more expensive than the baseline and increased cost about \$383 per pound of weight saved. The cost for the wing box was reduced 35%, for the horizontal stabilizer box, 42%, and for the vertical stabilizer box, 29%. The respective savings per pound of weight saved were approximately \$245, \$263, and \$168. The total cost for all four components was reduced \$254,000, or 15.3% from the baseline. Including the resizing benefits to the remainder of the structure, the total cost reduction to the aircraft structure was \$311,000, or 7%, from the baseline cost.

10.4 NEW CONCEPT COMPARISONS

In addition to the data contained in the preceeding paragrapns for the new concept aircraft having a honeycomb fuselage, comparable data are presented in Volume II for the new concept aircraft having an isogrid fuselage shell structure. The costs of these two new concept aircraft, unresized and resized, are compared to the baseline aircraft in Table CXI for the 300 aircraft program. The combined application of the new concepts to wing and empennage structural boxes together with the honeycomb fuselage results in a reduction of about 2.5 percent with resizing in Manufacturer's Weight Empty. However,

TABLE CVII LIFE CYCLE COST COMPARISON (NEW CONCEPTS - HONEYCOMB FUSELAGE)

RESOURCE ELEMENTS	BASELINE	NEW CONCEPT UNRESIZED	NEW CONCEPT RESIZED
100 AIRCRAFT QUANTITY			
ACQUISITION	2,143.5	2,066.4	2,036.6
OPERATIONS AND SUPPORT			
DIRECT			
MATERIALS/SPARES	467.5	452.7	445.0
PERSONNEL	434.9	426.5	424.0
POL	520.2	515.6	512.6
DEPOT MAINTENANCE	250.3	250.3	250.3
MISCELLANEOUS	5.0	4.9	4.8
INDIRECT			
BASE OPERATING SUPPORT	214.3	213.3	211.4
PLANNING ADDITIVES	32.7	32.0	31.7
SUBTOTAL	1,924.9	1,895.3	1,879.8
LIFE CYCLE COST	4,068.4	3,961.7	3,916.4
300 AIRCRAFT QUANTITY			
ACQUISITION	4,234.8	4,128.7	4,069.6
OPERATIONS AND SUPPORT			
DIRECT			
MATERIALS/SPARES	1,035.1	1,014.4	998.1
PERSONNEL	1,309.8	1,384.4	1,276.9
POL	1,566.7	1,552.9	1,543.7
DEPOT MAINTENANCE	753.9	753.9	753.9
MISCELLANEOUS	15.0	14.7	14.6
INDIRECT			
BASE OPERATING SUPPORT	645.5	642.5	636.6
PLANNING ADDITIVES	98.5	96.4	95.6
SUBTOTAL	5,424.5	5,359.2	5,319.4
LIFE CYCLE COST	9,659.3	9,487.9	9,389.0
500 AIRCRAFT QUANTITY			
ACQUISITION	6,084.5	5,947.4	5,859.1
OPERATIONS AND SUPPORT			
DIRECT			
MATERIALS/SPARES	1,536.6	1,509.3	1,484.4
PERSONNEL	2,184.7	2,142.4	2,129.8
POL	2,613.2	2,590.2	2,574.8
DEPOT MAINTENANCE	1,257.4	1,257.4	1,257.4
MISCELLANEOUS	25.0	24.5	24.3
INDIRECT			
BASE OPERATING SUPPORT	1,076.7	1,071.6	1,061.8
PLANNING ADDITIVES	164.3	160.8	159.5
SUBTOTAL	8,857.9	8,756.2	8,692.1
LIFE CYCLE COST	14,942.4	14,703.6	14,551.2

JANUARY 1973 DOLLARS-MILLIONS

TABLE CVIII IMPLICIT LABOR COMPLEXITY FACTORS FOR RESIZED NEW CONCEPT AIRCRAFT RELATIVE TO BASELINE AIRCRAFT (HONEYCOMB FUSELAGE - 300 AIRCRAFT PROGRAM)

AIRCRAFT COMPONENT	MANUFACTURING	QUALITY ASSURANCE	TOOLING	PLANNING
WING				
Box Structure	0.628	0.733	0.799	0.448
Remainder (Includes also Flaps, Ailerons, Balance Weights)	0.972	[illegible]	[illegible]	[illegible]
Subtotal	0.823	0.751	0.922	0.745
HORIZONTAL TAIL[1]				
Box Structure	0.512	0.674	0.976	0.366
Remainder	0.982	0.978	0.985	[illegible]
Subtotal	0.753	0.833	[illegible]	[illegible]
VERTICAL TAIL				
Box Structure	0.600	0.773	0.865	0.428
Remainder	0.983	0.982	0.983	[illegible]
Subtotal	0.833	[illegible]	[illegible]	[illegible]
FUSELAGE				
Fuselage Shell (Station 365-982)	1.210	1.512	1.219	0.868
Remainder	0.988	[illegible]	0.938	[illegible]
Subtotal	1.057	[illegible]	1.057	[illegible]
REMAINDER OF AIRCRAFT[1]	0.990	0.990	0.991	[illegible]
TOTAL	[illegible]	[illegible]	[illegible]	[illegible]

[1]Includes the following airframe systems

- landing gear (less rolling assembly)
- flight controls
- propulsion (less engine)
- fuel system
- auxiliary power unit
- instruments
- hydraulics
- pneumatics
- electrical
- avionics
- furnishings
- air conditioning
- ice protection
- handling gear

TABLE CIX IMPLICIT MATERIAL COST COMPLEXITY FACTORS FOR RESIZED NEW CONCEPT AIRCRAFT RELATIVE TO BASELINE AIRCRAFT (HONEYCOMB FUSELAGE - 300 AIRCRAFT PROGRAM)

AIRCRAFT COMPONENT	COMPLEXITY FACTOR
WING	
BOX STRUCTURE	0.857
REMAINDER (INCLUDES ALSO FLAPS, AILERONS, BALANCE WEIGHTS)	0.972
SUBTOTAL	0.936
HORIZONTAL TAIL	
BOX STRUCTURE	1.639
REMAINDER	0.983
SUBTOTAL	1.284
VERTICAL TAIL	
BOX STRUCTURE	3.010
REMAINDER	0.983
SUBTOTAL	1.709
FUSELAGE	
CENTER FUSELAGE SHELL (STATIONS 366 TO 982) & FLOOR PANELS	2.310
REMAINDER	0.970
SUBTOTAL	1.359

TABLE CX COST AND WEIGHT BENEFITS OF NEW CONCEPTS (HONEYCOMB FUSELAGE)

STRUCTURAL COMPONENT	WEIGHT - LB			PRODUCTION COST - $MILLIONS			
	BASELINE	RESIZED NEW CONCEPT	REDUCTION	BASELINE	RESIZED NEW CONCEPT	COST	Δ$/ΔLB
Wing Box	9,118	7,876	1,242	0.865	0.561	-0.304	-245.02
Horizontal Stabilizer Box	1,749	1,519	230	0.143	0.083	-0.060	-263.03
Vertical Stabilizer Box	1,475	1,280	195	0.111	0.079	-0.032	-167.88
Fuselage Shell And Floor	7,571	7,202	369	0.541	0.683	+0.142	383.00
COMPONENT TOTAL	19,913	17,877	2,036	1.660	1.406	-0.254	-124.75
AIRCRAFT STRUCTURE TOTAL	49,826	47,268	2,558	4.448	4.137	-0.311	-121.58

300 AIRCRAFT CUMULATIVE AVERAGE COST

the total life cycle cost is reduced about 3 percent relative to the baseline. With the isogrid fuselage, the weight and cost reductions are less. The resized new concept aircraft with the isogrid fuselage results in about a 2 percent reduction in Manufacturer's Weight Empty and about 1/2 percent less acquisition and life cycle costs. Although the resized aircraft with the isogrid fuselage weighs only slightly more than the resized honeycomb fuselage aircraft, the production cost is 3.7 percent higher. The aircraft cost increase is due to the higher cost and weight for the isogrid fuselage.

While the new structural design concepts when combined into the baseline aircraft provide relatively modest weight reductions, the honeycomb fuselage case results in a much larger relative cost improvement. In fact, the isogrid fuselage aircraft must be resized before the production cost becomes less than the baseline. This occurs for the honeycomb fuselage case, even with material cost increases which are partially offsetting to the labor reductions. These cost impact factors are readily apparent in Table CXII where all costs are normalized to those for the baseline. The honeycomb fuselage aircraft exhibits manufacturing and planning labor reductions and slight material cost increase. The isogrid fuselage aircraft provides less significant planning labor improvements, increased tooling, and much greater quality assurance labor and raw material cost.

Estimates were made of the total potential benefits of using the new concepts based on the present values of the life cycle costs. Since technology investments are required for the new concepts, the total benefits must be large enough to justify the investment. The benefits were calculated for the 300 aircraft procurement quantity deployed in sixteen squadrons of 16 aircraft each operating at 900 hours per year per aircraft. A discount rate of ten percent was used to roughly reflect the current decision making rate of the government. The present values, presented in Table CXIII, show that if the technology development costs are less than $120 million, the technology involved in the new concept aircraft with the honeycomb fuselage would be worthwhile for the C-15 application. If the technology development costs exceed $120 million, there must be additional applications to result in an investment pay-off.

TABLE CXI AIRCRAFT CHARACTERISTICS AND COST SUMMARY

CHARACTERISTIC	BASELINE AIRCRAFT	NEW CONCEPT AIRCRAFT			
		HONEYCOMB FUSELAGE		ISOGRID FUSELAGE	
		UNRESIZED	RESIZED	UNRESIZED	RESIZED
THRUST PER ENGINE - SLT, LB	14,900	[illegible]	14,532	14,900	14,697
WEIGHT SUMMARY - LB					
AMPR WEIGHT	79,016	77,171	76,054	77,937	77,298
MFG. WEIGHT EMPTY	98,724	96,579	96,348	97,645	96,767
OPERATORS WEIGHT EMPTY	103,240	101,320	99,853	102,155	101,274
TAKEOFF GROSS WEIGHT	150,000	150,000	146,310	150,000	147,872
COST WEIGHT	82,055	80,210	79,090	80,976	80,336
COST**					
RESOURCE ELEMENT					
DEVELOPMENT	659.0	638.5	631.3	636.9	651.7
PRODUCTION	3,575.8	3,490.2	3,438.3	3,653.7	3,565.1
ACQUISITION SUBTOTAL	4,234.8	4,128.7	4,069.6	4,310.6	4,216.8
OPERATIONS AND SUPPORT (20 YRS)	5,424.5	5,359.2	5,319.4	5,450.5	5,406.1
TOTAL LIFE CYCLE COST	9,659.3	9,487.9	9,389.0	9,761.1	9,623.0
*(PRODUCTION UNIT PRICE)	(10.165)	(9.914)	(9.767)	(10.394)	(10.137)

*(FLYAWAY PRICE ONLY)

**300 AIRCRAFT - JANUARY 1, 1973 DOLLARS, MILLIONS

TABLE CXII COST COMPARISON OF THE NEW CONCEPT AIRCRAFT RELATIVE TO THE BASELINE AIRCRAFT

RESOURCE ELEMENT	NEW CONCEPT AIRCRAFT			
	HONEYCOMB FUSELAGE		ISOGRID FUSELAGE	
	UNRESIZED	RESIZED	UNRESIZED	RESIZED
LABOR				
MANUFACTURING	0.946	0.932	1.020	0.975
TOOLING	1.068	0.913	1.047	1.038
PLANNING	0.911	0.909	0.976	0.936
QUALITY ASSURANCE	1.004	0.991	1.138	1.130
ENGINEERING DESIGN	0.964	0.950	0.901	0.900
ENGINEERING LABORATORY	1.000	1.000	1.058	1.058
FLIGHT TEST	1.000	1.000	1.058	1.058
PRODUCT SUPPORT	0.947	0.930	0.947	0.930
SUBTOTAL	0.955	0.940	1.018	[illegible]
MATERIAL				
MANUFACTURING - RAW MATERIAL AND PURCHASED PARTS	1.045	1.033	1.137	1.128
EQUIPMENT - INSTRUMENTS AND SPECIAL EQUIPMENT	1.000	0.987	1.000	0.993
TOOLING	0.918	0.909	1.045	1.036
PRODUCT SUPPORT	0.938	0.926	0.901	0.889
FLIGHT TEST	0.0	0.0	0.0	0.0
SUBTOTAL	1.017	1.004	1.058	1.050
SUBCONTRACTS				
ENGINES	1.000	0.975	1.000	0.986
AVIONICS	1.000	1.000	1.000	1.000
SUBTOTAL	1.000	0.981	1.000	0.989
UNIT PRICE	0.975	0.960	1.022	0.997

300 AIRCRAFT PROGRAM

TABLE CXIII PRESENT VALUE COMPARISONS OF LIFE CYCLE COSTS

CONFIGURATION	DOLLARS, MILLIONS	
	LIFE CYCLE COST	DELTA LIFE CYCLE COST
BASELINE	3553.7	0
UNRESIZED AIRCRAFT WITH HONEYCOMB FUSELAGE	3481.9	-71.8
RESIZED AIRCRAFT WITH HONEYCOMB FUSELAGE	3439.3	-120.3
UNRESIZED AIRCRAFT WITH ISOGRID FUSELAGE	3606.6	+46.9
RESIZED AIRCRAFT WITH ISOGRID FUSELAGE	3544.1	-15.6

SECTION XI

AIRCRAFT PERFORMANCE PAYOFF

The structural arrangement of the aircraft used in the following performance analysis consists of the following new design concepts: 1) integrally stiffened wing cover skins, 2) honeycomb sandwich fuselage shell and 3) honeycomb sandwich empennage cover skins.

The performance analysis of the aircraft having the isogrid fuselage shell is found in Volume II.

11.1 PERFORMANCE ANALYSIS

The performance payoff studies were conducted for three configurations of aircraft utilizing the new design concepts. These include: 1) unresized, or fixed, geometry; 2) completely resized airframe, including "rubberized" engines and 3) partially resized airframe with the baseline engines.

11.1.1 Unresized Aircraft

The unresized aircraft has the same external dimensions and engine thrust as the baseline aircraft. The weight reduction of 1850 lb. is due to a combination of new materials and internal geometry changes. This structural weight reduction results in a performance improvement over the baseline aircraft. The improvement may be taken as a reduction in field length, an increase in payload, or as an increase in mission radius. These performance improvement options are summarized in Table CXIV.

11.1.2 Resized Aircraft

The resized aircraft is the minimum weight configuration that has the same performance characteristics as the baseline aircraft. The reduction in structural weight has a cascading effect on total weight as the aircraft is resized. The wing and empennage areas are reduced, and the engines are smaller. Engine weight and performance are those of the JT8D-17 scaled linearly to the required size. The external geometry of the fuselage does not change due to the requirements of cargo space.

The total operator's weight empty reduction obtained by completely resizing the aircraft is 3390 lbs. The description of the resized aircraft is given in Table CXV.

The reduced wing area cuts the ferry range some 30 nautical miles due to less fuel volume available in the resized wing.

11.1.3 Resized Aircraft with Fixed Engine Thrust

The fixed engine thrust configuration was sized to minimize weight by reducing wing and empennage areas. This allows a greater wing and horizontal tail area reduction relative to the completely resized aircraft. However, the vertical tail area is larger due to the requirements imposed by the fixed engines. The fuselage external geometry was not changed.

The total operator's weight empty saved by using the baseline engine is 3150 lbs. The ferry range is reduced some 83 nautical miles (53 less than the completely resized aircraft) due to the smaller wing. The description of the partially resized aircraft is found in Table CXV.

TABLE CXIV UNRESIZED AIRCRAFT PERFORMANCE IMPROVEMENT OPTIONS				
OPTION	MID-POINT GROSS WEIGHT (LBS)	PAYLOAD CAPABILITY (LBS)	RADIUS CAPABILITY (N.MI.)	FIELD LENGTH MID-POINT (SL 103°F)
BASELINE	150,000	27,000	400	2,000
1	150,000	28,850	400	2,000
2	150,000	27,000	458	2,000
3	147,990	27,000	400	1,958

TABLE CXV RESIZED AIRCRAFT PERFORMANCE DATA			
AIRCRAFT DESCRIPTION	BASELINE AIRCRAFT	COMPLETELY RESIZED AIRCRAFT	PARTIALLY RESIZED (FIXED ENGINE SIZE)
PAYLOAD (LB)	27,000	27,000	27,000
RADIUS (N.MI.)	400	400	400
FIELD LENGTH, SL (103°F)(FT)	2,000	2,000	2,000
WING AREA (FT^2)	1,740	1,697	1,671
HORIZONTAL TAIL AREA (FT^2)	643	632	626
VERTICAL TAIL AREA (FT^2)	462	454	457
THRUST/ENG., SL (103°)(LB)	14,900	14,532	14,900
OPERATORS EMPTY WEIGHT (LB)	103,240	99,850	100,090
MID-POINT WEIGHT (LB)	150,000	146,310	146,570
FERRY RANGE (N.MI.)	2,420	2,390	2,337

SECTION XII

CONCLUSIONS AND RECOMMENDATIONS

The study requirement to devise, evaluate, and select new structural concepts and to identify the resulting effects on aircraft performance and life cycle costs provides a basis for conclusions and recommendations of possible interest and value for future planning and studies.

12.1 STUDY APPROACH

The study approach (see Figure 1), identifying structural integrity requirements, material properties, geometry efficiencies, cost rates, and manufacturing capabilities as the primary elements influencing concept definition, is supported by the study experience.

The study approach for concept selection, based on acquisition and life cycle cost, directly reflects the study goals of reduced structural weight and cost (see Section VI). The resulting criteria parameters are simple and objective and therefore of significant value in concept screening and selection as demonstrated in Section 6.2.

A simple "design-for-weight" preliminary design method is required to quantitatively integrate structural integrity requirements, material capabilities, geometry capabilities, and weight. An initial development and implementation of such a method was accomplished in the study (see Section 6.2). The method is a formal representation of the concept selection process in a simple chart format and provides visibility, traceability and most important, a quantitative relation between weight and the design parameters influencing weight. Therefore, the engineers' capability to identify the constraining problems and the required lower weight concept solutions is greatly enhanced.

The method also defines the weight parameter values required to implement the concept selection criteria. Additional refinement of, and experience with the procedure, are recommended. Currently recognized areas for further consideration include (1) further definition and incorporation of "geometry selection" parameters analogous to the already incorporated material selection parameters, (2) further definition and generalization of the charting rules for complex material and geometry conditions, (3) trial use of the material selection parameter for "walk-around" damage tolerance and (4) improvement of the material selection parameter for "depot level" damage tolerance.

A simple "design-for-cost" preliminary design method is also required to directly support the engineer in the concept definition process. The method would also define the cost parameter values required to implement the concept selection criteria. As currently envisioned, the method would provide cost buildup information from a chart format type manual. The primary material, fabrication, and assembly cost elements for a range of material, geometry, and joining options would be included. Where possible, existing study and experience cost data would also be included for calibration and comparative purposes.

12.2 MATERIALS

The most promising new metallic materials for use in future aircraft structures appear to be the aluminum alloys x7475 and x7050 for their combination of high tensile and ultimate strengths, damage tolerance capability, and low cost. The higher specific strength capabilities of titanium and beryllium are offset by their higher costs.

Additional crack propagation rate and fracture toughness data are required to supplement the data currently available in the Damage Tolerant Design Handbook (Reference 11). The smaller initial flaw sizes appearing in current damage tolerance criteria versions subsequent to Revision D require da/dn data extension into the 10^{-8} inches/cycle range. To support improved damage tolerance analyses of the future, the effects of temperature, cyclic rate, chemical environment, and spectra, as influencing crack tip plasticity and crack retardation, are also required.

Fatigue, damage tolerance, and ultimate strength data are required for new structural joining concepts such as padded hole, external clamping, weld bond, etc. Further evaluation of existing structural joining concepts incorporating increased attachment interference or hole cold working or both is also required. Fatigue and damage tolerance data are also required for basic "isogrid" panel structure.

A standardized approach to define estimated "B" value data from available typical data is required for strength and damage tolerance design properties. For this study, an approach for estimating "B" value strength data was used (see Appendix B). Since a fatigue type "scatter factor" approach (wherein the service life is increased by a factor to account for basic data variability) is not used for damage tolerance, an alternate "B" value approach is required for da/dn and K_c data also. This standard approach should then be applied to the basic data of Reference 11 to define "B" value capability and thereby preclude each user from duplicating the work. By standardizing the method and data, the variability in damage tolerance analysis results between users that may be introduced by differing data interpretations would be eliminated.

Methods for correlating existing data provide a means for estimating values under new parametric conditions as well as reducing the amount of additional test data required. This is both useful and economic, therefore data correlation approaches should be pursued. The approach for correlating fatigue data under various notch, specimen geometry, and material conditions that was used in the study is presented in Appendix B. Correlation approaches may also be possible for crack propagation and fracture data. These could include generation of full range da/dn curves with "R" ratio and K_c variation (an extension of Forman's work) and with further provision for temperature and chemical environment variation effects.

12.3 CRITERIA

The study premise that the relative and absolute severity of requirements for the individual failure modes strongly influences concept selection, weight, and cost is supported by the study experience (Section 6.2). Hence, all known and representable failure modes, including rigidity for flutter, should be included in studies of this nature to increase the pertinency of the concept selections and quantitativeness of the resulting value estimates. Realistic criteria based on calibration to existing experience and data are necessary to properly establish the "relative" and "absolute" severity levels. Hence, work in the "criteria" area may offer as significant a potential for weight and cost saving as that in the "new concepts" area.

Damage tolerance criteria are currently in an evolutionary phase. The study experience has indicated, for example, that differences in proposed initial flaw requirements between Revision D and tentative March 1974 criteria can result in significant capability differences (Section 6.2).

For example, use of the March 1974 criteria initial flaw size associated with "attachment interference benefit" can result in an otherwise damage tolerance critical area becoming very non-critical, thus influencing material, geometry and design stress level selection and resulting weight and possibly cost in a favorable manner. Selection of this initial flaw size should be based on a realistic "B" value approach (if not already so based) which reflects an acceptable probability that a minimum or greater "favorable benefit" level exists.

Under constant (Revision D) criteria and wing lower panel structure conditions, significantly higher damage tolerance capabilities are demonstrated for "walk around" relative to "depot" inspectability (Table XLI). Presuming a realistic relative criteria, "walk around" visual inspection provides a higher NDI efficiency level than depot level with larger crack size and higher frequency apparently being the favorable factors. The practicality and cost of applying the "walk around" approach to other critical components should be considered, perhaps in the form of much more frequent special visual inspections. A large percentage of the damage tolerance required safe period for depot inspection is generated at relatively small crack sizes which would require sophisticated NDI techniques to be applied over large surface areas for adequate detection. A realistic assessment of depot level detection capability (if not already reflected in the criteria) is also required.

12.4 ANALYSES

A computer code for growing multiple symmetric or asymmetric cracks from a hole through several elements with full spectra and accounting for variable interacting material, geometry, and crack size conditions is required. The inclusion and correlation to test data of a crack retardation model is also required. The parametric development and normalization of stress intensity correction factor data reflecting panel geometry effects (such as stiffener size, spacing and attachment rigidity, crack size, crack symmetry/asymmetry, etc.) as well as damage tolerance capability variation with the above type geometry variation is also recommended to identify favorable geometry factors.

12.5 DESIGN CONCEPTS

The wing cover panel studies (Section 6.2.1, 6.2.2) indicate that material and geometry options exist to substantially increase wing design stress levels above baseline levels, primarily through more efficient fatigue and compression geometry options. The fatigue options could include hole cold working or greater attachment interference or both, among other options; however all require further evaluation.

The integrally stiffened wing cover skins, with rib and bulkhead caps machined in, reduces the number of small detail parts required to assemble a wing box. The integral spar concept, machined from a forged billet, has less parts and saves structural weight. Similarly, the one-piece ribs and bulkheads offer the same advantages. The integral concepts are feasible due to the better properties of the emerging aluminum alloys. The fatigue life and damage tolerance criteria was met for the life of the airframe. The selection of this type of box structure will have an impact on the machining and forging capabilities of industry. There is a point where large machined components could become more expensive than built up structure due to the raw material costs.

The load intensities of both the horizontal and vertical stabilizer structural boxes were so low that a stiffened skin concept was not an efficient arrangement. The bonded aluminum honeycomb skin panels, including all spar caps, rib and bulkhead caps, proved to have merit. Both weight and cost savings were realized. Honeycomb panels and integrally machined spar and bulkhead webs eliminated many parts. The critical design condition for the vertical stabilizer was flutter, requiring stiffness in chordwise bending. The use of boron-epoxy inserts in the spar caps to obtain the stiffness reduced the weight by 150 pounds. Development testing of composite reinforced components must be done to insure structural compatibility for the life of the airframe.

The fuselage shell studies (Section 6.2.3) indicate that substantial portions of the baseline shell are at or near minimum skin gage as established by attachment countersink requirements. Elimination of countersink requirements by bonding (honeycomb concept studied) permitted reduction of the minimum gage and weight saving in the basic panel; however a substantial portion of the basic panel weight saving was negated by the panel edge weight penalty. The panel sizes, as developed in this study, were predicated on existing bonding facilities. These panels may be made much larger, thereby eliminating a portion of the weight penalty associated with the edge member splices. The design, a tension bolt attachment, was coordinated with manufacturing, and is considered as the most efficient manner of assembly for a honeycomb sandwich panel fuselage shell. The portion of the fuselage, extending the length of the cargo floor, was covered in the concept study. Similar weight and cost factors may be feasible for the aft section.

Consideration of a single face skin concept without a countersink constraint on the minimum gage (integral machined isogrid studied) permitted minimum skin gage reduction to honeycomb two-skin levels but no weight saving due to the minimum gage skin, rib, node and edge weight penalties. Since a "machined down" single face skin approach is constrained in a weight penalizing way by minimum dimensions for machining, an alternate "built-up" single face approach without countersink constraint and incorporating efficient thin gage stability elements may offer weight saving potential in lightly loaded areas.

12.6 MANUFACTURING METHODS

The design concept selected for the wing covers, spars, and bulkheads, and for the empennage spar and bulkhead webs is integrally stiffened. The wing cover panels were assumed to be machined from plate stock by numerically controlled equipment. A considerable savings in raw material and reduction in the amount of material removed would be realized if forging blanks of sufficient size could be obtained. Forging blanks of this size would require development of a sequenced forging operation utilizing overlapping segmented dies. Development problems could be reduced by design features which simplify the forging operation such as parallel stiffeners and standard stiffener and bulkhead spacing. The wing spars are machined from forging blanks produced by utilizing overlapping segmented forging dies. The bulkheads are integrally machined from forging blanks produced by current "state of the art" forging techniques.

The structural components of this study utilizing the honeycomb sandwich design concept were designed to be manufactured by existing equipment. The weight of panel edge treatment is a significant factor in the total weight of a honeycomb panel. This panel edge treatment weight could be reduced by increasing the size of the honeycomb panels. The increased panel sizes require larger autoclaves for bonding and curing of the panels and larger handling fixtures. The honeycomb sandwich design concept could be utilized for the aft segment of the fuselage from Station 982 to Station 1437 to further reduce weight and cost. The panels of the aft fuselage have a double curvature but require no special manufacturing techniques.

The use of large, integrally stiffened panels require special forming techniques. A favorable candidate for this operation is shot peen forming. Research and development in the shot peen forming of panels to simple and compound contours support peening techniques as being both economical and reliable. Further development is required to improve techniques and increase capability with emphasis on determining the degree and effect of stress distribution between peened and unpeened areas.

Conventional forming methods can be utilized for the horizontal and vertical stabilizer honeycomb sandwich panels and conventionally constructed fuselage components. Boron/epoxy reinforced aluminum extrusions were considered for extra stiffness in wing, floor, and vertical stabilizer assemblies. The high ratio of aluminum to boron in a typical extrusion cross-section complicates the machining of the extrusion but this problem can be handled by present in-house machining techniques using special metal matrix wheels at high surface speeds. Three methods of reinforcing aluminum extrusions were considered: 1) the application of boron-epoxy reinforcement to the upper cap of the stiffener, 2) the infiltration of the extrusion by boron fibers, and 3) the reinforcement of extrusions with boron/epoxy composite by pultrusion. The three methods of extrusion reinforcement require an effective chemical resistant adhesive system that cures at room temperature. Reinforcement of extrusions by pultrusion requires development of cost effective techniques and capabilities. The most promising reinforcement technique is the infiltration process where boron fibers are pulled through and cured inside a hole in the extrusion. The boron reinforcement is protected from the environment and warpage due to the mismatch of thermal coefficients of expansion between the aluminum extrusion and boron reinforcement is reduced. Development of methods to produce infiltrated reinforced extrusions between 50 and 60 feet in length with ability to reduce the amount of reinforcement area along the length of the extrusion is required.

The large size of the structural components of the advanced concepts reduces the number of mechanical attachments required in the advanced STOL transport. Several types of attachments that offer advantages over conventional types were considered and studies underway to determine the relative cost efficiency of these fastener systems. Improved coatings and lubricants for interference fit attachments can be used to expand the use of straight shank fasteners in areas of greater than 4D material thickness.

In honeycomb sandwich panels where attachments are installed, conventional techniques can be used to prevent the core from crushing and to transfer the load into the panel.

Adhesive bonding is another joining technique that can be used extensively in the advanced STOL transport. The honeycomb sandwich panels of the horizontal and vertical stabilizers use conventional adhesive systems. Adhesives can be used to bond the boron reinforcement to the stringers of the wing, to the vertical stabilizer spar caps, and to the cargo floor panels. Cold setting adhesives that are corrosion resistant are required for this operation, and several candidates should be evaluated to determine their efficiency. Development of a suitable adhesive system may be required.

APPENDIX A

USAF DAMAGE TOLERANCE CRITERIA
(REVISION D - 18 AUGUST 1972)

1.0 DEFINITIONS AND GENERAL REQUIREMENTS

1.1 DEFINITIONS

1.1.1 Degree of Inspectability

The degree of inspectability of each element of safety of flight structure shall be established in accordance with the following definitions.

1.1.1.1 In-Flight Evident Inspectable - Structure is in-flight evident inspectable if the nature and extent of damage occurring in flight will result directly in characteristics which make the flight crew immediately and unmistakably aware that significant damage has occurred and that the mission should not be continued.

1.1.1.2 Ground Evident Inspectable - Structure is ground evident inspectable if the nature and extent of damage being considered will be readily and unmistakably obvious to ground personnel without specifically inspecting the structure for damage.

1.1.1.3 Walkaround Inspectable - Structure is walkaround inspectable if the nature and extent of damage being considered is unlikely to be overlooked by personnel conducting a visual inspection of the structure. This inspection normally shall be a visual look at the exterior of the structure from ground level without removal of access panels or doors and without special inspection aids.

1.1.1.4 Special Visual Inspectable - Structure is special visual inspectable if the nature and extent of damage being considered is unlikely to be overlooked by personnel conducting a detailed visual inspection of the aircraft for the purpose of finding damaged structure. The procedure may include removal of access panels and doors, and may permit simple visual aids such as mirrors and magnifying glasses. Removal of paint, sealant, etc. and use of NDI techniques such as penetrant, x-ray, etc. are not part of a special visual inspection.

1.1.1.5 Depot or Base Level Inspectable - Structure is depot or base level inspectable if the nature and extent of damage being considered will be detected with a 90% probability at 95% confidence level for slow crack growth structure and with 90% probability at 50% confidence level for fail safe structure. The inspection procedures may include NDI techniques such as penetrant, x-ray, ultrasonic, etc. Accessibility considerations may include removal of those components designed for removal.

1.1.1.6 In-Service Non-Inspectable Structure - Structure is in-service non-inspectable if either damage size or accessibility preclude detection during one or more of the above inspections.

1.1.2 Frequency of Inspection

Frequency of inspection is the number of times that a particular type of inspection is to be conducted during the service life of the aircraft.

1.1.3 Minimum Period of Unrepaired Service Usage

Minimum period of unrepaired service usage is that period of time during which the appropriate level of damage (assumed initial or in-service) is presumed to remain unrepaired and allowed to grow within the structure.

1.1.4 Minimum Required Residual Strength (P_{XX})

The minimum required residual strength shall be as specified in Paragraph 1.2.2.

1.1.5 Minimum Assumed Initial Damage Size

The minimum assumed initial damage size is the smallest crack-like defect which shall be used as a starting point for analyzing residual strength and crack growth characteristics of the structure.

1.1.6 Minimum Assumed In-Service Damage Size

The minimum assumed in-service damage size is the smallest damage which shall be assumed to exist in the structure after completion of an in-service inspection.

1.1.7 Damage Growth Limit

Damage growth limit is the maximum amount of damage growth allowed within a specified interval so as not to degrade the residual strength below a specified minimum level.

1.1.8 Slow Crack Growth Structure

Slow crack growth structure consists of those design concepts where flaws or defects are not allowed to attain the critical size required for unstable rapid propagation.

1.1.9 Crack Arrest Fail Safe Structure

This is structure which is designed and fabricated such that unstable rapid propagation will be stopped within a continuous area of the structure prior to complete failure and the strength and safety of the remaining undamaged structure will not be degraded below a specified level for a specified period of unrepaired service usage.

1.1.10 Multiple Load Path-Fail Safe Structure

This is structure which is designed and fabricated in segments (with each segment consisting of one or more individual elements) such that failure of any single segment (i.e. load path) will not degrade the strength and safety below a specified level for a specified period of unrepaired service usage.

1.1.10.1 Multiple Load Path-Dependent Structure - Multiple load path structure is classified as dependent if, by design, a common source of cracking exists in adjacent load paths at one location due to the nature of the assembly or manufacturing procedures. An example of multiple load path-dependent structure is planked tension skin where individual members are spliced in the spanwise direction by common fasteners with common drilling and assembly operations.

1.1.10.2 Multiple Load Path-Independent Structure - Multiple load path structure is classified as independent if by design, it is unlikely that a common source of cracking exists in more than a single load path at one location due to the nature of assembly or manufacturing procedures.

1.2 GENERAL REQUIREMENTS

1.2.1 Analysis Requirements

It shall be a requirement to classify all safety of flight structure with regard to type of damage tolerance approach and degree of inspectability and perform the required analytical work necessary to demonstrate compliance with specific requirements in this specification. The analysis shall assume the presence of crack-like defects, placed in the most unfavorable orientation with respect to the applied stress and the material properties, and shall predict the growth behavior in the chemical, thermal, and sustained and cyclic stress environment to which that portion of the component shall be subjected. In addition, the interaction effects of variable loading shall be considered. Regardless of the damage tolerance concept, single initial flaws of the specified size shall be assumed to exist in each separate element of the structure. For structural elements where it is likely due to the fabrication and assembly operations that the flaws in two or more elements exist at the same location in the structure this shall be assumed.

1.2.2 Residual Strength Requirements

The minimum required residual strength is the minimum load which must be sustained by the aircraft with damage present without endangering safety of flight or degrading the performance of the aircraft for the specified minimum period of unrepaired service usage. This includes loss of strength, loss of stiffness, excessive permanent deformation, loss of control, or by reduction of the flutter speed below V_L. The minimum residual strength requirements are specified in Sections 2.0 through 4.0 in terms of the minimum load P_{XX} that the structure must be able to sustain at any time during the specified minimum period of unrepaired service usage with the specified damage present. The magnitude of P_{XX} varies with the overall degree of inspectability of the structure (e.g. P_{FE} applies to flight evident, P_{SV} applies to

1.2.2 Continued
special visual inspectable, etc). The P_{XX} load shall be determined from average load exceedance data and shall be that load that could occur once in 100 times the applicable inspection interval (e.g. P_{DM} is the load that could occur once in 100 depot or base level inspection intervals). For fail safe structure there is a requirement to sustain a minimum load, P_{YY}, at the instant of load path failure (or crack arrest) in addition to being able to sustain the load, P_{XX}, subsequent to load path failure (or crack arrest) at any time during the specified interval. The single load path failure (or crack arrest) load, P_{YY}, shall include a dynamic factor (D.F.). In lieu of test or analytical data to the contrary a dynamic factor of 1.15 shall be used. The magnitude of P_{YY} shall depend upon the overall inspectability and the specific inspectability of the intact structure for subcritical damage (i.e. damage less than failed load paths or arrested cracks). P_{YY} shall be determined per Table CXVI.

1.2.3 Test Requirements

1.2.3.1 Specimen Testing - Valid data shall be determined in accordance with the procedures set forth in the 1970 ASTM Standards Test Method E3999-70T, or as described in AFFDL-TR-69-111 or by alternate methods approved by the procuring agency. The materials from which the structure identified in Paragraph 1.2.1 are to be fabricated shall be controlled by a system of procedures and/or specifications which are sufficient to preclude the utilization in fracture critical areas of materials possessing K_{IC} (or K_C) values inferior to those assumed in design. Tests will be conducted on all billets, forgings, extrusions, plates, or other forms (from which final parts are to be finished) to evaluate the fracture toughness. A slice will be cut from these items, or integral projections thereof, at receiving inspections, so that specimens from each slice may be tested. These specimens shall have been heat treated with the same material from which they were cut. When sufficient data are available, sampling procedures may be instituted on approval of the Air Force.

1.2.3.2 Component Testing - Fail safe tests will be conducted on that structure which is considered to be fail safe to verify that the failure of a load path or rapid propagation of a crack will not result in loss of the entire structure. Tests will be performed during the preproduction design verification component test program and the full scale qualification test program. These tests will be conducted by pre-cracking a particular member to the critical crack length and applying the load P_{YY}. Tests will be conducted on selected critical structure, particularly slow crack growth components, to verify the analytical crack propagation rates. Initial flaws of the specified size will be initiated at the critical point(s) and propagation rates measured. These tests will be performed during the preproduction design verification test program and during the full scale qualification test program. Wherever possible, the structural components used for static test and fatigue test will be used to perform these tests. If in certain cases, this is not possible, then additional components will be fabricated for testing.

TABLE CXVI SINGLE LOAD PATH FAILURE LOAD		
OVERALL DEGREE OF INSPECTABILITY	INSPECTABILITY FOR MIN. ASSUMED IN-SERVICE SUB-CRITICAL DAMAGE SIZES	P_{YY}
In-Flight Evident	Walkaround Visual	D.F. X P_{WV}
	Special Visual	D.F. X P_{SV}
	Depot or Base Level	D.F. X P_{DM}
	Non-Inspectable	D.F. X P_{LT}
Ground Evident	Walkaround Visual	D.F. X P_{WV}
	Special Visual	D.F. X P_{SV}
	Depot or Base Level	D.F. X P_{DM}
	Non-Inspectable	D.F. X P_{LT}
Walkaround Visual	Walkaround Visual	D.F. X P_{WV}
	Special Visual	D.F. X P_{SV}
	Depot or Base Level	D.F. X P_{DM}
	Non-Inspectable	D.F. X P_{LT}
Special Visual	Special Visual	D.F. X P_{SV}
	Depot or Base Level	D.F. X P_{DM}
	Non-Inspectable	D.F. X P_{LT}
Depot or Base Level	Depot or Base Level	D.F. X P_{DM}
	Non-Inspectable	D.F. X P_{LT}
Non-Inspectable	Non-Inspectable	D.F. X P_{LT}

1.2.4 Fracture Control Plan

General guidelines for the fracture control plan are provided in 5.1.3 of MIL-STD-XXX.

2.0 SLOW CRACK GROWTH STRUCTURE

2.1 WALKAROUND INSPECTABLE

2.1.1 Frequency of Inspection

The frequency of inspection and inspection interval shall be specified in the system RFP, Prime Item Development Specification or other contract document as applicable (Table CXVII).

2.1.2 Minimum Period of Unrepaired Service Usage

The minimum period of unrepaired service usage shall be five (5) times the inspection interval specified in Paragraph 2.1.1.

2.1.3 Minimum Required Residual Strength

The minimum required residual strength shall be P_{WV}.

2.1.4 Minimum Assumed Initial Damage

The damage assumed to exist in new structure as a result of fabrication operations shall be an .050" long through the thickness crack emanating from one side of a hole. At locations other than holes the assumed initial damage size shall be $(a/Q) = .100$ where a is measured in the principal direction of crack growth and Q is the flaw shape parameter. A smaller initial flaw size may be assumed subsequent to a demonstration that all flaws larger than this assumed size have at least a 90% probability of detection with a 95% confidence using the selected production inspection procedure, equipment and personnel. This demonstration shall be subject to USAF approval. A smaller initial size may be assumed if proof test inspection is used. In this case the minimum assumed initial size shall be the calculated critical size at the proof test stress levels and temperature using the upper bound of the material K_{1C} data.

2.1.5 Minimum Assumed In-Service Damage Size

The smallest damage which can be presumed to exist in fuel tank structure after completion of a walkaround inspection shall be an uncovered open 2" through the thickness crack. A smaller through the thickness crack may be assumed only after it is shown (analytically or experimentally) that fuel leakage will occur and can be detected during the inspection. Other slow crack growth structure shall be assumed to be walkaround uninspectable.

2.1.6 Damage Growth Limits

2.1.6.1 Fabrication Damage - Initial damage as specified in Paragraph 2.1.4 shall not grow to critical size and cause failure of the structure due to the application of P_{DM} in the minimum period of unrepaired service usage specified in Paragraph 2.3.2.

TABLE CXVII SLOW CRACK GROWTH STRUCTURE

DEGREE OF INSPECTABILITY	FREQUENCY OF INSPECTION	MIN. PERIOD OF UNREPAIRED SERVICE USAGE (F_{XX})	MIN. REQ'D RESIDUAL STRENGTH (P_{XX})	MIN. ASSUMED INITIAL DAMAGE SIZES (a)	MIN. ASSUMED IN-SERVICE DAMAGE SIZES (1)	DAMAGE GROWTH LIMITS
IN FLIGHT EVIDENT	←		N/A			→
GROUND EVIDENT	←		N/A			→
WALK AROUND VISUAL	SPECIFIED IN CONTRACT DOCUMENTS (10 FLTS. TYPICAL)	5 X FREQ (F_{WV})	P_{WV}	a/Q = 0.10 OR 0.05" 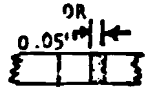 OR SMALLER IF DEMONSTRATED	2" Open Thru Crack Unless Detection Of Smaller Size Demonstrated	1 Shall not grow to critical @ P_{WV} in F_{WV} a Shall not grow to critical @ P_{DM} in F_{DM}
SPECIAL VISUAL	SPECIFIED IN CONTRACT DOCUMENTS (1 YR. TYP)	2 X FREQ (F_{SV})	P_{SV}			1 Shall not grow to critical @ P_{SV} in F_{SV} a Shall not grow to critical @ P_{DM} in F_{DM}
DEPOT OR BASE LEVEL	SPECIFIED IN CONTRACT DOCUMENTS (1/4 LIFE-TIME TYP.)	2 X FREQ (F_{DM})	P_{DM}		(a/Q)DM	1 Shall not grow to critical @ P_{DM} in F_{DM} a Shall not grow to critical @ P_{DM} in F_{DM}
NON INSPECTABLE	N/A	2 LIFETIMES (F_{LT})	P_{LT}		N/A	a Shall not grow to critical @ P_{LT} in F_{LT}

2.1.6.2 In-Service Damage - In-service damage size specified in Paragraph 2.1.5 shall not grow to critical size and cause failure of the structure due to the application of P_{WV} in the minimum period of unrepaired service usage specified in Paragraph 2.1.2.

2.2 SPECIAL VISUAL INSPECTABLE

2.2.1 Frequency of Inspection

The frequency of inspection and inspection intervals shall be specified in the system RFP, PIDS or other contract documents as applicable.

2.2.2 Minimum Period of Unrepaired Service Usage

The minimum period of unrepaired service usage shall be two (2) times the inspection interval specified in Paragraph 2.2.1.

2.2.3 Minimum Required Residual Strength

The minimum required residual strength shall be P_{SV}.

2.2.4 Minimum Assumed Initial Damage

The minimum assumed initial damage shall be as specified in Paragraph 2.1.4.

2.2.5 Minimum Assumed In-Service Damage Size

The smallest damage which can be presumed to exist in the structure after completion of special visual inspection shall be an uncovered open 2" through the thickness crack. A smaller through the thickness crack may be assumed only in those special cases where inspection statistics on similar structure or unique design features clearly indicate that smaller cracks can and will be found.

2.2.6 Damage Growth Limits

2.2.6.1 Fabrication Damage - Paragraph 2.1.5.1 applies.

2.2.6.2 In-Service Damage - In-service damage size specified in Paragraph 2.2.5 shall not grow to critical size and cause failure of the structure due to the application of P_{SV} in the minimum period of unrepaired service usage specified in Paragraph 2.2.2.

2.3 DEPOT OR BASE LEVEL INSPECTABLE

2.3.1 Frequency of Inspection

The frequency of inspection and inspection intervals shall be specified in the system RFP, PIDS or other contract documents as applicable.

2.3.2 Minimum Period of Unrepaired Service Usage

The minimum period of unrepaired service usage shall be two (2) times the inspection interval specified in Paragraph 2.3.1.

2.3.3 Minimum Required Residual Strength

The minimum required residual strength shall be P_{DM}.

2.3.4 Minimum Assumed Initial Damage

The minimum assumed initial damage shall be as specified in Paragraph 2.1.4.

2.3.5 The Minimum Assumed In-Service Damage Size

The smallest damage which can be presumed to exist in the structure after completion of a depot or base level inspection shall be as follows:

2.3.5.1 If the component is to be removed from the aircraft and completely inspected with NDI procedures equivalent to those performed during fabrication, the minimum assumed damage size shall be that specified in 2.1.4.

2.3.5.2 Where NDI techniques such as penetrant, magnetic particle or ultrasonics are applied to a component installed in the aircraft, the minimum assumed size shall be a through the thickness crack emanating from a fastener hole, having 0.250" of uncovered length. At other locations, the minimum assumed damage size shall be a/Q = 0.20".

2.3.5.3 Where visual inspection is used, a 2" uncovered open through the thickness crack shall be the minimum size.

2.3.5.4 Smaller flaw sizes may be assumed under Paragraphs 2.3.5.2 and 2.3.5.3 subsequent to a demonstration that all flaws larger than the selected size have at least a 90% probability of detection with a 95% confidence using the specified in-service inspection procedures and equipment. This demonstration shall be subject to USAF approval.

2.3.5.5 Smaller flaw sizes may be assumed under 2.3.5.2 and 2.3.5.3 if depot or base level proof test inspection is used. In this case the minimum assumed sizes shall be calculated critical sizes at the proof test stress levels and temperatures using the upper bound of the material K_{1C} data.

2.3.6 Damage Growth Limits

2.3.6.1 Fabrication Damage - Paragraph 2.1.6.1 applies.

2.3.6.2 In-Service Damage - In-service damage size specified in Paragraph 2.3.5 shall not grow to critical size and cause failure of the structure due to the application of P_{DM} in the minimum period of unrepaired service usage specified in Paragraph 2.3.2.

2.4 NON-INSPECTABLE

2.4.1 Frequency of Inspection

The frequency of inspection is not applicable.

2.4.2 Minimum Period of Unrepaired Service Usage

The minimum period of unrepaired service usage shall be two (2) design lifetimes.

2.4.3 Minimum Required Residual Strength

The minimum required residual strength shall be P_{LT}.

2.4.4 Minimum Assumed Initial Damage

The minimum assumed initial damage shall be as specified in Paragraph 2.1.4.

2.4.5 Minimum Assumed In-Service Damage Size

The minimum assumed in-service damage size is not applicable.

2.4.6 Damage Growth Limits

The initial damage as specified in Paragraph 2.1.4 shall not grow to critical size and cause failure of the structure due to the application of P_{LT} in the minimum period of unrepaired service usage as specified in Paragraph 2.4.2.

3.0 FAIL SAFE - MULTIPLE LOAD PATH (MLP) STRUCTURE

3.1 IN-FLIGHT EVIDENT

3.1.1 Frequency of Inspection

Not applicable.

3.1.2 Minimum Period of Unrepaired Service Usage

The minimum period of unrepaired service usage shall be that period of time between that when the damage becomes evident and the completion of an immediate return to base (Table CXVIII).

3.1.3 Minimum Required Residual Strength

The minimum required residual strength shall be P_{FE} subsequent to load path failure and P_{YY} at time of load path failure.

3.1.4 Minimum Assumed Initial Damage

3.1.4.1 Intact New Structure - The damage assumed to exist in each load path of new structure as a result of fabrication operations shall be an .020" long through the thickness crack emanating from one side of a hole. At locations other than holes the assumed initial damage sizes shall be (a/Q) = .030" where a is measured in the principal direction of crack growth and Q is the flaw shape parameter. A smaller initial flaw size may be assumed subsequent to a demonstration that all flaws larger than this assumed size have at least a 90% probability of detection with a 50% confidence level using the selected production inspection procedure, equipment, and personnel. This demonstration shall be subject to USAF approval.

3.1.4.2 Remaining Structure at Time of and Subsequent to Load Path Failure - The damage assumed to exist adjacent to the primary failure in the remaining MLP dependent structure at time of and following the failure of a load path shall be equal to an .020" long through the thickness crack emanating from one side of a hole or damage level equal to (a/Q) = .030" at locations other than holes, plus the amount of growth Δa which occurs prior to load path failure. The damage assumed to exist adjacent to the primary failure in each load path of the remaining MLP independent structure at time of and following the failure of a load path shall be equal to an .010" radius semicircular corner crack emanating from one side of a hole or damage equal to (a/Q) = 0.010" at locations other than holes, plus the amount of growth Δa which occurs prior to load path failure.

3.1.5 Minimum Assumed In-Service Damage Size

The minimum assumed in-service damage size shall be a failed load path.

3.1.6 Damage Growth Limits

TABLE CXVIII FAIL SAFE - MULTIPLE LOAD PATH STRUCTURE

DEGREE OF INSPECTABILITY	FREQUENCY OF INSPECTION	MIN PERIOD OF UNREPAIRED SERVICE USAGE (F_{XX})	MIN REQ'D RESIDUAL STRENGTH (P_{XX})	MIN ASSUMED INITIAL DAMAGE SIZE: INTACT NEW STRUCTURE (a_1)	MIN ASSUMED INITIAL DAMAGE SIZE: REMAINING STRUCTURE: DEPENDENT LOAD PATH (a_2)	MIN ASSUMED INITIAL DAMAGE SIZE: REMAINING STRUCTURE: INDEPENDENT LOAD PATH (a_3)	MIN ASSUMED IN-SERVICE DAMAGE SIZE	DAMAGE GROWTH LIMITS
IN FLIGHT EVIDENT	N/A	RETURN TO BASE (F_{FE})	P_{FE}	a/Q = .03 .02" or Smaller If Demonstrated	Failed Load Path Plus $a_1 + \Delta a$ in adjacent load paths or 2" crack Plus $a_1 + \Delta a$ in adjacent load paths	Failed load path plus a/Q = .01 or .01 + Δa in adjacent load paths or 2" crack plus a/Q = .01 or .01 + Δa in adjacent load paths	a_2 or a_3	a_1 Shall not grow to critical @ P_{DM} in F_{DM} a_2 or a_3 Shall not grow to critical @ P_{FE} in F_{FE}
GROUND EVIDENT	EVERY FLIGHT	ONE FLIGHT (F_{GE})	P_{GE}					a_1 Shall not grow to critical @ P_{DM} in F_{DM} a_2 or a_3 Shall not grow to critical @ P_{GE} in F_{GE}
WALK AROUND VISUAL	SPECIFIED IN CONTRACT DOCUMENTS (10 FLTS TYPICAL)	5 X FREQ (F_{WV})	P_{WV}					a_1 Shall not grow to critical @ P_{DM} in F_{DM} a_2 or a_3 Shall not grow to critical @ P_{WV} in F_{WV}
SPECIAL VISUAL	SPECIFIED IN CONTRACT DOCUMENTS (ONE YEAR TYPICAL)	2 X FREQ (F_{SV})	P_{SV}					a_1 Shall not grow to critical @ P_{DM} in F_{DM} a_2 or a_3 Shall not grow to critical @ P_{SV} in F_{SV}
DEPOT OR BASE LEVEL	SPECIFIED IN CONTRACT DOCUMENTS (1/4 LIFE-TIME TYPICAL)	2 X FREQ (F_{DM})	P_{DM}				(a/Q)DM as specified in 2.3.5	a_1 Shall not grow to critical @ P_{DM} in F_{DM} a_2 Or a_3 Shall not grow to critical @ P_{DM} in F_{DM} (a/Q)DM Shall not grow to critical @ P_{DM} in F_{DM}
NON INSPECTABLE	N/A	ONE LIFETIME (F_{LT})	P_{LT}				N/A	a_1 Shall not grow to critical @ P_{LT} in F_{LT} a_2 or a_3 Shall not grow to critical @ P_{LT} in F_{LT}

3.1.6.1 Intact New Structure - Initial damage as specified in Paragraph 3.1.4.1 shall not grow to critical size and cause failure of a load path due to the application of P_{DM} in the minimum period of unrepaired service usage specified in Paragraph 3.5.2. If the structure is not inspectable for sub-critical cracks, the initial damage specified in Paragraph 3.1.4.1 shall not grow to critical size and cause failure of a load path due to the application of P_{LT} in one lifetime.

3.1.6.2 In Remaining Structure Subsequent to Load Path Failure - Damage as specified in Paragraph 3.1.4.2 shall not grow to critical size and cause failure of the remaining structure due to the application of P_{FE} in the minimum period of unrepaired service usage specified in Paragraph 3.1.2.

3.2 GROUND EVIDENT

3.2.1 Frequency of Inspection

The frequency of inspection shall be once per flight.

3.2.2 Minimum Period of Unrepaired Service Usage

The minimum period of unrepaired service usage shall be one (1) complete flight.

3.2.3 Minimum Residual Strength

The minimum residual strength shall be P_{GE} subsequent to load path failure and P_{YY} at time of load path failure.

3.2.4 Minimum Assumed Initial Damage

3.2.4.1 Damage In Intact New Structure - The damage in intact new structure shall be as specified in Paragraph 3.1.4.1.

3.2.4.2 Damage In Remaining Structure - The damage in remaining structure at time of and subsequent to load path failure shall be as specified in Paragraph 3.1.4.2.

3.2.5 Minimum Assumed In-Service Damage Size

The minimum assumed in-service damage size shall be a failed load path.

3.2.6 Damage Growth Limits

3.2.6.1 Intact New Structure - Paragraph 3.1.6.1 applies.

3.2.6.2 In Remaining Structure Subsequent to Load Path Failure - Damage as specified in Paragraph 3.1.4.2 shall not grow to critical size and cause failure of the remaining structure due to the application of P_{GE} in the minimum period of unrepaired service usage specified in Paragraph 3.2.2.

3.3 WALKAROUND VISUAL INSPECTABLE

3.3.1 Frequency of Inspection

The frequency of inspection and inspection interval shall be specified in the system RFP, PIDS or other contract document as applicable.

3.3.2 Minimum Period of Unrepaired Service Usage

The minimum period of unrepaired service usage shall be five (5) times the walkaround inspection interval specified in Paragraph 3.3.1.

3.3.3 Minimum Residual Strength

The minimum residual strength shall be P_{WV} subsequent to in-service inspection, and P_{YY} at time of load path failure.

3.3.4 Minimum Assumed Initial Damage

3.3.4.1 Damage In Intact New Structure

The damage in intact new structure shall be as specified in Paragraph 3.1.4.1.

3.3.4.2 Remaining Structure Subsequent to Load Path Failure and Intact Structure Subsequent to In-Service Inspection - The damage assumed to exist adjacent to the primary failure in the remaining MLP dependent structure at time of and following the failure of a load path (or significant damage to the load path) shall be equal to an .020" long through the thickness crack emanating from one side of a hole or damage equal to a/Q = .030" at locations other than holes, plus the amount of growth Δa which occurs prior to load path failure or prior to in-service inspection. The damage assumed to exist adjacent to the primary failure in each load path of the remaining MLP independent structure at time of and following failure of a load path (or significant damage to the load path) shall be equal to an .010" radius semi-circular corner crack emanating from one side of a hole or damage equal to a/Q = 0.010" at locations other than holes, plus the amount of growth Δa which occurs prior to a load path failure or prior to in-service inspection.

3.3.5 Minimum Assumed In-Service Damage

The minimum assumed in-service damage shall be as specified in Paragraph 2.1.5 or a failed member, whichever is applicable.

3.3.6 Damage Growth Limits

3.3.6.1 Intact New Structure - Paragraph 3.1.6.1 applies.

3.3.6.2 Intact Structure - Subsequent to In-Service Inspection - If the detectable damage is less than a failed load path then the minimum assumed damage in one load path shall be as specified in Paragraph 2.1.5. This damage plus the damage assumed to exist in the remaining structure at the time of inspection as defined in Paragraph 3.3.4.2, shall not grow to critical size and cause failure of the structure due to the application of P_{WV} in the minimum period of unrepaired service usage specified in Paragraph 3.3.2.

3.3.6.3 Remaining Structure - Subsequent to Load Path Failure - If the in-service detectable damage size is a failed load path then the damage in the remaining structure as defined in Paragraph 3.3.4.2 shall not grow to critical size and cause failure of the remaining structure due to the application of P_{WV} in the minimum period of unrepaired service usage specified in Paragraph 3.3.2.

3.4 SPECIAL VISUAL INSPECTABLE

3.4.1 Frequency of Inspection

The frequency of inspection and inspection intervals shall be specified in the systems RFP, PIDS or other contract document as applicable.

3.4.2 Minimum Period of Unrepaired Service Usage

The minimum period of unrepaired service usage shall be two (2) times the special visual inspection interval specified in Paragraph 3.4.1.

3.4.3 Minimum Required Residual Strength

The minimum required residual strength shall be P_{SV} subsequent to in-service inspection, and P_{YY} at time of load path failure.

3.4.4 Minimum Assumed Initial Damage

The minimum assumed initial damage shall be as specified in Paragraph 3.3.4.

3.4.5 Minimum Assumed In-Service Damage

The minimum assumed in-service damage shall be as specified in Paragraph 2.2.5 or a failed member, whichever is applicable.

3.4.6 Damage Growth Limits

3.4.6.1 Intact New Structure - Paragraph 3.1.6.1 applies.

3.4.6.2 Intact Structure - Subsequent to In-Service Inspection - If the in-service detectable damage size is less than a failed load path then the minimum

3.4.6.2 Continued
assumed damage in one load path shall be as specified in Paragraph 2.2.4. This damage plus the damage assumed to exist in the remaining structure at the time of inspection as defined in Paragraph 3.3.4.2 shall not grow to critical size and cause failure of the structure due to the application of P_{SV} in the minimum period of unrepaired service usage as specified in Paragraph 3.4.2.

3.4.6.3 Remaining Structure - Subsequent to Load Path Failure - If the in-service detectable damage is a failed load path, then the damage in the remaining structure as defined in Paragraph 3.3.4.2 shall not grow to critical size and cause failure of the structure due to the application of P_{SV} in the minimum period of unrepaired service usage as specified in Paragraph 3.4.2.

3.5 DEPOT OR BASE LEVEL INSPECTABLE

3.5.1 Frequency of Inspection

The frequency of inspection and inspection intervals shall be specified in the system RFP, PIDS or other contract documents as applicable.

3.5.2 Minimum Period of Unrepaired Service Usage

The minimum period of unrepaired service usage shall be two (2) times the depot or base level inspection interval specified in Paragraph 3.5.1.

3.5.3 Minimum Residual Strength

The minimum residual strength shall be P_{DM} subsequent to in-service inspection, and P_{YY} at time of load path failure.

3.5.4 Minimum Assumed Initial Damage

The minimum assumed initial damage shall be as specified in Paragraph 3.3.4.

3.5.5 Minimum Assumed In-Service Damage

The minimum assumed in-service damage shall be as specified in Paragraph 2.3.5 or a failed member whichever is applicable.

3.5.6 Damage Growth Limits

3.5.6.1 Intact New Structure - Paragraph 3.1.6.1 applies.

3.5.6.2 Intact Structure - Subsequent to In-Service Inspection - If the in-service detectable damage is less than a failed load path, then the minimum assumed damage in one load path shall be as specified in Paragraph 2.3.5. This damage plus the damage assumed to exist in the remaining structure at the time of inspection as defined in Paragraph 3.3.4.2 shall not grow to

3.5.6.2 Continued
critical size and cause failure of the structure due to the application of P_{DM} in the minimum period of unrepaired service usage as specified in Paragraph 3.5.2.

3.5.6.3 Remaining Structure - Subsequent to Load Path Failure - If the in-service detectable damage is a failed load path, then the damage in the remaining structure as defined in Paragraph 3.3.4.2 shall not grow to critical size and cause failure of the remaining structure due to the application of P_{DM} in the minimum period of unrepaired service usage specified in Paragraph 3.5.2.

3.6 IN-SERVICE NON-INSPECTABLE

3.6.1 Frequency of Inspection

Not applicable.

3.6.2 Minimum Period of Unrepaired Service Usage

The minimum period of unrepaired service usage shall be one (1) design service lifetime.

3.6.3 Minimum Residual Strength

The minimum residual strength shall be P_{LT} subsequent to load path failure, and P_{YY} at time of load path failure.

3.6.4 Minimum Assumed Initial Damage

The minimum assumed initial damage shall be as specified in Paragraph 3.3.4.

3.6.5 Minimum Assumed In-Service Damage

Not applicable

3.6.6 Damage Growth Limits

3.6.6.1 Intact New Structure - Initial damage as specified in Paragraph 3.3.4.1 shall not grow to critical size and cause failure of a load path due to the application of P_{LT} in the minimum period of unrepaired service usage specified in Paragraph 3.6.2.

3.6.6.2 Remaining Structure - Subsequent to Load Path Failure - Initial damage in the remaining structure subsequent to load path failure, as specified in Paragraph 3.3.4.2 shall not grow to critical size and cause failure of the remaining structure due to the application of P_{LT} in the minimum period of unrepaired service usage specified in Paragraph 3.6.2.

4.0 FAIL SAFE - CRACK ARREST STRUCTURE

4.1 IN-FLIGHT EVIDENT

4.1.1 Frequency of Inspection

Not applicable.

4.1.2 Minimum Period of Unrepaired Service Usage

The minimum period of unrepaired service usage shall be that period of time between that when the damage becomes evident and completion of an immediate return to base (Table CXIX).

4.1.3 Minimum Required Residual Strength

The minimum required residual strength shall be P_{YY} at time of crack arrest and P_{FE} subsequent to crack arrest.

4.1.4 Minimum Assumed Initial Damage

4.1.4.1 Intact New Structure - The damage in intact new structure shall be as specified in Paragraph 3.1.4.1.

4.1.4.2 Remaining Structure at Time of and Subsequent to Crack Arrest - The damage assumed to exist in the remaining structure following arrest of a rapidly propagating crack shall depend upon the particular geometry. In conventional skin stringer (or frame) construction this shall be assumed as two panels (bays) of cracked skin plus the broken central stringer (or frame). Where tear straps are provided between stringers (or frames), this damage shall be assumed as cracked skin between tear straps plus the broken central stringer (or frame). Other configurations shall assume equivalent damage as mutually agreed upon by the contractor and the A.F.

4.1.5 Minimum Assumed In-Service Damage

The minimum assumed in-service damage shall be as specified in Paragraph 4.1.4.2.

4.1.6 Damage Growth Limits

4.1.6.1 Intact New Structure - Initial damage as specified in Paragraph 3.1.4.1 shall not grow to the size which would cause an initial rapid propagation due to the application of P_{DM} in the minimum period of unrepaired service usage specified in Paragraph 4.5.2. If the structure is not inspectable for subcritical cracks, the initial damage specified in 3.1.4.1 shall not grow to the size which would cause an initial rapid crack propagation due to the application of P_{LT} in one lifetime.

TABLE CXIX FAIL SAFE - CRACK ARREST STRUCTURE

DEGREE OF INSPECTABILITY	FREQUENCY OF INSPECTION	MIN. PERIOD OF UNREPAIRED SERVICE USAGE (F_{XX})	MIN. REQUIRED RESIDUAL STRENGTH (P_{XX})	MIN ASSUMED INITIAL DAMAGE SIZE		MIN. ASSUMED IN-SERVICE DAMAGE SIZE (1)	DAMAGE GROWTH LIMITS
				INTACT NEW STRUCTURE a_1	IN REMAINING STRUCTURE a_2		
IN FLIGHT EVIDENT	N/A	RETURN TO BASE (F_{FE})	P_{FE}			2 Cracked Skin Panels Plus Failed Central Stringer (Or Equivalent)	a_1 Shall not cause initial rapid propagation @ P_{DM} In F_{DM} 1 Shall not cause complete failure @ P_{FE} in F_{FE}
GROUND EVIDENT	EVERY FLIGHT	ONE FLIGHT (F_{GE})	P_{GE}	$a/0 = 0.03$ 0.02" 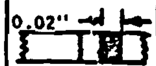	2 Cracked Skin Panels Plus Failed Central stringer (or equivalent)		a_1 Shall not cause initial rapid propagation at P_{DM} in F_{DM} 1 Shall not cause complete failure @ P_{GE} In F_{GE}
WALK AROUND VISUAL	SPECIFIED IN CONTRACT DOCUMENTS (10 FLIGHTS TYPICAL)	5 X FREQ (F_{WV})	P_{WV}	Or Smaller If. Demonstrated		a_2 or 2" or Greater through crack in skin at failed stringer whichever is applicable	a_1 Shall not cause initial rapid propagation @ P_{DM} in F_{DM} 1 Shall not cause complete failure @ P_{WV} in F_{WV}
SPECIAL VISUAL	SPECIFIED IN CONTRACT DOCUMENTS (ONE YEAR TYPICAL)	2 X FREQ (F_{SV})	P_{SV}			Smaller crack if demonstrated	a_1 Shall not cause initial rapid propagation @ P_{DM} in F_{DM} 1 Shall not cause complete failure @ P_{SV} in F_{SV}
DEPOT OR BASE LEVEL	SPECIFIED IN CONTRACT DOCUMENTS (1/4 LIFE-TIME TYPICAL)	2 X FREQ (F_{DM})	P_{DM}			$(a/Q)_{DM}$ As specified in 2.3.5 or a_2	a_1 Shall not cause initial rapid propagation @ P_{DM} in F_{DM} 1 Shall not cause complete failure @ P_{DM} in F_{DM}

4.1.6.2 Remaining Structure Subsequent to Crack Arrest - Damage as specified in Paragraph 4.1.4.2 shall not grow to the size required to cause complete structural failure due to the application of P_{FE} in the minimum period of unrepaired service usage specified in Paragraph 4.1.2.

4.2 GROUND EVIDENT

4.2.1 Frequency of Inspection

The frequency of inspection shall be once per flight.

4.2.2 Minimum Period of Unrepaired Service Usage

The minimum period of unrepaired service usage shall be one (1) complete flight.

4.2.3 Minimum Required Residual Strength

The minimum required residual strength shall be P_{GE} subsequent to crack arrest and P_{YY} at time of crack arrest.

4.2.4 Minimum Assumed Initial Damage

4.2.4.1 Intact New Structure - The damage in intact new structure shall be as specified in Paragraph 3.1.4.1.

4.2.4.2 Remaining Structure at Time of and Subsequent to Crack Arrest - The damage in remaining structure at time of and subsequent to crack arrest shall be as specified in Paragraph 4.1.4.2.

4.2.5 Minimum Assumed In-Service Damage

The minimum assumed in-service damage shall be as specified in Paragraph 4.1.4.2.

4.2.6 Damage Growth Limits

4.2.6.1 Intact New Structure - Paragraph 4.1.6.1 applies.

4.2.6.2 Remaining Structure Subsequent to Crack Arrest - Damage as specified in Paragraph 4.1.4.2 shall not grow to the size required to cause complete structural failure due to the application of P_{GE} in the minimum period of unrepaired service usage specified in Paragraph 4.2.2.

4.3 WALKAROUND VISUAL INSPECTABLE

4.3.1 Frequency of Inspection

The frequency of inspection shall be as specified in the system RFP, PIDS or other contract documents as applicable.

4.3.2 Minimum Period of Unrepaired Service Usage

The minimum period of unrepaired service usage shall be five (5) times the walkaround inspection interval specified in Paragraph 4.3.1.

4.3.3 Minimum Required Residual Strength

The minimum required residual strength shall be P_{WV} subsequent to in-service inspection, and P_{YY} at time of crack arrest.

4.3.4 Minimum Assumed Initial Damage

4.3.4.1 Intact New Structure - The damage in intact new structure shall be as specified in Paragraph 3.1.4.1.

4.3.4.2 Remaining Structure at Time of and Subsequent to Crack Arrest - The damage in remaining structure at time of and subsequent to crack arrest shall be as specified in Paragraph 4.1.4.2.

4.3.5 Minimum Assumed In-Service Damage

The minimum assumed in-service damage shall be as specified in Paragraph 2.1.5 (assumed to be located at an inaccessible, failed stringer or frame), or specified in Paragraph 4.1.4.2, whichever is applicable.

4.3.6 Damage Growth Limits

4.3.6.1 Intact New Structure - Paragraph 4.1.6.2 applies.

4.3.6.2 Intact Structure - Subsequent to In-Service Inspection - If the in-service detectable damage is less than an arrested crack as described in Paragraph 4.1.4.2, then the minimum assumed damage as specified in Paragraph 4.3.5 shall not grow to the size required to cause complete structural failure due to the application of P_{WV} in the minimum period of unrepaired service usage specified in Paragraph 4.3.2.

4.3.6.3 Remaining Structure Subsequent to Crack Arrest - Damage as specified in Paragraph 4.3.5 shall not grow to the size required to cause complete structural failure due to the application of P_{WV} in the specified period of unrepaired usage specified in Paragraph 4.3.2.

4.4 SPECIAL VISUAL INSPECTABLE

4.4.1 Frequency of Inspection

The frequency of inspection shall be as specified in the system RFP, PIDS or other contract documents as applicable.

4.4.2 Minimum Period of Unrepaired Service Usage

The minimum period of unrepaired service usage shall be two (2) times the special visual inspection interval specified in Paragraph 4.4.1.

4.4.3 Minimum Required Residual Strength

The minimum required residual strength shall be P_{SV} subsequent to in-service inspection, and P_{YY} at time of crack arrest.

4.4.4 Minimum Assumed Initial Damage

4.4.4.1 Intact New Structure - The damage in intact new structure shall be as specified in Paragraph 3.1.4.1.

4.4.4.2 Rem· .ng Structure - The damage in remaining structure at time of and subsequent to crack arrest shall be as specified in Paragraph 4.1.4.2.

4.4.5 Minimum Assumed In-Service Damage

The minimum assumed in-service damage shall be as specified in Paragraph 2.2.5 (assumed to be located at an inaccessible, failed stringer or frame), or as specified in Paragraph 4.1.4.2, whichever is applicable.

4.4.6 Damage Growth Limits

4.4.6.1 Intact New Structure - Paragraph 4.1.6.2 applies.

4.4.6.2 Intact Structure - Subsequent to In-Service Inspection - If the in-service detectable damage is less than an arrested crack as described in Paragraph 4.1.4.2, then the minimum assumed damage as specified in Paragraph 4.4.5 shall not grow to the size required to cause complete structural failure due to the application of P_{SV} in the minimum period of unrepaired service usage specified in Paragraph 4.4.2.

4.4.6.3 Remaining Structure Subsequent to Crack Arrest - Damage as specified in Paragraph 4.1.4.2 shall not grow to the size required to cause complete structural failure due to the application of P_{SV} in the minimum period of unrepaired service usage specified in Paragraph 4.4.2.

4.5 DEPOT OR BASE LEVEL INSPECTABLE

4.5.1 Frequency of Inspection

The frequency of inspection shall be specified in the system RFP, PIDS or other contract documents, as applicable.

4.5.2 Minimum Period of Unrepaired Service Usage

The minimum period of unrepaired service usage shall be two (2) times the depot or base level inspection interval specified in Paragraph 4.5.1

4.5.3 Minimum Required Residual Strength

The minimum required residual strength shall be P_{DM} subsequent to in-service inspection and P_{YY} at time of crack arrest.

4.5.4 Minimum Assumed Initial Damage

4.5.4.1 Intact New Structure - The damage in intact new structure shall be as specified in Paragraph 3.1.4.1,

4.5.4.2 Remaining Structure - The damage in remaining structure at time of and subsequent to crack arrest shall be as specified in Paragraph 4.1.4.2.

4.5.5 Minimum Assumed In-Service Damage

The minimum assumed in-service damage shall be as specified in Paragraph 2.3.5 (assumed to be located at an inaccessible failed stringer or frame), or as specified in Paragraph 4.1.4.2, whichever is applicable.

4.5.6 Damage Growth Limits

4.5.6.1 Intact New Structure - Paragraph 4.1.6.2 applies.

4.5.6.2 Intact Structure - Subsequent to In-Service Inspection - If the in-service detectable damage is less than an arrested crack as described in Paragraph 4.1.4.2, then the minimum assumed damage as specified in Paragraph 4.5.5 shall not grow to the size required to cause complete structural failure due to the application of P_{DM} in the minimum period of unrepaired service usage specified in Paragraph 4.5.2.

4.5.6.3 Remaining Structure Subsequent to Crack Arrest - Damage as specified in Paragraph 4.5.5 shall not grow to the size required to cause complete structural failure due to the application of P_{DM} in the minimum period of unrepaired service usage specified in Paragraph 4.5.2.

4.6 NON-INSPECTABLE STRUCTURE

In service non-inspectable crack arrest structure shall not be allowed.

APPENDIX B

MATERIAL DATA ANALYSES

1.0 MATERIAL STRENGTH PROPERTIES

The structure of the baseline airplane is designed to the "B" values of the state-of-the-art materials for F_{tu}, F_{ty}, F_{cy} and F_{su}. Since most of the new materials have only "S" values for the design properties, it becomes necessary to estimate "B" values for a valid strength and weight comparison.

It is proposed to estimate the "B" values by using the analysis method outlined in Section 9.0 of the MIL-HDBK-5. The equation for "A" values is $A = \bar{X} - K_A$ (SD) where $\bar{X}$ is the mean, or typical, value; K_A is the one-sided tolerance limit factor corresponding to a proportion at least 0.99 of a normal distribution and a confidence coefficient of 0.95 and SD is the standard deviation. Similarly, "B" values are given by the equation $B = \bar{X} - K_B$ (SD). X and SD are the same values as for the "A" value equation, and K_B is the one-sided tolerance limit factor corresponding to a proportion to at least 0.90 of a normal distribution and a confidence coefficient of 0.95. By solving the two equations simultaneously, the standard deviation value SD is determined as follows:

$$A = \bar{X} - K_A\,(SD) \text{ or } \bar{X} = A + K_A\,(SD) \tag{48}$$

$$B = \bar{X} - K_B\,(SD) \text{ or } \bar{X} = B + K_B\,(SD) \tag{49}$$

$$\text{where } SD = \frac{B-A}{K_A - K_B}$$

The terms K_A and K_B, as defined in MIL-HDBK-5, are 2.684 and 1.527, respectively. Therefore, $K_A - K_B = 1.157$ and SD = 1/1.157 (B-A), or 0.8643 (B-A). Based on the assumption that "S" values are equal to "A" values, then $\bar{X}$ can be determined from equation (1). If the values for F_{tu}, F_{ty}, F_{cy} and F_{su} are listed as typical, they will be taken equal to $\bar{X}$.

A trend for certain values of (B-A) has been noted for various wrought forms of aluminum and titanium alloys as taken from MIL-HDBK-5. The values of (B-A) found in Tables CXX and CXXI will be assumed typical for the same wrought products for the new alloys of both aluminum and titanium.

The values for "B" calculated in this manner are enclosed in parentheses and noted as estimated values in Tables X, XI and CXXII thru CXXV. The same trend is valid for all four static strength properties of aluminum and titanium.

The same correlation procedure is applied to the steel alloys evaluated. Table CXXVI has listed various steel alloy properties as taken from the MIL-HDBK-5 document. Applicable factors were applied to the properties listed in Table CXXIV to obtain "B" values. These values are enclosed in parentheses and noted as estimated.

Data for beryllium was sparse; however, "B" values were estimated in the same manner as for the steel alloys.

TABLE CXX CORRELATION OF MATERIAL PROPERTY

MATERIAL			F_{tu} (KSI)		B-A (KSI)
ALLOY	FORM	GAUGE	A	B	
7075-T6	Clad Sheet	.063 - .187	73	75	2
7079-T6	Clad Sheet	.063 - .187	70	72	2
7178-T6	Clad Sheet	.063 - .187	80	82	2
7075-T6	Clad Sheet	.040 - .249	78	80	2
7178-T6	Clad Sheet	.045 - .249	84	86	2
7075-T651	Clad Plate	.250 - .499	74	76	2
7178-T651	Clad Plate	.250-1.500	81	83	2
7075-T651	Plate	.250-1.000	77	79	2
7178-T651	Plate	.250-1.500	83	85	2
7075-T6	Die Forging	≤ 1.000	75	78	3
7075-T6	Die Forging	1.001-2.000	74	77	3
7075-T652	Die Forging	≤ 1.000	75	78	3
7075-T652	Die Forging	1.001-2.000	74	77	3
7075-T6	Extrusion	≤ .249	78	82	4
7075-T6	Extrusion	.250-2.999	81	85	4
7178-T6	Extrusion	.062-.249	84	88	4

TABLE CXXI CORRELATION OF TITANIUM MATERIAL PROPERTY

MATERIAL			F_{ty} (KSI)		B-A (KSI)
ALLOY	FORM	GAUGE	A	B	
Ti-6-4	Sheet (Ann)	≤ .187	134	139	5
Ti-6-6-2	Sheet (Ann)	≤ .107	155	160	5
Ti-8M	Sheet (Ann)	≤ .187	125	130	5
Ti-5-2.5	Sheet (Ann)	≤ .187	120	125	5
Ti-5-2.5	Plate (Ann)	.187-.250	120	125	5
Ti-6-4	Bar (Ann)	≤ 3.000	132	137	5
Ti-6-4	Extr (Ann)	≤ 2.000	131	137	6
Ti-4-3-1	Sheet (Sta)	≤ .187	175	182	7
Ti-6-4	Bar (Sta)	≤ .500	164	172	8
Ti-6-4	Bar (Sta)	.501-1.000	151	160	9
Ti-6-4	Bar (Sta)	1.001-1.500	147	157	10
Ti-6-4	Bar (Sta)	1.501-2.000	139	146	7
Ti-6-4	Extr (Sta)	≤ .500	155	163	8
Ti-6-4	Extr (Sta)	.501-.750	151	157	6
Ti-6-4	Extr (Sta)	.751-1.000	147	153	7

TABLE CXXII CANDIDATE ALUMINUM ALLOYS

FORM	ALLOY		F_{tu} KSI	F_{tu}/ρ 10^3 INCH	F_{ty} KSI	F_{ty}/ρ 10^3 INCH	F_{cy} KSI	F_{cy}/ρ 10^3 INCH	F_{su} KSI	F_{su}/ρ 10^3 INCH	E_c 10^3 KSI	E_c/ρ 10^6 INCH	ρ LB/IN^3	0.7 SECANT STRESS KSI	SHAPE FACTOR (n)	K_c KSI$\sqrt{\text{INCH}}$	K_{Ic}	K_{Ic}/ρ	$(K_{Ic}/F_{ty})^2$	STRESS CORROSION: THRESHOLD σ_{th} KSI	K_{ISCC}	K_{ISCC}/ρ	FATIGUE 10^7 CYCLES σ_{max} $K_t=1$ KSI	σ_{max} $K_t=3$ KSI	σ_{max}/ρ $K_t=1$	σ_{max}/ρ $K_t=3$	CRACK GROWTH $\Delta a/\Delta N$	$\Delta a/\Delta N/\rho$	REFERENCES
DIE FORGING	7049-T73		(8)		(8)		(8)		(8)		10.6	104	.102										55	23	539	225			5,28,29
	≤ 1.0	L	75	735	65	637	67	657	44	431				66.1	(20)														5,13,28
		LT																									12.8	123	
		TL																											
		ST	74	725	64	627	66	647												42									
		SL																											
	1.0 to 2.0	L	75	735	65	637	67	657	44	431				66.1	(20)														
		LT															30	294	.213										13
		TL															25	245	.160										
		ST	73	717	63	618	65	637												42									
		SL															24	235	.145		20	1.89							13
	2.0 to 4.0	L	74	725	64	627	66	647	44	431				67.0	(20)														
		LT																											
		TL																											
		ST	73	717	63	618	65	637												42									
		SL																											
	4.0 to 5.0	L	73	717	63	618	65	637	42	412				66.0	(20)														
		LT																											
		TL																											
		ST	71	696	61	598	63	618												42									
		SL																											
	7050-T73		((8))		((8))		((8))		((8))		(10.6)	104	.102																
	≤ 2.9	L	69	677	58	568	61	598	42	402				61.2	(20)	(130)		1273	5.00				55	23	539	225	(16)	157	25
		LT															(34)	334	.364										
		TL															(26)	255	.215										
		ST	65	647	56	549	58	568												(47)									
		SL															(22)	216	.154										

* ... as applicable

( ) Estimated, B values based on actual S values

(( )) Estimated, B values based on estimated S values

(20) Assumed values for 'n' (0.7 secant stress calculated)

TABLE CXXII CANDIDATE ALUMINUM ALLOYS (CONT'D)

FORM	ALLOY		F_{tu} KSI	F_{tu}/ρ 10^3 INCH	F_{ty} KSI	F_{ty}/ρ 10^3 INCH	F_{cy} KSI	F_{cy}/ρ 10^3 INCH	F_{su} KSI	F_{su}/ρ 10^3 INCH	E_c 10^3 KSI	E_c/ρ 10^6 INCH	ρ LB/IN^3	0.7 SECANT STRESS KSI	SHAPE FACTOR (n)	K_c KSI$\sqrt{\text{INCH}}$	K_{Ic}	K_{Ic}/ρ	$(K_{Ic}/F_{ty})^2$	STRESS CORROSION: THRESHOLD σ_{th} KSI	K_{ISCC}	K_{ISCC}/ρ	FATIGUE 10^7 CYCLES σ_{max} $K_t=1$ KSI	σ_{max} $K_t=3$ KSI	σ_{max}/ρ $K_t=1$	σ_{max}/ρ $K_t=3$	CRACK GROWTH $\Delta a/\Delta N$	$\Delta a/\Delta N/\rho$	REFERENCES
DIE FORGING	7050-T736		(8)		(8)		(8)		(8)		10.6	104	.102										55	23	539	225			17
	≤ 2.0	L	75	77	65	637	67	647	--	43				66.0	(20)														14,17,55
		LT															32	314	.242								16	157	
		TL															25	245	.180										
		ST	71	696	59	578	61	607												35									13,21
		SL															22	216	.139		27	2.55							27
	2.0 to 4.0	L	74	725	64	627	66	647						65.0	(20)														21
		LT																											
		TL																			25	2.36							27,56
		ST	70	686	58	569	60	588												35									
		SL																			23	2.17							17
	7075-T6		8		8		8		8		10.4	103	.101										55	23	545	228			5
	≤ 1.0	L	78	772	67	663	70	693	45	446				71.4	(20)					35									5,14,15,16
		LT																		25							10	99	
		TL																											
		ST	75	743	65	644	68	673												7									13
		SL																											
	1.0 to 2.0	L	77	762	66	653	69	683	44	436				70.3	(20)														17
		LT															26	257	.142										
		TL															23	228	.118										
		ST	74	733	64	634	67	663																					
		SL															17	168	.064										
	2.0 to 3.0	L	76	752	65	644	68	673	43	426				69.2	(20)														
		LT																											
		TL																											
		ST	73	723	63	624	66	653																					
		SL																											

* ... as applicable

( ) Estimated, B values based on actual S values

(( )) Estimated, B values based on estimated S values

(20) Assumed values for 'n' (0.7 secant stress calculated)

TABLE CXXII CANDIDATE ALUMINUM ALLOYS (CONT'D)

Form	Alloy		Ftu KSI	Ftu/ρ	Fty KSI	Fty/ρ	Fcy KSI	Fcy/ρ	Fsu KSI	Fsu/ρ	Ec	Ec/ρ	ρ	0.7 Secant Stress KSI	Shape Factor n	Kc	KIc	KIc/ρ	[illegible]	Stress Corrosion Smooth KSI	Stress Corrosion Notched	Stress Corrosion Notched	Fatigue	Fatigue	Fatigue	Fatigue	Crack Growth	Crack Growth	References
DIE FORGING	7075-T73		(B)		(B)		(B)		(B)		10.4	103	.101										55	23	545	228			5
	≤ 3.0	L	69	683	59	584	61	604	42	416				61.7	(20)					50									5,14,17,1
		LT															31	307	.286	48							12.9	123	
		TL															25	248	.200										
		ST	65	644	56	554	58	574												43									13
		SL															20	198	.126										
	7175-T66		(B)		(B)		(B)		(B)		10.5	104	.101										55	23	545	228			57,58
	≤ 3.0	L	82	681	79	782	81	802						83.2	[20]					60									
		LT															29	287	.135								(10)	99	
		TL																											
		ST	80	792	69	683	73	723												8									
		SL																			3	0.29							
	7175-T736		(B)		(B)		(B)		(B)		10.7	103	.101										55	23	545	228			
	≤ 1.0	L	79	782	69	683	70	693	46	455				71.3	(20)					50									57,59,60,61
		LT															34	337	.243	48							13	129	
		TL															32	317											
		ST	74	733	65	644	68	673												35									
		SL															27	267	.173		20	1.07							13
	1.0 to 2.0	L	79	782	69	683	70	693	46	455				71.3	(20)														
		LT																											
		TL																											
		ST	74	733	65	644	67	663																					
		SL																											
	2.0 to 3.0	L	79	782	69	683	70	693	46	455				71.3	(20)														
		LT																											
		TL																											
		ST	74	733	65	644	66	653																					
		SL																											

[illegible]

[ ] Estimated, ρ values based on actual [illegible] values

([ρ]) Estimated, [illegible] values based on estimated [illegible] values

(20) Assumed values for n. (0.7 secant stress calculated)

TABLE CXXII CANDIDATE ALUMINUM ALLOYS (CONT'D)

Form	Alloy		Ftu KSI	Ftu/ρ	Fty KSI	Fty/ρ	Fcy KSI	Fcy/ρ	Fsu KSI	Fsu/ρ	Ec	Ec/ρ	ρ	0.7 Secant Stress KSI	Shape Factor n	Kc	KIc	KIc/ρ	[illegible]	Stress Corrosion Smooth KSI	Stress Corrosion Notched	Stress Corrosion Notched	Fatigue	Fatigue	Fatigue	Fatigue	Crack Growth	Crack Growth	References
HAND FORGING	7049-T73		(B)		(B)		(B)		(B)		10.6	104	.102										55	23	539	225			5,28
	2.0 to 3.0	L	74	725	64	627	67	657	41	402				68.1	(20)														13,28,62
		LT	74	725	62	608	64	627									28	275	.191								12.5	123	
		TL															23	225	.138										
		ST	72	706	61	598																							
		SL															20	196	.107	46									
	3.0 to 4.0	L	72	706	62	606	64	627	40	392				64.9	(20)														
		LT	72	706	60	588	62	608																					
		TL																											
		ST	70	686	59	578														44									
		SL																											
	4.0 to 5.0	L	71	696	59	578	61	598	39	382				51.7	(20)														
		LT	70	686	59	578	61	598																					
		TL																											
		ST	69	676	58	569														42									
		SL																											
	7050-T73652		(B)		(B)		(B)		(B)		10.6	104	.102										55	23	539	225			17
	≤ 2.0	L	75	735	66	647	66	647	44	431				67.0	(20)														17,35
		LT	74	725	64	627	68	667									36	353	.298								16	157	
		TL																											
		ST																		32									13,17,25
		SL															22	216											
		TS															25	245											
	2.0 to 3.0	L	75	735	65	637	65	637						65.9	(20)														
		LT	73	716	63	618	67	657																					
		TL																											
		ST	70	686	58	569	65	637												31									17
		SL																											

[illegible]

[ ] Estimated, ρ values based on actual [illegible] values

([ρ]) Estimated, [illegible] values based on estimated [illegible] values

(20) Assumed values for n. (0.7 secant stress calculated)

TABLE CXXII CANDIDATE ALUMINUM ALLOYS (CONT'D)

Form	Alloy		Ftu ksi	Ftu/ρ	Fty ksi	Fty/ρ	Fcy ksi	Fcy/ρ	Fsu ksi	Fsu/ρ	Ec	Ec/ρ	ρ	0.7 Secant stress ksi	Shape factor	[illegible]	[illegible]	[illegible]	[illegible]	Stress corrosion			Fatigue				Crack growth		References
Hand forging	7175-T736		(8)		(8)		(8)		(8)		10.6	135	.101										55	23	539	225			61
	≤ 3.0	L	76	745	66	647	67	657	45	441				68.1	(20)														
		LT	74	725	63	618	66	647																			(10)	99	
		TL																											
		ST	72	706	63	618	66	647																					
		SL																											
Extrusion	7049-T73511		(8)		(8)		(8)		(8)		10.6	104	.102										55	23	539	225			57
	≤ 2.9	L	78	765	68	667	68	667	46	451				69.1	(20)														11,57,63
		LT	74	725	64	627	70	686									33	323	.266								11	108	
		TL															23	226	.129										
		ST																		42									
		SL															20	190	.098		20	1.89							
		LS																			26	2.45							
	7049-T76511		(8)		(8)		(8)		(8)		10.6	104	.102										55	23	539	225			57
	≤ 2.9	L	82	804	74	725	74	725	48	471				75.6	(20)														27,63
		LT	80	784	72	706	76	745									33		.200								(10)	98	
		TL															23		.102										
		ST																		25									
		SL															20												
	7050-T736511		(8)		(8)		(8)		(8)		10.6	101	.102										55	23	539	225			17
	≤ .249	L	79	775	71	696	73	716	47	461				74.5	(20)														
		LT																									(13)	127	
		TL																											
		ST																											
		SL																											
	.250 to .499	L	81	794	72	706	74	725						75.6	(20)														
		LT																											
		TL																											
		ST																											
		SL																											

( ) Estimated, ρ values based on actual values

(20) Assumed values for n. (0.7 secant stress calculated)

((E)) Estimated, values based on estimated values

TABLE CXXII CANDIDATE ALUMINUM ALLOYS (CONT'D)

Form	Alloy		Ftu ksi	Ftu/ρ	Fty ksi	Fty/ρ	Fcy ksi	Fcy/ρ	Fsu ksi	Fsu/ρ	Ec	Ec/ρ	ρ	0.7 Secant stress ksi	Shape factor	[illegible]	[illegible]	[illegible]	[illegible]	Stress corrosion			Fatigue				Crack growth		References
Extrusion	7050-T736511																												
	0.50 to 1.50	L	82	804	74	725	74	725						75.6	(20)														
		LT																											
		TL																											
		ST																		35									17
		SL															23												
	7050-T76511		(8)		(8)		(8)		(8)		10.6	104	.102										55	23	539	225			17,21
	≤ .249	L	82	804	74	725	75	735	48	471				77.7	(20)														
		LT	81	794	73	716	76	745																					
		TL																											
		ST																											
		SL																											
	.250 to .499	L	85	833	77	755	78	765						81.0	(20)														
		LT	84	824	[illegible]	735	79	775								90		882	1.37								11.5	113	30
		TL																											
		ST																											
		SL																											
	1.00 to 1.50	L	85	833	76	745	77	755						77.7	(20)														
		LT	82	804	72	706	76	745									38	372	.250		35	3.30							17,27
		TL																		54									
		ST																											
		SL															22			25	20	1.89							17,27
	7075-T6		8		8		8		8		10.7	106	.101										55	23	545	220			5
	≤ .249	L	82	812	74	733	74	733	44	436				75.4	22.5					60									14,15,19
		LT	80	792	70	693	76	752												50							10	98	
		TL																											
		ST															19	188	.074	8									
		SL																											

( ) Estimated, ρ values based on actual values

(20) Assumed values for n. (0.7 secant stress calculated)

((E)) Estimated, values based on estimated values

TABLE CXXII CANDIDATE ALUMINUM ALLOYS (CONT'D)

Form	Alloy		Ftu KSI	Ftu/ρ	Fty KSI	Fty/ρ	Fcy KSI	Fcy/ρ	Fsu KSI	Fsu/ρ	Ec	Ec/ρ	ρ	Secant stress KSI	Shape	n		/ρ		KSI	Static corrosion			Fatigue				Crack growth		References
EXTRUSION	.250 to .499	L	85	842	77	762	77	762	45	446				78.6	22.5	85		842	1.22	.80										
		LT	81	802	72	713	78	772												.50										
		TL																												
		ST																												
		SL																												
	7075-T76		a		a		a		a		10.7	106	.101											58	23	545	228			13, 64
	.062 to .249	L	74	733	55	544	[illegible]	694	40	396				65.9	(29)															
		LT	71	703	61	604	66	653																				(12)	118	
		TL																												
		ST																												
		SL																												
			(8)		(8)		(8)		(8)																					
	.250 to .499	L	76	752	66	653	66	653	42	416				70.2	(20)															
		LT	73	723	62	614	67	663																						
		TL																												
		ST																												
		SL																												
			8		8		8		6																					
	.500 to .749	L	76	752	67	663	67	663	42	416				68.0	(20)															
		LT	73	723	62	614	67	663																						
		TL																												
		ST															21	208	.114	25										
		SL																												
PLATE	2024-T351		a		a		a		a		10.8	108	0.100											(45)	(13)	450	180	(14)	180	5,13
	2.000 to 3.000	L	67	670	49	490	40	400	37	370				43.6	11					15										
		LT	63	630	44	443	46	463									31	310	.42	20										
		TL															23	230	.45											
		ST																		8										
		SL															22	232	.27											

* Based on 100 data

( ) Estimated, ρ values based on Actual values

(( )) Estimated, ρ values based on estimated values

( ) Assumed values for n (Secant stress calculated)

TABLE CXXII CANDIDATE ALUMINUM ALLOYS (CONT'D)

Form	Alloy		Ftu KSI	Ftu/ρ	Fty KSI	Fty/ρ	Fcy KSI	Fcy/ρ	Fsu KSI	Fsu/ρ	Ec	Ec/ρ	ρ	Secant stress KSI	Shape	n		/ρ		KSI	Static corrosion			Fatigue				Crack growth		References
PLATE	7050-T73651		(8)		(8)		(8)		(8)		10.6	104	.102												23	539	225			17,21
	2.0	L	72	706	63	617	64	627	43	422																				
		LT	72	706	65	637	67	657						64.9	(20)		36	353	.307									16	152	12,22,23
		TL															32	314	.212		36	3.83								13
		ST																												
		SL															26	255	.155		26	2.45								17,24
	7050-T7651		(8)		(8)		(8)		(8)		10.6	104	.102											55	23	539	225			17
	2.0	L	79	775	71	696		696	46	451				72.1	13													16	132	25
		LT	80	784	63	617	72	706									34	333	.329											13
		TL															28	275	.155		70	1.89								
		ST																		75										
		SL															24	235	.127											
	7075-T7351		(8)		(8)		(8)		(8)		10.6	105	.101											55	23	545	228			
	.250 to 1.000	L	71	703	59	584			576	41	406			58.5	(20, 122**)			1200	4.26	50										5,13
		LT	71	703	223	58	574		578								30	297	.258	58								12.5	124	
		TL															28	287	.243		28	2.54								
		ST																												
		SL															22	218	.115	43	26	1.89								
	7075-T7651		(8)		(8)		(8)		(8)		10.6	105	.101											55	23	545	228			5
	.250 to .499	L	73	723	63	624	62	614	43	426				72.7	(20)					47										5,9,11
		LT	74	732	63	624	65	644								75		743	7.42	49								12	119	
		TL														62		.614	.969											
		ST																												
		SL																												
	1.0 to 2.0	L	73	723	65	414	63	624	43	426				61.7	(20)					49										13,17,59
		LT	73	723	64	634	64	634									27	267	.130	49										
		TL															23	226	.130											
		ST																		28										
		SL															22	222			(36)	3.61								27

* Based on 100 data

** (LT) direction

( ) Estimated, ρ values based on Actual values

(( )) Estimated, ρ values based on estimated values

( ) Assumed values for n (Secant stress calculated)

TABLE CXXII CANDIDATE ALUMINUM ALLOYS (CONT'D)

Form	Alloy		Ftu ksi	Ftu/ρ	Fty ksi	Fty/ρ	Fcy ksi	Fcy/ρ	Fsu ksi	Fsu/ρ	Et	Ec/ρ	ρ	Secant stress ksi	Shape factor	Kc ksi	KIc ksi√in	KIc/ρ	[illegible]	Stress corrosion ksi	Stress corrosion [illegible]	Stress corrosion [illegible]	Fatigue [illegible]	Fatigue [illegible]	Fatigue [illegible]	Fatigue [illegible]	Crack growth [illegible]	Crack growth/ρ	References
PLATE	7475-T651		(B)		(B)		(B)		(B)		10.6	105	101										55	23	545	228			26
	.250 to .499	L	79	782	69	683	69	683	46	455				70.2	(20)					50									
		LT	80	792	69	683	72	713									40	396	.34	45	40	3.27					(12)	119	
		TL															35	347	.26		.31	2.92							
		ST																		8									
		SL															27				9	.649							
	7475-T7351		(B)		(B)		(B)		(B)		10.6	105	101										55	23	545	228			26
	.250 to .499	L	73	693	59	584	58	574	41	406				58.5	(20)														
		LT	71	703	59	584	61	604								(160)		1581	2.8										
		TL																											
		ST																											
		SL																											
	1.5 to 2.0	L	69	683	58	574	57	564	43	426				52.4	20					47									
		LT	70	693	58	574	60	594									50	495	.743	42	50	4.72					14	138	17,24,27
		TL															45	446	.603		45	4.25							24
		ST	67	663	55	545	59	584												42									
		SL															33	327	.360		33	3.11							
	7475-T7651		(B)		(B)		(B)		(B)		10.6	105	101										55	23	545	228			
	.250 to .499	L	72	713	62	614	60	594	43	426				60.6	(20)														25
		LT	73	723	62	614	64	634																			14	138	
		TL																											
		ST																											
		SL																											
	1.0 to 1.5	L	71	703	61	604	60	594	41	406				60.6	(20)					50									17,25,27
		LT	72	713	61	604	63	624									43	426	.497	.45	43	4.06					14	139	
		TL															38	376	.388		.35	3.30							
		ST																		.25		2.64							
		SL															29	287			28								

[illegible]

( ) Estimated, ρ values based on actual values

((B)) Estimated, values based on estimated values

(20) Assumed values for [illegible] secant stress calculated)

TABLE CXXII CANDIDATE ALUMINUM ALLOYS (CONT'D)

Form	Alloy		Ftu ksi	Ftu/ρ	Fty ksi	Fty/ρ	Fcy ksi	Fcy/ρ	Fsu ksi	Fsu/ρ	Et	Ec/ρ	ρ	Secant stress ksi	Shape factor	Kc ksi	KIc ksi√in	KIc/ρ	[illegible]	Stress corrosion ksi	Stress corrosion [illegible]	Stress corrosion [illegible]	Fatigue [illegible]	Fatigue [illegible]	Fatigue [illegible]	Fatigue [illegible]	Crack growth [illegible]	Crack growth/ρ	References
SHEET (CLAD)	2024-T3		B		B		B		B		10.7	107	100										(43)	23	430	230			
	.063 to .249	L	64	640	47	470	39	390	40	400				38.0	10.7					35							18	140	5,6,7,8
		LT	63	630	42	420	45	450								175		1750	12.26	35									6,9,10
		TL														148		1480	11.30		8	.748							
		ST																											
		SL																											
	7050-T76		((B))		((B))		((B))		((B))		10.6	104	102										(40)	(21)	382	206			
	.020 to .063	L	79	774	72	706	73	716	47	461				74.5	(20)														20
		LT	79	774	70	686	76	745								60		588	.695								14	132	
		TL																											
		ST																											
		SL																											
	7075-T6		B		B		B		B		10.5	104	101										40	21	336	208			5
	.063 to .187	L	75	743	62	663	66	653	45	446				67.9	11.6					46									5,6
		LT	75	743	65	644	69	683								(60)		594	.756	46							10	99	
		TL														57		564	.769		(45)	4.29							8
		ST																											
		SL																											
	7475-T61		(B)		(B)		(B)		(B)		10.5	104	101										40	21	396	208			26
	.040 to .062	L	71	703	63	624	62	614	44	436				62.8	(20)														
		LT	71	703	61	604	65	644																					
		TL																											
		ST																											
		SL																											
	.063 to .187	L	72	713	64	634	63	624	44	436				63.0	(20)					(46)									65,66
		LT	72	713	62	614	66	653								133		1317	4.32	(46)	(91)	6.67					13	129	
		TL														122		1208	3.06										
		ST																											
		SL																											

[illegible]

( ) Estimated, ρ values based on actual values

((B)) Estimated, values based on estimated values

(20) Assumed values for [illegible] secant stress calculated)

TABLE CXXII CANDIDATE ALUMINUM ALLOYS (CONT'D)

FORM	ALLOY		Ftu KSI	Ftu/ρ	Fty KSI	Fty/ρ	Fcy KSI	Fcy/ρ	Fsu KSI	Fsu/ρ	E	E/ρ	ρ	Secant Stress KSI	Shape Factor	Kc	KIc	KIc/ρ					Fatigue				Crack Growth		REFERENCES
SHEET (CLAD)	7475-T61 (Cont'd)		(B)		(B)		(B)		(B)		10.5	.104	.101										40	21	396	208			26
	.188 to .249	L	74	.733	65	.644	64	.634	46	.455				64.9	(20)														
		LT	74	.733	62	.624	67	.663																					
		TL																											
		ST																											
		SL																											
	7475-T761		(B)		(B)		(B)		(B)		10.5	.104	.101										40	21	396	208			26
	.040 to .062	L	68	.673	58	.574	57	.564	42	.416				57.5	18.5														
		LT	68	.673	57	.564	59	.584																					
		TL																											
		ST																											
		SL																											
	.063 to .187	L	69	.681	57	.564	59	.564	43	.426				56.5	19.5					(.41)									
		LT	69	.683	58	.564	60	.594								145		1436	6.04	(.41)							16	139	65,66
		TL														137		1356	5.58										
		ST																											
		SL																											
	.188 to .249	L	71	.703	62	.614	59	.584	44	.436				59.6	19.5														
		LT	71	.703	59	.584	61	.604																					
		TL																											
		ST																											
		SL																											
SHEET (BARE)	7050-T76		(B)		(B)		(B)		(B)		10.6	.104	.102										45	19	441	186			13,17
	.040 to .250	L	80	.784	73	.716	74	.725	48	.471				75.6	(20)														
		LT	80	.784	71	.696	72	.755								75		.735	1.06										
		TL														62		.608	.76								16	137	
		ST																											

( ) Estimated, P values based on Actual (S) Values

((B)) Estimated, ? values based on estimated (S) values

(20) Assumed values for n (?) secant stress calculated)

TABLE CXXII CANDIDATE ALUMINUM ALLOYS (Concluded)

FORM	ALLOY		Ftu KSI	Ftu/ρ	Fty KSI	Fty/ρ	Fcy KSI	Fcy/ρ	Fsu KSI	Fsu/ρ	E	E/ρ	ρ	Secant Stress KSI	Shape Factor	Kc	KIc	KIc/ρ					Fatigue				Crack Growth		REFERENCES
SHEET (BARE)	7075-T76		(B)		(B)		(B)		(B)		10.5	.104	.101										45	19	446	188			5
	.125 to .249	L	76	.731	66	.634	65	.624	46	.455				63.8	(20)					.49									5,6,11,12
		LT	75	.743	64	.634	67	.663								75		.742	1.32	48	(47)	6.48					12	119	13
		TL														62		.614	.838										
		ST																											
		SL																											
	7475-T61		(B)		(B)		(B)		(B)		10.5	.104	.101										45	19	.446	.188			26
	.040 to .249	L	77	.762	68	.673	67	.663	47	.465				88.1	(20)					(.46)									65,66,67
		LT	77	.762	66	.653	70	.693								133		1317	3.03	(.46)	(.31)	8.67					14	139	56
		TL														122		1208	1.??										
		ST																											
		SL																											
	7475-T761		(B)		(B)		(B)		(B)		10.5	.124	.101										45	19	.446	.188			26
	.040 to .249	L	73	.723	63	.624	62	.614	45	.446				62.8	(20)					(.44)									56,65,66,67
		LT	73	.723	62	.614	65	.644								145		1436	5.10	.46	(.106)	10.1							
		TL														137		1356	7.21								16	139	
		ST																											
		SL																											
		L																											
		LT																											
		TL																											
		ST																											
		SL																											
		L																											
		LT																											
		TL																											
		ST																											
		SL																											

( ) Estimated, P values based on Actual (S) Values

((B)) Estimated, ? values based on estimated (S) values

(20) Assumed values for n (?) secant stress calculated)

TABLE CXXIII CANDIDATE TITANIUM ALLOYS

FORM	ALLOY		Ftu KSI	Ftu/ρ 10³ IN	Fty KSI	Fty/ρ 10³ IN	Fcy KSI	Fcy/ρ 10³ IN	Fsu KSI	Fsu/ρ 10³ IN	Ec 10³ KSI	Ec/ρ 10⁶ IN	ρ LB/IN³	0.7 Secant Stress KSI	Shape Factor (n)	Kc KSI√IN	KIc KSI√IN	KIc/ρ	(KIc/Fty)² IN	Stress Corrosion σth KSI	KIscc	KIscc/Kc	Fatigue 10^7 cycles σ max unnotched KSI	σ max notched KSI	σ max/ρ unnotched	σ max/ρ notched	Crack Growth Δa/ΔN	Δa/ρ	REFERENCES
EXTRUSION	Ti-6-4 (ANN)		B		B		B		B		16.4	103	.160										114	54	713	338			69
	≤2.0	L	137	85?	126	775	132	825	89	556				135.8	(20)														
		LT	139	854	128	800	13?	856																			(20)	125	
		TL																											
		ST																											
		SL																											
	Ti-6-4 (STA)		B		B		B		B		16.4	103	.160										129	52	806	325			69
	≤.50	L	163	101?	147	91?	157	981	99	619				164.2	17.1						**								13
		LT	163	101?	147	91?	157	981													43	2.99							
		TL																											
		ST																											
		SL																											
	.51 to .75	L	157	981	143	894	153	956	96	600				159.7	17.1														
		LT	157	981	145	906	155	969																					
		TL																											
		ST																											
		SL																											
	.76 to 1.00	L	151	956	140	875	150	938	93	581				156.4	17.1														13
		LT	153	[illegible]	142	888	152	950																			(20)	125	
		TL																											
		ST																											
		SL																											
	Ti-6-6-2 (ANN)		(B)		(B)		((B))		((B))		17.5	107	.164										136	50	829	305			69,70
	≤2.0	L	151	921	141	860	143	872	100	610				147.3	(20)														63
		LT																									(19)	116	
		TL																											
		ST																											
		SL																											

* [illegible]

( ) Estimated, B values based on Actual S values

((B)) Estimated, B values based on estimated S values

(20) Assumed values for "n" (0.7 secant stress calculated)

** LS Direction.

TABLE CXXIII CANDIDATE TITANIUM ALLOYS (CONT'D)

FORM	ALLOY		Ftu KSI	Ftu/ρ 10³ IN	Fty KSI	Fty/ρ 10³ IN	Fcy KSI	Fcy/ρ 10³ IN	Fsu KSI	Fsu/ρ 10³ IN	Ec 10³ KSI	Ec/ρ 10⁶ IN	ρ LB/IN³	0.7 Secant Stress KSI	Shape Factor (n)	Kc KSI√IN	KIc KSI√IN	KIc/ρ	(KIc/Fty)² IN	Stress Corrosion σth KSI	KIscc	KIscc/Kc	Fatigue 10^7 cycles σ max unnotched KSI	σ max notched KSI	σ max/ρ unnotched	σ max/ρ notched	Crack Growth Δa/ΔN	Δa/ρ	REFERENCES
EXTRUSION	Ti-6-6-2 (STA)		(B)		(B)		((B))		((B))		17.5	107	.164										152	58	927	354			
	≤.50	L	17?	10??	15?	10??	17?	104?	118	720				177.8	(20)														69
		LT																									(22)	134	
		TL																											
		ST																											
		SL																											
	.51 to 1.5	L	167	1018	162	988	165	1006						171.2	(20)														
		LT																											
		TL																											
		ST																											
		SL																											
PLATE	Ti-6-4 (ANN)		B		B		B		B		16.4	103	.160										114	54	713	338			69
	.188 to 2.0	L	1??	844	12?	75?	13?	81?	[illegible]	4?4				134.8	(20)														71,72
		LT	13?	[illegible]	13?	81?	13?	8??									70	41?	.314								20	125	
		TL																											
		ST																											
		SL																											
	Ti-6-4 (STA)		(B)		(B)		((B))		((B))		16.4	103	.160										129	52	806	325			69
	.187 to .750	L	165	1031	15?	938	15?	956	100	625				158.7	(20)														13,25,71,72
		LT	165	1031	159	938	160	1000									68	375	.188								22	118	71
		TL																											
		ST																											
		SL																											
	1.0 to 2.0	L	150	938	14?	875	142	888	[illegible]	544				146.7	(20)														25
		LT	1?8		140	875	14?	90?																					
		TL																											
		ST																											
		SL																											

* [illegible]

( ) Estimated, B values based on Actual S values

((B)) Estimated, B values based on estimated S values

(20) Assumed values for "n" (0.7 secant stress calculated)

TABLE CXXIII CANDIDATE TITANIUM ALLOYS (CONT'D)

FORM	ALLOY		Ftu KSI	Ftu/ρ	Fty KSI	Fty/ρ	Fcy KSI	Fcy/ρ	Fsu KSI	Fsu/ρ	Ec	Ec/ρ	ρ	Secant stress KSI	Shape factor	Kc	KIc	K/ρ	(K/Fty)²	Stress corrosion			Fatigue				Crack growth		REFERENCES
PLATE	Ti-6-4 (Beta Ann)		((B))		((B))		((B))		[(B)]		16.4	103	.160										114	54	713	338			
	.187 to .50	L	135	844	120	750	133	831	81	506				136.9	(20)														25,69,71,74
		LT															75	469	.391								23	144	
		TL																											
		ST																											
		SL																											
	Ti-6-6-2 (Ann)		B		B		B		(B)		17.5	107	.164										[illegible]	50	829	305			5,70
	.187 to 4.0	L	150	915	140	854	142	866	102	591				146.2	(20)														69,71,73 72,75,76
		LT															51	311	.133								19	116	
		TL																											
		ST																											
		SL																											
	Ti-6-6-2 (STA)		(B)		(B)		((B))		((B))		17.5	107	.164										152	58	927	354			5,70
	.187 to 1.5	L	175	1067	167	1006	168	1024	115	701				174.5	(20)														69,73,77 71,72
		LT															37	226	.260								22	134	
		TL																											
		ST																											
		SL																											
	Ti-6-6-2 (Beta Ann)		(B)		(B)		(B)		((B))		17.5	107	.164										136	50	829	305			
	.187 to 2.0	L	155	945	145	884	147	896	102	622				151.6	(20)														13,69,71
		LT															60	366	.171								26	159	
		TL																											
		ST																											
		SL																											
	Ti-8-8-2-3 (STA)**		((B))		((B))		((B))		((B))		(15.5)	86	.175										75	33	429	188			69
	≥1.0	L	175	1000	165	943	170	972	110	629				177.0	(20)														11,24,78
		LT															56	320	.107								32	183	
		TL															53	303											
		ST																											
		SL																											

( ) Estimated, B values based on Actual S values
((B)) Estimated, B values based on estimated S values

(20) Assumed values for n (0.7 secant stress calculated)
** Very low ductility in this strength range.

TABLE CXXIII CANDIDATE TITANIUM ALLOYS (CONT'D)

FORM	ALLOY		Ftu KSI	Ftu/ρ	Fty KSI	Fty/ρ	Fcy KSI	Fcy/ρ	Fsu KSI	Fsu/ρ	Ec	Ec/ρ	ρ	Secant stress KSI	Shape factor	Kc	KIc	K/ρ	(K/Fty)²	Stress corrosion			Fatigue				Crack growth		REFERENCES
PLATE	Ti-6-22-22 (STA)		((B))		((B))		((B))		((B))		(18.0)	111	.162										135	45	833	278			
	.187 to .50	L	180	1111	170	1049	182	1123	115	710				189.6	(20)														30,79,80
		LT																									20	123	
		TL																											
		ST																											
		SL																											
	.501 to 1.5	L	173	1068	161	994	125	1080	113	698				181.9	(20)														
		LT															70	.432	.109										
		TL															55	.340	.118										
		ST	174	1074	162	1000	178	1099																					
		SL																											
	Ti-10-6-44 (STA)		((B))				((B))		((B))		14.8	85	.174										125	43	718	247			
	.187 to 2.0	L	175	1006	165	948	167	960	110	632				174.9	(20)														69,74,81
		LT															60	345	.132								20	116	
		TL																											
		ST																											
		SL																											
SHEET	Ti-6-4 (Ann)		B		B		B		B		16.4	103	.160										114	54	713	338			69
	≤.187	L	139	869	131	819	138	863	81	506				140.8	(50)														13,69,77,82
		LT	139	869	131	819	138	863								192		1200	2.15								21	131	
		TL														156		994	1.47										13
		ST																											
		SL																											
	Ti-6-4 (STA)		(B)		(B)		(B)		(B)		14.4	103	.160										129	52	[illegible]	325			69
	≤.187	L	165	1031	150	938	159	994	105	656				163.1	(30)														69,73,8?,83
		LT	165	1031	150	938	167	1044								82		513	.299								20	125	
		TL																											
		ST																											
		SL																											

( ) Estimated, B values based on Actual S values
((B)) Estimated, B values based on estimated S values

(20) Assumed values for n (0.7 secant stress calculated)

TABLE CXXIII CANDIDATE TITANIUM ALLOYS (CONT'D)

Form	Alloy	Dir.	Ftu (KSI)	Ftu/ρ (10^3 inch)	Fty (KSI)	Fty/ρ (10^3 inch)	Fcy (KSI)	Fcy/ρ (10^3 inch)	Fsu (KSI)	Fsu/ρ (10^3 inch)	Ec (10^3 KSI)	Ec/ρ (10^6 inch)	ρ (lb/in^3)	0.7 Secant Stress (KSI)	Shape Factor (n)	Kc* (KSI√in)	KIc	Kc/ρ	(KIc/Fty)^2 (inch)	Stress Corrosion Smooth σth (KSI)	Stress Corrosion Notched KIscc	KIscc/Ec	Fatigue 10^7 Cycles σmax	Fatigue 10^7 Cycles σmax	Fatigue σmax/ρ	Fatigue σmax/ρ	Crack Growth Δa/ΔN	Crack Growth Δa/ρ	References
SHEET	Ti-6-6-2 (Ann)		B		B		((B))		((B))		17.5	107	.164										136	50	829	365			69,70
	≤.187	L	160	976	152	927	154	939	104	634				157.4	(30)														11,69,73
		LT			154	939																							
		TL																											
		ST																											
		SL																											
	Ti-6-6-2 (STA)		(B)		(B)		(B)		(B)		17.5	107	.164										152	58	927	354			69,70
	≤.187	L	175	1067	165	1006	165	1006	115	702				169.0	(30)														11,69,73
		LT																											
		TL																											
		ST																											
		SL																											
	Ti-38-6-44 (STA)		(B)		(B)		((B))		((B))		14.8	85	.174										125	43	218	247			
	≤.187	L	185	1128	175	1067	179	1091	115	661				185.0	(30)														69,74
		LT	185	1128	175	1067																							
		TL																											
		ST																											
		SL																											
	Ti-8-8-2-3 (STA)		((B))		((B))		((B))		((B))		(15.4)	88	.175										30	28	423	171			24,69,78,84
	≥.060	L	165	943	150	857	183	1046	105	600				190.0	(30)														
		LT	180	1029	165	943	197	1126																					
		TL														48		274	.102										
		ST																											
		SL																											
	Ti-8-8-2-3 (STOA)		((B))		((B))		((B))		((B))		15.4	88	.175																
	≥.060	L	150	857	140	800	146	834	90	514				149.6	(30)														69,84
		LT														110		629	.61[illegible]										
		TL																											
		ST																											
		SL																											

* Kc or KIc as applicable

( ) Estimated, "B" values based on Actual "S" Values

((B)) Estimated, "B" values based on estimated "S" values

(30) Assumed values for n (0.7 secant stress calculated)

TABLE CXXIII CANDIDATE TITANIUM ALLOYS (Concluded)

Form	Alloy	Dir.	Ftu (KSI)	Ftu/ρ (10^3 inch)	Fty (KSI)	Fty/ρ (10^3 inch)	Fcy (KSI)	Fcy/ρ (10^3 inch)	Fsu (KSI)	Fsu/ρ (10^3 inch)	Ec (10^3 KSI)	Ec/ρ (10^6 inch)	ρ (lb/in^3)	0.7 Secant Stress (KSI)	Shape Factor (n)	Kc* (KSI√in)	KIc	Kc/ρ	(KIc/Fty)^2 (inch)	Stress Corrosion Smooth σth (KSI)	Stress Corrosion Notched KIscc	KIscc/Ec	Fatigue 10^7 Cycles σmax	Fatigue 10^7 Cycles σmax	Fatigue σmax/ρ	Fatigue σmax/ρ	Crack Growth Δa/ΔN	Crack Growth Δa/ρ	References
SHEET	Ti-8-1-1 (Mill Ann)		(B)		(B)		(B)		(B)		18.0	114	.158										106	44**	671	278			69
	.020 to .187	L	150	949	140	886	148	937	96	608				150.9	(30)														5,13,70
		LT	150	949	140	886	148	937																					
		TL														138		.873	.972										
		ST																											
		SL																											
	Ti-6 -1 (Duplex Ann)		(B)		(B)		(B)		((B))		18.0	114	.158										106	44**	671	278			13,69
	.020 to .187	L	140	886	125	791	132	835	92	582				134.1	(30)														
		LT	140	886	125	791	132	835																					
		TL														250		1582	4.00										
		ST																											
		SL																											

* Kc or KIc as applicable

( ) Estimated, "B" values based on Actual "S" Values

((B)) Estimated, "B" values based on estimated "S" values

(30) Assumed values for n (0.7 secant stress calculated)

** Computed

TABLE CXXIV CANDIDATE STEEL ALLOYS

Form	Alloy		Ftu ksi	Ftu/ρ	Fty ksi	Fty/ρ	Fcy ksi	Fcy/ρ	Fsu ksi	Fsu/ρ	Ec	Ec/ρ	ρ	0.7 secant stress ks	Shape factor (n)	Kc	KIc	KIc/ρ	Stress corrosion				Fatigue				Crack growth		References
SHEET	PH 15-7 (RH 950)		(B)		(B)		((B))		((B))		30.0	106	.277										72	36	240	130			85,86
	.01 to .187	L	235	844	215	758	218	786	148	534					(10.3)														
		LT																											
		TL																											
		ST																											
		SL																											
	Marage 250		(B)		(B)		((B))		((B))		28.5	95	.300																
	.01 to .187	L	260	867	250	833			146	483						128		427	262										13,86
		LT																											
		TL																											
		ST																											
		SL																											
OTHER WROUGHT PRODUCTS	HP-9-4-.30		(B)		((B))		((B))		((B))		29.6	104	.284											52		183			
		L	225	792	190	669	211	743	162	500				217.5 (15)															87,88
		LT																									30	106	
		TL															105	375	325										
		ST																		198									
		SL																			30	1.01							
	Marage 250		(B)		((B))		((B))		((B))		28.5	95	.300										75	36	250	120			
		L	255	850	245	817			145	483																			11,13,88
		LT															80	267	102								38	127	
		TL																											
		ST																											
		SL																			40	1.40							
	300M		(B)		((B))		((B))		((B))		29.0	102	.283										166	65	508	230			
		L	280	989	232	820	242	855	170	601				252.3 (15)															5,13,90
		LT															60	212	067										
		TL															60	212											
		ST																		140									
		SL																			15	.517							

* Kc or KIc as applicable

( ) Estimated, ρ' values based on Actual 'S' Values

((B)) Estimated, 'S' values based on estimated 'S' values

(20) Assumed values for 'n' (0.7 secant stress calculated)

TABLE CXXIV CANDIDATE STEEL ALLOYS (Concluded)

Form	Alloy		Ftu ksi	Ftu/ρ	Fty ksi	Fty/ρ	Fcy ksi	Fcy/ρ	Fsu ksi	Fsu/ρ	Ec	Ec/ρ	ρ	0.7 secant stress ks	Shape factor (n)	Kc	KIc	KIc/ρ	Stress corrosion				Fatigue				Crack growth		References
OTHER WROUGHT PRODUCTS	HP 310		((B))		((A))		((B))		((B))				(.283)																
		L	305	1078	260	919	270	954	185	654																			91,92
		LT															57	201											
		TL															51	180											
		ST																											
		SL																											
		TS															52	184											
		L																											
		LT																											
		TL																											
		ST																											
		SL																											
		L																											
		LT																											
		TL																											
		ST																											
		SL																											
		L																											
		LT																											
		TL																											
		ST																											
		SL																											
		L																											
		LT																											
		TL																											
		ST																											
		SL																											

* Kc or KIc as applicable

( ) Estimated, ρ' values based on Actual 'S' Values

((B)) Estimated, 'S' values based on estimated 'S' values

(20) Assumed values for 'n' (0.7 secant stress calculated)

TABLE CXXV CANDIDATE BERYLLIUM ALLOYS																													
FORM	ALLOY		F_{tu} KSI	F_{tu}/ρ	F_{ty} KSI	F_{ty}/ρ	F_{cy} KSI	F_{cy}/ρ	F_{su} KSI	F_{su}/ρ	E_c	E_c/ρ	ρ	SECANT STRESS KSI	SHAPE FACTOR (n)	K_c	K_{Ic}	K/ρ	$(K/F_{ty})^2$	STRESS CORROSION SMOOTH	NOTCHED	NOTCHED	FATIGUE	FATIGUE	FATIGUE	FATIGUE	CRACK GROWTH	CRACK GROWTH	REFERENCES
SHEET	PS 20 or SR 200E		B		B		((B))		((B))		42.0	627	.067										(63)	(42)	940	627			5,93
	.050 to .069	L	72	1045	50	746	52	776	37	552				48.5	(20)														94,95,96 97
		LT	70	1045	50	746	52	776									18**	269	.130								23	312	
		TL																											
		ST																											
		SL																											
	HIP PRESSED BLOCK		((B))		((B))		((B))				42.0	627	.067																98,99
		L	60	896	40	597	40	597						36.8	(20)														
		LT	60	896	40	597	42	597									(18)**	263	.130										
		TL																											
		ST																											
		SL																											

* K_c or K_{Ic} as appropriate

( ) Estimated, "B" values based on actual "S" values

((B)) Estimated, "C" values based on estimated "S" values

(20) Assumed values for "n" (0.7 secant stress calculated)

** Some uncertainty whether this is Kc or KIc.

TABLE CXXVI CORRELATION OF STEEL MATERIAL PROPERTIES														
MATERIAL		F_{tu} (KSI)		B-A	F_{ty} (KSI)		B-A	F_{cy} (KSI)		B-A	F_{su} (KSI)		B-A
ALLOY	H.T.	A	B	(KSI)	A	B	(KSI)	A	B	(KSI)	A	B	(KSI)
PH 13-8 Mo	H950	213	219	6	190	201	11						
PH 13-8 Mo	H1000	195	205	10	187	197	10						
9Ni-4Co-.45C	Baintic	257	262	5	212	218	6	236	242	6	152	155	3
PH 14-8 Mo	SRH 950	209	220	11	190	202	12						
PH 14-8 Mo	SRH1050	190	201	11	189	192	12						
17-7 PH	TH1050	177	184	7	150	169	19	158	178	20	115	120	5
AISI 301	1/2 Hard	141	151	10	93	110	17	63	72	9	77	82	5

For the purposes of this study, a fatigue correlation analysis has been assumed to estimate the stress at R = 0 when only R =0.1 data is available. Several titanium alloys were studied to determine a trend in ratios for stress levels at R =0.1 and R = 0. The fatigue data was obtained from constant life charts in the MIL-HDBK-5 document. The data were normalized to the value at R = 0.1. The results are in Table CXXVII. The ratios shown for the various alloys, whether annealed or STA, will be applied to the same class of material alloys to determine stress at R = 0. Since the material in question is a Beta alloy, graphs were made of a similar Beta alloy for annealed and for STA conditions for values of K_t =1.0 and K_t = 3.0. The graphs are presented in Figures 194 and 195, respectively. The fatigue data for Ti-8Mo-8V-2Fe-3Al, in the STA condition, was ratioed by the factors indicated and included in the final report. The values so calculated are in Table CXXIII.

A second method that can be used to obtain values for maximum stress at R = 0 when data is given for other values of R is as follows: construct a constant life (Goodman) diagram as shown in Figure 196; use three data points; 1) tension ultimate, 2) compression yield and 3) the maximum stress at applicable value of R, to define the curve as shown. The value of maximum stress for R = 0 may then be obtained.

The tangent modulus is an important material data that is used in all column and panel compression strength allowable analyses. This data is very sparse and those available are mostly typical curves. The stress/strain curves, in conjunction with tangent modulus curves, are all plotted as typical values in MIL-HDBK-5. This, by definition, does not agree with the "B" values that are listed in the tables. One example of this is shown in Figure 197 for 7075-T6511 extrusion material.

Both curves, in Figure 197, were plotted with the same value for the shape factor "n" as determined from the typical stress/strain charts by the Ramberg-Osgood equation. However, the equation was modified to use the secant modulus of the compression yield in lieu of the 0.7 secant modulus. Likewise, the second data point was at a secant modulus half way between the elastic modulus and the compressive yield secant modulus. This is shown on Figure 198. This modification changes the value of the constant in the equation for strain and the equation to determine the shape factor.

The reason for the equation modification was to obtain a better mathematical fit of the stress/strain curves. Some of the available curves ended before the 0.7 secant stress value, and others had compression yield stress values somewhat removed from the 0.7 secant stress.

The Ramberg-Osgood basic equation for strain is

$$\epsilon = \frac{\sigma}{E} + K(\sigma)^n \qquad (50)$$

and by choosing two sets of known coordinates of stress and strain from a curve, the values of "K" and "n" can be determined as follows:

From equation (50)

$$K = \frac{\epsilon - \sigma/E}{\sigma^n} \qquad (51)$$

TABLE CXXVII TITANIUM FATIGUE DATA CORRELATION										
ALLOY	K_t	σ AT $N = 10^5$					$\sigma_t / \sigma_{R=.1}$			
		R					R			
		-.2	0	.1	.2	.4	-.2	0	.2	.4
Ti-8-1-1 Sheet	1.0	94	105	110	115	124	.855	.955	1.045	1.127
Ti-4-3-1 Sheet (Sta)	1.0	87	95	99	104	116	.879	.960	0.051	1.172
Ti-6-4 Bar	1.0	111	118	122	126	131	.910	.967	1.033	1.074
Ti-6-4 Sheet	1.0	104	112	117	122	132	.889	.957	1.043	1.128
Ti-13-11-3 Sheet (Ann)	1.0	66	74	78	83	95	.846	.945	1.064	1.218
Ti-13-11-3 Sheet (Sta)	1.0	56	60	63	67	78	.889	.952	1.063	1.238
Ti-8-1-1 Sheet	2.57	44	50	53	57	68	.830	.943	1.075	1.283
Ti-4-3-1 Sheet (Sta)	2.82	55	59	62	65	73	.887	.952	1.048	1.177
Ti-6-4 Bar	3.30	63	69	72	76	84	.875	.944	1.056	1.167
Ti-6-4 Sheet	2.82	50	53	56	60	72	.893	.946	1.071	1.286
Ti-13-11-3 Sheet (Ann)	3.00	28	32	34	37	46	.824	.941	1.088	1.353
Ti-13-11-3 Sheet (Sta)	3.00	28	30	32	34	38	.875	.938	1.063	1.188

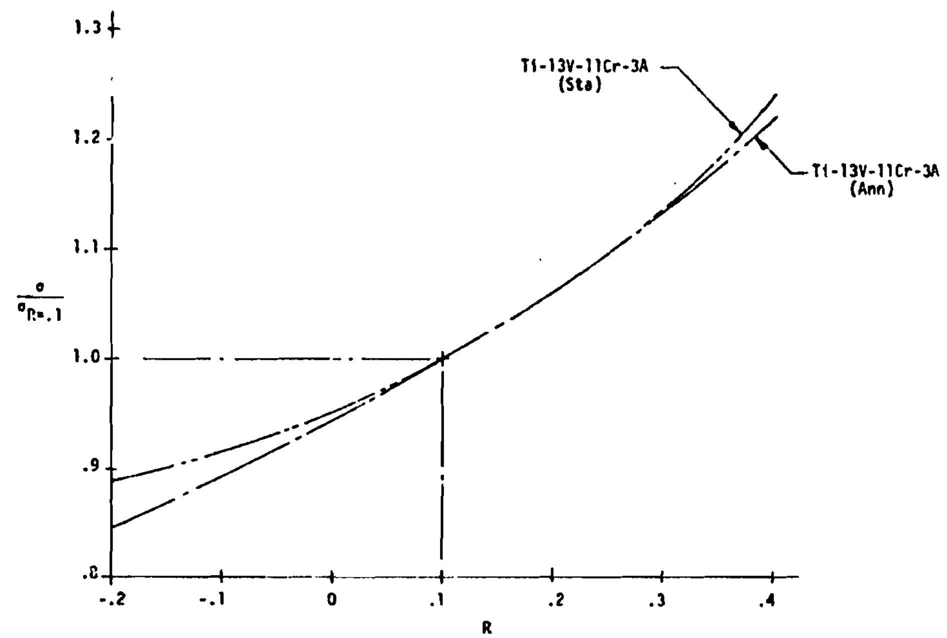

Figure 194 BETA TITANIUM FATIGUE DATA CORRELATION (K_t = 1.0)

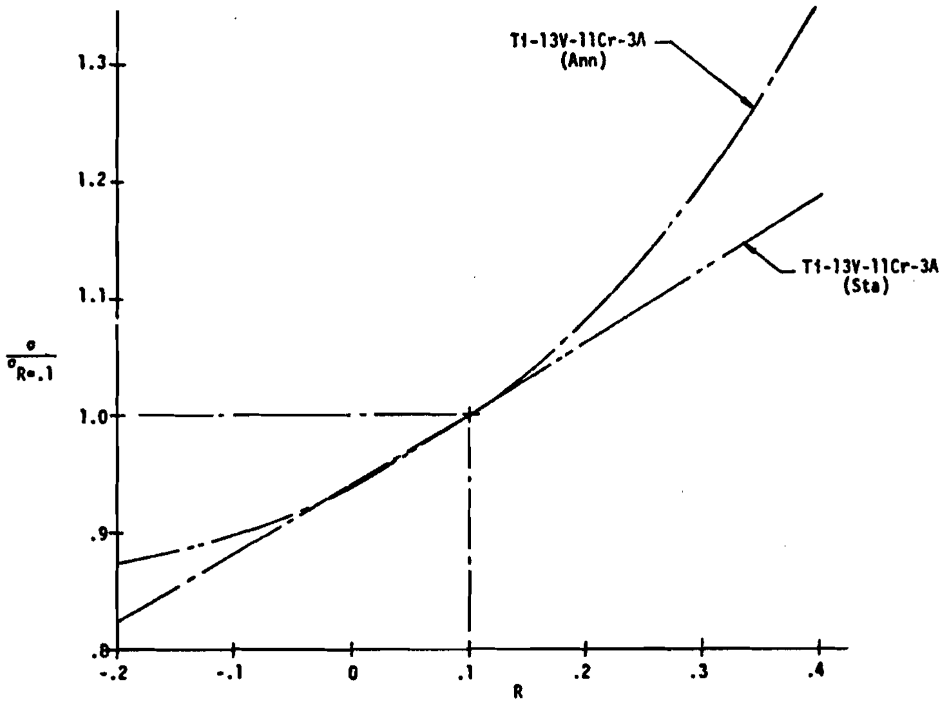

Figure 195 BETA TITANIUM FATIGUE DATA CORRELATION (K_t = 3.0)

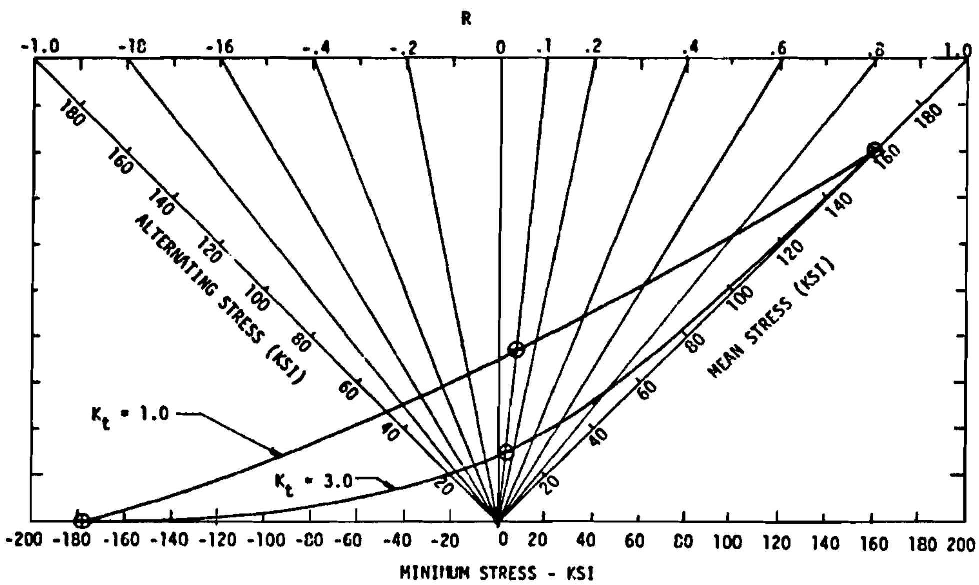

Figure 196 CONSTANT LIFE DIAGRAM TO DETERMINE MAXIMUM STRESS FOR R = 0

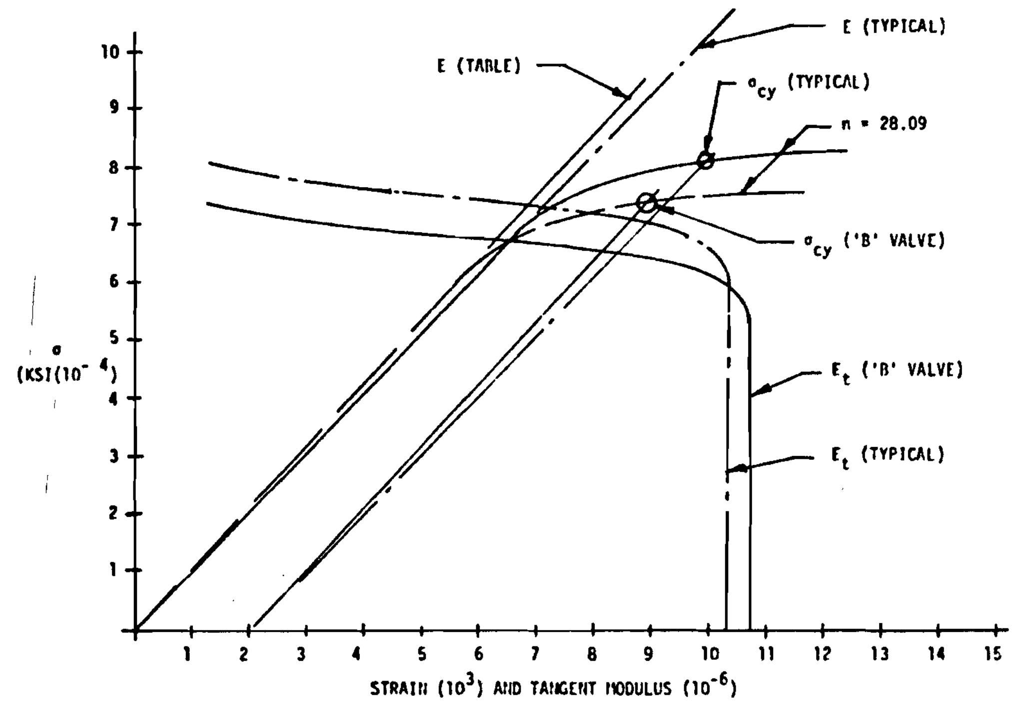

Figure 197 "B" VALUE STRESS/STRAIN DIAGRAM DEVELOPMENT (7075-T6511 EXTRUSION)

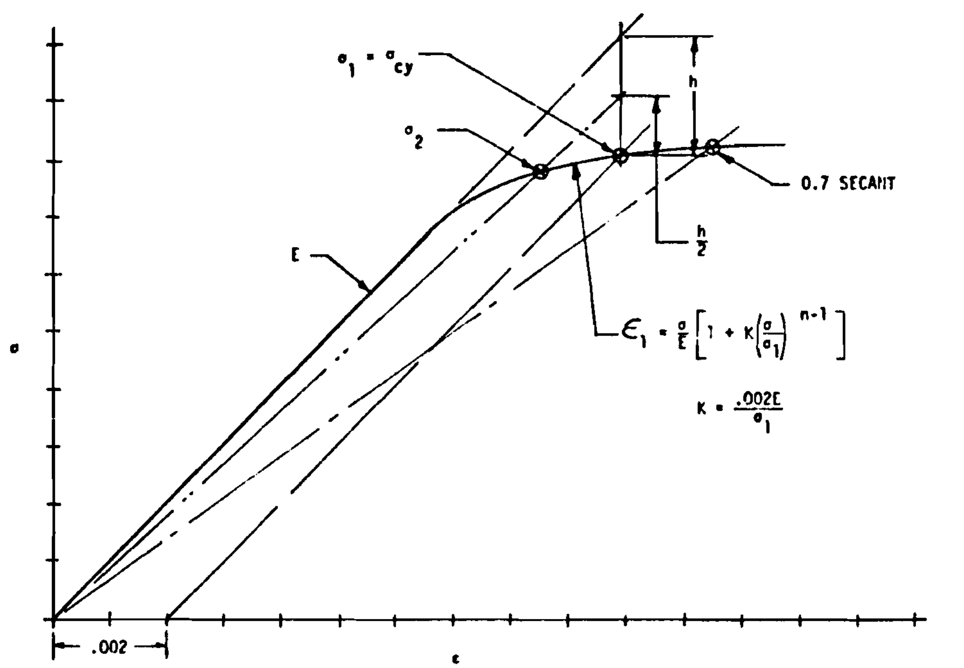

Figure 198 COMPRESSIVE STRESS/STRAIN DATA BY MODIFIED RAMBERG-OSGOOD EQUATION

Let (σ_1, ϵ_1) define the set of coordinates for compression yield such that

$$\sigma = \sigma_1 = X_1 E \epsilon_1 \text{ and } \epsilon = \epsilon_1 = \frac{\sigma_1}{X_1 E}$$

then
$$K = \frac{\sigma_1}{E(\sigma_1)^n} \left(\frac{1-X_1}{X_1}\right) \tag{52}$$

and equation (50) becomes

$$\epsilon = \frac{\sigma}{E} + \left(\frac{1-X_1}{X_1}\right) \left(\frac{\sigma_1}{E}\right) \left(\frac{\sigma}{\sigma_1}\right)^n \tag{53}$$

Let (σ_2, ϵ_2) define the second set of coordinates whose secant modulus is midway between the compression yield secant modulus and the elastic modulus such that $\sigma = \sigma_2 = X_2 E \epsilon_2$ and $\epsilon = \epsilon_2 = \sigma_2 / X_2 E$. These values substituted into equation (53) give

$$\frac{\sigma_2}{X_2 E} = \frac{\sigma_2}{E} + \left(\frac{1-X_1}{X_1}\right) \left(\frac{\sigma_1}{E}\right) \left(\frac{\sigma_2}{\sigma_1}\right)^n \tag{54}$$

or

$$\frac{\sigma_2}{E} \left(\frac{1-X_2}{X_2}\right) = \left(\frac{1-X_1}{X_1}\right)\left(\frac{\sigma_1}{E}\right)\left(\frac{\sigma_2}{\sigma_1}\right)^n \tag{55}$$

since, by definition, the secant modulus of the second data point is midway between the elastic and compression yield modulii, the relation of X_2 to X_1 is

$$X_2 = \frac{1+X_1}{2}$$

and this value substituted into equation (55) gives

$$\left(\frac{\sigma_1}{\sigma_2}\right) = \frac{1+X_1}{X_1} \left(\frac{\sigma_1}{\sigma_2}\right) \tag{56}$$

The value of "n" is then obtained from equation (56) by taking the log of both sides to give

$$n = 1 + \left[\text{LOG} \left(\frac{1+X_1}{X_1}\right) \Big/ \text{LOG} \left(\frac{\sigma_1}{\sigma_2}\right)\right] \tag{57}$$

which is the Ramberg-Osgood equation. The value of X_1 is determined from the strain at compression yield as follows:

$$\epsilon_{\sigma_1} = 0.002 + \frac{\sigma_1}{E} = \frac{\sigma_1}{X_1 E} \tag{58}$$

from which

$$X_1 = \frac{\sigma_1}{0.002E + \sigma_1} \tag{59}$$

and substituting this into equation (53) gives

$$\epsilon = \left(\frac{\sigma}{E}\right)\left[1 + \left(\frac{0.002E}{\sigma_1}\right)\left(\frac{\sigma}{\sigma_1}\right)^{n-1}\right] \tag{60}$$

and into equation (57) gives

$$n = 1 + \left[\mathrm{LOG}\left(\frac{0.002E}{\sigma_1} + 2\right) \Big/ \mathrm{LOG}\left(\frac{\sigma_1}{\sigma_2}\right)\right] \tag{61}$$

The equation for the tangent modulus is then

$$E_t = E_c \Big/ \left[1 + \left(\frac{0.002E}{\sigma_1}\right)(n)\left(\frac{\sigma}{\sigma_1}\right)^{n-1}\right] \tag{62}$$

The values for the 0.7 secant stress, as listed in the material properties Tables X, XI, and CXXII thru CXXV were calculated by the following method: Equate the basic stress/strain curve and the 0.7 secant modulus line thus

$$\epsilon = \epsilon_{0.7} = \frac{\sigma_{0.7}}{0.7E} = \frac{\sigma_{0.7}}{E}\left[1 + \frac{0.002E}{\sigma_1}\left(\frac{\sigma_{0.7}}{\sigma_1}\right)^{n-1}\right] \tag{63}$$

and solving for $\sigma_{0.7}$ as follows:

$$1 = 0.7 + 0.7\left(\frac{0.002E}{\sigma_1}\right)\left(\frac{\sigma_{0.7}}{\sigma_1}\right)^{n-1} \tag{64}$$

or

$$(n-1)\ (\mathrm{LOG}\ \sigma_{0.7} - \mathrm{LOG}\ \sigma_1) = \mathrm{LOG}\left(\frac{3\sigma_1}{0.014E}\right) \tag{65}$$

from this

$$\mathrm{LOG}\ \sigma_{0.7} = \mathrm{LOG}\ \sigma_1 + \frac{\mathrm{LOG}\left(\frac{3\sigma_1}{0.014E}\right)}{n-1} \tag{66}$$

then

$$\sigma_{0.7} = 10^{\left(\mathrm{LOG}\ \sigma_1 + \frac{\mathrm{LOG}\ (3\sigma_1/0.014E)}{n-1}\right)} \tag{67}$$

The search for valid stress/strain curves has not produced the desired data base for determining the compressive tangent modulus for the various materials.

An attempt was made to determine if a pattern existed for values of the shape factor "n" for aluminum. This was based on all the compressive stress/strain curves included in MIL-HDBK-5. The results of the study are listed in Table CXXVIII. The values shown are taken from typical curves. The values for the shape factor range approximately from 11 to 56. It should be noted that the elastic compressive modulus taken from the typical curves differs from the values found in the table for several of the alloys.

A study was made to determine the impact of the shape factors on the weight of a stiffened skin compression panel. The equation for column stability is:

$$\frac{F_c}{E_t} = \frac{\pi^2}{(L'/\rho)^2} \tag{68}$$

The term F_c/E_t is the material property data and is obtained from a tangent modulus curve as shown in Figure 199. Various combinations of F_c and E_t are possible, depending on the shape factor used, for each F_c/E_t ratio. As noted, the highest value for F_c occurs with the highest shape factor; hence, less panel weight is possible when the material modulus curve shape factor is as large as possible. A series of computer runs were made to determine the weight variations for integrally stiffened skins made from 7050-T7651 plate and assuming values for the shape factor of 10, 20, 30, 40 and 50. The results are listed in Table CXXIX. The weights were normalized to the "n" = 20 and are plotted in Figure 200. The range in weight differences is some ±3.5% around the normal n = 20. Consequently, the shape factor for all aluminum alloys that were not available will be 20 for this study. Stress/strain curves were drawn by an in-house computer program for each of the materials and are found in Figure 201. The values for the shape factor "n" for titanium, steel and beryllium were estimated by the same type of analysis.

Therefore, unless specific values for "n" were calculated from stress/strain data curves, the values are 10 and 30, respectively, for titanium and steel. The shape factor used for beryllium was 20. The stress/strain curves for each are found in Figures 202 through 204, respectively.

TABLE CXXVIII RAMBERG-OSGOOD SHAPE FACTOR COMPARISON

MATERIAL	FORM	E * $10^{(-6)}$ PSI	E + $10^{(-6)}$ PSI	F_{cy} (KSI)	F_2 (KSI)	n
7075-T6 o	Sheet	10.5	10.0	66	61	11.59
7075-T651 o	Plate	10.6	10.0	66	61	11.59
7075-T6	Extr	10.7	10.2	81	78	22.51
7075-T6	Bar	10.5	10.1	70	65	12.17
7075-T651	Plate	10.6	10.6	76	71.5	14.49
7075-T62	Plate	-	10.5	80.5	77	19.35
7075-T7351	Extr	10.7	10.4	66	65	56.00
7079-T651	Plate	10.6	10.4	74	72.5	41.27
7079-T62	Plate	-	10.5	72	70	30.44
7178-T6	Sheet	10.5	10.3	79.5	74.5	13.55
7178-T62	Plate	-	10.5	88	85	24.24
7178-T6 o	Plate	-	9.7	72	67	12.39
7475-T761	Sheet	-	10.5	68	65	19.55

* From Table CXXII + From Chart o Clad

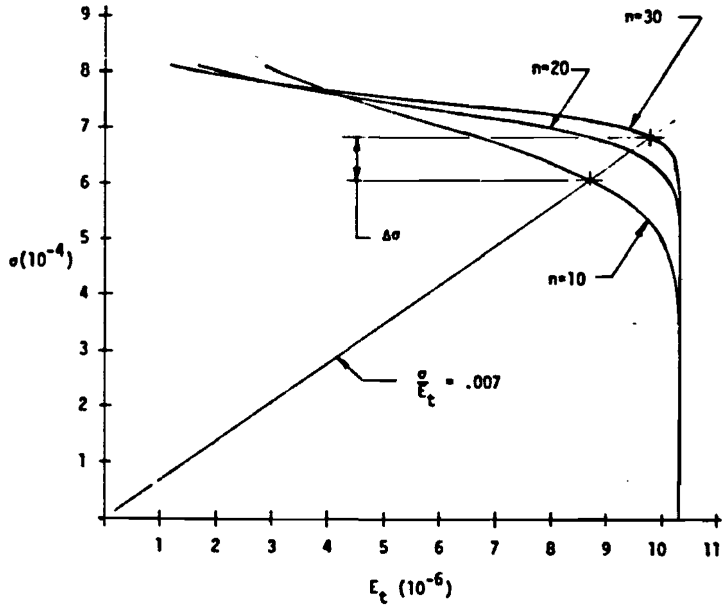

Figure 199 TANGENT MODULUS CURVES FOR VARIOUS VALUES OF "n"

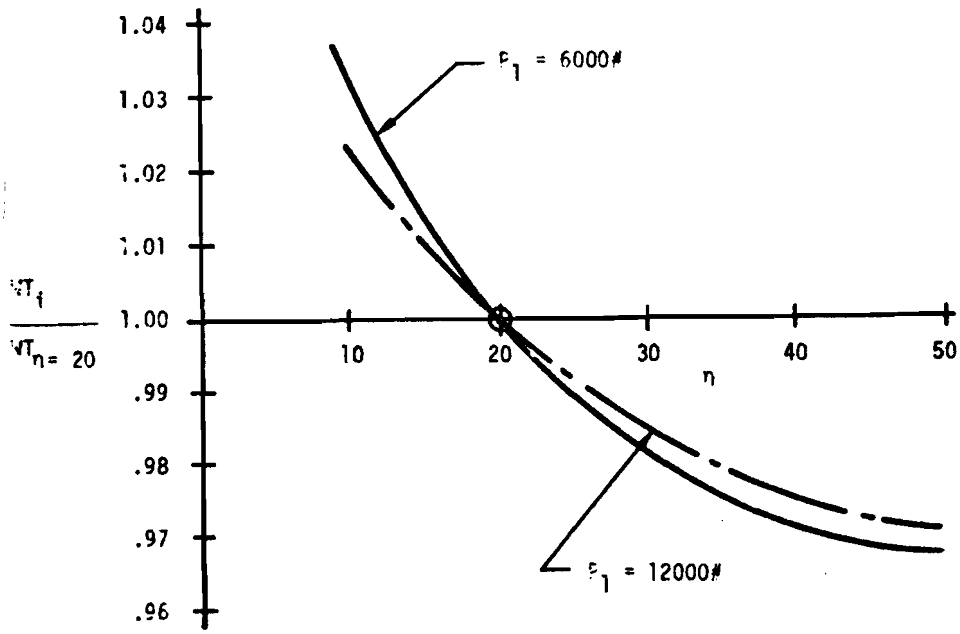

Figure 200 EFFECT ON PANEL WEIGHT DUE TO VARIOUS VALUES OF SHAPE FACTOR 'n'

TABLE CXXIX COMPRESSION PANEL WEIGHT COMPARISON					
LOAD P_i (#/IN)	LENGTH (IN)	SHAPE FACTOR 'n'	STRESS (PSI)	WEIGHT $\#/FT^2$	$\frac{WT_i}{WT_{n=20}}$
6000	24.5	10	41500	2.082	1.0327
↕		20	42860	2.016	1.0000
↕		30	43660	1.979	0.9816
↕		40	44100	1.959	0.9717
6000		50	44300	1.951	0.9678
12000		10	54800	3.154	1.0227
↕		20	56000	3.084	1.0000
↕		30	56900	3.037	0.9849
↕		40	57400	3.008	0.9753
12000		50	57700	2.994	0.9708

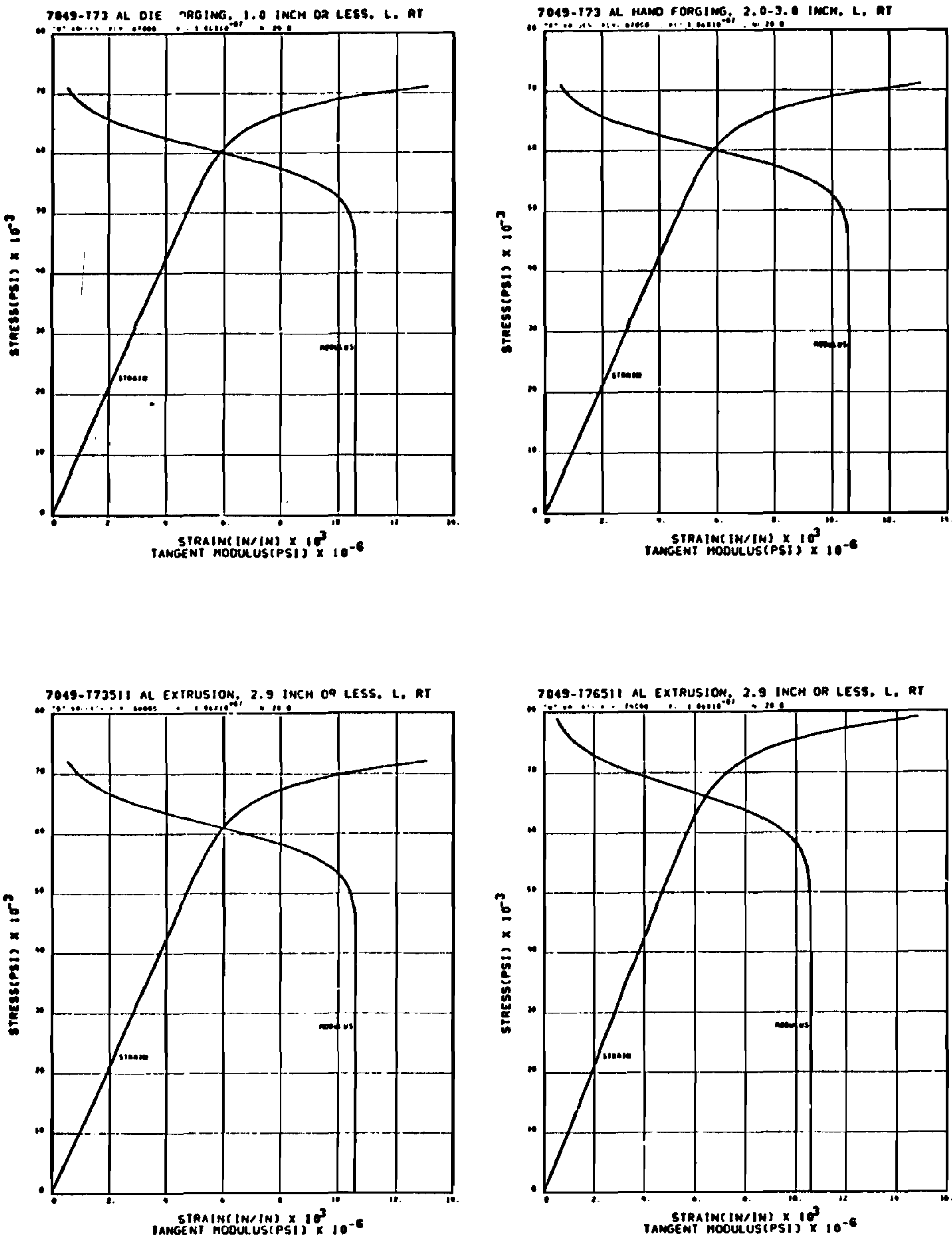

Figure 201 STRESS-STRAIN CHARTS FOR ALUMINUM

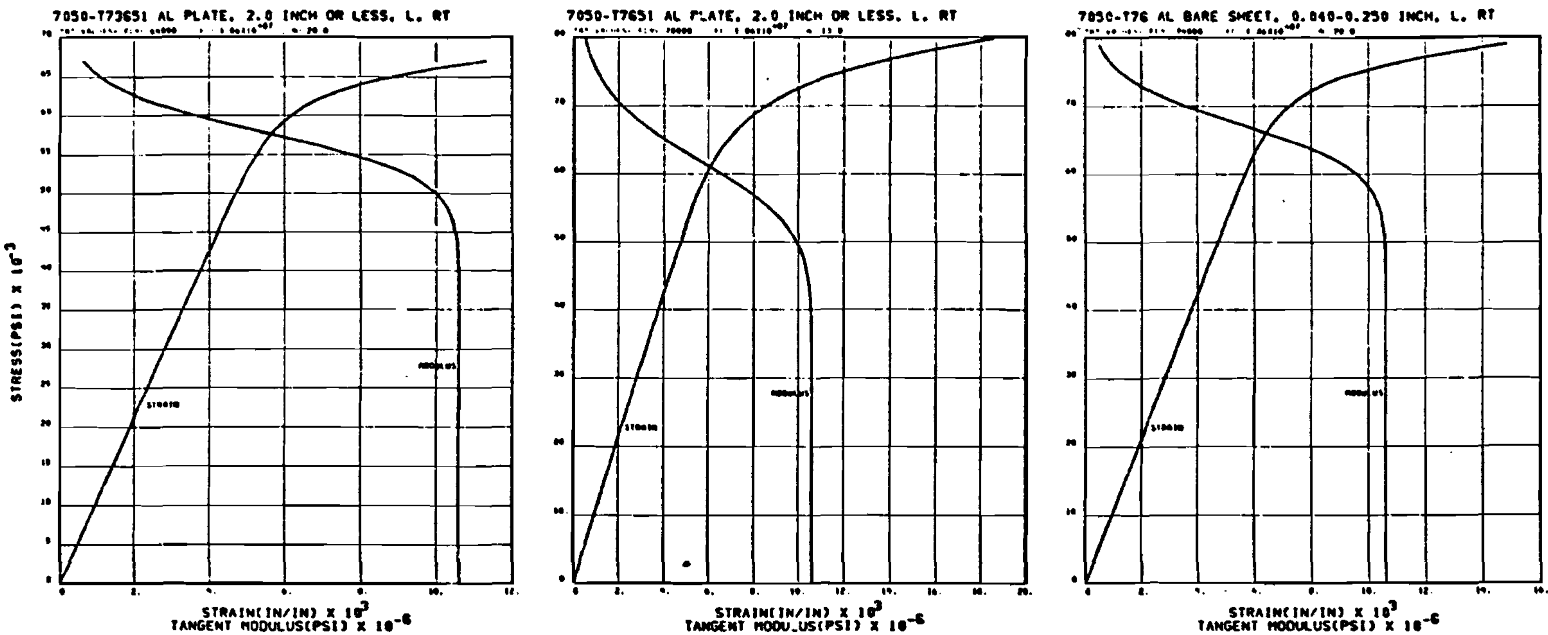

Figure 201 STRESS-STRAIN CHARTS FOR ALUMINUM -- Continued

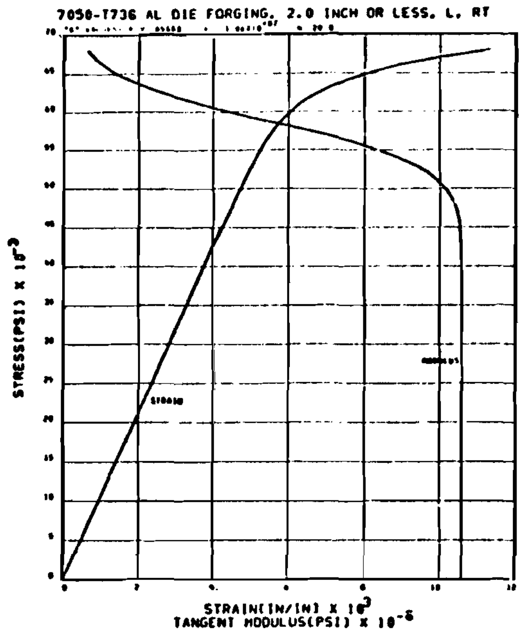

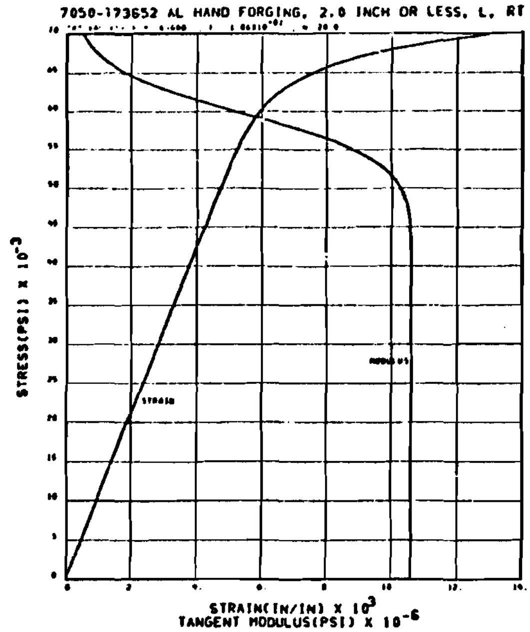

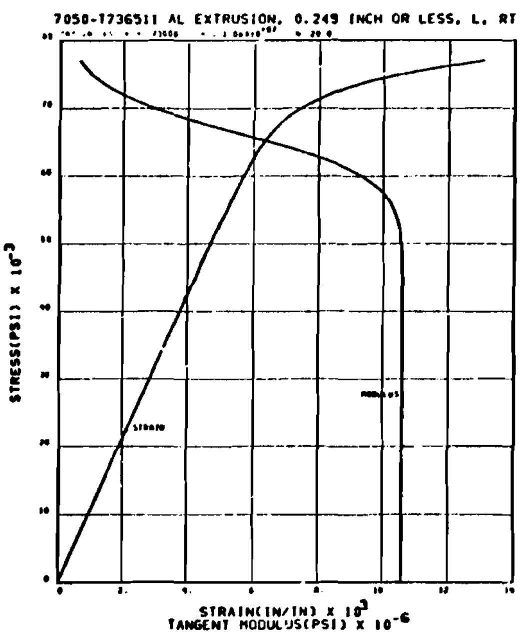

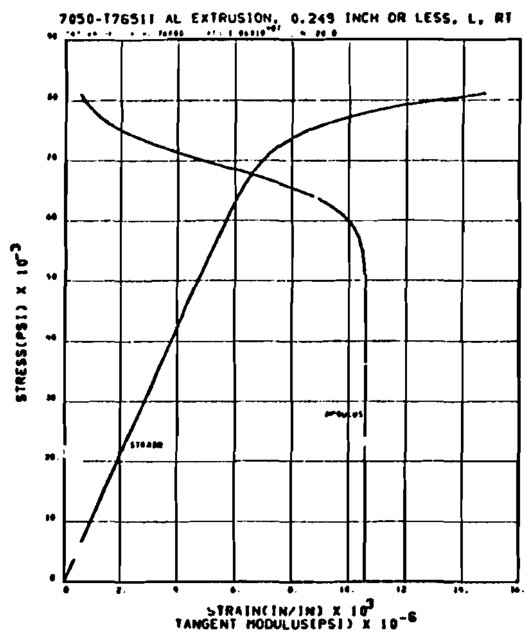

Figure 201 STRESS-STRAIN CHARTS FOR ALUMINUM -- Continued

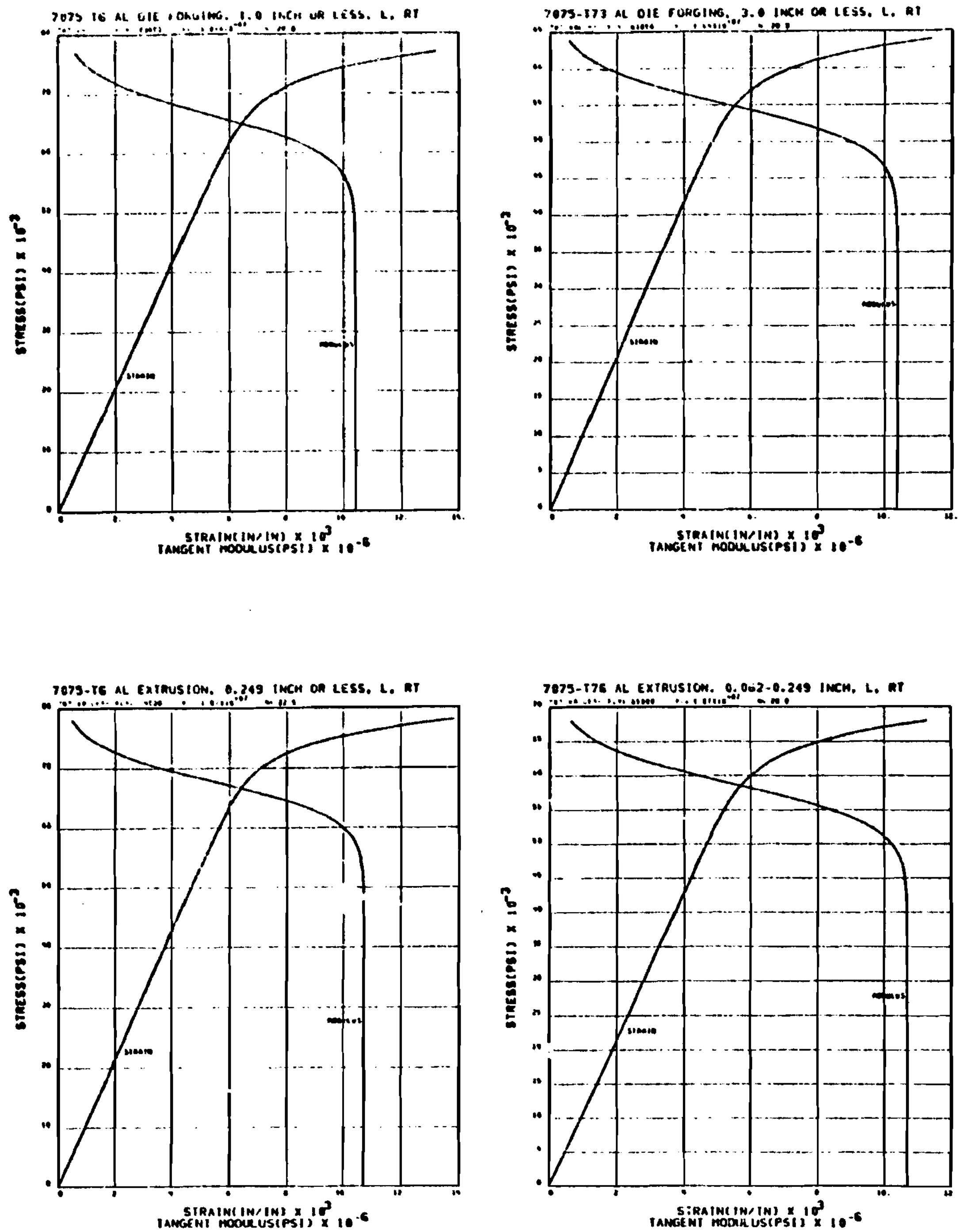

Figure 201 STRESS-STRAIN CHARTS FOR ALUMINUM -- Continued

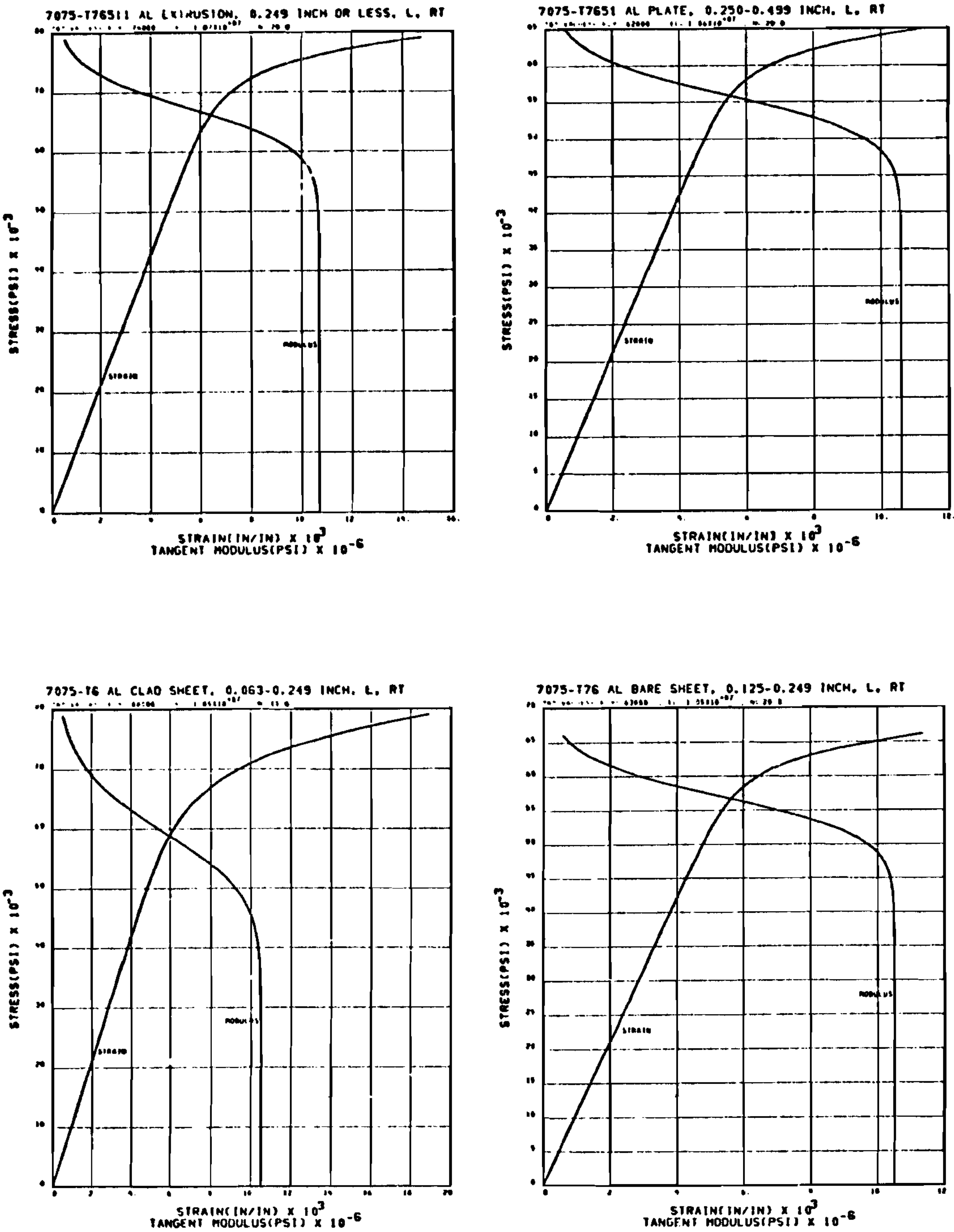

Figure 201 STRESS-STRAIN CHARTS FOR ALUMINUM -- Continued

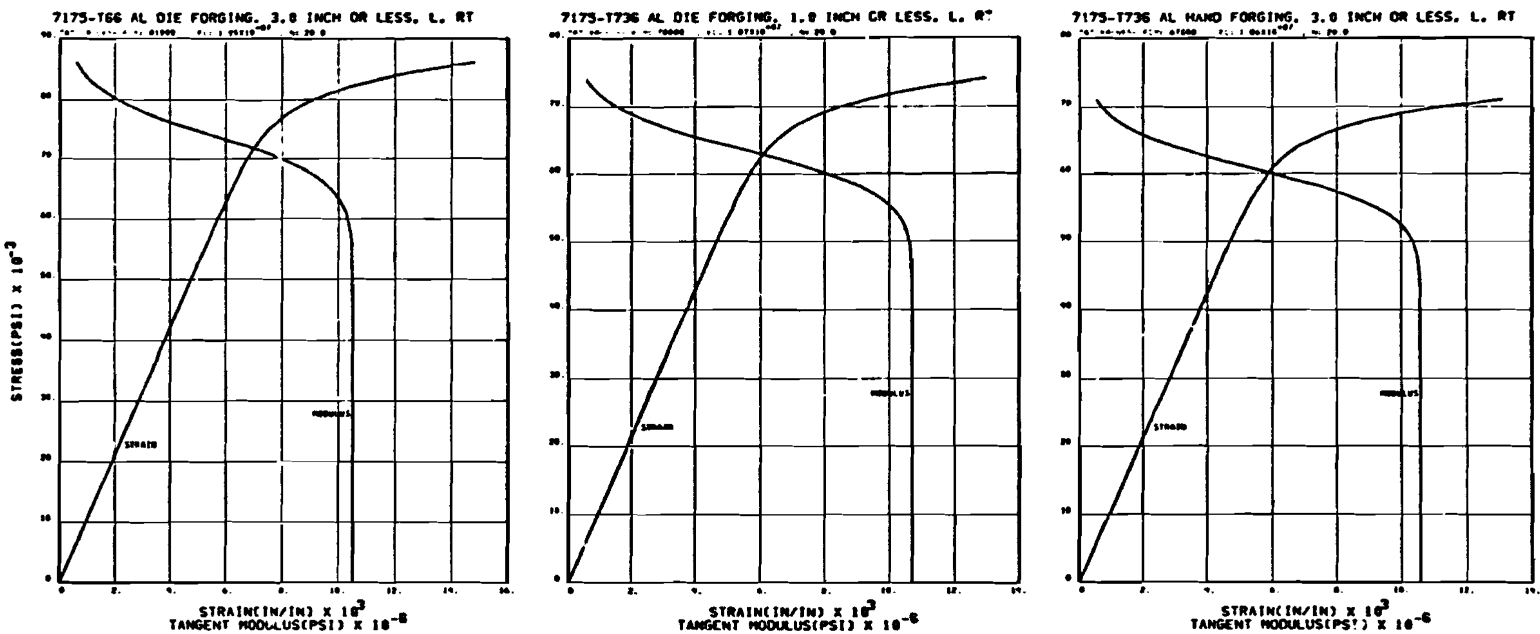

Figure 201 STRESS-STRAIN CHARTS FOR ALUMINUM -- Continued

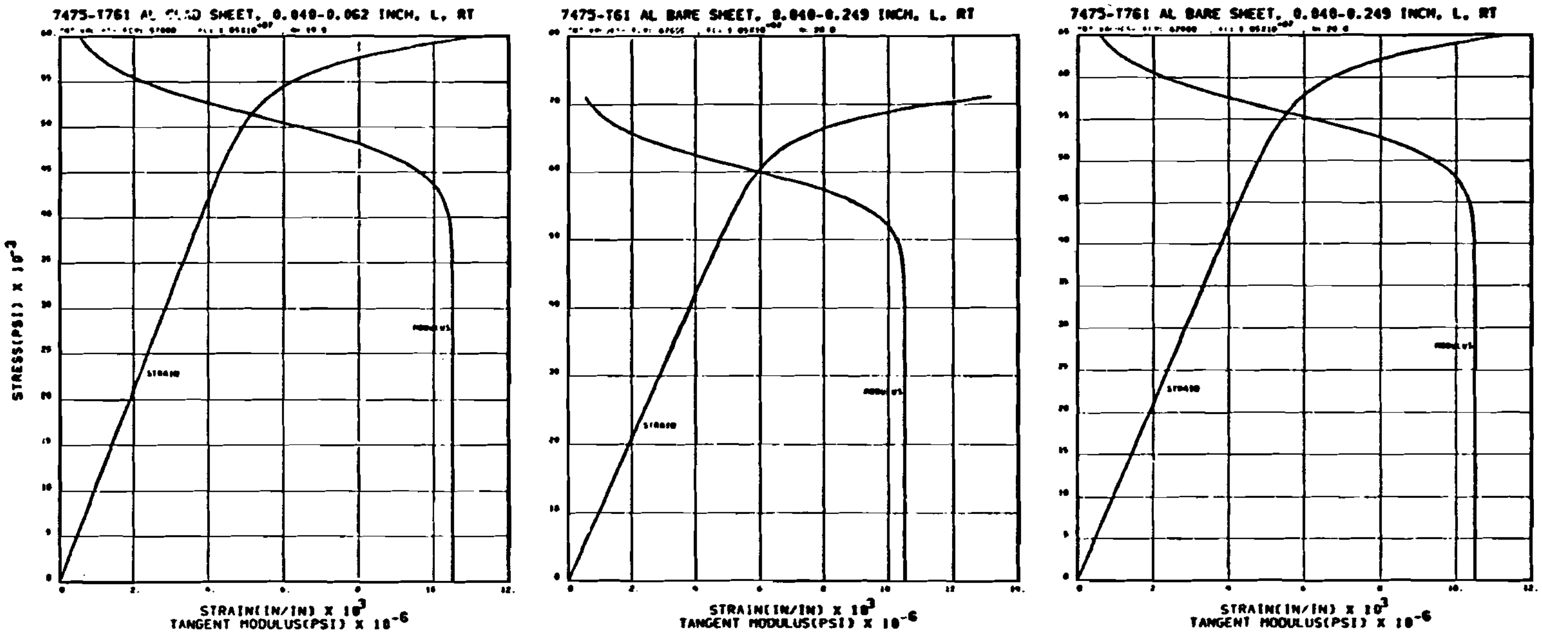

Figure 201 STRESS-STRAIN CHARTS FOR ALUMINUM -- Continued

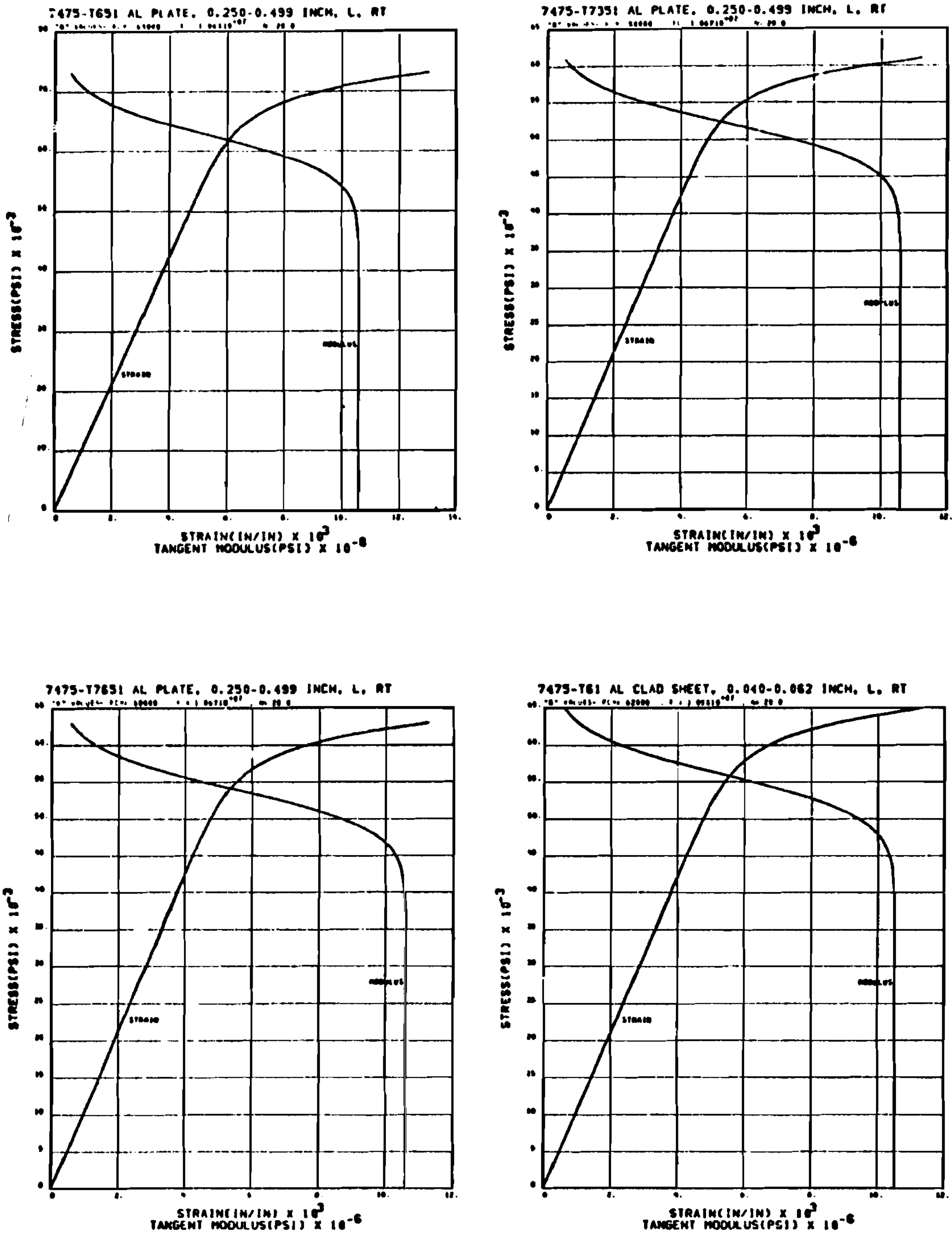

Figure 201 STRESS-STRAIN CHARTS FOR ALUMINUM -- Concluded

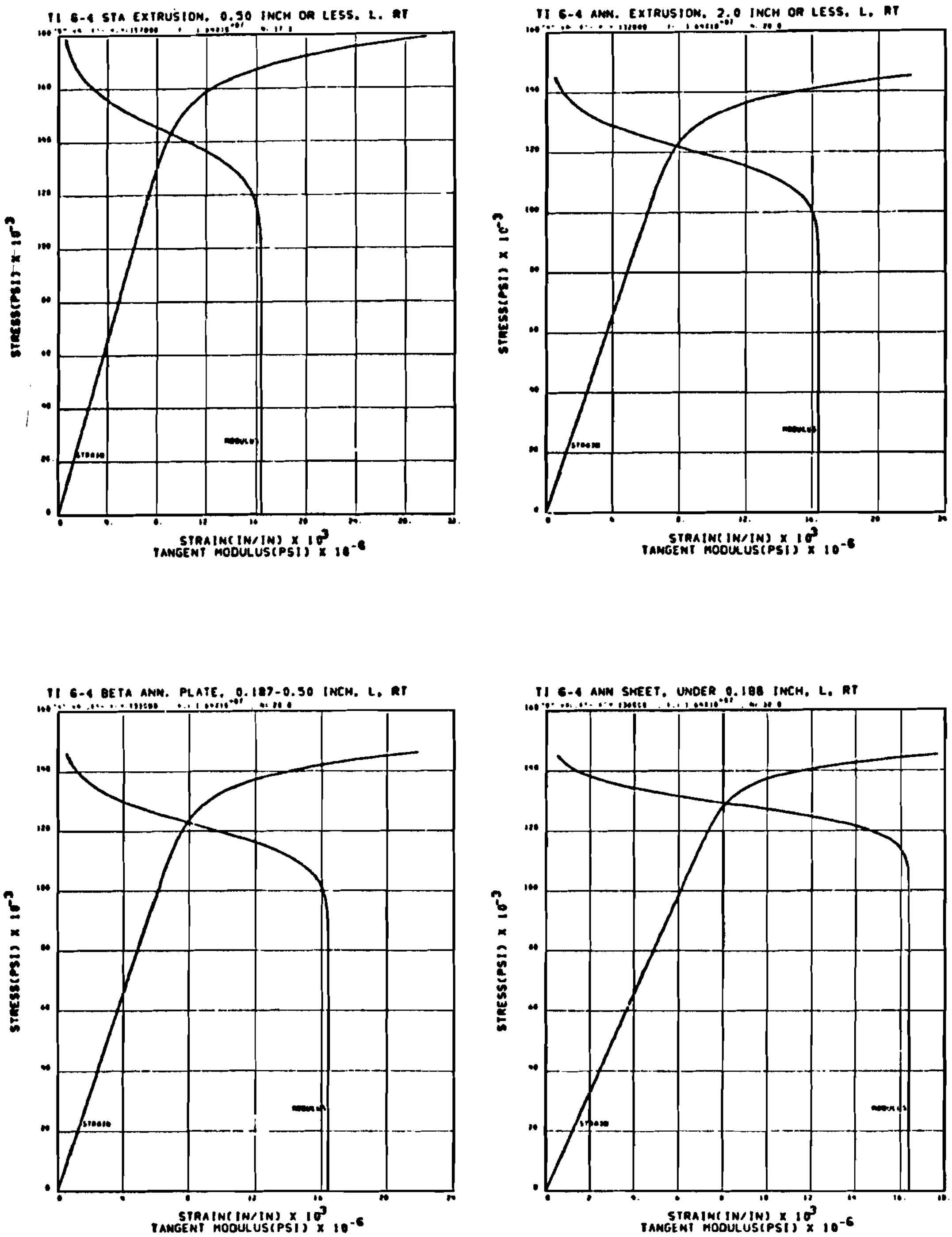

Figure 202 STRESS-STRAIN CHARTS FOR TITANIUM

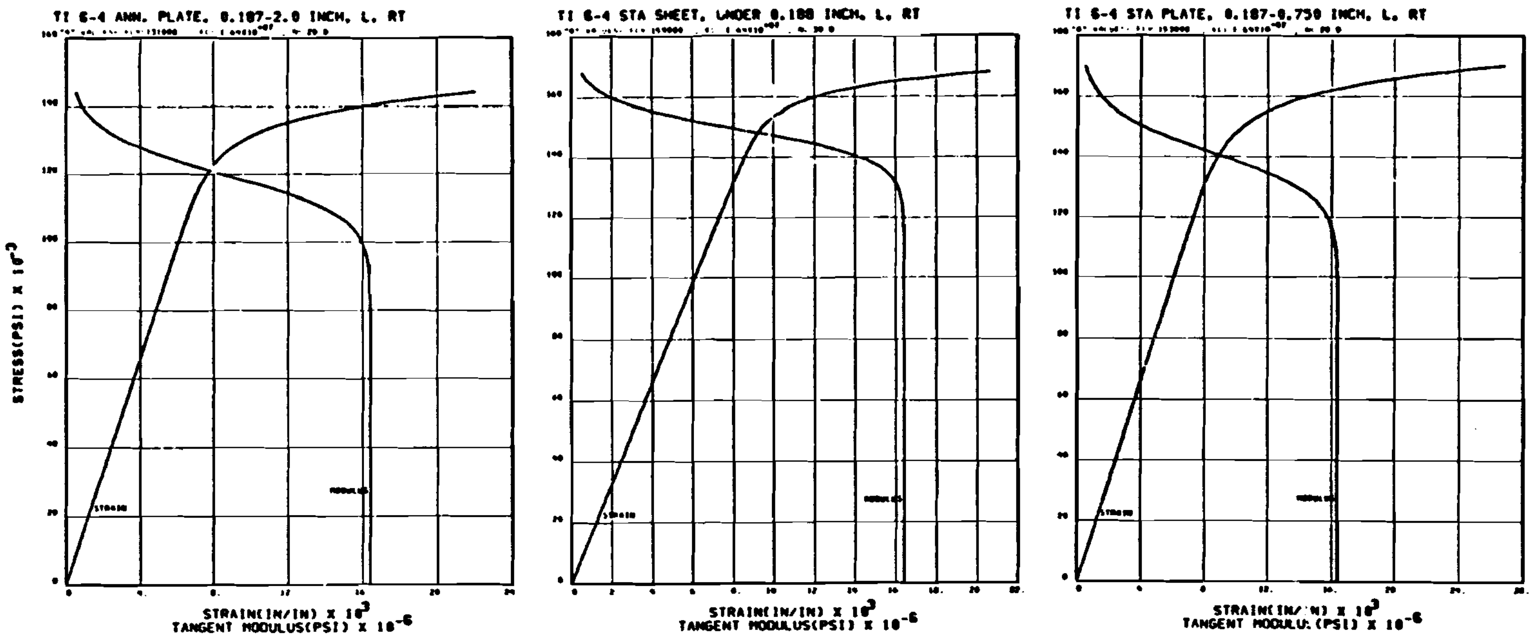

Figure 202 STRESS-STRAIN CHARTS FOR TITANIUM -- Continued

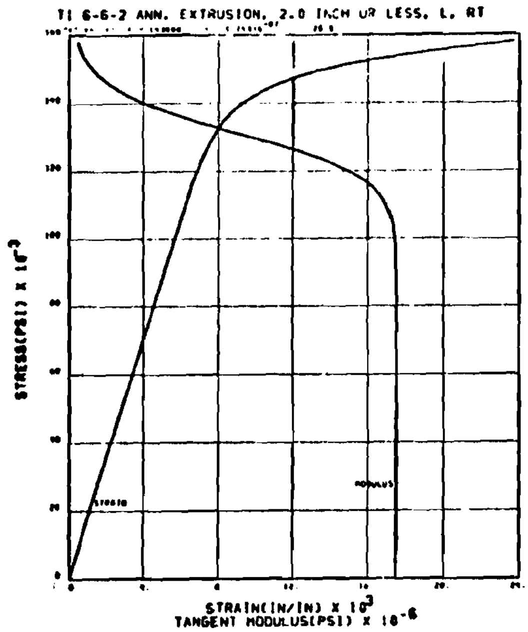

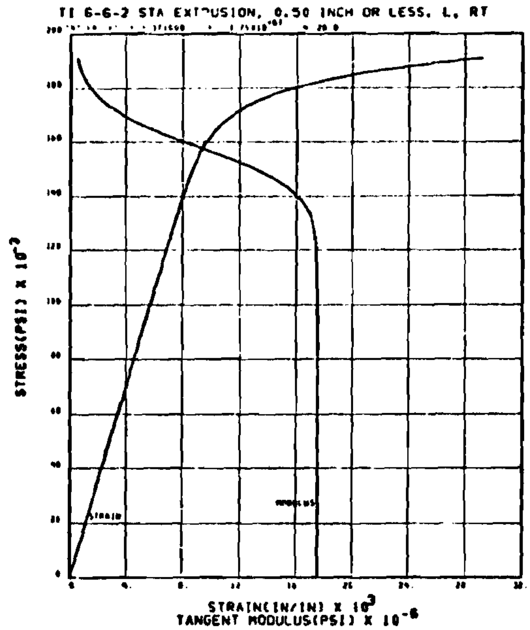

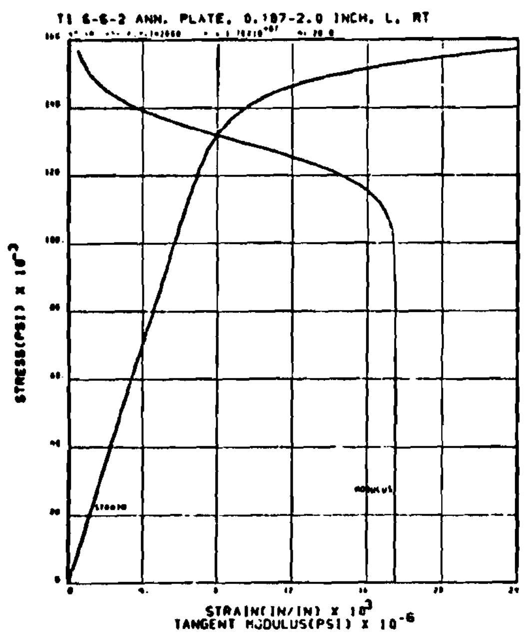

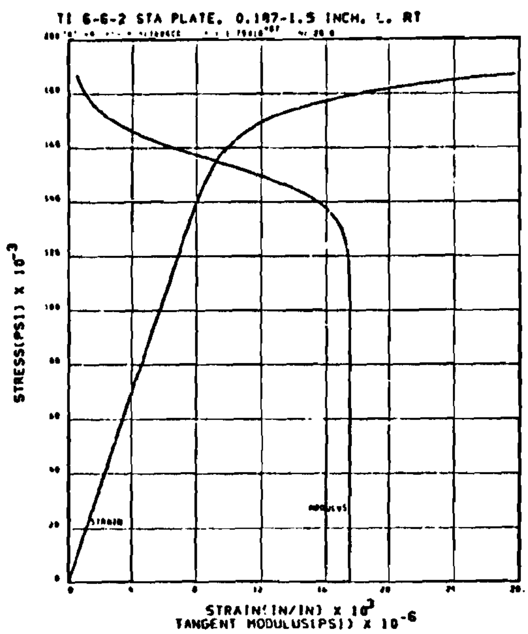

Figure 202 STRESS-STRAIN CHARTS FOR TITANIUM -- Continued

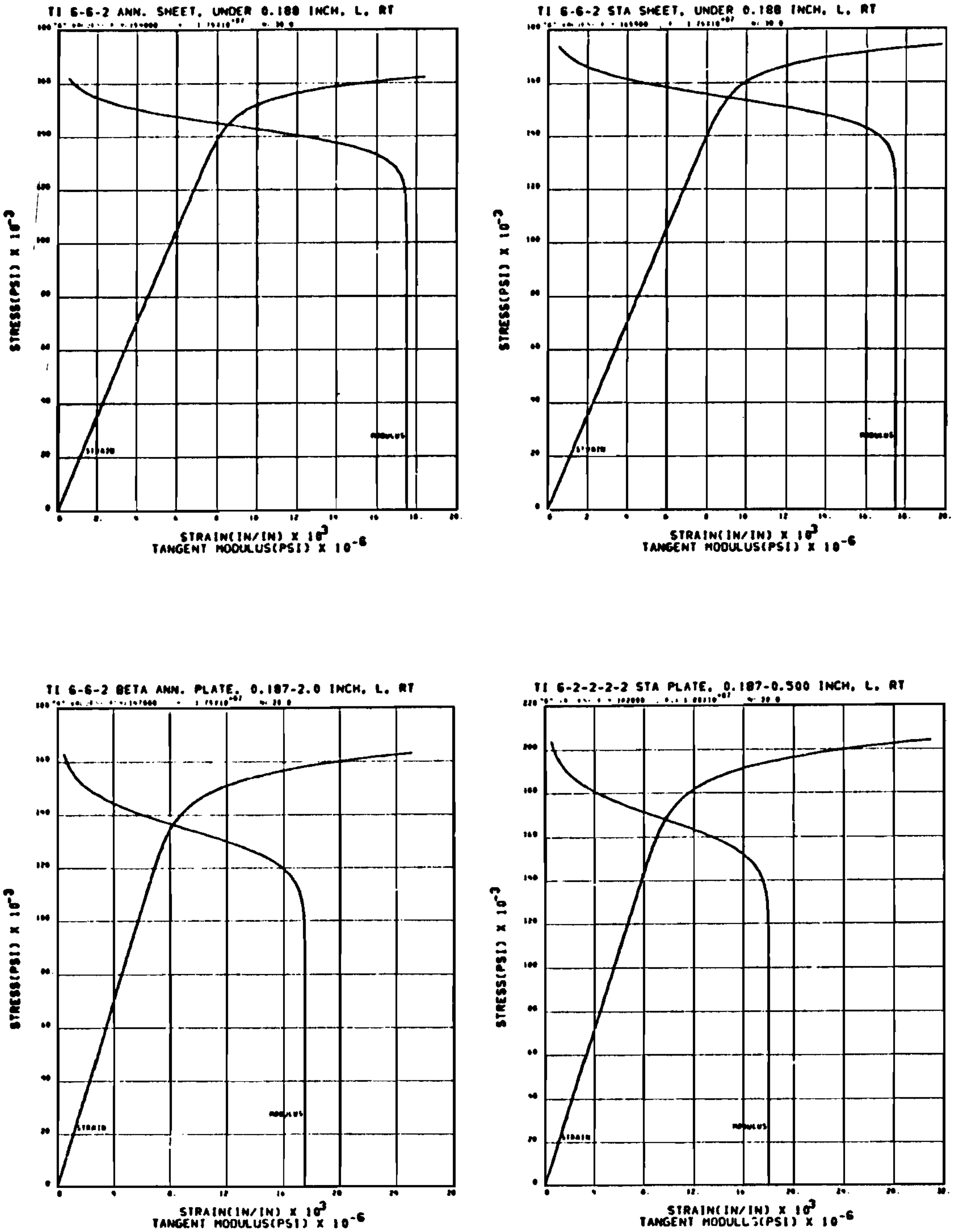

Figure 202 STRESS-STRAIN CHARTS FOR TITANIUM -- Continued

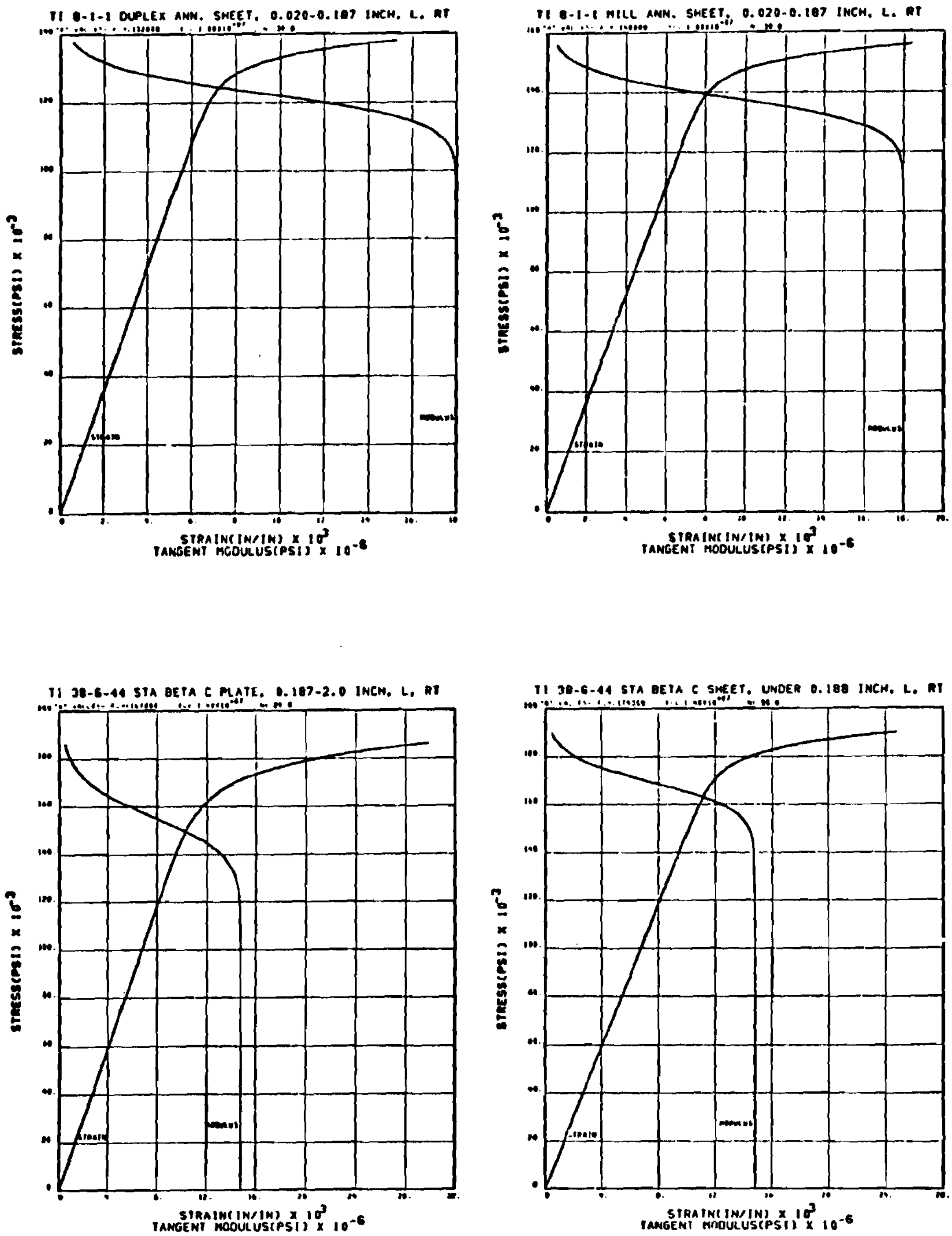

Figure 202 STRESS-STRAIN CHARTS FOR TITANIUM -- Continued

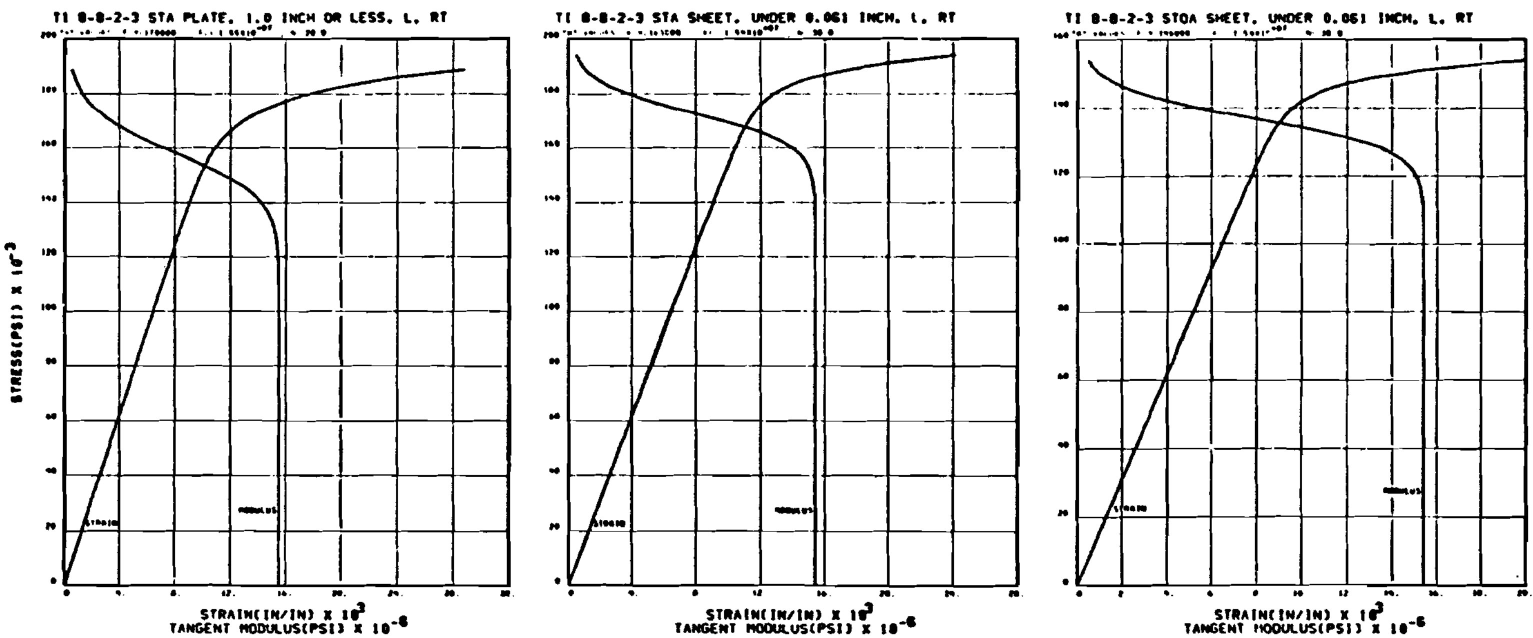

Figure 202 STRESS-STRAIN CHARTS FOR TITANIUM -- Concluded

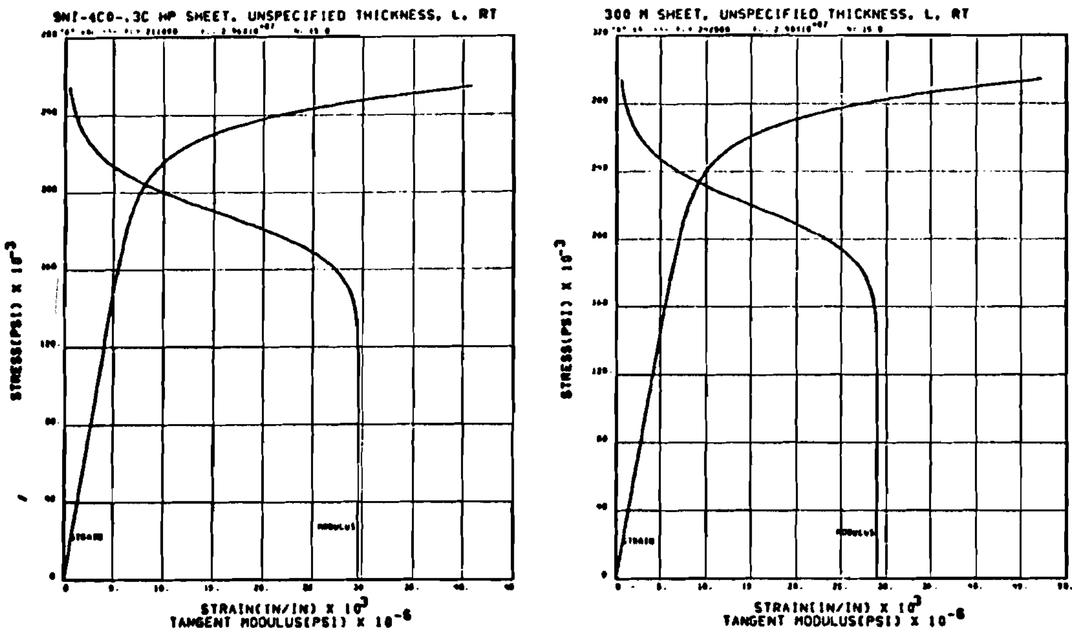

Figure 203 STRESS-STRAIN CHARTS FOR STEEL

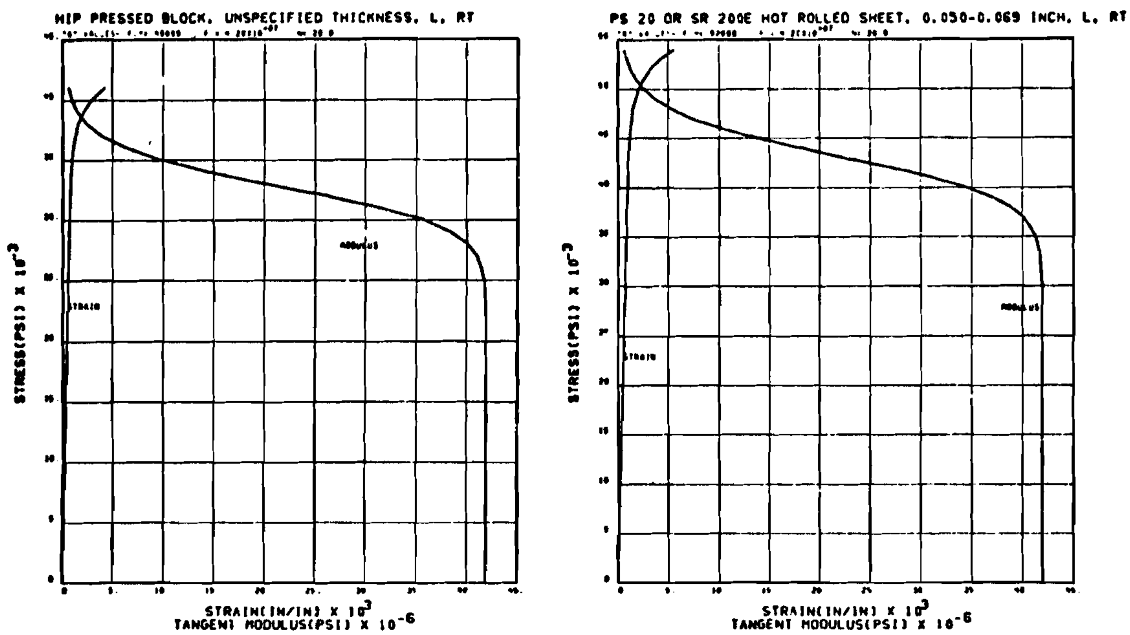

Figure 204 STRESS-STRAIN CHARTS FOR BERYLLIUM

2.0 CORRELATION OF NOTCHED SPECIMEN FATIGUE DATA

The material selection criteria developed for the study (Section 3.1), as well as the fatigue analyses to be made on new concepts, require the definition of fatigue data under specified conditions. Although significant quantities of fatigue data have been generated and reported in the literature through the years, data for specific notch conditions are often not available. A general approach for extending existing data to new conditions has, therefore, been considered and is discussed in this section.

The fatigue strength of structures subjected to operational environments is influenced by many factors. Notched coupon S-N data primarily reflects materials and simple notch factors (as noted in Table CXXX). thereby providing a basis for material selection and an initial approximation of structural performance. The factors reflected include material type, alloy and grain size; specimen failure point, notch geometry and size; stress magnitude, gradient and ratio R; and cycles to failure N under constant amplitude stress conditions.

The influence of failure point location and stress gradient is qualitatively illustrated in Figure 205. Fatigue strength decreases as surrounding material "support" to the failure point decreases, such that at corner edge conditions, the minimum strength occurs. Coupled with a stress concentration, e.g., at a notch, this defines the specimen initial failure point and therefore is a primary interest. (NOTE: "Rounding off" of critical edges provides a potential for fatigue strength improvement.) Also related to the "support" factor, decreasing stress gradient results in decreasing fatigue strength, as indicated. Zero gradient data is generally associated witn axial loading tests of unnotched specimen (i.e., $K_t = 1$); gradient data, with notched specimens ($K_t > 1$).

Comparison of notched-to-unnotched data therefore provides a basis for relating gradient effects to a convenient standard for which data is also more readily available.

Development of a fatigue data correlation procedure therefore requires the definition and use of stress concentration factors (Figure 206).

The theoretical stress factor (K_t) is defined on net section conditions assuming an ideal material (i.e., grain size is very small). An experimentally determined stress factor (K_n) is defined by accounting for real material conditions through a grain size factor (ρ'). Since specimen width (as indicated by the curve) has an influential effect on local stress magnitude (and gradient), it logically will also have an effect on fatigue capability. Therefore, K_t or K_n is a required parameter in fatigue data correlation.

The stress concentration factor in fatigue (K_f) is formed at constant N and R conditions by comparison of unnotched to notched specimen maximum cyclic stress levels as defined in Figure 207. A comparison at various N and R values provides the basis for establishment of an average value of K_f as illustrated in Figure 208 for one set of notched data and a material type. Plotting notched and unnotched specimen stress levels corresponding to various N and R conditions results in a typical curve as shown. The slope of the straight line (elastic) portion of the curve represents the average value of K_f.

TABLE CXXX APPLICABILITY OF NOTCHED COUPON S-N DATA					
ITEM	STRUCTURE FATIGUE STRENGTH FACTOR	NOTCHED COUPON S-N DATA DIRECTLY REPRESENTS FACTOR YES	LIMITED	NO	REMARKS
(a)	Material (type, alloy, grain size, etc.)	X			
(b)	Item (a) and notch geometry	X			
(c)	Item (b) and notch "by-passing" load[1]	X			[1] Generally representative of basic panel structure.
(d)	Item (c) and attachment interference load[1]		← - - - -	X[2]	[2] "Correction" factor required.
(e)	Item (b) and notch "source" load[3]		← - - - -	X[2]	[3] Generally representative of local splice structure.
(f)	Item (e) and attachment interference load[3]		← - - - -	X[2]	[4] Remark [2]. When most damaging loads are also the high loads, less "correction" required.
(g)	Items (d), (f) and influence of high spectrum loads		← - - - -	X[4]	

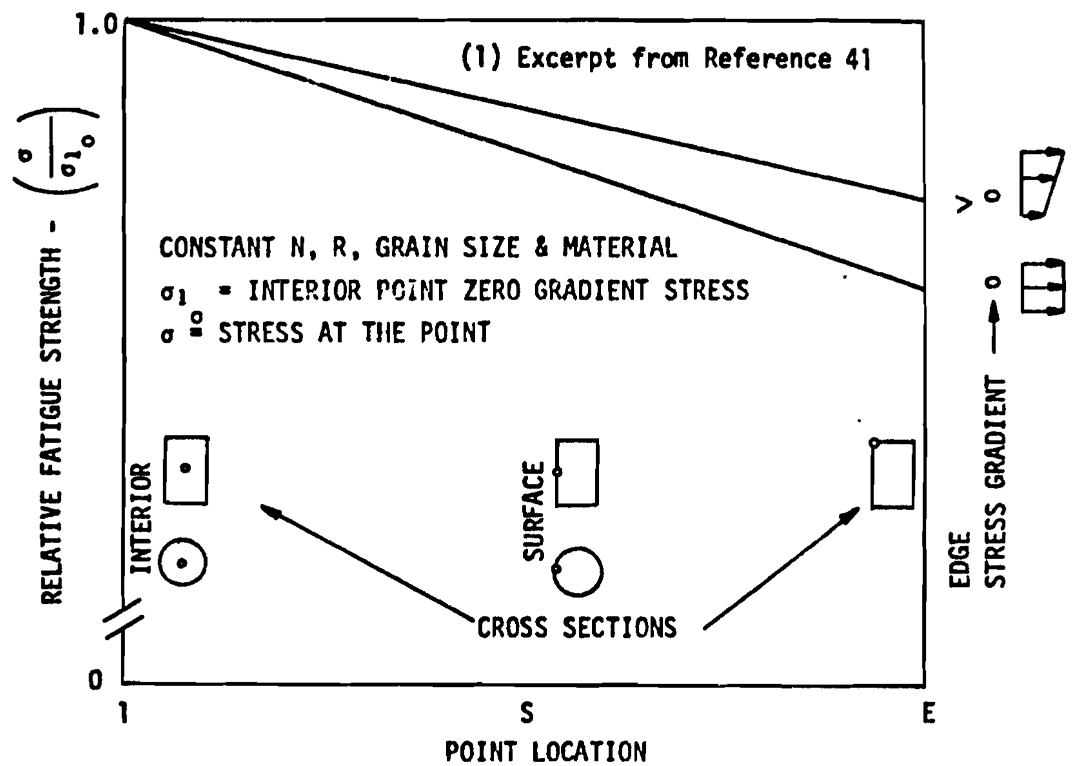

Figure 205 FATIGUE STRENGTH RELATIVE TO POINT LOCATION AND STRESS GRADIENT (1)

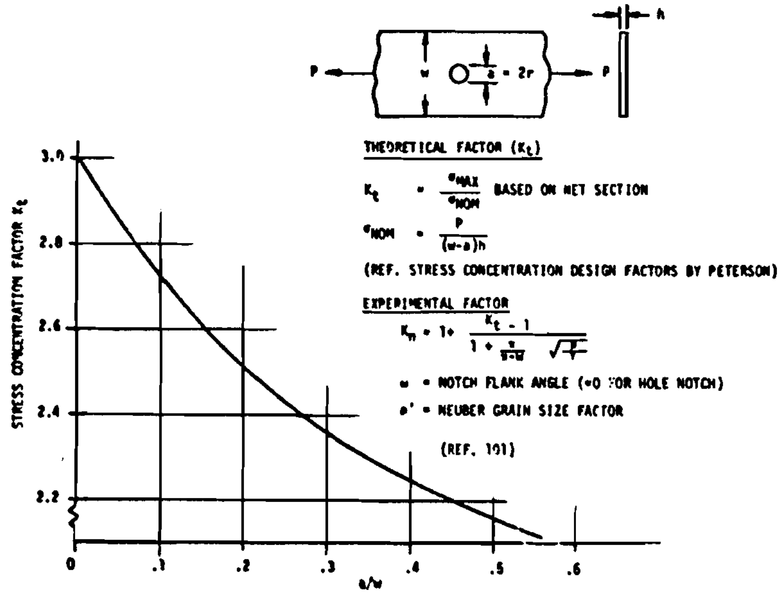

Figure 206 STRESS CONCENTRATION FACTOR DEFINITIONS

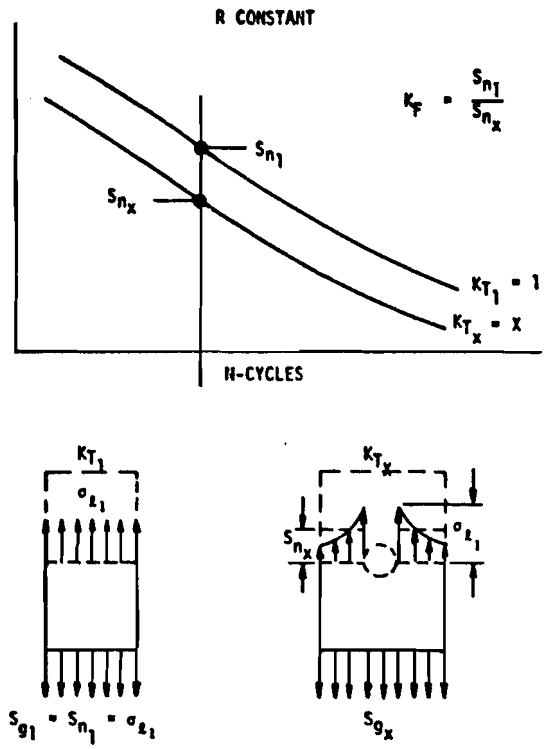

Figure 207 FATIGUE STRENGTH RELATIONSHIP BETWEEN NOTCHED AND UNNOTCHED SPECIMEN

Thus, each set of notched data for each material may be represented by a unique single value of K_f and K_t.

Recognizing that K_f and K_t are normally greater than or equal to unity permits formation of a convenient "notch sensitivity" parameter $q = \frac{K_f - 1}{K_t - 1}$ (Reference 55) where the limits q = 0 and 1 correspond to K_f = 1 and = K_t, respectively. The limiting value q = 1 indicates that the fatigue stress concentration factor is equal to the theoretical stress concentration factor, a condition which is approached (but generally not attained). For a constant notch radius-to-specimen width ratio (i.e., K_t = constant), a wider specimen (and corresponding larger notch radii) would have lower stress gradient (and fatigue strength) conditions and a q approaching unity. Therefore, it is logical to plot q versus notch radius r since fatigue strength is most sensitive to these geometric variables.

Basic S-N data (primarily developed by NACA and Battelle) on 2024-T3 bare sheet and 7075-T6 bare and clad sheet have been evaluated (in Reference 41) to establish the fatigue factors, K_f (Figures 209 through 211). The data represents hole, edge and fillet notches, $1 \lesssim K \lesssim 5$ and $0.0156 \lesssim r \lesssim 1.5$ in. Basic parameters (in accordance with the described approach) are summarized in Table CXXXI. The data points normalize fairly well (Figures 209 through 211) considering the inherent scatter in fatigue. The trends, in general, support the previous discussion; however, it should be recognized that the absolute value of q is based on the theoretical stress concentration factor K_t. Values of K_t are established on the basis of "ideal material" properties, including the assumption of small grain size dimension with respect to notch radius r, which could result in significant error, especially for low values of r. Neuber (Reference 56) provides for a modified stress concentration factor K_n which includes grain size and notch flank angle factors, ρ' and w, respectively.

$$K_n = 1 + \frac{K_t - 1}{1 + \frac{\pi}{\pi - w}\sqrt{\rho'/r}} \qquad (69)$$

For $\rho' = 0$, corresponding to ideal material conditions, $K_n = K_t$. For $\rho' > 0$, corresponding to actual material conditions, $K_n < K_t$. If K_n were to be used in lieu of K_t, this would result in generally increased and more realistic absolute values of notch sensitivity q. Since now the grain size effect would be normalized, the value 1 - q would also be a truer indication of the significance of stress gradient. However, for material evaluation purposes, this is considered to be more of an academic than a practical consideration. Hence, K_t is retained as the normalizing parameter. However, the above relationship is useful in that rearranging and assuming $K_n = K_f$ permits evaluation of a pseudo ρ' (= ρ'_f) for "best fit" of the (q) data.

$$q = \frac{K_f - 1}{K_t - 1} = \frac{K_n - 1}{K_t - 1} = \frac{1}{1 + \frac{\pi}{\pi - w}\sqrt{\rho'_f/r}} \qquad (70)$$

Average values of ρ'_f for r < 0.500 inches are established in Table CXXXI which result in the fitted curves shown in Figures 209 through 211.

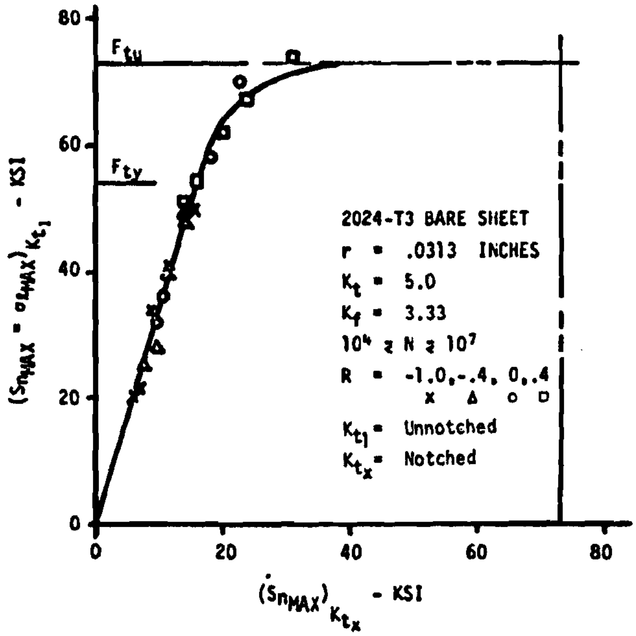

Figure 208 TYPICAL FATIGUE STRENGTH RELATIONSHIP OF NOTCHED-TO-UNNOTCHED SPECIMEN

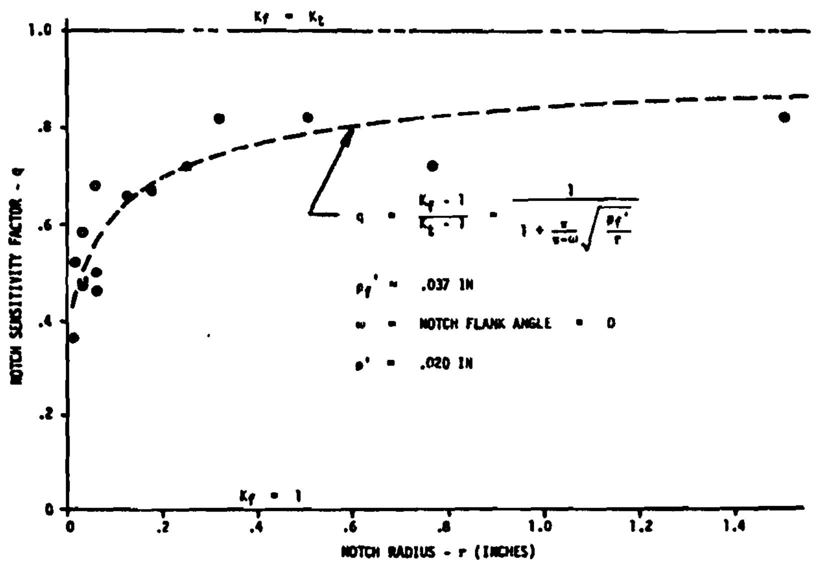

Figure 209 NOTCH SENSITIVITY OF 2024-T3 SHEET (BARE)

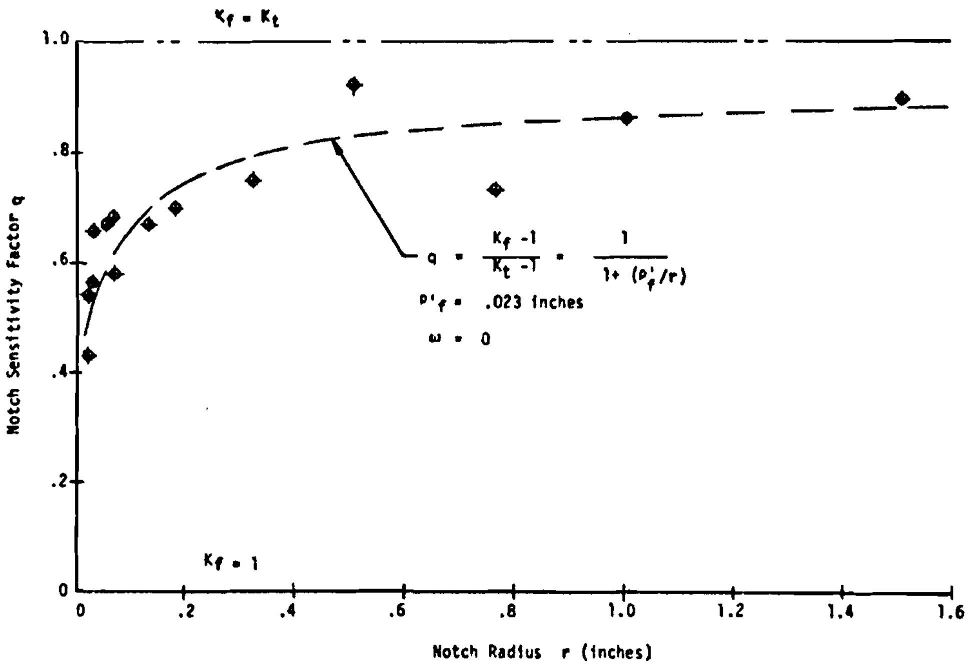

Figure 210 NOTCH SENSITIVITY OF 7075-T6 SHEET (BARE)

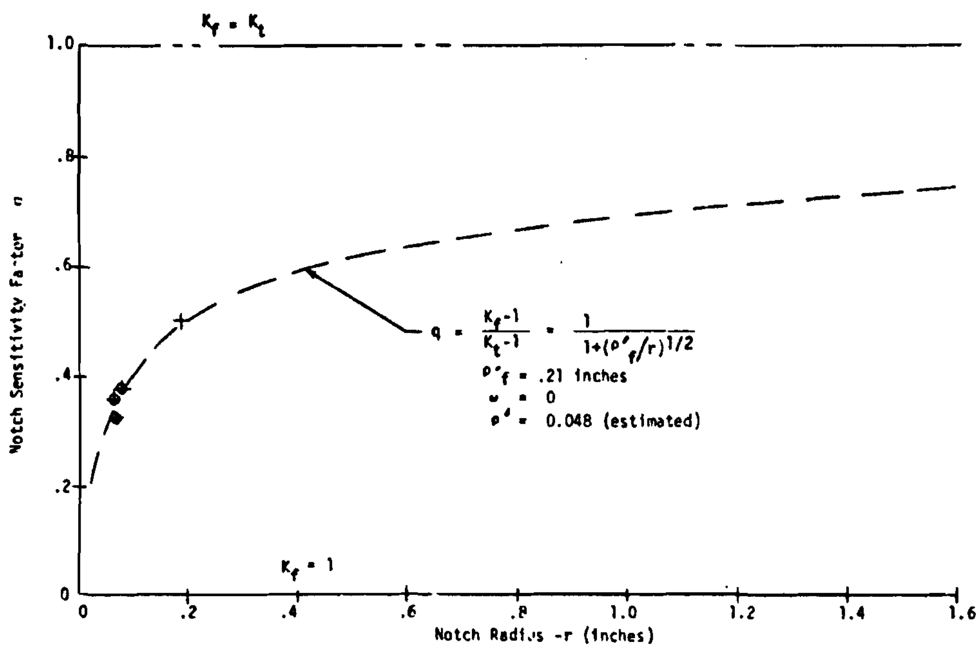

Figure 211 NOTCH SENSITIVITY OF 7075-T6 SHEET (CLAD)

TABLE CXXXI ALUMINUM ALLOY "NOTCH SENSITIVITY" DATA (REF. 41)

MATERIAL FACTORS	NOTCH[(1)] RADIUS r (in)	THEOR. SCF K_t	FATIGUE SCF K_f	$\frac{K_f - 1}{K_t - 1}$ " q	$r\left(\frac{1}{q} - 1\right)^2$ " ρ'_f (in)
2024-T3	1.500 H	2.0	1.82	.82	.0727
Bare	.760 E	1.5	1.36	.72	.1155
Sheet	.500 H	2.16	1.95	.82	.0242
F_{Tu} (L) = 73 KSI	.3175E	2.0	1.82	.82	.0153
	.250 H	2.67	2.20	.72	.0380
	.1736F	2.0	1.67	.67	.0418
	.125 H	2.67	2.10	.66	.0331
	.0625H	2.91	1.95	.50	.0625
	.0625H	2.43	1.66	.46	.0855
	.057 E	4.0	3.05	.68	.0126
	.0313E	5.0	3.33	.58	.0164
	.0313H	2.91	1.90	.47	.0400
	.0313H	2.67	1.80	.48	.0366
	.0195F	4.0	2.56	.52	.0166
	.0156H	2.82	1.65	.36	.0494
				AVE	(.037)
7075-T6	1.500 H	2.0	1.90	.90	.0181
Bare	1.00 H	2.16	2.00	.86	.0258
Sheet	.760 E	1.50	1.37	.74	.0930
F_{Tu} (L) = 83 KSI	.500 H	2.16	2.07	.92	.0039
	.3175E	2.00	1.75	.75	.0351
	.174 F	2.00	1.70	.70	.0321
	.125 H	2.16	1.78	.67	.0300
	.0625H	2.91	2.30	.68	.0138
	.0625H	2.43	1.83	.58	.0333
	.057 E	4.0	3.02	.67	.0138
	.0313E	5.0	3.64	.66	.0083
	.0313H	2.91	2.07	.56	.0190
	.0195F	4.0	2.62	.54	.0141
	.0156H	2.82	1.78	.43	.0272
				AVE	(.023)
7075-T6	.1875H	2.43	1.72	.50	.188
Clad	.078 H	2.60	1.60	.38	.207
Sheet	.0625H	2.60	1.57	.36	.198
F_{Tu} (L) = 75 KSI	.0625H	2.43	1.47	.33	.258
					(.21)

(1) Notch Flank Angle = 0 Radians

NOTCH TYPE: H = Hole, E = Edge, F = Fillet

The notch sensitivity trends are applicable for all values of N and R for which the stress level $S_{n(K_t=1)} \leq 1.10\ F_{ty}$. A plasticity correction factor to K_f is required for higher stress levels. The trends can be used to create notched ($K_t = x$) S-N data from unnotched ($K_t = 1$) data merely by identifying the desired condition of r (and K_t), establishing q (and K_f) and applying the definition of K_f (Figure 207).

$$S_{n(K_t = x)} = S_{n(K_t = 1)} / K_f \qquad (71)$$

The trends also can be used to convert available notched data to equivalent unnotched specimen data and then, if desired, to new conditions of r and K_t, as described. Representative $K_t = 1$ basic S-N data for 2024-T3 and 7075-T6 bare sheet is shown on Figures 212 and 213. Similar data on these and other materials appears in Reference 5.

Consideration of readily available MIL-HDBK-5 titanium alloy data resulted in a limited number of data points as shown in Figure 214. Extrapolation to higher notch radii may be accomplished by selection of a representative curve. This, however, points up the problem of limited data for many materials and alloys which may be of interest in the study. In order to further generalize the approach described above to accommodate newer materials where less fatigue data is available, it is desirable to establish a correlation, if possible, between the material notch sensitivity characteristics and other material properties (F_{tu}, F_{ty}, E, etc.) for which more data exists. Since notch sensitivity has been related to ρ'_f, the fatigue grain size factor, it may be possible to establish relationships between ρ'_f and ρ', the Neuber grain size factor, and thence between ρ' and basic material properties such as F_{ty} (Reference 57).

Investigation of available aluminum and titanium data indicates that a degree of correlation between ρ'_f and ρ' may exist as shown in Figure 215. Data relating ρ' and material strength properties (Table CXXXII) also show a degree of correlation as can be seen in Figure 216. General trends appear to exist for the various materials as indicated by the trend lines through the data points. It is of interest that the titanium trend line is counter to that of aluminum and steel.

Assuming that the trend relationships are valid, the procedure can be used to obtain missing fatigue data. For a given material and yield strength, ρ' and ρ'_f may be identified and for a selected notch radius (and specimen width), q, K_t and K_f identified. However, a relationship between one of these parameters and $S_{n_{max}}(K_t = 1)$ is still required to permit definition of S-N data based on knowledge of F_{ty} only. Preliminary checks have not revealed any simple correlation. This might be expected, considering that apparently none have been published.

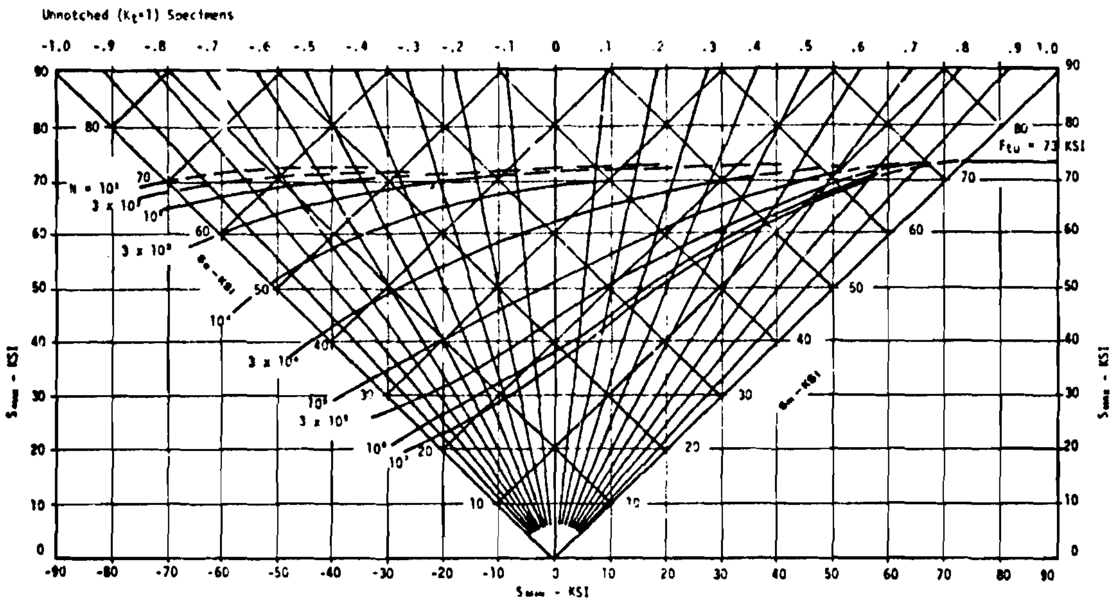

Figure 212 AXIAL FATIGUE CONSTANT-LIFE CURVES FOR 2024-T3 ALUMINUM BARE SHEET

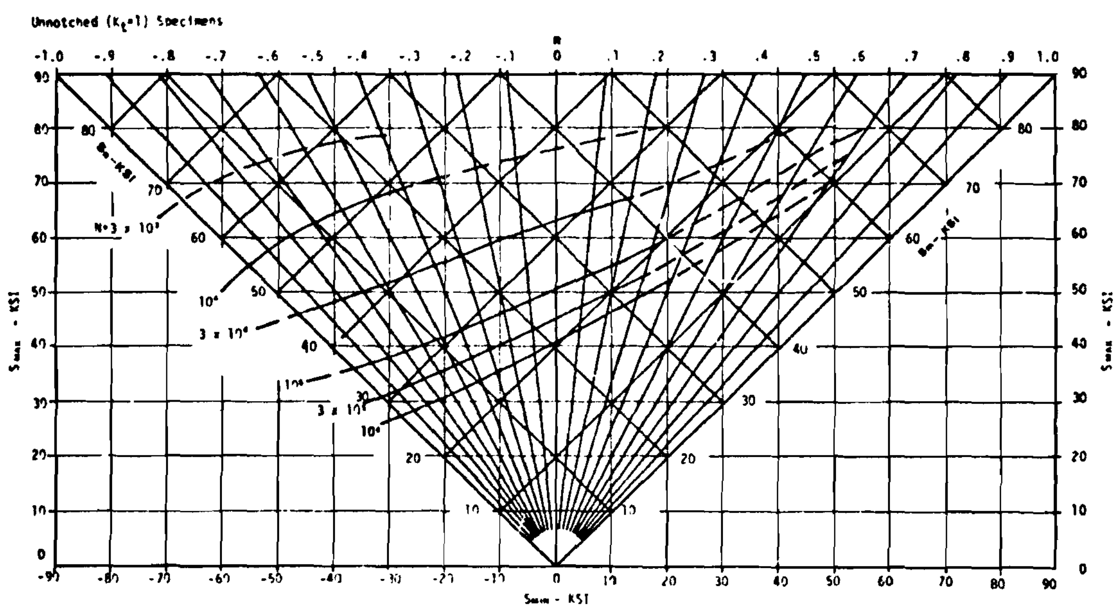

Figure 213 AXIAL FATIGUE CONSTANT-LIFE CURVES FOR 7075-T6 ALUMINUM BARE SHEET

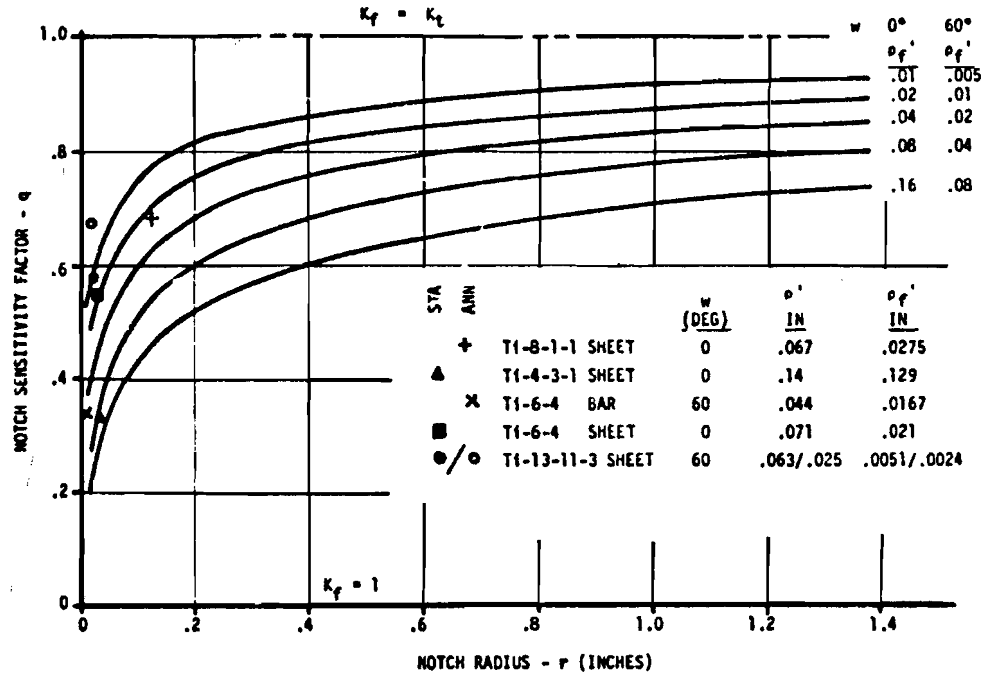

Figure 214 NOTCH SENSITIVITY OF SOME TITANIUM ALLOYS

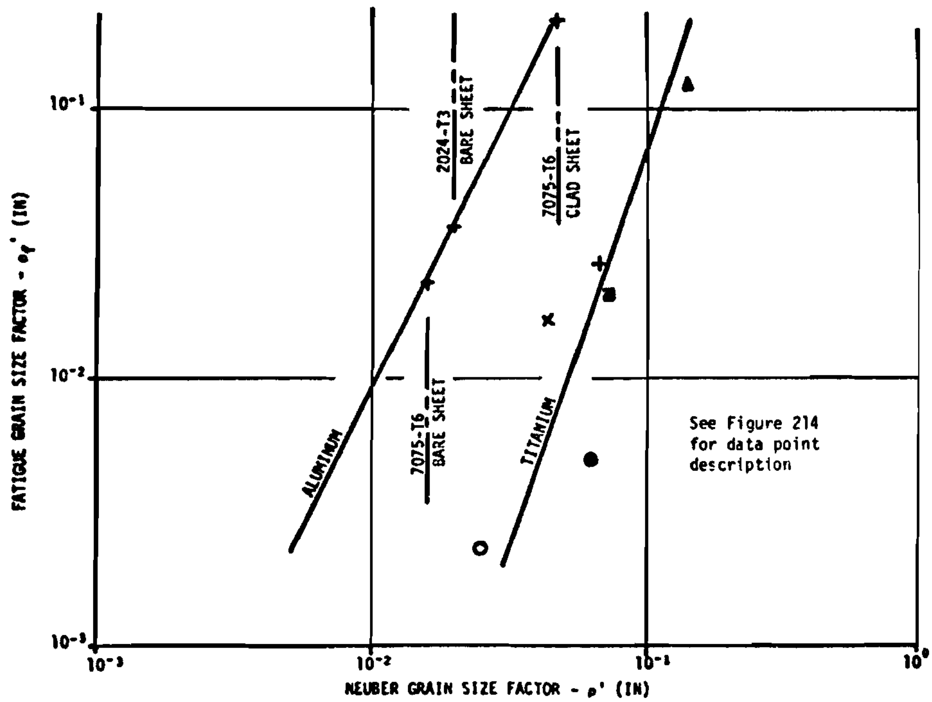

Figure 215 GRAIN SIZE FACTOR RELATIONSHIPS

TABLE CXXXII MATERIAL GRAIN SIZE FACTOR CORRELATION TO STRENGTH PROPERTIES(1)

Material	Alloy	Product Form	Ftu (L) (KSI)	Fty (L) (KSI)	ρ' (IN)
Aluminum	2014-T6	Rod, bar	72.7	65.1	.020
Aluminum	2024-T4	Rod, bar	77	55.3	.0'8
Aluminum	2024-T3	Bare sheet	73	54	.020
Aluminum	7075-T6	Rod, bar	87.2	77.6	.014
Aluminum	7075-T6	Bare sheet	82.5	76.0	.017
Titanium	8Al-1Mo-1V	Sheet	148.	136.	.067
Titanium	4Al-3Mo-1V (Sta)	Sheet	196.	167.	.14
Titanium	6Al-4V (Annealed)	Bar	136.5	128.5	.044
Titanium	6Al-4V (Sta)	Sheet	172.	158.	.071
Titanium	13V-11Cr-3Al (Annealc)	Sheet	138.5	132.8	.025
Titanium	13V-11Cr-3Al (Sta)	Sheet	174.5	156.7	.063
Steel	AISI4340	Bar	125.	115 Est	.0023
Steel	AISI4340	Bar	158.5	146.9	.001
Steel	AISI4340	Bar	208.	187 Est	.0002
Steel	AISI4340	Bar	266.	232.	.000009
Steel	300M	Forging	290.	242.	.000009
Steel	PH15-7Mo (TH1050)	Sheet	201.	196.	.011
Steel	17-4PH (H900)	Bar	201.5	194.5	.0002[illegible]
Steel	Inconel 718	Sheet	197.	164.	.00014

(1) Room temperature data from Reference 10

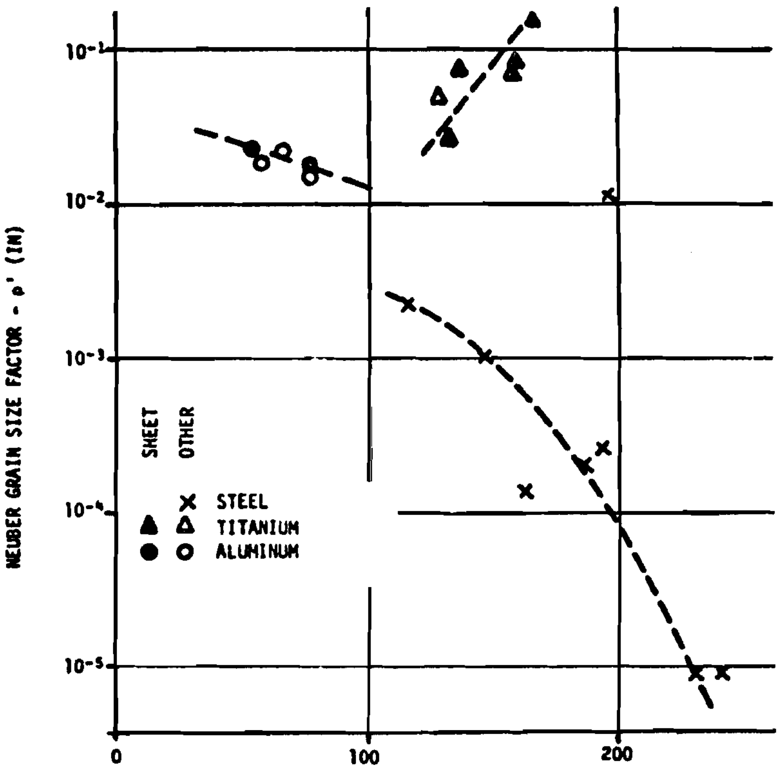

Figure 216 CORRELATION OF NEUBER GRAIN SIZE FACTOR TO YIELD STRENGTH

REFERENCES

1. Harmon, M. B. et. al.; "Medium STOL Aircraft Structural Loads", Douglas Aircraft Co., MDC Report No. J6638, June 1974.

2. Denke, P. H., "A Generalized Digital Computer Analysis of Statically Indeterminate Structures", Douglas Aircraft Co., DAC Paper #834, September, 1959.

3. Denke, P. H., "A Computerized Static & Dynamic Structural Analysis System-Part III, Engineering Aspects & Mathematical Formulation of the Problem", Douglas Aircraft Co., DAC Paper 3213, Presented to the SAE International Automotive Congress and Exposition, January, 1965.

4. Pickard, J. and Morris, R. C., "Format Fortran Matrix Abstraction Technique", Douglas Aircraft Co., Air Force Report AFFDL-TR-66-207, Volume II, V, VI, VII & Supplements, August 1970.

5. Anonymous, "Military Standardization Handbook Metallic Materials and Elements for Aerospace Vehicles and Structures", MIL-HDBK-5B, September 1, 1971.

6. Turley, R. V., "Design Property Data for New Aluminum Alloys" - Vol 1 - Summary, Douglas Aircraft Co., Report No. MDC-J5873/01, March, 1973.

7. Sprowls, D. O., "Resistance of Wrought High Strength Aluminum Alloys to Stress Corrosion", ALCOA Technical Paper No. 17, 1962.

8. Hahn, G. T., Simon, R., "Metallurgical Control of Fatigue Crack Growth in High Strength Aluminum Alloys", AD745989, AFML TR-72-48, May, 1972.

9. Wang, D., "A Study of Modeling Methods for Failsafe Design & Testing", Douglas Aircraft Co., Report No. J0240, September, 1969.

10. Kaufman, J. G., "Fracture Toughness Testing, Including Screening and Quality Control Testing in the Aluminum Industry", ALCOA Report No. 9-72-18, July 72.

11. Anonymous, "Damage Tolerant Design Handbook", Battelle Columbus Laboratories MCIC-HB-01, December, 1972.

12. Rosenkranz, C. et. al., "Advanced Lightweight Fighter Structural Concept Study", AFFDL-TR-72-98, July, 1972.

13. Garland, K., "Fracture Toughness of X7475-T61 Aluminum Alloy Sheet", McDonnell Aircraft Company Report No. 604-431, August 17, 1971.

14. Mayer, L. W., "ALCOA Alloy 7050", ALCOA Green Letter No. 220, April, 1973.

15. Staley, J. T., "Further Development of Aluminum Alloy X7050", Aluminum Company of America, NASA Contract No. N00019-71-C-0131 Final Report, May 8, 1972.

REFERENCES (Continued)

16. Dubensky, R. G., "Fatigue Crack Propagation in 2024-T3 & 7075-T6 Aluminum Alloys at High Stress", NASA CR-1732, March, 1971.

17. Anonymous, "Computed Design Mechanical Properties of 7175-T736 Hand Forgings (F33615-71-1571) Preliminary Data", Attachment 5 to A3-250-AB00-53, Forty-Fifth Meeting of MIL-HDBK-5 Coordination Committee, April, 1973.

18. Brownhill, D. J. et. al., "Mechanical Properties, Including Fracture Toughness and Fatigue, Corrosion Characteristics and Fatigue Crack Propagation Rates of Stress Relieved Aluminum Alloy Hand Forgings" - AD868376, AFML TR-70-10, February, 1970.

19. Danielson, G. R., Deneff, G. V., et. al., "Advanced Military Tanker Wing/ Fuselage Structural Concept Study", AFFDL-TR-72-89, July, 1972.

20. Staley, J. T., Evancho, J. W., "Development of a Cladding Alloy for 7050-T76 Sheet and Quenching Characteristics of Aluminum Alloy 7050", ALCOA Research Laboratories, NASA Contract N00019-72-C-0146.

21. Davies, R. E., "Design Mechanical Properties, Fracture Toughness, Fatigue Properties, Exfoliation and Stress Corrosion Resistance of 7050 Sheet, Plate, Extrusions, Hand Forgings, Die Forgings", Contract NASA N00019-72-C-0512, 5th Letter Progress Report, April 4, 1973.

22. Dill, H. D., Rich, D. L., "Evaluation of Aluminum Plate Alloys 7075-T7351, X7050-T73651 & 2021-T81, McDonnell Douglas Corp., Report No. MDC-A1755, May, 1972.

23. Davis, D. F. et. al., "AMS ADP Fighter Wing Concepts Study", General Dynamics, Convair Division, AFFDL-TR-73-50, Preliminary Draft, Material Test Data, May, 1973.

24. Davies, R. E., Kaufman, J. G., "Design Mechanical Properties of 7050 Sheet, Plate, Hand Forgings & Extrusions", Aluminum Co. of America, NASA Contract-N00019-72-C-0512 Item 0002, 9th Bi-Monthly Progress Letter Report, December 12, 1973.

25. Figge, F. A., et. al., "AMS ADP Fighter Wing Concepts Study", Northrop Corp., AFFDL-TR-73-52, Preliminary Draft, Materials Test Data, May, 1973.

26. Turley, R. V., Ross, S. V., "Design Property Data for New Aluminum Alloys", Vol. II - Data Handbook, Douglas Aircraft Company, Report No. MDC-J5873/02, March 20, 1973.

27. Larner, H., "Proposed Revisions to ALCOA Green Letter No. 216, ALCOA 467 Process X7475", Memorandum to B. J. Alperin, Douglas Aircraft Co., May 1973.

28. Anonymous, "Aluminum Alloy Forgings (7049-T73)", AMS 4111, November 1970.

29. Anonymous, "Computer Design Mechanical Properties of 7049-T73 Die Forgings", Item 71-20, Forty-Fifth Meeting of MIL-HDBK-5 Coordination Committee, April 1973.

REFERENCES (Continued)

30. Bigham, C. R. et. al., "AMS ADP Cargo Wing Concepts Study", Lockheed GA, Co., AFFDR-TR-73-51, Preliminary Draft, Materials Test Data, May 1973.

31. Emero, D. H. & Spunt, L., "Optimization of Multirib & Multiweb Wing Box Structures Under Shear and Moment Loads", AIAA 6th Structures and Materials Conference, Palm Springs, California, April 1965.

32. Crawford, R. F. and Burns, A. B., "Strength, Efficiency, and Design Data for Beryllium Structures", Lockheed Missiles and Space Company, ASD TR 61-692, February, 1962.

33. Wilhem, D. P., "Fracture Mechanics Guidelines for Aircraft Structure Applications, AFFDL-TR-69-111, February 1970.

34. Schofield, B. E., "The Combined Effect of Torsional Stiffness & Compressive Load Requirements on Wing Panel Weight", Douglas Aircraft Co., Report DAC No. 33877, July 1967.

35. Schofield, B. E., "Computer- Aided Design of Skin Stiffened Compression Panels", AIAA/ASME 8th Structures, Structural Dynamics & Materials Conference, Palm Springs, March 1967.

36. U.S. Department of Defense, "Structural Sandwich Composites", MIL-HDBK-23A, December 30, 1968.

37. Shanley, F. R., "Weight-Strength Analysis of Aircraft Structures", Dover Publications, Inc. 1960.

38. "Study to Assess the Utility of Advanced Materials in Aircraft Structures (U)", Contract AF33(615)-5085, Douglas Aircraft Company Report No. DAC 56087A (Secret), October 1967.

39. Kenyon, R. E., "Techniques for Estimating Weapon System Structural Costs", General Dynamics, AFFDL-TR-71-74, April 1972.

40. Grandt, A. F. and Gallagher, J. P., "Developing an Infinite Life Design Procedure for Fastener Holes Utilizing Fracture Mechanics", Air Force Materials and Flight Dynamics Laboratories, Technical Memorandum LLP72-3, September 1972.

41. Deneff, G. V., "Fatigue Prediction Study", Douglas Aircraft Company, WADD TR 61-153, May 1961.

42. Lall, T. R., "Structural Backup Data, Book 6 - Fatigue and Damage Tolerance", Douglas Aircraft Company, Report DAC No. J6454, February 1974.

43. Abelkis, P. R., and Bobovski, W. P., "Fatigue Strength Design and Analysis of Aircraft Structures - Part II, Fatigue Life Analysis Computer Program - Users Manual", AFFDL-TR-66-197.

REFERENCES (Continued)

44. Swift, T., "The Effects of Fastener Flexibility and Stiffener Geometry on the Stress Intensity in Stiffened Cracked Sheets", DAC Report No. J6502, February 1974.

45. Liu, A. F., "Stress Intensity Factor for a Corner Crack", Engineering Fracture Mechanics, 1972, Vol. 4, Pergamon Press.

46. Packman, P. F., et al., "The Applicability of a Fracture Mechanics - Nondestructive Testing Design Criterion for Aerospace Structures", Metals Engineering Quarterly, Vol. 9, No. 3, August 1969.

47. Pearson, H. S., "Critical Crack Size Compared with NDT Capability", Pratt & Whitney Aircraft, 15 July 1973.

48. Southworth, H., "Practical Sensitivity Limits of Production Nondestructive Testing Methods in Aluminum and Steel", AFML IR-1, November 1973.

49. Frederick, S. F., "Service Life of Re-usable Structures Based on NDT", McDonnell Douglas Astronautics Company (Western Division) Report MDC G2668, December 1971.

50. Tiede, D. A., "Improved Detection of Tight Defects in Aluminum by Application of a Tensile Load", McDonnell Douglas Astronautics Company (Western Division) Report MDC G2081, 1971.

51. Anderson, R. T., et al., "Detection of Fatigue Cracks by Nondestructive Testing Methods" Convair Aerospace Division, Report No. GDCA-DBG73-002, March 1973.

52. Hagemaier, D. T., "Nondestructive Testing of Bonded Honeycomb Structures", Nondestructive Testing; Part 1, December 1971; Part 2, February 1972.

53. Hagman, E. L., "Fatigue Crack Detection Through Organic Coatings", Douglas Aircraft Company, M&PE Report No. LR-DAC-6835 dated 5/29/73.

54. Anonymous, "USAF Cost and Planning Factors", AFM 173-10, Cost and Economic Analysis Division, Directorate of Management Analysis, Comptroller of the Air Force, dated 1 July 1973.

55. Garland, K., "Evaluation of 7050-T736 Die Forgings," McDonnell Douglas Report No. 514-131.10, February 20, 1973.

56. McCarty, et. al., "AMS ADP Cargo Fuselage Concepts Study," Boeing Co., AFFDL-TR-73-53, Preliminary Draft, Materials Test Data, May 1973.

57. Turley, R. V., Ross, S. V., "Design Property Data for New Aluminum Alloys - Vol. III - Test Data," Douglas Aircraft Company Report No. MDC - J5873/02, March 20, 1973.

58. Hyatt, W. V., "Use of Precracked Specimens in Stress Corrosion Testing of High Strength Aluminum Alloys," Corrosion - NACE, 26-11, p. 487, November 1970.

REFERENCES (Continued)

59. Kaufman, J. G., "Fracture Toughness Testing, Including Screening and Quality Control Testing in the Aluminum Industry," ALCOA Report No. 9-72-18, July, 1972.

60. Jones, R. E., "Fracture Toughness and Fatigue Crack Growth of 7175-T736 Aluminum Alloy Forging at Several Temperatures," AD748257, AFML TR-72-1, February, 1972.

61. Anonymous, "Computed Design Mechanical Properties of 7175-T736 Hand Forgings (F33615-71-1571), Preliminary Data," Attachment 5 to A3-250-AB00-53, Forty-fifth Meeting of Mil-HDBK-5 Coordination Committee, April 1973.

62. Van Orden, J. M., "Evaluation of 7049-T73 Aluminum Alloy Hand Forged Billet," Lockheed California Company Report No. LR 23447, February, 1970.

63. Jones, R. E., "Mechanical Properties of 7049-T73 and 7049-T76 Aluminum Alloy Extrusions at Several Temperatures," AFML-TR-72-2, February 1972.

64. Anonymous, "Proposed Design Mechanical Properties of Aluminum Alloy 7075 Extrusions" Item 72-16, Forty Fifth Meeting of Mil-HDBK-5 Coordination Committee, April 1973.

65. Wang., D., "Unpublished 1972 IRAD Data," Douglas Aircraft Company.

66. Dickson, J. A., "ALCOA 467 Process X7475 Alloy," ALCOA Green Letter (Rev.) October, 1971.

67. Newcomber, R. E., "Improved Aluminum Alloys," McDonnell Douglas Corporation Report No. A 1666, May, 1972.

68. Cervay, R. R., "Engineering Design Data for Aluminum Alloy 7475 in the T761 and T61 Condition," AD 753709, AFML-TR-72-173, September, 1972.

69. Wood, R. A., Favor, R. J., "Titanium Alloys Handbook," Metals and Ceramics Information Center, Battelle Columbus Laboratories, MCIC-HB-02, December, 1972.

70. Anonymous, "Aircraft Designers Handbook for Titanium and Titanium Alloys," AFML-TR-67-142, March, 1967.

71. Pitman, W. A., et al., "Preliminary Design Technical Summary - Phase IA - Wing Carrythrough Structure for an Advanced Metallic Air Vehicle," AFFDL-TR-72-65, July, 1972.

72. Neu, C. W., "Effect of Grain Orientation on Susceptibility of Two Titanium Plate Alloys to Stress Corrosion," AD 745293, June, 1972.

73. Sommer, A. W., Martin, G. R., "Design Allowables for Titanium Alloys," 857807, June, 1969.

REFERENCES (Continued)

74. Anonymous, "Advanced Metallic Air Vehicle Structure Program," General Dynamics, Convair Division, AFFDL-TR-73-1, January 1973.

75. Amateau, M. F., et al., "The Effect of Microstructure on Fatigue Crack Propagation in Ti-6AL-6V-2 Sn Alloy," AD 733335, October 1971.

76. Garland, K., Newcomber, R. E., "Methods to Obtain Fracture Toughness of Titanium Alloy," McDonnell Douglas Report, MDC A1123, June, 1971.

77. Anonymous, "Advanced Metallic Air Vehicle Structure Program," General Dynamics, Fort Worth, Texas, AFFDL-TR-72-75, June, 1972.

78. Mechanical Property Data, Ti-8Mo-8V-2Fe-3AL Alloy" AFML Contract F33615-72-C-1280, Battelle, Draft March, 1973.

79. Anonymous, "Mechanical Property Data Ti-6AL-2Zr-2Sn-2MO-2CR Alloy," Battelle Columbus Laboratories, Contract No. F33615-72-C-1280, April, 1973.

80. Bartolo, L. J., et al., "Deep-Hardenable Titanium Alloy," RMI Company, Contract No. F33615-72-C-1152, Preliminary Draft, March 1973.

81. Anonymous, Unpublished Data, General Dynamics, Convair Division, November, 1973.

82. Crooker, T. W., "The Role of Fracture Toughness in Low Cycle Fatigue Crack Propagation for High Strength Alloys," AD 747243, January, 1972.

83. Freed, C. N., et al., "Effect of Sheet Thickness on the Fracture Toughness Resistance K_c Parameter for Titanium Alloys," AD 753198, November, 1972.

84. Lenning, G. (TMCA), Private Communication to S. M. Weiman, Douglas Aircraft Company, June 13, 1973.

85. Anonymous, "Armco Advanced Materials Data Manual," Armco Steel Corp., 1966.

86. Anonymous, "Aerospace Structural Metals Handbook," AFML-TR-68-115, 1973.

87. Bullock, D. F., et al., "Evaluation of the Mechanical Properties of 9 Ni-4Co Steel Forgings," AFML-TR-68-57, March, 1968.

88. Hall, L. R., Masters, J. N., "Investigation of Stress and Mechanical Environments on the Prediction of Fracture in Aircraft Structural Materials," Boeing Company, AFSC Contract Number F33615-71-C-1687, June 1971 to December 1972.

89. Anonymous, "Report to the NASA Research and Technology Advisory Committee on Materials and Structures," NASA - Marshall Space Flight Center, January, 1973.

REFERENCES (Concluded)

90. Thrash, C. V., "Steel 300M (Vacuum Melted)," Douglas Aircraft Material Specification (DMS 1935), February 3, 1969.

91. Ault, R. T., et al., "Development of an Improved Ultra-High Strength Steel for Forged Aircraft Components," AFML-TR-27, February, 1971.

92. Hughes, B. G., Republic Steel Corporation, "Private Communication of Unpublished Data," to R. Gassner, Douglas Aircraft Company, May 31, 1973.

93. Deel, O. L., Hyler, W. S., "Engineering Data on Newly Developed Structural Materials," AFML-TR-67-418, April, 1968.

94. Anderson, R. H., "Evaluation of Beryllium Sheet," McDonnell Douglas Corporation, Report No. DAC 59539, April, 1968.

95. Conrad, H., et al., "The Fracture Toughness of Beryllium," Journal of Testing and Evaluation," p. 88, March 1973.

96. Finn, J. M., et al., "Design, Fabrication and Ground Testing of the F-4 Beryllium Rudder," AFFDL-TR-67-68, April, 1967.

97. Finn, J. M., et al., "Design, Fabrication, Testing and Evaluation of Damage Tolerant Beryllium Structures," AFFDL-TR-68-108, August, 1968.

98. Strock, R., K. B. Industries. Producers estimated minimum properties, telecon with R. H. Anderson, MDC, September 14, 1973.

99. Anderson, R. H., McDonnell Douglas Corporation Telecon with Brush Wellman Corporation re: unpublished data on fracture toughness, September 14, 1973.

100. Peterson, R. E., "Stress Concentration Design Factors," John Wiley and Sons, Inc., New York.

101. Neuber, Heinz, "Theory of Notch Stresses, Principles for Exact Stress Calculation," English Translation of the German Version for the David Taylor Model Basin, U.S. Navy (Publisner, J. W. Edwards, Ann Arbor, Michigan, 1946).

102. Dieter, George E., Jr., "Mechanical Metallurgy," McGraw Hill, P. 121, 1961.

END

DATE

FILMED

4-10-75

NTIS